

9106270146 910618
PDR ADOCK 05000315
PDR

AMERICAN ELECTRIC POWER
SERVICE CORPORATION

- ☒ APPROVED IN GENERAL
☐ APPROVED EXCEPT AS NOTED
☐ NOT APPROVED
☐ FOR REFERENCE ONLY

BY Paul H. Scherf DATE 1/4/90

D. C. COOK UNIT 2 LOW TEMPERATURE OVERPRESSURE

PROTECTION SYSTEM (LTOPS) SETPOINT EVALUATION

(COPY 2 OF 3)

I&C COPY

JUNE 1989

WESTINGHOUSE ELECTRIC CORPORATION

10

11

12

13

14

15

16

17

18

19

20

21

22

23

24

25

26

27

28

29

30

31

32

33

34

35

36

37

38

39

40



INDEX

<u>Section</u>	<u>Page No.</u>
Introduction.....	S.1
Summary of Results.....	S.2
1.0 Description of the Low Temperature Transients.....	1.1
1.1 General Description.....	1.2
1.2 Operation.....	1.2
1.3. Potential Overpressure Transients.....	1.5
1.3.1 Summary of Mass Input Transients.....	1.5
1.3.1.1 Inadvertent Safety Injection.....	1.5
1.3.1.2 Charging/Letdown Flow Mismatch.....	1.7
1.3.2 Summary of Heat Input Transients.....	1.7
1.3.2.1 Actuation of Pressurizer Heaters.....	1.7
1.3.2.2 Loss of RHRS Cooling.....	1.8
1.3.2.3 RCP Startup With Temperature Asymmetry.....	1.8
1.3.2.4 Relative Severity of the Heat Input Transients.....	1.10
1.4 Summary of Transient Evaluation.....	1.10
2.0 Description of the LTOPS Setpoint Algorithm.....	2.1
2.1 Pressure Limits Selection.....	2.1
2.2 Mass Input Considerations.....	2.7
2.3 Heat Input Considerations.....	2.7
2.4 Final Setpoint Selection.....	2.8
3.0 LTOPS Setpoint Analysis for D.C. Cook Unit 2.....	3.1
3.1 Operational Limits.....	3.2
3.2 PORV Stroke Time.....	3.5
3.3 PORV Operation.....	3.5
3.4 Mass Input Considerations.....	3.6
3.5 Heat Input Considerations.....	3.11
3.6 Specifications for Mass Input Transients.....	3.18
3.7 Specifications for Heat Input Transients.....	3.19
3.8. Setpoint Evaluation.....	3.20

10

11

12

13

14

15

16

17

18

19

20

21

22

23

24

25

26

27

28

29

30

31

32

33

34

35

36

37

38

39

40

41

42

43

44

45

46

47

48

49

50

INDEX (Cont'd)

Section

Page No.

4.0 Correlation to WOG LTOPS Setpoint Methodology.....	4.1
4.1 WOG Methodology LTOPS Setpoints.....	4.1
4.2 LOFTRAN/WOG Correlation.....	4.10
4.3 Impact of Steam Generator Tube Plugging.....	4.14

100

100

100

100

100

100

100

100

100

100

100

100

100

100

100

100

100

100

100

100

100

100

100

100

100

100

100

D. C. COOK UNIT 2 LOW TEMPERATURE OVERPRESSURE PROTECTION SYSTEM SETPOINT ANALYSIS

INTRODUCTION

USNRC Regulatory Guide 1.99 Revision 2, "Radiation Embrittlement of Reactor Vessel Materials," dated May, 1988 became official with it's publication in the Federal Register on June 8, 1988. The guide revises the general procedures acceptable to the NRC staff for calculating the effects of neutron radiation embrittlement of the low alloy steels currently used for light water cooled reactor vessels.

Appendix G of 10 CFR Part 50 provides the fracture toughness requirements for reactor pressure vessels under certain conditions. To ensure that the Appendix G limits are not exceeded during any anticipated operational occurrence, technical specification pressure-temperature limits are provided during low temperature operations. The embrittlement algorithm specified by revision 2 of Regulatory Guide 1.99 is more conservative than revision 1, and requires that these limits be re-calculated.

The Low Temperature Overpressure Protection System (LTOPS) provides protection against exceeding the vessel ductility limits, as expressed by the Appendix G pressure-temperature limits, during cold shutdown, heatup, and cooldown operations. The limits resulting from implementation of the new revision to Regulatory Guide 1.99, requires that the LTOPS setpoints be re-evaluated. The purpose of this report is, in part, to document the re-evaluation.

This report includes a study of the sensitivity of the LTOPS setpoint on pressurizer PORV opening time, and a correlation that benchmarks the results of the analysis to that of the algorithm described in the report "Pressure Mitigating Systems Transient Analysis Results" (July 1977). This report was prepared for the Westinghouse Owners Group (acronymed "WOG") on Reactor Coolant System Overpressurization by Westinghouse Electric Corporation. The purpose of the correlation is to provide American Electric Power Corporation a



means of determining LTOPS setpoints equivalent to those obtained from the relatively sophisticated LOFTRAN based analysis described here, by using a simple methodology; i.e., the WOG report. The correlation remains valid as long as certain plant parameters are unchanged. These are: instrumentation time delays, pressurizer PORV flow characteristics, and pressurizer PORV full flow C(v).

The organization of this report, apart from the introductory comments and the summary statement, is in four sections: the first and second sections describe, respectively, the justification for the design basis transients and the algorithm used for the setpoint analysis; the third section documents the analysis specific to D. C. Cook unit 2, and the fourth section provides the correlation to the WOG methodology referenced in the introduction to this report.

Summary of Results

The result of the analysis is summarized by Figures S.1 and S.2, illustrating, respectively, the dependency of the maximum allowed LTOPS setpoint on PORV opening time for reactor vessel exposures of 12 EFPY and 32 EFPY. A minimum setpoint limit, for RCP number 1 seal protection, does not exist. This is due to the fact that, given the 4 second PORV closure time, there is not enough separation (white space) between the steady-state pressure-temperature limit and the minimum RCS pressure requirements for an RCP start, to umbrella the pressure swing resulting from either a heat injection or mass injection event. As the closure time decreases, the pressure undershoot would become less severe. At the current 435 psig setpoint, with single PORV operation, the peak pressure would remain below the Appendix G limit provided the PORV stroke open times remained below 6.5 seconds, with vessel exposures to 12 EFPY; or 3.5 seconds, with vessel exposures to 32 EFPY.

Figure S.3 provides the correlation that benchmarks the results of the "LOFTRAN" based analysis to the results obtained from application of the algorithm described in the "WOG" report. These curves are used to compensate for some of the conservatisms or nonconservatisms, depending on the selected PORV stroke open time, inherent in the WOG methodology. These correlations

100

100

100

100

100

100

100

100

100

100

100

100

100

100

100

100

100

are independent of Appendix G limits, and will remain valid as long as certain plant parameters (pressurizer PORV flow characteristics and $C(v)$, and instrumentation signal delays) are unchanged.

Utilization of the curves requires that the LTOPS setpoint first be determined using the "WOG" methodology. At the PORV opening time corresponding to that selected for the "WOG" calculation, determine the "LOFTRAN" analysis setpoint from the ordinate by linearly interpolating between the two curves bounding the predetermined "WOG" setpoint.

100

100



100

100

100



100

100

100

100



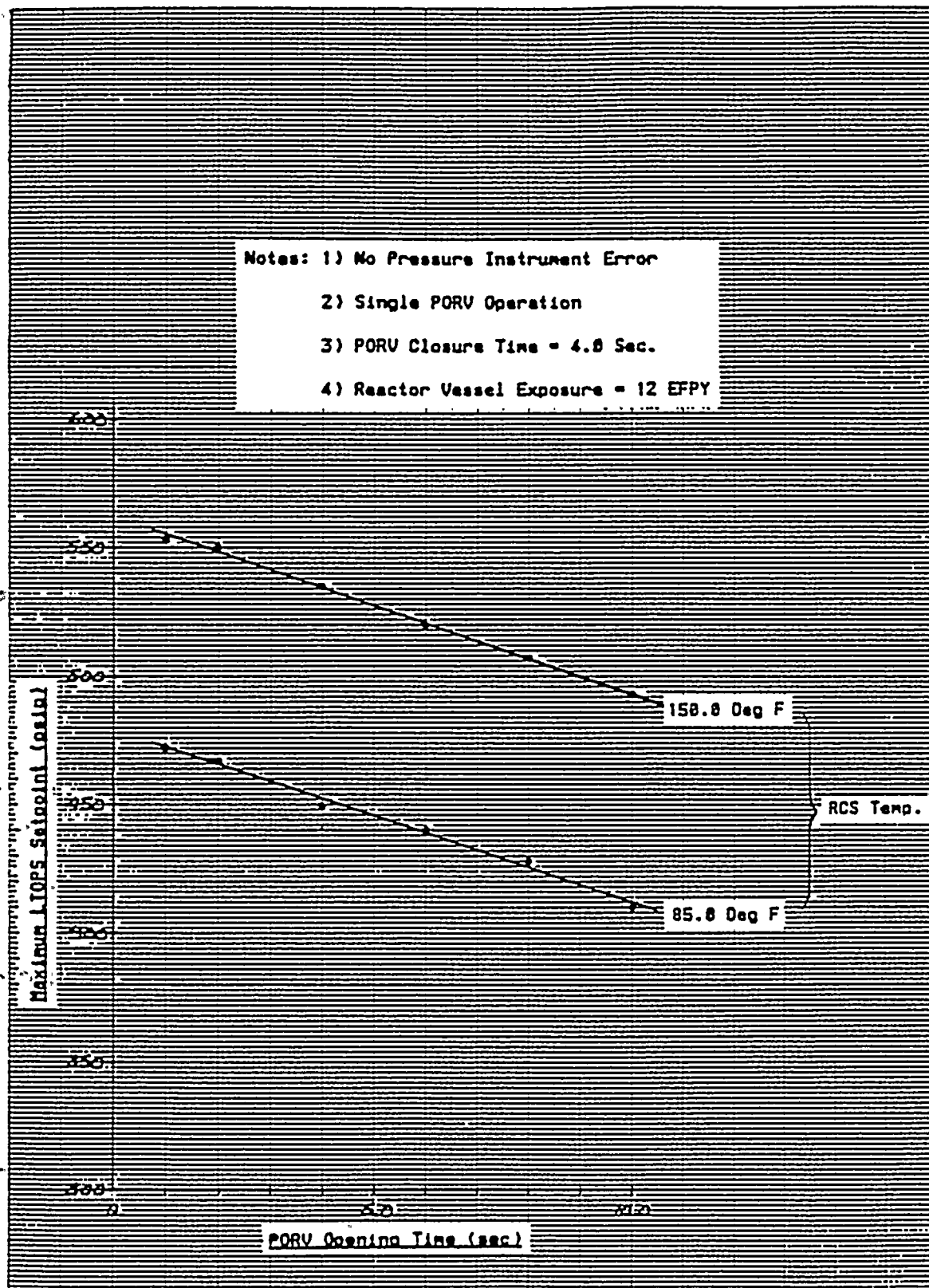


Figure S.1 PORV LTOP Setpoint vs. Valve Opening Time at 12 EFY

100-100000

100-100000

100-100000

100-100000

100-100000

100-100000

100-100000

100-100000

100-100000

100-100000

100-100000

100-100000

100-100000

100-100000

100-100000

- Notes: 1) No Pressure Instrument Error
 2) Single PORV Operation
 3) PORV Closure Time = 4.8 Sec.
 4) Reactor Vessel Exposure = 32 EFPY

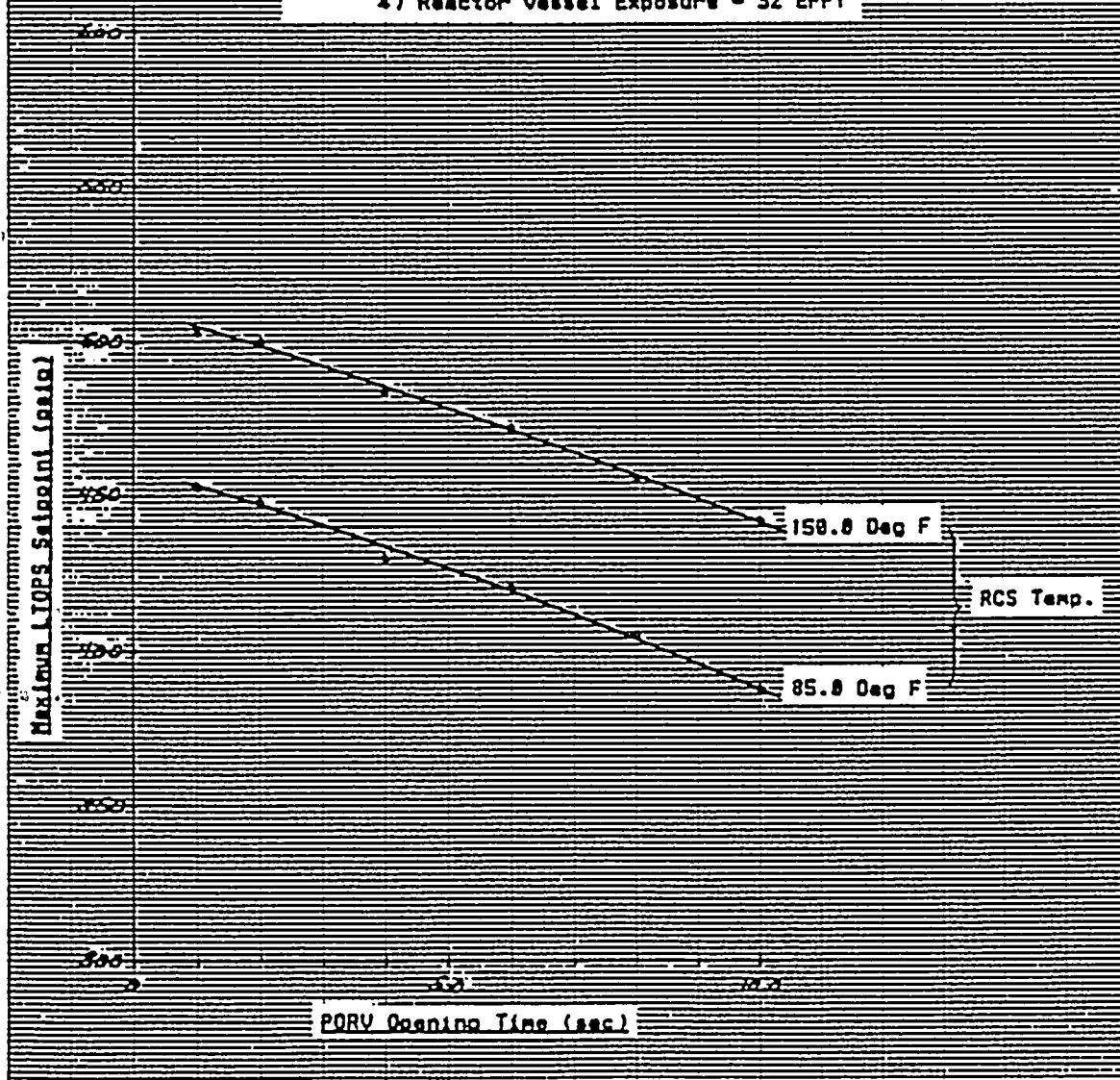


Figure S.2 PORV LTOP Setpoint vs. Valve Opening Time at 32 EFPY

10/10/10

10/10/10

10/10/10

10/10/10

10/10/10

10/10/10

10/10/10

10/10/10

10/10/10

10/10/10

10/10/10

10/10/10

10/10/10

10/10/10

10/10/10

10/10/10

10/10/10

10/10/10

10/10/10

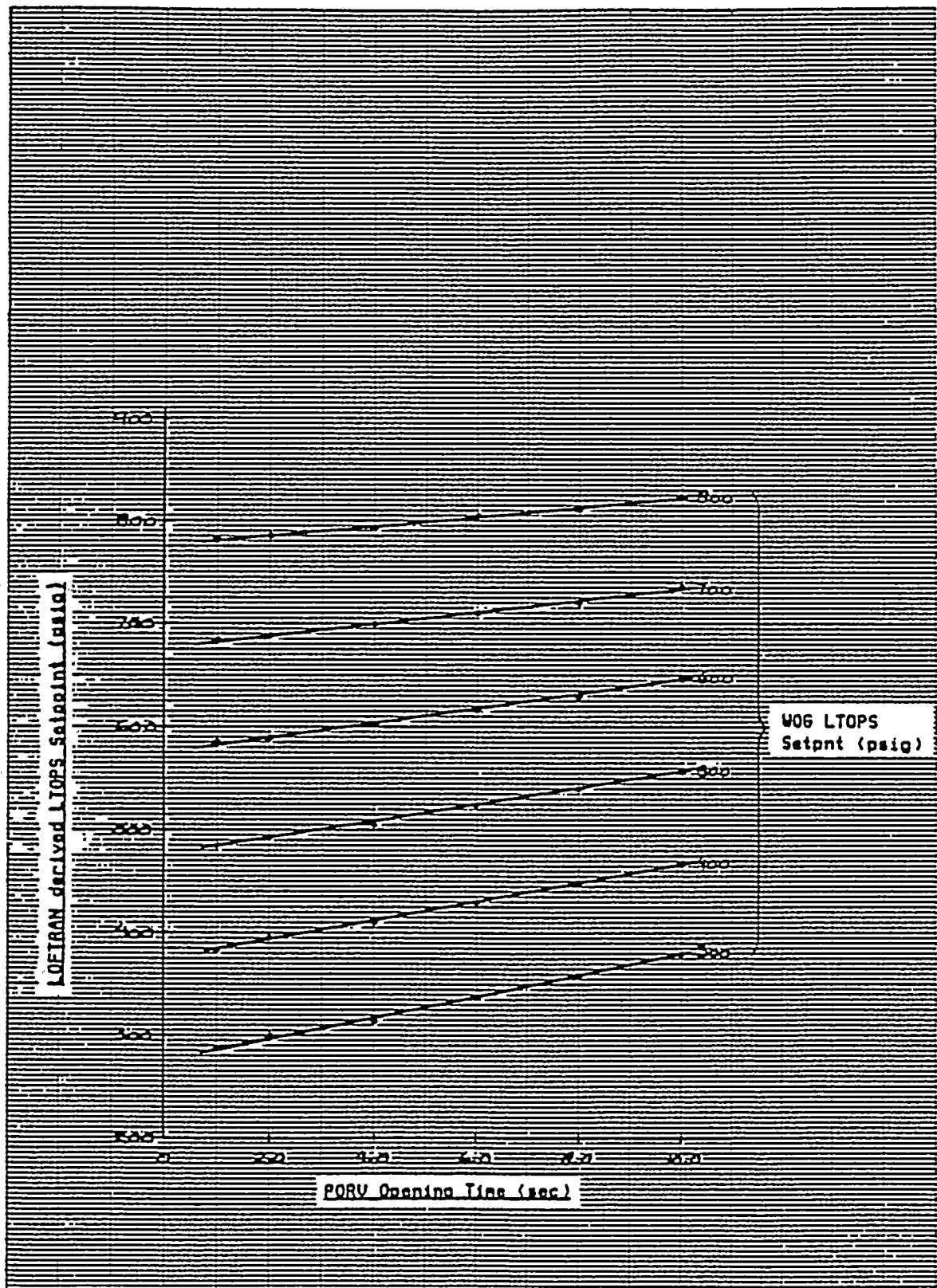


Figure S.3 LOFTRAN/WOG LTOPS Setpoint Correlation vs. Pressurizer PORV Opening Time

100

100

100

100

100

100

100

100

100

100

100

100

100

100

100

100

100

100

100

100

100

100

100

100

100

100

100

100

100

1.0 DESCRIPTION OF THE LOW TEMPERATURE PRESSURE TRANSIENTS

Overpressure protection for the reactor coolant system (RCS) is achieved by means of self-actuated steam safety valves located high in the steam space of the pressurizer. These safety valves have a set pressure based on the RCS design pressure and are intended to protect the system against transients initiated in the plant when the RCS is operating near its normal temperature. To avoid brittle fracture at low reactor vessel metal temperatures, the allowable system pressure is progressively reduced from the nominal system design pressure as temperature is decreased. Therefore, supplemental overpressure mitigation provisions for the reactor vessel must be available when the RCS, and hence the reactor vessel, is at reduced temperatures. This supplemental protection, utilizing the power operated relief valves (PORVs), is known as the Low Temperature Overpressure Protection System (LTOPS).

The PORVs are designed to limit the RCS pressure during normal operational transients when the reactor is at power by discharging steam to the pressurizer relief tank (PRT), thus avoiding the need for the code safety valves to function. The flow capacity and stroke time of the PORVs is selected to avoid a reactor trip during a large step load decrease. In addition, the valves are utilized for pressure relief (water, gas, or a mixture) as a part of the LTOPS, and when performing this function will also discharge to the PRT. The setpoint for the LTOPS function is selected so that if one valve fails to actuate when required, the second valve will be able to mitigate the transient.

Normally, when the RCS is at a temperature below 350°F, the RCS is open to the Residual Heat Removal System (RHRS) for the purposes of removing residual heat from the core, providing a path for letdown to the purification subsystem, and controlling the RCS pressure when the plant is operating in a water solid mode. The RHRS is provided with selfactuating water relief valves to prevent overpressurizing this relatively low pressure system due to events originating either from within the system itself or from transients transmitted from the RCS. The RHRS relief valves will mitigate pressure transients originating in the RCS to maximum pressure values determined by the relief valves set

10

11

12

13

14

15

16

17

18

19

20

21

22

23

24

25

26

27

28

29

30

31

32

33

34

35

36

37

38

39

40

41

42

43

44

45

46

47

48

49

50

51

52

53

54

pressure plus a pressure accumulation above the set pressure dependent on the liquid volume magnitude of the transient.

The low pressure RHRS is normally isolated from the high design pressure RCS during operation at temperatures above 350°F by two isolation valves in series. Because of the NRC required automatic closure feature designed to prevent inadvertent overpressurization of the RHRS, spurious closure of the RHRS isolation valves is a creditable event. The LTOPS is intended to provide overpressure mitigation for the RCS, considering those transients which might occur when the RHRS isolation valves are inadvertently closed, thus isolating the RHRS water relief valves from the RCS.

1.1 GENERAL DESCRIPTION

The LTOPS is designed to provide the capability, during relatively low temperature reactor coolant system operation, to prevent the RCS pressure from exceeding 10CFR50 Appendix G limits. The LTOPS is provided in addition to the administrative controls to prevent overpressure transients and as a supplement to the RCS overpressure mitigating function of the residual heat removal system water relief valves. The system is designed with redundant components to assure its performance in the event of the failure of any single active component.

The power operated relief valves located near the top of the pressurizer, together with additional actuation logic from the wide range pressurizer channels, are utilized to mitigate potential RCS overpressure transients which might occur if the RHR water relief valves are isolated from the RCS. LTOPS provides the additional relief capacity for the specific transients which would not be mitigated by the RHRS relief valves and thereby maintain the system pressure below the limits specified by Appendix G requirements.

1.2 OPERATION

During normal plant heatup, the RCS is open to the RHRS and is operated in a water solid mode until the steam bubble is formed in the pressurizer. During

20

20

20

20

20

20

20

20

20

20

20

20

20

20

20

20

20

20

20

20

20

20

20

20

150°F see 7032
152°F
160°F

these low-temperature low-pressure operating conditions, the LTOPS is armed and in a ready status to mitigate pressure transients which might occur if the RHRS is inadvertently isolated. After the steam bubble is formed and the pressurizer water level is at its' normal value for no-load operation, the RHRS is manually isolated from the RCS and the plant heatup continues. Pressure surge control is provided by the steam bubble. When the reactor coolant temperature has increased above a preset value (152°F, in the case of D. C. Cook Unit 2) the LTOPS is disarmed.

During a normal plant cooldown, the LTOPS is armed as the reactor coolant temperature is decreased below the preset value. At this time there is a steam bubble in the pressurizer and the water level is at the normal level for no-load operation. The RHRS has been placed in service by opening the suction isolation valves, thus making the RHRS water relief valves available to mitigate pressure transients. When the coolant temperature has been reduced to about 160°F by the operation of the RHRS, the steam bubble may be quenched and the reactor coolant pumps stopped. From this point on in the cooldown, the plant is water solid and if the RHRS becomes inadvertently isolated, the LTOPS will be in an active status ready to mitigate those pressure transients that might occur.

When the RCS is operated in the water solid mode, the pressure is automatically controlled by the low pressure letdown valve in the Chemical and Volume Control System (CVCS). This valve senses the pressure in the letdown line (ref Figure 1.1) and maintains the pressure at the selected control value by throttling the letdown flow from the RCS. At this time, the charging flow into the RCS is set at a constant value and is controlled by the charging flow control valve. It should be noted that the pressure being controlled is that in the letdown line which then indirectly controls the pressure in the RCS. However, if the pressure drop through the RHRS and the bypass line into the CVCS is changed by throttling of valves or changing the flow rate through the RHRS, the RCS pressure will also change since the location of the controlled pressure is in the letdown line.

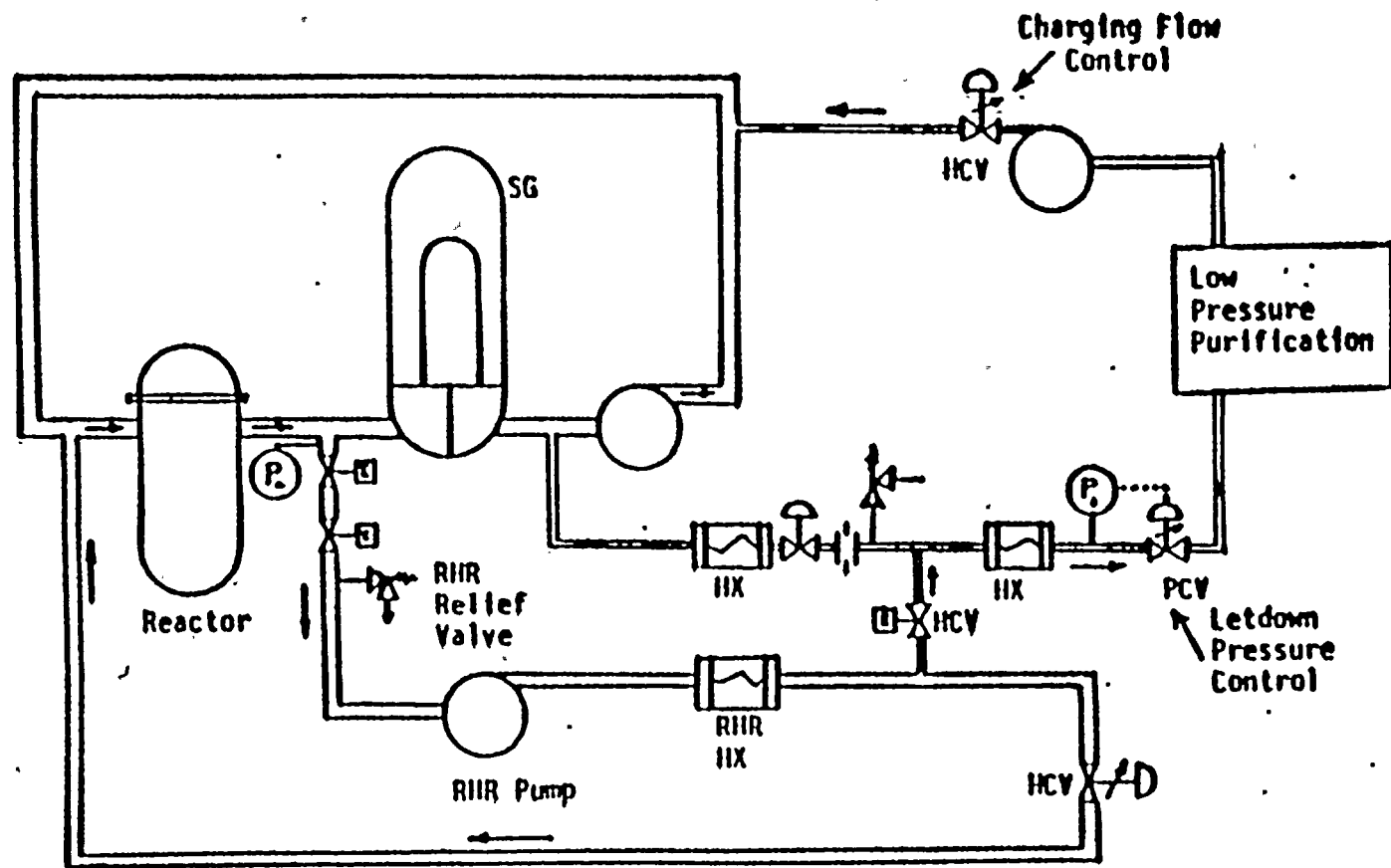


Figure 1.1 Typical Low Pressure Coolant/Purification Flow Path

1

2

3

4

5

6

7

8

9

10

11

12

13

14

15

16

17

18

19

20

21

22

23

24

25

26

27

28

29

30

31

32

33

34

35

36

37

38

39

40

41

42

43

44

45

46

47

48

49

50

51

52

53

54

55

56

57

58

59

60

61

62

63

64

65

66

67

68

69

70

71

72

73

74

75

76

77

78

79

80

81

82

83

84

85

86

87

88

89

90

91

92

93

94

95

96

97

98

99

100

101

102

103

104

105

106

107

108

109

110

111

112

113

114

115

116

117

118

119

120

121

122

123

124

125

126

127

128

129

130

131

132

133

134

135

136

137

138

139

140

141

142

143

144

145

146

147

148

149

150

151

152

153

154

155

156

157

158

159

160

161

162

163

164

165

166

167

168

169

170

171

172

173

174

175

176

177

178

179

180

181

182

183

184

185

186

187

188

189

190

191

192

193

194

195

196

197

198

199

200

201

202

203

204

205

206

207

208

209

210

211

212

213

214

215

216

217

218

219

220

221

222

223

224

225

226

227

228

229

230

231

232

233

234

235

236

237

238

239

240

241

242

243

244

245

246

247

248

249

250

251

252

253

254

255

256

257

258

259

260

261

262

263

264

265

266

267

268

269

270

271

272

273

274

275

276

277

278

279

280

281

282

283

284

285

286

287

288

289

290

291

292

293

294

295

296

297

298

299

300

301

302

303

304

305

306

307

308

309

310

311

312

313

314

315

316

317

318

319

320

321

322

323

324

325

326

327

328

329

330

1.3 POTENTIAL OVERPRESSURE TRANSIENTS

During low temperature operations, reactor coolant system overpressurization transients can be caused by either of two types of events: mass input or heat input. Both types result in more rapid pressure changes when the RCS is water solid. However, at reactor temperatures below 350°F, the RCS must be aligned to the Residual Heat Removal System to remove core decay heat and the water relief valves will be available to mitigate pressure transients which might occur. Also, there will generally be a steam bubble in the pressurizer when the reactor coolant temperature is above about 150°F during plant cooldown so that water solid conditions are limited to relatively low temperature conditions. Therefore, the descriptions of the two types of transients imply that the RCS is water solid at a low temperature.

1.3.1 Summary of Mass Input Transients

1.3.1.1 Inadvertent Safety Injection

Inadvertent actuation of safety injection events include full system (both trains), single train, or single component within a train actuation. Each of the three types of events are discussed separately. Full system actuation would include the opening of the isolation valves on all SI accumulators, startup of all low-head and high-head safety injection pumps and isolation of the normal letdown path to the Chemical and Volume Control System. Such an event would result in unacceptably large volumes of water being forced into the RCS. Therefore, such events must be prevented by strict administrative controls. These controls require the blocking of the automatic SI actuation circuits, immobilizing the SI accumulator motor operated isolation valves, and locking out power to the high-head SI pumps. In a typical Westinghouse design, the low-head safety injection pumps (the RHR pumps) are normally in operation and aligned to take their suction from the RCS, and not from the refueling water storage tank, during low pressure and low temperature plant operations. Therefore, even if a spurious start signal was received, the low-head SI pumps would not function to inject RWST water into the RCS.

100

100

100

100

100

100

100

100

100

100

100

100

100

100

100

100

100

100

100

100

100

100

100

100

100

100

100

100

100

100

100

100

100

100

100

100

100

100

100

100

100

100

100

100

100

100

100

100

100

100

100

100

100

100

100

100

100

100

100

The probability of a single train actuation is about the same as a full system actuation, since the signals which call for safety injection, both manual and automatic, are normally processed through the engineered safety feature logic circuits such that a signal, whether spurious or not, will impact both trains. Therefore, since the SI system is essentially immobilized at low temperature, single train inadvertent actuation is considered no more likely than full system actuation.

For those plant designs in which the charging pumps serve the second function of high head SI pumps, e.g. the Cook units, a spurious safety injection signal would realign the valving to transfer from the charging function to the safety injection function. Therefore, the one operating charging pump which is not locked out will deliver through the safety injection flow path to the RCS.

However, the RHRS would remain open to the RCS at this time and the RHRS relief valves would mitigate the resulting RCS pressure transient.

Inadvertent actuation of a single component would require that an operator selectively unlock the electrical power to the component and then cause the component to be energized. The most probable way for this event to occur would be during periodic surveillance testing required by the technical specifications or during post maintenance checkout of the component.

Deliberate opening of an SI accumulator isolation valve while the accumulator is pressurized with gas is not considered probable because there is no technical specification to test the isolation valves at shutdown, and prudent maintenance procedures for the valves would likely require that the compressed gas in the accumulator be removed.

Post maintenance checkout or periodic surveillance tests however, might be attempted on a high head safety injection pump providing an opportunity for operator error to cause an inadvertent single pump injection event.

Therefore, a single safety injection pump startup event during surveillance testing or following maintenance is considered a potential mass input transient. Since the RHRS would be open to the RCS at this time, the RHRS relief valves would mitigate the resulting RCS pressure transient.

• 434

4-7 40-45

12

94

52

[Faint handwritten notes at the bottom of page 70]

●

100

44

10

59

7

-Ag-

44

274

Figure 1

1940

2

3

1

2

1

2

2

●●●●●

1

1.3.1.2 Charging/Letdown Flow Mismatch

Charging/letdown flow mismatch events can be postulated to occur in a number of ways. One way would involve the complete termination of letdown: closure of the letdown control valve, isolation of the RHRS/CVCS crossover path, or closure of the RHRS inlet isolation valves caused by malfunctions of the control systems. A second way would involve an increase in the charging flow by either operator or instrument error such that the charging flow exceeds the prevailing letdown flow.

The most severe mass input transient would occur if the letdown flow controls failed to the zero flow condition while the charging flow controls failed to the full flow condition. This failure mode would result in the maximum charging/letdown flow mismatch event but does not result in the isolation of the RHRS relief valves from the RCS. Therefore, the RHRS relief valves would mitigate this transient and prevent an overpressure condition in either the RHRS or the RCS.

The most likely way that a charging/letdown flow mismatch would occur is for the RHRS (and relief valves) to be inadvertently isolated from the RCS by spurious closure of the RHRS inlet isolation valves. Such a spurious closure is credible due to the presence of the automatic closing signal required by the NRC. Since this spurious valve closure event causes an RCS pressure transient by stopping the letdown flow and concurrently isolates the RHRS relief valves from the RCS, it is considered a "design basis" transient for the LTOPS.

1.3.2 Summary of Heat Input Transients

1.3.2.1 Actuation of Pressurizer Heaters

The inadvertent actuation of the pressurizer heaters when the pressurizer is filled solid will cause a slow rise in the water temperature with a consequent increase in pressure of the constant volume RCS, if the installed automatic pressure control equipment is not in service. Since the pressure transient is



very slow, the operator should recognize and terminate the transient before an unacceptable pressure is reached. The RHRS is open to the RCS whenever the pressurizer is filled solid, in accordance with administrative controls. Therefore, the RHRS relief valves will be actuated, negating the need for the LTOPS, if the operator does not intervene and stop the transient. This case is not considered significant to the design of either the RHRS relief valves or the LTOPS.

1.3.2.2 Loss of RHR Cooling

A loss of residual heat removal cooling while the pressurizer is filled solid could be caused by a loss of flow malfunction in the component cooling water or the service water systems, or the closure of the RHRS inlet isolation valves. The continual release of core residual heat into the reactor coolant, with no heat rejection into the environs, would cause a slow rise in the coolant temperature and pressure. Since the transient is slow, the operator should respond and either restore the RHRS valves to their open position, restore cooling, or limit the RCS pressure by venting the pressurizer. This transient is not considered significant to the design of the LTOPS since it is a relatively slow transient compared to the heat input transient resulting from the startup of a reactor coolant pump in combination with an RCS/SG temperature asymmetry.

1.3.2.3 RCP Startup With Temperature Asymmetry

During plant heatup and cooldown operations, typical administrative controls require that at least one reactor coolant pump be maintained in operation whenever the reactor coolant temperature is greater than 160°F. Therefore, the large volumetric flow throughout the RCS will maintain an isothermal condition in the RCS. The steam generator secondary side water immediately surrounding the tubes will also remain at a temperature near that of the circulating reactor coolant on the primary side.

During normal cooldown operations, when the reactor coolant temperature has decreased below 160°F the reactor coolant pumps may be stopped. Subsequently,

4

2

2

57



23

●

10

1. By Agreement, the parties have agreed to the following:

• • 2014-2015

34

7



DE LA B. I. 2. 3. 4. 5. 6. 7. 8. 9. 10. 11. 12. 13. 14. 15. 16. 17. 18. 19. 20. 21. 22. 23. 24. 25. 26. 27. 28. 29. 30. 31. 32. 33. 34. 35. 36. 37. 38. 39. 40. 41. 42. 43. 44. 45. 46. 47. 48. 49. 50. 51. 52. 53. 54. 55. 56. 57. 58. 59. 60. 61. 62. 63. 64. 65. 66. 67. 68. 69. 70. 71. 72. 73. 74. 75. 76. 77. 78. 79. 80. 81. 82. 83. 84. 85. 86. 87. 88. 89. 90. 91. 92. 93. 94. 95. 96. 97. 98. 99. 100. 101. 102. 103. 104. 105. 106. 107. 108. 109. 110. 111. 112. 113. 114. 115. 116. 117. 118. 119. 120. 121. 122. 123. 124. 125. 126. 127. 128. 129. 130. 131. 132. 133. 134. 135. 136. 137. 138. 139. 140. 141. 142. 143. 144. 145. 146. 147. 148. 149. 150. 151. 152. 153. 154. 155. 156. 157. 158. 159. 160. 161. 162. 163. 164. 165. 166. 167. 168. 169. 170. 171. 172. 173. 174. 175. 176. 177. 178. 179. 180. 181. 182. 183. 184. 185. 186. 187. 188. 189. 190. 191. 192. 193. 194. 195. 196. 197. 198. 199. 200. 201. 202. 203. 204. 205. 206. 207. 208. 209. 210. 211. 212. 213. 214. 215. 216. 217. 218. 219. 220. 221. 222. 223. 224. 225. 226. 227. 228. 229. 230. 231. 232. 233. 234. 235. 236. 237. 238. 239. 240. 241. 242. 243. 244. 245. 246. 247. 248. 249. 250. 251. 252. 253. 254. 255. 256. 257. 258. 259. 260. 261. 262. 263. 264. 265. 266. 267. 268. 269. 270. 271. 272. 273. 274. 275. 276. 277. 278. 279. 280. 281. 282. 283. 284. 285. 286. 287. 288. 289. 290. 291. 292. 293. 294. 295. 296. 297. 298. 299. 300. 301. 302. 303. 304. 305. 306. 307. 308. 309. 310. 311. 312. 313. 314. 315. 316. 317. 318. 319. 320. 321. 322. 323. 324. 325. 326. 327. 328. 329. 330. 331. 332. 333. 334. 335. 336. 337. 338. 339. 340. 341. 342. 343. 344. 345. 346. 347. 348. 349. 350. 351. 352. 353. 354. 355. 356. 357. 358. 359. 360. 361. 362. 363. 364. 365. 366. 367. 368. 369. 370. 371. 372. 373. 374. 375. 376. 377. 378. 379. 380. 381. 382. 383. 384. 385. 386. 387. 388. 389. 390. 391. 392. 393. 394. 395. 396. 397. 398. 399. 400. 401. 402. 403. 404. 405. 406. 407. 408. 409. 410. 411. 412. 413. 414. 415. 416. 417. 418. 419. 420. 421. 422. 423. 424. 425. 426. 427. 428. 429. 430. 431. 432. 433. 434. 435. 436. 437. 438. 439. 440. 441. 442. 443. 444. 445. 446. 447. 448. 449. 450. 451. 452. 453. 454. 455. 456. 457. 458. 459. 460. 461. 462. 463. 464. 465. 466. 467. 468. 469. 470. 471. 472. 473. 474. 475. 476. 477. 478. 479. 480. 481. 482. 483. 484. 485. 486. 487. 488. 489. 490. 491. 492. 493. 494. 495. 496. 497. 498. 499. 500. 501. 502. 503. 504. 505. 506. 507. 508. 509. 510. 511. 512. 513. 514. 515. 516. 517. 518. 519. 520. 521. 522. 523. 524. 525. 526. 527. 528. 529. 530. 531. 532. 533. 534. 535. 536. 537. 538. 539. 540. 541. 542. 543. 544. 545. 546. 547. 548. 549. 550. 551. 552. 553. 554. 555. 556. 557. 558. 559. 560. 561. 562. 563. 564. 565. 566. 567. 568. 569. 570. 571. 572. 573. 574. 575. 576. 577. 578. 579. 580. 581. 582. 583. 584. 585. 586. 587. 588. 589. 590. 591. 592. 593. 594. 595. 596. 597. 598. 599. 600. 601. 602. 603. 604. 605. 606. 607. 608. 609. 610. 611. 612. 613. 614. 615. 616. 617. 618. 619. 620. 621. 622. 623. 624. 625. 626. 627. 628. 629. 630. 631. 632. 633. 634. 635. 636. 637. 638. 639. 640. 641. 642. 643. 644. 645. 646. 647. 648. 649. 650. 651. 652. 653. 654. 655. 656. 657. 658. 659. 660. 661. 662. 663. 664. 665. 666. 667. 668. 669. 670. 671. 672. 673. 674. 675. 676. 677. 678. 679. 680. 681. 682. 683. 684. 685. 686. 687. 688. 689. 690. 691. 692. 693. 694. 695. 696. 697. 698. 699. 700. 701. 702. 703. 704. 705. 706. 707. 708. 709. 710. 711. 712. 713. 714. 715. 716. 717. 718. 719. 720. 721. 722. 723. 724. 725. 726. 727. 728. 729. 730. 731. 732. 733. 734. 735. 736. 737. 738. 739. 740. 741. 742. 743. 744. 745. 746. 747. 748. 749. 750. 751. 752. 753. 754. 755. 756. 757. 758. 759. 760. 761. 762. 763. 764. 765. 766. 767. 768. 769. 770. 771. 772. 773. 774. 775. 776. 777. 778. 779. 780. 781. 782. 783. 784. 785. 786. 787. 788. 789. 790. 791. 792. 793. 794. 795. 796. 797. 798. 799. 800. 801. 802. 803. 804. 805. 806. 807. 808. 809. 810. 811. 812. 813. 814. 815. 816. 817. 818. 819. 820. 821. 822. 823. 824. 825. 826. 827. 828. 829. 830. 831. 832. 833. 834. 835. 836. 837. 838. 839. 840



1

五

91.

①

~~SECRET~~ REF ID: A67890 DATE: 10/1/81

4

17

42

42

1

14

16

isothermal conditions may no longer exist. The reactor coolant temperature will be decreased below 160°F by heat rejection through the RHRS. The steam generator contained water (both primary and secondary) may remain at a relatively constant temperature, greater than the RCS temperature, due to little or no circulation through the tubes. Therefore, a significant temperature asymmetry may develop between the primary water contained in the steam generator and the rest of the RCS. If a reactor coolant pump were to be started, the sudden heat input into the reactor coolant from the steam generator would cause a rapid increase in reactor coolant temperature. If the event were to occur while the pressurizer is filled solid, a rapidly increasing pressure transient would occur.

In accordance with typical administrative controls, the plant will be under water solid conditions only while the RHRS is in service, and at least one reactor coolant pump will be in operation at reactor coolant temperatures above 160°F. Therefore, this type of heat input transient will be limited to initial coolant temperatures below 160°F. Since it is not practical to determine a representative temperature for the large stagnant volume of secondary water in the steam generator, the operator will not be aware that the temperature may be substantially different from the remainder of the reactor coolant. From the initial isothermal temperature of 160°F when the RCP is stopped, the bulk reactor coolant temperature is unlikely to decrease below 110°F without some extraordinary cooling means, while the steam generator water may remain near 160°F. Therefore, the differential temperature is not expected to be greater than 50°F for this type of heat input transient.

If the RHRS is inadvertently isolated from the RCS by closure of the isolation valves, as by a spurious operation of the required auto/close interlock, while the plant is water solid and in mode 4, typical technical specifications require that a reactor coolant pump be restarted within one hour if an RHR loop cannot be returned to service. During the potential one hour delay period, a temperature asymmetry in the reactor coolant loops, due to the continued input of cold seal injection water, could develop and not be

1

2

3

4

5

6

7

8

9

10

11

12

13

14

15

16

17

18

19

20

21

22

23

24

25

26

27

28

29

30

31

32

33

34

35

36

37

38

39

40

41

42

43

44

45

46

47

48

49

50

51

52

53

54

55

56

57

58

59

60

61

62

63

64

65

66

67

68

69

70

71

72

73

74

75

76

77

78

79

80

81

82

83

84

85

86

87

88

89

90

91

92

93

94

95

96

97

98

99

100

101

102

103

104

105

106

107

108

109

110

111

112

113

114

115

116

117

118

119

120

121

122

123

124

125

126

127

128

129

130

131

132

133

134

135

136

137

138

139

140

141

142

143

144

145

146

147

148

149

150

151

152

153

154

155

156

157

158

159

160

161

162

163

164

165

166

167

168

169

170

171

172

173

174

175

176

177

178

179

180

181

182

183

184

185

186

187

188

189

190

191

192

193

194

195

196

197

198

199

200

201

202

203

204

205

206

207

208

209

210

211

212

213

214

215

216

217

218

219

220

221

222

223

224

225

226

227

228

229

230

231

232

233

234

235

236

237

238

239

240

241

242

243

244

245

246

247

248

249

250

251

252

253

254

255

256

257

258

259

260

261

262

263

264

265

266

267

268

269

270

271

272

273

274

275

276

277

278

279

280

281

282

283

284

285

286

287

288

289

290

291

292

293

294

295

296

297

298

299

300

301

302

303

304

305

306

307

308

309

310

311

312

313

314

315

316

317

318

319

320

321

322

323

324

325

326

327

328

329

330

<

apparent to the operator. Then when the reactor coolant pump is restarted, an increasing pressure transient will occur as the cold water contained in the steam generator/RCP cross-over pipe mixes with the rest of the RCS water.

1.3.2.4 Relative Severity of the Heat Input Transients

Figure 1.2 compares the relative severity of the pressure transients resulting from the heat input cases discussed in the previous paragraphs, as analyzed for the Westinghouse Owners Group. From an inspection of the figure, it is evident that the heat input cases from pressurizer heaters and decay heat are less significant than those for the cases with a loop asymmetry. Therefore, these less significant cases are not considered for the setpoint analysis.

Similarly, the loop seal (cross-over pipe) asymmetry case is seen to result in a relatively small pressure transient compared to the potential excursion possible from the steam generator/RCS temperature asymmetry cases. The "design basis" case for the setpoint determination is therefore the temperature asymmetry between the steam generator and the RCS.

1.4 SUMMARY OF TRANSIENT EVALUATION

Based on the previous discussion, most of the identified mass input and heat input transients which might occur while the plant is water solid, will be mitigated by the water relief valves in the RHRS. However, for those remote cases which occur or are caused by the RHRS having become isolated from the RCS, the LTOPS may be called upon to mitigate certain increasing pressure transients. Specifically, the LTOPS design basis transients are: 1) the mass input transient caused by a normal charging/letdown flow mismatch after termination of letdown flow, and 2) the heat input transient caused by the restart of a RCP when the RHRS is not open to the RCS.



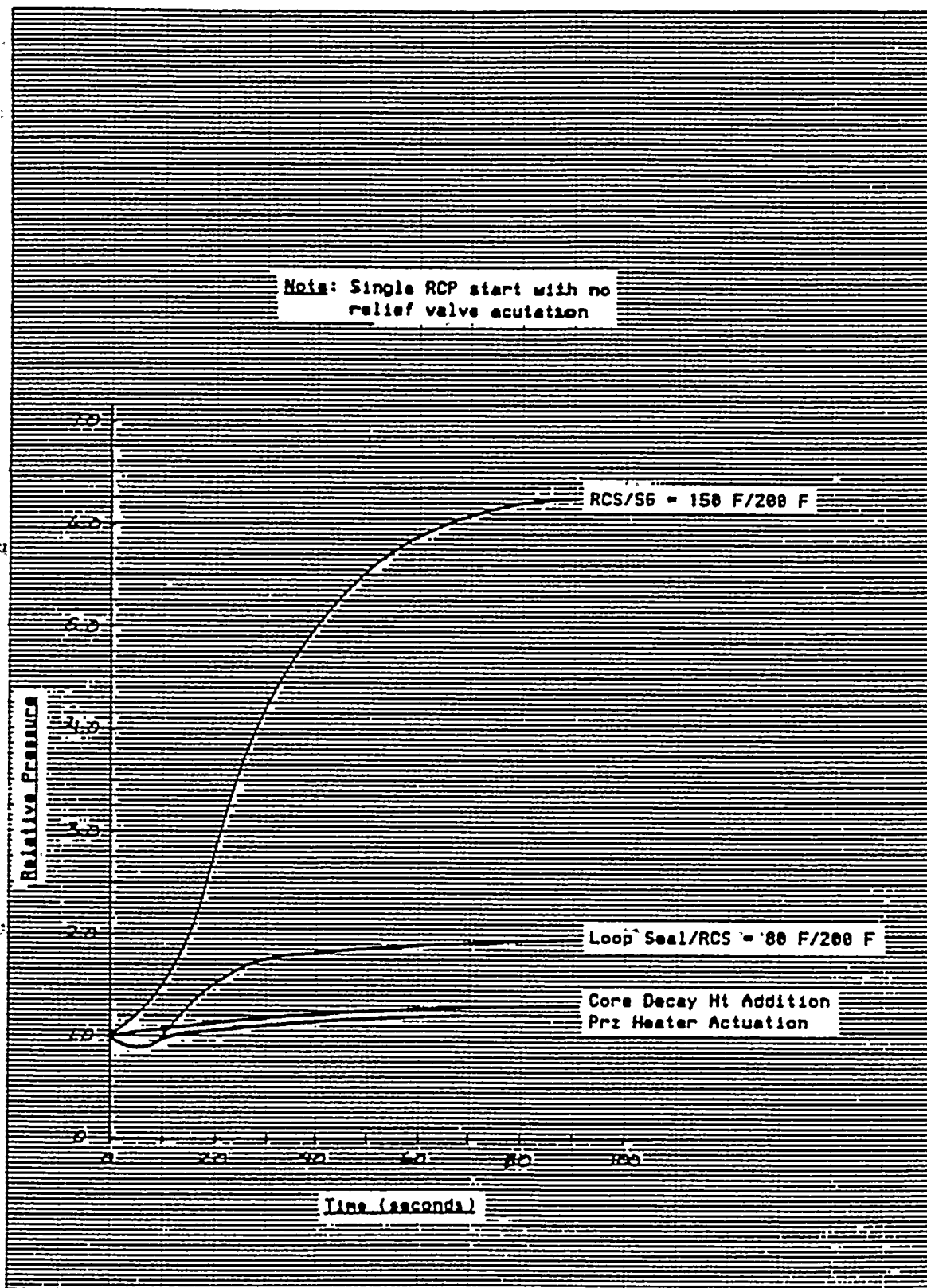


Figure 1.2 Relative RCS Pressure Transients Resulting From Heat Input Events

51

52

53

54

55

56

57

58

59

60

61

62

63

64

65

66

67

68

69

70

71

72

73

74

75

76

77

78

79

80

81

82

83

84

85

86

87

88

89

90

91

92

93

94

95

2.0 DESCRIPTION OF THE LTOPS SETPOINT ALGORITHM

The determination of the low temperature overpressure protection setpoint is based on a local version of the LOFTRAN code. The LOFTRAN code predicts plant transient thermal/hydraulic behavior by modeling the reactor coolant system, including the steam generators, pressurizer (including PORVs), and reactor coolant pumps, as well as the control and protection systems, selected valving, and some balance of plant systems. Two versions of the LOFTRAN code were utilized: the first version, used for the mass input calculations, collapses the several RCS loops into a single loop model; the second version, used for the heat input calculation, models each loop explicitly.

The selection of the proper LTOPS setpoint requires the consideration of a number of system parameters. Among these are the following:

1. Volume of the reactor coolant involved in the transient.
2. RCS pressure signal transmission delay.
3. Volumetric capacity of the relief valves vs. opening position.
4. Stroke time of the relief valves (opening and closing). If the pressure undershoot is important, the closure time is required.
5. Mass input rate into the RCS.
6. Heat transfer characteristics of the steam generators.
7. Initial temperature asymmetry between the RCS and steam generator secondary water.
8. Mass of steam generator secondary water.
9. RCP startup dynamics.
10. RCP No. 1 seal delta P requirements. Important if a lower setpoint limit is to be specified for RCP seal protection.
11. Appendix G pressure/temperature limits for the reactor vessel.

2.1 PRESSURE LIMITS SELECTION

The function of the LTOPS is to prevent the RCS pressure from increasing above the PORV piping/structural analysis limits and the limits prescribed by the allowable pressure-temperature characteristics for the specific reactor vessel

100

100

100

100

100

100

100

100

100

100

100

100

100

100

100

100

100

100

100

100

100

100

100

100

100

100

100

100

100

100

100

100

100

100

100

100

100

100

100

100

100

material in accordance with the rules given in Appendix G to 10CFR50. For the Cook units, a constant pressure setpoint, independent of temperature, is employed so that the limits considered for this particular case must meet the most restrictive segment of the Appendix G curves when compared to the overpressure transient as a function of temperature. The PORV piping/structural limits are well above those pressures of concern here, and are generally considerations only for those plants whose PORV setpoints are functions of temperature.

A characteristic pressure-temperature relationship is shown in Figure 2.1, illustrating the allowable system pressure increases with increasing temperature. This type of curve sets the nominal upper limit on the pressure, which should not be exceeded during RCS increasing pressure transients. When a relief valve is actuated to mitigate an increasing pressure transient, the release of a volume of coolant through the valve will cause the pressure increase to be slowed and reversed as illustrated by Figure 2.2. The system pressure then decreases, as the relief valve discharges coolant, until a reset pressure is reached where the valve is signalled to close. Note that the pressure continues to decrease below the reset pressure as the valve closes. The nominal lower limit on the pressure during the transient is selected based on a requirement of the reactor coolant pump No. 1 seal to maintain a nominal 200 psi differential pressure across the seal faces.

The nominal upper limit (based on the minimum of Appendix G requirements or the PORV piping limitations) and the nominal RCP No. 1 seal lower limit pressure values create an acceptable pressure range into which the PORV setpoints must be fit. An illustration of these limits along with the setpoint selection range is shown in Figures 2.3 and 2.4. In the event that the setpoint selection range is insufficient to accommodate both the Appendix G and the RCP No. 1 seal limit, the Appendix G limit will take precedence.

100-100000

100-100000

100-100000

100-100000

100-100000

100-100000

100-100000

100-100000

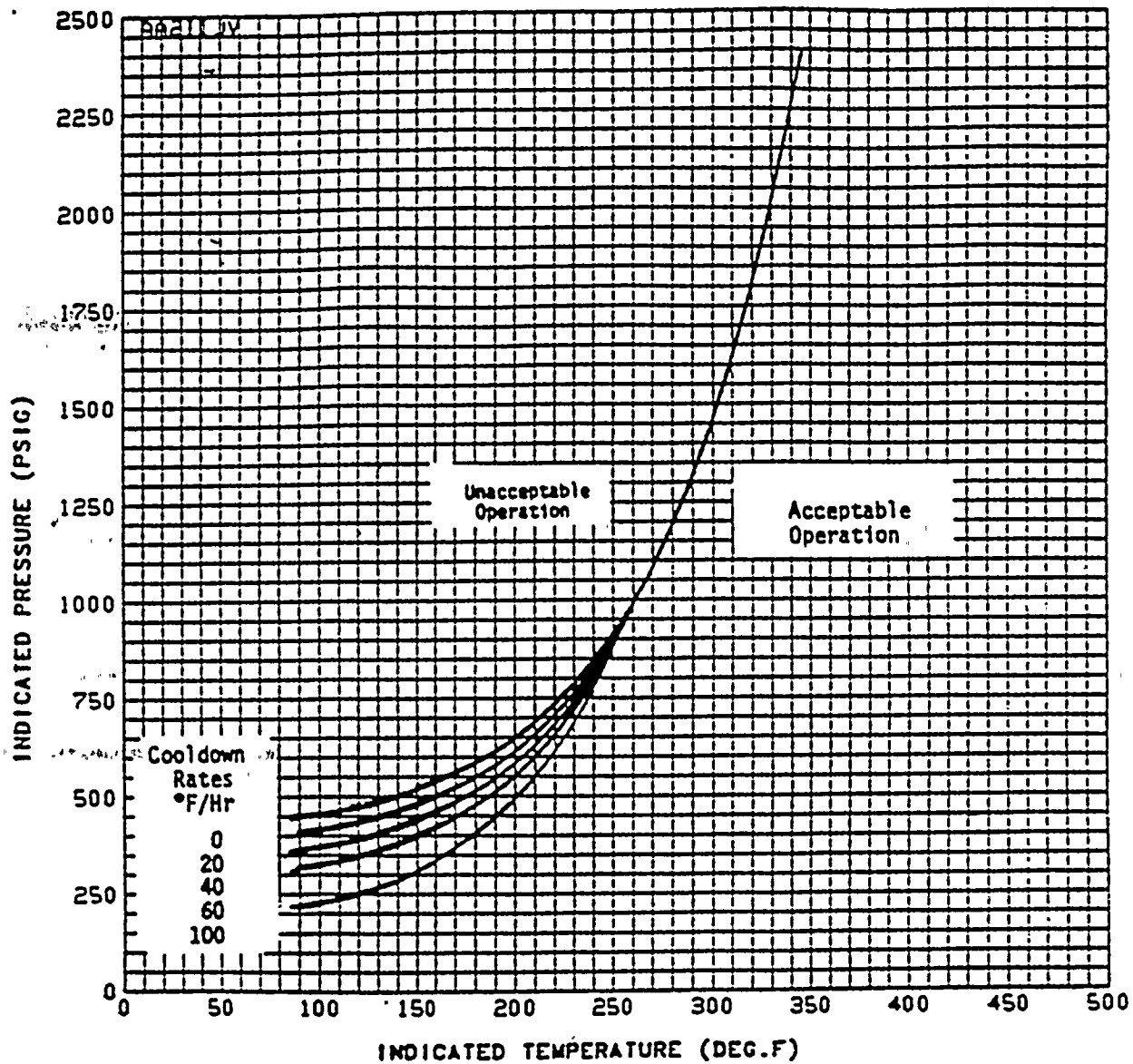


Figure 2.1 Typical Appendix G P/T Characteristics



RECEIVED

1

2

3

4

5

6

7

8

9

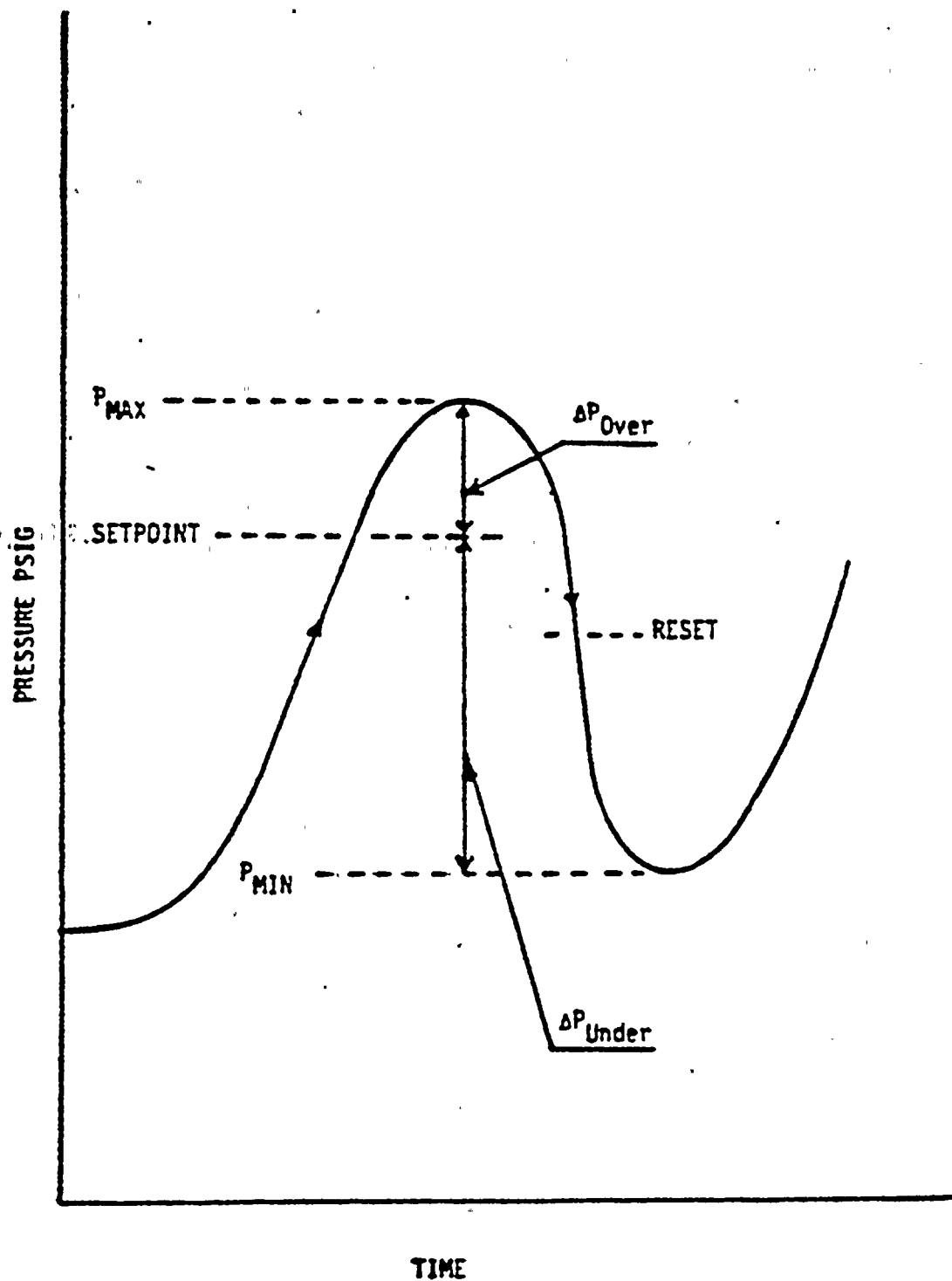


Figure 2.2 Typical Pressure Transient

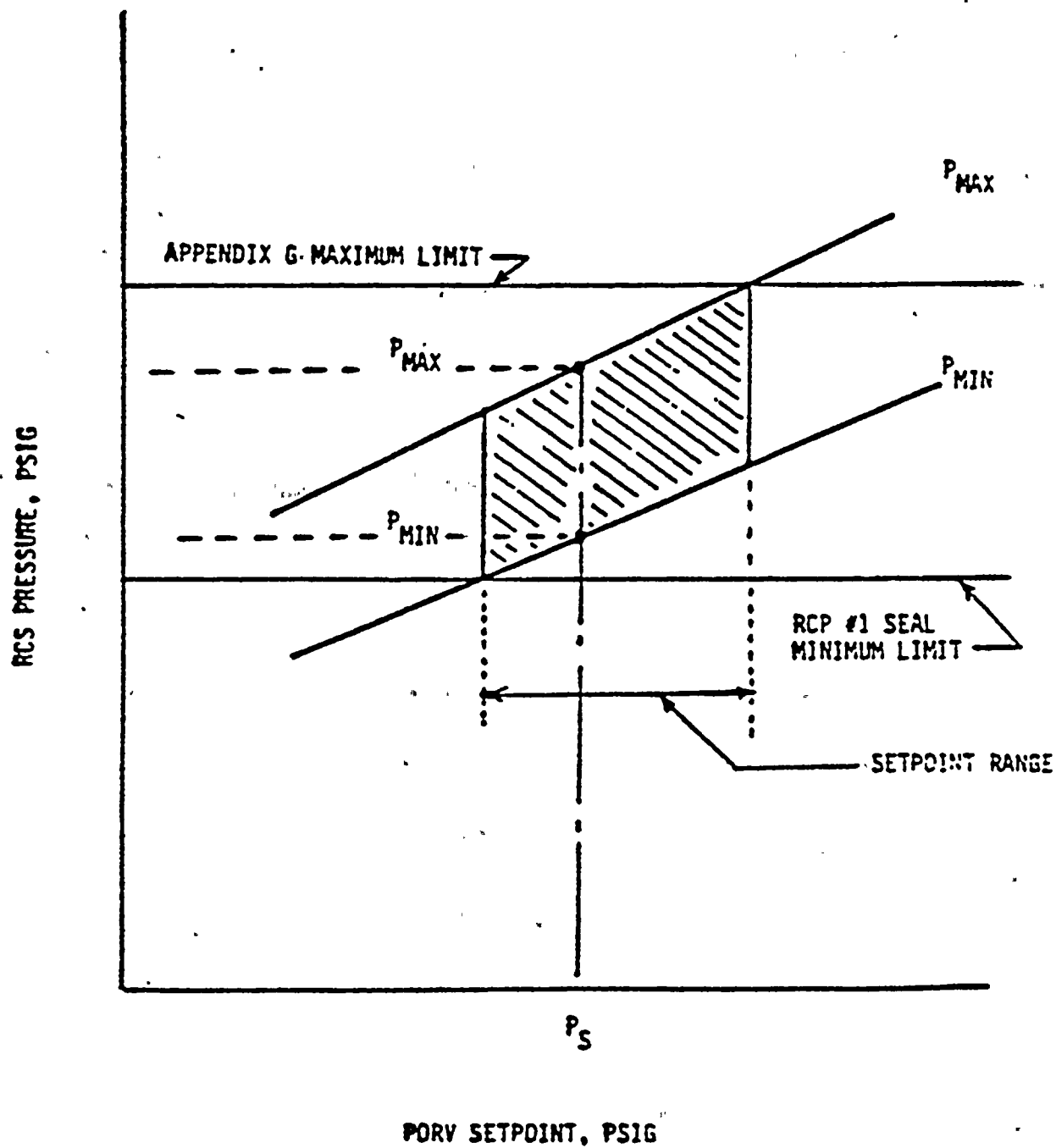


Figure 2.3 Setpoint Determination (Mass Input)

100

100

100

100

100

100

100

100

100

100

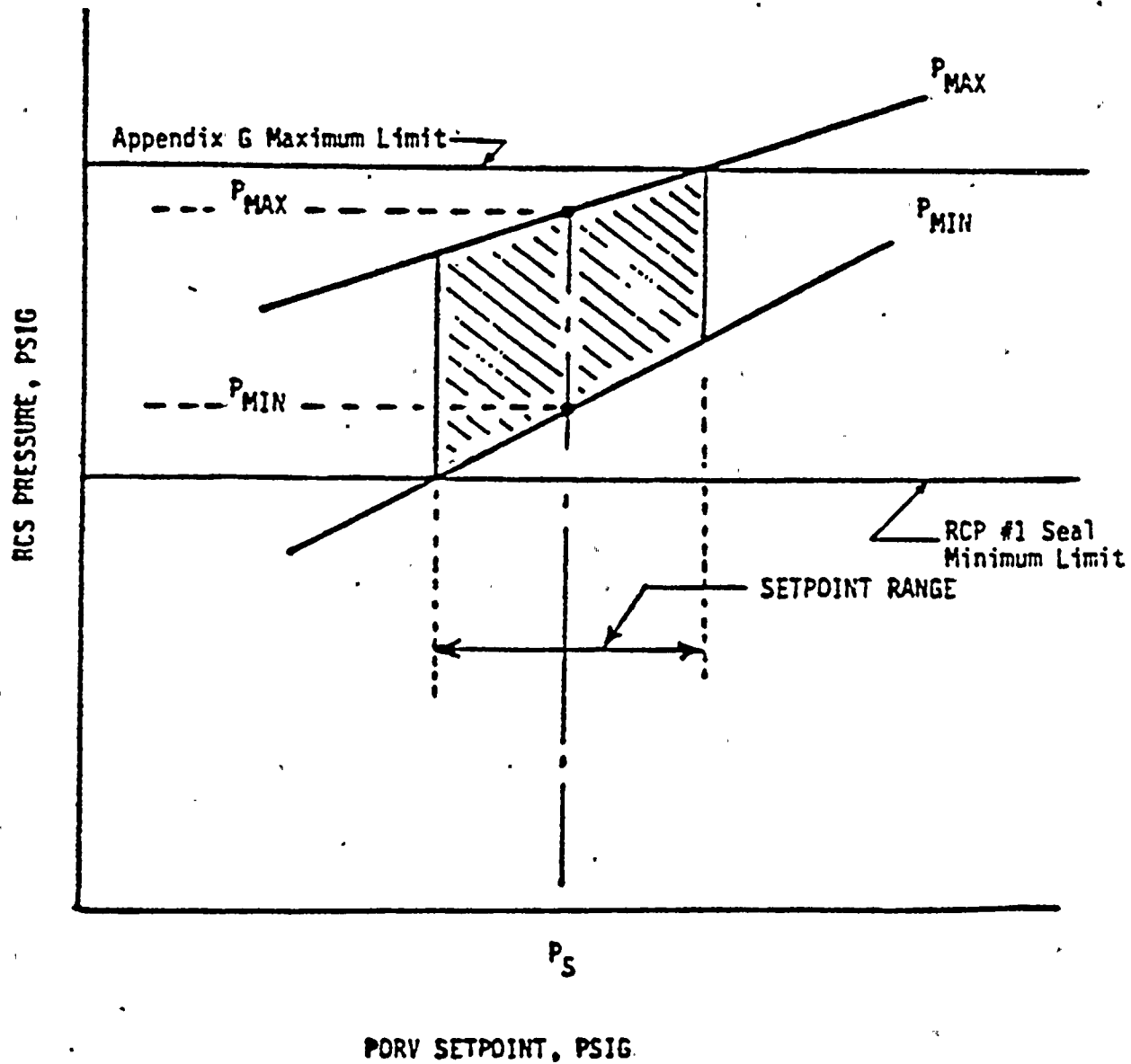


Figure 2.4 Setpoint Determination (Heat Input)

1
2
3
4
5
6
7
8
9
10
11
12
13
14
15
16
17
18
19
20
21
22
23
24
25
26
27
28
29
30
31
32
33
34
35
36
37
38
39
40
41
42
43
44
45
46
47
48
49
50
51
52
53
54
55
56
57
58
59
60
61
62
63
64
65
66
67
68
69
70
71
72
73
74
75
76
77
78
79
80
81
82
83
84
85
86
87
88
89
90
91
92
93
94
95
96
97
98
99
100

THE UNITED STATES OF AMERICA

DEPARTMENT OF JUSTICE

2.2 MASS INPUT CONSIDERATIONS

For a particular mass input transient to the RCS, the relief valve will be signalled to open at a specific pressure setpoint. However, as shown in Figure 2.2, there will be a pressure overshoot during the delay time before the valve starts to move and during the time the valve is moving to the full open position. This overshoot is dependent on the dynamics of the system and the input parameters (e.g. mass flow rate), and results in a maximum system pressure somewhat higher than the set pressure. Similarly, there will be an undershoot while the valve is relieving, both due to the reset pressure being below the setpoint and to the delay in stroking the valve closed. The maximum and minimum pressures reached in the transient are a function of the selected setpoint and must fall within the acceptable pressure range shown in Figure 2.3. A number of mass input cases are run at various LTOPS setpoints selected to bound the expected setpoint range and over a range of mass injection rates. From these runs, a locus of the maximum and minimum pressure values is generated over the expected setpoint range, as shown in Figure 2.3. The shaded area represents the acceptable range from which to select the setpoint. The mass injection cases are conservatively analyzed at low temperature where the bulk modulus of the fluid is greatest. The resulting overshoot is therefore worst case, and evaluating mass injection events at higher temperatures is not required.

2.3 HEAT INPUT CONSIDERATIONS

The heat input case is analyzed in about the same way as the mass input case except that the locus of transient pressure values vs. selected setpoints are determined for several values of the initial RCS temperature. This heat input evaluation provides a range of acceptable setpoints dependent on the reactor coolant temperature, whereas the mass input case is limited to the most restrictive low temperature conditions only. The shaded area on Figure 2.4 highlights the acceptable range for a heat input transient for a particular initial reactor coolant temperature.



2.4 FINAL SETPOINT SELECTION

By superimposing the results of the several mass input and heat input cases evaluated (from a series of figures such as 2.3 and 2.4), the range of allowable setpoints can be determined that will satisfy both mass input and heat input considerations. As previously stated, the selection of the pressure setpoints for the PORVs is based on the use of nominal upper and lower limits. Use of nominal values is justified based on the recognized high degree of conservatism inherent in the 10 CFR 50 Appendix G pressure-temperature limits.

SECRET

4

453

2

11

—

● 1997年12月1日

— 64 —









2.

$$x \in \mathbb{R}^n, y \in \mathbb{R}^m, z \in \mathbb{R}^k, w \in \mathbb{R}^l$$

10

$$1 \leq n \leq \infty, \quad \mathbb{R}^n \rightarrow \mathbb{R}^n, \quad \mathbb{R}^n \rightarrow \mathbb{R}^n$$

47

1

花

100

42

3.0 LTOPS SETPOINT ANALYSIS FOR THE D. C. COOK UNIT 2

The LTOPS setpoint analysis presented in this section was developed for the American Electric Power Corporation's D. C. Cook unit 2 using the algorithm described in the previous section. The analysis evaluates the impact of PORV opening times up to 10 seconds on the value of the setpoint required to maintain overpressures below the 10CFR50 Appendix G limits. PORV closure time is assumed to be 4 seconds for all cases. In addition, this section documents the development of the correlation benchmarking the results of the analysis to that of the algorithm described in Westinghouse Owners Group (WOG) report referenced in the introduction to this report.

The LTOPS currently installed at Cook Unit 2 features a constant value setpoint program (i.e. a program independent of temperature) with an enable/disable reactor coolant system temperature of 152°F. The program setpoint is currently 435 psig for both PORV's.

The analysis assumes overpressurization transients resulting from either mass injection or heat input events under 4-loop water solid conditions, with the replacement model 51F steam generators. The mass injection transient occurs as a result of the operation of a single centrifugal charging pump concurrent with a spurious loss of letdown. The allowable charging configuration is limited by technical specification to a single centrifugal charging pump in operational modes 5 and 6. The safety injection pumps are required to be racked out in these modes. The heat injection event results from the start of a reactor coolant pump assuming that the primary water in the steam generator is 50°F warmer than the water contained in the rest of the reactor coolant system. The temperature asymmetry can develop during a cooldown maneuver following the shutoff of the reactor coolant pumps and continued cooling with the RHR system. No credit is taken for the RHR relief valves for either of the overpressure scenarios. The setpoint selection is based on the most restrictive of either the mass injection or heat input cases.

A constraint required for the analysis is the assumption of the failure of one of the PORV's. The design basis for the overpressure events require that

1

2

3

4

5

6

7

8

9

10

11

12

13

14

15

16

17

18

19

20

21

THE

THE

THE

THE

THE

THE

THE

THE

THE

THE

THE

THE

THE

either PORV provide adequate relieving capability in the event of a single valve failure.

Code Description

The evaluation of the cold overpressure mitigation system setpoints is based on local versions of the LOFTRAN code. Two versions of the code were utilized: LOFT12, used for the mass input calculations, collapses the several RCS loops into a single loop model; and LOFT4, which models each loop explicitly, for the heat input calculation.

3.1 OPERATIONAL LIMITS

The pressure-temperature limit curves (Appendix G curves) based on revision 2 of USNRC Regulatory Guide 1.99, have been generated for reactor vessel exposures of 12 and 32 effective full power years (EFPY). The setpoint evaluation is based on the steady-state cooldown limit, where the technical difference between a steady-state cooldown limit and a steady-state heatup limit is the assumed location of the flaw; i.e., inside or outside of the vessel. The steady-state limit provides the greatest operational margin and has been accepted by the NRC with the justification that "most pressure transients have occurred during isothermal metal conditions." The steady-state limits are shown in Figure 3.1 and, in digitized form, in Table 3.1. The curves also include the 800 psig PORV piping load limit.

The analysis assumes nominal values; i.e., pressure instrumentation uncertainties are not included. This is consistent with standard Westinghouse practice. Use of the Appendix G limits without instrumentation uncertainty is justified on the basis of the large amount of conservatism (recognized by the NRC) inherent in the development of the limits.

The 800 psig piping limit results from an analysis of water hammer effects on relief valve piping for certain classes of rapidly opening relief valves (e.g., Garrett valves) under water solid conditions. The Garrett valves are solenoid operated with a rapidly increasing flow vs. stem position curve.



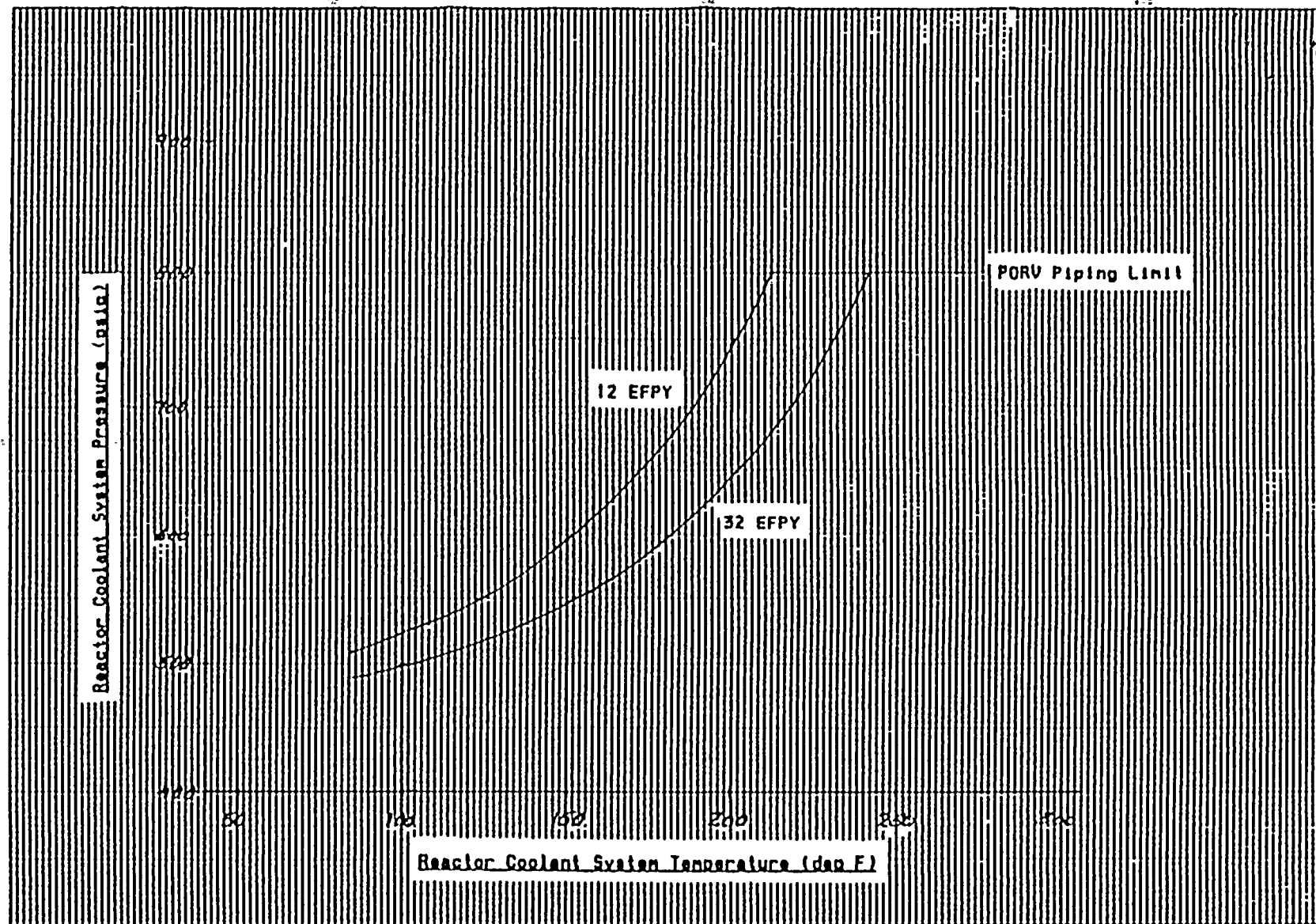


Figure 3.1 Reactor Coolant System Steady-State Pressure -- Temperature Limits at 12 and 32 EFPY



TABLE 3.1

STEADY-STATE COOLDOWN PRESSURE/TEMPERATURE LIMITS

RCS Temp (deg F)	<u>RCS Pressure (psig)</u>		RCS Temp (deg F)	<u>RCS Pressure (psig)</u>	
	<u>12 EFPY</u>	<u>32 EFPY</u>		<u>12 EFPY</u>	<u>32 EFPY</u>
85.0	509.2	490.2	165.0	629.1	568.3
90.0	513.3	492.8	170.0	642.1	576.9
95.0	517.8	495.7	175.0	656.3	586.1
100.0	522.6	498.8	180.0	671.5	595.9
105.0	527.7	502.1	185.0	687.7	606.6
110.0	533.2	505.7	190.0	705.2	618.0
115.0	539.0	509.6	195.0	724.1	630.4
120.0	545.4	513.8	200.0	744.2	643.5
125.0	552.2	518.2	205.0	766.0	657.7
130.0	559.6	523.0	210.0	789.3	673.0
135.0	567.5	528.2	215.0	814.5	689.3
140.0	576.1	533.8	220.0	841.4	707.0
145.0	585.1	539.6	225.0	870.4	726.0
150.0	594.9	546.0	230.0	901.6	746.3
155.0	605.5	552.9	235.0	935.0	768.2
160.0	616.9	560.4	240.0	970.8	791.7
			245.0	1009.6	817.0

100-100000

100-100000

100-100000

100-100000

100-100000

100-100000

100-100000

100-100000

When a characteristic curve of this type is combined with Garrett's typically rapid stroke time (less than two seconds) the valve becomes effectively full open or full closed within a few tenths of a second, thus setting the conditions for a water hammer.

The flow through an air operated relief valve, when compared to solenoid valves, is much less sensitive to stem position. When combined with the relatively slow opening and closing times characteristic of these types of valves, the water hammer effects will be much reduced, if not effectively eliminated. Evaluation of water hammer forces on the piping of air operated valves has not been performed by Westinghouse. The practice has been to assume the conservative position of taking the worst case results (the Garrett analysis) and applying them to all LTOPS setpoint evaluations, regardless of the relief valve employed.

3.2 PORV STROKE TIME

As instructed by American Electric Power Corporation, the LTOPS analysis also includes a parameter study on valve opening time in order to determine the relationship between opening time and LTOPS setpoint. The parametric study was performed assuming 6 different valve opening times, ranging from 1.0 sec. to 10 seconds. This was considered a broad enough range to cover all reasonable opening time measurements.

The PORV closing time selected for the analysis was set at 4.0 seconds, independent of the opening time. The closure time selection has no impact on the overpressure transient (an Appendix G consideration), but does impact the underpressure transient (important for the protection of the reactor coolant pump No. 1 seal). The characteristic of the transient is such that as closure time increases, the underpressure becomes more severe.

3.3 PORV OPERATION

The design basis for an overpressure event requires that either PORV provide adequate relieving capability in the event of a single valve failure.

[illegible]

Therefore, the setpoint analysis is based on the assumption of single valve operation.

The setpoint analysis includes the effect of time delays associated with the transmission of the wide range reactor coolant system pressure signal. A conservative value of 0.95 seconds was utilized for the analysis. The breakdown of the time delay is as follows:

Pressure sensing line transport delay	0.15 sec.
Pressure transmitter delay	0.25 sec.
Electronics delay	0.10 sec.
Solenoid actuation delay	0.10 sec.
Valve Chamber (Pneumatic) delay	<u>0.35</u> sec.
Total	0.95 sec

With the exception of the pressure transmitter delay, the factors comprising the total delay time are Westinghouse generic estimates for air operated pressurizer relief valves. D. C. Cook Unit 2 features two Foxboro wide range (Model N-EIIGH-HIM2-A) pressure transmitters. Westinghouse instrumentation group had no information on Foxboro transmitters, so the delay time of 0.25 seconds was obtained directly from Foxboro's Product Information Group.

The flow characteristics (valve $C(v)$ vs. valve stroke) for the pressurizer power operated relief valves were obtained from American Electric Power Co. and are shown by Figure 3.2. The percent at full flow $C(v)$ corresponding to selected percent of valve stroke values is listed in Table 3.2.

3.4 MASS INPUT CONSIDERATIONS

The mass injection transient is assumed to occur as a result of the operation of a single centrifugal charging pump in combination with a sudden loss of letdown. The allowable charging configuration is limited by technical specifications in operational modes 5 and 6, where the Cook units LTOPS is enabled. The charging flow, assuming that the normal and alternate flow paths are both open, as a function of reactor coolant system pressure is shown in Figure 3.3. The data in tabular form is given in Table 3.3.

100-100000

100-100000

100-100000

100-100000

100-100000

100-100000

100-100000

100-100000

100-100000

100-100000

100-100000

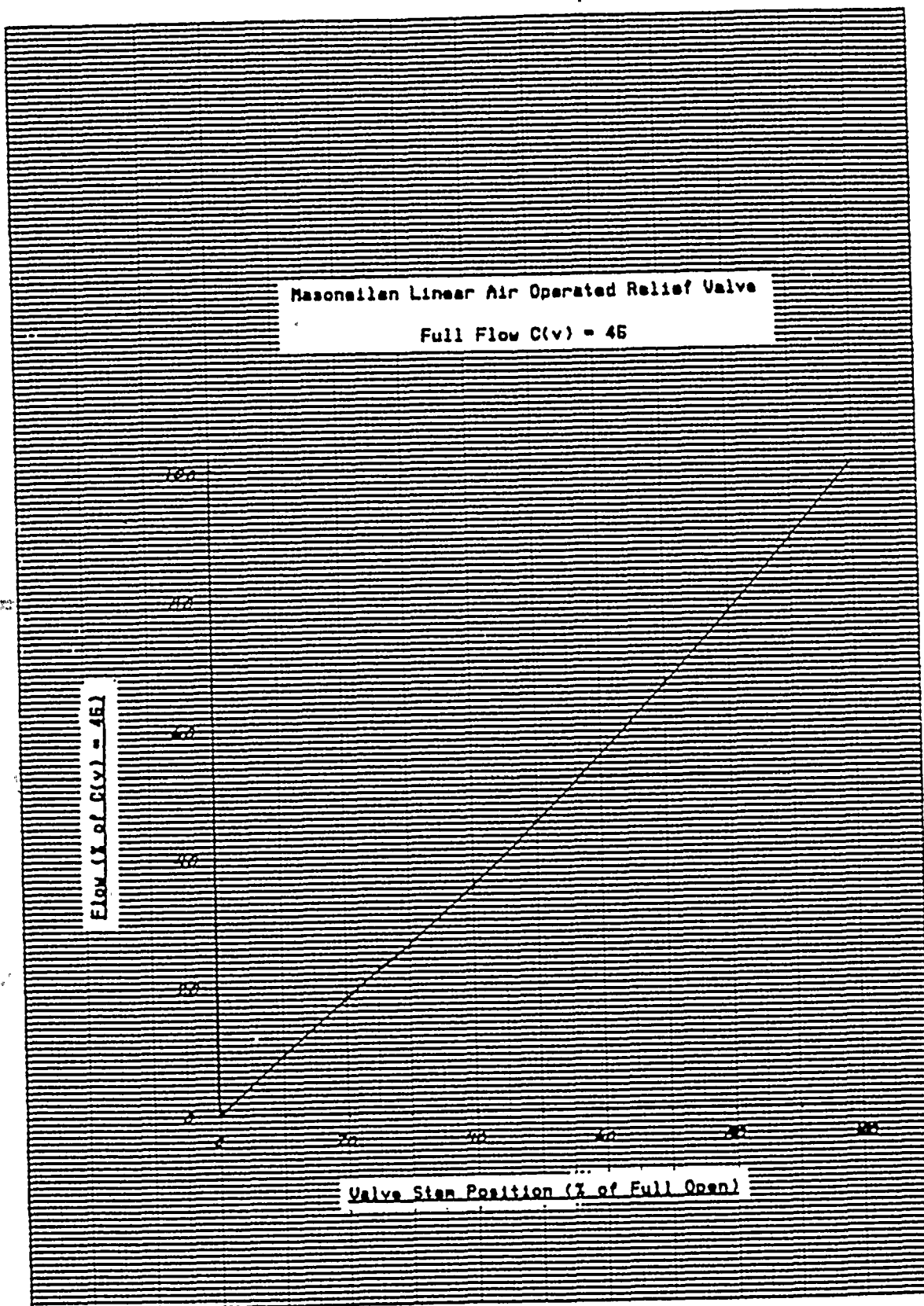


Figure 3.2 Pressurizer PORV Flow Characteristic Curve

1
2
3
4
5
6
7
8
9
10
11
12
13
14
15
16
17
18
19
20
21
22
23
24
25
26
27
28
29
30
31
32
33
34
35
36
37
38
39
40
41
42
43
44
45
46
47
48
49
50
51
52
53
54
55
56
57
58
59
60
61
62
63
64
65
66
67
68
69
70
71
72
73
74
75
76
77
78
79
80
81
82
83
84
85
86
87
88
89
90
91
92
93
94
95
96
97
98
99
100

1
2
3
4
5
6
7
8
9
10
11
12
13
14
15
16
17
18
19
20
21
22
23
24
25
26
27
28
29
30
31
32
33
34
35
36
37
38
39
40
41
42
43
44
45
46
47
48
49
50
51
52
53
54
55
56
57
58
59
60
61
62
63
64
65
66
67
68
69
70
71
72
73
74
75
76
77
78
79
80
81
82
83
84
85
86
87
88
89
90
91
92
93
94
95
96
97
98
99
100



TABLE 3.2

PRESSURIZER PORV CHARACTERISTICS*PORV Opening

<u>% Valve</u> <u>Stroke</u>	<u>% Valve</u> <u>C(v)</u>	<u>% Valve</u> <u>Stroke</u>	<u>% Valve</u> <u>C(v)</u>
0.0	0.0	60.0	56.0
10.0	9.0	70.0	66.0
30.0	26.0	80.0	77.0
40.0	35.0	90.0	88.0
50.0	45.0	100.0	100.0

PORV Closing

<u>% Valve</u> <u>Stroke</u>	<u>% Valve</u> <u>C(v)</u>	<u>% Valve</u> <u>Stroke</u>	<u>% Valve</u> <u>C(v)</u>
0.0	100.0	50.0	45.0
10.0	88.0	60.0	35.0
20.0	77.0	70.0	26.0
30.0	66.0	90.0	9.0
40.0	56.0	100.0	100.0

*Based on the characteristic curve shown in Figure 3.2.



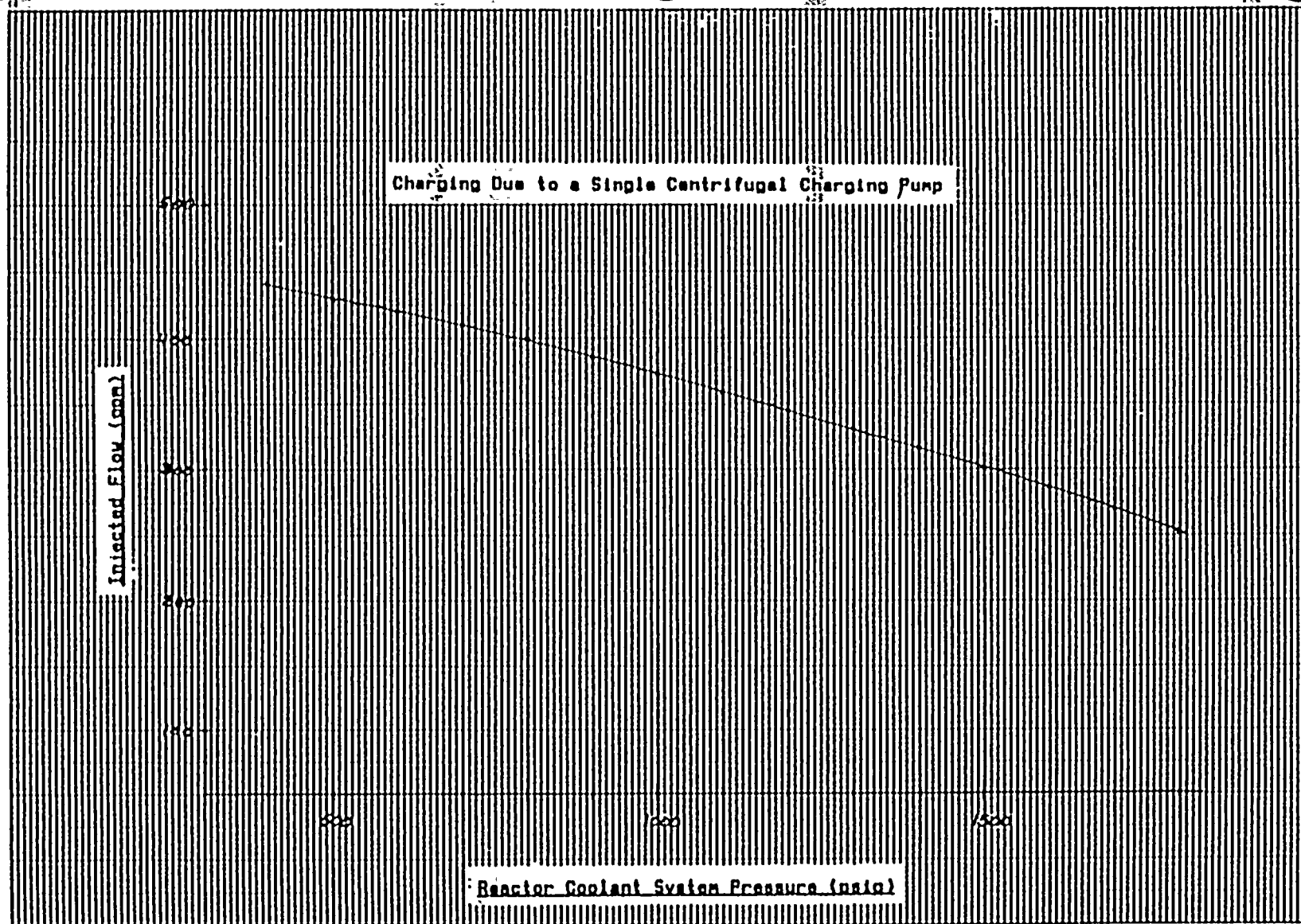


Figure 3.3 Mass Injection Flow vs. RCS Pressure

100

100

100

100

100

100

100

TABLE 3.3

MAXIMUM CHARGING FLOW AT RCS PRESSURE*

<u>RCS Press.</u> <u>(psig)</u>	<u>Charging</u> <u>Flow (gpm)</u>	<u>RCS Press.</u> <u>(psig)</u>	<u>Charging</u> <u>Flow (gpm)</u>
400	439.2	1100	358.3
500	429.7	1200	344.1
600	420.2	1300	329.8
700	410.7	1400	315.2
800	399.9	1500	300.5
900	386.2	1600	285.6
1000	372.3	1700	268.9
		1800	251.5

*Based on single centrifugal charging pump operation.

一、

二、

三、

四、

五、

六、

The mass input case was conservatively analyzed at low temperature, 85°F, where the pressure transient resulting from a mass input shows the greatest overshoots and undershoots. No other calculations were performed at different temperatures, for the reason that this is the worst case situation and the D. C. Cook Unit 2 LTOPS setpoint is independent of temperature.

Mass injection rates ranging from 100 to 600 gpm were selected for the mass input parameter study portion of the analysis. This range was based on analyses performed for units similar to D. C. Cook Unit 2, and provides a good definition of the relationship between mass input and the resulting pressure transient. The results of the LOFTRAN runs are presented in Figures 3.4 through 3.9 for the both overpressure and underpressure transients.

3.5 HEAT INPUT CONSIDERATIONS

The heat input mechanism, from the discussion in Section 1.3.2, is based on a single reactor coolant pump startup with a temperature asymmetry existing between the primary water held up in the steam generator tubes and the water in the remainder of the reactor coolant system. The magnitude of the asymmetry depends on the previous plant operation which allowed the asymmetry to develop. For this study, it was considered conservative to assume a maximum asymmetry of 50°F as the design basis, since much higher differences would be difficult to develop.

The heat input cases were analyzed at RCS temperatures of 85°F and 150°F (steam generator temperatures of 135°F and 200°F respectively). The characteristic behavior of the overpressure transient resulting from a heat input event is to become more severe with increasing RCS temperature. This required the additional LOFTRAN runs at increased temperatures in order to provide assurance that the increase in pressure overshoot with temperature did not exceed that of the Appendix G limit, as the heat injection events began to dominate.



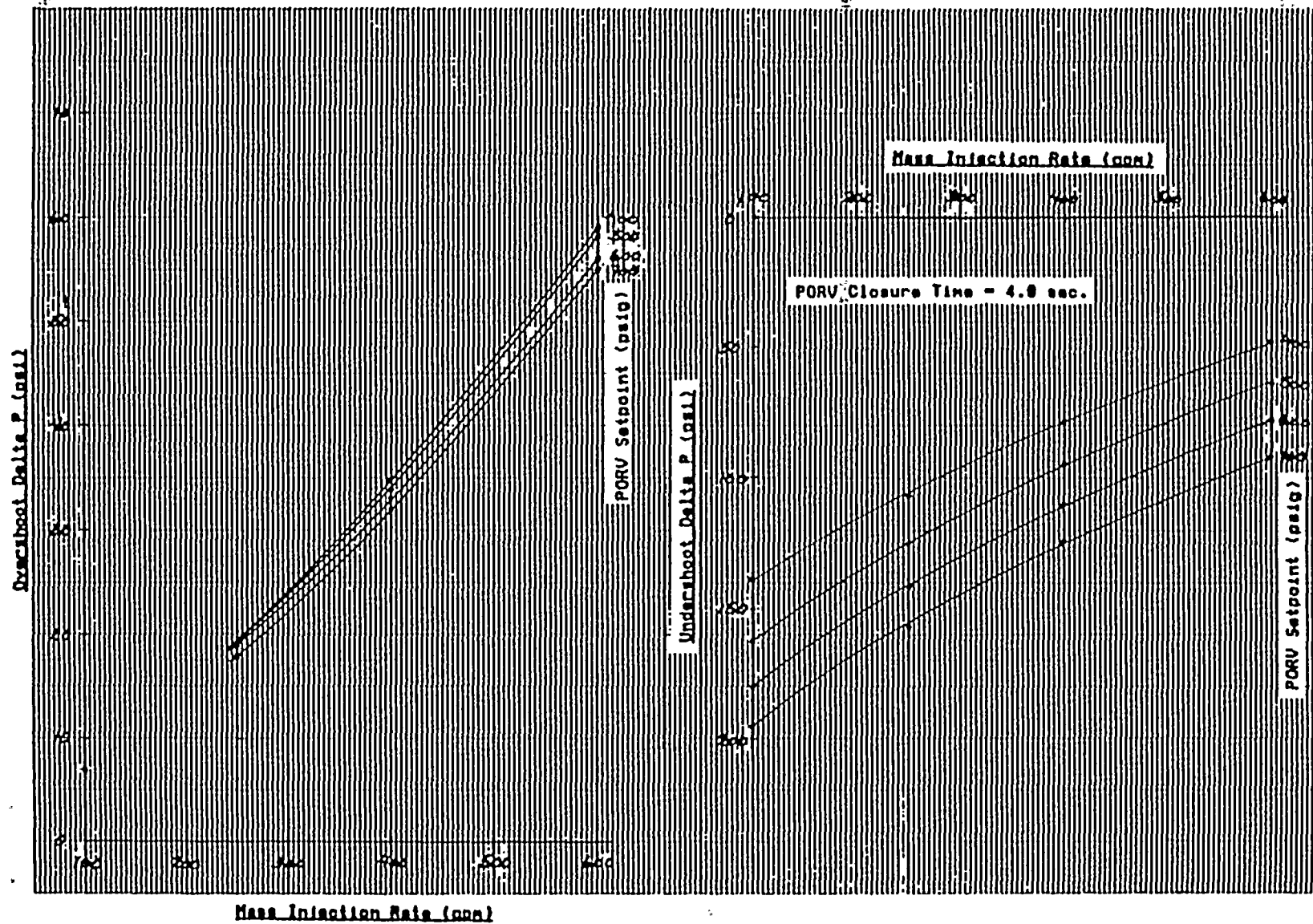


Figure 3.4 Overshoot and Undershoot ΔP Values vs. Mass Injection Rate at PORV Stroke open time of 1.0 Sec.



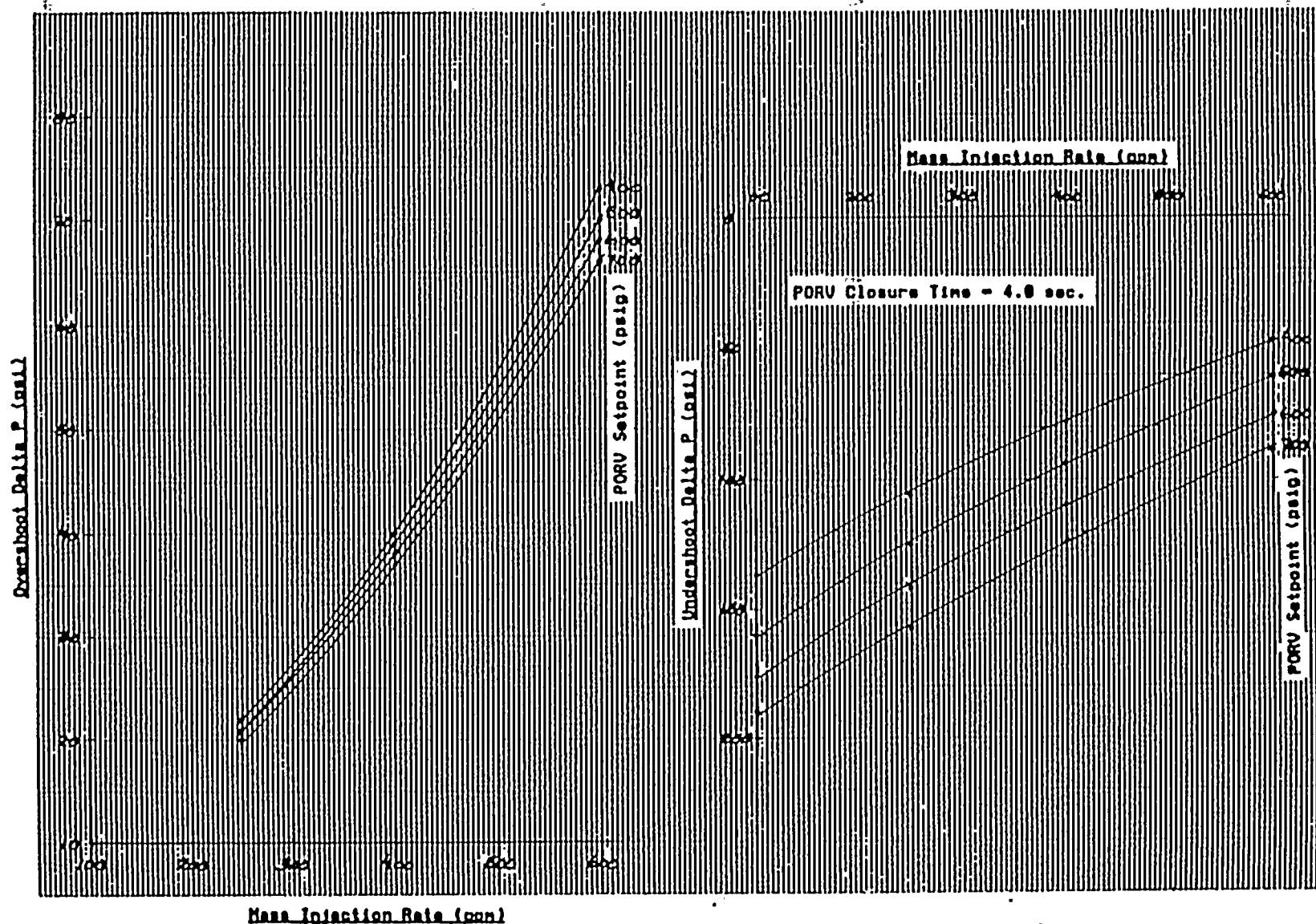


Figure 3.5 Overshoot and Undershoot ΔP Values vs. Mass Injection Rate at PORV Stroke Open Time of 2.0 Sec.

1

2

3

4

5

6

7

8

9

10

11

12

13

14

15

16

17

18

19

20

21

22

23

24



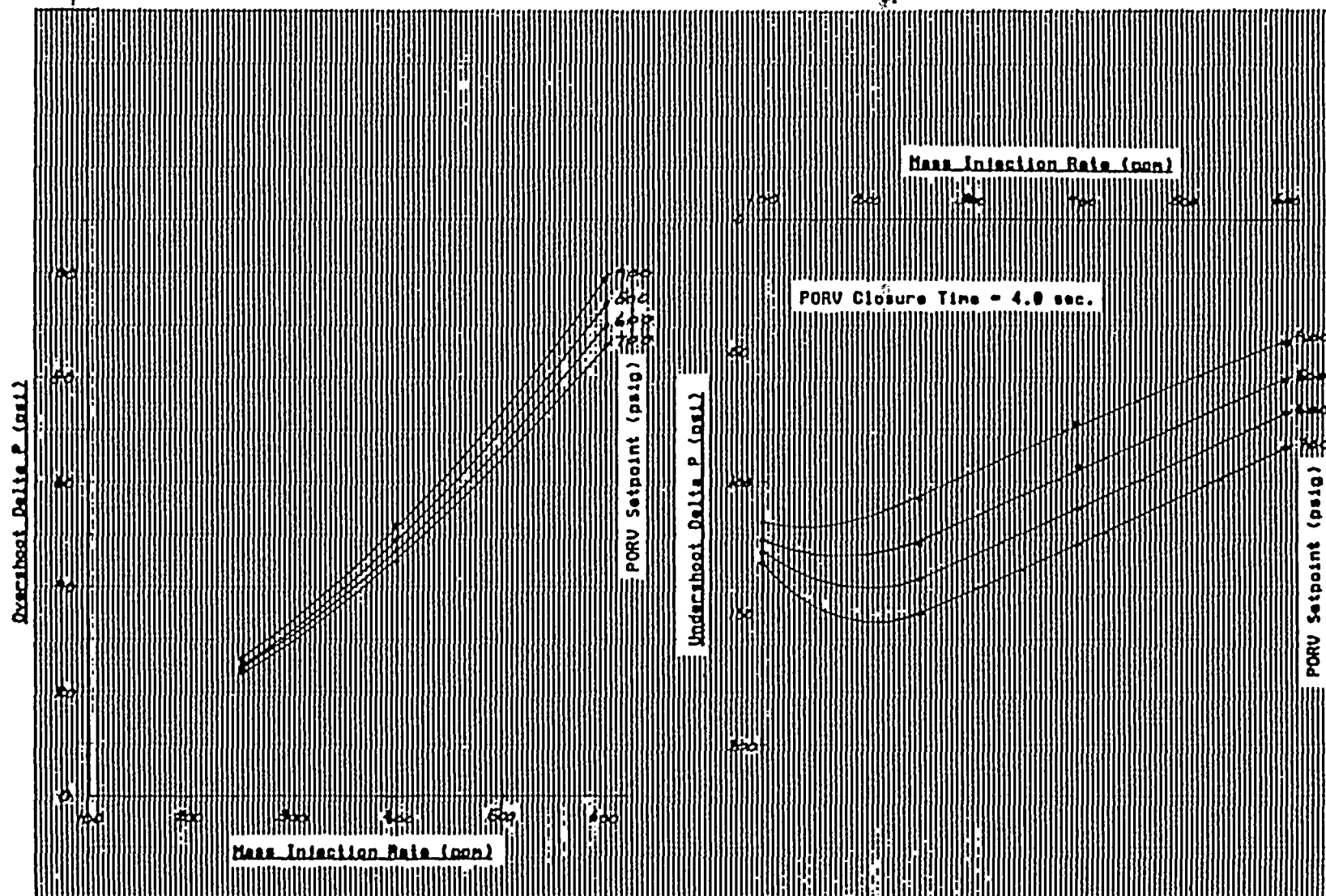


Figure 3.6 Overshoot and Undershoot ΔP Values vs. Mass Injection Rate at PORV Stroke Open Time of 4.0 Sec.

100-100000-100000

100-100000-100000

100-100000-100000

100-100000-100000

100-100000-100000

100-100000-100000

100-100000-100000

100-100000-100000

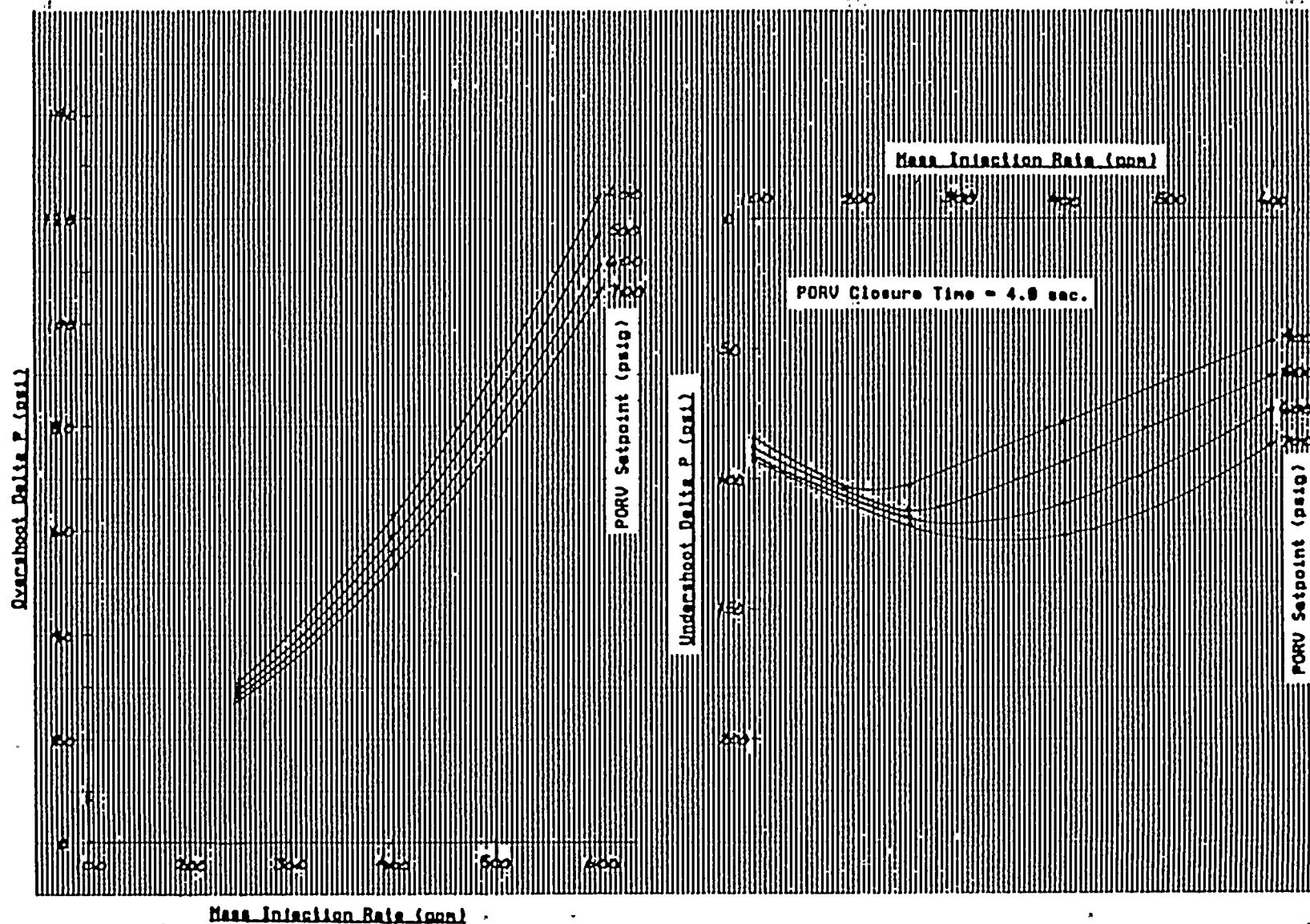


Figure 3.7 Overshoot and Undershoot ΔP Values vs. Mass Injection Rate at PORV Stroke Open Time of 6.0 Sec.



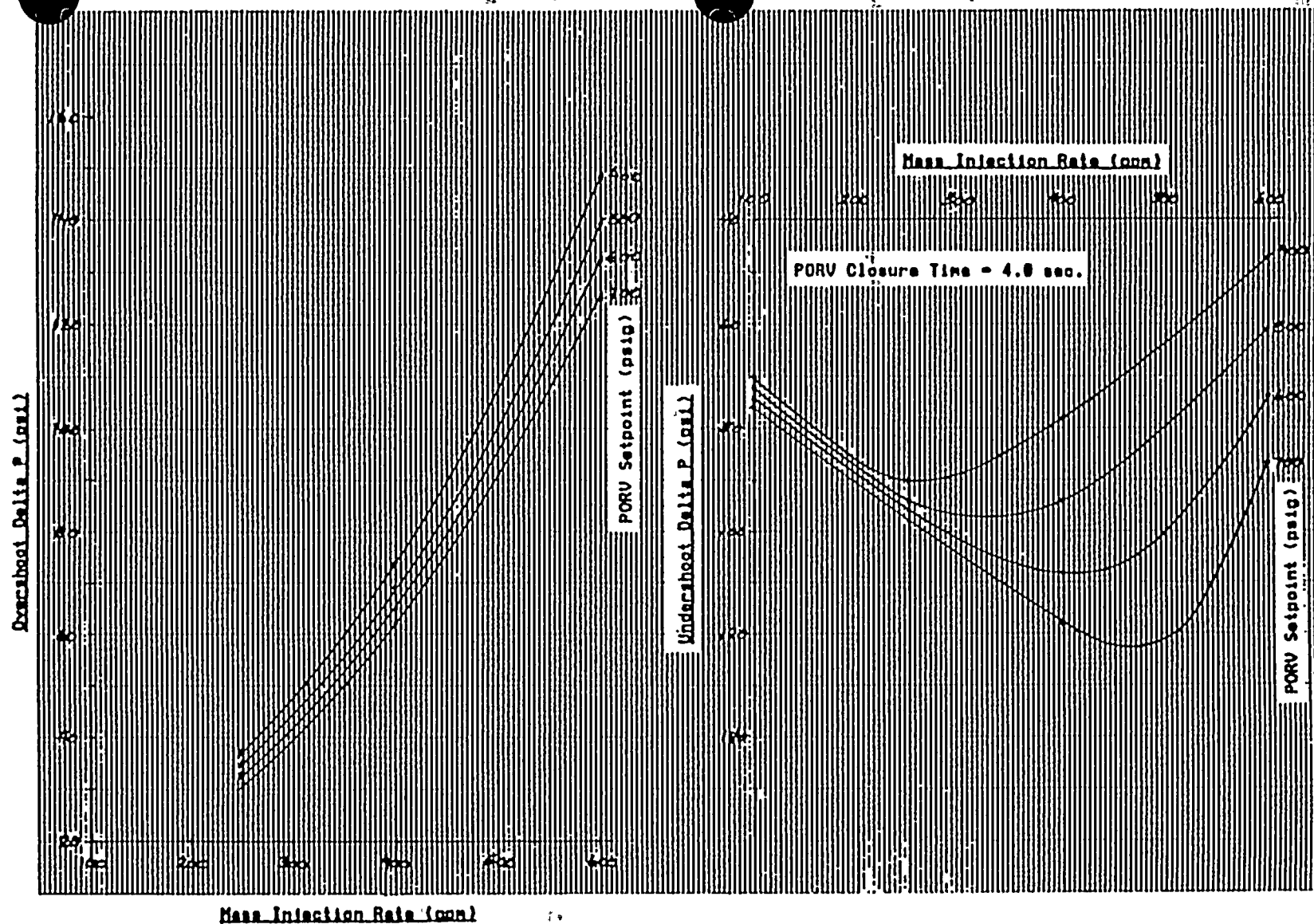


Figure 3.8 Overshoot and Undershoot ΔP Values vs. Mass Injection Rate at PORV Stroke Open Time of 8.0 Sec.

1

2

3

4

5

6

7

8

9

10

11

12

13

14

15

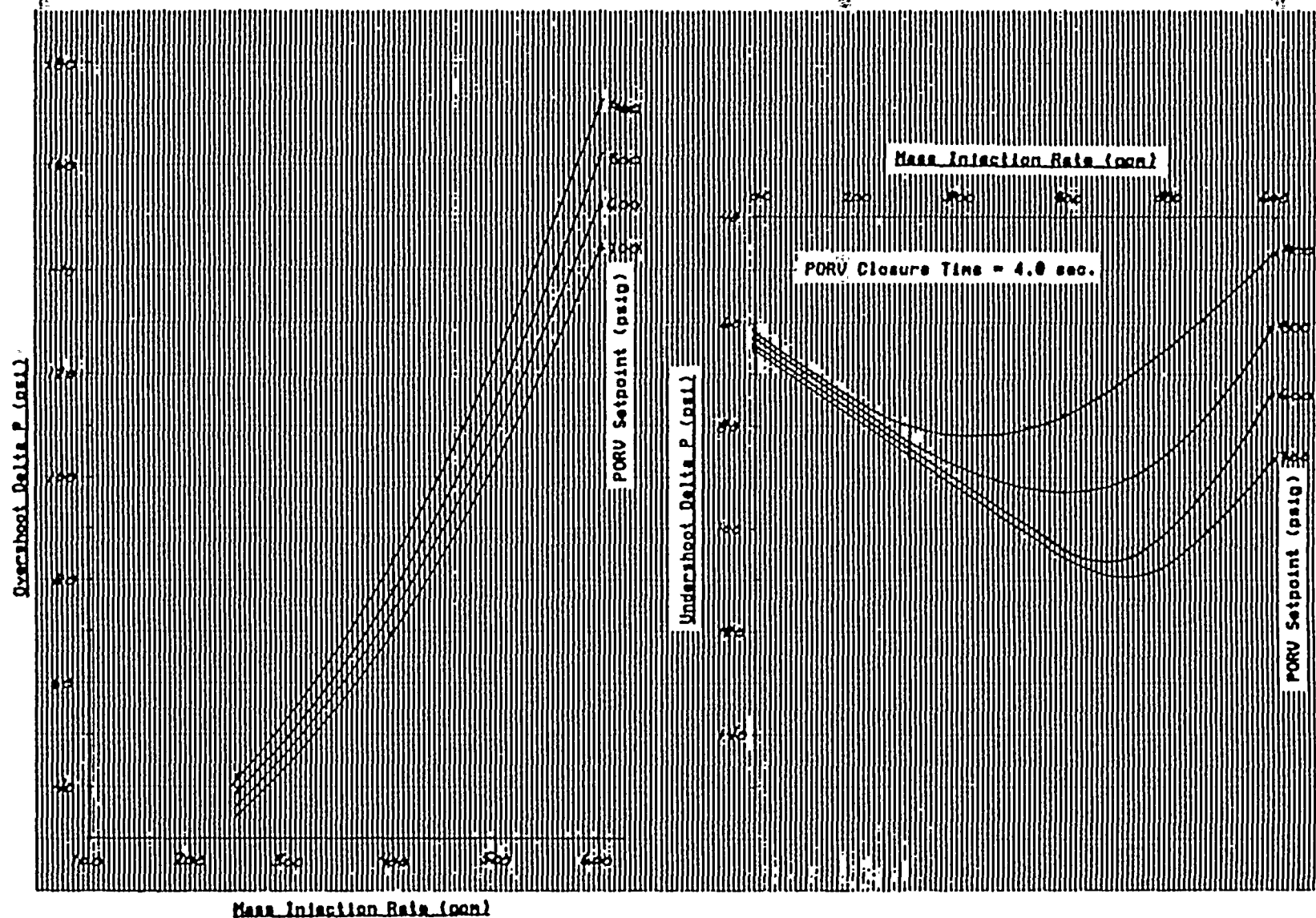


Figure 3.9 Overshoot and Undershoot ΔP Values vs. Mass Injection Rate at PORV Stroke Open Time of 10.0 Sec.

10

11

12

13

14

15

16

17

18

19

20

21

22

23

24

25

26

27

3.6 SPECIFICATION FOR MASS INPUT TRANSIENTS

Temperatures:

Reactor Coolant System temperature = 85°F

Reactor Coolant System Volume:

RCS volume = 12,509 cu. ft. for the D. C. Cook units

Initial Reactor Coolant System Pressure:

The initial RCS pressure was assumed to be 200 psi less than the setpoint pressure. This is conservative and assures that the transient is well defined by the time the PORV setpoint is reached. Given this definition, the overpressure is essentially insensitive to the initial pressure selection.

Reactor Coolant Relief Capacity:

The transient is analyzed assuming the failure of one PORV.

PORV Characteristics:

LTOPS Setpoints = 400, 500, 600, 700 psig

PORV flow characteristics are shown in Figure 3.2

Opening Time = 1.0, 2.0, 4.0, 6.0, 8.0, 10.0 sec.

Closing time = 4.0 sec.

$C(v) = 46$



Mass Injection Flow Capability:

Mass input Rates = 100, 250, 400, 600 gpm

Maximum charging flow corresponding to LTOPS setpoint pressure.
(Ref. Table 3.3)

Pressure Signal Transmission Characteristics:

Time delay to PORV stem motion = 0.95 sec.

3.7 SPECIFICATION FOR HEAT INPUT TRANSIENTS

System Temperatures:

SG/RCS temperature difference = 50°F

Steam generator (heat source) temperature = 135°F, 200°F

Reactor Coolant System Volume:

The same as that used for the mass injection cases.

Initial Reactor Coolant System Pressure:

The initial RCS pressure = 200 psi less than the LTOPS setpoint pressure

Reactor Coolant System Relief Capability:

The same as that for the mass injection cases

PORV Relief Characteristics:

The same as that for the mass injection cases.

Steam Generator Design Characteristics:

S/G tube heat transfer surface area = 54,500 sq. ft.

S/G type = 51F (D. C. Cook Unit 2 replacement steam generator)

Reactor Coolant Pump:

RCP type = 93A

Pressure Signal Transmission Characteristics:

The same as that for the mass injection cases.

3.8 SETPOINT EVALUATION

The impact of variable mass injection rates and PORV opening times on overshoot and undershoot values is provided by Table 3.4. The information provided by this table is based on the pressure overshoot/undershoot relationship with mass injection rate shown in composite Figures 3.4 through 3.9. The overshoot value was determined from the overshoot curves presented in these figures for the maximum mass injection rates consistent with single centrifugal charging pump injection flow (from Figure 3.3, or the tabulation shown in Table 3.3) for the indicated PORV setpoint. The undershoot value was conservatively estimated from the maximum delta P value below the indicated setpoint. In some cases (PORV opening times of 1 sec. and 2 sec.) the minimum delta P was estimated by extrapolating the undershoot to zero mass injection. This provides a basis for estimating the setpoint requirement for reactor coolant number 1 seal protection.

The overshoot and undershoot pressures resulting from the heat injection events are shown in Tables 3.5 and 3.6 as functions of setpoint pressure and PORV opening time. The tables summarize the results of LOFTRAN runs performed for RCS temperatures of 85 and 150°F, respectively. The evaluation was



TABLE 3.4

Max Overshoot/Undershoot Delta P Values vs PORV Opening Time Due to Mass InjectionD. C. Cook Unit 2

Setpt Press. (psig)	Mass Inj. Rate (gpm)	Overshoot/Undershoot Values (psi) vs. PORV Opening Time (sec)*											
		1.0		2.0		4.0		6.0		8.0		10.0	
		Over	Under	Over	Under	Over	Under	Over	Under	Over	Under	Over	Under
400.0	439.2	439.0	231.0	446.0	232.0	460.0	282.0	473.0	296.0	487.0	310.0	499.0	318.0
500.0	429.7	538.0	302.0	542.0	303.0	555.0	372.0	566.0	388.0	578.0	403.0	588.0	407.0
600.0	420.2	635.0	381.0	641.0	388.0	651.0	460.0	560.0	482.0	671.0	492.0	681.0	493.0
700.0	410.7	733.0	465.0	738.0	479.0	747.0	547.0	755.0	576.0	765.0	577.0	773.0	591.0

* PORV Closure time = 4.0 sec.

- Notes:
1. Mass injection rate obtained from RCS pressure vs. single pump charging flow.
 2. Overshoot obtained from max delta P overshoot vs. mass injection flow curve.
 3. Undershoot obtained from max delta P undershoot vs. mass injection flow.

1

2

3

4

5

6

7

8

9

10

11

12

13

14

15

16

17

18

19

20

21

22

23

24

25

26

27

28

29

30

31

32

33

34

35

36

37

38

39

40

41

42

43

44

45

46

47

48

49

50

51

52

53

54

55

56

57

58



TABLE 3.5

Max Overshoot/Undershoot Delta P Values vs PORV Opening Time Due to Heat InjectionD. C. Cook Unit 2

Setpoint Pressure (psig)	Overshoot/Undershoot Values (psi) vs. PORV Opening Time (sec)*											
	1.0		2.0		4.0		6.0		8.0		10.0	
	<u>Over</u>	<u>Under</u>	<u>Over</u>	<u>Under</u>	<u>Over</u>	<u>Under</u>	<u>Over</u>	<u>Under</u>	<u>Over</u>	<u>Under</u>	<u>Over</u>	<u>Under</u>
400.0	418.0	265.0	420.0	266.0	423.0	289.0	427.0	311.0	431.0	323.0	435.0	330.0
500.0	517.0	329.0	518.0	335.0	521.0	372.0	525.0	400.0	528.0	416.0	531.0	426.0
600.0	617.0	422.0	618.0	426.0	621.0	463.0	624.0	496.0	627.0	513.0	629.0	523.0
700.0	716.0	502.0	717.0	510.0	720.0	557.0	723.0	593.0	726.0	610.0	728.0	621.0

* Valve Closure time = 4.0 sec.

RCS temperature = 85.0°F

S/G temperature = 135.0°F

10

10

10

10

10

10

10

10

10

TABLE 3.6

Max Overshoot/Undershoot Delta P Values vs PORV Opening Time Due to Heat InjectionD. C. Cook Unit 2

Setpoint Pressure (psig)	<u>Overshoot/Undershoot Values (psi) vs. PORV Opening Time (sec)*</u>											
	<u>1.0</u>		<u>2.0</u>		<u>4.0</u>		<u>6.0</u>		<u>8.0</u>		<u>10.0</u>	
	<u>Over</u>	<u>Under</u>	<u>Over</u>	<u>Under</u>	<u>Over</u>	<u>Under</u>	<u>Over</u>	<u>Under</u>	<u>Over</u>	<u>Under</u>	<u>Over</u>	<u>Under</u>
400.0	438.0	278.0	445.0	279.0	459.0	295.0	475.0	311.0	490.0	311.0	505.0	324.0
500.0	540.0	338.0	547.0	342.0	562.0	381.0	576.0	395.0	589.0	407.0	602.0	408.0
600.0	639.0	419.0	646.0	433.0	659.0	468.0	672.0	487.0	685.0	493.0	697.0	495.0
700.0	739.0	512.0	745.0	516.0	757.0	563.0	770.0	579.0	782.0	581.0	793.0	585.0

* Valve Closure time = 4.0 sec.

RCS temperature = 150.0°F

S/G temperature = 200.0°F

100

100

100

100

100

100

100

100

100

100

100

100

100

100

100

100

100

100

100

100

100

100

100

100

100

100

100



stopped at this point (150°F) since it became evident that the most limiting temperature with respect to Appendix G criteria was at 85°F and that the mass injection events are dominant.

The data from these tables (both mass injection and heat injection) is presented in Figures 3.10 through 3.21, showing the maxima and minima system pressure as a function of setpoint pressure for the valve opening times selected for the study. Figures 3.10 through 3.15 show the pressure extrema at an RCS temperature of 85°F, and Figures 3.16 through 3.21 show the extrema at 150°F. Also included on these figures is the Appendix G pressure limit at 12 and 32 EFPY, and the minimum system pressure for an RCP start. The Appendix G limits (ref. Figure 3.1) correspond to the RCS temperature assumed for the calculation shown by the figure. The RCP seal limit was selected to correspond to the minimum system pressure specified by D. C. Cook for reactor coolant fill and vent operations (325 psig). At other times, "the system pressure is governed by the requirement to maintain 200 psid across the number 1 RCP seal." It is assumed that the differential pressure requirement across the seal plus the volume control tank pressure and the static head in the number 1 seal leakoff line will be no more than 325 psig; the value specified for fill and vent.

The intersection of these limits (Appendix G and RCP seal) with the most limiting of the maxima and minima curves due to mass and/or heat injection events forms the basis for the construction of Figures 3.22 and 3.23. These figures show, respectively, the dependency of the maximum allowed LTOPS setpoint on valve opening time for reactor vessel exposures of 12 EFPY and 32 EFPY. The minimum setpoint limit (RCP protection) has not been shown, since the "white space" is generally not large enough to meet both the RCP number 1 seal requirements and the Appendix G limit.

100-100000

100-100000

100-100000

100-100000

100-100000

100-100000

100-100000

100-100000

100-100000

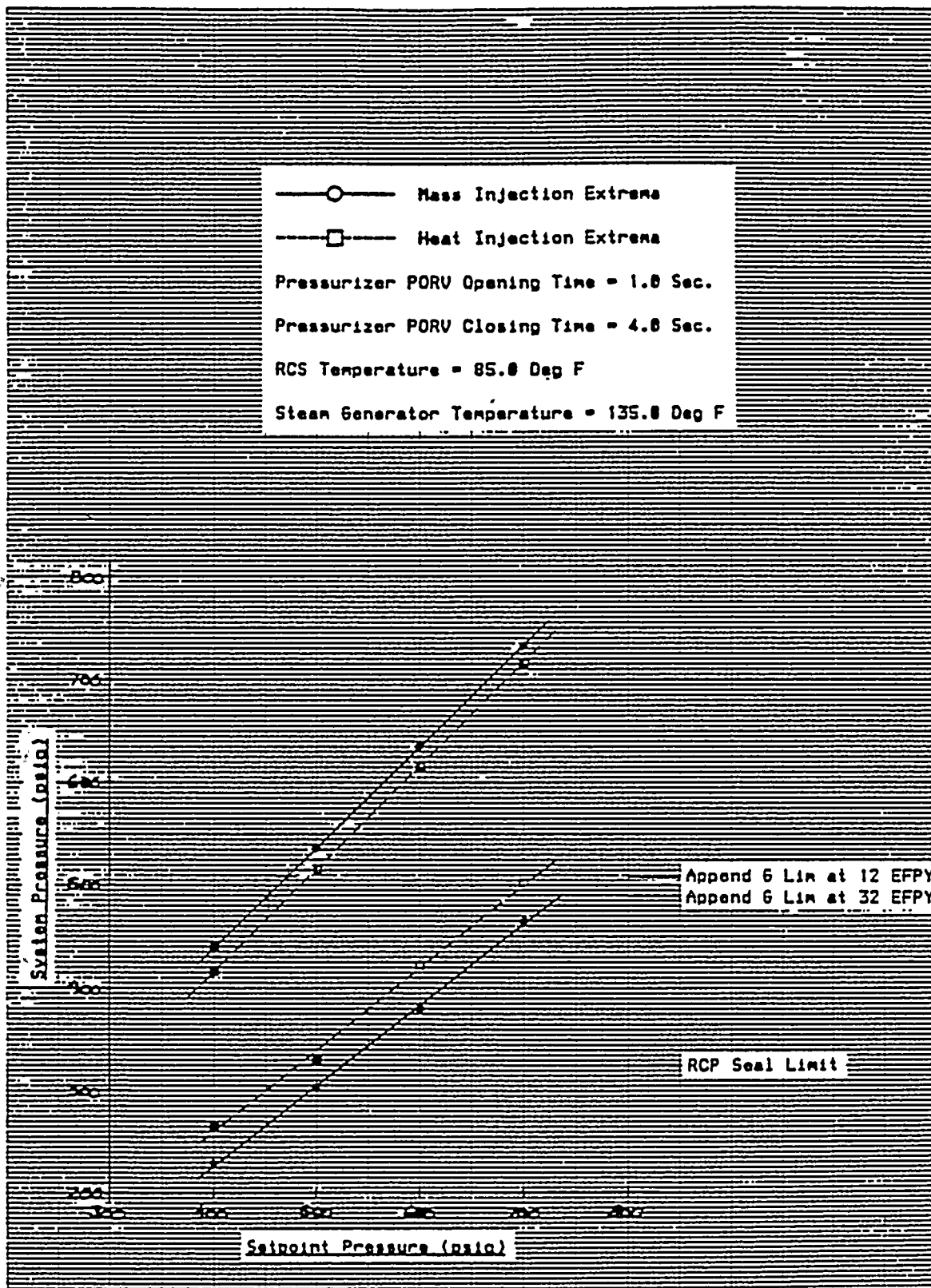


Figure 3.10. RCS Pressure Extrema vs. Setpoint Pressure at PORV
 Stroke Open Time of 1.0 Sec. and RCS Temperature of 85°F

100

100

100

100

100

100

100

100

100

100

100

100

100

100

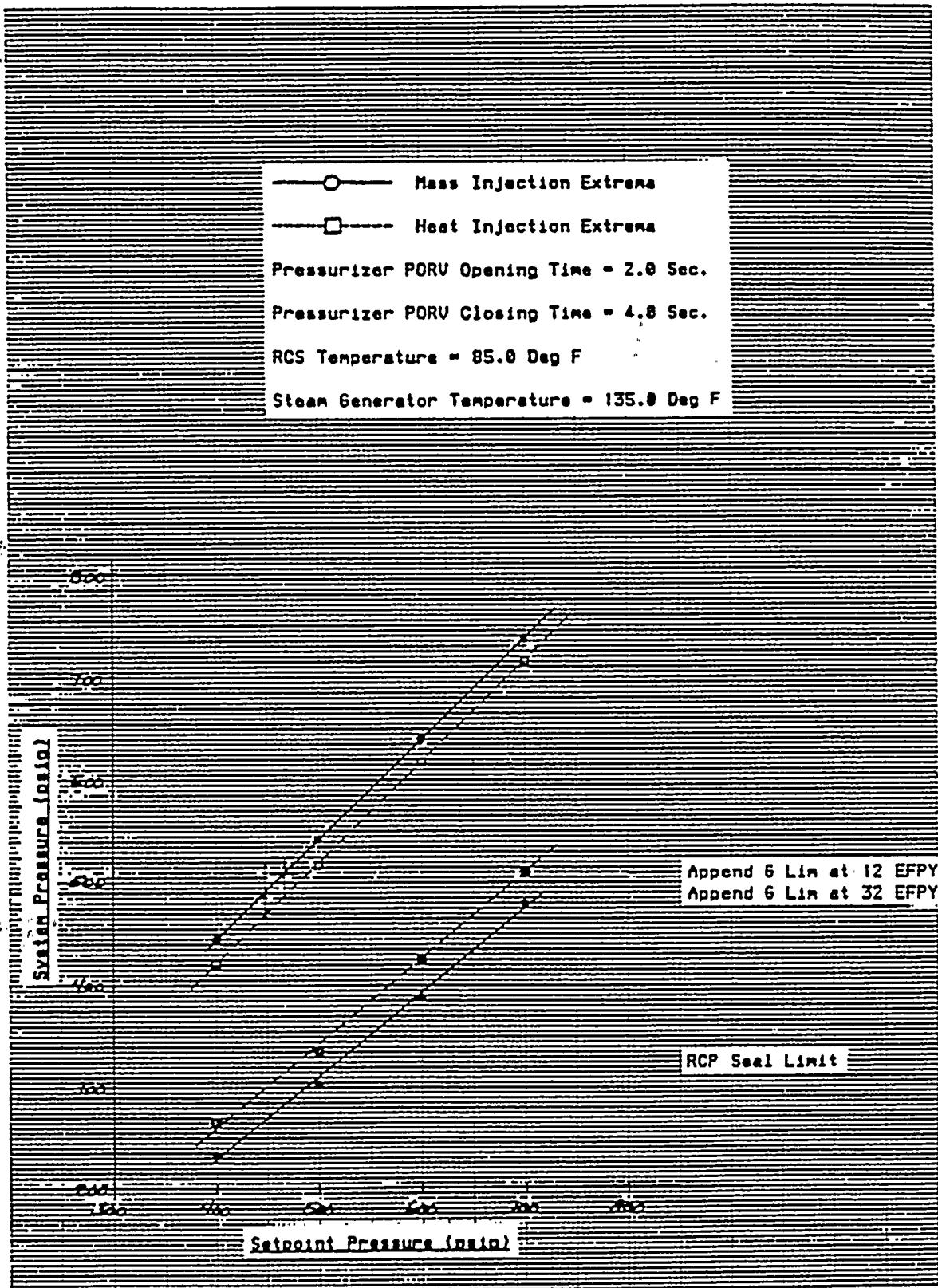


Figure 3.11 RCS Pressure Extrema vs. Setpoint Pressure at PORV
 Stroke Open Time of 2.0 Sec. and RCS Temperature of 85°F

100

100

100

100

100

100

100

100

100

100

100

100

100

100

100

100

100

100

100

100

100

100

100

100

100

100

100

100

100

100

100

100

100

100

100

100

100

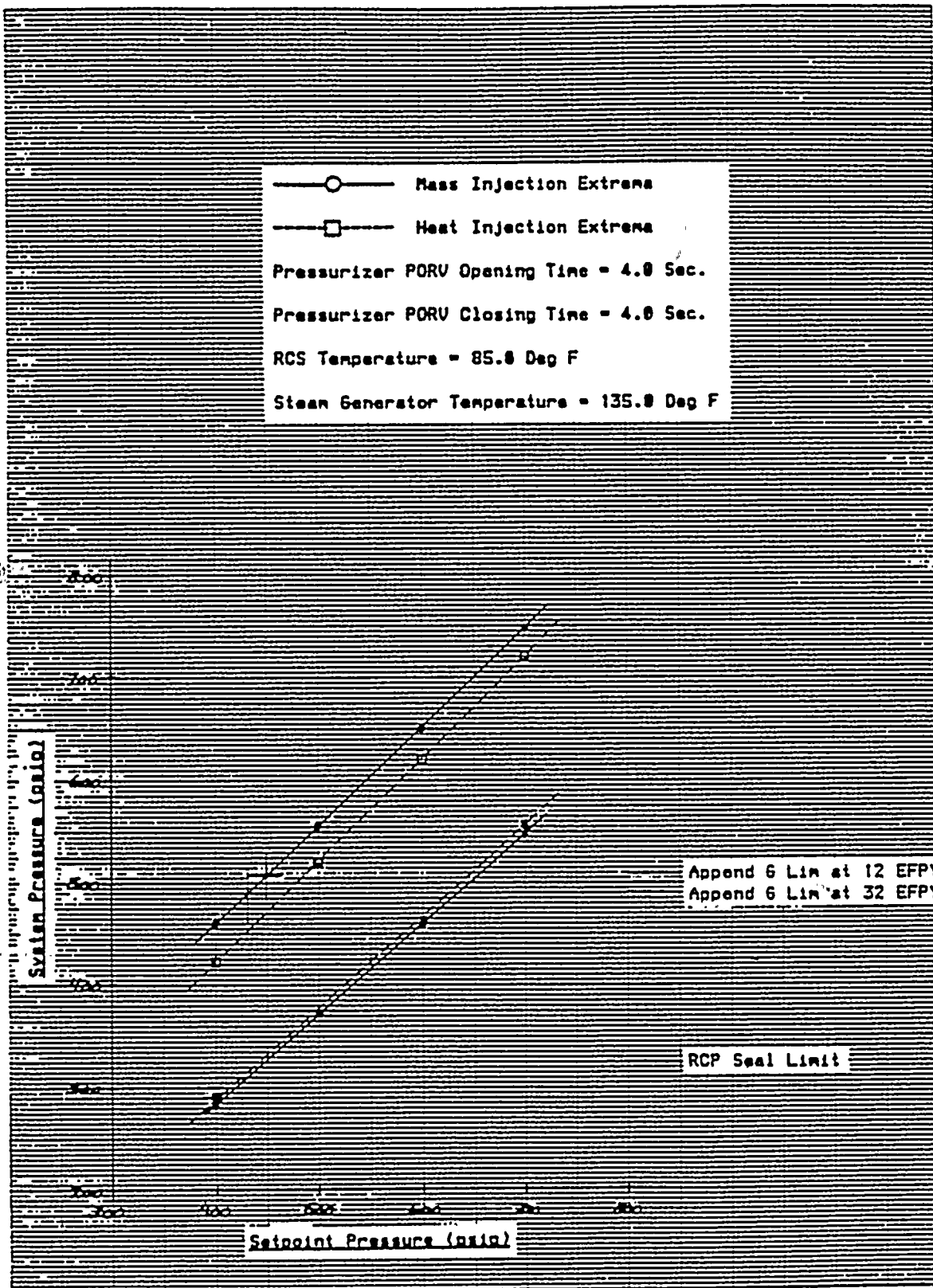


Figure 3.12 RCS Pressure Extrema vs. Setpoint Pressure at PORV
Stroke Open Time of 4.0 Sec. and RCS Temperature of 85°F

100-100000

100-100000

100-100000

100-100000

100-100000

100-100000

100-100000

100-100000

100-100000

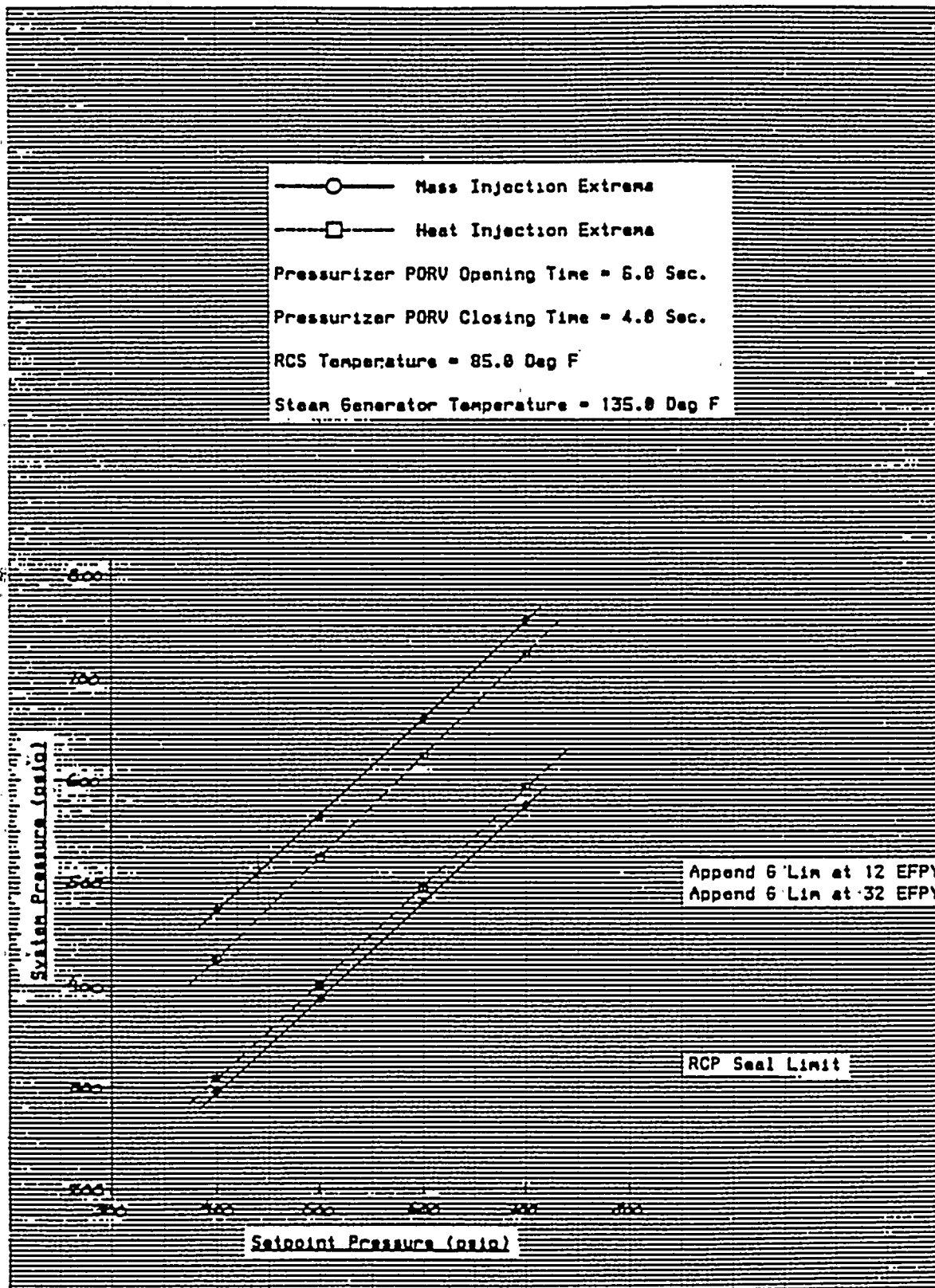


Figure 3.13 RCS Pressure Extrema vs. Setpoint Pressure at PORV
 Stroke Open Time of 6.0 Sec. and RCS Temperature of 85°F

100

100

100

100

100

100

100

100

100

100

100

100

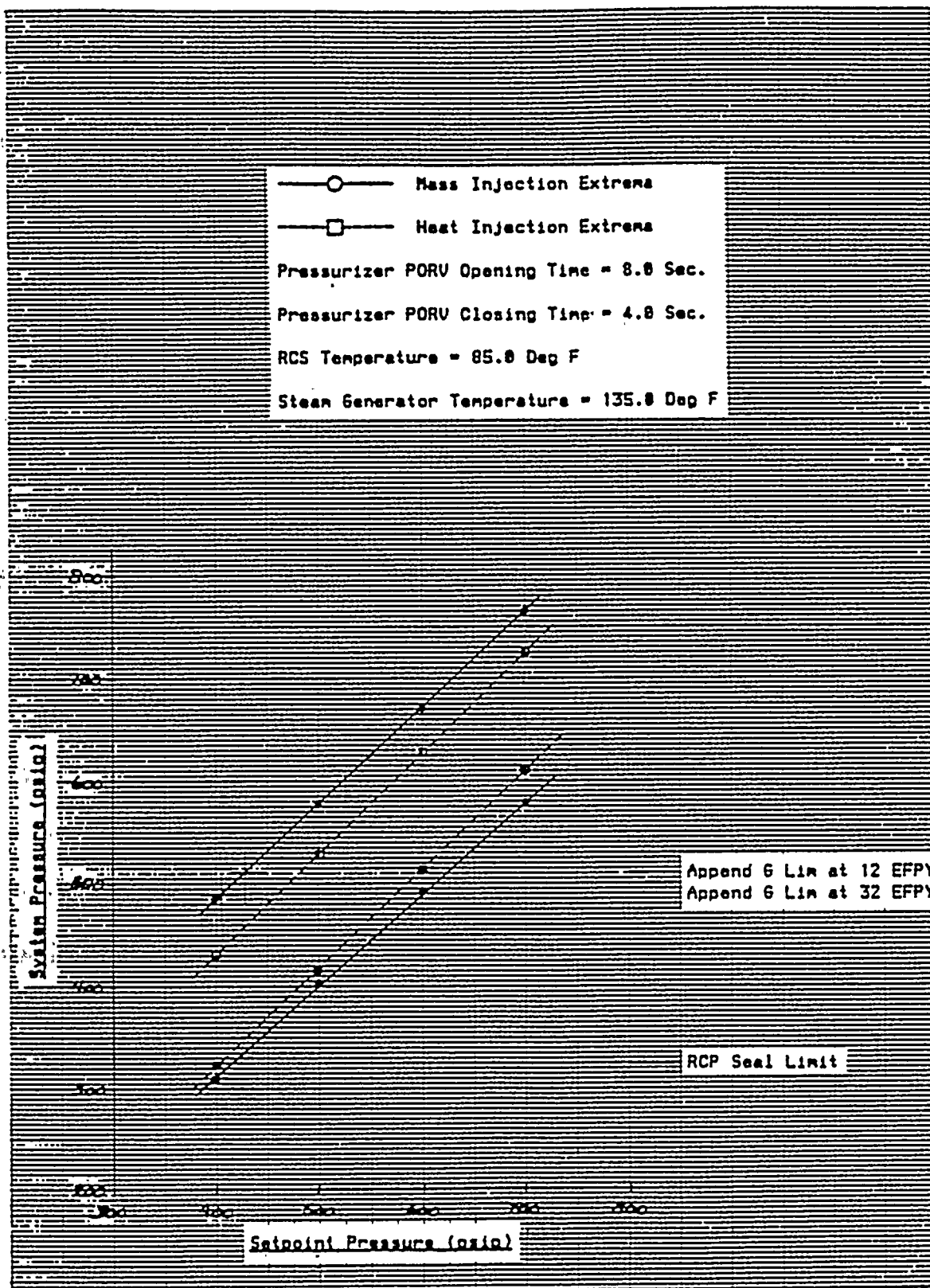


Figure 3.14 RCS Pressure Extrema vs. Setpoint Pressure at PORV
 Stroke Open Time of 8.0 Sec. and RCS Temperature of 85°F

100-100000

100-100000

100-100000

100-100000

100-100000

100-100000

100-100000

100-100000

100-100000

100-100000

100-100000

100-100000

100-100000

100-100000

100-100000

100-100000

100-100000

100-100000

100-100000

100-100000

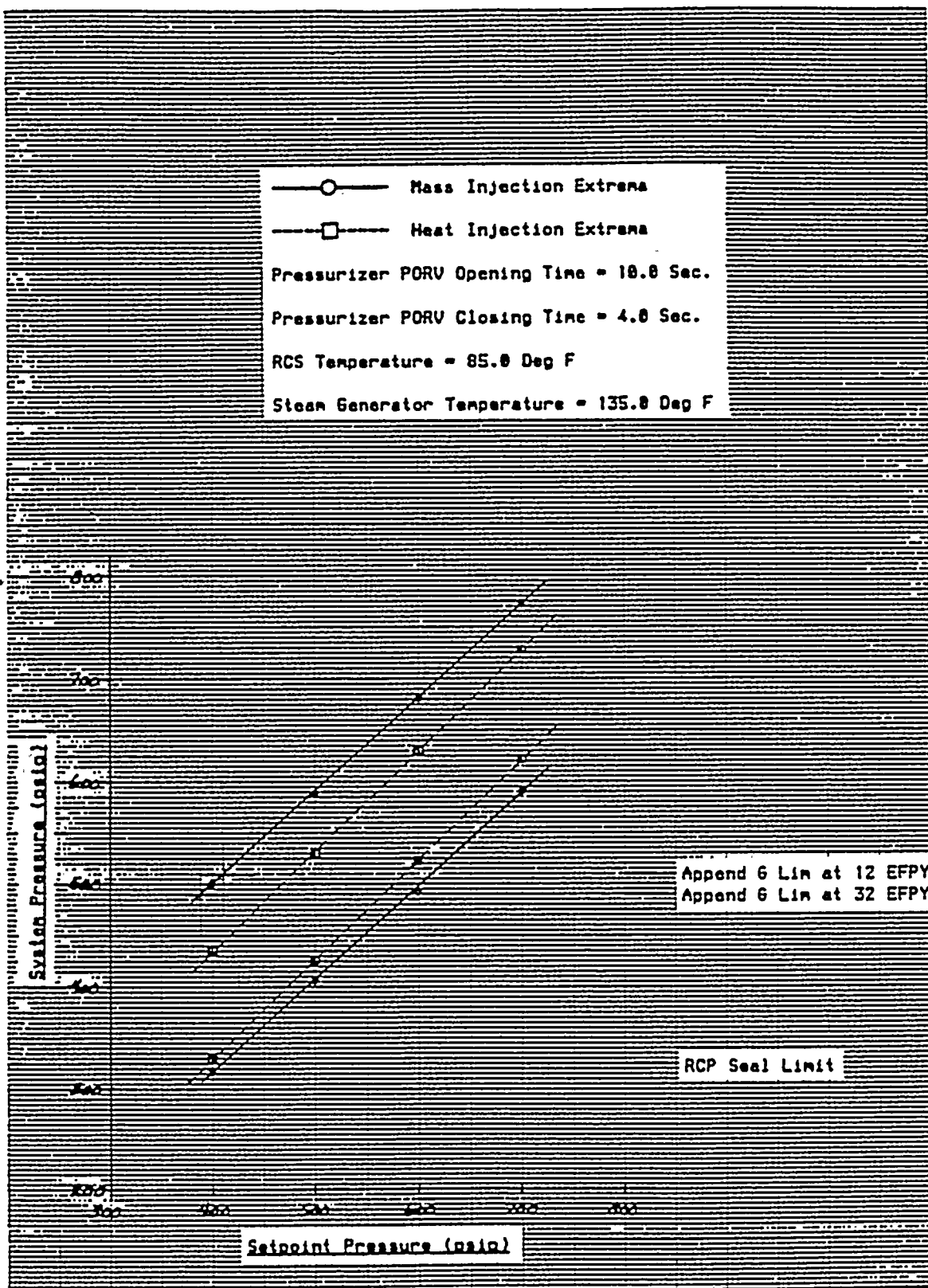


Figure 3.15 RCS Pressure Extrema vs. Setpoint Pressure at PORV
 Stroke Open Time of 10.0 Sec. and RCS Temperature of 85°F



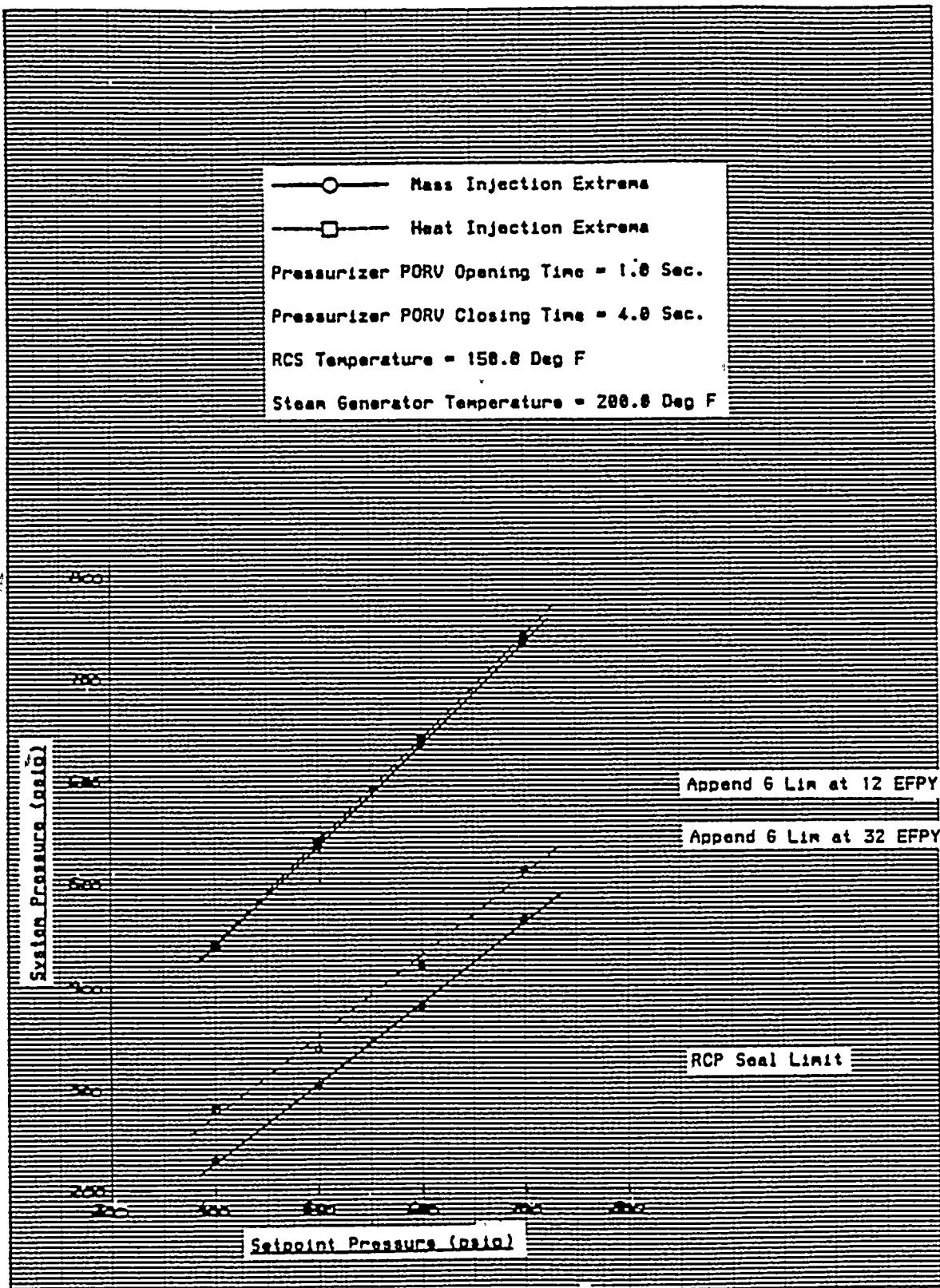


Figure 3.16 RCS Pressure Extrema vs. Setpoint Pressure at PORV
Stroke Open Time of 1.0 Sec. and RCS Temperature of 150°F

100

100

100

100

100

100

100

100

100

100

100

100

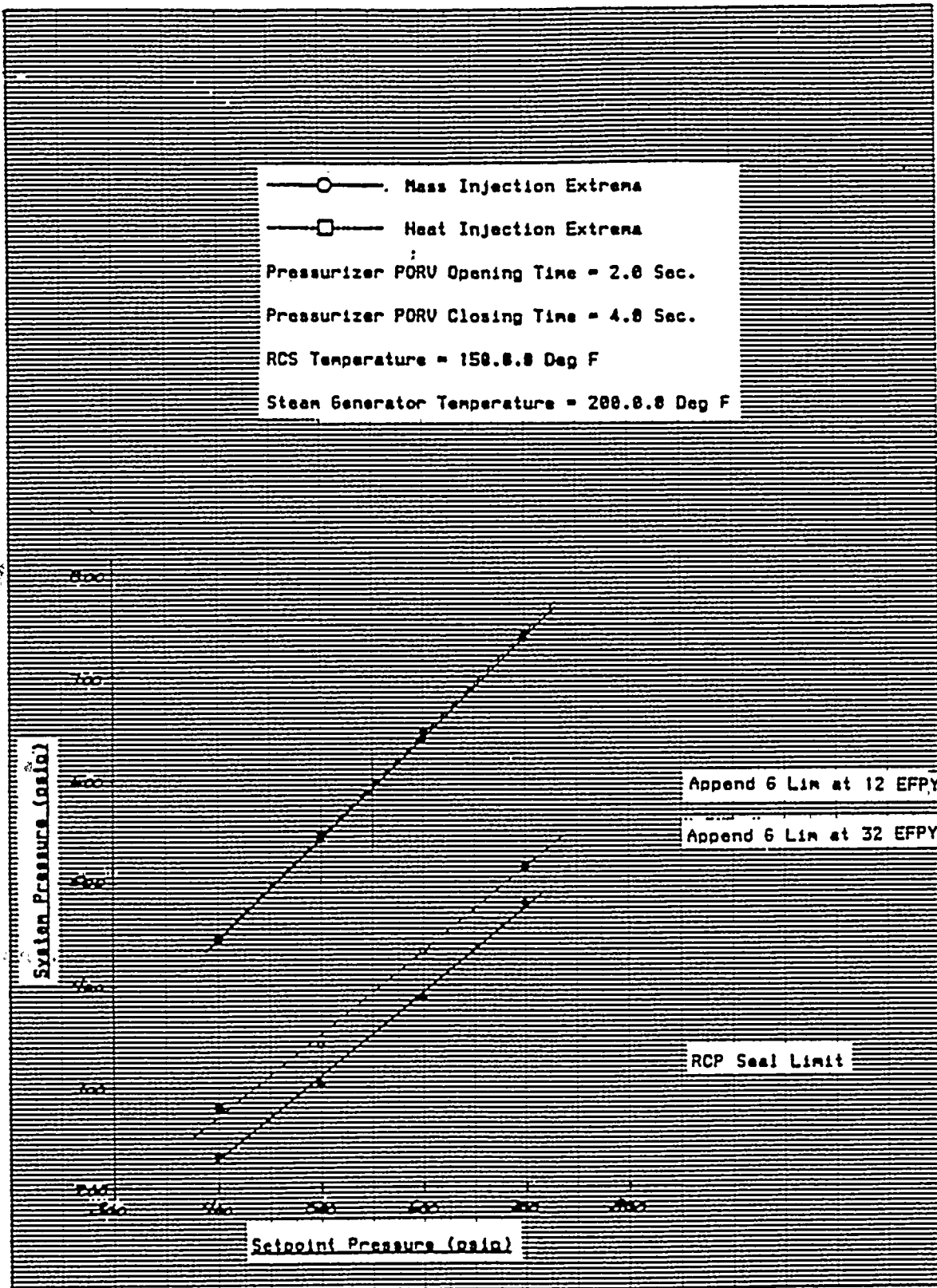


Figure 3.17. RCS Pressure Extrema vs. Setpoint Pressure at PORV
Stroke Open Time of 2.0 Sec. and RCS Temperature of 150°F

100

100

100

100

100

100

100

100

100

100

100

100

100

100

100

100

100

100

100

100

100

100

100

100

100



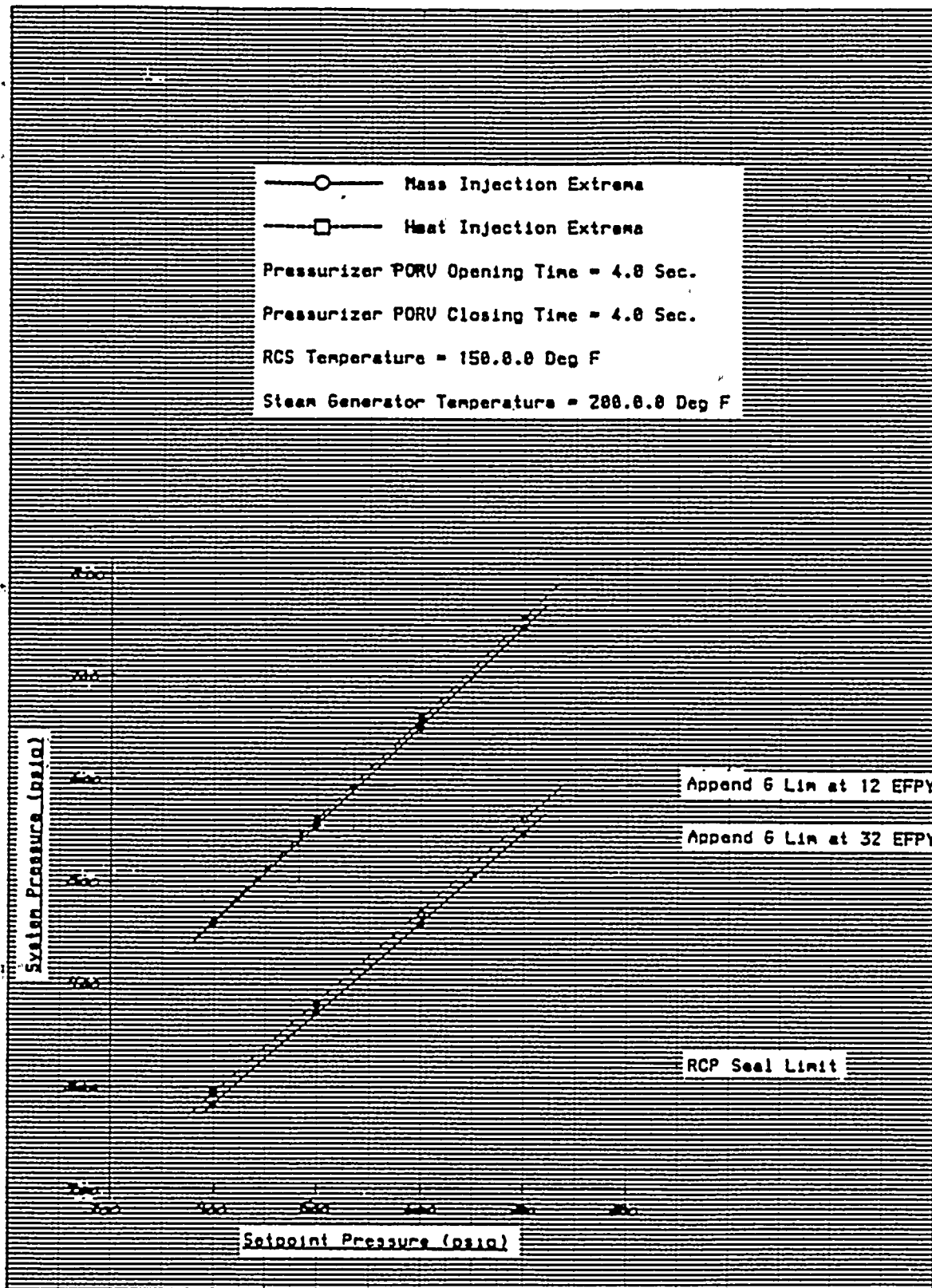


Figure 3.18 RCS Pressure Extrema vs. Setpoint Pressure at PORV Stroke Open Time of 4.0 Sec. and RCS Temperature at 150°F

1
2
3
4
5
6
7
8
9
10
11
12
13
14
15
16
17
18
19
20
21
22
23
24
25
26
27
28
29
30
31
32
33
34
35
36
37
38
39
40
41
42
43
44
45
46
47
48
49
50
51
52
53
54
55
56
57
58
59
60
61
62
63
64
65
66
67
68
69
70
71
72
73
74
75
76
77
78
79
80
81
82
83
84
85
86
87
88
89
90
91
92
93
94
95
96
97
98
99
100

101

102

103

104

105

106

107

108

109

110

111

112

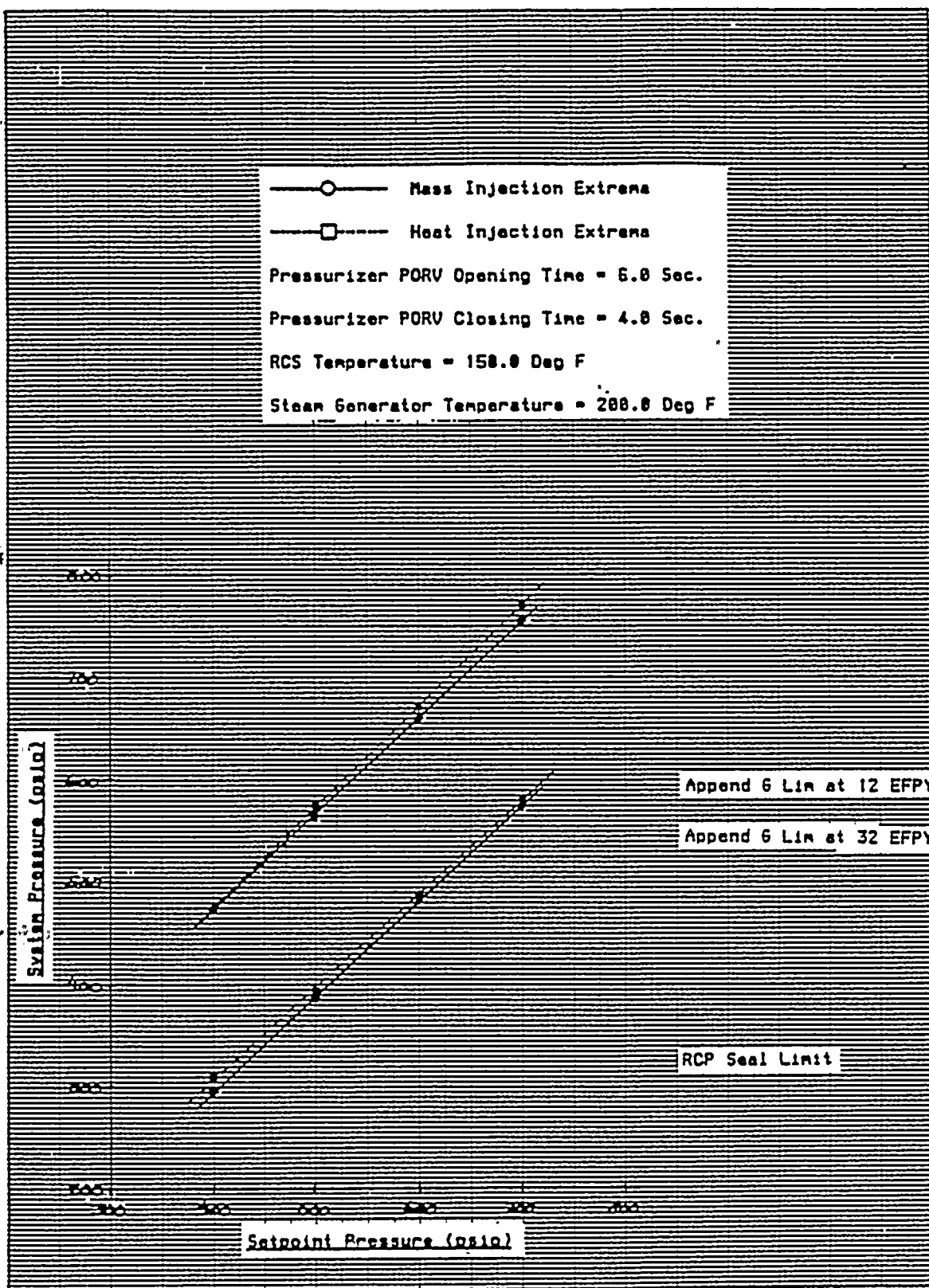


Figure 3.19 RCS Pressure Extrema vs. Setpoint Pressure at PORV
Stroke Open Time of 6.0 Sec. and RCS Temperature of 150°F

100-100000

100-100000

100-100000

100-100000

100-100000

100-100000

100-100000

100-100000

100-100000

100-100000

100-100000

100-100000

100-100000

100-100000

100-100000

100-100000

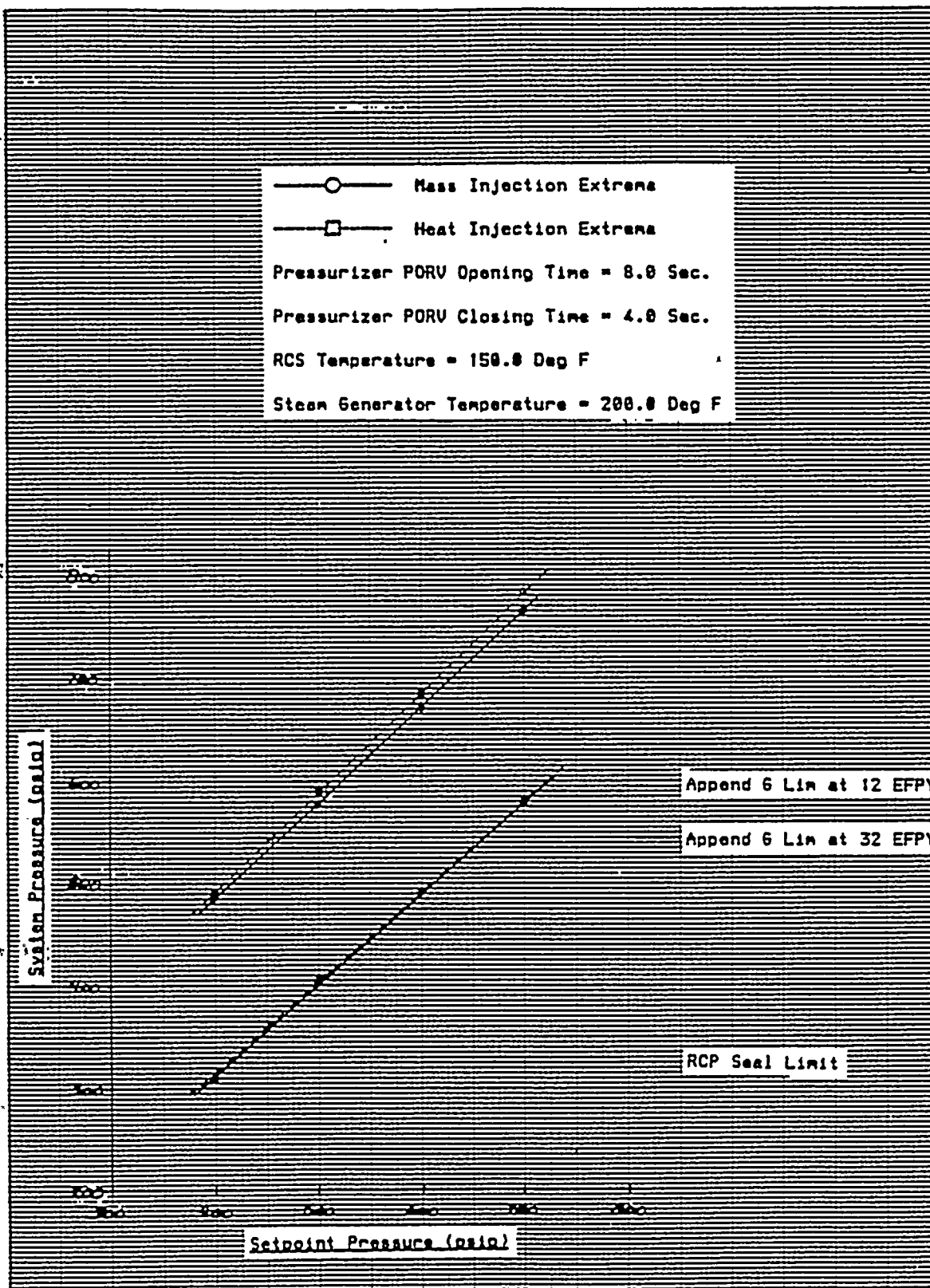


Figure 3.20 RCS Pressure Extrema vs. Setpoint Pressure at PORV
 Stroke Open Time of 8.0 Sec. and RCS Temperature of 150°F



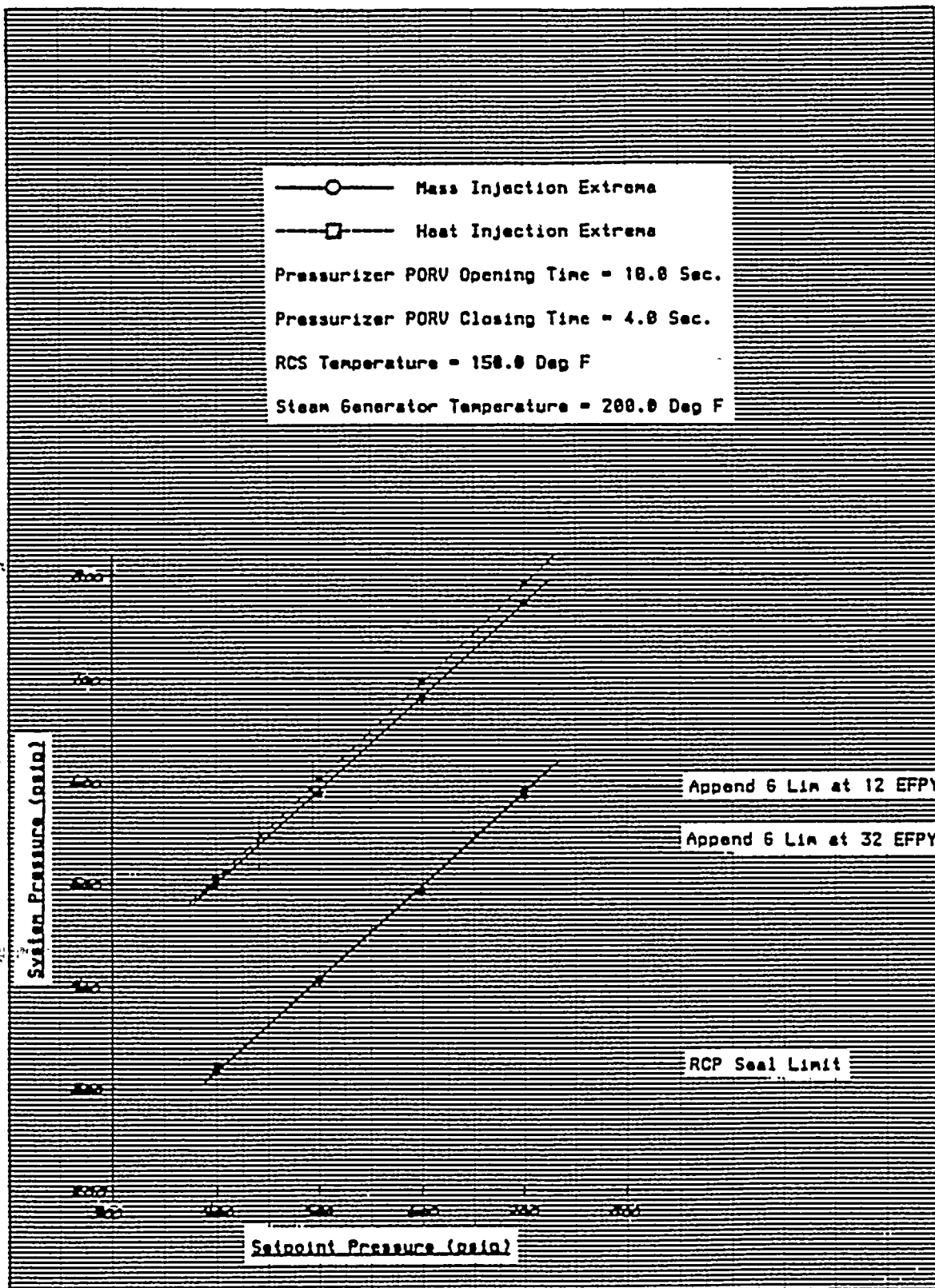


Figure 3.21 RCS Pressure Extrema vs. Setpoint Pressure at PORV
Stroke Open Time of 10.0 Sec. and RCS Temperature of 150°F

● 2014 年 1 月 1 日起

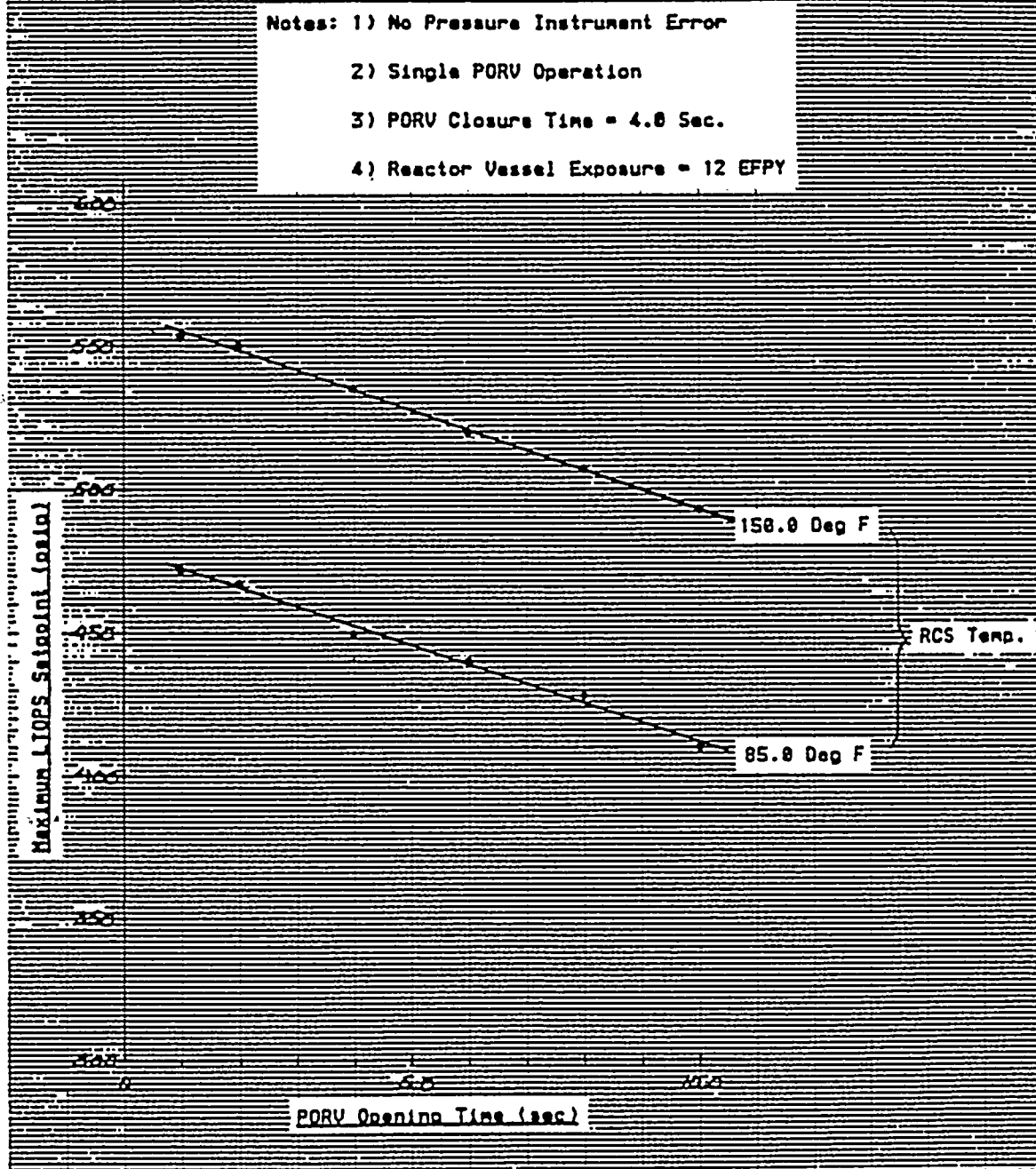


Figure 3.22 PORV LTOP Setpoint at 12 EFPY vs. Valve Opening Time

1. The first part of the document is a list of names and addresses of the members of the committee.

2. The second part of the document is a list of names and addresses of the members of the committee.

3. The third part of the document is a list of names and addresses of the members of the committee.

4. The fourth part of the document is a list of names and addresses of the members of the committee.

5. The fifth part of the document is a list of names and addresses of the members of the committee.

6. The sixth part of the document is a list of names and addresses of the members of the committee.

7. The seventh part of the document is a list of names and addresses of the members of the committee.

8. The eighth part of the document is a list of names and addresses of the members of the committee.

9. The ninth part of the document is a list of names and addresses of the members of the committee.

10. The tenth part of the document is a list of names and addresses of the members of the committee.

11. The eleventh part of the document is a list of names and addresses of the members of the committee.

12. The twelfth part of the document is a list of names and addresses of the members of the committee.

13. The thirteenth part of the document is a list of names and addresses of the members of the committee.

14. The fourteenth part of the document is a list of names and addresses of the members of the committee.

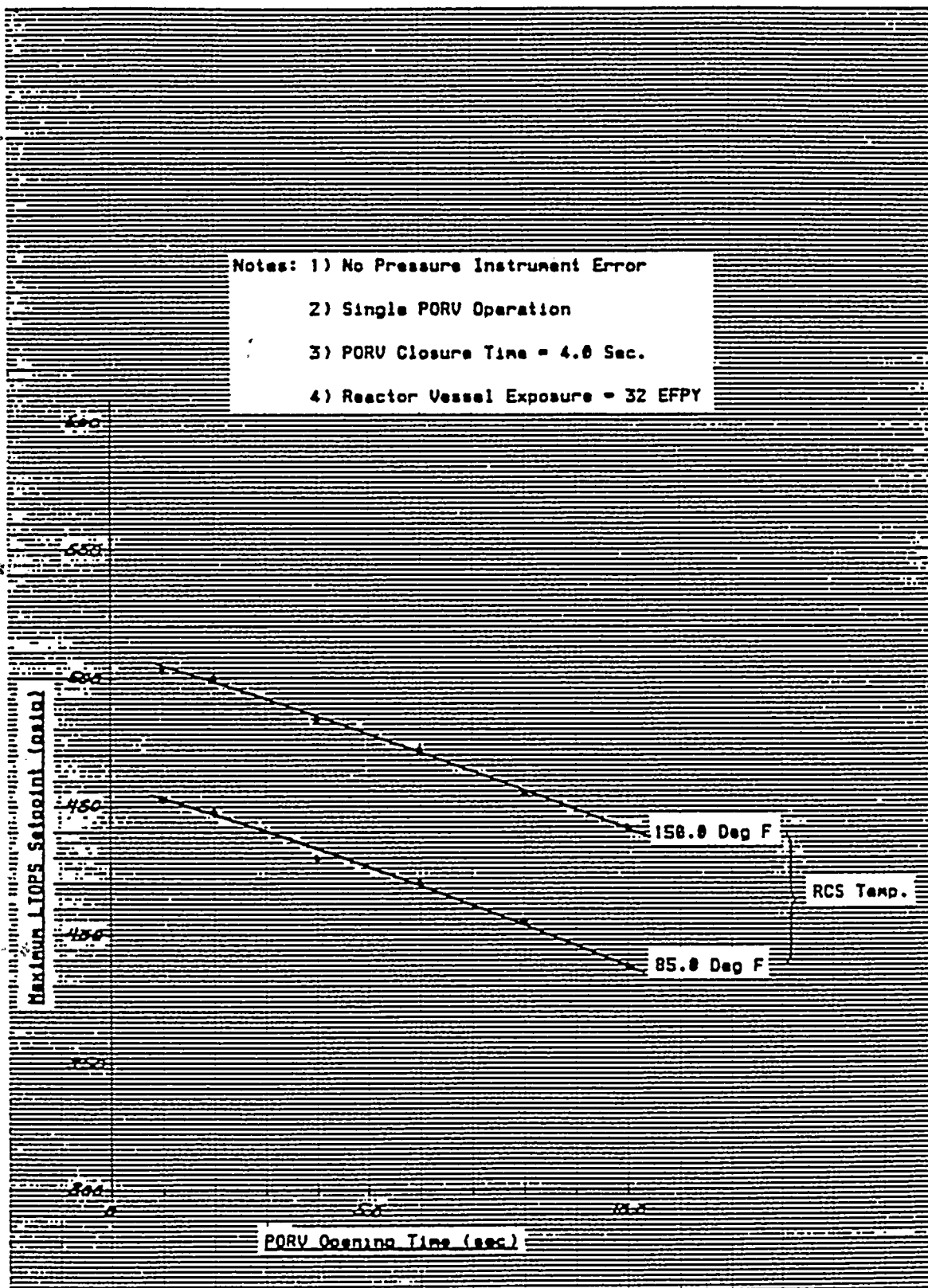


Figure 3.23 PORV LTOP Setpoint at 32 EFY vs. Valve Opening Time



4.0 CORRELATION TO WOG LTOPS SETPOINT METHODOLOGY

As part of the LTOPS setpoint analysis performed for D. C. Cook Unit 2, American Electric Power Corporation requested a correlation that benchmarks the results of the analysis to that of the algorithm described in the report prepared for the Westinghouse Owners Group (acronymed WOG) on Reactor Coolant System Over-pressurization by Westinghouse Electric Corporation. The reason for the request was to provide a means to determine the equivalent LOFTRAN derived setpoints from the execution of a relatively simple algorithm; i.e., the WOG report.

The correlation assumes a mass injection event, only. This is justified on the following bases: 1) the LTOPS at D. C. Cook unit 2 features a setpoint independent of temperature; 2) the most limiting condition is at low temperature, and 3) the mass injection event dominates at low temperatures. Under these conditions, as will be shown, the correlation takes the form of a series of curves of "LOFTRAN" setpoints plotted against pressurizer PORV opening time, with the "WOG" setpoints as a parametric.

4.1 WOG METHODOLOGY LTOPS SETPOINTS

The WOG methodology, for mass injection events, determines the resulting over-pressure from a 4-factor formula; the derivation, of which, is provided in the WOG report referenced in the introduction to this report:

$$\Delta P = \Delta P(\text{Ref}) * F(v) * F(s) * F(z)$$

The factors comprising the formula are determined from a series of linear relationships with known (or assumed) plant parameters. For convenience, these relationships are reproduced here from WOG report, and are shown as Figures 4.1 through 4.4. For the parameter study performed here, it is convenient to express these figures analytically:

$$\Delta P(\text{Ref}) = \frac{82}{60} * (\text{Mass Injection Rate, lbm/sec})$$

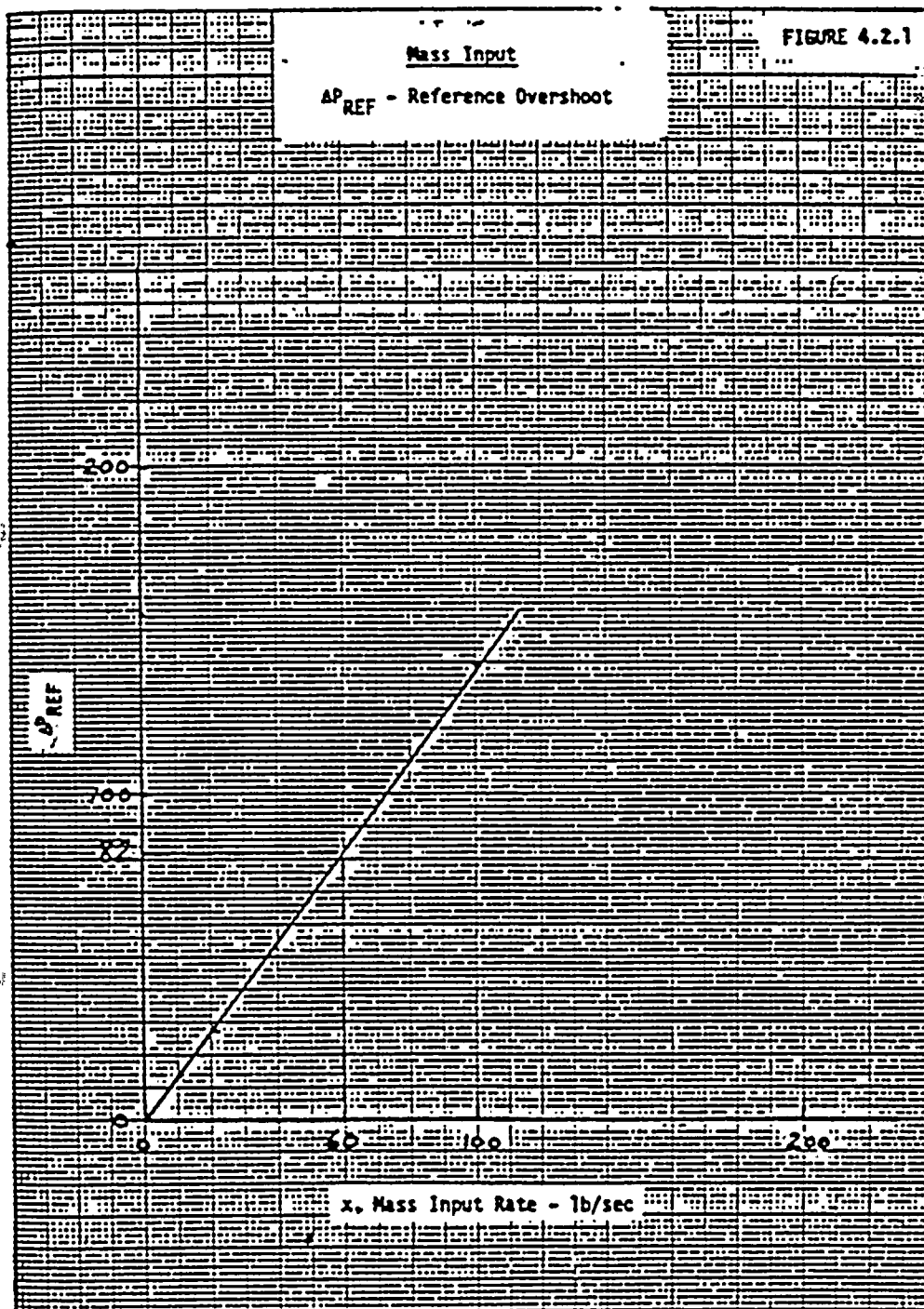


Figure 4.1 Delta P (Ref) vs. Mass Injection Rate

1

2

3

4

5

6

7

8

9

10

11

12

13

14

15

16

17

18

19

20

21

22

23

24

25

26

27

28

29

THE UNITED STATES OF AMERICA

DO hereby certify that

the within and foregoing is a true and correct copy

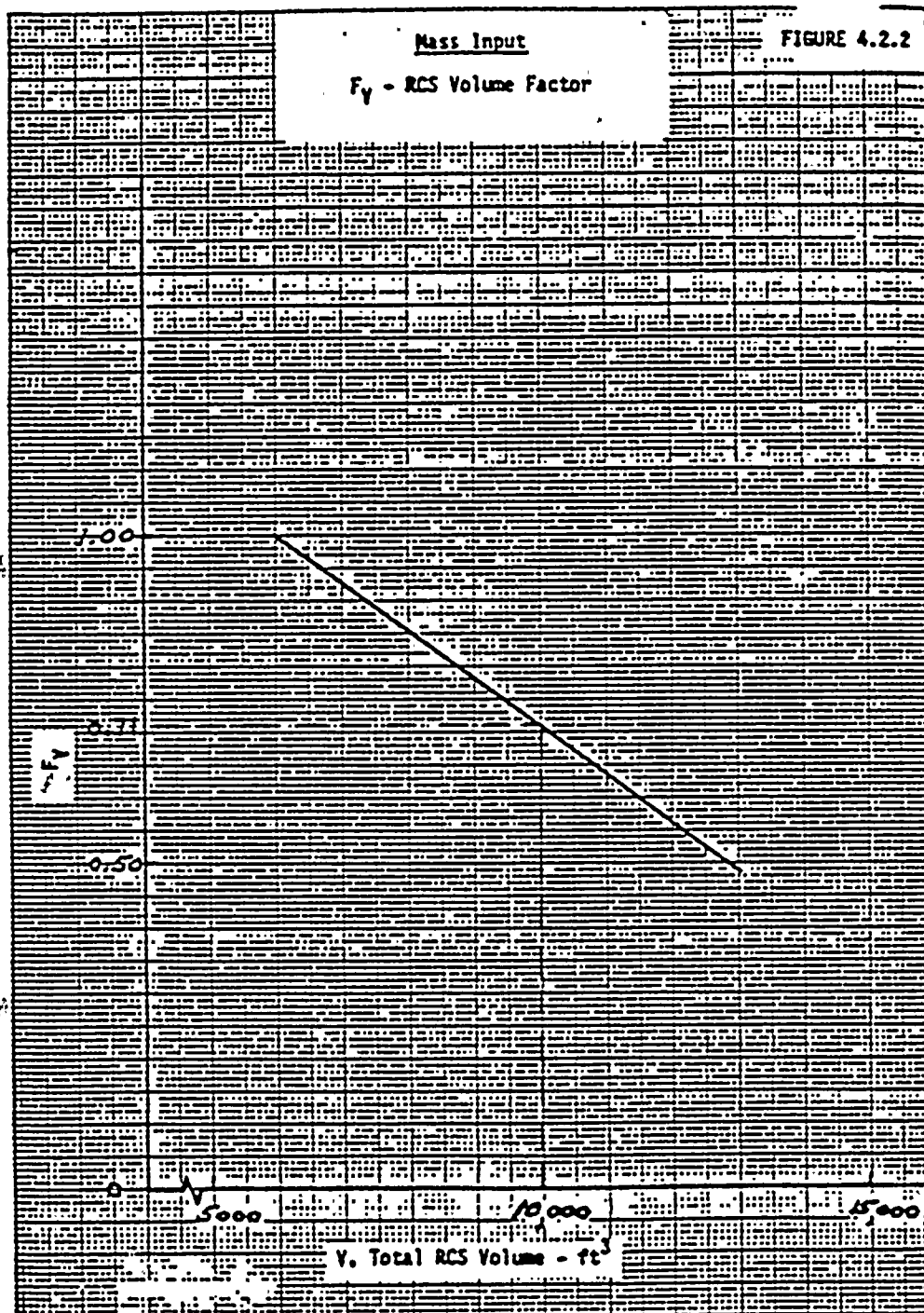


Figure 4.2 Volume Factor, $F(v)$, vs. RCS Total Volume



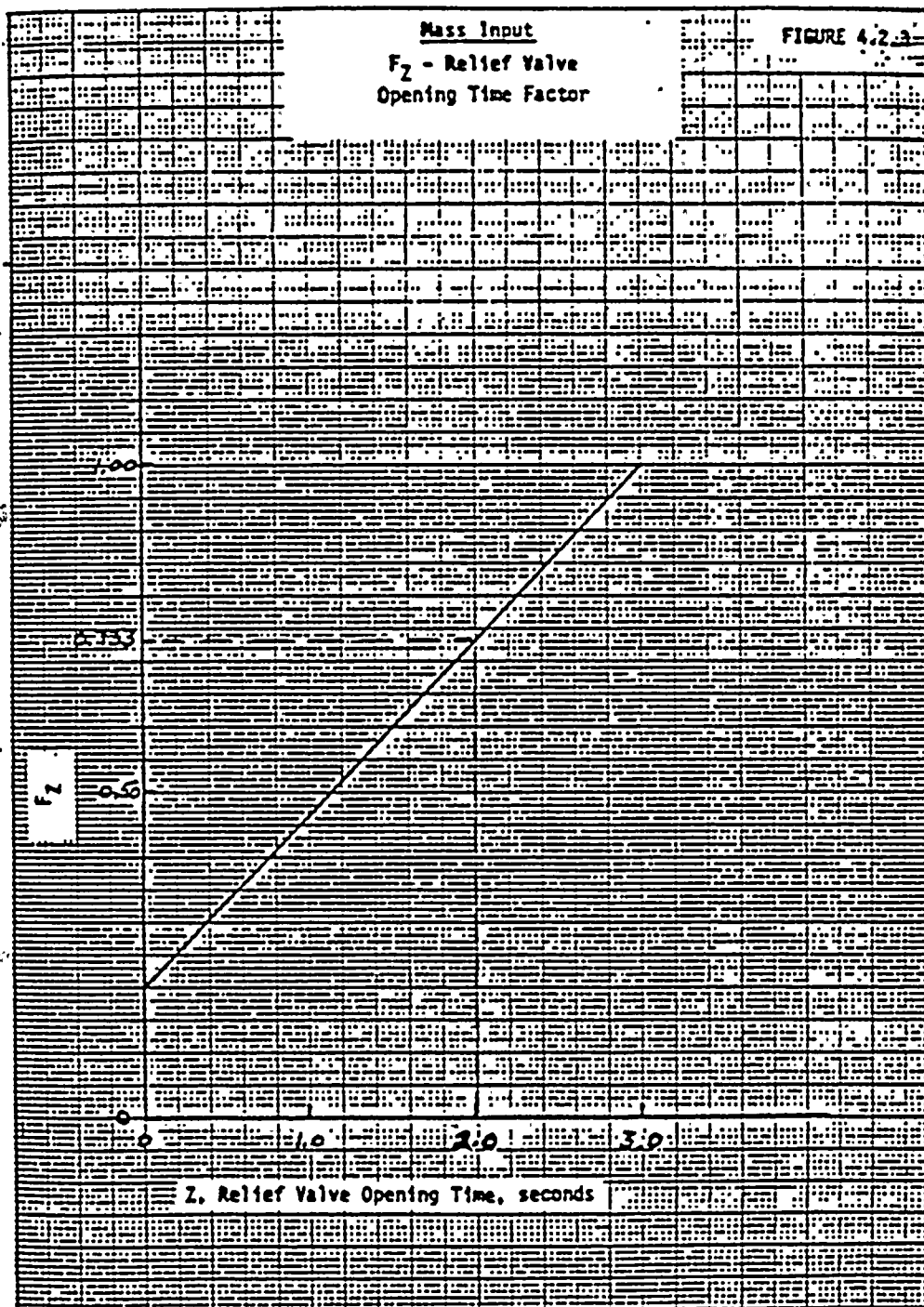


Figure 4.3 PORV Opening Time Factor, $F(z)$, vs. Valve Opening Time

7.

8

→

4

—

100

1

•

45

52

9

•

歌

2

2

●



1

1. The first group of people who are interested in the results of the study are the researchers themselves. They want to know how well the study was conducted and whether the results are reliable and valid. They also want to know how the study was funded and whether there were any conflicts of interest.

Hauls	1. Yellow perch (%)	2. Rock bass (%)	3. Striped bass (%)	4. White perch (%)
1	10	10	10	10
2	40	20	20	20
3	70	40	30	30
4	90	60	40	35
5	95	70	50	38
6	98	75	55	40
7	100	78	58	40
8	100	80	60	40
9	100	80	60	40
10	100	80	60	40

2010年12月10日

100

• • •

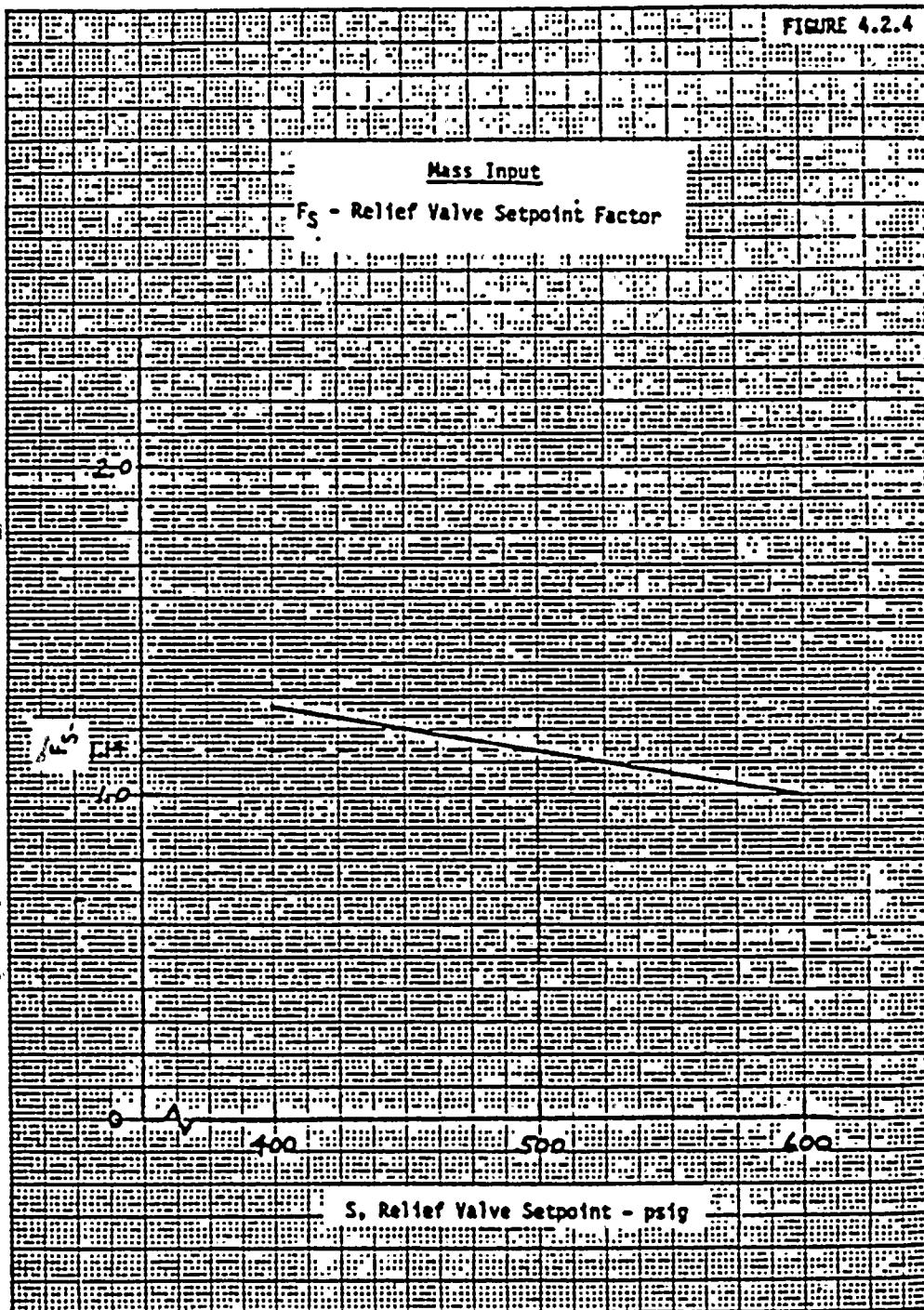


Figure 4.4 LTOPS Setpoint Factor, $F(s)$, vs. LTOPS Setpoint

11

12

13

14

15

16

17

18

19

20

21

22

23

24

25

26

$$F(v) = 1.435 - (0.725E-4) * (\text{RCS Volume, cu.ft.})$$

$$= 0.53 \text{ for Cook unit 2. (Cook unit 2 cold RCS volume} = 12509.2 \text{ cu.ft.)}$$

$$F(s) = 1.810 - (0.00135) * (\text{PORV Setpoint, psig})$$

$$F(z) = 0.200 + (0.267) * (\text{PORV Opening Time, sec.})$$

The overpressures resulting from the application of these factors are documented in tabular form below and through page 4.9, for the several PORV opening times selected for the analysis. A summary of the overpressures is given on page 4.9.

Mass Injection Overpressures at PORV Opening Time = 1.0 sec.

	<u>LTOPS Setpoint (psig)</u>			
	<u>400</u>	<u>500</u>	<u>600</u>	<u>700</u>
Inj. Mass (ref Table 3.3)				
(gpm)	439.2	429.7	420.2	410.7
(lbm/sec.)	60.96	59.64	58.32	57.01
Delta P(Ref)	83.31	81.51	79.70	77.91
F(v)	0.53	0.53	0.53	0.53
F(s)	1.270	1.135	1.000	0.865
F(z)	0.467	0.467	0.467	0.467
Delta P (psig)	26.20	22.90	19.70	16.70
Overpressure (psig)	426.2	522.9	619.7	716.7

422

1

2

3

4

5

6

7

8

9

10

11

12

13

14

15

16

17

18

19

20

21

22

23

24

25

26

27

28

29

30

31

32

33

34

35

36

37

38

39

40

Mass Injection Overpressures at PORV Opening Time = 2.0 sec.

	<u>LTOPS Setpoint (psig)</u>			
	<u>400</u>	<u>500</u>	<u>600</u>	<u>700</u>
Inj. Mass (ref Table 3.3)				
(gpm)	439.2	429.7	420.2	410.7
(lbm/sec.)	60.96	59.64	58.32	57.01
Delta P(Ref)	83.31	81.51	79.70	77.91
F(v)	0.53	0.53	0.53	0.53
F(s)	1.270	1.135	1.000	0.865
F(z)	0.734	0.734	0.734	0.734
Delta P (psig)	41.20	36.00	31.00	26.20
Overpressure (psig)	441.2	536.0	631.0	726.2

Mass Injection Overpressures at PORV Opening Time = 4.0 sec.

	<u>LTOPS Setpoint (psig)</u>			
	<u>400</u>	<u>500</u>	<u>600</u>	<u>700</u>
Inj. Mass (ref Table 3.3)				
(gpm)	439.2	429.7	420.2	410.7
(lbm/sec.)	60.96	59.64	58.32	57.01
Delta P(Ref)	83.31	81.51	79.70	77.91
F(v)	0.53	0.53	0.53	0.53
F(s)	1.270	1.135	1.000	0.865
F(z)	1.268	1.268	1.268	1.268
Delta P (psig)	71.10	62.20	53.60	45.30
Overpressure (psig)	471.1	562.2	653.6	745.3

1

2

3

4

5

6

7

8

9

10

11

12

13

14

15

16

17

18

19

20

21

22

23

24

25

26

27

28

29

30

31

32

33

34

35

36

37

38

39

40

41

42

43

44

45

46

47

48

49

50

51

52

53

54

55

56

57

58

59

60

61

62

63

64

65

66

67

68

69

70

71

72

73

74

75

76

77

78

79

80

81

82

83

84

85

86

87

88

89

90

91

92

93

94

95

96

97

98

99

100

101

102

103

104

105

106

107

108

109

110

111

112

113

114

115

116

117

118

119

120

121

122

123

124

125

126

127

128

129

130

131

132

133

134

135

136

137

138

139

140

141

142

143

144

145

146

147

148

149

150

151

152

153

154

155

156

157

158

159

160

Mass Injection Overpressures at PORV Opening Time = 6.0 sec.

	<u>LTOPS Setpoint (psig)</u>			
	<u>400</u>	<u>500</u>	<u>600</u>	<u>700</u>
Inj. Mass (ref Table 3.3)				
(gpm)	439.2	429.7	420.2	410.7
(lbm/sec.)	60.96	59.64	58.32	57.01
Delta P(Ref)	83.31	81.51	79.70	77.91
F(v)	0.53	0.53	0.53	0.53
F(s)	1.270	1.135	1.000	0.865
F(z)	1.802	1.802	1.802	1.802
Delta P (psig)	101.0	88.40	76.10	64.40
Overpressure (psig).	501.0	588.4	676.1	764.4

Mass Injection Overpressures at PORV Opening Time = 8.0 sec.

	<u>LTOPS Setpoint (psig)</u>			
	<u>400</u>	<u>500</u>	<u>600</u>	<u>700</u>
Inj. Mass (ref Table 3.3)				
(gpm)	439.2	429.7	420.2	410.7
(lbm/sec.)	60.96	59.64	58.32	57.01
Delta P(Ref)	83.31	81.51	79.70	77.91
F(v)	0.53	0.53	0.53	0.53
F(s)	1.270	1.135	1.000	0.865
F(z)	2.336	2.336	2.336	2.336
Delta P (psig)	131.0	114.5	98.70	83.40
Overpressure (psig).	531.0	614.5	698.7	783.4

1

2

3

4

5

6

7

8

9

10

11

12

13

14

15

16

17

18

19

20

21

22

23

24

25

26

27

28

29

30

31

32

33

Mass Injection Overpressures at PORV Opening Time = 10.0 sec.

	<u>LTOPS Setpoint (psig)</u>			
	<u>400</u>	<u>500</u>	<u>600</u>	<u>700</u>
Inj. Mass (ref Table 3.3)				
(gpm)	439.2	429.7	420.2	410.7
(lbm/sec.)	60.96	59.64	58.32	57.01
Delta P(Ref)	83.31	81.51	79.70	77.91
F(v)	0.53	0.53	0.53	0.53
F(s)	1.270	1.135	1.000	0.865
F(z)	2.870	2.870	2.870	2.870
Delta P (psig)	160.9	140.7	121.2	102.5
Overpressure (psig).	560.9	640.7	721.2	802.5

RCS Overpressure Summary

<u>PORV Opening Time (sec)</u>	<u>LTOPS Setpoint (psig)</u>			
	<u>400</u>	<u>500</u>	<u>600</u>	<u>700</u>
1.0	426.2	522.9	619.7	716.7
2.0	441.2	536.0	631.0	726.2
4.0	471.1	562.2	653.6	745.3
6.0	501.0	588.4	676.1	764.4
8.0	531.0	614.5	698.7	783.4
10.0	560.9	640.7	721.2	805.5

1000

1000

1000

1000

1000

1000

1000

1000

1000

The summary is shown in Figure 4.5, illustrating the high degree of linearity of the peak system pressure as a function of setpoint pressure. The peak system pressure, resulting from implementation of the WOG methodology, can therefor be expressed as a linear function of setpoint pressure:

$$1) \text{ Peak System Press} = A + B*(P_{sp}^{WOG})$$

and the peak system pressure must be less than the Appendix G limit. The coefficients of the equation have been determined by performing a least-squares fit on the peak pressures (from the above table) as a function of setpoint pressure:

PORV Opening Time (sec)	Coefficients	
	A	B
1.0	38.81	0.9683
2.0	61.10	0.9500
4.0	105.35	0.9140
6.0	149.63	0.8779
8.0	194.13	0.8414
10.0	234.21	0.8143

4.2 LOFTRAN/WOG Correlation

The system overpressures determined from the LOFTRAN based analysis are also quite linear (reference Figures 3.10 through 3.15), and can be expressed as linear functions of setpoint pressure for each of the PORV opening times:

$$2) \text{ Peak System Press} = C + D*(P_{sp}^{LOFT})$$



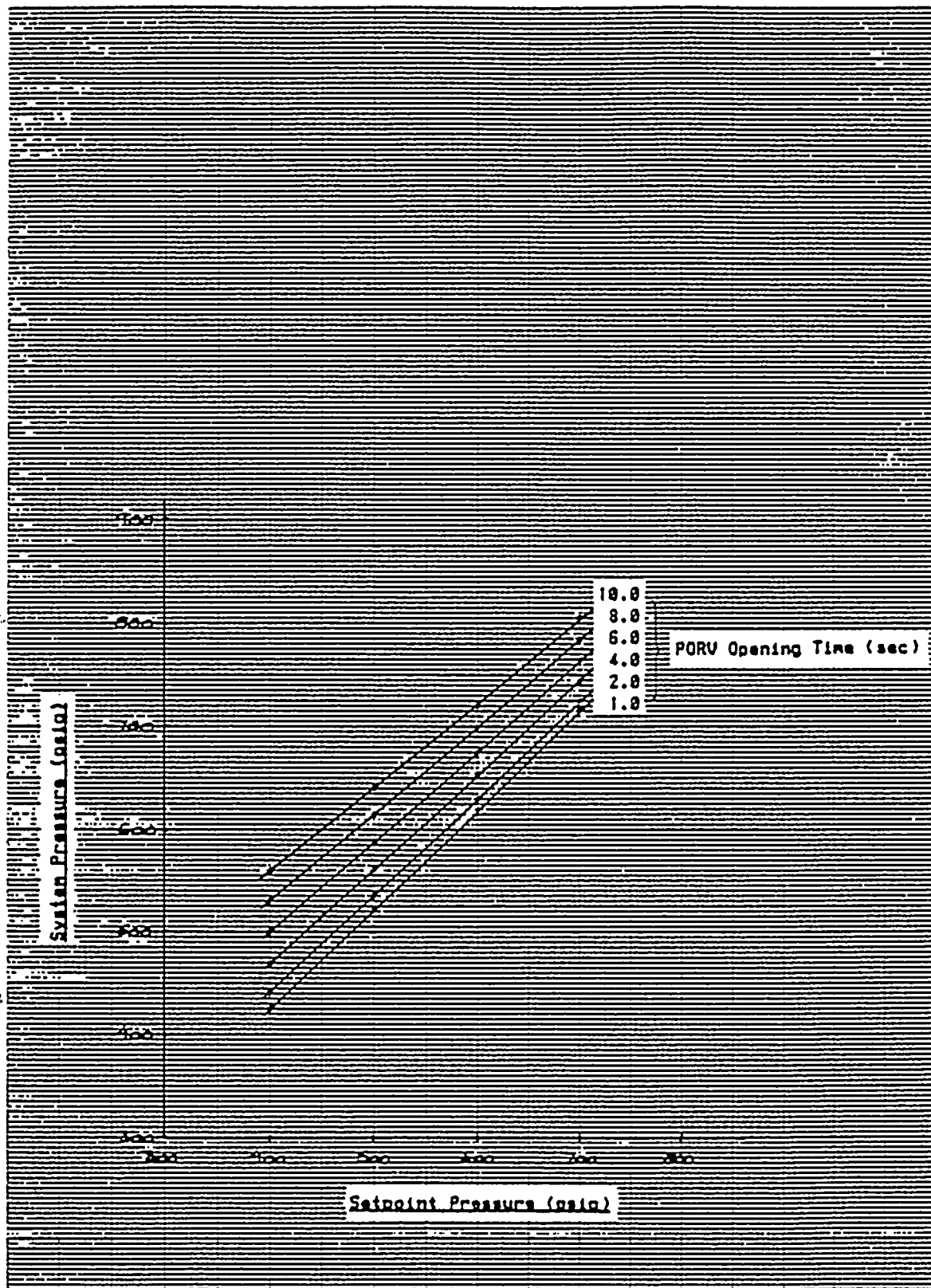


Figure 4.5 Maximum RCS Overpressure Based on "WOG" Methodology vs. LTOPS Setpoint Pressure

100

100

100

100

100

100

100

100

100



with the peak system pressures required to be less than the Appendix G limit. A least-squares fit of the data in Table 3.4 results in the following coefficients:

PORV Opening Time (sec)	Coefficients	
	C	D
1.0	47.80	0.9790
2.0	55.50	0.9750
4.0	76.90	0.9570
6.0	96.50	0.9400
8.0	115.40	0.9270
10.0	132.00	0.9150

The peak system pressure determined by either the WOG algorithm or the LOFTRAN based analyses must be less than the Appendix G limit. Therefore, at the limit, the overpressure determined from equation 1 must be equal to the overpressure determined from equation 2:

$$C + D(P_{sp}^{LOFT}) = A + B(P_{sp}^{WOG})$$

$$\text{or } P_{sp}^{LOFT} = \frac{A - C}{D} + \frac{B}{D} (P_{sp}^{WOG})$$

20

21

22

23

24

25

26

27

28

29

30

31

32

33

34

35

36

37

38

39

40

41

42

43

44

45

46

47

48

49

50

51

52

53

54

55

56

57

58

59

60

61

62

63

64

65

66

67

68

69

70

71

72

73

74

75

76

77

78

79

80

81

82

83

84

85

86

87

88

89

90

91

92

93

94

95

96

97

98

99

100

101

102

103

104

105

106

107

108

109

110

111

112

113

114

115

116

117

118

119

120

121

122

123

124

125

126

127

128

129

130

131

132

133

134

135

136

137

138

139

140

141

142

143

144

145

146

147

148

149

150

151

152

153

154

155

156

157

158

159

160

161

162

163

164

165

166

167

168

169

170

171

172

173

174

175

176

177

178

179

180

181

182

183

184

185

186

187

188

189

190

191

192

193

194

195

196

197

198

199

200

201

202

203

204

205

206

207

208

209

210

211

212

213

214

215

216

217

218

219

220

221

222

223

224

225

226

227

228

229

230

231

232

233

234

235

236

237

238

239

240

241

242

243

244

245

246

247

248

249

250

251

252

253

254

255

256

257

258

259

260

261

262

263

264

265

266

267

268

269

270

271

272

273

274

275

276

277

278

279

280

281

282

283

284

285

286

287

288

289

290

291

292

293

294

295

296

297

298

299

300

301

302

303

304

305

306

307

308

309

310

311

312

313

314

315

316

317

318

319

320

321

322

323

324

325

326

327

328

329

330

331

332

333

334

335

336

337

338

339

340

341

342

343

344

345

346

347

348

349

The coefficients resulting from the combined equations (1) and (2) are as follows:

PORV Opening Time (sec)	Coefficients	
	$\frac{A - C}{D}$	$\frac{B}{D}$
1.0	-9.18	0.9891
2.0	5.74	0.9744
4.0	29.73	0.9551
6.0	56.52	0.9339
8.0	84.93	0.9077
10.0	111.70	0.8899

Using the above table of coefficients, the LOFTRAN equivalent LTOPS setpoints corresponding to a series of selected WOG setpoints is tabulated below:

Summary of LOFTRAN Equivalent LTOPS Setpoints (psig)

PORV Opening Time (sec)	LTOPS Setpoint (psig) Based on WOG Algorithm					
	<u>300</u>	<u>400</u>	<u>500</u>	<u>600</u>	<u>700</u>	<u>800</u>
1.0	287.6	386.5	485.4	584.3	683.2	782.1
2.0	298.1	395.5	492.9	590.4	687.8	785.3
4.0	316.3	411.8	507.3	602.8	698.3	793.8
6.0	336.7	430.1	523.5	616.9	710.3	803.6
8.0	357.2	448.0	538.8	629.6	720.3	811.1
10.0	378.7	467.7	556.7	645.6	734.6	823.6

100-100000

100-100000

1

100-100000

1

100-100000

100-100000

100-100000

1

100-100000

100-100000

100-100000

100-100000

100-100000

100-100000

100-100000

100-100000

100-100000

100-100000

100-100000

100-100000

100-100000

100-100000

100-100000

100-100000



The tabulation is shown graphically in Figure 4.6, and plots the LOFTRAN derived LTOPS setpoint as a function of PORV opening time; parametric with the WOG LTOPS setpoint. This figure is used to translate the LTOPS setpoint derived from application of the WOG methodology to the LOFTRAN equivalent value.

Utilization of the figure requires that the LTOPS setpoint first be determined using the WOG methodology. At the PORV opening time corresponding to that selected for the WOG calculation, determine the LOFTRAN analysis setpoint from the ordinate by linearly interpolating between the two curves bounding the WOG setpoint.

4.3 IMPACT OF STEAM GENERATOR TUBE PLUGGING

Both the LOFTRAN and the WOG based analyses were performed assuming no tubes plugged in the steam generators. The impact of tube plugging is a small reduction in RCS volume; the consequence, of which, is slightly higher overpressures as a result of mass injection events, and reduced overpressures from heat input events. The heat input events are reduced in importance because of the reduction in heat transfer surface area of the steam generators.

The importance of tube plugging with respect to its impact on LTOPS setpoints is accounted for by the $F(v)$ term in the WOG methodology (reference Figure 4.2), and is directly translatable to the LOFTRAN based analysis through the correlation developed in this chapter. As a worst case example, reducing the number of steam generator tubes by 15% over all four steam generators, results in a reduction in RCS cold volume of 492.6 cu.ft. (based on an average tube length of 69.77 ft., a tube O.D. of 0.875 inches, and a wall thickness of 0.050 inches). This represents a fractional reduction in initial RCS volume of a bit less than 4% (i.e., 0.0394). The impact on overpressure can be determined from the $F(v)$ equation in section 4.1. Without tube plugging (RCS volume = 12509.2 cu.ft.), $F(v) = 0.53$. With 15% of the tubes plugged (RCS volume = 12016.6 cu.ft.), $F(v)$ increases to 0.56. This represents an increase in the delta overpressure of 1.068, almost a 7% increase.

100-100000

100-100000

100-100000

100-100000

100-100000

100-100000

100-100000

100-100000

100-100000

100-100000

100-100000

100-100000



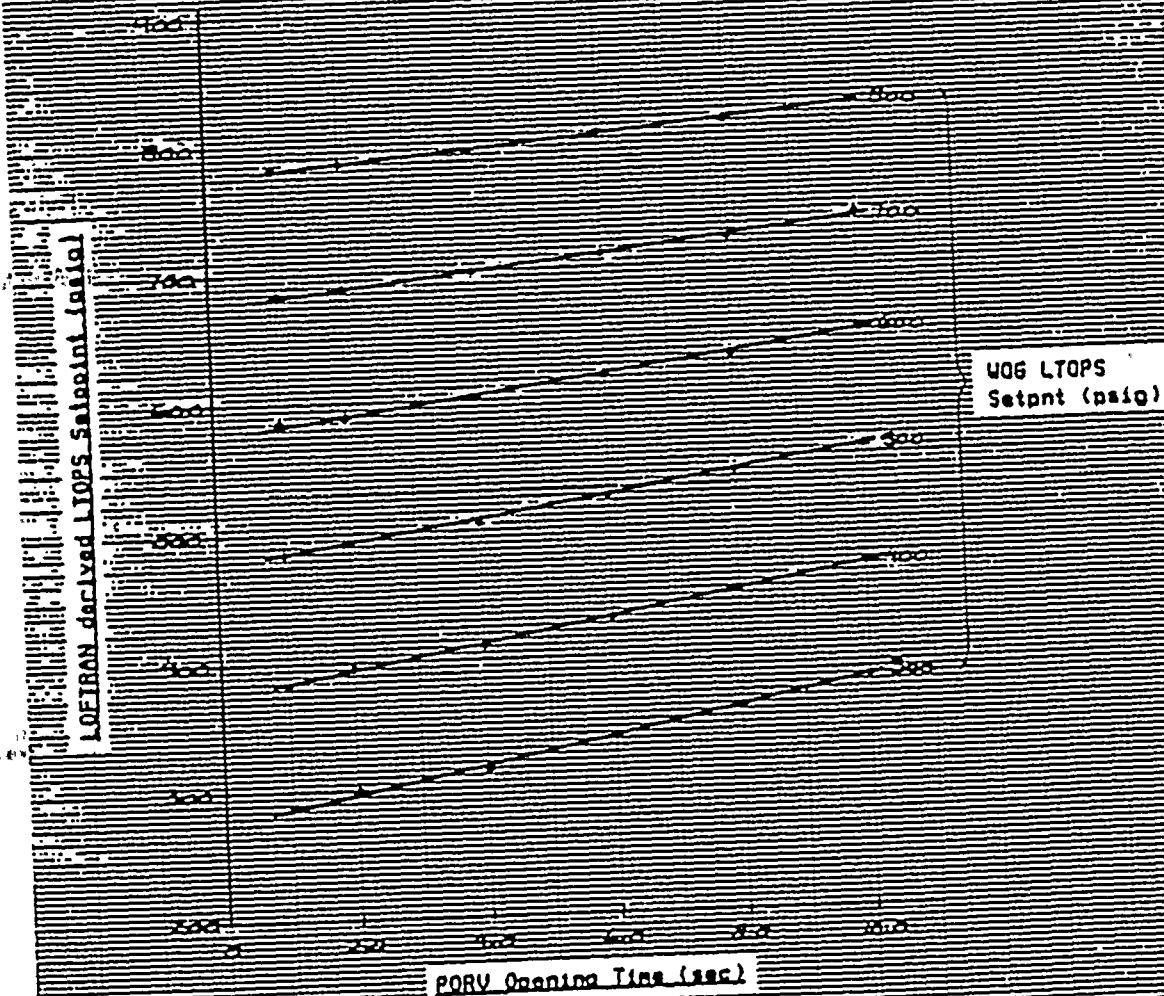


Figure 4.6 LOFTRAN/WOG Setpoint Correlation vs. PORV Opening Time

100-100000

100-100000

100-100000

100-100000

100-100000

100-100000

100-100000

100-100000

100-100000

100-100000

100-100000

100-100000

100-100000

100-100000

100-100000

100-100000

100-100000

100-100000

SECTION 4

OPERATING INSTRUCTIONS

DATA AND TROUBLE-SHOOTING

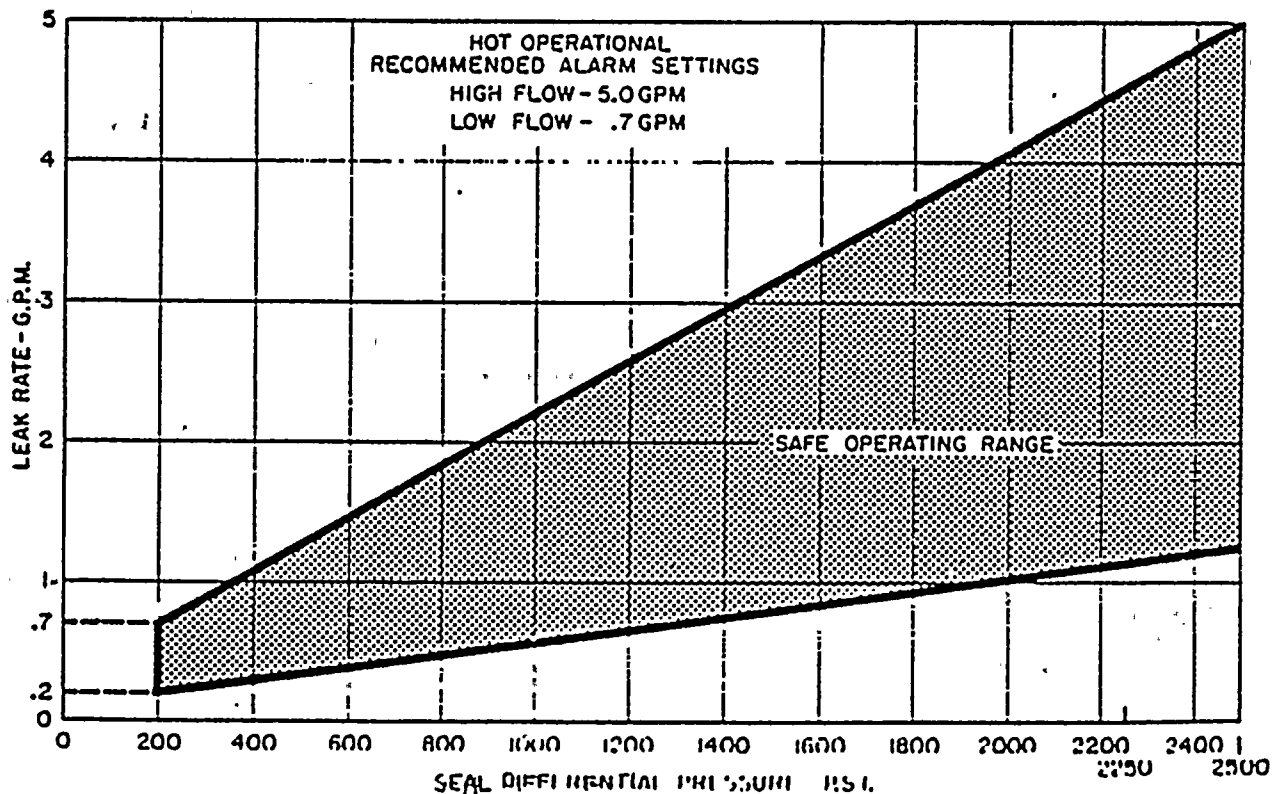
From Westinghouse
Instruction and Operating Book
(PP-045)

4.1 NORMAL, MINIMUM, AND MAXIMUM OPERATING VALUES

4.1.1 Pump

1. No. 1 Seal

ITEM	UNIT	NORMAL	MINIMUM	MAXIMUM	NOTES*
Flow	gpm	See Figure 4-0	0.2	5.0	1, 2, 3
Temperature	degrees F	100 - 190	60	235	4
Pressure	psig	2250	325	2485	5
ΔP	psi	2217	200	2470	---



93A00028-1

FIGURE 4-0 No. 1 Seal Performance Parameters

4-1
Rev. 1

*Notes

1. During heatup or cooldown, when the system water pressure is 1000 psig or below, leak-off flow may be insufficient to cool the bearing and seal components. When the leak-off flow is below 1 gpm, the seal bypass valve should be opened. This permits a limited flow to bypass the No. 1 seal through a non-adjustable orifice block (external to the pump itself).
2. If the leak-off flow is less than 0.2 gpm, it is probable that minor foreign matter is restricting the flow at the seal face inlet. The seal faces act like a filter. Foreign particles in the order of 25 - 40 microns can collect between the faces and restrict the flow. Increasing the seal differential pressure (ΔP) may clear the seal. If it does not, decrease the seal differential pressure to 100 psi and turn the pump rotor by hand. Do not start the pump motor if the seal flow is below the specified minimum.
3. If a slow increase in the No. 1 seal leak-off flow is observed, i.e. over a period of several weeks or more, Westinghouse should be notified to provide guidance. During this period the pump may be operated and the No. 1 seal leak-off valve should be left open. The seal leak-off flow should not be permitted to exceed the limits of the safe operating range of Figure 4-0. If these conditions do not exist, the procedures for emergency operation shown under the No. 2 seal should be followed.
4. This temperature is measured by a thermocouple at the outlet of the No. 1 seal. The maximum value shown should not be exceeded either in normal service or during a loss-of-injection condition.
5. The minimum loop pressure (325 psig) applies only during the filling and venting operation. The minimum loop pressure for subsequent operations is controlled by the minimum ΔP across the No. 1 seal (200 psi).

2. No. 2 Seal

ITEM	UNIT	NORMAL	MINIMUM	MAXIMUM	NOTES*
Flow	gph	3	Negligible	5	1
Temperature	degrees F	N/A	N/A	N/A	2
Inlet Pressure	psi	33	15	75	-
ΔP	psi	30	11	73	3
Flow	gpm	8	4	12	4
Temperature	degrees F	N/A	N/A	N/A	2
ΔP	psi	2235	N/A	N/A	4

*Notes

Normal operation - No. 1 seal operative.

2. The No. 2 seal temperature will vary with the No. 1 seal temperature and is not considered informative.

10

11

12

13

14

15

16

17

18

19

20

21

22

23

24

25

26

27

28

29

30

31

32

33

34

35

36

37

38

39

40

41

42

43

3. Established by prevailing system conditions.

4. Emergency operation - No. 1 seal inoperative, with a primary pressure drop occurring across the No. 2 seal. The following action should be taken:

- a. Close the No. 1 leak-off valve within five minutes.
- b. Prepare for pump shutdown. The pump may be operated for a period not to exceed an additional 30 minutes. During this period, the reactor power should be ramped down to the N-1 allowable power level, where N is the number of operating RC pumps.
- c. Secure the pump.
- d. Do not restart the pump until the cause of the seal malfunction has been determined.

3. No. 3 Seal

ITEM	UNIT	NORMAL	MINIMUM	MAXIMUM	NOTES*
Flow	cc/hr	100	Negligible	200	1
Temperature	degrees F	N/A	N/A	N/A	2
ΔP	psi	3	2	4	3
Flow	gph	2	N/A	N/A	4
Temperature	degrees F	N/A	N/A	N/A	2
ΔP	psi	15	N/A	N/A	4

*Notes

1. Normal operation - No. 1 seal operative.
2. The No. 3 seal temperatures are not considered informative.
3. The seal differential pressure is established by the head tank.
4. Emergency operation - No. 1 seal inoperative, with a primary pressure drop occurring across the No. 2 seal. Refer to note 4 of paragraph 4.1.1.1.

4. Injection Water

ITEM	UNIT	NORMAL	MINIMUM	MAXIMUM	NOTES*
Flow	gpm	8	6	12	1
Temperature	degrees F	130	60	150	2
Pressure	psig	N/A	N/A	N/A	3

1

2

3

4

5

6

7

8

9

10

11

12

13

14

15

16

17

18

19

20

21

22

23

24

25

26

27

28

29

30

31

32

33

34

35

36

37

THE FOLLOWING IS A LIST OF THE NAMES OF THE PERSONS WHO WERE

*Notes

1. The normal flow distribution is 5 gpm into the system and 3 gpm for the seal supply.
 2. If the injection water is increased to 150°F, the reactor coolant temperature should be adjusted to a temperature not to exceed 400°F.
 3. Injection water pressure is adjusted to obtain the required flow.
5. Thermal Barrier Cooling Water

ITEM	UNIT	NORMAL	MINIMUM	MAXIMUM	NOTES*
Flow	gpm	40	35	60	1
Temperature	degrees F	80	60	105	-
Pressure	psi	150	N/A	200	2

*Notes

1. Water shall be supplied from the non-radioactive component cooling system.
2. Pressure shall be adequate to ensure the required flow.

6. Bearing Water

ITEM	UNIT	NORMAL	MINIMUM	MAXIMUM	NOTES*
Temperature	degrees F	160.	Ambient	225	1

*Note

1. Refer to paragraph 4.5.1, items 1 and 2 (Loss of Injection Water and High Temperature of Injection Water).

7. Seal Purge Water

The No. 3 seal is fitted with a connection for purge water to minimize the buildup of boric acid crystals at the top of the seal. If purge flow is considered necessary, 2 to 4 gph of cool, clean, demineralized, non-borated water should be injected. The purge water drains out through the normal No. 3 seal leak-off line. When purge water is used, the flows of the table in paragraph 4.1.1.3 do not apply.

8. Alarm Settings

Alarm settings should be set in accordance with the maximum or minimum values shown on the preceding charts.

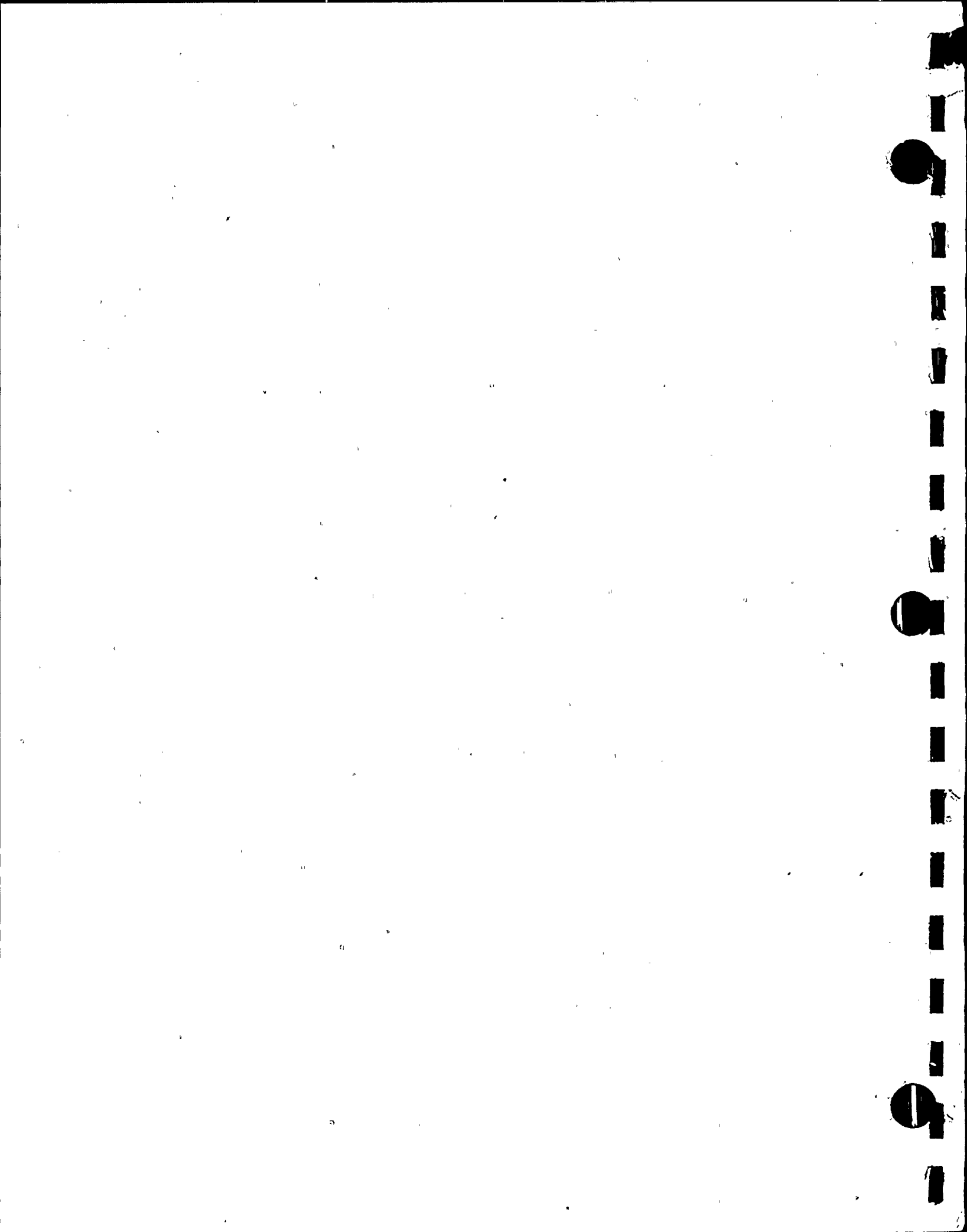
LICENSING REPORT FOR STORAGE DENSIFICATION
OF D.C. COOK SPENT FUEL POOL

INDIANA MICHIGAN POWER COMPANY

by

Holtec International

AEPSC Contract No. C-7926
Holtec Project 00480



HOLTEC INTERNATIONAL

REVIEW AND CERTIFICATION LOG

DOCUMENT NAME: LICENSING REPORT FOR STORAGE DENSIFICATION
OF D.C. COOK SPENT FUEL POOL

HOLTEC DOCUMENT I.D. NO. HI-90488
HOLTEC PROJECT NO. 00480
CUSTOMER/CLIENT: AMERICAN ELECTRIC POWER
(INDIANA MICHIGAN POWER CO.)

REVISION BLOCK				
ISSUE NO.	AUTHOR & DATE	REVIEWER & DATE	Q.A. MANAGER & DATE	APPROVED* BY & DATE
ORIGINAL	<i>Y.W. Wang</i> SING 6/14/90	<i>Alan Soter</i> A.S. 6/16/90	<i>M. Soter</i> M. Soter 6/19/90	<i>Y.W. Wang</i> SING 6/19/90
REVISION 1	<i>Y.W. Wang</i> WANG 10/2/90	<i>Y.W. Wang</i> SING 10/1/90	<i>M. Soter</i> M. Soter 10/2/90	<i>Y.W. Wang</i> SING 10/2/90
REVISION 2	<i>Y.W. Wang</i> YW 3/23/91	<i>Alan Soter</i> A.S. 3/28/91	<i>M. Soter</i> M. Soter 3/23/91	<i>Alan Soter</i> A.S. 3/25/91
REVISION 3	<i>Y.W. Wang</i> YW 5/23/91	<i>Alan Soter</i> A.S. 5/23/91	<i>M. Soter</i> M. Soter 5/23/91	<i>Y.W. Wang</i> SING 5/23/91
REVISION 4	<i>Y.W. Wang</i> YW 6/26/91	<i>Alan Soter</i> A.S. 6/26/91	<i>M. Soter</i> M. Soter 6/26/91	<i>Alan Soter</i> A.S. 6/26/91
REVISION 5	<i>Y.W. Wang</i> YW 6/31/91	<i>Alan Soter</i> A.S. 6/31/91	<i>M. Soter</i> M. Soter 6/31/91	<i>Y.W. Wang</i> SING 6/31/91
REVISION 6	<i>Y.W. Wang</i> YW 7/10/91	<i>Y.W. Wang</i> SING 7/10/91	<i>M. Soter</i> M. Soter 7/10/91	<i>Y.W. Wang</i> SING 7/10/91

NOTE: Signatures and printed names are required in the review block.

* Must be Project Manager or his Designee.

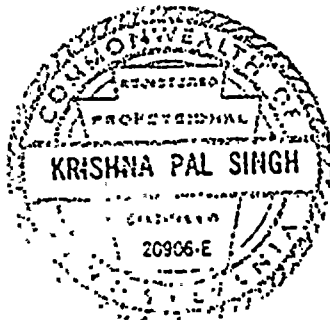
This document conforms to the requirement of the design specification and the applicable sections of the governing codes.

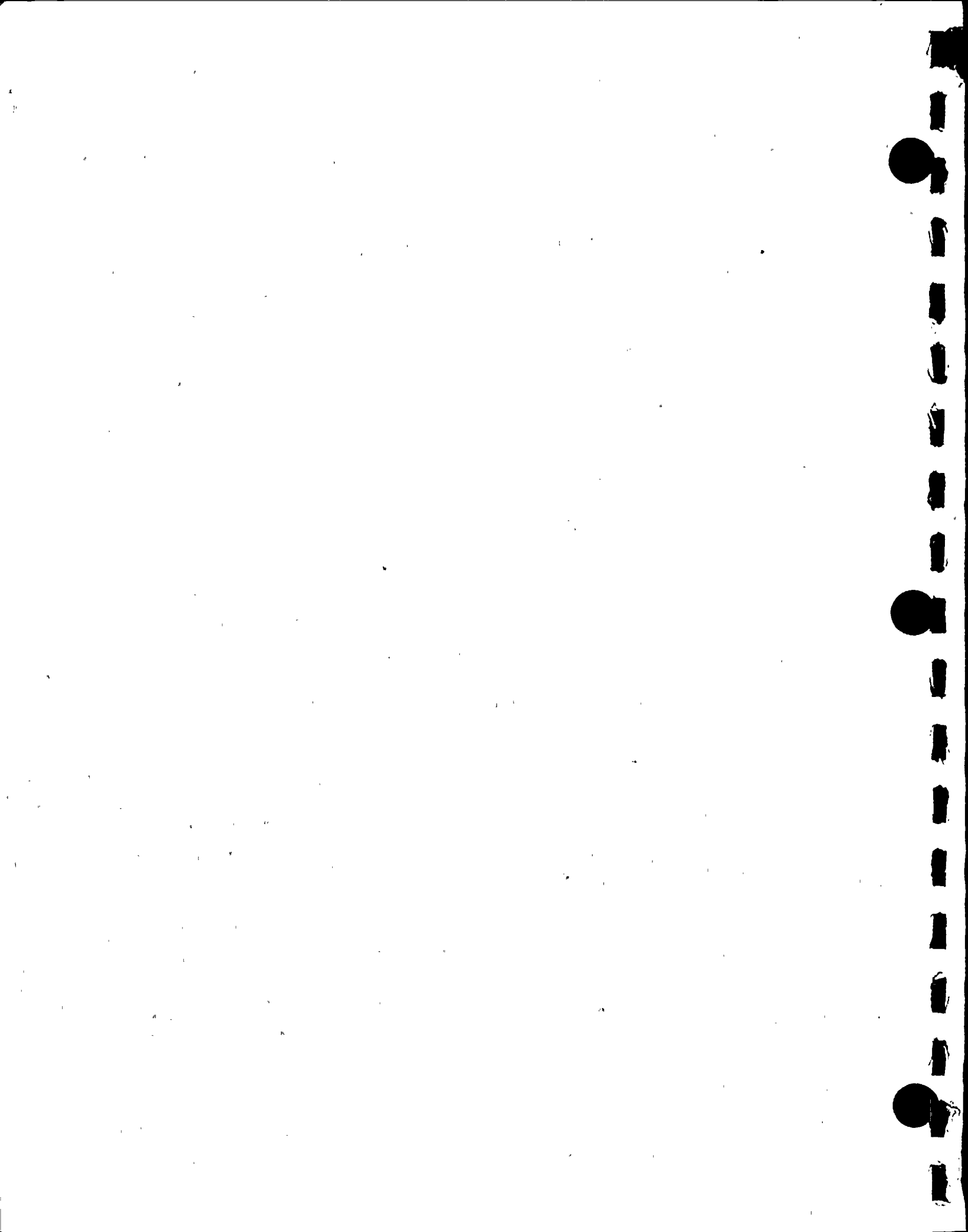
This document bears the ink stamp of the professional engineer who is certifying this document.

Y.W. Wang

Professional Engineer

SEAL





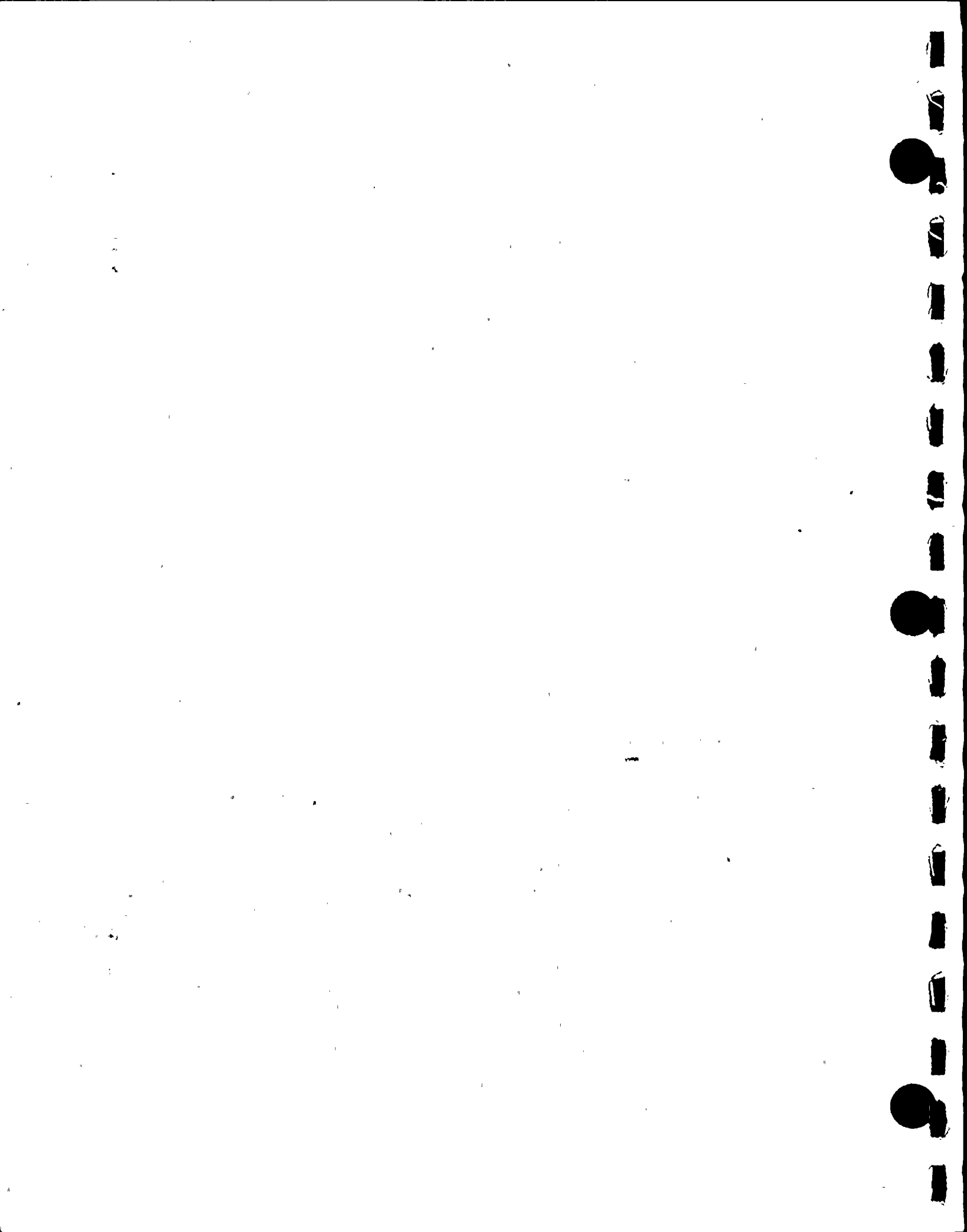
SUMMARY OF REVISIONS

Revision 1 contains the following number of pages of text
(including tables, but excluding figures):

Title Page	1
Review and Certification Log	1
Summary of Revisions Page	1
Table of Contents	4
List of Figures	3
Section 1	8
Section 2	17
Section 3	8
Section 4	(later)
Section 5	23
Section 6	48
Section 7	5
Section 8	13
Section 9	(later)
Section 10	11

Revision 2 contains the following number of pages of text
(including tables and figures):

Title Page	1
Review and Certification Log	1
Summary of Revisions Page	1
Table of Contents	4
List of Figures	3
Section 1	8
Section 2	18
Section 3	14
Section 4	Not included in Revision 2
Section 5	33
Section 6	78
Section 7	5
Section 8	17
Section 9	Not included in Revision 2
Section 10	Not included in Revision 2



SUMMARY OF REVISIONS

Revision 3 contains the following number of pages of text
(including tables and figures):

Title Page	1
Review and Certification Log	1
Summary of Revisions Page	2
Table of Contents	4
List of Figures	3
Section 1	9
Section 2	19
Section 3	14
Section 4	34
Appendix A to Section 4	9
Section 5	33
Section 6	76
Section 7	5
Section 8	17
Section 9	11
Section 10	5
Section 11	4

Revision 4 contains the same number of pages as Revision 3 with
these exceptions:

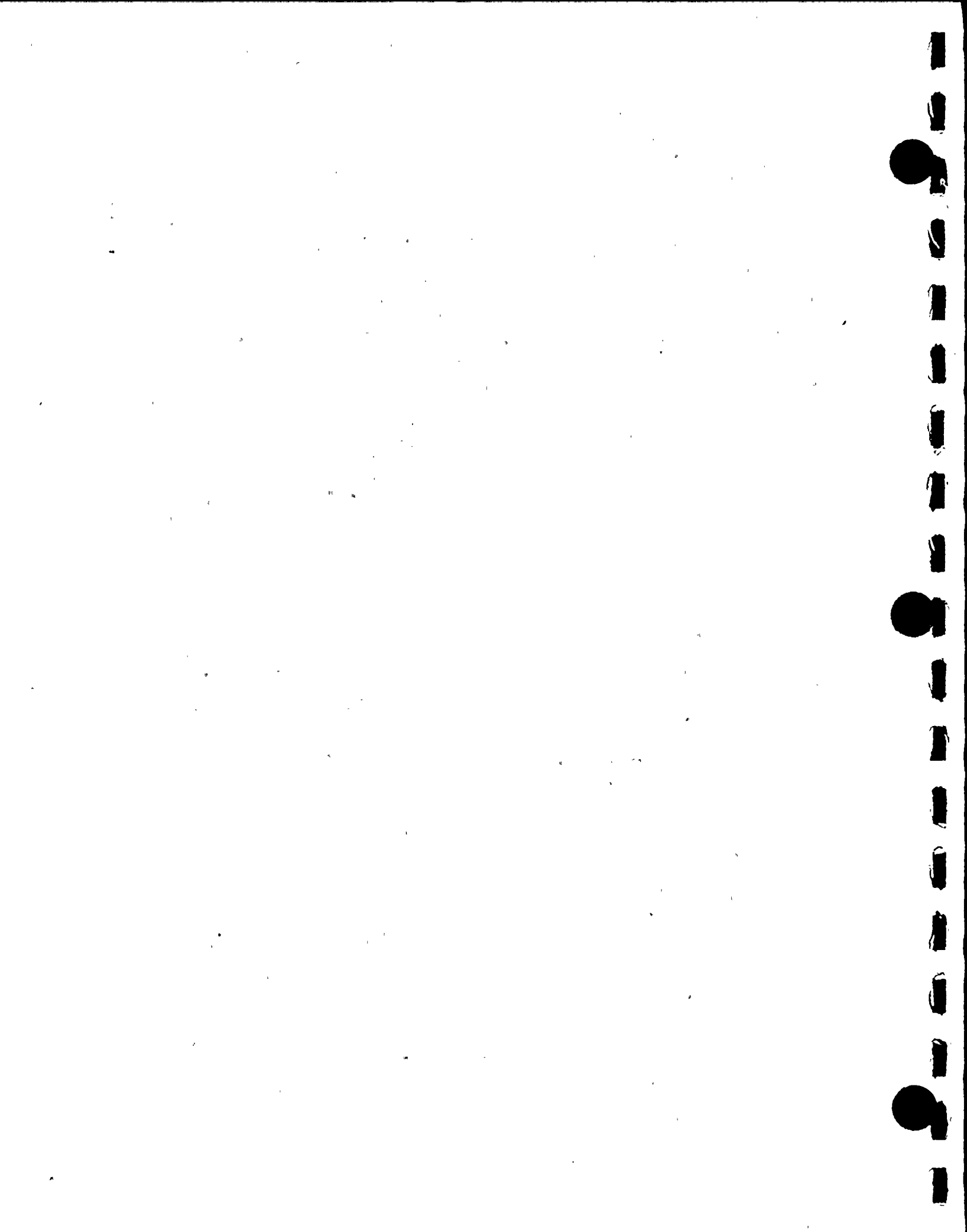
List of Tables (added to Rev. 4): 3

Sections revised in Rev. 4 now contain the following number of
pages:

Section 1	9
Section 2	18
Section 4	35
Section 5	34
Section 9	11

Individual pages revised and transmitted in Revision 4 are:

Pages 3-1, 3-3, 3-4, 6-6, 6-15, 6-18, 6-28, 6-30, 7-4, 7-5,
7-6, 8, 7 and 10-2.



SUMMARY OF REVISIONS

Holtec Report HI-90488

Revision 5

The following is revised in Revision 5:

Pages 4-8 and 4-9
Section 9
Appendix A
Page v of Table of Contents

Revision 6

The following pages are revised in Revision 6:

List of Figures
Table of Contents (page v)

2-1

4-15, 4-16

5-2, 5-3, 5-5, 5-6, 5-8, 5-9, 5-10, 5-12, 5-15, 5-16, 5-17, 5-18,
5-19, 5-20, 5-21, 5-24 through 5-38

6-3, 6-4, 6-35

7-2, 7-4

8-6, 8-7, 8-13

10-4

11-3



TABLE OF CONTENTS

1.0	INTRODUCTION	1-1
2.0	MODULE DATA	2-1
2.1	Synopsis of New Modules	2-1
2.2	Mixed Zone Two Region Storage (MZTR)	2-1
2.3	Material Considerations	2-4
2.3.1	Introduction	2-4
2.3.2	Structural Materials	2-4
2.3.3	Poison Material	2-4
2.3.4	Compatibility with Coolant	2-7
2.4	Existing Rack Modules and Proposed Reracking Operation	2-7
3.0	CONSTRUCTION OF RACK MODULES	3-1
3.1	Fabrication Objective	3-1
3.2	Mixed Zone Two Region Storage	3-2
3.3	Anatomy of Rack Modules	3-2
3.4	Codes, Standards and Practices for the D.C. Cook Spent Fuel Pool Racks	3-5
3.5	Materials of Construction	3-9
4.0	CRITICALITY SAFETY ANALYSES	4-1
4.1	Design Basis	4-1
4.2	Summary of Criticality Analyses	4-4
4.2.1	Normal Operating Conditions	4-4
4.2.2	Abnormal and Accident Conditions	4-6
4.3	Reference Fuel Storage Cells	4-8
4.3.1	Reference Fuel Assembly	4-8
4.3.2	High Density Fuel Storage Cells	4-9



TABLE OF CONTENTS (continued)

4.4	Analytical Methodology	4-10
4.4.1	Reference Design Calculations	4-10
4.4.2	Fuel Burnup Calculations and Uncertainties	4-12
4.4.3	Effect of Axial Burnup Distribution	4-13
4.5	Criticality Analyses and Tolerances	4-15
4.5.1	Nominal Design	4-15
4.5.2	Uncertainties due to Manufacturing Tolerances	4-15
4.5.2.1	Boron Loading Tolerances	4-15
4.5.2.2	Boral Width Tolerance	4-16
4.5.2.3	Tolerance in Cell Lattice Spacing	4-16
4.5.2.4	Stainless Steel Thickness Tolerances	4-16
4.5.2.5	Fuel Enrichment and Density Tolerances	4-16
4.5.3	Water-gap Spacing Between Modules	4-17
4.5.4	Eccentric Fuel Positioning	4-17
4.6	Abnormal and Accident Conditions	4-17
4.6.1	Temperature and Water Density Effects	4-17
4.6.2	Dropped Fuel Assembly	4-18
4.6.3	Lateral Rack Movement	4-18
4.6.4	Abnormal Location of a Fuel Assembly	4-19
4.7	Existing Spent Fuel	4-19
4.8	References	4-21
5.0	THERMAL-HYDRAULIC CONSIDERATIONS	
5.1	Introduction	5-1
5.2	Spent Fuel Cooling System Description	5-2
5.2.1	System Functions	5-2
5.2.2	System Description	5-3
5.2.3	Performance Requirements	5-4
5.3	Decay Heat Load Calculations	5-4



TABLE OF CONTENTS (continued)

5.4	Discharge Scenarios	5-5
5.5	Bulk Pool Temperatures	5-6
5.6	Local Pool Water Temperature	5-11
5.6.1	Basis	5-11
5.6.2	Model Description	5-12
5.7	Cladding Temperature	5-13
5.8	Blocked Cell Analysis	5-16
5.9	References for Section 5	5-16
6.0	RACK STRUCTURAL CONSIDERATIONS	6-1
6.1	Introduction	6-1
6.2	Analysis Outline	6-2
6.3	Artificial Slab Motions	6-3
6.4	Outline of Single Rack 3-D Analysis	6-5
6.5	Dynamic Model for the Single Rack Analysis	6-7
6.5.1	Assumptions	6-9
6.5.2	Model Description	6-11
6.5.3	Fluid Coupling	6-12
6.5.4	Damping	6-13
6.5.5	Impact	6-13
6.6	Assembly of the Dynamic Model	6-14
6.7	Time Integration of the Equations of Motion	6-17
6.7.1	Time History Analysis Using Multi-Degree of Freedom Rack Model	6-17
6.7.2	Evaluation of Potential for Inter-Rack Impact	6-19
6.8	Structural Acceptance Criteria	6-19
6.9	Material Properties	6-21

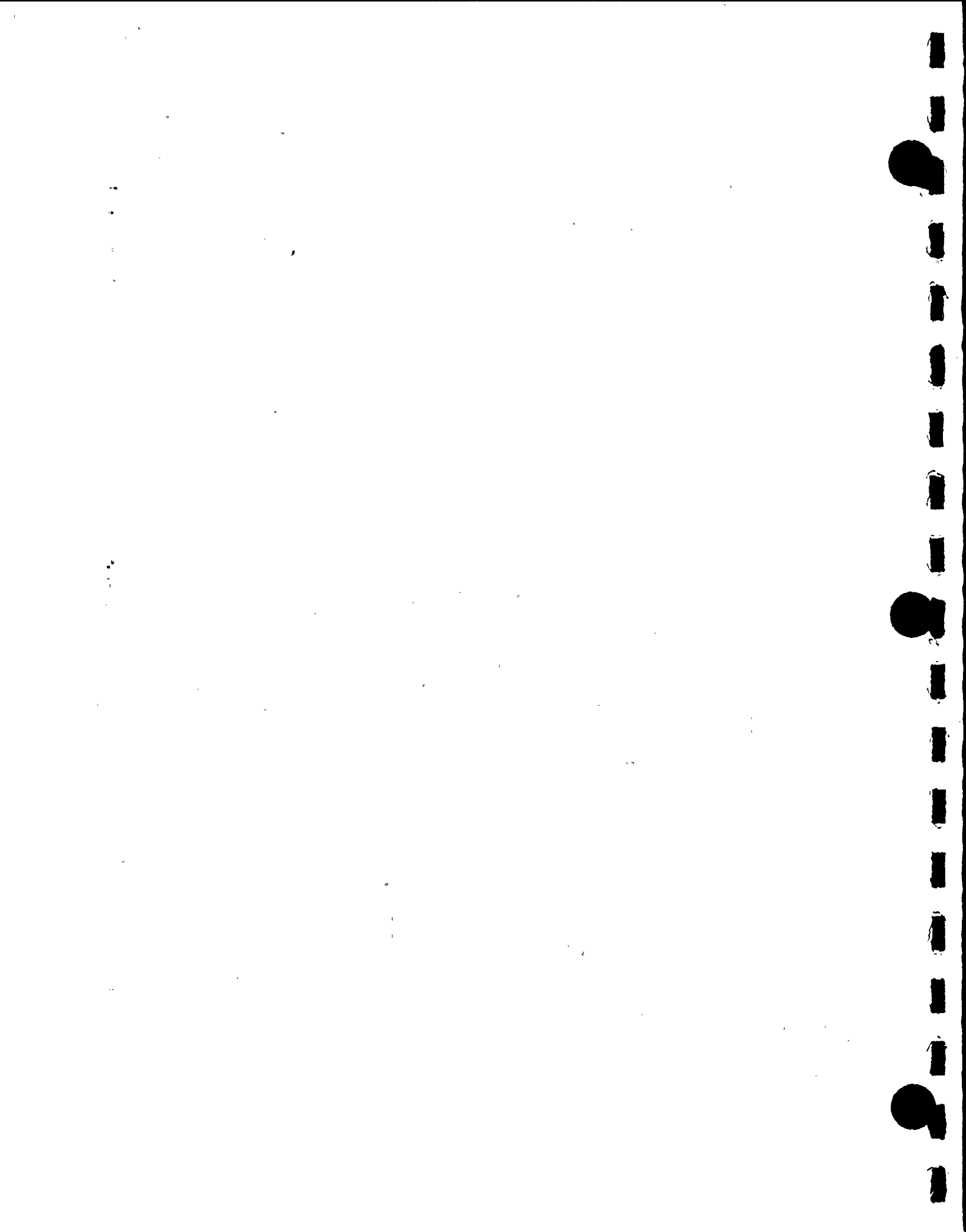


TABLE OF CONTENTS (continued)

6.10	Stress Limits for Various Conditions	6-22
6.10.1	Normal and Upset Conditions (Level A or Level B)	6-22
6.10.2	Level D Service Limits	6-25
6.11	Results for the Analysis of Spent Fuel Racks Using a Single Rack Model and 3-D Seismic Motion	6-25
6.12	Impact Analyses	6-28
6.12.1	Impact Loading between Fuel Assembly and Cell Wall	6-28
6.12.2	Impacts between Adjacent Racks	6-28
6.13	Weld Stresses	6-31
6.13.1	Baseplate to Rack Welds and Cell-to-Cell Welds	6-29
6.13.2	Heating of an Isolated Cell	6-30
6.14	Whole Pool Multi-Rack Analysis	6-30
6.14.1	Multi-Rack Model	6-32
6.14.2	Results of Multi-Rack Analysis	6-34
6.15	Bearing Pad Analysis	6-36
6.16	References for Section 6	6-37
7.0	ACCIDENT ANALYSIS AND MISCELLANEOUS STRUCTURAL EVALUATIONS	7-1
7.1	Introduction	7-1
7.2	Refueling Accidents	7-1
7.2.1	Dropped Fuel Assembly	7-1
7.3	Local Buckling of Fuel Cell Walls	7-2
7.4	Analysis of Welding Joints in Rack due to Isolated Hot Cell	7-3
7.5	Crane Uplift Load of 3000 lbs.	7-4
7.6	References for Section 7	7-4

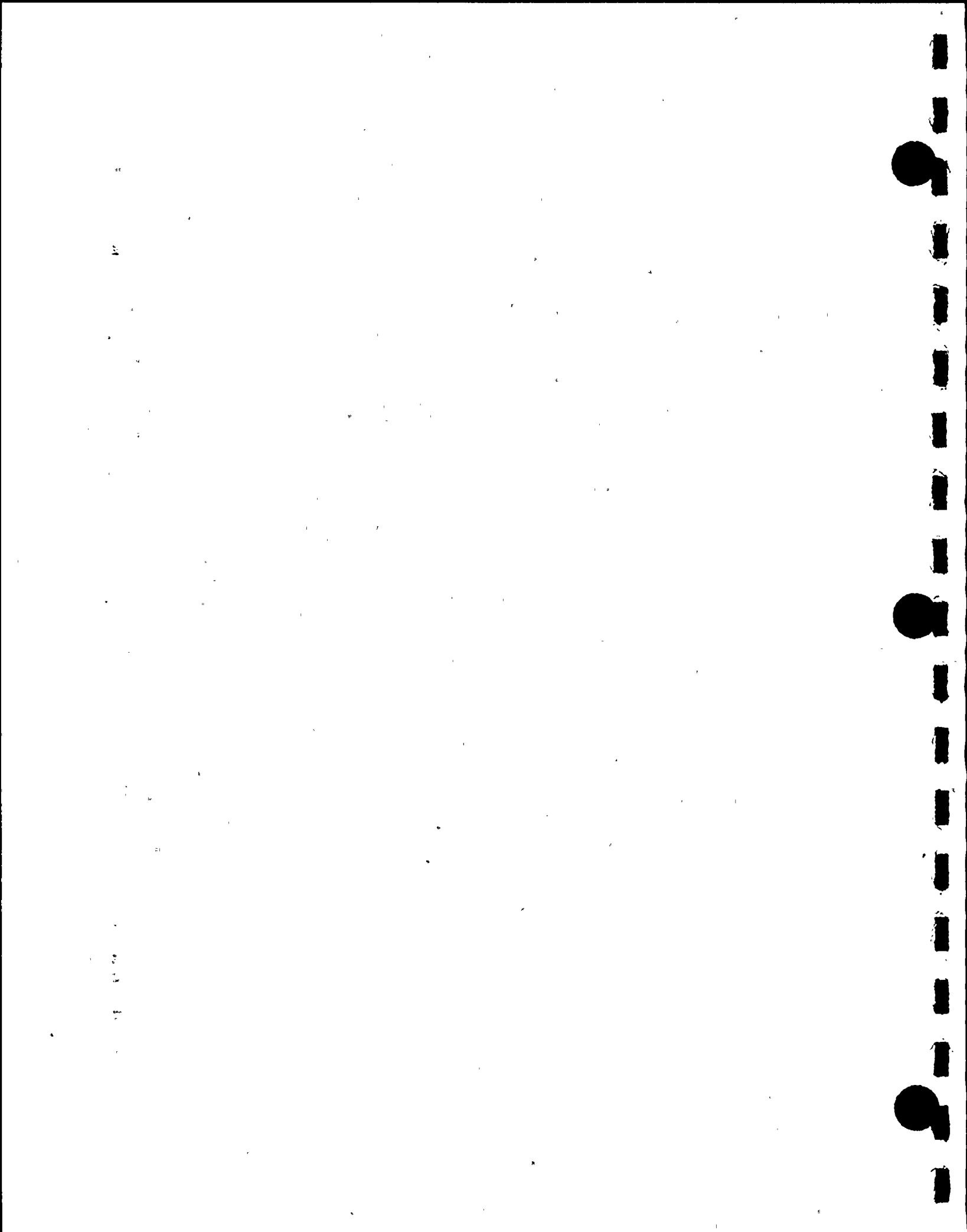


TABLE OF CONTENTS

8.0	STATIC AND DYNAMIC ANALYSES OF FUEL POOL STRUCTURE	
8.1	Introduction	8-1
8.2	General Features of the Model	8-3
8.3	Loading Conditions	8-6
8.4	Results of Analyses	8-10
8.5	Pool Liner	8-11
8.6	Conclusions	8-11
8.7	References for Section 8	8-12
9.0	RADIOLOGICAL EVALUATION	9-1
9.1	Fuel Handling Accident	9-1
9.1.1	Assumptions and Source Term Calculations	9-1
9.1.2	Results	9-4
9.2	Solid Radwaste	9-5
9.3	Gaseous Releases	9-5
9.4	Personnel Exposures	9-5
9.5	Anticipated Exposure during Reracking	9-6
9.6	References for Section 9	9-8
10.0	IN-SERVICE SURVEILLANCE PROGRAM	10-1
10.1	Purpose	10-1
10.2	Coupon Surveillance	10-2
10.2.1	Description of Test Coupons	10-2
10.2.2	Benchmark Data	10-3
10.2.3	Coupon Reference Data	10-3
10.2.4	Accelerated Surveillance	10-4
10.2.5	Post-Irradiation Tests	10-4
10.2.6	Acceptance Criteria	10-4
10.3	References for Section 10	10-5

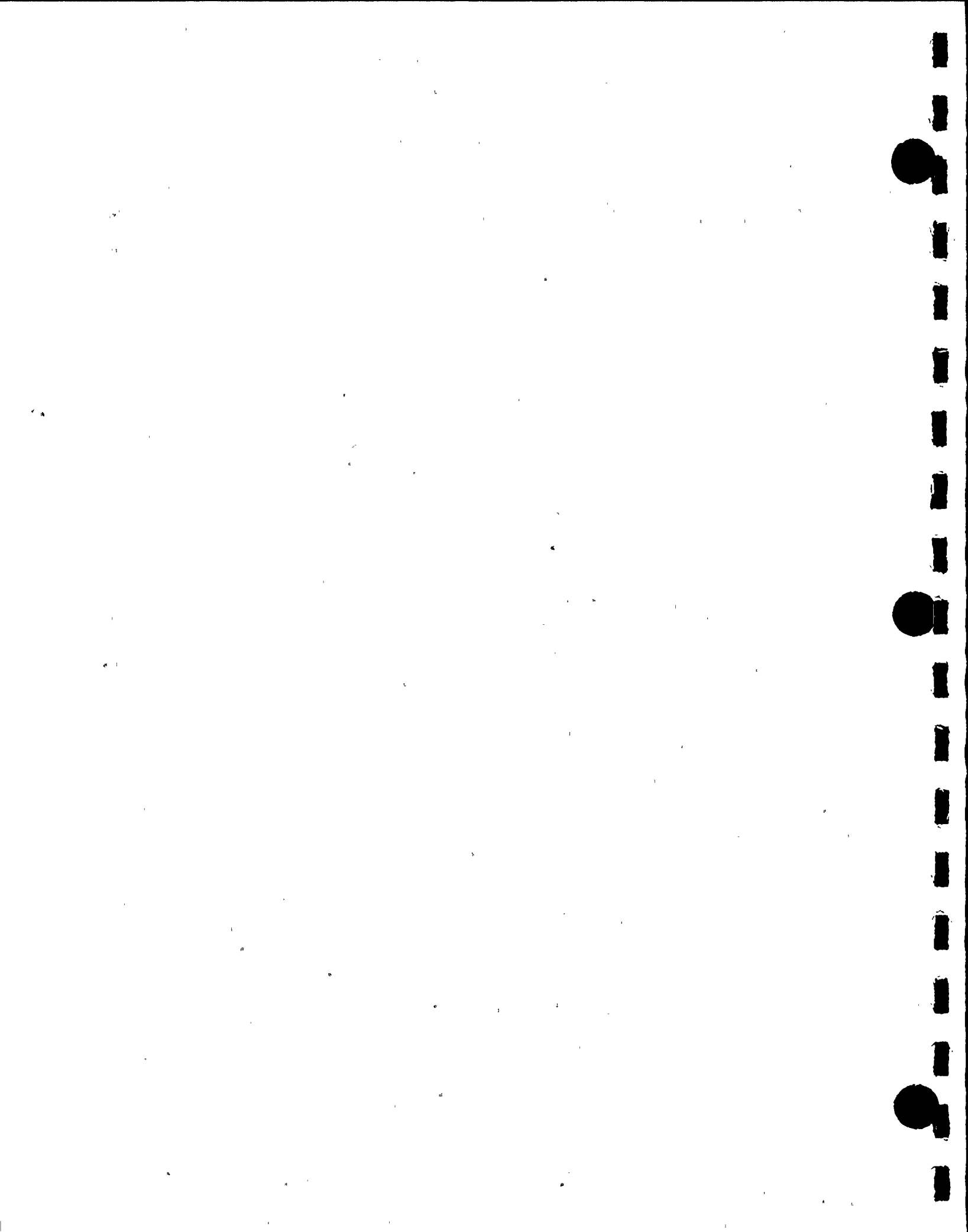


TABLE OF CONTENTS

11.0 COST/BENEFIT ANALYSIS	11-1
11.1 Introduction	11-1
11.2 Project Cost Assessment	11-1
11.3 Resource Commitment	11-3
11.4 Environment Assessment	11-3

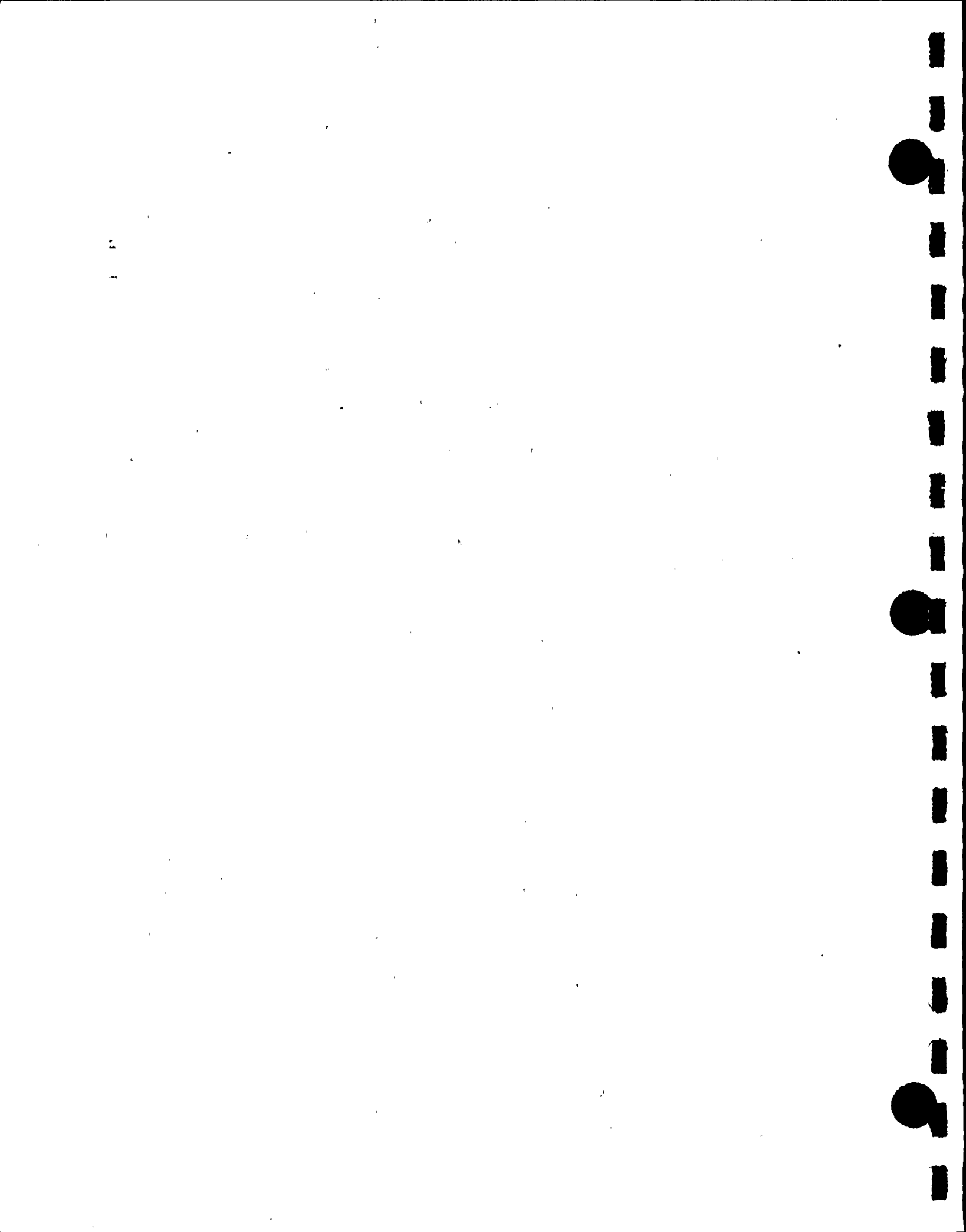
LIST OF TABLES

Table 1.1.1	Discharge Schedule
Table 1.1.2	Available Storage in the Donald C. Cook Pool
Table 1.1.3	Rack Module Data, Existing and Proposed Racks
Table 2.1.1	Module Data
Table 2.1.2	Common Module Data
Table 2.1.3	Module Data
Table 2.3.1	Boral Experience List (Domestic and Foreign)
Table 2.3.2	1100 Alloy Aluminum Physical and Mechanical Properties
Table 2.3.3	Chemical Composition (by weight) - Aluminum (1100 Alloy)
Table 2.3.4	Boron Carbide Chemical Composition, Weight & Boron Carbide Physical Properties
Table 4.1	Summary of Criticality Safety Analyses Normal Storage Configurations
Table 4.2	Summary of Criticality Safety Analyses Interim Checkerboard Loading
Table 4.3	Reactivity Effects of Abnormal and Accident Conditions
Table 4.4	Design Basis Fuel Assembly Specifications
Table 4.5	Reactivity Effects of Manufacturing Tolerances
Table 4.6	Effect of Temperature and Void on Calculated Reactivity of Storage Rack
Table 5.4.1	Fuel Specific Power and Pool Capacity Data
Table 5.4.2	Data for Scenarios 1 through 3



LIST OF TABLES (continued)

Table 5.4.3	Data for Scenarios 1 through 3
Table 5.5.1	Pool Bulk Temperature and Heat Generation Rate Data
Table 5.5.2	Time-to-Boil for Various Discharge Scenarios
Table 5.6.1	Peaking Factor Data
Table 5.6.2	Data for Local Temperatures
Table 5.7.1	Local and Cladding Temperature Output Data for the Maximum Pool Water Condition (Case 1)
Table 6.3.1	Correlation Coefficient
Table 6.5.1	Degrees of Freedom
Table 6.6.1	Numbering System for Gap Elements and Friction Elements
Table 6.6.2	Typical Input Data for Rack Analyses (lb-inch units)
Table 6.9.1	Rack Material Data (200°F) Support Material Data (200°F)
Table 6.11.1	Stress Factors and Rack-to-Fuel Impact Load
Table 6.11.2	Rack Displacements and Support Loads
Table 6.14.1	Rack Numbering and Weight Information
Table 6.14.2	Maximum Displacements from WPMR Run MP1
Table 6.14.3	Maximum Displacements from WPMR Run MP2
Table 6.14.4	Maximum Displacements from WPMR Run MP3
Table 6.14.5	Maximum Rack Displacements and Foot Load
Table 8.4.1	Safety Factors for Bending of Pool Structure Regions



LIST OF TABLES (continued)

Table 9.1	Inventories and Constants of Significant Fission Product Radionuclides
Table 9.2	Data and Assumptions for the Evaluation of the Fuel Handling Accident
Table 9.3	Typical Concentrations of Radionuclides in the Spent Fuel Pool Water
Table 9.4	Preliminary Estimate of Person-Rem Exposures During Reracking
Table 11.1	Donald C. Cook Nuclear Plant Worst Case Spent Fuel Inventory



• • • • •

• • • • •

• • • • •

LIST OF FIGURES

- Figure 2.1.1 Cook Spent Fuel Pool Layout
(upper bound cell count 3616 cells)
- Figure 3.3.1 Seam Welding Precision Formed Channels
- Figure 3.3.2 Composite Box Assembly
- Figure 3.3.3 Array of Cells for Non-Flux Trap Modules
- Figure 3.3.4 Adjustable Support Leg
- Figure 3.3.5 Elevation View of Rack Module
- Figure 4.1 Normal Storage Pattern (Mixed Three Zone)
- Figure 4.2 Interim Storage Pattern (Checkerboard)
- Figure 4.3 Acceptable Burnup Domain in Regions 2 & 3
- Figure 4.4 Fuel Storage Cell Cross Section
- Figure 4.5 KENO Calculational Model
- Figure 4.6 Equivalent Enrichment for Spent Fuel at
Various Burnups for Initial Enrichment
of 4.95%
- Figure 4.7 Effect of Water-Gap Spacing Between
Modules on System Reactivity
- Figure 4.8 Acceptable Burnup Domain in Regions 2 & 3
Showing Existing Spent Fuel Assemblies
- Figure 5.5.1 Pool Bulk Temperature Model
- Figure 5.5.2 Donald C. Cook SFP Normal Discharge,
One Cooling Train, Case 1a
- Figure 5.5.3 Donald C. Cook SFP Normal Discharge,
One Cooling Train, Case 1b
- Figure 5.5.4 Donald C. Cook SFP Normal Discharge,
Two Cooling Trains, Case 2
- Figure 5.5.5 Donald C. Cook SFP Full Core Offload
Two Cooling Trains, Case 3
- Figure 5.5.6 Donald C. Cook SFP Full Core Offload
One Cooling Train, Case 4
- Figure 5.5.7 Cook SFP Loss of Cooling Scenario, Case 1a

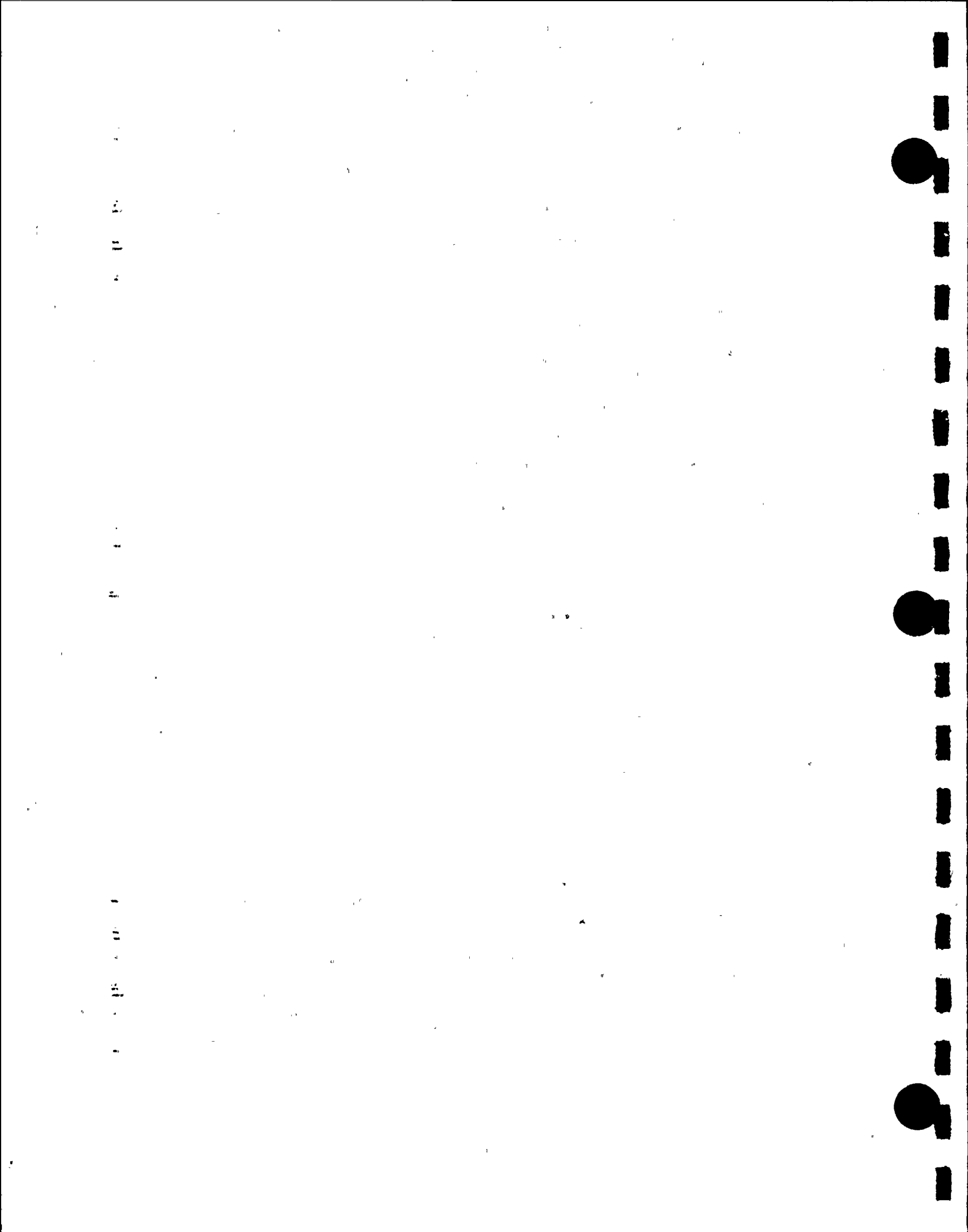
100-1-100

LIST OF FIGURES
(continued)

Figure 5.5.8	Cook SFP Loss of Cooling Scenario, Case 1b
Figure 5.5.9	Cook SFP Loss of Cooling Scenario, Case 2
Figure 5.5.10	Cook SFP Loss of Cooling Scenario, Case 3
Figure 5.5.11	Cook SFP Loss of Cooling Scenario, Case 4
Figure 5.6.1	Idealization of Rack Assembly
Figure 5.6.2	Thermal Chimney Flow Model
Figure 5.6.3	Convection Currents in the Pool
Figure 6.2.1	Pictorial View of Rack Structure
Figure 6.3.1	DBE - N-S Acceleration Time History
Figure 6.3.2	DBE - E-W Acceleration Time History
Figure 6.3.3	DBE - Vertical Acceleration Time History

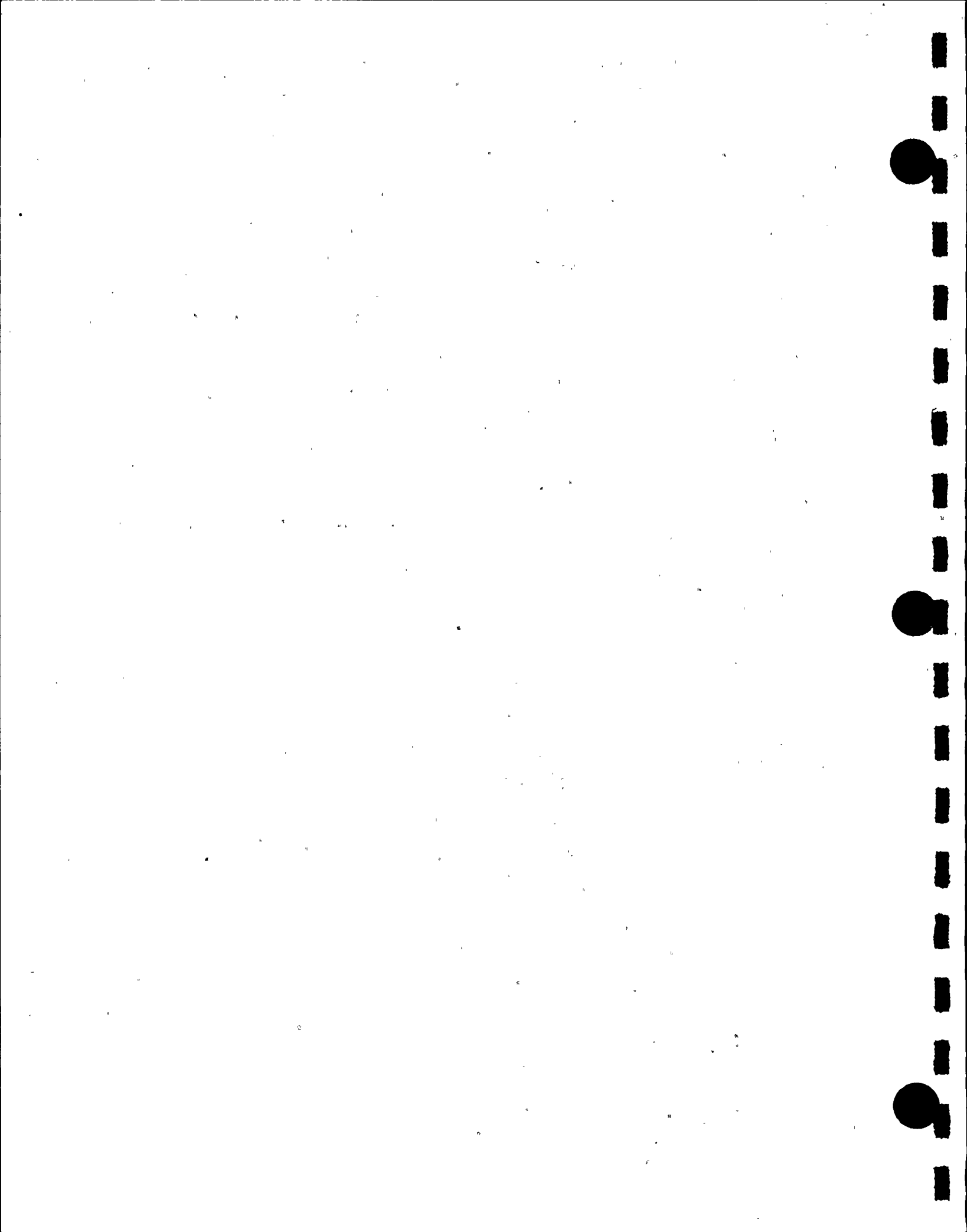
LIST OF FIGURES (continued)

Figure 6.3.4	Horizontal Design Spectrum and N-S Time History Spectrum (5% damping)
Figure 6.3.5	Horizontal Design Spectrum and E-W Time History Spectrum (5% damping)
Figure 6.3.6	Vertical Design and Time History Derived Spectra (5% damping)
Figure 6.3.7	OBE - N-S Acceleration Time History
Figure 6.3.8	OBE - E-W Acceleration Time History
Figure 6.3.9	OBE - Vertical Acceleration Time History
Figure 6.3.10	Horizontal Design Spectrum and Time History Derived N-S Spectrum (2% damping)
Figure 6.3.11	Horizontal Design Spectrum and E-W Time History Derived Spectrum (2% damping)
Figure 6.3.12	Vertical Design and Time History Derived Spectra (2% damping)



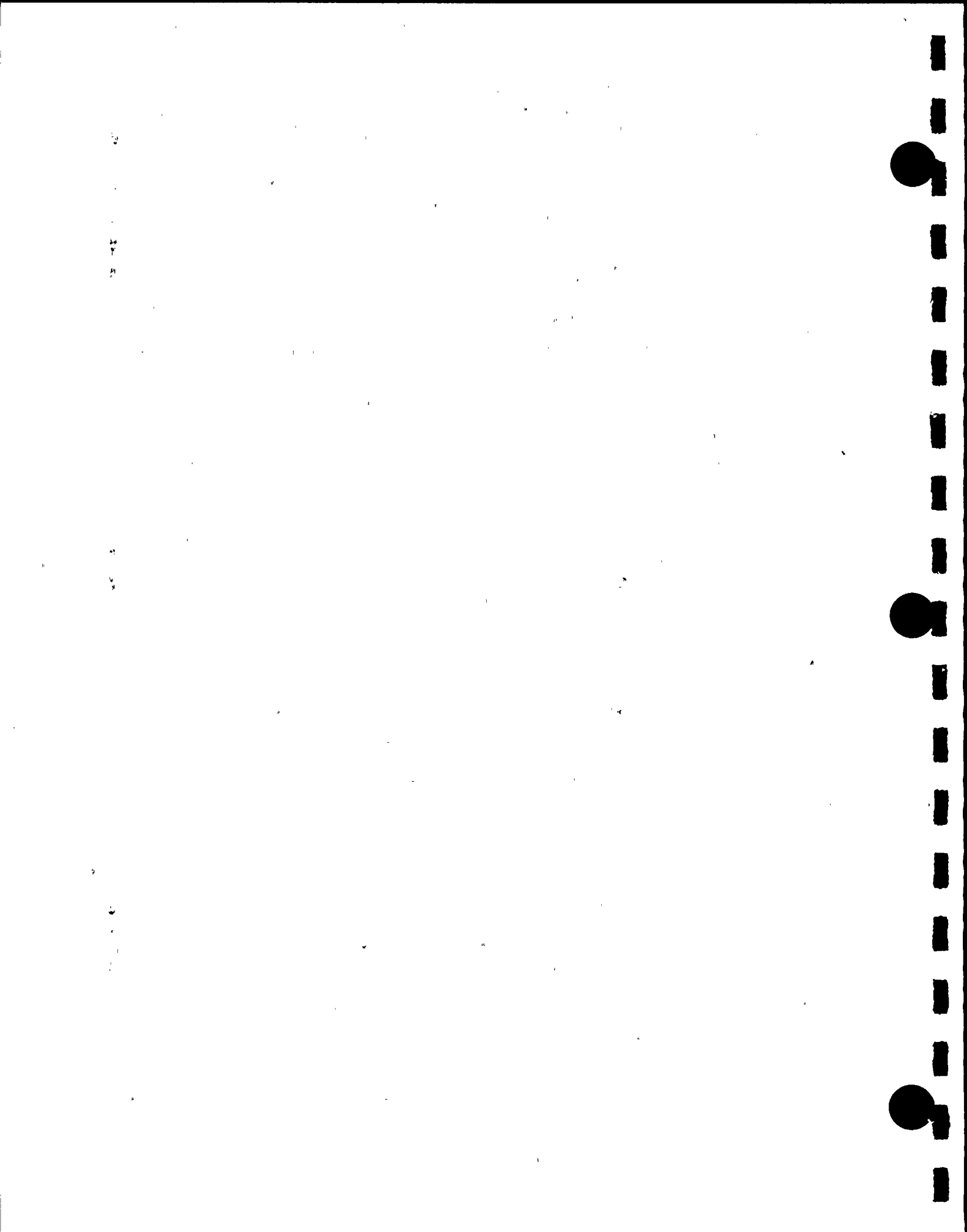
LIST OF FIGURES
(continued)

Figure 6.5.1	Schematic Model for DYNARACK
Figure 6.5.2	Rack-to-Rack Impact Springs
Figure 6.5.3	Impact Spring Arrangement at Node i
Figure 6.5.4	Degrees of Freedom Modelling Rack Motion
Figure 6.5.5	Rack Degrees of Freedom for X-Z Plane Bending
Figure 6.5.6	Rack Degrees of Freedom for Y-Z Plane Bending
Figure 6.6.1	2-D View of Rack Module
Figure 6.14.1	Rack and Foot Pedestal Numbering for Cook Multi-Rack Model
Figure 6.14.2	Cook Pool Multi-Rack Seismic Analysis, Run MP2 Rack 16 to Rack 17 South Corner Dynamic Gap at Rack Top
Figure 6.14.3	Cook Pool Multi-Rack Seismic Analysis, Run MP2 Rack 16 to Rack 17 South Corner Dynamic Gap at Rack Top
Figure 6.14.4	Cook Pool Multi-Rack Seismic Analysis, Run MP3 Rack 12 to Rack 18 WEst Corner Dynamic Gap at Rack Top
Figure 6.14.5	Cook Pool Multi-Rack Seismic Analysis, Run MP3 Rack 12 to Rack 18 East Corner Dynamic Gap at Rack Top
Figure 7.3.1	Loading on Rack Wall
Figure 7.4.1	Welded Joint in Rack
Figure 8.2.1	Isometric View of Cook Spent Fuel Pool
Figure 8.2.2	Overall Finite Model of Cook Pool Top View
Figure 8.2.3	Overall Finite Model of Cook Pool Bottom View
Figure 8.3.1	Pedestal Load vs. Time



1.0 INTRODUCTION

Donald C. Cook is a twin unit pressurized water nuclear power reactor installation owned and operated by Indiana Michigan Power Company. Donald C. Cook received its construction permit from the AEC in March, 1969, and its operating License in October, 1974 for Unit 1 and December 1977 for Unit 2. The two reactors went into commercial operation in August, 1975 (Unit 1) and July, 1978 (Unit 2), respectively. The Donald C. Cook fuel storage system is made up of a fuel pool 58'-3 1/8" long x 39'-1 9/16" wide with an integral cask laydown area. The pool presently contains 1367 spent fuel storage assemblies and 36 miscellaneous hardware items. Thus, out of the total installed storage capacity of 2050 storage cells, 1403 storage cells are presently occupied. Since the full core has 193 fuel assemblies for both Donald C. Cook reactors, maintaining full core offload capability from one reactor implies that 1857 storage cells (2050 minus 193) are available for normal offload storage. Table 1.1.1 provides the data on previous and projected fuel assembly discharge in the Donald C. Cook spent fuel pool. Table 1.1.2, constructed from Table 1.1.1 data, indicates that Donald C. Cook will lose full core discharge capability (for one reactor) in 1995. This projected loss of full core discharge capability prompted the present undertaking to increase spent fuel storage capability in the Donald C. Cook pool.



The purpose of this licensing submittal is to rerack the Donald C. Cook pool and equip it with new poisoned high density storage racks containing 3613 storage cells. The reracking also entails relocation of the thimble plug tool, spent fuel handling tool, Rod Cluster Control Assembly (RCCA) change tool, and Burnable Poison Rod Assembly (BPRA) tool brackets to the South wall adjacent to the cask pit.

Twenty three free-standing poisoned rack modules positioned with a prescribed and geometrically controlled gap between them will contain a total of 3613 storage cells (including 3 triangle cells located at the SW, NW and NE corners of the pool). Out of these cells, the peripheral cells located in each rack module are flux-trap cells*, and the interior ones are of the so-called non-flux trap type. The storage cells suitable for storing fresh fuel (up to 5% enrichment) are uniquely identified (see Section 4.0, Figures 4.1 and 4.2), and are surrounded by non-flux trap cells which have a burnup restriction on the fuel which they can store. Consistent with the concept of two region storage, the placement of fuel with a given burnup in the allowable location is administratively controlled. No credit is taken for soluble boron in normal refueling and full core offload storage conditions.

* A flux trap construction implies that there is a water gap between adjacent storage cells such that the neutrons emanating from a fuel assembly are thermalized before reaching an adjacent fuel assembly.



It is noted that the proposed reracking effort will increase the number of licensed storage locations to 3613 and, as indicated in Table 1.1.2, will extend the date of loss of full core discharge capability through the year 2008. Table 1.1.3 presents key comparison data for existing and proposed rack modules for Donald C. Cook.

The new spent fuel storage racks are free-standing and self supporting. The principal construction materials for the new racks are SA240-Type 304 stainless steel sheet and plate stock, and SA564-630 (precipitation hardened stainless steel) for the adjustable support spindles. The only non-stainless material utilized in the rack is the neutron absorber material which is boron carbide and aluminum-composite sandwich available under the patented product name "Boral".

The new racks are designed and analyzed in accordance with Section III, Division 1, Subsection NF of the ASME Boiler and Pressure Vessel (B&PV) Code. The material procurement, analysis, and fabrication of the rack modules conform to 10CFR 50 Appendix B requirements.

This Licensing Report documents the design and analyses performed to demonstrate that the new spent fuel racks satisfy all governing requirements of the applicable codes and standards, in particular, "OT Position for Review and Acceptance of Spent Fuel Storage and Handling Applications", USNRC (1978) and 1979 Addendum thereto.



The safety assessment of the proposed rack modules involved demonstration of its thermal-hydraulic, criticality and structural adequacy. Hydrothermal adequacy requires that fuel cladding will not fail due to excessive thermal stress, and that the steady state pool bulk temperature will remain within the limits prescribed for the spent fuel pool to satisfy the pool structural strength constraints. Demonstration of structural adequacy primarily involves analysis showing that the free-standing rack modules will not impact with each other or with the pool walls under the postulated Design Basis Earthquake (DBE) and Operating Basis Earthquake (OBE) events, and that the primary stresses in the rack module structure will remain below the ASME B&PV Code allowables. The structural qualification also includes analytical demonstration that the subcriticality of the stored fuel will be maintained under accident scenarios such as fuel assembly drop, accidental misplacement of fuel outside a rack, etc.

The criticality safety analysis shows that the neutron multiplication factor for the stored fuel array is bounded by the USNRC limit of 0.95 (OT Position Paper) under assumptions of 95% probability and 95% confidence. Consequences of the inadvertent placement of a fuel assembly are also evaluated as part of the criticality analysis. The criticality analysis also sets the requirements on the length of the B-10 screen and the areal B-10 density.

This Licensing Report contains documentation of the analyses performed to demonstrate the large margins of safety with respect to all USNRC specified criteria. This report also contains the results of the analysis performed to demonstrate the integrity of the fuel pool reinforced concrete structure, and an appraisal of



radiological considerations. A cost/benefit analysis demonstrating reracking as the most cost effective approach to increase the on-site storage capacity of the Donald C. Cook Nuclear Plant has also been performed and synopsized in this report.

All computer programs utilized in performing the analyses documented in this licensing report are identified in the appropriate sections. All computer codes are benchmarked and verified in accordance with Holtec International's nuclear Quality Program.

The analyses presented herein clearly demonstrate that the rack module arrays possess wide margins of safety from all three - thermal-hydraulic, criticality, and structural - vantage points. The No Significant Hazard Consideration evaluation submitted to the Commission along with this Licensing Report is based on the descriptions and analyses synopsized in the subsequent sections of this report.



Table 1.1.1
DISCHARGE SCHEDULE

<u>Cycle</u>	<u>Month/ Year</u>	<u>Number of Assemblies Discharged</u>	<u>Cumulative Inventory In the Pool</u>
1A*	12/1976	65	65
2A	4/1978	64	129
3A	4/1979	64	193
1B**	10/1979	80	273
4A	5/1980	65	338
2B	5/1981	92	430
5A	5/1981	64	494
6A	7/1982	64	558
3B	11/1982	72	630
7A	7/1983	80	710
4B	3/1984	92	802
8A	4/1985	80	882
5B	2/1986	88	970
9A	6/1987	80	1050
6B	5/1988	80	1130
10A	3/1989	80	1210
7B	6/1990	77	1282
11A	10/1990	80	1362
8B	11/1991	76	1438
12A	2/1992	80	1518
9B	3/1993	80	1598
13A	6/1993	80	1678
10B	7/1994	80	1758
14A	10/1994	80	1838
11B	11/1995	80	1918
15A	4/1996	80	1998
12B	3/1997	80	2078
16A	8/1997	80	2158
13B	7/1998	80	2238

* A - Reactor Unit 1
 ** B - Reactor Unit 2

Table 1.1.1 (continued)

DISCHARGE SCHEDULE

<u>Cycle</u>	<u>Month/ Year</u>	<u>Number of Assemblies Discharged</u>	<u>Cumulative Inventory In the Pool</u>
17A*	12/1998	80	2318
14B**	1/2001	80	2398
18A	4/2000	80	2478
15B	5/2001	80	2558
19A	8/2001	80	2638
16B	9/2002	80	2718
20A	12/2002	80	2798
17B	1/2004	80	2878
21A	6/2004	80	2958
18B	5/2005	80	3038
22A	10/2005	80	3118
19B	9/2006	80	3198
23A	2/2007	80	3278
20B	1/2008	80	3358
24A	7/2008	80	3438
21B	7/2009	80	3518

* A - Reactor Unit 1
** B - Reactor Unit 2

11

11

Table 1.1.2

AVAILABLE STORAGE IN THE DONALD C. COOK POOL

NUMBER OF STORAGE LOCATIONS AVAILABLE

<u>Cycle</u>	<u>Month/ Year</u>	<u>With Present Licensed Capacity (2050 Locations)</u>	<u>After Reracking (3616 Locations)</u>
7B	6/1990	768	2334
11A	10/1990	688	2254
8B	11/1991	612	2178
12A	2/1992	532	2098
9B	3/1993	452	2018
13A	6/1993	372	1938
10B	7/1994	292*	1858
14A	10/1994	212	1778
11B	11/1995	132**	1698
15A	4/1996	52***	1618
12B	3/1997		1538
16A	8/1997		1458
13B	7/1998		1378
17A	12/1998		1298
14B	1/2000		1218
18A	4/2000		1138
15B	5/2001		1058
19A	8/2001		978
16B	9/2002		898
20A	12/2002		818
17B	1/2004		738
21A	6/2004		658
18B	5/2005		578
19B	9/2006		418
23A	2/2007		338*
20B	1/2008		258
24A	7/2008		178**
21B	7/2009		98
25A	11/2009		18***

* Date of loss of full core offload capability from both reactors.

** Date of loss of full core offload capability for one reactor.

*** Date of loss of normal discharge capability.

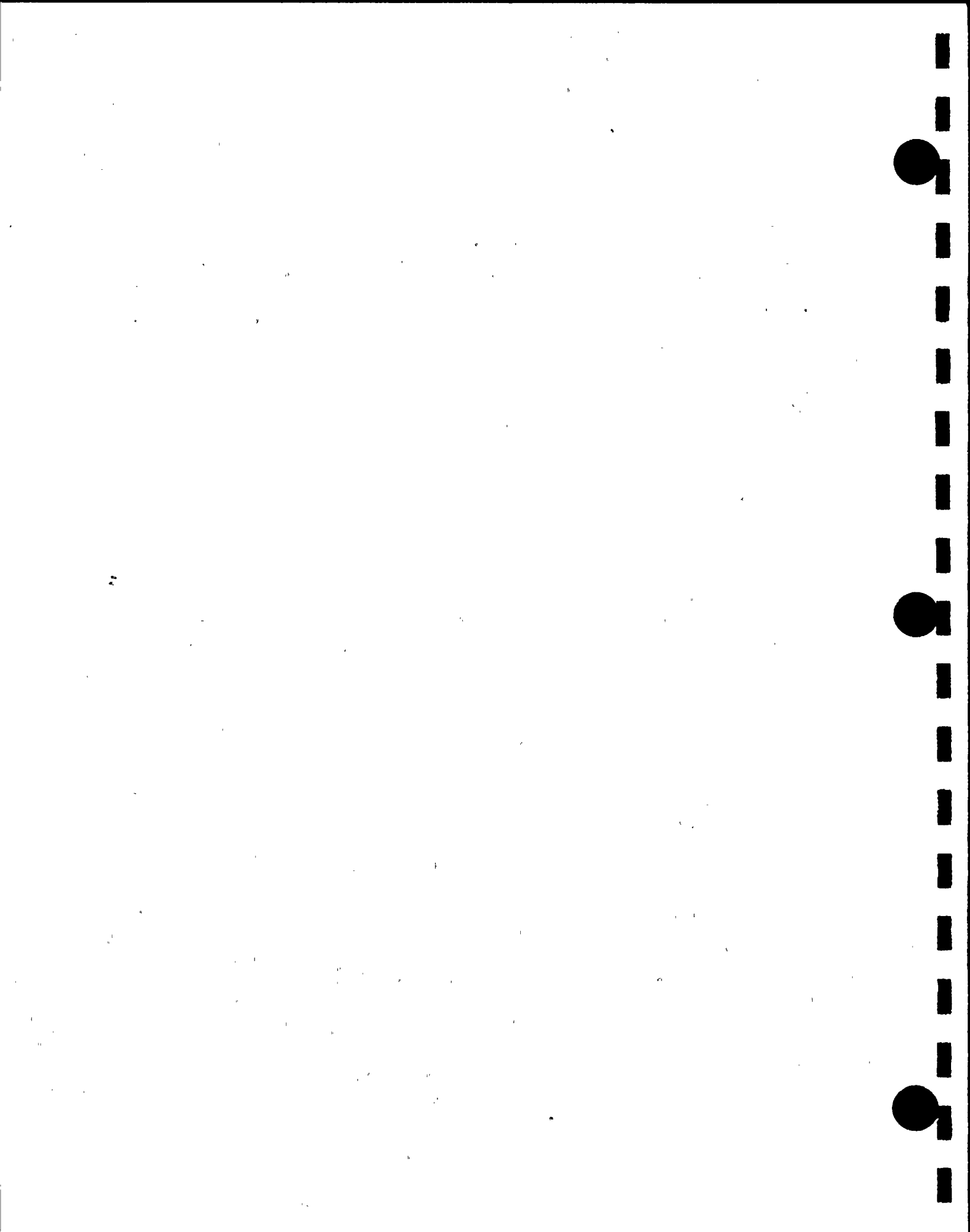


Table 1.1.3

RACK MODULE DATA, EXISTING AND PROPOSED RACKS

<u>ITEM</u>	<u>EXISTING RACKS</u>	<u>PROPOSED RACKS</u>
Number of cells	2050	3616*
Number of modules	20	23
Neutron Absorber	Boral	Boral
(Nom.) cell pitch, inch	10.5"	8.97"
(Nom.) cell opening size, inch	8.884 ± 0.124	8.75" ± 0.04

* Include three triangular corner storage cells.



2.0 MODULE DATA

2.1 Synopsis of New Modules

The Donald C. Cook spent fuel pool consists of a 39'-1 9/16" x 58'-3 1/8" rectangular pit with a 10'-4" x 10'-6" space designated for cask handling operations. The pool is connected to the fuel transfer canal through a weir gate on the West wall. This gate is normally closed.

At the present time, the Donald C. Cook pool contains medium density racks with a 10.5" nominal assembly center-to-center pitch. There is a total of 2050 storage cells in the pool. There are two sizes of modules, 10x10 and 10x11. The 10x10 module weighs 33,800 lb. and the 10x11 module weighs 37,200 lb.

Figure 2.1.1 shows the module layout for the Donald C. Cook pool after the proposed reracking campaign. As shown in Figure 2.1.1 and tabulated in Table 2.1.1, there are twenty-three racks containing a total of 3613 storage cells with a 8.97" nominal pitch.

The essential cell data for all storage cells is given in Table 2.1.2. The physical size and weight data on the modules may be found in Table 2.1.3. In summary, the present reracking application will increase the licensed storage capacity of the Donald C. Cook pool from 2050 to 3613 cells.

2.2 Mixed Zone Three Region Storage (MZTR):

The high density spent fuel storage racks in the Donald C. Cook pool will provide storage locations for up to 3613 fuel assemblies and will be designed to maintain the stored fuel, having an initial enrichment of up to 5 wt% U-235, in a safe, coolable, and subcritical configuration during normal discharge and full core offload storages and postulated accident conditions.



All rack modules for Donald C. Cook spent fuel pool are of the so-called "free-standing" type such that the modules are not attached to the pool floor nor do they require any lateral braces or restraints. These rack modules will be placed in the pool in their designated locations using a specifically designed lifting device, and the support legs remotely leveled (using a telescopic removable handling tool) by an operator on the fuel handling bridge. The leveling operations are done when the support legs are lifted off the floor. Except for the crane, no additional lifting equipment is needed while leveling is being performed.

As described in detail in Section 3, all modules in the Donald C. Cook pool are of "non-flux trap" construction. However, the module baseplates extend out by $7/8$ " (nominal), such that the nominal gap between the adjacent walls of two neighboring racks is 2" (nom.). Thus, although there is a single screen of neutron absorber panel between two fuel assemblies stored in the same rack, there are two poison panels with a water flux trap (2" wide) between them for fuel assemblies located in cells in two facing modules. Out of these flux trap locations, and peripheral cell locations (cells adjacent to pool walls) a certain number of storage cells are designated for storing fresh fuel. In addition, as described in Section 4, a certain number of interior cells in each rack are designated for storing fresh fuel of 5% wt. U-235 (max.) enrichment. In this manner, a sufficient number of locations without any burnup restriction (Region I cells) are identified to enable unrestricted full core offload of the Donald C. Cook reactor in the spent fuel pool. These so-called Region I cells are identified in Section 4 of this report. The remaining storage cells have enrichment/burnup restrictions. Appropriate restrictions on the enrichment/burnup of the stored fuel in Region II and Region III cells are presented in Section 4.



1
2
3
4
5
6
7
8
9
10
11
12
13
14
15
16
17
18
19
20
21
22
23
24
25
26
27
28
29
30
31
32
33
34
35
36
37
38
39
40
41
42
43
44
45
46
47
48
49
50
51
52
53
54
55
56
57
58
59
60
61
62
63
64
65
66
67
68
69
70
71
72
73
74
75
76
77
78
79
80
81
82
83
84
85
86
87
88
89
90
91
92
93
94
95
96
97
98
99
100

Each rack module is supported by at least four legs which are remotely adjustable. Thus, the racks can be made vertical and the top of the racks can easily be made co-planar with each other. The rack module support legs are engineered to accommodate variations of the pool floor. The support legs also provide an under rack plenum for natural circulation of water through the storage cells. The placement of the racks in the spent fuel pool has been designed to preclude any support legs from being located over existing obstructions on the pool floor.

The Donald C. Cook racks are subjected to mandated seismic loadings per the plant UFSAR. The Design Basis Earthquake (DBE) and Operating Basis Earthquake (OBE) seismic response spectra are provided and synthetic time histories are generated. These acceleration time histories are applied as inertia loads (see Section 6.3).

Under these seismic events, the rack modules have four designated locations of potential impact:

- (i) Support leg to bearing pad
- (ii) Storage cell to fuel assembly contact surfaces
- (iii) Baseplate edges
- (iv) Rack top corners

The support leg to pool slab bearing pad impact would occur whenever the rack support foot lifts off the pool floor during a seismic event. The "rattling" of the fuel assemblies in the storage cell is a natural phenomenon associated with seismic conditions. The baseplate and rack top corners impacts would occur if the rack modules tend to slide or tilt towards each other during the postulated DBE or OBE seismic events. Section 6 of this report presents the analysis methodology and results for all three locations of impact, and establishes the structural integrity of the racks under the load combinations specified for plant conditions required by the NRC.

10 10 10 10 10

10 10 10 10 10



A bearing pad, made of austenitic stainless steel, is interposed between the support foot and the liner such that the loads transmitted to the slab by the rack module under steady state as well as seismic conditions are diffused into the pool slab, and allowable local concrete surface pressures are not exceeded. Section 8 of this report presents the detailed pool structure analysis.

2.3 Material Considerations

2.3.1 Introduction

Safe storage of nuclear fuel in the Donald C. Cook spent fuel pool requires that the materials utilized in the fabrication of racks be of proven durability and be compatible with the pool water environment. This section provides the necessary information on this subject.

2.3.2 Structural Materials

The following structural materials are utilized in the fabrication of the spent fuel racks:

- a. ASME SA240-304 for all sheet metal stock.
- b. Internally threaded support legs: ASME SA240-304.
- c. Externally threaded support spindle: ASME SA564-630 precipitation hardened stainless steel.
- d. Weld material - per the following ASME specification: SFA 5.9 ER308.

2.3.3 Poison Material

In addition to the structural and non-structural stainless material, the racks employ Boral, a patented product of AAR Brooks & Perkins, as the thermal neutron absorber material. A brief description of Boral, and its fuel pool experience list follows.

Boral is a thermal neutron absorbing material composed of boron carbide and 1100 alloy aluminum. Boron carbide is a compound



having a high boron content in a physically stable and chemical inert form. The 1100 alloy aluminum is a light-weight metal with high tensile strength which is protected from corrosion by a highly resistant oxide film. The two materials, boron carbide and aluminum, are chemically compatible and ideally suited for long-term use in the radiation, thermal and chemical environment of a spent fuel pool.

Boral's use in the spent fuel pool as the neutron absorbing material can be attributed to the following reasons:

- (i) The content and placement of boron carbide provides a very high removal cross section for thermal neutrons.
- (ii) Boron carbide, in the form of fine particles, is homogenously dispersed throughout the central layer of the Boral.
- (iii) The boron carbide and aluminum materials in Boral do not degrade as a result of long-term exposure to gamma radiation.
- (iv) The thermal neutron absorbing central layer of Boral is clad with permanently bonded surfaces of aluminum.
- (v) Boral is stable, strong, durable, and corrosion resistant.

The passivation process of Boral in an aqueous environment results in the generation of hydrogen gas. If the generation rate of hydrogen is too rapid, then swelling of Boral may occur. Laboratory studies by Boral's supplier indicate that the rate of hydrogen generation is a strong function of the so-called impurities in the chemical composition of the boron carbide powder, namely sodium hydroxide and boron oxide. AAR Brooks & Perkins has instituted a strict program of monitoring of the chemistry of boron carbide used in the manufacturing of Boral to ensure that no swelling of the panels will occur. Furthermore,



1

2

3

4

randomly selected coupons of Boral panels from production runs are subjected to swelling test checks to preclude any possibility of swelling of Boral.

Boral is manufactured by AAR Brooks & Perkins under the control and surveillance of a computer-aided Quality Assurance/Quality Control Program that conforms to the requirements of 10CFR50 Appendix B, "Quality Assurance Criteria for Nuclear Power Plants and Fuel Reprocessing Plants". As indicated in Table 2.3.1, Boral has been licensed by the USNRC for use in numerous BWR and PWR spent fuel storage racks and has been extensively used in overseas nuclear installations.

Boral Material Characteristics

Aluminum: Aluminum is a silvery-white, ductile metallic element that is abundant in the earth's crust. The 1100 alloy aluminum is used extensively in heat exchangers, pressure and storage tanks, chemical equipment, reflectors and sheet metal work.

It has high resistance to corrosion in industrial and marine atmospheres. Aluminum has atomic number of 13, atomic weight of 26.98, specific gravity of 2.69 and valence of 3. The physical/mechanical properties and chemical composition of the 1100 alloy aluminum are listed in Tables 2.3.2 and 2.3.3.

The excellent corrosion resistance of the 1100 alloy aluminum is provided by the protective oxide film that develops on its surface from exposure to the atmosphere or water. This film prevents the loss of metal from general corrosion or pitting corrosion and the film remains stable between a pH range of 4.5 to 8.5.

11 25 1 24



Boron Carbide: The boron carbide contained in Boral is a fine granulated powder that conforms to ASTM C-750-80 nuclear grade Type III. The particles range in size between 60 and 200 mesh and the material conforms to the chemical composition and properties listed in Table 2.3.4.

2.3.4 Compatibility with Coolant

All materials used in the construction of the Donald C. Cook racks have an established history of in-pool usage. Their physical, chemical and radiological compatibility with the pool environment is an established fact at this time. As noted in Table 2.3.1, Boral has been used in both vented and unvented configurations in fuel pools with equal success. Consistent with the recent practice, the Donald C. Cook rack construction allows full venting of the Boral space. Austenitic stainless steel (304) is widely used in nuclear power plants.

2.4 Existing Rack Modules and Proposed Reracking Operation

The Donald C. Cook fuel pool currently has medium density rack modules containing a total of 2050 storage cells in twenty modules. At the time of the proposed reracking operation, approximately 1678 cells (between 6/1993 and 7/1994) out of 2050 locations will be occupied with spent fuel. There is sufficient number of open (unoccupied) cells in the pool to permit relocation of all fuel such that the existing modules can be emptied and removed from the pool, and new modules installed in a programmed manner.

A remotely engagable lift rig, which is designed to meet the criteria of NUREG-0612 "Control of Heavy Loads of Nuclear Power Plants", will be used to lift the empty modules. Auxiliary Building Cranes will be used for this purpose. A module change-out



scheme and procedure will be developed which ensures that all modules being handled are empty when the module is moving at a height which is more than 12" above the pool floor.

The Auxiliary Building has two overhead cranes which ride on rails that traverse the entire fuel handling area of the building. Each crane has a main hook rated at 150 tons. These hooks are single failure proof (SFP) (up to 60 tons). In addition there is an auxiliary hoist on the East Crane rated at 20 tons.

Pursuant to the defense-in-depth approach of NUREG-0612, the following additional measures of safety will be undertaken for the reracking operation.

- (i) The crane and hoist will be given a preventive maintenance checkup and inspection within 3 months of the beginning of the reracking operation.
- (ii) The crane hook will be used to lift no more than 50% of its single failure proof capacity of 60 tons at any time during the reracking operation. (The maximum weight of any module and its associated handling tool is 24 tons).
- (iii) The old fuel racks will be lifted no more than 6" above the pool floor and held in that elevation for approximately 10 minutes before beginning the vertical lift.
- (iv) The rate of vertical lift will not exceed 6' per minute.
- (v) The rate of horizontal movement will not exceed 6' per minute.
- (vi) Preliminary safe load paths have been developed. The "old" or "new" racks will not be carried over any region of the pool containing fuel.
- (vii) The rack upending or laying down will be carried out in an area which is not overlapping to any safety related component.
- (viii) All crew members involved in the reracking operation will be given training in the use of the lifting and upending equipment. The training



seminar will utilize videotapes of the actual lifting and upending rigs on typical modules to be installed in the pool. Every crew member will be required to pass a written examination in the use of lifting and upending apparatus administered by the rack designer.

- (ix) Referring to Figure 2.1.1, it is noted that the fuel handling bridge crane cannot access storage cells facing the east wall and several locations in the southwest corner. Therefore, it will be necessary to load the inaccessible cells with fuel when the rack is staged a certain distance (approximately 20 inches) from the pool wall. Having loaded these cells, the module will be lifted approximately 4 inches above the pool liner, and laterally transported to its final designated locations. A fuel shuffling and rack installation sequence has been developed to ensure that all heavy load handling criteria of NUREG-0612 are satisfied. The rack handling rig is designed with consideration of the rack module weight along with the contained fuel assembly mass.

The fuel racks will be brought directly into the Auxiliary Building through the access door which is at ground level (609' elevation). This direct access to the building greatly facilitates the rack removal and installation effort.

The "old" racks will be decontaminated to the extent practical on-site and approved for shipping per the requirements of 10 CFR71 and 49 CFR 171-178, be housed in shipping containers, and transported to a processing facility for volume reduction. Non-decontaminatable portions of the racks will be shipped to a licensed radioactive waste burial site or returned to site for storage if disposal access is unavailable. The volume reduction is expected to reduce the overall volume of the racks to about 1/10th of their original value.

All phases of the reracking activity will be conducted in accordance with written procedures which will be reviewed and approved by I&M.

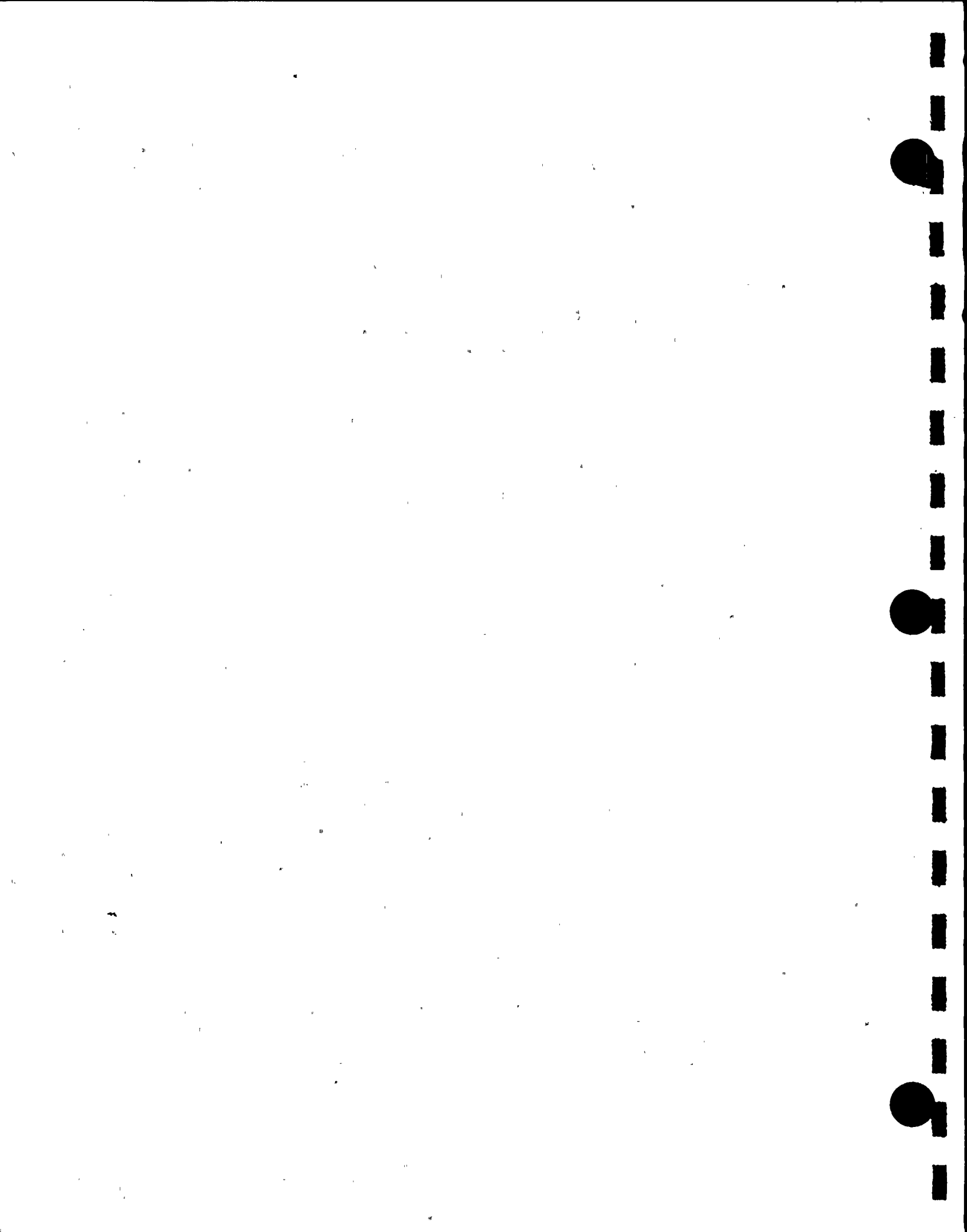


Table 2.1.1

MODULE DATA

<u>Module I.D.</u>	<u>Quantity</u>	<u>Array Cell Size</u>	<u>Total Cell Count for this Module Type</u>
A**	5	13x14	910
B	4	12x14	672
C	4	13x12	624
D	2	12x12	288
E	4	13x11	572
F	2	12x11	264
G	1	12x10	120
H*	<u>1</u>	13x14 - (8x2)	<u>166</u>
Total	23		3616

* Non-rectangular module.

** Three of the A modules have one triangle cell to accommodate pool corner curvature.



Table 2.1.2
COMMON MODULE DATA

Storage cell inside dimension:	8.75" \pm 0.04"
Storage cell height (above the baseplate):	168 \pm 1/16"
Baseplate thickness:	0.75" (nominal)
Support leg height:	5.25" (nominal)
Support leg type:	Remotely adjustable legs
Number of support legs:	4 (minimum)
Remote lifting and handling provision:	Yes
Poison material:	Boral
Poison length:	144"
Poison width:	7.5"
Cell Pitch:	8.97" (nominal)

Table 2.1.3

MODULE DATA

<u>Module I.D.</u>	<u>Dimensions (inch)*</u>		<u>Shipping Weight (kips)</u>
	<u>East-West</u>	<u>North-South</u>	
A	117-3/16	126-3/16	25.7
B	108-1/8	126-3/16	23.7
C	117-3/16	108-1/8	22.5
D	108-1/8	108-1/8	20.9
E	117-3/16	99-1/16	20.8
F	108-1/8	99-1/16	19.3
G	108-1/8	90-1/8	17.7
H	117-3/16	126-3/16	23.9

* All dimensions are bounding rectangular envelopes rounded to the nearest one sixteenth of an inch.

12

104 4 50



Table 2.3.1

BORAL EXPERIENCE LIST (Domestic and Foreign)

Pressurized Water Reactors

Plant	Utility	Vented Construc- tion	Mfg. Year
Bellefont 1, 2	Tennessee Valley Authority	No	1981
Donald C. Cook 1, 2	Indiana & Michigan Electric	No	1979
Indian Point 3	NY Power Authority	Yes	1987
Maine Yankee	Maine Yankee Atomic Power	Yes	1977
Salem 1, 2	Public Service Elec & Gas	No	1980
Seabrook	New Hampshire Yankee	No	---
Sequoyah 1,2	Tennessee Valley Authority	No	1979
Yankee Rowe	Yankee Atomic Power	Yes	1964/1983
Zion 1,2	Commonwealth Edison Co.	Yes	1980
Byron 1,2	Commonwealth Edison Co.	Yes	1988
Braidwood 1,2	Commonwealth Edison Co.	Yes	1988
Yankee Rowe	Yankee Atomic Electric	Yes	1988
Three Mile Island I	GPU Nuclear	Yes	1990

Boiling Water Reactors

Browns Ferry 1,2,3	Tennessee Valley Authority	Yes	1980
Brunswick 1,2	Carolina Power & Light	Yes	1981
Clinton	Illinois Power	Yes	1981
Cooper	Nebraska Public Power	Yes	1979
Dresden 2,3	Commonwealth Edison Co.	Yes	1981
Duane Arnold	Iowa Elec. Light & Power	No	1979
J.A. Fitzpatrick	NY Power Authority	No	1978
E.I. Hatch 1,2	Georgia Power	Yes	1981
Hope Creek	Public Service Elec & Gas	Yes	1985
Humboldt Bay	Pacific Gas & Electric	Yes	1986
LaCrosse	Dairyland Power	Yes	1976
Limerick 1,2	Philadelphia Electric	No	1980
Monticello	Northern States Power	Yes	1978
Peachbottom 2,3	Philadelphia Electric	No	1980
Perry, 1,2	Cleveland Elec. Illuminating	No	1979
Pilgrim	Boston Edison	No	1978
Shoreham	Long Island Lighting	Yes	---
Susquehanna 1,2	Pennsylvania Power & Light	No	1979
Vermont Yankee	Vermont Yankee Atomic Power	Yes	1978/1986
Hope Creek	Public Service Elec & Gas	Yes	1989



41

Table 2.3.1 (continued)

Foreign Installations Using Boral

France

12 PWR Plants	Electricite de France
---------------	-----------------------

South Africa

Koeberg 1,2	ESCOM
-------------	-------

Switzerland

Beznau 1,2	Nordostschweizerische Kraftwerke AG
Gosgen	Kernkraftwerk Gosgen-Daniken AG

Taiwan

Chin-Shan 1,2	Taiwan Power Company
---------------	----------------------

Kuosheng 1,2	Taiwan Power Company
--------------	----------------------

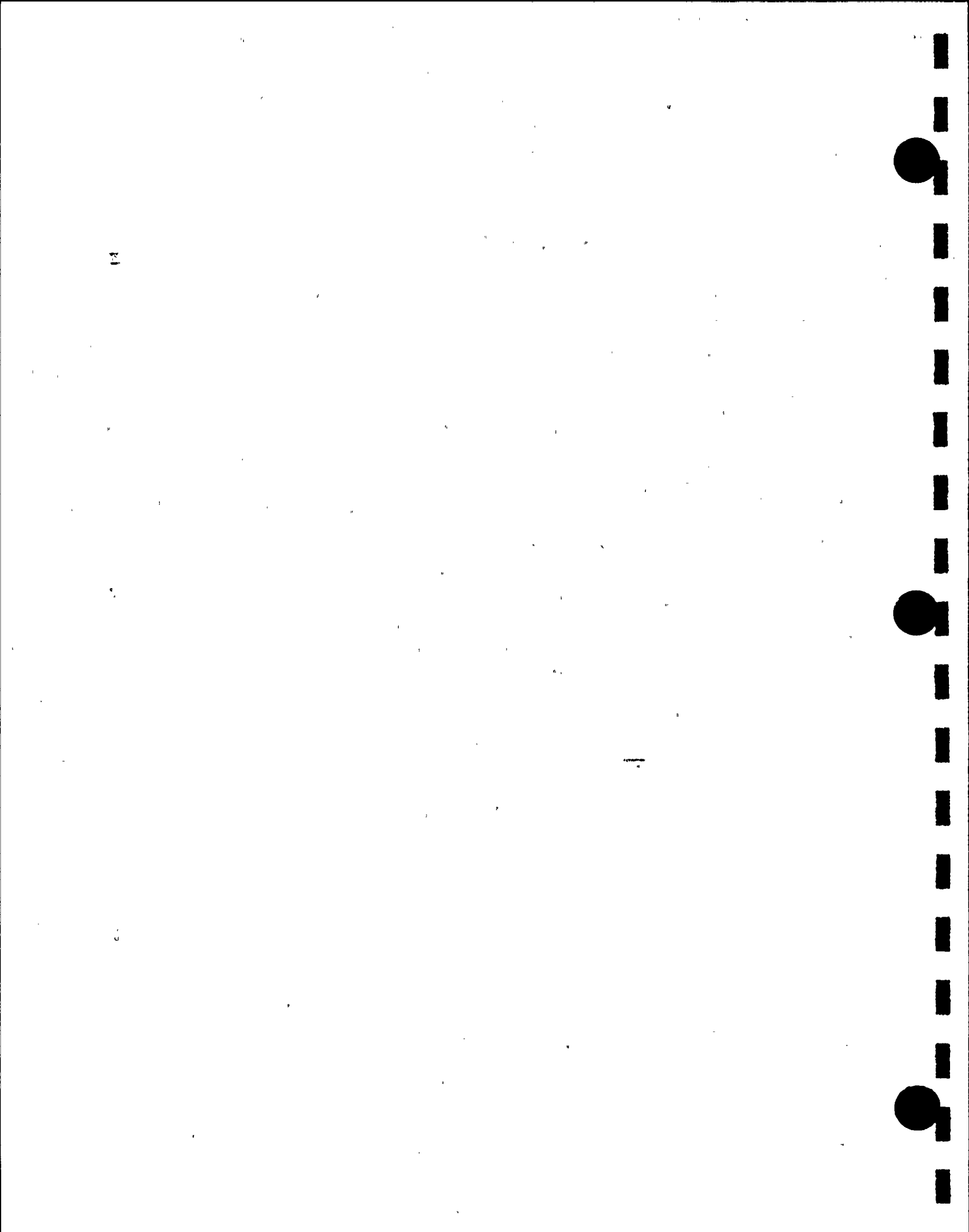


Table 2.3.2

1100 ALLOY ALUMINUM PHYSICAL AND MECHANICAL PROPERTIES

Density	0.098 lb/cu. in. 2.713 gm/cc
Melting Range	1190-1215 deg. F 643-657 deg. C
Thermal Conductivity (77 deg. F)	128 BTU/hr/sq ft/deg. F/ft 0.53 cal/sec/sq cm/deg. C/cm
Coef. of Thermal Expansion (68-212 deg. F)	13.1 x 10 ⁻⁶ /deg. F 23.6 x 10 ⁻⁶ /deg. C
Specific heat (221 deg. F)	0.22 BTU/lb/deg. F 0.23 cal/gm/deg. C
Modulus of Elasticity	10x10 ⁶ psi
Tensile Strength (75 deg. F)	13,000 psi annealed 18,000 psi as rolled
Yield Strength (75 deg. F)	5,000 psi annealed 17,000 psi as rolled
Elongation (75 deg. F)	35-45% annealed 9-20% as rolled
Hardness (Brinell)	23 annealed 32 as rolled
Annealing Temperature	650 deg. F 343 deg. C



Table 2.3.3

CHEMICAL COMPOSITION (by weight) - ALUMINUM (1100 Alloy)

99.00% min.	Aluminum
1.00% max.	Silicone and Iron
0.05-0.20% max.	Copper
.05% max.	Manganese
.10% max.	Zinc
.15% max.	others each

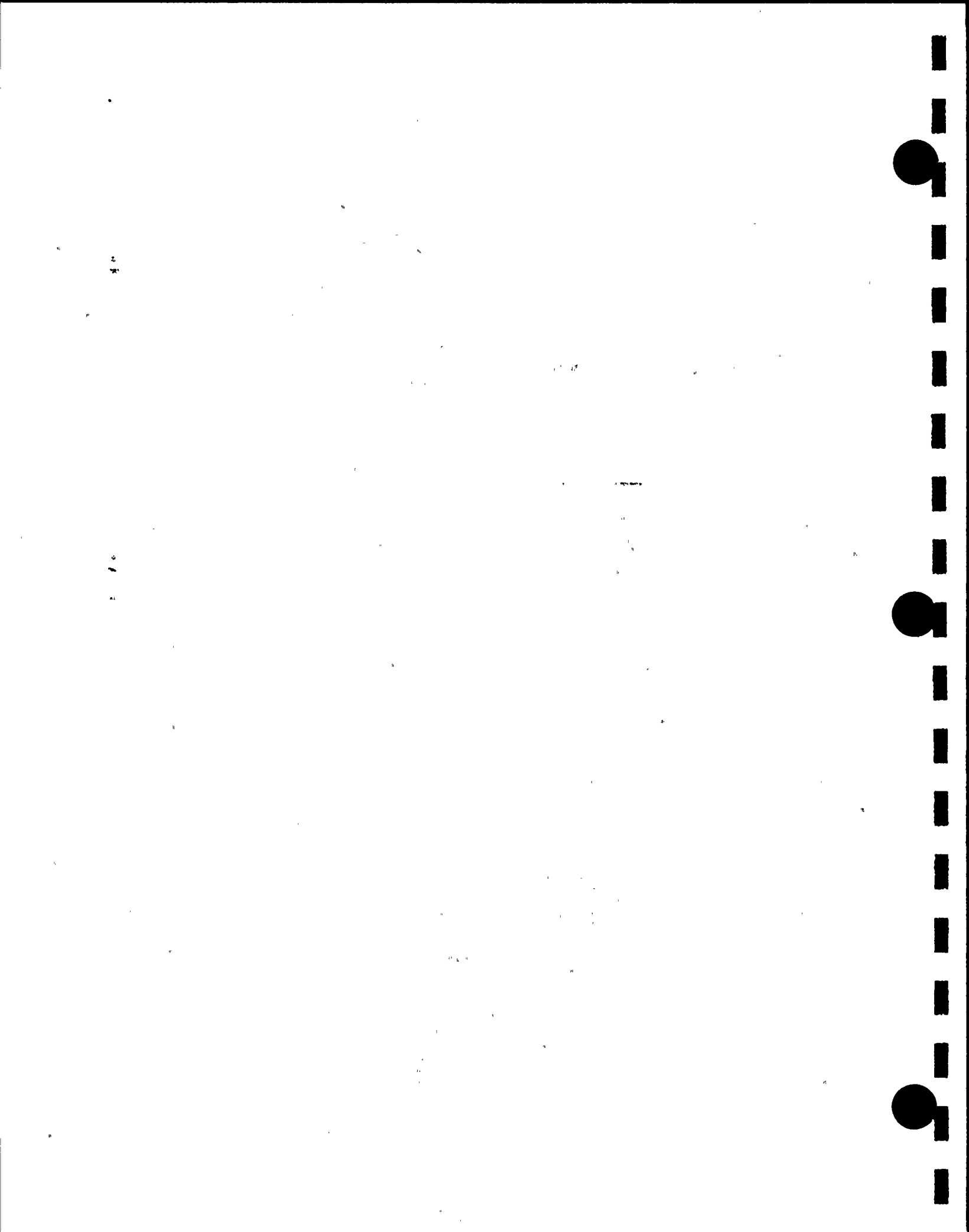


Table 2.3.4

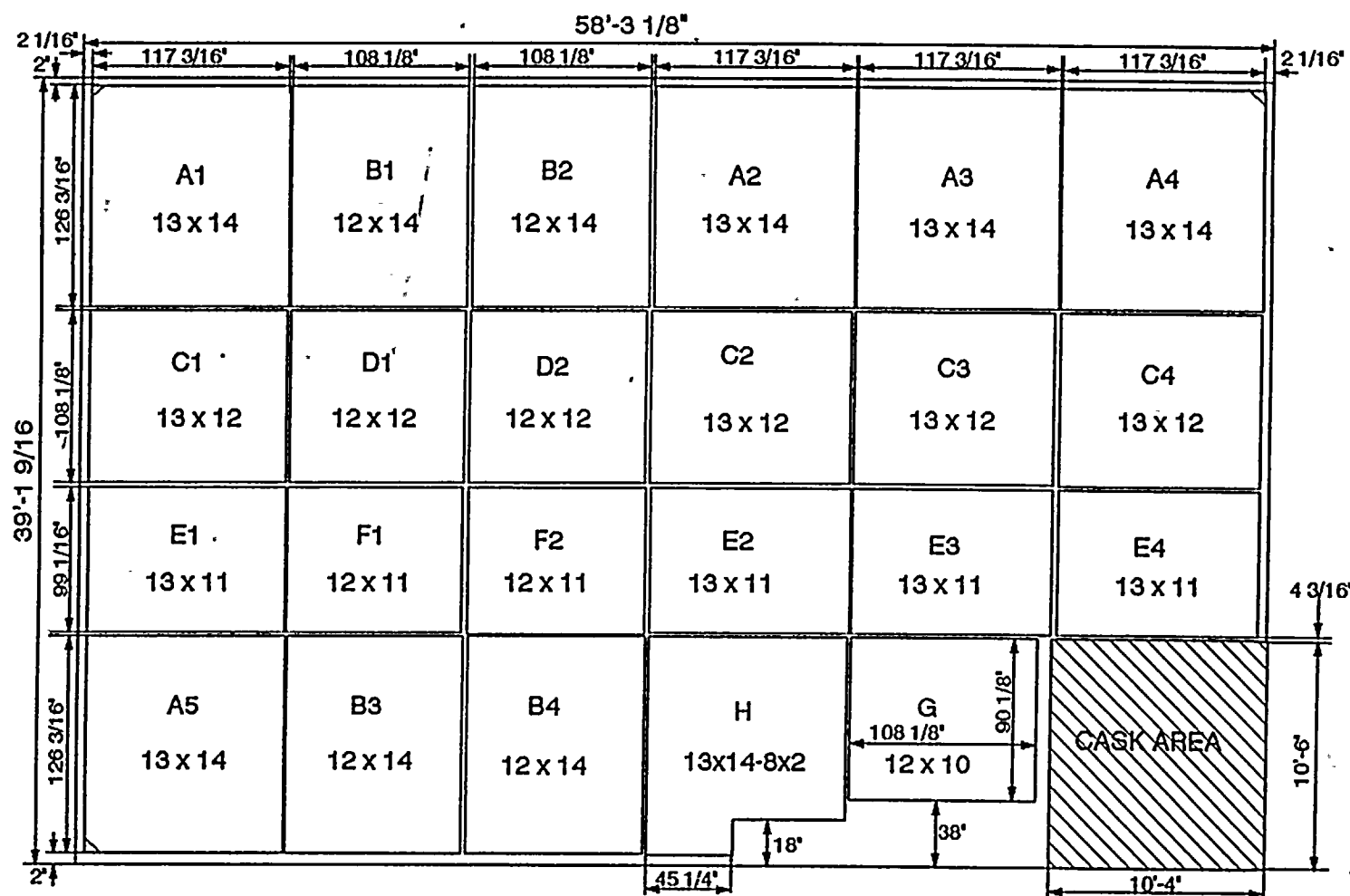
BORON CARBIDE CHEMICAL COMPOSITION, Weight %

Total boron	70.0 min.
B ¹⁰ isotopic content in natural boron	18.0
Boric oxide	3.0 max.
Iron	2.0 max.
Total boron plus total carbon	94.0 min.

BORON CARBIDE PHYSICAL PROPERTIES

Chemical formula	B ₄ C
Boron content (weight)	78.28%
Carbon content (weight)	21.72%
Crystal Structure	rombohedral
Density	2.51 gm./cc-0.0907 lb/cu. in.
Melting Point	2450 ⁰ C (4442 ⁰ F)
Boiling Point	3500 ⁰ C (6332 ⁰ F)
Microscopic thermal-neutron cross-section	600 barn





Typical Rack-to-Rack Gap: 2"

Total Storage: 3616 cells (Include 3 triangular corner cells)

FIGURE 2.1.1 COOK SPENT FUEL POOL LAYOUT



3.0

CONSTRUCTION OF RACK MODULES

The object of this section is to provide a description of rack module construction for the Donald C. Cook spent fuel pool to enable an independent appraisal of the adequacy of the design. Similar rack structure designs have recently been used in previous licensing efforts for Kuosheng Units 1 & 2 (Taiwan Power Company); J.A. FitzPatrick (New York Power Authority); Indian Point 2 (Consolidated Edison Company of New York, Inc.); Three Mile Island Unit 1 (GPU Nuclear); and Hope Creek 1 (Public Service Electric & Gas Company). A list of applicable codes and standards is also presented.

3.1

Fabrication Objective

The requirements in manufacturing the high density storage racks for the Donald C. Cook fuel pool may be stated in four interrelated points:

- (1) The rack module will be fabricated in such a manner that there is no weld splatter on the storage cell surfaces which would come in contact with the fuel assembly.
- (2) The storage locations will be constructed so that redundant flow paths for the coolant are available.
- (3) The fabrication process involves operational sequences which permit immediate verification by the inspection staff.
- (4) The storage cells are connected to each other by austenitic stainless steel corner welds which leads to a honeycomb lattice construction. The extent of welding is selected to "detune" the racks from the seismic input motion of the Operating Basis Earthquake (OBE) and Design Basis Earthquake (DBE).



11
12
13
14

15
16

17
18

3.2 Mixed Zone Two Region Storage

All rack modules designed and fabricated for the Donald C. Cook spent fuel pool are of the so-called "non-flux trap" type. In the non-flux trap modules, a single screen of the poison panel is interposed between two fuel assemblies. The poison material utilized in this project is Boral, which does not require lateral support to prevent slumping due to the inherent stiffness. However, accurate dimensional control of the poison location is essential for nuclear criticality and thermal-hydraulic considerations. The design and fabrication approach to realize this objective is presented in the next sub-section.

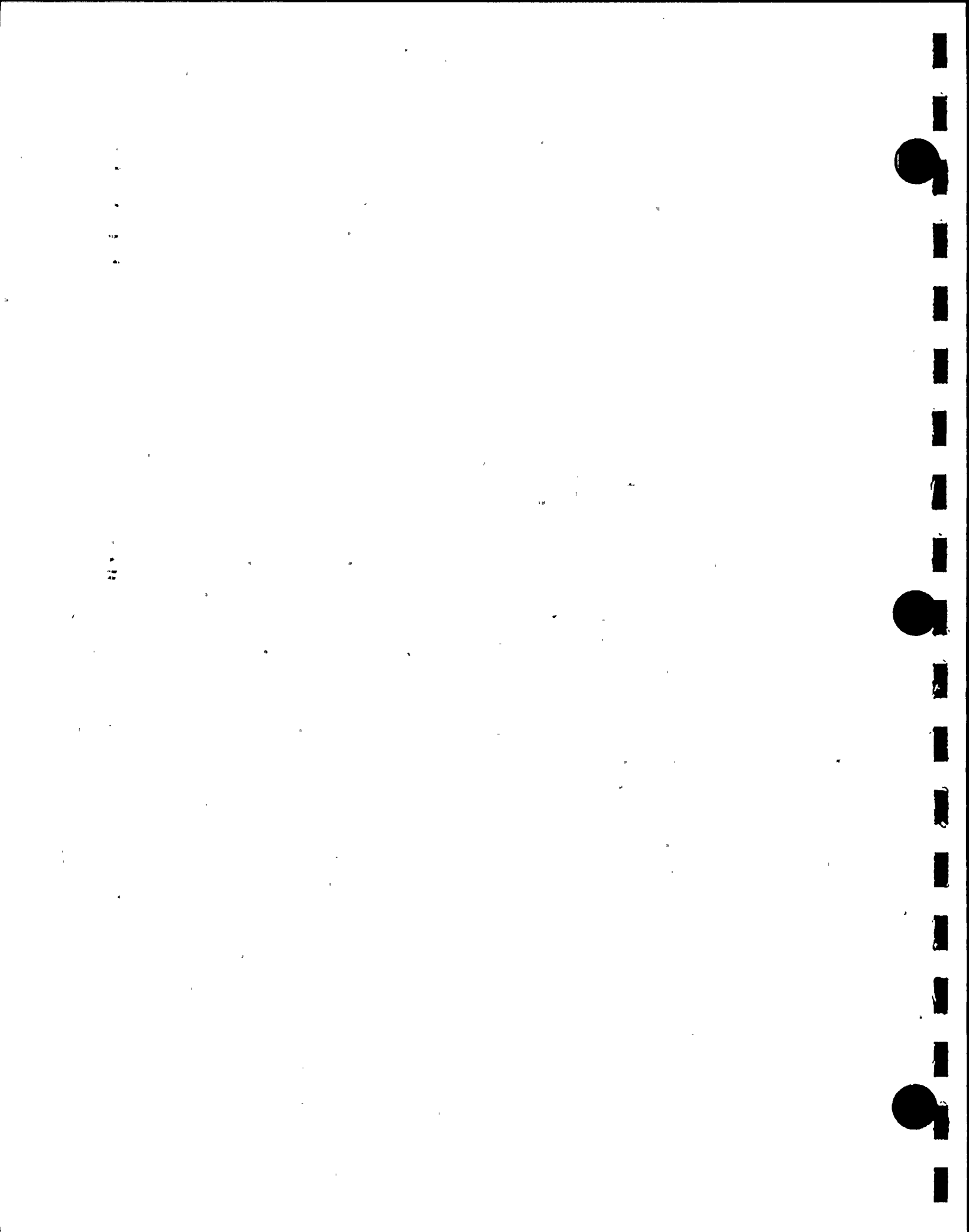
3.3 Anatomy of Rack Modules

As stated earlier, the storage cell locations have a single poison panel between adjacent austenitic stainless steel surfaces. The significant components of the rack module are: (1) the storage box subassembly (2) the baseplate, (3) the thermal neutron absorber material, (4) picture frame sheathing, and (5) support legs.

- (1) The rack module manufacturing begins with fabrication of the box. The "boxes" are fabricated from two precision formed channels by seam welding in a machine equipped with copper chill bars and pneumatic clamps to minimize distortion due to welding heat input. Figure 3.3.1 shows the box.

The minimum weld penetration will be 80% of the box metal gage which is 0.075" (14 gage). The boxes are manufactured to 8.75" I.D. (nominal inside dimension).

The design objective calls for installing Boral with minimal surface loading. This is accomplished by die forming a "picture frame sheathing" as shown in Figure



3.3.2. This sheathing is 0.035" thick and is made to precise dimensions such that the offset is .010" to .005" greater than the poison material thickness.

As shown in Figure 3.3.1, each box has four lateral 1" diameter holes punched near its bottom edge to provide auxiliary flow holes. The edges of the sheathing and the box are welded together to form a smooth edge. The box, with integrally connected sheathing, is referred to as the "composite box".

The "composite boxes" are arranged in a checkerboard array to form an assemblage of storage cell locations (Figure 3.3.3). The inter-box welding and pitch adjustment are accomplished by small longitudinal connectors. Further details are given later in this section.

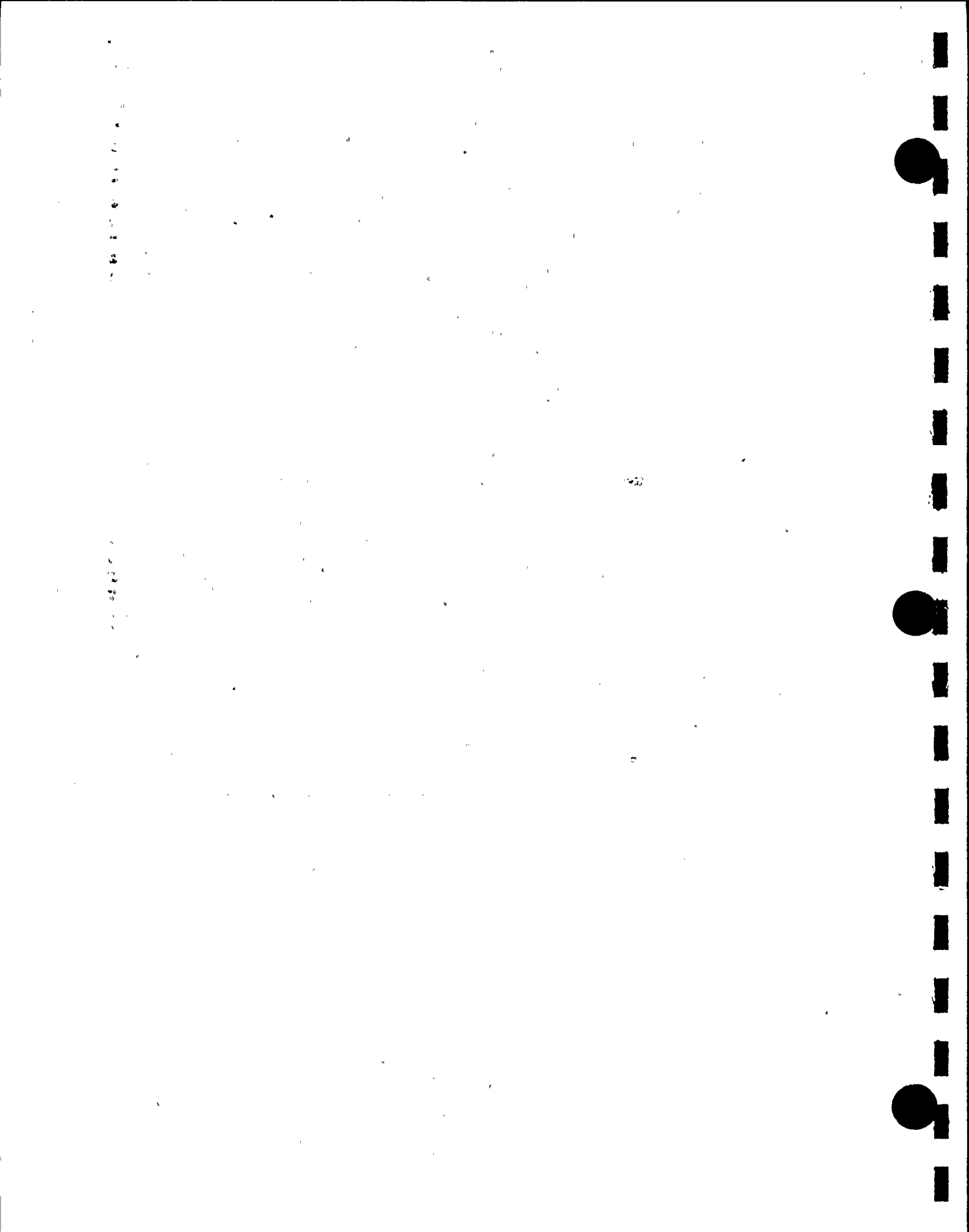
This assemblage of box assemblies is welded edge-to-edge as shown in Figure 3.3.3, resulting in a honeycomb structure with axial, flexural and torsional rigidity depending on the extent of intercell welding provided. It can be seen from Figure 3.3.3 that the edges of each interior box are connected to the contiguous boxes resulting in a well defined path to resist shear.

- (2) Baseplate: The baseplate provides a continuous horizontal surface for supporting the fuel assemblies.

The baseplate is attached to the cell assemblage by fillet welds. The baseplate in each storage cell has a 5" diameter flow hole. The baseplate is 3/4" thick to withstand accident fuel assembly drop loads postulated and discussed in Section 7 of this report.

- (3) The thermal neutron absorber material: As mentioned in the preceding section, Boral is used as the thermal neutron absorber material.

- (4) Picture Frame Sheathing: As described earlier, the sheathing serves as the locator and retainer of the poison material. Figure 3.3.2 shows a schematic of the sheathing.



The poison material is placed in the customized flat depression region of the sheathing, which is next laid on a side of the "box". The precision of the shape of the sheathing obtained by die forming guarantees that the poison sheet installed in it will not be subject to surface compression. The flanges of the sheathing (on all four sides) are attached to the box using skip welds. The sheathing serves to locate and position the poison sheet accurately, and to preclude its movement under seismic conditions.

- (5) Support Legs: All support legs are the adjustable type (Figure 3.3.4). The top portion is made of austenitic steel material. The bottom part is made of SA564-630 stainless steel to avoid galling problems.

Each support leg is equipped with a readily accessible socket to enable remote leveling of the rack after its placement in the pool. Lateral holes in the support leg provide the requisite coolant flow path.

An elevation cross-section of the rack module shown in Figure 3.3.5 shows two box cells, and a developed cell in elevation. The Boral panels and their location are also indicated in this figure. The boral panels are positioned such that the entire enriched fuel portion of the fuel assembly is enveloped by the thermal neutron absorber material.

The joint between the composite box arrays and the baseplate is made by single fillet welds which provide a minimum of 7" of connectivity between each cell wall and the baseplate surface.

As shown in Figure 3.3.4, the support leg is gusseted to provide an increased section for load transfer between the support legs and the cellular structure above the baseplate. Use of the gussets also minimizes heat input induced distortions of the support/baseplate contact region.



3.4 Codes, Standards, and Practices for the Donald C. Cook Spent Fuel Pool Racks

The fabrication of the rack modules for the Donald C. Cook spent fuel pool is performed under a strict quality assurance system suitable for manufacturing and complying with the provisions of 10CFR50 Appendix B.

The following codes, standards and practices will be used as applicable for the design, construction, and assembly of the spent fuel storage racks. Additional specific references related to detailed analyses are given in each section.

a. Codes and Standards for Design and Testing

- (1) AISC Manual of Steel Construction, 8th Edition, 1980.
- (2) ANSI N210-1976, "Design Objectives for Light Water Reactor Spent Fuel Storage Facilities at Nuclear Power Stations".
- (3) American Society of Mechanical Engineers (ASME), Boiler and Pressure Vessel Code, Section III, Subsection NF, 1989.
- (4) ASNT-TC-1A, June, 1980 American Society for Nondestructive Testing (Recommended Practice for Personnel Qualifications).
- (5) ASME Section V - Nondestructive Examination
- (6) ASME Section IX - Welding and Brazing Qualifications
- (7) Building Code Requirements for Reinforced Concrete, ACI318-89/ACI318R-89.



- (8) Code Requirements for Nuclear Safety Related Concrete Structures, ACI 349-85 and Commentary ACI 349R-85
- (9) Reinforced Concrete Design for Thermal Effects on Nuclear Power Plant Structures, ACI 349.1R-80 .
- (10) ACI Detailing Manual - 1980
- (11) ASME NQA-2, Part 2.7 "Quality Assurance Requirements of Computer Software for Nuclear Facility Applications (draft).
- (12) ANSI/ASME, Qualification and Duties of Personnel Engaged in ASME Boiler and Pressure Vessel Code Section III, Div. 1, Certifying Activities, N626-3-1977.

b. Material Codes

- (1) American Society for Testing and Materials (ASTM) Standards - A-240.
- (2) American Society of Mechanical Engineers (ASME), Boiler and Pressure Vessel Code, Section II - Parts A and C, 1989.

c. Welding Codes

ASME Boiler and Pressure Vessel Code, Section IX-Welding and Brazing Qualifications (1986) or later issue accepted by USNRC.

d. Quality Assurance, Cleanliness, Packaging, Shipping, Receiving, Storage, and Handling Requirements

- (1) ANSI N45.2.2 - Packaging, Shipping, Receiving, Storage and Handling of Items for Nuclear Power Plants.
- (2) ANSI 45.2.1 - Cleaning of Fluid Systems and Associated Components during Construction Phase of Nuclear Power Plants.



2

3

4

5

6

7

- (3) ASME Boiler and Pressure Vessel, Section V, Nondestructive Examination, 1983 Edition, including Summer and Winter Addenda, 1983.
- (4) ANSI - N16.1-75 Nuclear Criticality Safety Operations with Fissionable Materials Outside Reactors.
- (5) ANSI - N16.9-75 Validation of Calculation Methods for Nuclear Criticality Safety.
- (6) ANSI - N45.2.11, 1974 Quality Assurance Requirements for the Design of Nuclear Power Plants.
- (7) ANSI 14.6-1978, "Special Lifting Devices for Shipping Containers weighing 10,000 lbs. or more for Nuclear Materials".
- (8) ANSI N45.2.6, Qualification of Inspection and Testing Personnel.
- (9) ANSI N45.2.8, Installation, Inspection.
- (10) ANSI N45.2.9, Records.
- (11) ANSI N45.2.10, Definitions.
- (12) ANSI N45.2.12, QA Audits.
- (13) ANSI N45.2.13, Procurement.
- (14) ANSI 45.2.23, QA Audit Personnel.

e. Other References

(In the references below, RG is NRC Regulatory Guide)

- (1) RG 1.13 - Spent Fuel Storage Facility Design Basis, Rev. 2 (proposed).
- (2) RG 1.123 - (endorses ANSI N45.2.13) Quality Assurance Requirements for Control of Procurement of Items and Services for Nuclear Power Plants.
- (3) RG 1.124 - Service Limits and Loading Combinations for Class 1 Linear Type Component Supports, Rev. 1.



- (4) RG 1.25 - Assumptions Used for Evaluating the Potential Radiological Consequences of a Fuel Handling Accident in the Fuel Handling and Storage Facility of Boiling and Pressurized Water Reactors.
- (5) RG 1.28 - (endorses ANSI N45.2) - Quality Assurance Program Requirements, June, 1972.
- (6) RG 1.29 - Seismic Design Classification, Rev. 3.
- (7) RG 1.31 - Control of Ferrite Content in Stainless Steel Weld Metal, Rev. 3.
- (8) RG 1.38 - (endorses ANSI N45.2.2) Quality Assurance Requirements for Packaging, Shipping, Receiving, Storage and Handling of Items for Water-Cooled Nuclear Power Plants, March, 1973.
- (9) RG 1.44 - Control of the Use of Sensitized Stainless Steel.
- (10) RG 1.58 - (endorses ANSI N45.2.2) Qualification of Nuclear Power Plant Inspection, Examination, and Testing Personnel, Rev. 1, September, 1980.
- (11) RG 1.64 - (endorses ANSI N45.2.11) Quality Assurance Requirements for the Design of Nuclear Power Plants, October, 1973.
- (12) RG 1.71 - Welder Qualifications for Areas of Limited Accessibility.
- (13) RG 1.74 - (endorses ANSI N45.2.10) Quality Assurance Terms and Definitions, February, 1974.
- (14) RG 1.85 - Materials Code Case Acceptability ASME Section III, Division 1.
- (15) RG 1.88 - (endorses ANSI N45.2.9) Collection, Storage and Maintenance of Nuclear Power Plant Quality Assurance Records, Rev. 2, October, 1976.
- (16) RG 1.92 - Combining Modal Responses and Spatial Components in Seismic Response Analysis.

- (17) RG 3.41 - Validation of Calculation Methods for Nuclear Criticality Safety.
- (18) General Design Criteria for Nuclear Power Plants, Code of Federal Regulations, Title 10, Part 50, Appendix A (GDC Nos. 1, 2, 61, 62, and 63).
- (19) NUREG-0800, Standard Review Plan, Sections 3.2.1, 3.2.2, 3.7.1, 3.7.2, 3.7.3, 3.8.4.
- (20) "OT Position for Review and Acceptance of Spent Fuel Storage and Handling Applications," dated April 14, 1978, and the modifications to this document of January 18, 1979. (Note: OT stands for Office of Technology).
- (21) NUREG-0612, "Control of Heavy Loads at Nuclear Power Plants".
- (22) Regulatory Guide 8.8, "Information Relative to Ensuring that Occupational Radiation Exposure at Nuclear Power Plants will be as Low as Reasonably Achievable (ALARA).
- (23) 10CFR50 Appendix B, Quality Assurance Criteria for Nuclear Power Plants and Fuel Reprocessing Plants
- (24) 10CFR21 - Reporting of Defects and Non-Compliance

3.5

Materials of Construction.

Storage Cell:	ASME SA240-304
Baseplate:	ASME SA240-304
Support Leg (female):	ASME SA240-304
Support Leg (male):	Ferritic stainless steel (anti-galling material) ASME SA564-630
Poison:	Boral



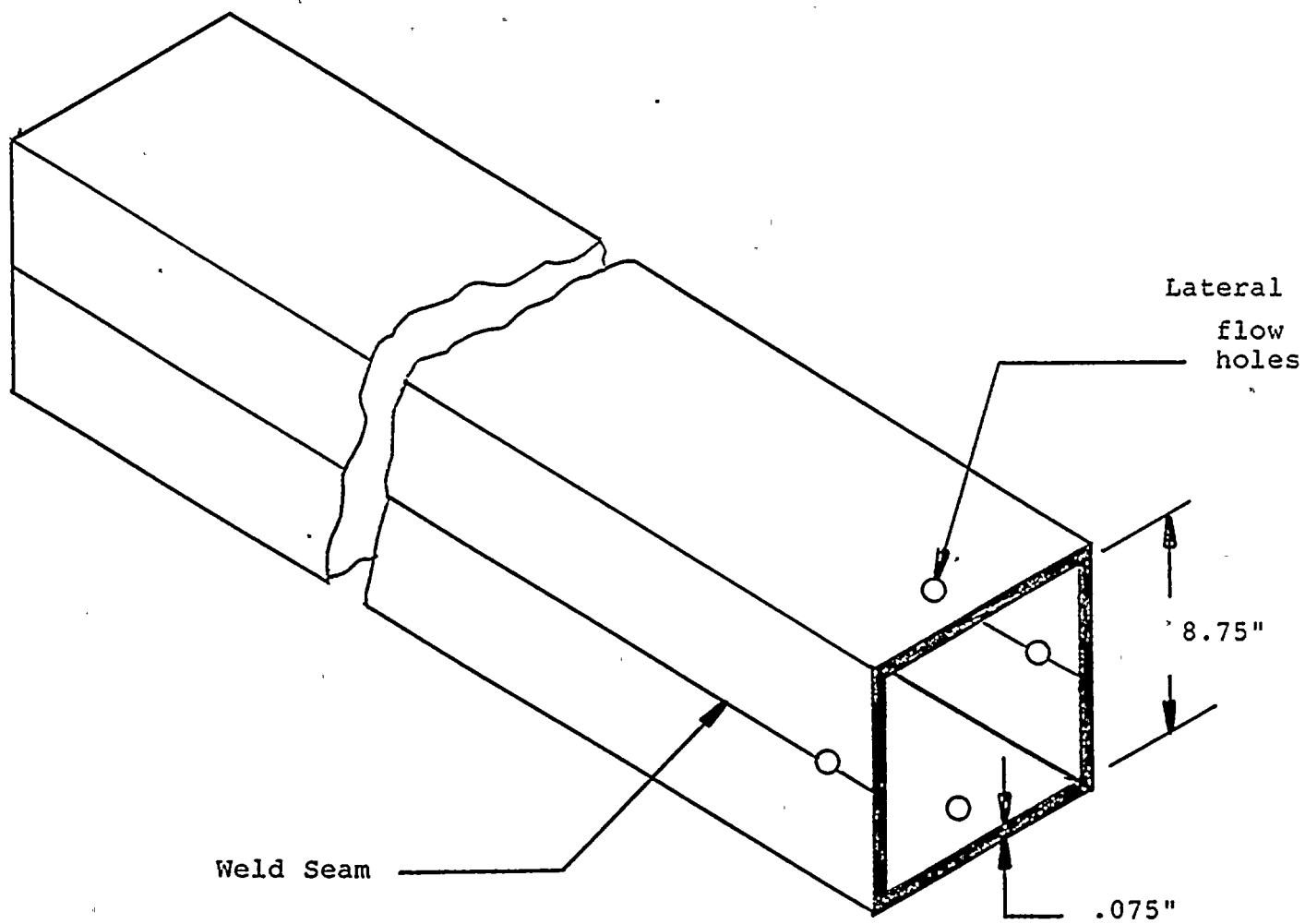


Figure 3.3.1 SEAM WELDING PRECISION FORMED CHANNELS



3-11

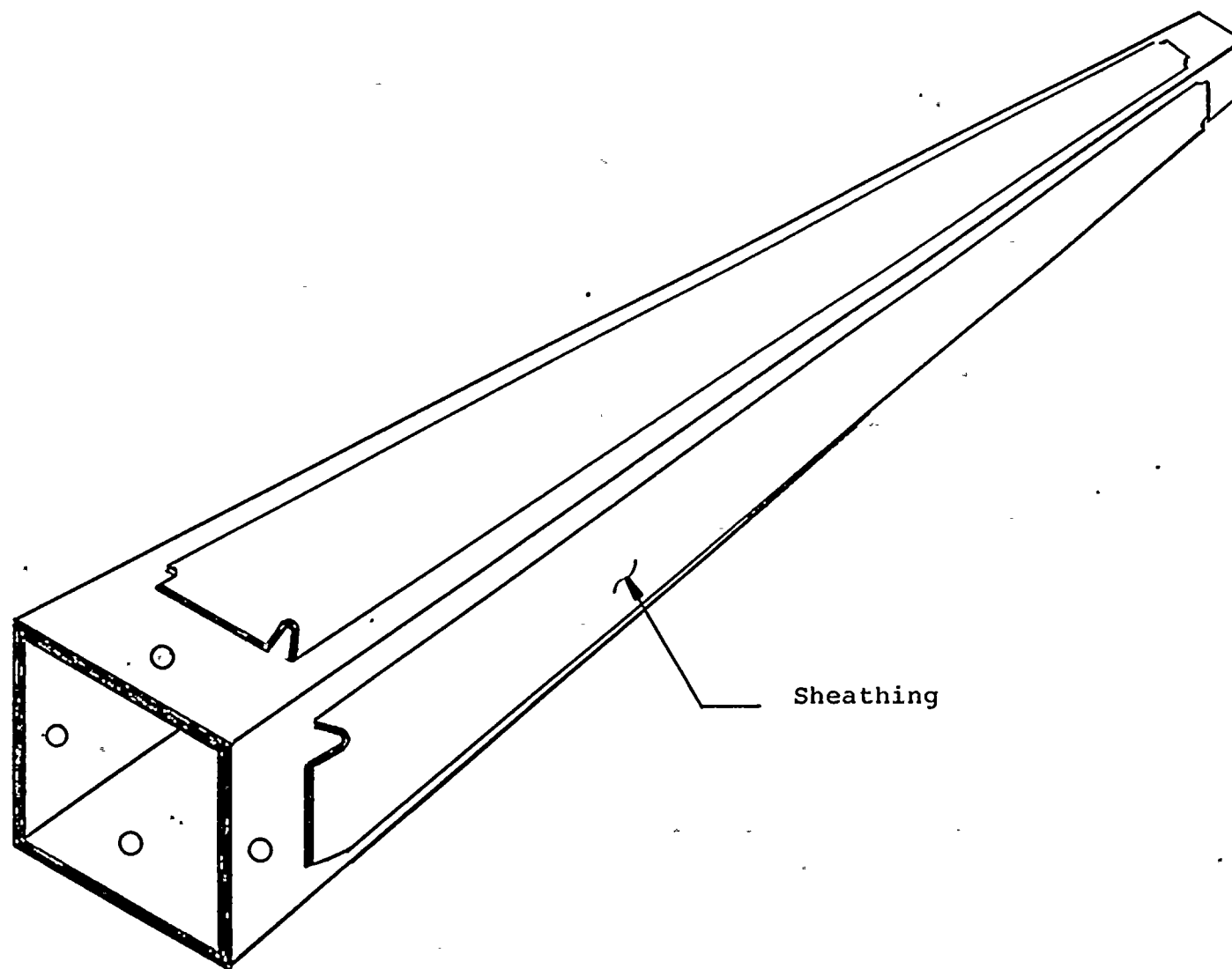


Figure 3.3.2 COMPOSITE BOX ASSEMBLY

55

11

12



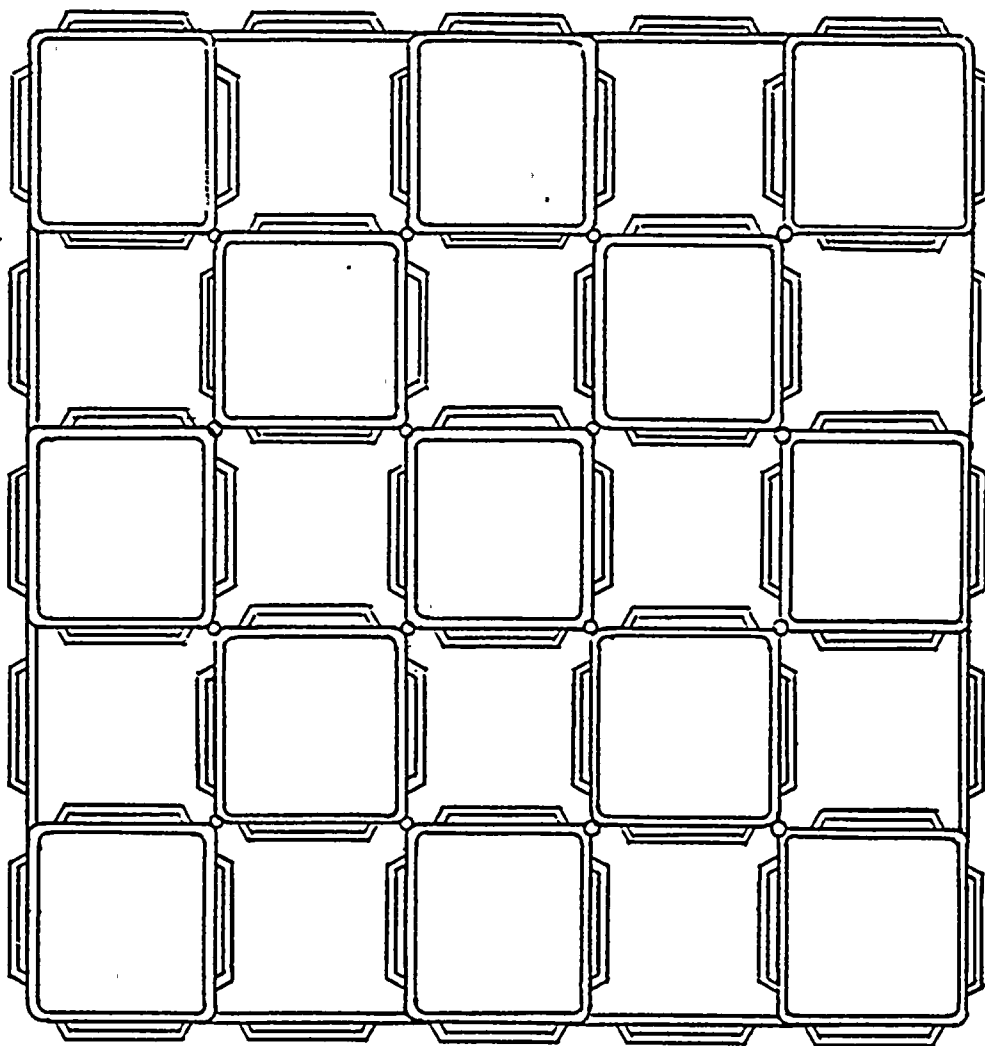


Figure 3.3.3 ARRAY OF CELLS FOR NON-FLUX TRAP MODULES



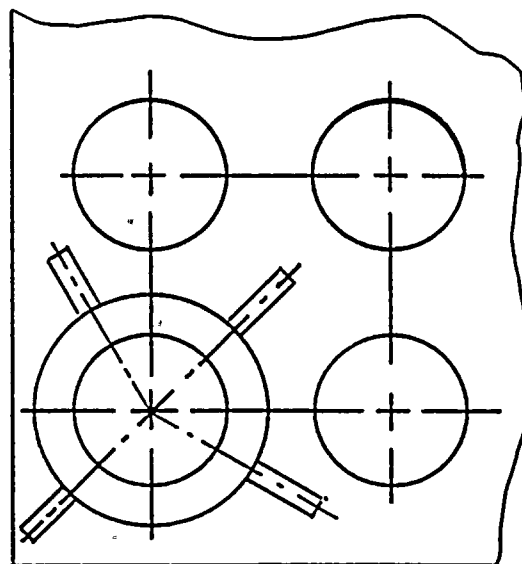
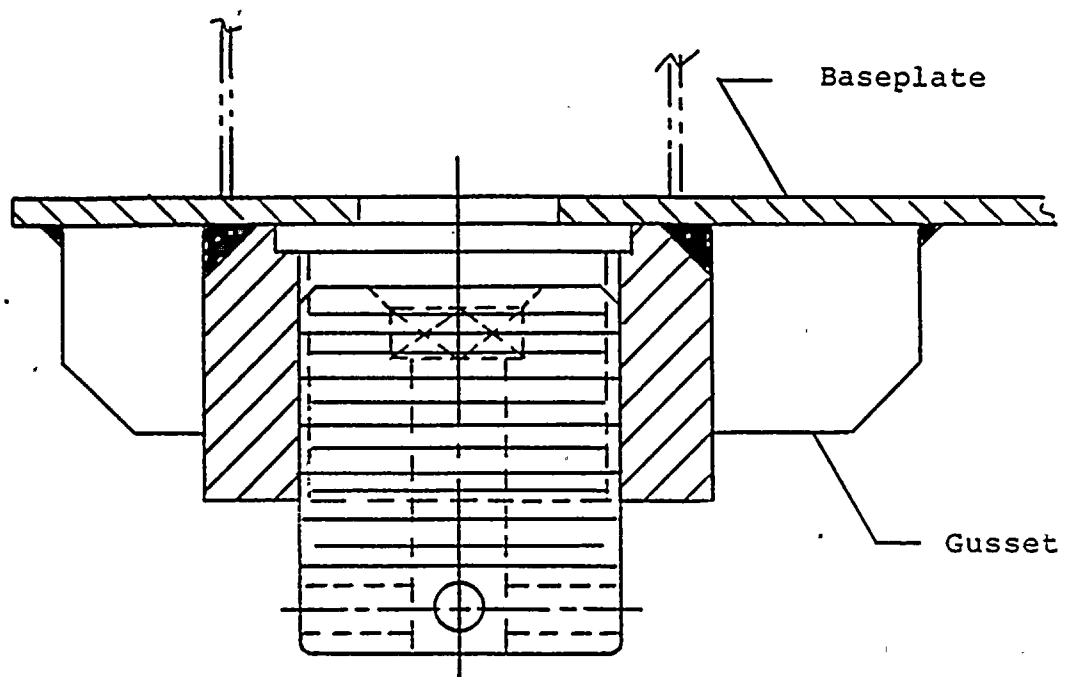


Figure 3.3.4 ADJUSTABLE SUPPORT LEG



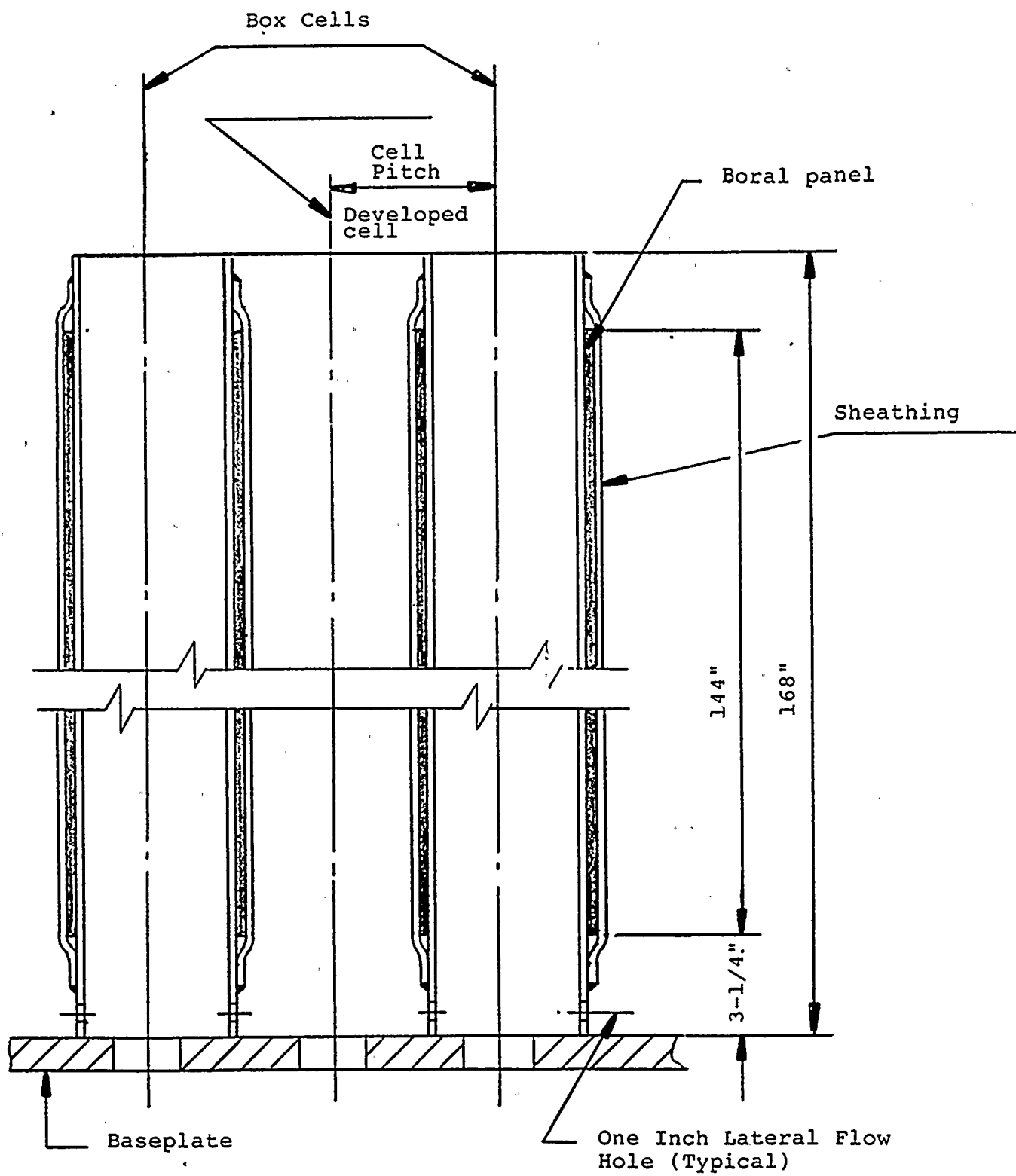


Figure 3.3.5 ELEVATION VIEW OF RACK MODULE



4.0 CRITICALITY SAFETY ANALYSES

4.1 Design Basis

The high density spent fuel storage racks for Donald C. Cook Nuclear Plant are designed to assure that the effective neutron multiplication factor (k_{eff}) is equal to or less than 0.95 with the racks fully loaded with fuel of the highest anticipated reactivity, and flooded with unborated water at the temperature within the operating range corresponding to the highest reactivity. The maximum calculated reactivity includes a margin for uncertainty in reactivity calculations including mechanical tolerances. All uncertainties are statistically combined, such that the final k_{eff} will be equal to or less than 0.95 with a 95% probability at a 95% confidence level.

Applicable codes, standards, and regulations or pertinent sections thereof, include the following:

- o General Design Criteria 62, Prevention of Criticality in Fuel Storage and Handling.
- o USNRC Standard Review Plan, NUREG-0800, Section 9.1.2, Spent Fuel Storage, Rev. 3 - July 1981
- o USNRC letter of April 14, 1978, to all Power Reactor Licensees - OT Position for Review and Acceptance of Spent Fuel Storage and Handling Applications, including modification letter dated January 18, 1979.
- o USNRC Regulatory Guide 1.13, Spent Fuel Storage Facility Design Basis, Rev. 2 (proposed), December 1981.
- o ANSI ANS-8.17-1984, Criticality Safety Criteria for the Handling, Storage and Transportation of LWR Fuel Outside Reactors.



To assure the true reactivity will always be less than the calculated reactivity, the following conservative assumptions were made:

- o Moderator is assumed to be unborated water at a temperature within the operating range that results in the highest reactivity (determined to be 20 °C).
- o The effective multiplication factor of an infinite radial array of fuel assemblies was used (see section 4.4.1) except for the boundary storage cells where leakage is inherent.
- o Neutron absorption in minor structural members is neglected, i.e., spacer grids are analytically replaced by water.

The design basis fuel assembly is a 15 x 15 (Standard) Westinghouse containing UO_2 at a maximum initial enrichment of 4.95 ± 0.05 wt% U-235 by weight. For fuel assemblies with natural UO_2 blankets, the enrichment is that of the central enriched zone. Calculations confirmed that this reference design fuel assembly was the most reactive of the assembly types expected to be stored in the racks. Three separate storage regions are provided in the spent fuel storage pool, with independent criteria defining the highest potential reactivity in each of the two regions as follows:

- o Region 1 is designed to accommodate new fuel with a maximum enrichment of 4.95 ± 0.05 wt% U-235, or spent fuel regardless of the discharge fuel burnup.
- o Region 2 is designed to accommodate fuel of 4.95% initial enrichment burned to at least 50,000 MWD/MtU (assembly average), or fuel of other enrichments with a burnup yielding an equivalent reactivity.
- o Region 3 is designed to accommodate fuel of 4.95% initial enrichment burned to at least 38,000 MWD/MtU (assembly average), or fuel of other enrichments with a burnup yielding an equivalent reactivity.



The water in the spent fuel storage pool normally contains soluble boron which would result in large subcriticality margins under actual operating conditions. However, the NRC guidelines, based upon the accident condition in which all soluble poison is assumed to have been lost, specify that the limiting k_{eff} of 0.95 for normal storage be evaluated in the absence of soluble boron. The double contingency principle of ANSI N-16.1-1975 and of the April 1978 NRC letter allows credit for soluble boron under other abnormal or accident conditions since only a single independent accident need be considered at one time. Consequences of abnormal and accident conditions have also been evaluated, where "abnormal" refers to conditions which may reasonably be expected to occur during the lifetime of the plant and "accident" refers to conditions which are not expected to occur but nevertheless must be protected against.



4.2 Summary of Criticality Analyses

4.2.1 Normal Operating Conditions

The design basis layout of storage cells for the three regions is shown in Figure 4.1. In this configuration, the fresh fuel cells (Region 1) are located alternately along the rack periphery (where neutron leakage reduces reactivity) or along the boundary between two storage modules (where the water gap provides a flux-trap which reduces reactivity). High burnup fuel in Region 2 affords a low-reactivity barrier between fresh fuel assemblies and Region 3 fuel of intermediate burnup. There are at the present time, an adequate number of spent fuel assemblies to nearly fill and "block off" the Region 2 barrier locations (see Section 4.7). Thus, the administrative controls required are comparable to a conventional two-region storage rack design.

Prior to approaching the reactor end-of-life, not all storage cells are needed for spent fuel. Therefore, an alternative configuration may be used in which the internal cells are loaded in a checkerboard pattern of fresh fuel (or fuel of any burnup) with empty cells, as indicated in Figure 4.2. This configuration is intended primarily to facilitate a full core unload when needed, prior to the time the racks are beginning to fill up.

Figure 4.3 define the acceptable burnup domains and illustrates the limiting burnup for fuel of various initial enrichments for both Region 2 (upper curve) or Region 3 (lower curve), both of which assume that the fresh fuel (Region 1) is enriched to 4.95% U-235. Criticality analyses show that the most reactive configuration occurs along the boundary between modules with the reactivity of

100 100 100 100

100

100 100 100



the edge configuration being slightly lower*. The bounding criticality analyses are summarized in Table 4.1 for the design basis storage condition (which assumes the single accident condition of the loss of all soluble boron) and in Table 4.2 for the interim checkerboard loading arrangement. The calculated maximum reactivity of 0.940 (same for both the normal storage condition and the interim checkerboard arrangement) is within the regulatory limit of a k_{eff} of 0.95. This maximum reactivity includes calculational uncertainties and manufacturing tolerances (95% probability at the 95% confidence level), an allowance for uncertainty in depletion calculations and the evaluated effect of the axial distribution in burnup. Fresh fuel of less than 4.95% enrichment would result in lower reactivities. As cooling time increases in long-term storage, decay of Pu-241 results in a continuous decrease in reactivity, which provides an increasing subcriticality margin with time. No credit is taken for this decrease in reactivity other than to indicate conservatism in the calculations.

The burnup criteria identified above (Figure 4-3) for acceptable storage in Region 2 and Region 3 can be implemented in appropriate administrative procedures to assure verified burnup as specified in the proposed Regulatory Guide 1.13, Revision 2. Administrative procedures will also be employed to confirm and assure the presence of soluble poison in the pool water during fuel handling operations, as a further margin of safety and as a precaution in the event of fuel misplacement during fuel handling operations.

* The thick base-plate on the rack modules extend beyond the storage cells and provide assurance that the necessary water-gap between modules is maintained.

Page 1 of 1

2

3



For convenience, the minimum (limiting) burnup data in Figure 4.3 for unrestricted storage may be described as a function of the initial enrichment, E, in weight percent U-235 by fitted polynomial expressions as follows;

For Region 2 Storage

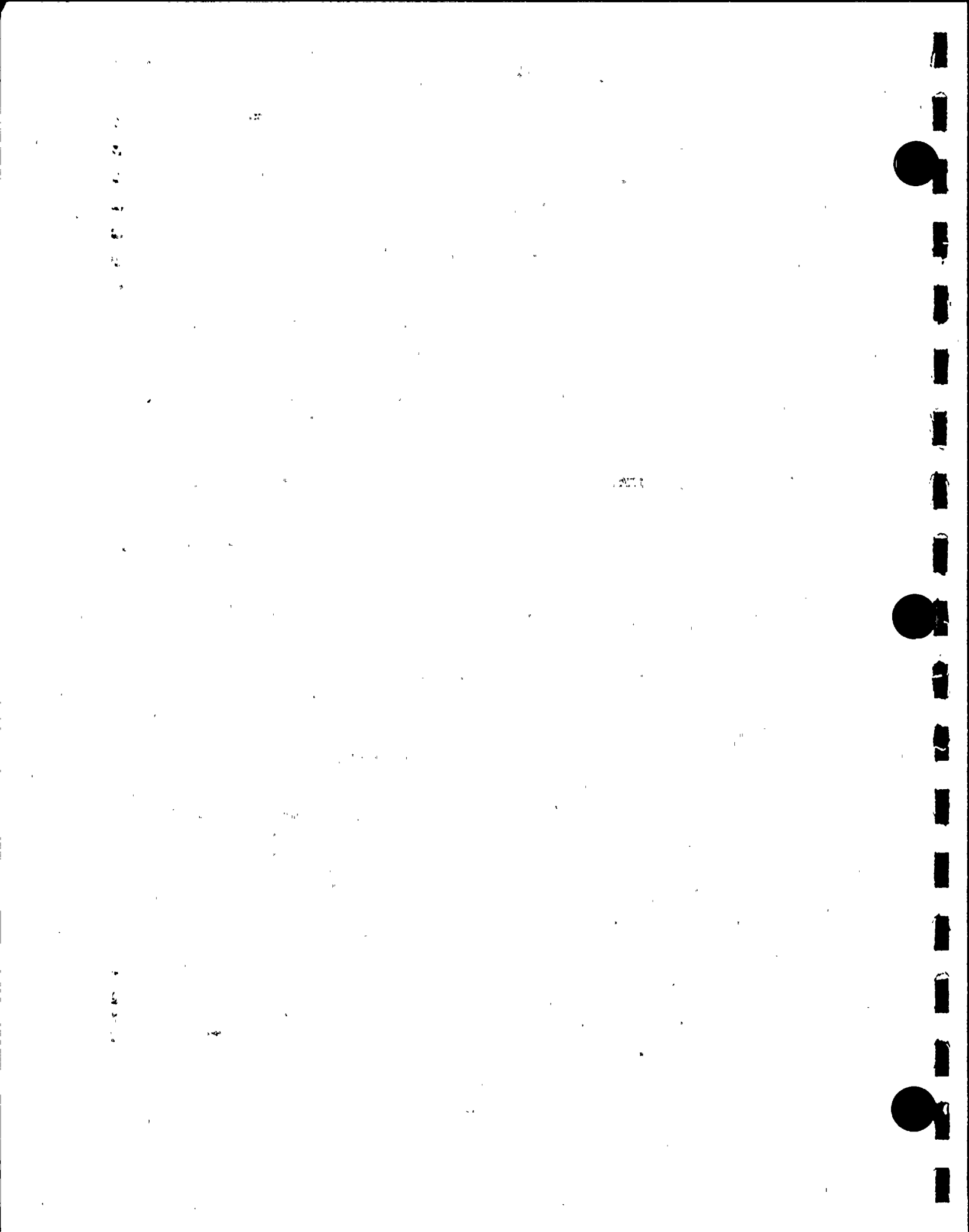
$$\begin{aligned} \text{Minimum Burnup in MWD/MTU} &= \\ &- 22,670 + 22,220 E - 2,260 E^2 + 149 E^3 \end{aligned}$$

For Region 3 Storage

$$\begin{aligned} \text{Minimum Burnup in MWD/MTU} &= \\ &- 26,745 + 18,746 E - 1,631 E^2 + 98.4 E^3 \end{aligned}$$

4.2.2 Abnormal and Accident Conditions

Although credit for the soluble poison normally present in the spent fuel pool water is permitted under abnormal or accident conditions, most abnormal or accident conditions will not result in exceeding the limiting reactivity (k_{eff} of 0.95) even in the absence of soluble poison. The effects on reactivity of credible abnormal and accident conditions are discussed in Section 4.7 and summarized in Table 4.3. Of these abnormal or accident conditions, only one has the potential for a more than negligible positive reactivity effect.



The inadvertent misplacement of a fresh fuel assembly has the potential for exceeding the limiting reactivity, should there be a concurrent and independent accident condition resulting in the loss of all soluble poison. Administrative procedures to assure the presence of soluble poison during fuel handling operations will preclude the possibility of the simultaneous occurrence of the two independent accident conditions. The largest reactivity increase (+ 0.065 δk) would occur if a new fuel assembly of 4.95% enrichment were to be positioned in a Region 2 location with the remainder of the rack fully loaded with fuel of the highest permissible reactivity. Under this accident condition, credit for the presence of soluble poison is permitted by NRC guidelines*, and calculations indicate that 550 ppm soluble boron would be adequate to reduce the k_{eff} to the calculated k_{eff} (0.940) and approximately 450 ppm would be sufficient to assure that the limiting k_{eff} of 0.95 is not exceeded.

*Double contingency principle of ANSI N16.1-1975, as specified in the April 14, 1978 NRC letter (Section 1.2) and implied in the proposed revision to Reg. Guide 1.13 (Section 1.4, Appendix A).

100-1000

4.3 Reference Fuel Storage Cells

4.3.1 Reference Fuel Assembly

The design basis fuel assembly, described in Figure 4.4, is a 15 x 15 array of fuel rods with 21 rods replaced by 20 control rod guide tubes and 1 instrument thimble. Table 4.4 summarizes the fuel assembly design specifications and the expected range of significant manufacturing tolerances. As shown below, initial cell calculations with CASMO-3 indicated that the W 15 x 15 fuel exhibited a slightly higher reactivity in the storage rack cell than either the W 17 x 17 standard or optimized (OFA) fuel or the ANF fuel assembly designs.

<u>Fuel type</u>	<u>Enrichment</u>	<u>Burnup</u> <u>MWD/KgU</u>	<u>Cell</u> <u>k_{eff}</u>
<u>W</u> 15 x 15	2.5	0	1.0261
<u>W</u> 15 x 15	2.5	10	0.9210
<u>W</u> 17 x 17 OFA	2.5	0	1.0205
<u>W</u> 17 x 17 OFA	2.5	10	0.9144
<u>W</u> 17 x 17 Stnd	2.5	0	1.0217
<u>W</u> 17 x 17 Stnd	2.5	10	0.9188
ANF 15 x 15	2.5	0	1.0148
ANF 17 x 17	2.5	0	1.0126
<u>W</u> 15 x 15	4.95	0	1.1941
<u>W</u> 15 x 15	4.95	40	0.9204
<u>W</u> 17 x 17 OFA	4.95	0	1.1933
<u>W</u> 17 x 17 OFA	4.95	40	0.9149
<u>W</u> 17 x 17 Stnd	4.95	0	1.1880
ANF 15 x 15	4.95	0	1.1857
ANF 17 x 17	4.95	0	1.1883
Highest values			

20 13

11

10000

Based upon the calculations listed above, the Westinghouse 15 x 15 rod design was used as the basis for the criticality calculations.

4.3.2 High Density Fuel Storage Cells

The nominal spent fuel storage cell used for the criticality analyses of the Donald C. Cook spent fuel storage cells is shown in Figure 4.4. Each storage cell is composed of Boral absorber panels positioned between a 8.75-inch I.D., 0.075-inch thick inner stainless steel box, and a 0.035-inch outer stainless steel sheath which forms the wall of the adjacent cell. The fuel assemblies are normally located in the center of each storage cell on a nominal lattice spacing of 8.97 ± 0.04 inches. The Boral absorber has a thickness of 0.101 ± 0.005 inch and a nominal B-10 areal density of 0.0345 g/cm^2 .

11
12
13

14
15
16
17
18
19
20
21
22
23
24
25
26
27
28
29
30
31
32
33
34
35
36
37
38
39
40
41
42
43
44
45
46
47
48
49
50
51
52
53
54
55
56
57
58
59
60
61
62
63
64
65
66
67
68
69
70
71
72
73
74
75
76
77
78
79
80
81
82
83
84
85
86
87
88
89
90
91
92
93
94
95
96
97
98
99
100



4.4 Analytical Methodology

4.4.1 Reference Design Calculations

In the fuel rack analyses, the primary criticality analyses of the high density spent fuel storage racks were performed with the KENO-5a computer code package⁽¹⁾; using the 27-group SCALE* cross-section library⁽²⁾ and the NITAWL subroutine for U-238 resonance shielding effects (Nordheim integral treatment). Depletion analyses and determination of equivalent enrichments were made with the two-dimensional transport theory code, CASMO-3⁽³⁾. Benchmark calculations, presented in Appendix A, indicate a bias of 0.0000 with an uncertainty of ± 0.0024 for CASMO-3 and 0.0090 ± 0.0021 (95%/95%) for NITAWL-KENO-5a. In tracking long-term (30-year) reactivity effects of spent fuel stored in Region 2 of the fuel storage rack, previous CASMO calculations confirmed a continuous reduction in reactivity with time (after Xe decay) due primarily to Pu-241 decay and Am-241 growth.

KENO-5a Monte Carlo calculations inherently include a statistical uncertainty due to the random nature of neutron tracking. To minimize the statistical uncertainty of the KENO-calculated reactivity, a minimum of 500,000 neutron histories in 1000 generations of 500 neutrons each, are accumulated in each calculation. For the design calculation for the racks, 1,250,000 histories were used to confirm convergence of the KENO-5a calculation.

Figure 4.5 represents the basic geometric model used in the KENO-5a calculations. This model effectively describes a repeating array of 10 storage cells in the X-direction separated by a 2-inch water

*"SCALE" is an acronym for Standardized Computer Analysis for Licensing Evaluation, a standard cross-section set developed by ORNL for the USNRC.

10 11 12 13 14 15 16 17 18 19 20 21 22 23 24 25 26 27 28 29 30 31 32 33 34 35 36 37 38 39 40 41 42 43 44 45 46 47 48 49 50 51 52 53 54 55 56 57 58 59 60 61 62 63 64 65 66 67 68 69 70 71 72 73 74 75 76 77 78 79 80 81 82 83 84 85 86 87 88 89 90 91 92 93 94 95 96 97 98 99 100

10 11 12 13 14 15 16 17 18 19 20 21 22 23 24 25 26 27 28 29 30 31 32 33 34 35 36 37 38 39 40 41 42 43 44 45 46 47 48 49 50 51 52 53 54 55 56 57 58 59 60 61 62 63 64 65 66 67 68 69 70 71 72 73 74 75 76 77 78 79 80 81 82 83 84 85 86 87 88 89 90 91 92 93 94 95 96 97 98 99 100

10 11 12 13 14 15 16 17 18 19 20 21 22 23 24 25 26 27 28 29 30 31 32 33 34 35 36 37 38 39 40 41 42 43 44 45 46 47 48 49 50 51 52 53 54 55 56 57 58 59 60 61 62 63 64 65 66 67 68 69 70 71 72 73 74 75 76 77 78 79 80 81 82 83 84 85 86 87 88 89 90 91 92 93 94 95 96 97 98 99 100



gap between modules and an infinite array of cells in the Y-direction (periodic boundary conditions). In the axial (Z) direction, the full length 144-inch fuel assembly was described with a 30-cm water reflector. A similiar model was used for calculations of the rack peripheral cells where the calculations were made with both water and concrete reflectors (a concrete reflector gave a slightly higher reactivity by 0.004 δk).

Larger models, encompassing an entire storage module (half of an 11 x 11 array, run for 1,250,000 neutron histories to assure convergence) confirmed results obtained with the smaller infinite array model. The larger model was also used to confirm the reactivity calculation for the checkerboard arrangement with fresh fuel and empty cells in Region 3 and in the investigation of the consequences of potential accident conditions with a misplaced fresh fuel assembly. In addition, the corner intersection was explicitly modeled and, as expected, gave a lower reactivity than the reference design calculation.

In the CASMO-3 geometric model (cell), each fuel rod and its cladding were described explicitly and reflecting boundary conditions (zero neutron current) were used in the axial direction and at the centerline of the Boron and steel plates between storage cells. These boundary conditions have the effect of creating an infinite array of storage cells in all directions and provide a conservative estimate of the uncertainties in reactivity attributed to manufacturing tolerances.

Because NITAWL-KENO-5a does not have burnup capability, burned fuel was represented by fuel of equivalent enrichment as determined by CASMO-3 calculations in the storage cell (i.e. an enrichment which yields the same reactivity in the storage cell as the burned fuel).

11

12

13

14



Figure 4.6 shows this equivalent enrichment for fuel of 4.95% initial enrichment at various discharge burnups, evaluated in the storage cell.

4.4.2 Fuel Burnup Calculations and Uncertainties

CASMO-3 was used for burnup calculations in the hot operating condition. CASMO-3 has been extensively benchmarked (Appendix A and Refs. 2 and 7) against critical experiments (including plutonium-bearing fuel). In addition to burnup calculations, CASMO-3 was used for evaluating the small reactivity increments (by differential calculations) associated with manufacturing tolerances.

Since there are no critical experiment data with spent fuel for determining the uncertainty in burnup-dependent reactivity calculations, an allowance for uncertainty in reactivity* was assigned based upon the assumption of 5% uncertainty in burnup. This is approximately equivalent to 5% of the total reactivity decrement. At the design basis burnups of 38 and 50 MWD/KgU, the uncertainties in burnup are ± 1.9 and ± 2.5 MWD/KgU respectively. To evaluate the reactivity consequences of the uncertainties in burnup, independent calculations were made with fuel of 36,100 and 47,500 MWD/MtU burnup in Regions 2 and 3, and the incremental change from the reference burnups assumed to represent the net uncertainties in reactivity. These calculations resulted in an incremental reactivity uncertainty of $\pm 0.0047 \delta k$ in Region 2 (isolation barrier at 50 MWD/KgU burnup) and ± 0.0019 for Region 3 (at 38 MWD/KgU burnup). In the racks, the fresh unburned fuel in Region 1 strongly dominate the reactivity which tends to minimize the reactivity consequences of uncertainties in burnup. The

*Only that portion of the uncertainty due to burnup. Other uncertainties are accounted for elsewhere.

10 11 12 13 14 15 16 17 18 19 20 21 22 23 24 25 26 27 28 29 30 31 32 33 34 35 36 37 38 39 40 41 42 43 44 45 46 47 48 49 50 51 52 53 54 55 56 57 58 59 60 61 62 63 64 65 66 67 68 69 70 71 72 73 74 75 76 77 78 79 80 81 82 83 84 85 86 87 88 89 90 91 92 93 94 95 96 97 98 99 100

101 102 103 104 105 106 107 108 109 110 111 112 113 114 115 116 117 118 119 120 121 122 123 124 125 126 127 128 129 130 131 132 133 134 135 136 137 138 139 140 141 142 143 144 145 146 147 148 149 150

151 152 153 154 155 156 157 158 159 160 161 162 163 164 165 166 167 168 169 170 171 172 173 174 175 176 177 178 179 180 181 182 183 184 185 186 187 188 189 190 191 192 193 194 195 196 197 198 199 200

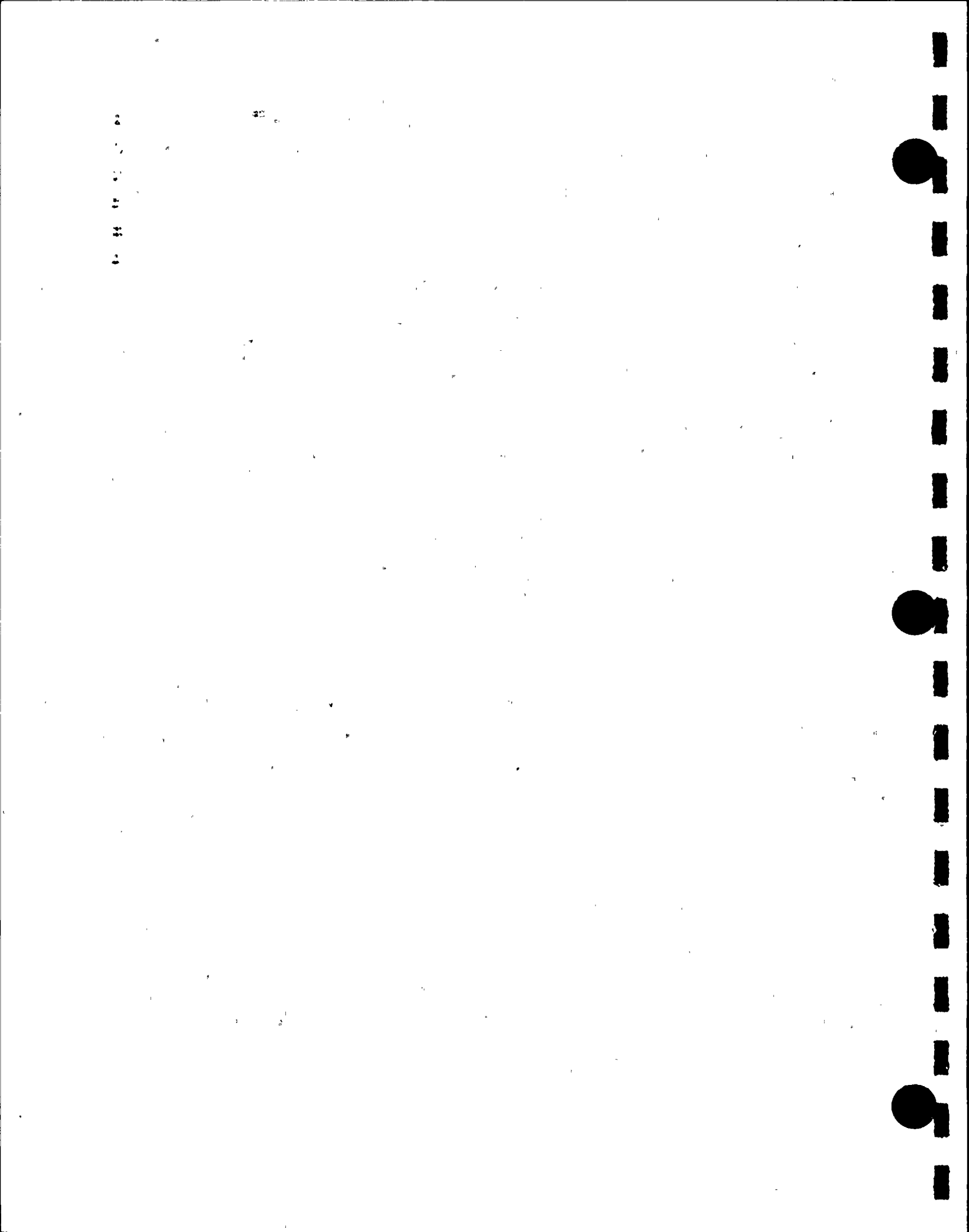


allowance for uncertainty in burnup calculations is a conservative estimate, particularly in view of the substantial reactivity decrease with time as the spent fuel ages.

4.4.3 Effect of Axial Burnup Distribution

Initially, fuel loaded into the reactor will burn with a slightly skewed cosine power distribution. As burnup progresses, the burnup distribution will tend to flatten, becoming more highly burned in the central regions than in the upper and lower ends, as may be seen in the curves compiled in Ref. 4. At high burnup, the more reactive fuel near the ends of the fuel assembly (less than average burnup) occurs in regions of lower reactivity worth due to neutron leakage. Consequently, it would be expected that over most of the burnup history, distributed burnup fuel assemblies would exhibit a slightly lower reactivity than that calculated for the average burnup. As burnup progresses, the distribution, to some extent, tends to be self-regulating as controlled by the axial power distribution, precluding the existence of large regions of significantly reduced burnup. Among others, Turner⁽⁵⁾ has provided generic analytic results of the axial burnup effect based upon calculated and measured axial burnup distributions. These analyses confirm the minor and generally negative reactivity effect of the axially distributed burnup. The trends observed, however, suggest the possibility of a small positive reactivity effect at high burnup.

Calculations were made with KENO-5a in three dimensions, based upon the typical axial burnup distribution of spent fuel (that observed at the Surrey plant was taken as representative). In these calculations, the axial height of the burned fuel was divided into a number of axial zones (6-inch intervals near the more significant top of the fuel), each with an enrichment equivalent to the burnup



of that zone. These calculations resulted in an incremental reactivity increase of 0.0037 δk for the reference design case. Fuel of lower initial enrichments (and lower burnup) would have a smaller (or negative) reactivity effect as a result of the axial variation in burnup. These estimates are conservative since smaller axial increments in the calculations have been shown to result in lower incremental reactivities⁽⁵⁾.



24
25
26

2422

27

4.5 Criticality Analyses and Tolerances

4.5.1 Nominal Design

For the nominal storage cell design, the NITAWL-KENO-5a calculation resulted in a bias-corrected k_{∞} of 0.9250 ± 0.0012 (95%/95%), which, when combined with all known uncertainties and the axial burnup effect, results in a k_{∞} of 0.929 ± 0.011 or a maximum k_{∞} of 0.940 with a 95% probability at the 95% confidence level⁽⁶⁾.

For the interim loading pattern of checkerboarded fuel and empty cells in Region 3, calculations resulted in essentially the same reactivity as the reference design within the normal KENO-5a statistics (maximum k_{∞} of 0.940, including all allowances and uncertainties, see Table 4.2).

4.5.2 Uncertainties Due to Manufacturing Tolerances

The uncertainties due to manufacturing tolerances are summarized in Table 4-5 and discussed below.

4.5.2.1 Boron Loading Tolerances

The Boral absorber panels used in the storage cells are nominally 0.101 inch thick, 7.50-inch wide and 144-inch long, with a nominal B-10 areal density of 0.0345 g/cm^2 . The vendors manufacturing tolerance limit is $\pm 0.0045 \text{ g/cm}^2$ in B-10 content which assures that at any point, the minimum B-10 areal density will not be less than 0.030 g/cm^2 . Differential KENO-5a calculations for the reference design with the minimum tolerance B-10 loading results in an incremental reactivity of $+ 0.00614 \delta k$ uncertainty.

1000

1000

1000

1000



4.5.2.2 Boral Width Tolerance

The reference storage cell design uses a Boral panel with an initial width of 7.50 ± 0.06 inches. For the maximum tolerance of 0.06 inch, the differential CASMO-3 calculated reactivity uncertainty is $\pm 0.0009 \delta k$.

4.5.2.3 Tolerances in Cell Lattice Spacing

The manufacturing tolerance on the inner box dimension, which directly affects the storage cell lattice spacing between fuel assemblies, is ± 0.06 inches. This corresponds to an uncertainty in reactivity of $\pm 0.0015 \delta k$ determined by differential CASMO-3 calculations.

4.5.2.4 Stainless Steel Thickness Tolerances

The nominal stainless steel thickness is 0.075 ± 0.005 inch for the inner stainless steel box and 0.035 ± 0.003 inch for the Boral cover plate. The maximum positive reactivity effect of the expected stainless steel thickness tolerances was calculated (CASMO-3) to be $+ 0.0009 \delta k$.

4.5.2.5 Fuel Enrichment and Density Tolerances

The design maximum enrichment is 4.95 ± 0.05 wt% U-235. Separate CASMO-3 burnup calculations were made for fuel of the maximum enrichment (5.00%) and for the maximum UO_2 density (10.50 g/cc). Reactivities in the storage cell were then calculated using the restart capability in CASMO-3 and equivalent enrichments determined for the reference fuel burnups of 38 and 50 MWD/KgU. The incremental reactivities between these calculations and the reference CASMO-3 cases, were conservatively taken as the



sensitivity to small enrichment and density variations. For the tolerance on U-235 enrichment, the uncertainty in k_0 is $\pm 0.0034 \delta k$ and for fuel density is ± 0.0035 .

4.5.3 Water-gap Spacing Between Modules

The water-gap between modules constitute a neutron flux-trap for the outer (peripheral) row of storage cells. Calculations with KENO-5a were made for various water-gap spacings (Figure 4.7). From these data, it was determined that the incremental reactivity consequence (uncertainty) for the minimum water-gap tolerance of $\pm 1/4$ inch is $\pm 0.0045 \delta k$. The racks are constructed with the base plate extending beyond the edge of the cells. This assures that a minimum spacing of 1.75 inch between storage modules is maintained under all credible conditions.

4.5.4 Eccentric Fuel Positioning

The fuel assembly is assumed to be normally located in the center of the storage rack cell. Infinite array calculations were made using KENO-5a for a single cell with the fuel assemblies centered and with the assemblies assumed to be in the corner of the storage rack cell (four-assembly cluster at closest approach). These calculations indicated that the reactivity uncertainty could be as much as $\pm 0.0019 \delta k$.

4.6 Abnormal and Accident Conditions

4.6.1 Temperature and Water Density Effects

The moderator temperature coefficient of reactivity is negative; a moderator temperature of 20°C (68°F) was assumed for the reference designs, which assures that the true reactivity will always be lower over the expected range of water temperatures. Temperature

10 50 41 11 43 40

10 48 11



effects on reactivity have been calculated and the results are shown in Table 4.6. With soluble poison present, the temperature coefficients of reactivity would differ from those inferred from the data in Table 4.6. However, the reactivities would also be substantially lower at all temperatures with soluble boron present, and the data in Table 4.6 is pertinent to the higher-reactivity unborated case.

4.6.2 Dropped Fuel Assembly

For a drop on top of the rack, the fuel assembly will come to rest horizontally on top of the rack with a minimum separation distance from the fuel in the rack of more than 12 inches, including the potential deformation under seismic or accident conditions. At this separation distance, the effect on reactivity is insignificant ($<0.0001 \delta k$). Furthermore, soluble boron in the pool water would substantially reduce the reactivity and assure that the true reactivity is always less than the limiting value for any conceivable dropped fuel accident.

4.6.3 Lateral Rack Movement

Lateral motion of the rack modules under seismic conditions could potentially alter the spacing between rack modules. However, the maximum rack movement has been determined to be less than the tolerance on the water-gap spacing. Furthermore, soluble poison would assure that a reactivity less than the design limitation is maintained under all accident or abnormal conditions.



1
2
3
4
5
6
7
8
9
10
11
12
13
14
15
16
17
18
19
20
21
22
23
24
25
26
27
28
29
30
31
32
33
34
35
36
37
38
39
40
41
42
43
44
45
46
47
48
49
50
51
52
53
54
55
56
57
58
59
60
61
62
63
64
65
66
67
68
69
70
71
72
73
74
75
76
77
78
79
80
81
82
83
84
85
86
87
88
89
90
91
92
93
94
95
96
97
98
99
100

101
102
103
104
105
106
107
108
109
110
111
112
113
114
115
116
117
118
119
120
121
122
123
124
125
126
127
128
129
130
131
132
133
134
135
136
137
138
139
140
141
142
143
144
145
146
147
148
149
150
151
152
153
154
155
156
157
158
159
160
161
162
163
164
165
166
167
168
169
170
171
172
173
174
175
176
177
178
179
180
181
182
183
184
185
186
187
188
189
190
191
192
193
194
195
196
197
198
199
200

201
202
203
204
205
206
207
208
209
210
211
212
213
214
215
216
217
218
219
220
221
222
223
224
225
226
227
228
229
230
231
232
233
234
235
236
237
238
239
240
241
242
243
244
245
246
247
248
249
250
251
252
253
254
255
256
257
258
259
260
261
262
263
264
265
266
267
268
269
270
271
272
273
274
275
276
277
278
279
280
281
282
283
284
285
286
287
288
289
290
291
292
293
294
295
296
297
298
299
300

1000

1000

4.6.4 Abnormal Location of a Fuel Assembly

The abnormal location of a fresh unirradiated fuel assembly of 4.95 wt% enrichment could, in the absence of soluble poison, result in exceeding the design reactivity limitation (k_{∞} of 0.95). This could occur if a fresh fuel assembly of the highest permissible enrichment were to be either positioned outside and adjacent to a storage rack module or inadvertently loaded into either a Region 2 or Region 3 storage cell. Calculations (KENO-5a) showed that the highest reactivity, including uncertainties, for the worst case postulated accident condition (fresh fuel assembly in Region 2) would exceed the limit on reactivity in the absence of soluble boron. Soluble boron in the spent fuel pool water, for which credit is permitted under these accident conditions, would assure that the reactivity is maintained substantially less than the design limitation. It is estimated that a soluble poison concentration of 550 ppm boron would be sufficient to maintain k_{∞} at the reference design value of 0.940 under the maximum postulated accident condition. Approximately 450 ppm boron would be required to limit the maximum reactivity to a k_{eff} of 0.95.

4.7 Existing Spent Fuel

As of May 1990, there were 1596 spent fuel assemblies in storage at the Donald C. Cook plant, including those now in the reactor and their projected burnups at discharge. Figure 4.8 superimposes the enrichment-burnup combination of these fuel assemblies on the curves defining the acceptable burnup domains. As may be seen in this figure, most of the spent fuel now in storage falls well into the acceptable domain for the barrier fuel (Region 2). The number of fuel assemblies meeting the enrichment-burnup criteria for storage in Region 2 is 1390 which will nearly fill the 1447 Region 2 storage locations. Twelve fuel assemblies (discharged

1. 2. 3. 4. 5. 6. 7. 8. 9. 10. 11. 12. 13. 14. 15. 16. 17. 18. 19. 20. 21. 22. 23. 24. 25. 26. 27. 28. 29. 30. 31. 32. 33. 34. 35. 36. 37. 38. 39. 40. 41. 42. 43. 44. 45. 46. 47. 48. 49. 50. 51. 52. 53. 54. 55. 56. 57. 58. 59. 60. 61. 62. 63. 64. 65. 66. 67. 68. 69. 70. 71. 72. 73. 74. 75. 76. 77. 78. 79. 80. 81. 82. 83. 84. 85. 86. 87. 88. 89. 90. 91. 92. 93. 94. 95. 96. 97. 98. 99. 100.



prematurely for various reasons) will need to be kept in a Region 1 storage location, and the remaining 194 assemblies may be stored in Region 3 locations. Future discharge batches may reasonably be expected to have a preponderance of highly burned fuel capable of being stored in Region 2 (or in Region 3 once Region 2 is filled). An appreciable number of spent fuel assemblies have enrichment-burnup combinations well in excess of the design basis and this provides further conservatism in the criticality safety of the spent fuel storage rack design.

100-100-100



4.8 References

1. Green, Lucious, Petrie, Ford, White, and Wright, "PSR-63-/NITAWL-1 (code package) NITAWL Modular Code System For Generating Coupled Multigroup Neutron-Gamma Libraries from ENDF/B", ORNL-TM-3706, Oak Ridge National Laboratory, November 1975.
2. R.M. Westfall et. al., "SCALE: A Modular System for Performing Standardized Computer Analysis for Licensing Evaluation", NUREG/CR-0200, 1979. Volume 2, Section F11, "KENO-5a An Improved Monte Carlo Criticality Program with Supergrouping".
3. A. Ahlin, M. Edenius, and H. Haggblom, "CASMO - A Fuel Assembly Burnup Program", AE-RF-76-4158, Studsvik report.

A. Ahlin and M. Edenius, "CASMO - A Fast Transport Theory Depletion Code for LWR Analysis", ANS Transactions, Vol. 26, p. 604, 1977.

"CASMO-3 A Fuel Assembly Burnup Program, Users Manual", Studsvik/NFA-87/7, Studsvik Energitechnik AB, November 1986
4. H. Richings, Some Notes on PWR (W) Power Distribution Probabilities for LOCA Probabilistic Analyses, NRC Memorandum to P.S. Check, dated July 5, 1977.
5. S. E. Turner, "Uncertainty Analysis - Burnup Distributions", presented at the DOE/SANDIA Technical Meeting on Fuel Burnup Credit, Special Session, ANS/ENS Conference, Washington, D.C., November 2, 1988
6. M.G. Natrella, Experimental Statistics National Bureau of Standards, Handbook 91, August 1963.



Table 4.1

SUMMARY OF CRITICALITY SAFETY ANALYSES
NORMAL STORAGE CONFIGURATION

| | |
|---|---|
| Design Basis burnups at 4.95%
± 0.05% initial enrichment | 0 in Region 1
50 in Region 2
38 in Region 3 |
| Temperature for analysis | 20°C (68°F) |
| Reference k_{∞} (KENO-5a) | 0.9160 |
| Calculational bias, $\delta k^{(1)}$ | 0.0090 |
| Uncertainties | |
| Bias statistics (95%/95%) | ± 0.0021 |
| KENO-5a statistics (95%/95%) | ± 0.0012 |
| Manufacturing Tolerances | ± 0.0064 |
| Water-gap | ± 0.0045 |
| Fuel enrichment | ± 0.0034 |
| Fuel density | ± 0.0035 |
| Burnup (38 MWD/KgU) | ± 0.0019 |
| Burnup (50 MWD/KgU) | ± 0.0047 |
| Eccentricity in position | ± 0.0019 |
| | ----- |
| Statistical combination
of uncertainties ⁽²⁾ | ± 0.0110 |
| Axial Burnup Effect | 0.0037 |
| Total | 0.9287 ± 0.0110 |
| Maximum Reactivity (k_{∞}) | 0.940 |

(1) See Appendix A

(2) Square root of sum of squares.

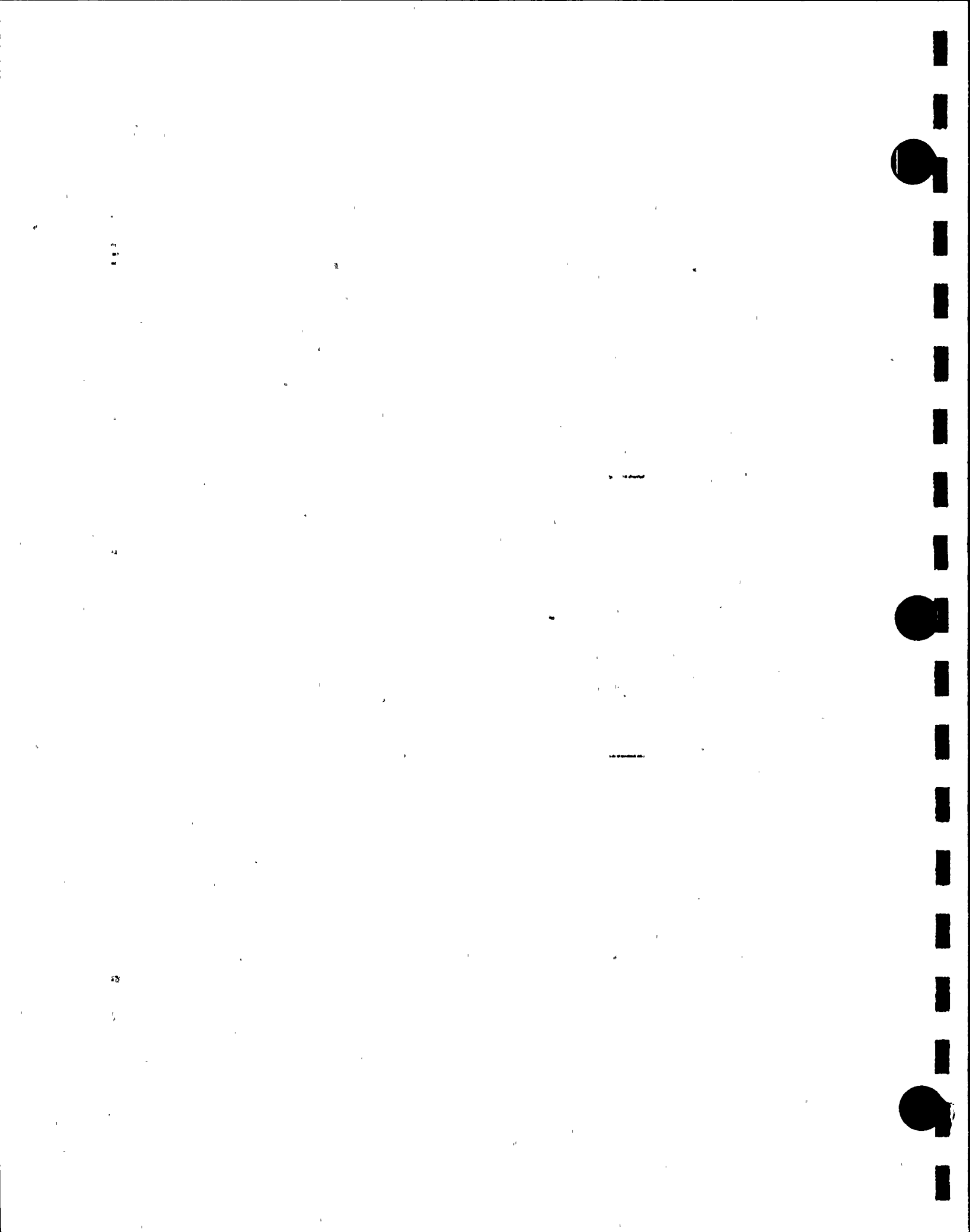


Table 4.2

SUMMARY OF CRITICALITY SAFETY ANALYSES
INTERIM CHECKERBOARD LOADING

| | |
|---|---|
| Design Basis burnups at 4.95%
± 0.05% initial enrichment | 0 in Region 1
50 in Region 2
Region 3 -CHECKERBOARD
(FRESH FUEL AND EMPTY) |
| Temperature for analysis | 20°C (68°F) |
| Reference k_{∞} (KENO-5a) | 0.9168 |
| Calculational bias, $\delta k^{(1)}$ | 0.0090 |
| Uncertainties (Assumed same as the reference case) | |
| Bias statistics (95%/95%) | ± 0.0021 |
| KENO-5a statistics (95%/95%) | ± 0.0012 |
| Manufacturing Tolerances | ± 0.0064 |
| Water-gap | ± 0.0045 |
| Fuel enrichment | ± 0.0034 |
| Fuel density | ± 0.0035 |
| Burnup (38 MWD/KgU) | NA |
| Burnup (50 MWD/KgU) | ± 0.0047 |
| Eccentricity | ± 0.0019 |
| Statistical combination
of uncertainties ⁽²⁾ | ± 0.0108 |
| Axial Burnup Effect | 0.0037 |
| Total | 0.9295 ± 0.0108 |
| Maximum Reactivity (k_{∞}) | 0.940 |

(1)

See Appendix A

(2)

Square root of sum of squares.



Table 4.3

REACTIVITY EFFECTS OF ABNORMAL AND ACCIDENT CONDITIONS

| Accident/Abnormal Conditions | Reactivity Effect |
|-----------------------------------|---|
| Temperature increase (above 68°F) | Negative (Table 4.6) |
| Void (boiling) | Negative (Table 4.6) |
| Assembly dropped on top of rack | Negligible ($<0.0001 \delta k$) |
| Lateral rack module movement | (Included in Tolerances) |
| Misplacement of a fuel assembly | Positive (0.065 Max δk)
(controlled by soluble
poison) |

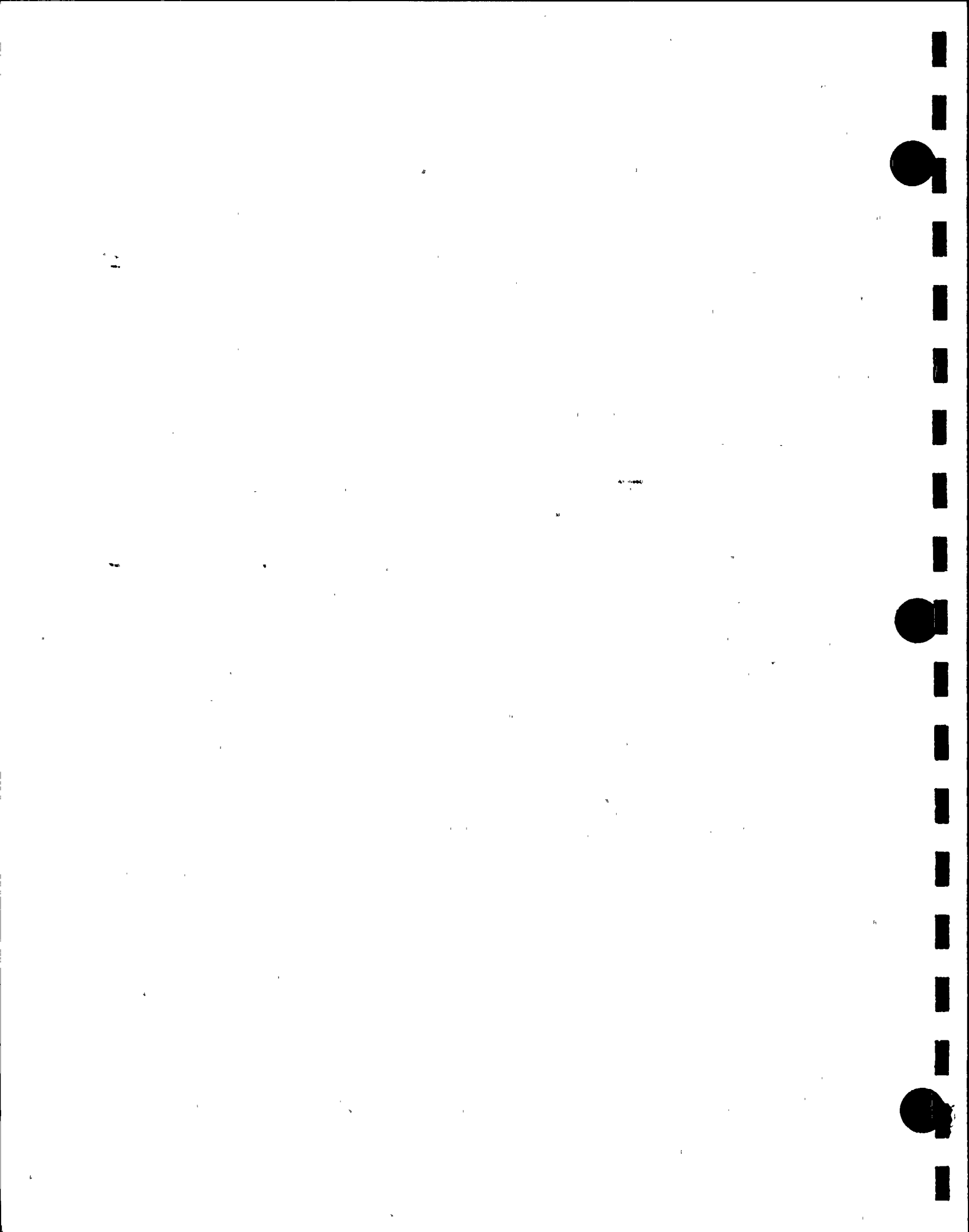


Table 4.4
DESIGN BASIS FUEL ASSEMBLY SPECIFICATIONS

FUEL ROD DATA

| | |
|--------------------------------------|--------------|
| Outside diameter, in. | 0.422 |
| Cladding thickness, in. | 0.0243 |
| Cladding inside diameter, in. | 0.3734 |
| Cladding material | Zr-4 |
| Pellet density, % T.D. | 95.0 |
| Stack density, g UO ₂ /cc | 10.29 ± 0.20 |
| Pellet diameter, in. | 0.3659 |
| Maximum enrichment, wt % U-235 | 4.95 ± 0.05 |

FUEL ASSEMBLY DATA

| | |
|--|---------|
| Fuel rod array | 15 x 15 |
| Number of fuel rods | 204 |
| Fuel rod pitch, in. | 0.563 |
| Number of control rod guide and
instrument thimbles | 21 |
| Thimble O.D., in. (nominal) | 0.533 |
| Thimble I.D., in. (nominal) | 0.499 |

11-1-5



Table 4.5

| Reactivity Effects of Manufacturing Tolerances | |
|--|--|
| <u>Tolerance</u> | <u>Incremental Reactivity, δk</u> |
| Boron-10 loading ($\pm 0.0045 \text{ g/cm}^2$) | ± 0.0061 |
| Boral Width ($\pm 1/16 \text{ inch}$) | ± 0.0009 |
| Lattice spacing ($\pm 0.04 \text{ inch}$) | ± 0.0015 |
| Stainless Thickness ($\pm 0.005 \text{ inch}$) | ± 0.0009 |
| Total (statistical sum) | ± 0.0064 |

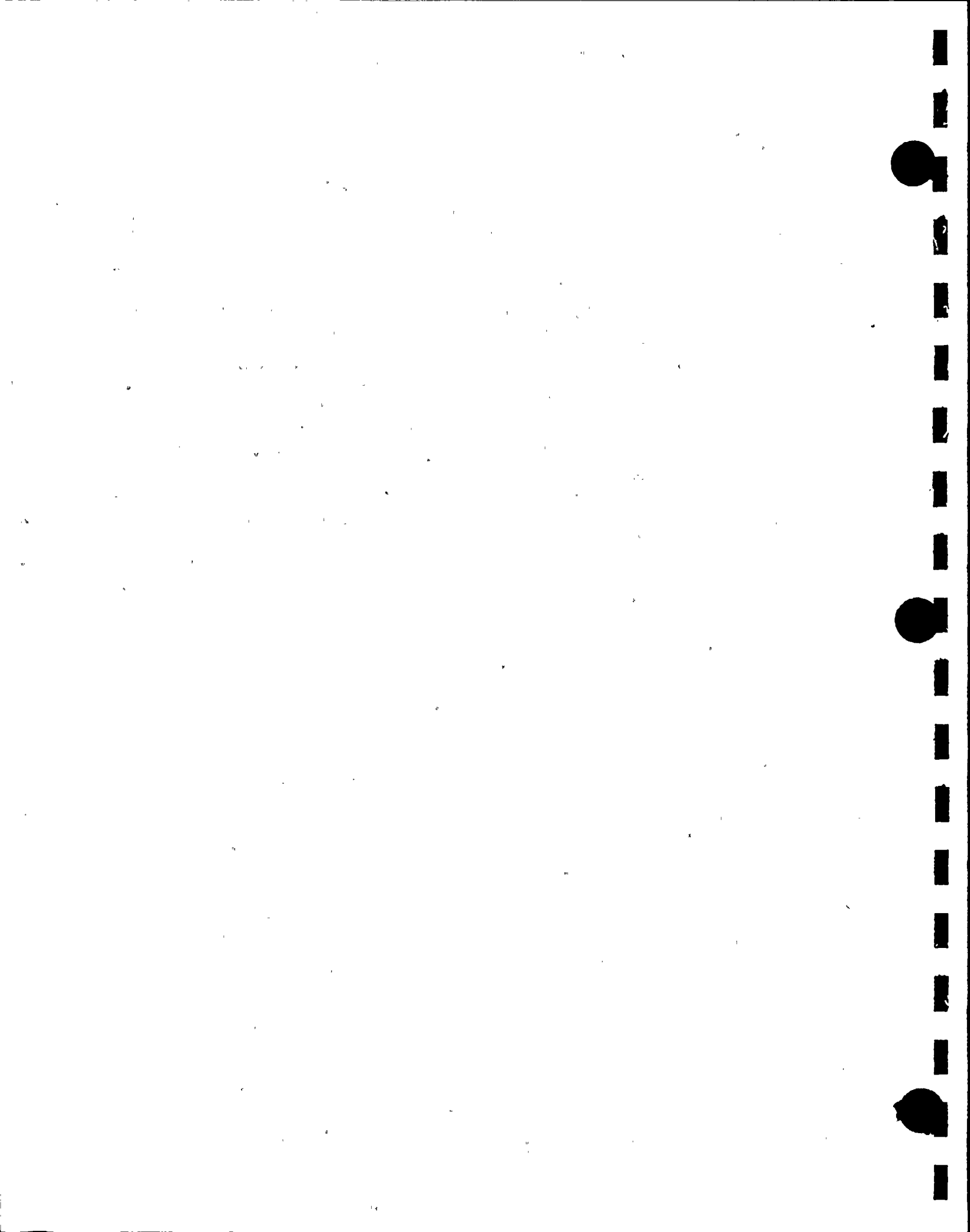


Table 4.6

EFFECT OF TEMPERATURE AND VOID ON CALCULATED
REACTIVITY OF STORAGE RACK

| Case | Incremental Reactivity Change, δk | |
|--------------------------|---|-----------|
| | Region 1 | Region 2 |
| 20°C (68°F) | Reference | Reference |
| 40°C (104°F) | -0.003 | -0.002 |
| 66°C (150°F) | -0.009 | -0.005 |
| 90°C (194°F) | -0.013 | -0.010 |
| 122°C (252°F) | -0.024 | -0.015 |
| 122°C (252°F) + 20% void | -0.071 | -0.061 |

11
12
13

14
15

16
17
18
19

20

Approved

in accordance



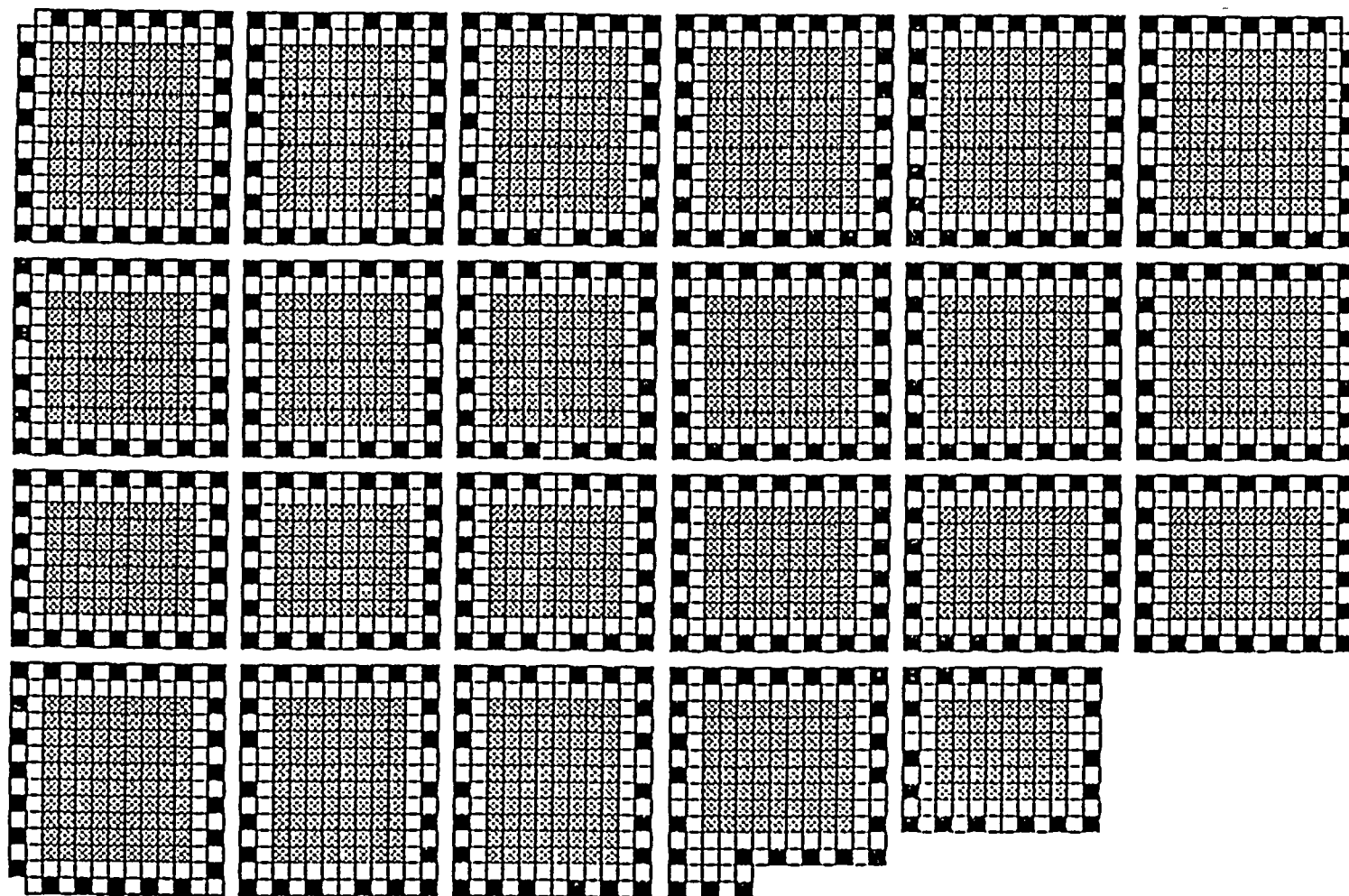


Fig. 4-1 NORMAL STORAGE PATTERN (MIXED THREE ZONE)

■ 504 REGION 1 CELLS

□ 1415 REGION 2 CELLS

▣ 1694 REGION 3 CELLS



10
11
12
13
14
15
16
17
18
19
20
21
22
23
24
25
26
27
28
29
30
31
32
33
34
35
36
37
38
39
40
41
42
43
44
45
46
47
48
49
50
51
52
53
54
55
56
57
58
59
60
61
62
63
64
65
66
67
68
69
70
71
72
73
74
75
76
77
78
79
80
81
82
83
84
85
86
87
88
89
90
91
92
93
94
95
96
97
98
99
100

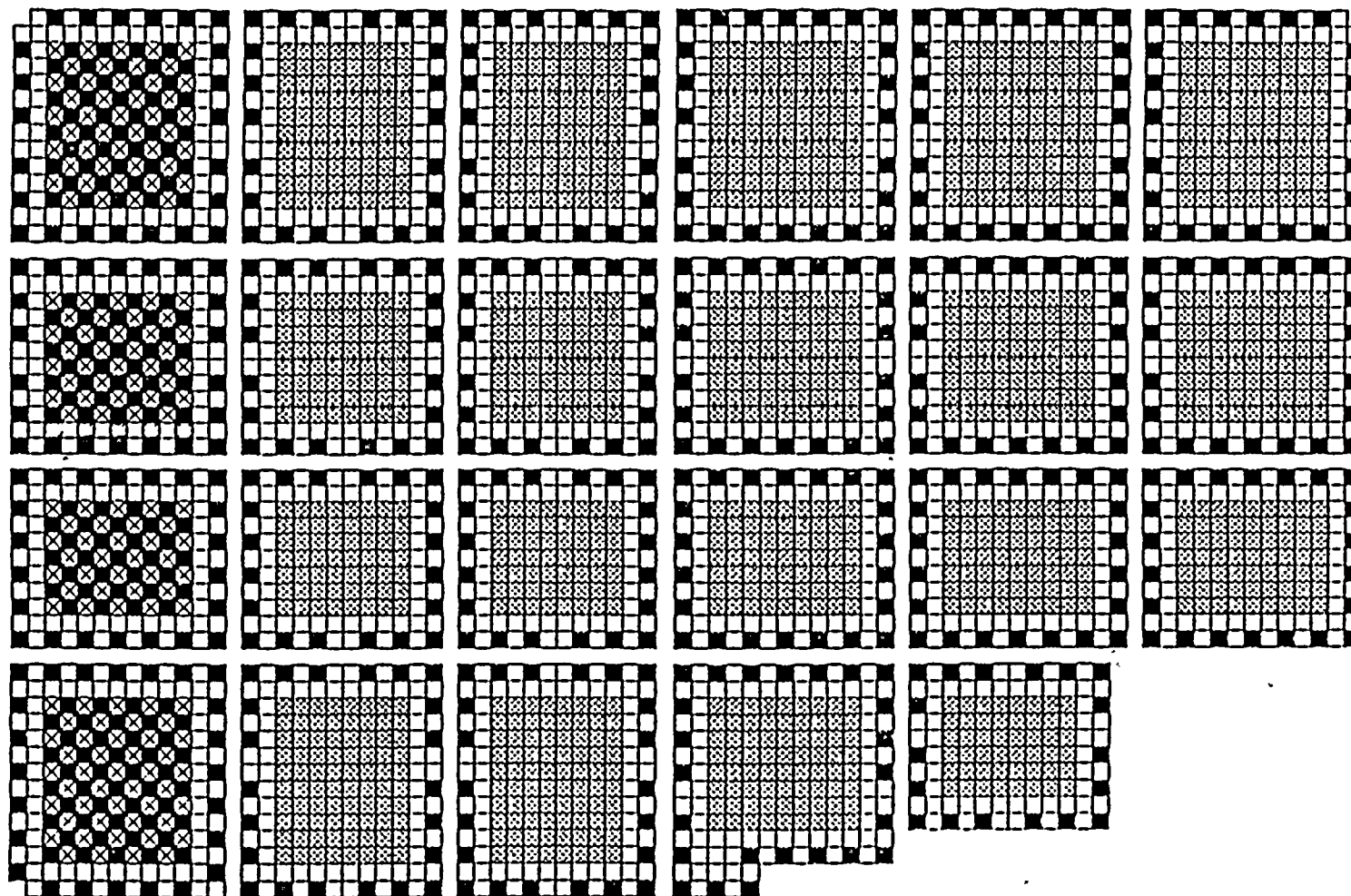
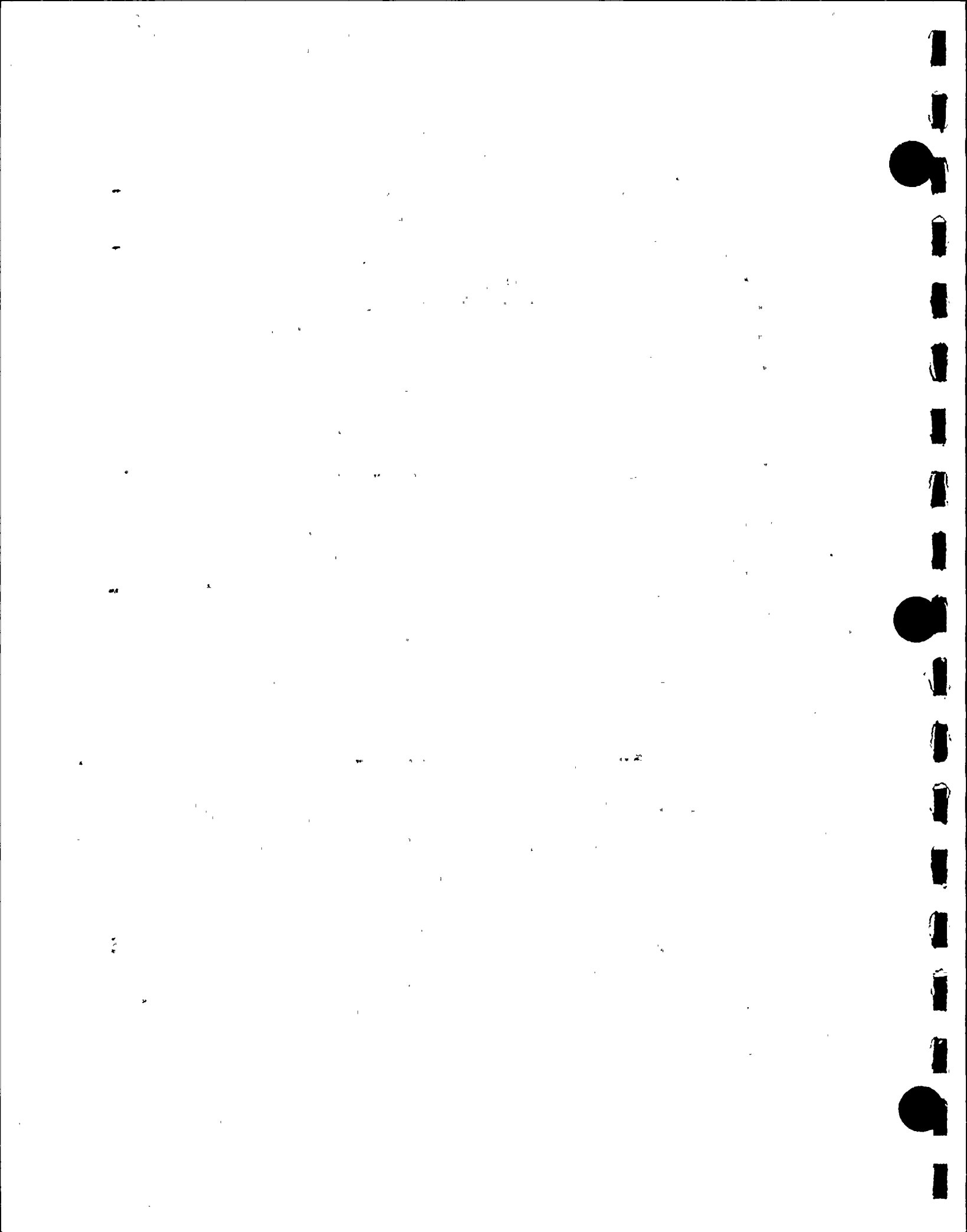


Fig. 4-2 INTERIM STORAGE PATTERN (CHECKERBOARD)

⊗ 158 EMPTY LOCATIONS ■ 661 REGION 1 CELLS □ 1415 REGION 2 CELLS ⊞ 1379 REGION 3 CELLS



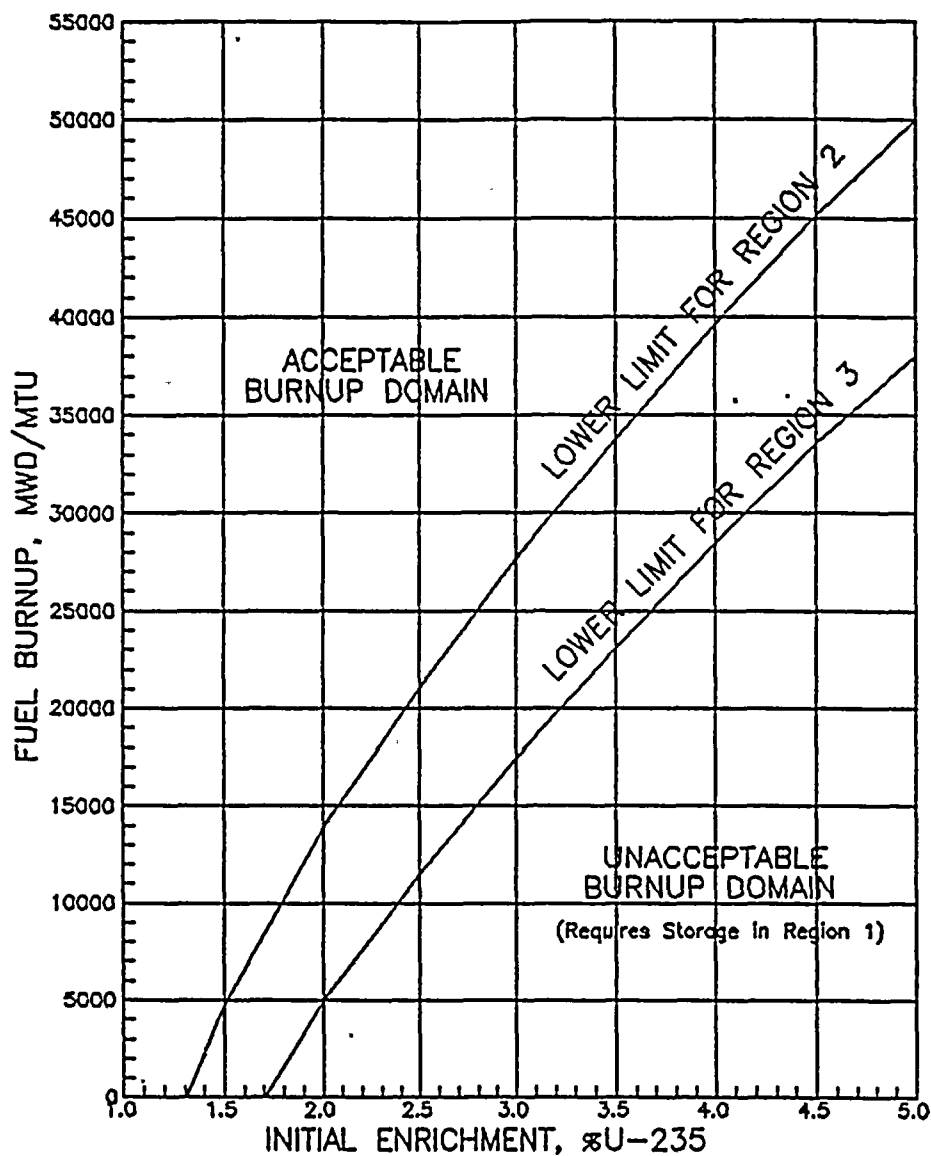


Fig. 4-3 ACCEPTABLE BURNUP DOMAIN IN REGIONS 2 & 3



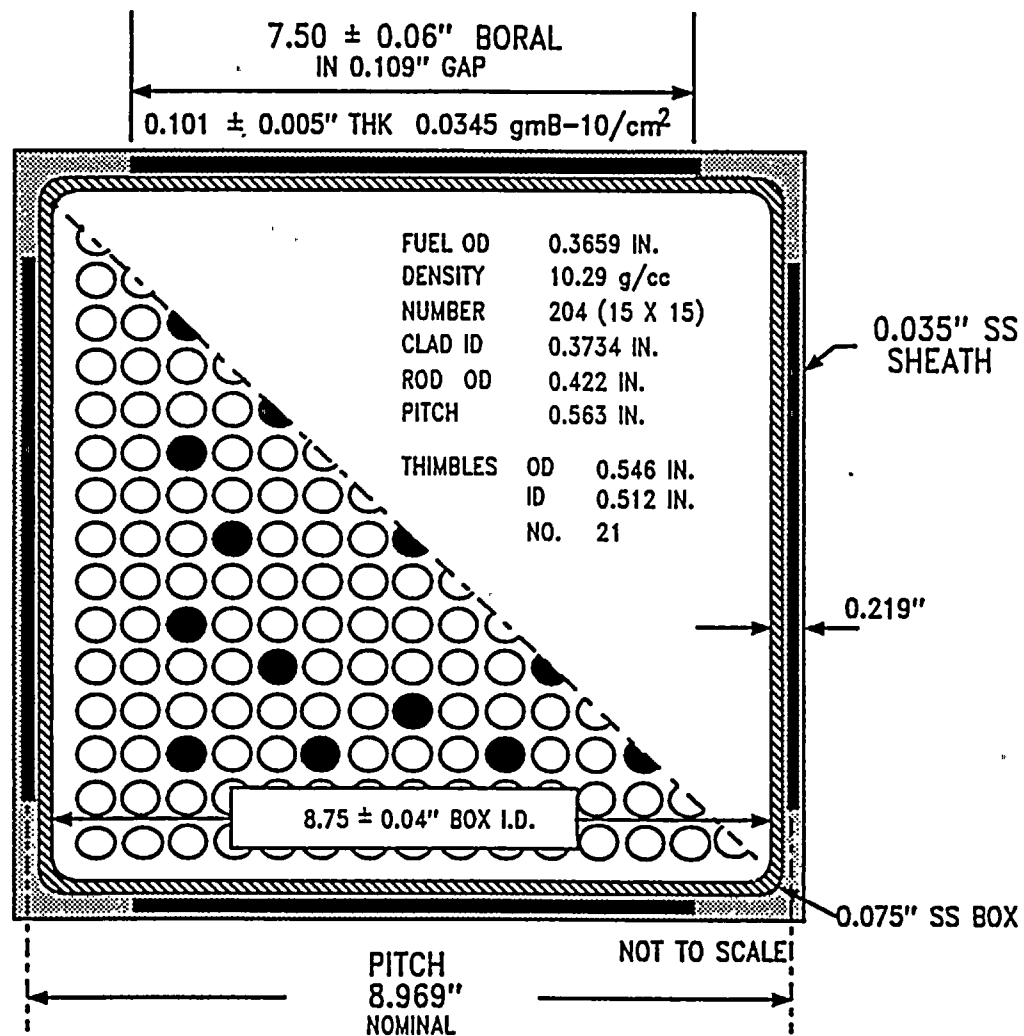


FIG. 4-4 FUEL STORAGE CELL CROSS SECTION



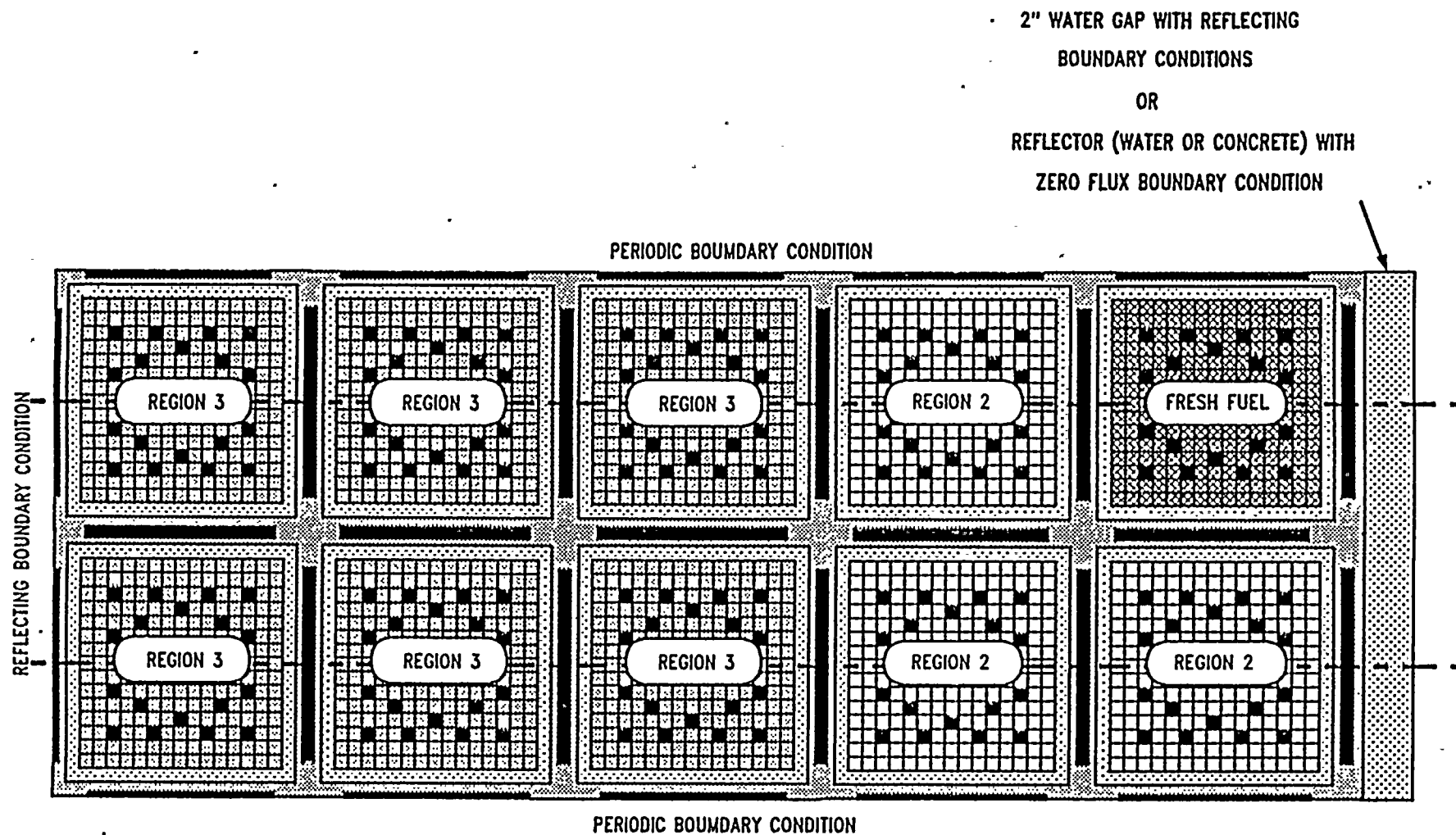
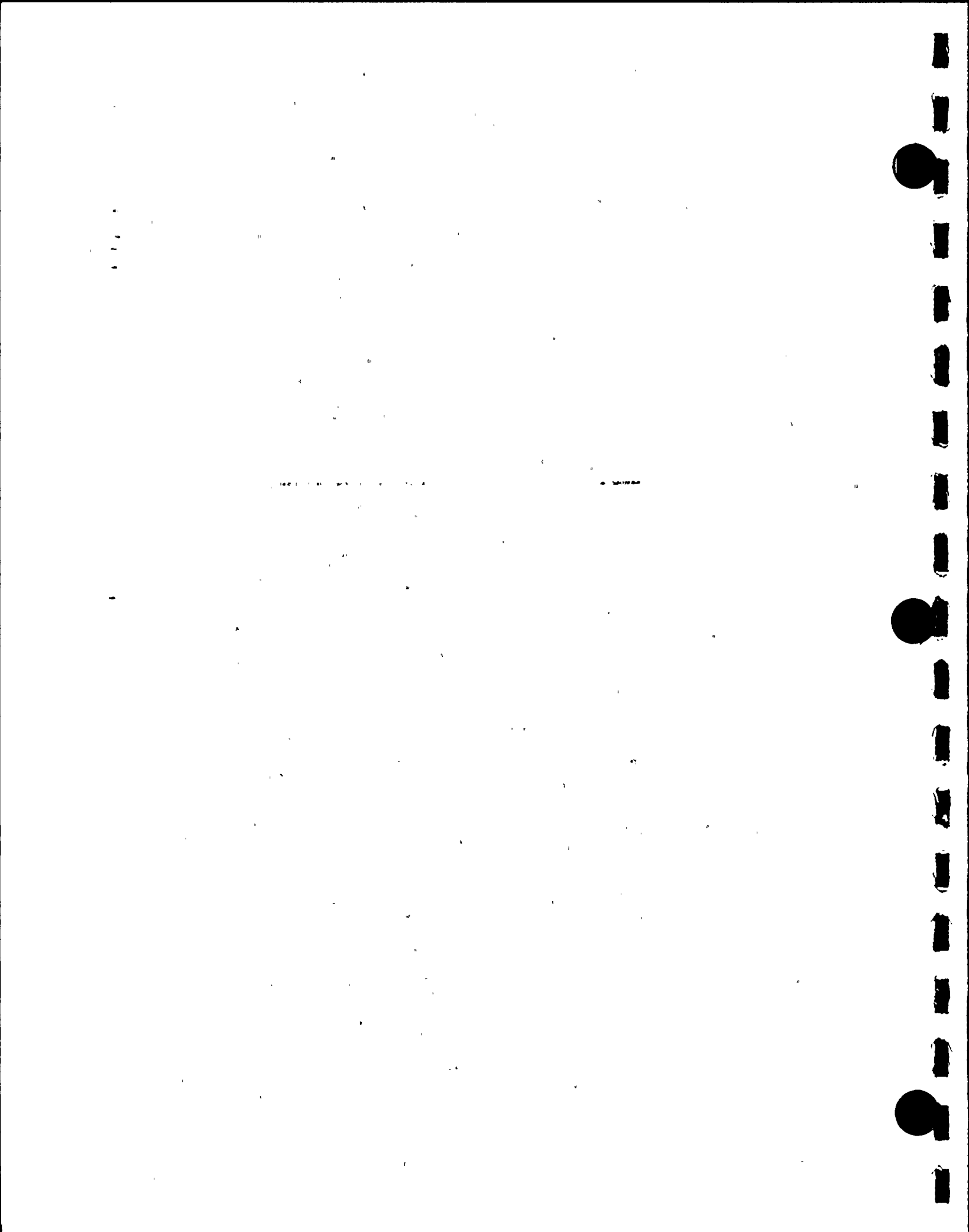


FIG. 4-5 KENO CALCULATIONAL MODEL



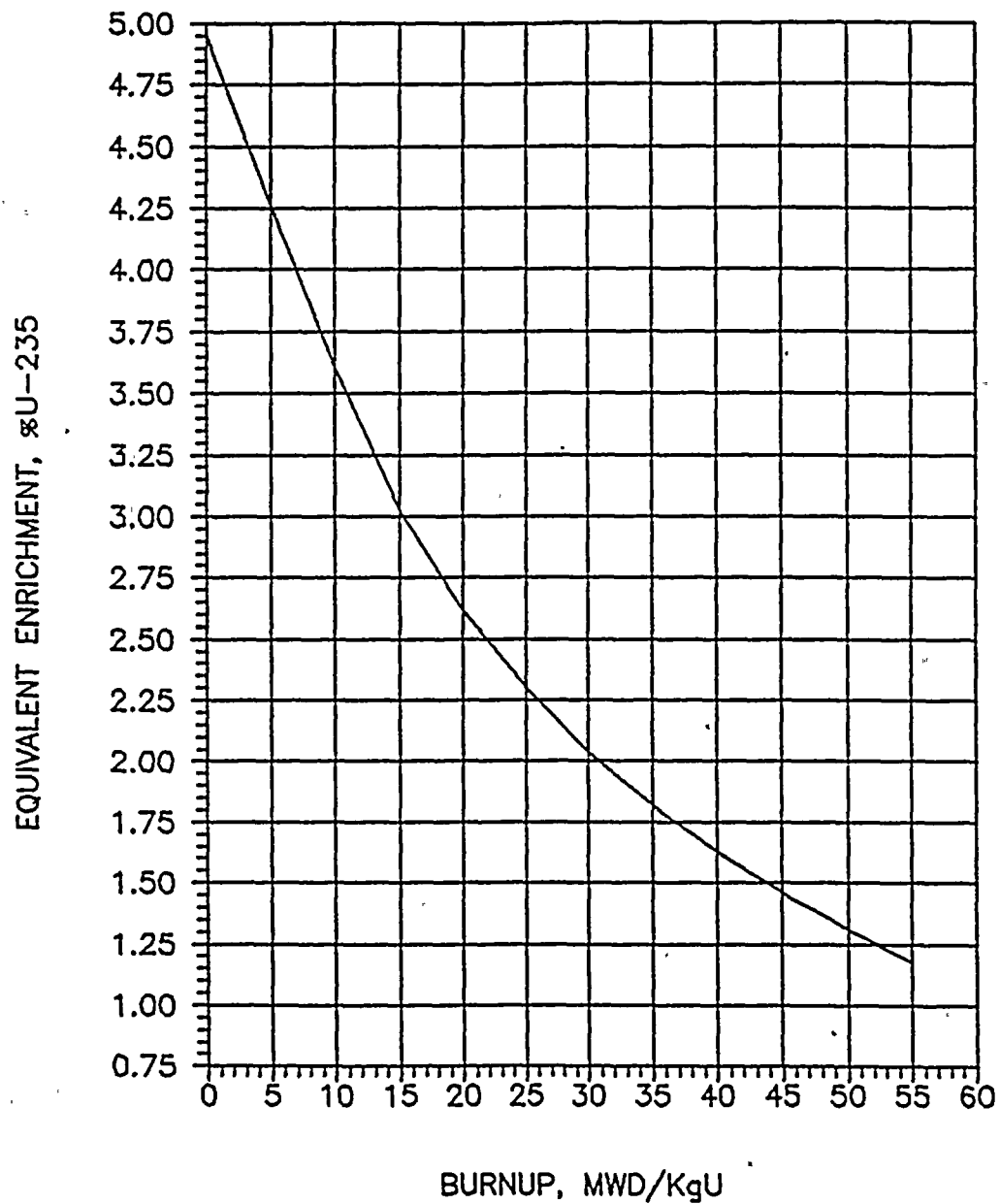
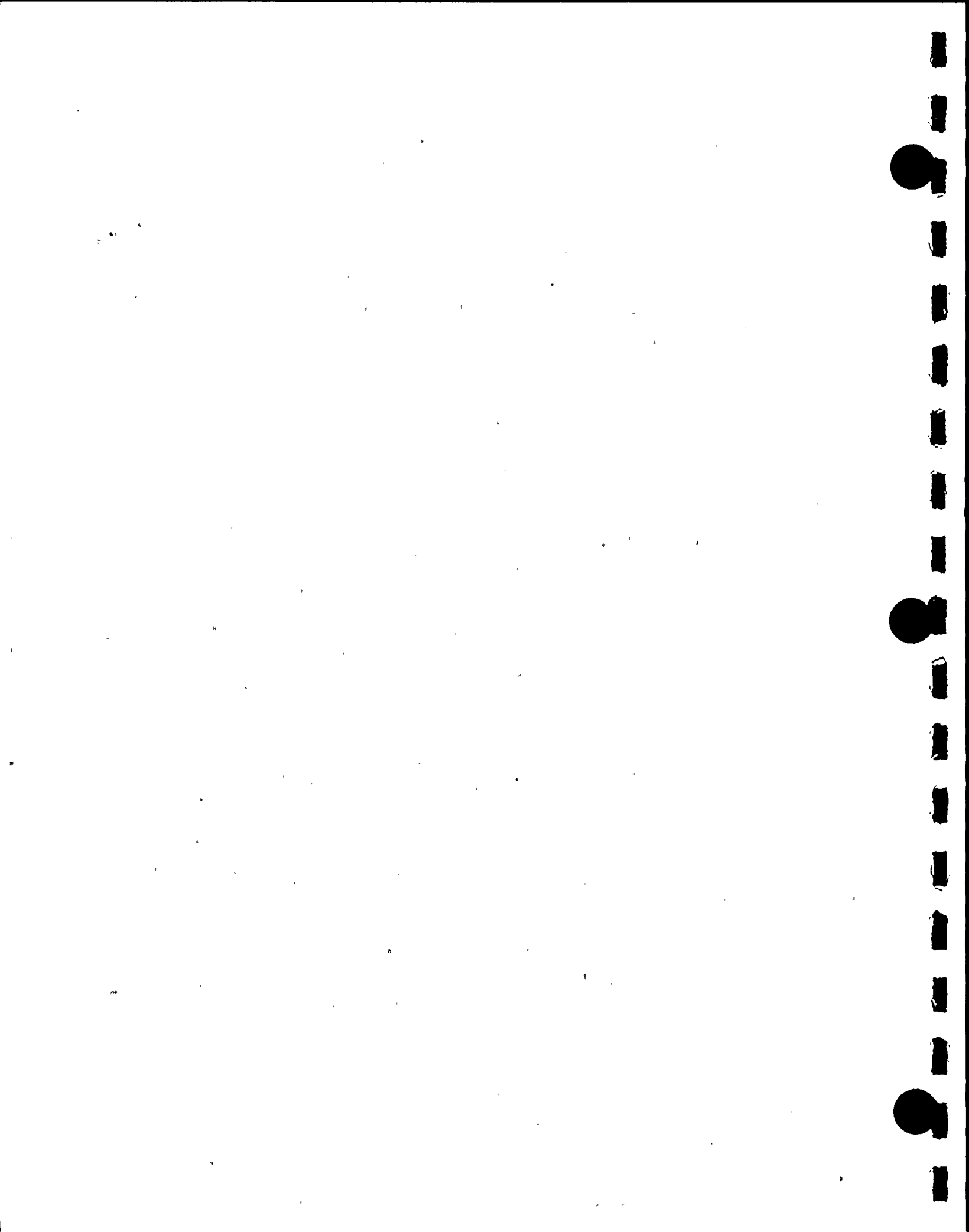


Fig. 4-6 EQUIVALENT ENRICHMENT FOR SPENT FUEL AT VARIOUS BURNUPS FOR INITIAL ENRICHMENT OF 4.95%



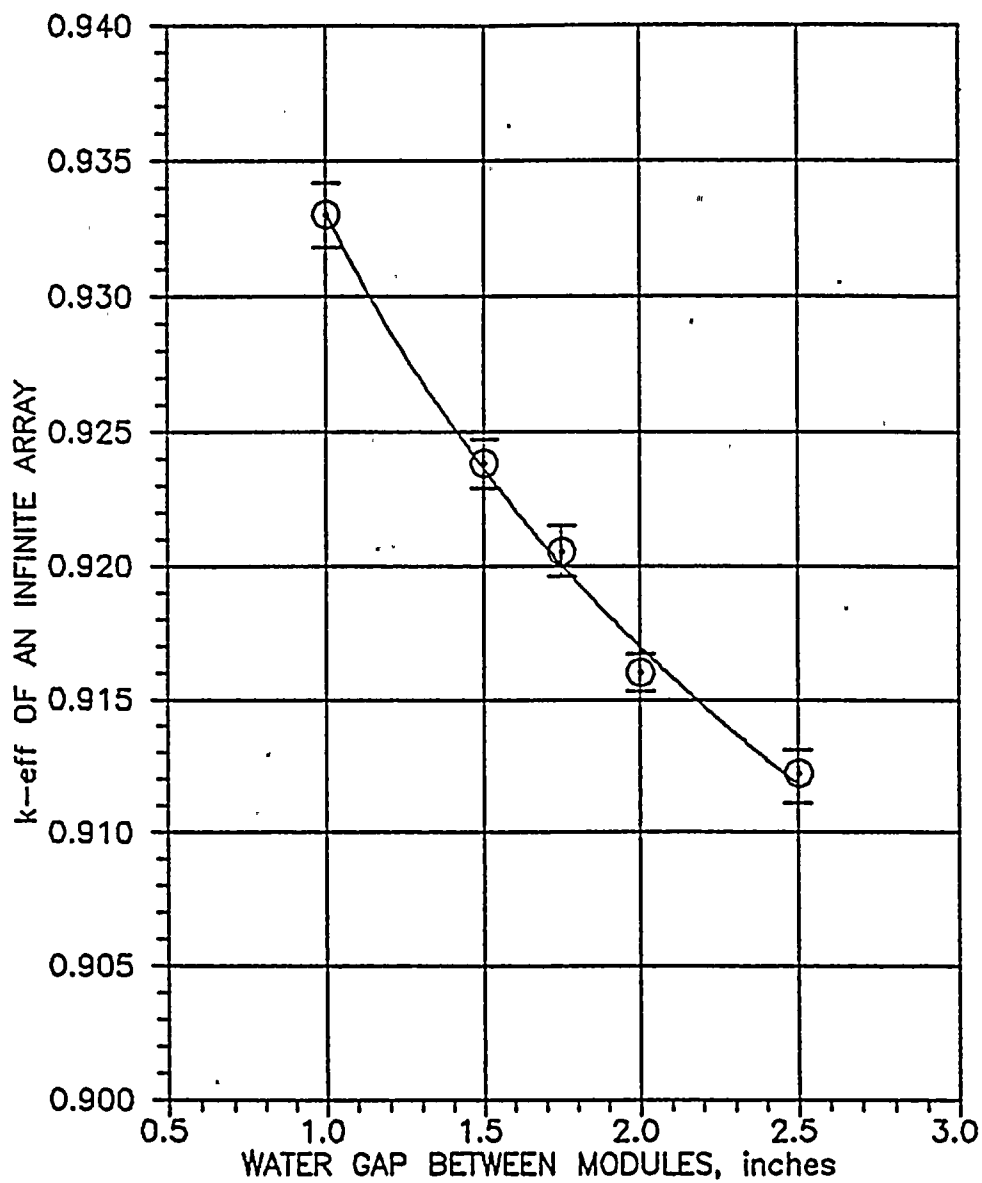
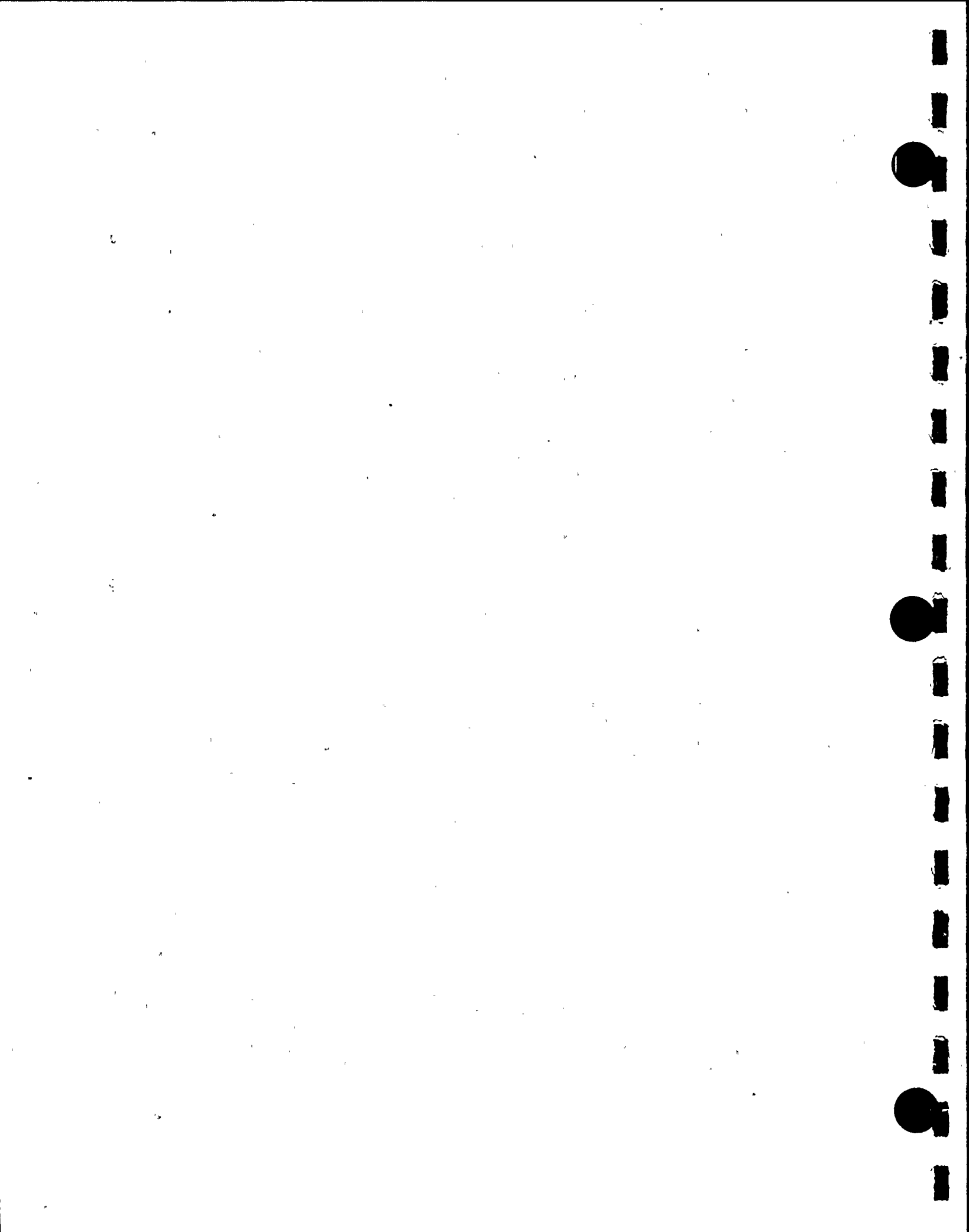


Fig. 4-7 EFFECT OF WATER-GAP SPACING BETWEEN MODULES ON SYSTEM REACTIVITY



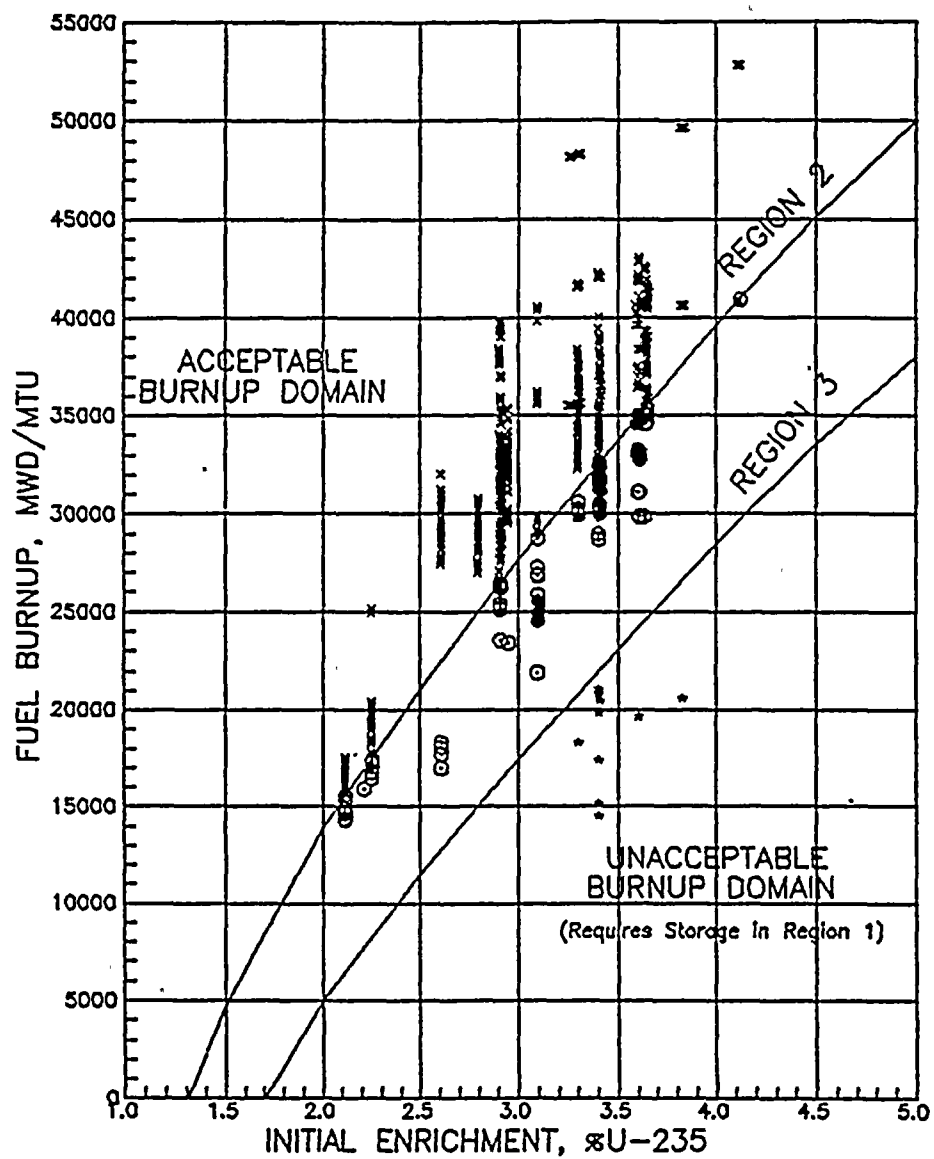
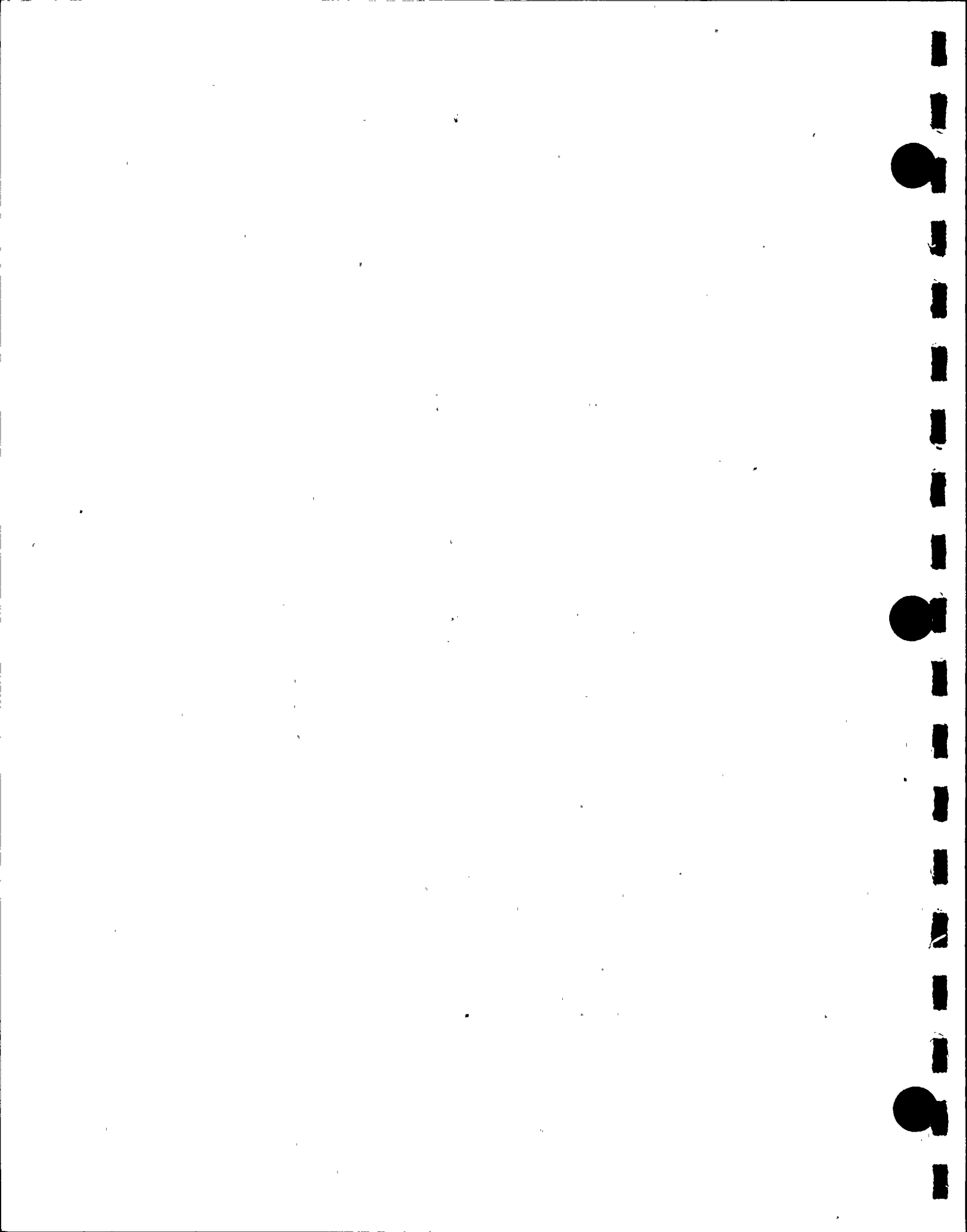


Fig. 4-8 ACCEPTABLE BURNUP DOMAIN IN REGIONS 2 & 3
SHOWING EXISTING SPENT FUEL ASSEMBLIES



APPENDIX A

BENCHMARK CALCULATIONS

by

Stanley E. Turner, PhD, PE

HOLTEC INTERNATIONAL

January 1991

1000

1000

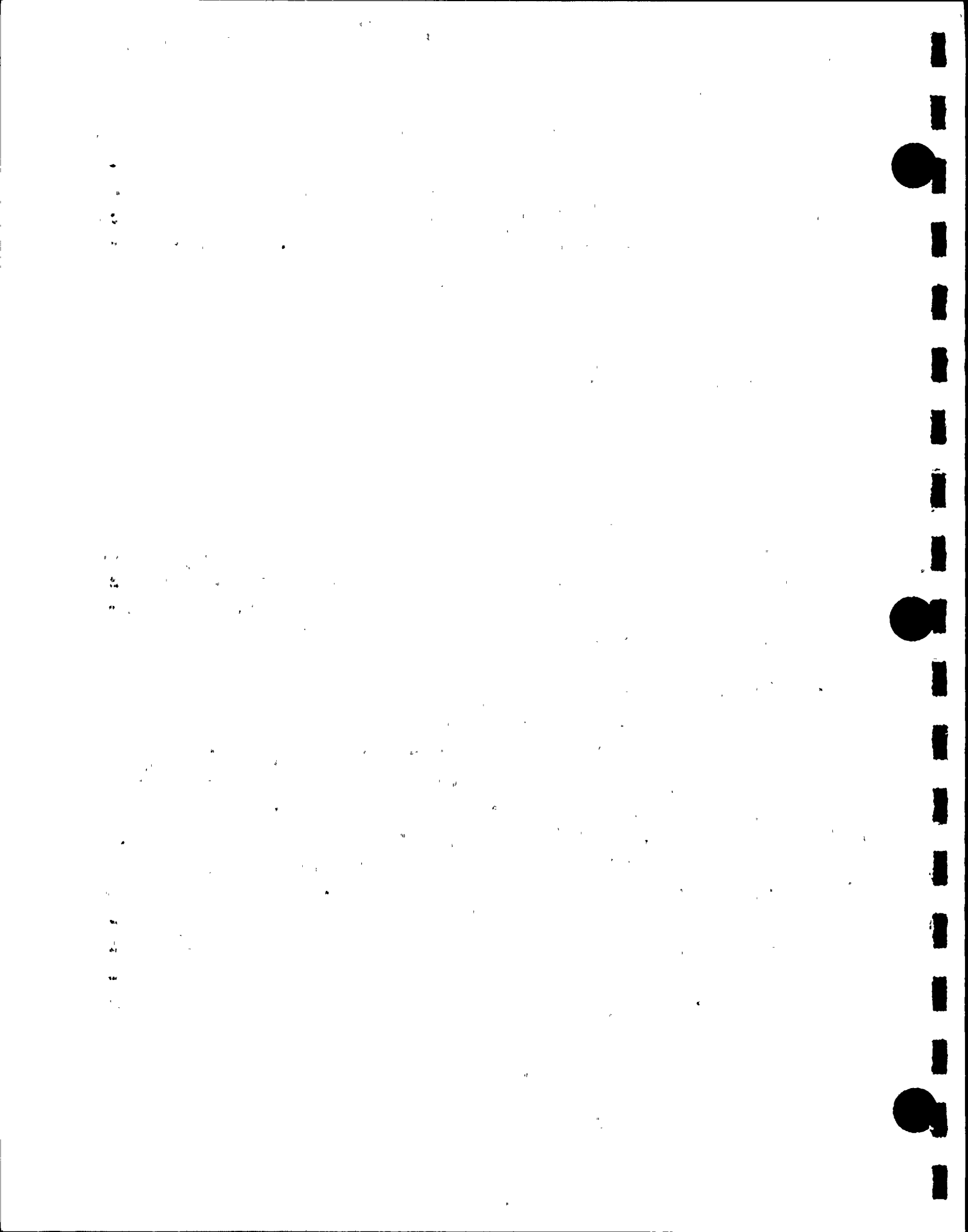
1000



The objective of this benchmarking study is to verify both the NITAWL-KENO-5a^(1,2) methodology with the 27-group SCALE cross-section library and the CASMO-3 code⁽³⁾ for use in criticality safety calculations of high density spent fuel storage racks. Both calculational methods are based upon transport theory and have been benchmarked against critical experiments that simulate typical spent fuel storage rack designs as realistically as possible. Results of these benchmark calculations with both methodologies are consistent with corresponding calculations reported in the literature.

Results of the benchmark calculations show that the 27-group (SCALE) NITAWL-KENO-5a calculations consistently underpredict the critical eigenvalue by $0.0090 \pm 0.0021 \delta k$ (with a 95% probability at a 95% confidence level) for critical experiments⁽⁴⁾ that are as representative as possible of realistic spent fuel storage rack configurations and poison worths.

Extensive benchmarking calculations of critical experiments with CASMO-3 have also been reported⁽⁵⁾, giving a mean k_{eff} of 1.0004 ± 0.0011 for 37 cases. With a K-factor of $2.14^{(6)}$ for 95% probability at a 95% confidence level, and conservatively neglecting the small overprediction, the CASMO-3 bias then becomes 0.0000 ± 0.0024 . CASMO-3 and NITAWL-KENO-5a intercomparison calculations of infinite arrays of poisoned cell configurations (representative of typical spent fuel storage rack designs) show very good agreement, confirming that 0.0000 ± 0.0024 is a reasonable bias and uncertainty for CASMO-3 calculations. Reference 5 also documents good agreement of heavy nuclide concentrations for the Yankee core isotopics, agreeing with the measured values within experimental error.

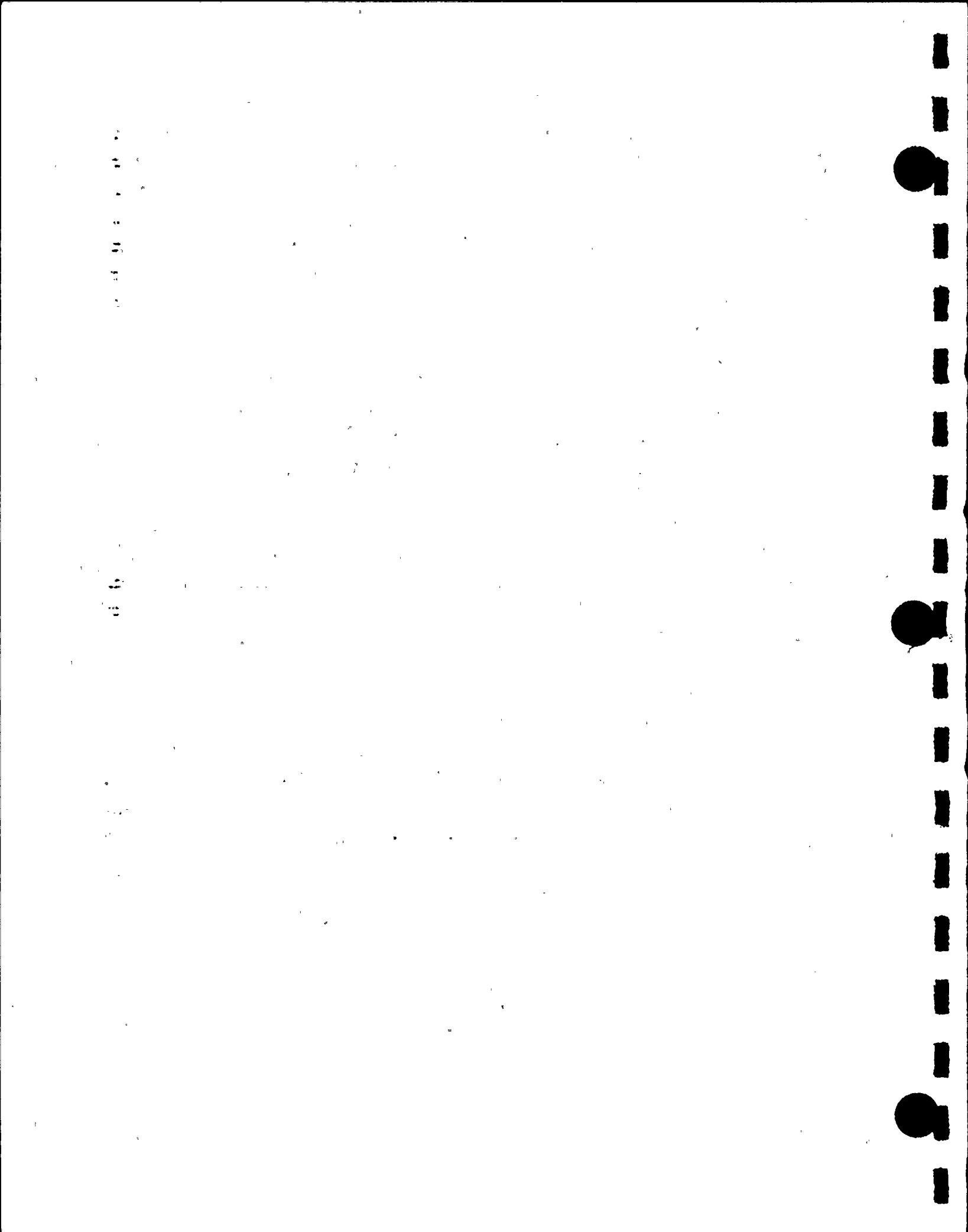


The benchmark calculations reported here confirm that either the 27-group (SCALE) NITAWL-KENO or CASMO-3 calculations are acceptable for criticality analysis of high-density spent fuel storage racks. Reference calculations for the rack designs should be performed with both code packages to provide independent verification.

2.0 NITAWL-KENO 5a BENCHMARK CALCULATIONS

Analysis of a series of Babcock & Wilcox critical experiments⁽⁴⁾, including some with absorber panels typical of a poisoned spent fuel rack, is summarized in Table 1, as calculated with NITAWL-KENO-5a using the 27-group SCALE cross-section library and the Nordheim resonance integral treatment in NITAWL. Dancoff factors for input to NITAWL were calculated with the Oak Ridge SUPERDAN routine (from the SCALE⁽²⁾ system of codes). The mean for these calculations is 0.9910 ± 0.0033 (1σ standard deviation of the population). With a one-sided tolerance factor corresponding to 95% probability at a 95% confidence level⁽⁶⁾, the calculational bias is $+ 0.0090$ with an uncertainty of ± 0.0021 for the sixteen critical experiments analyzed.

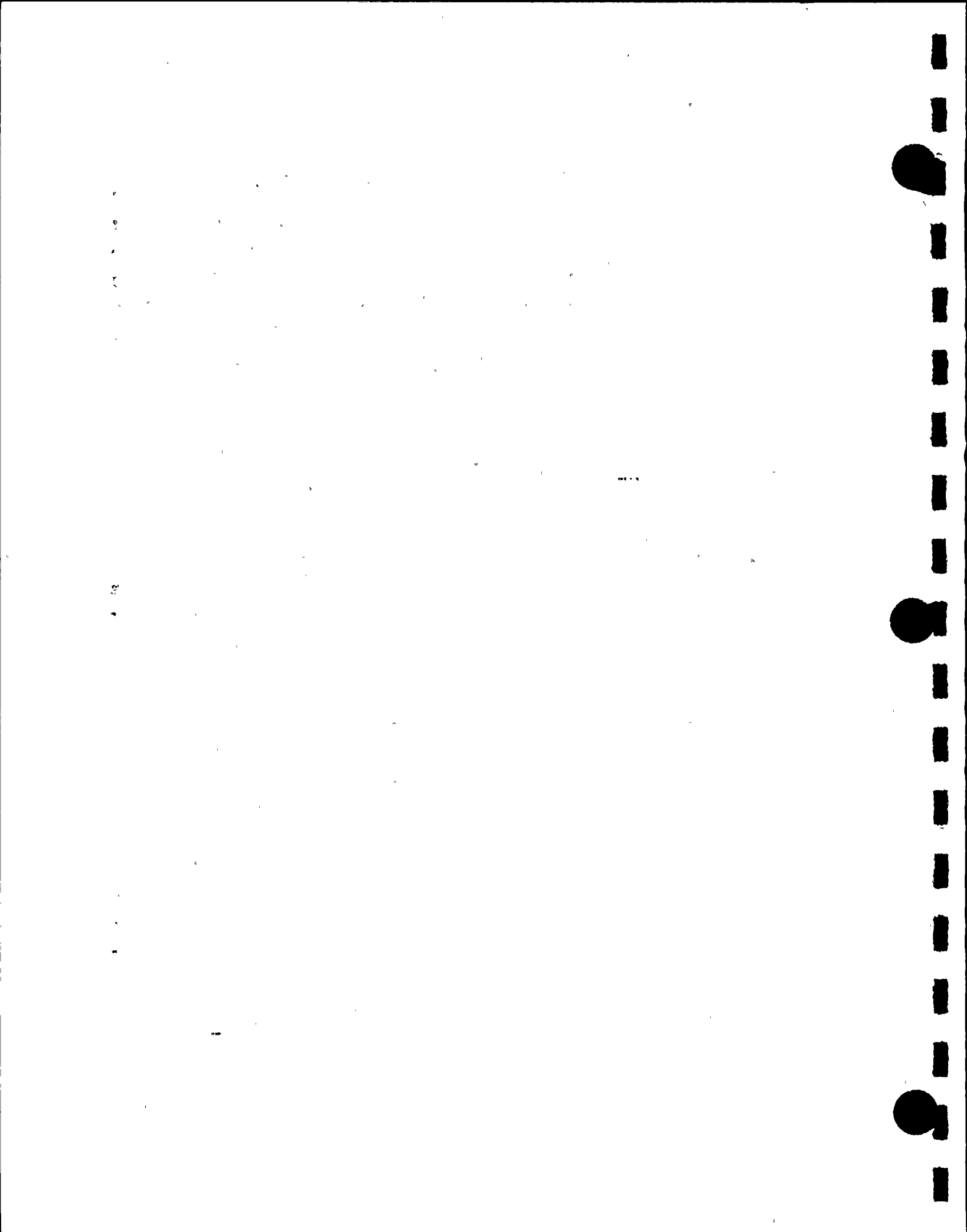
Similar calculational deviations have been reported by ORNL⁽⁷⁾ for some 54 critical experiments (mostly clean critical without strong absorbers), obtaining a mean bias of 0.0100 ± 0.0013 (95%/95%). These published results are in good agreement with the results obtained in the present analysis and lend further credence to the validity of the 27-group NITAWL-KENO-5a calculational model for use in criticality analysis of high density spent fuel storage racks. No trends in k_{eff} with intra-assembly water gap, with absorber panel reactivity worth, with enrichment or with poison concentration were identified.



Additional benchmarking calculations were also made for a series of French critical experiments⁽⁹⁾ at 4.75% enrichment and for several of the BNWL criticals with 4.26% enriched fuel. Analysis of the French criticals (Table 2) showed a tendency to overpredict the reactivity, a result also obtained by ORNL⁽¹⁰⁾. The calculated k_{eff} values showed a trend toward higher values with decreasing core size. In the absence of a significant enrichment effect (see Section 3 below), this trend and the overprediction is attributed to a small inadequacy in NITAWL-KENO-5a in calculating neutron leakage from very small assemblies.

Similar overprediction was also observed for the BNWL series of critical experiments⁽¹¹⁾, which also are small assemblies (although significantly larger than the French criticals). In this case (Table 2), the overprediction appears to be small, giving a mean k_{eff} of 0.9990 ± 0.0037 (1σ population standard deviation). Because of the small size of the BNWL critical experiments and the absence of any significant enrichment effect, the overprediction is also attributed to the failure of NITAWL-KENO-5a to adequately treat neutron leakage in very small assemblies.

Since the analysis of high-density spent fuel storage racks generally does not entail neutron leakage, the observed inadequacy of NITAWL-KENO-5a is not significant. Furthermore, omitting results of the French and BNWL critical experiment analyses from the determination of bias is conservative since any leakage that might enter into the analysis would tend to result in overprediction of the reactivity.



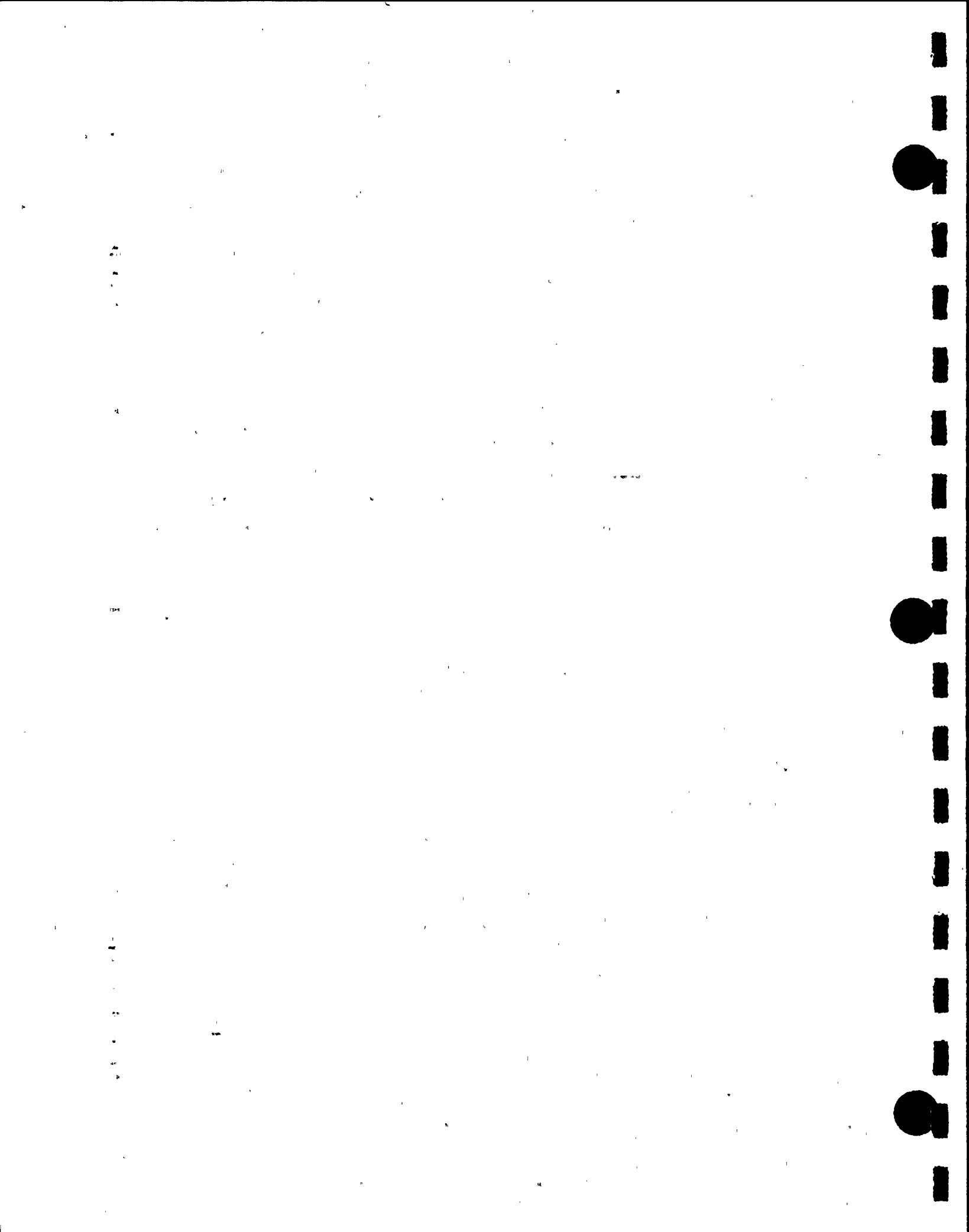
3. CASMO-3 BENCHMARK CALCULATIONS

The CASMO-3 code is a multigroup transport theory code utilizing transmission probabilities to accomplish two-dimensional calculations of reactivity and depletion for BWR and PWR fuel assemblies. As such, CASMO-3 is well-suited to the criticality analysis of spent fuel storage racks, since general practice is to treat the racks as an infinite medium of storage cells, neglecting leakage effects.

CASMO-3 is a modification of the CASMO-2E code and has been extensively benchmarked against both mixed oxide and hot and cold critical experiments by Studsvik Energiteknik⁽⁵⁾. Reported analyses⁽⁵⁾ of 37 critical experiments indicate a mean k_{eff} of 1.0004 ± 0.0011 (1 σ). To independently confirm the validity of CASMO-3 (and to investigate any effect of enrichment), a series of calculations were made with CASMO-3 and with NITAWL-KENO-5a on identical poisoned storage cells representative of high-density spent fuel storage racks. Results of these intercomparison calculations* (shown in Table 3) are within the normal statistical variation of KENO calculations and confirm the bias of 0.0000 ± 0.0024 (95%/95%) for CASMO-3.

Since two independent methods of analysis would not be expected to have the same error function with enrichment, results of the intercomparison analyses (Table 3) indicate that there is no significant effect of fuel enrichment over the range of enrichments involved in power reactor fuel. Furthermore, neglecting the French and BNWL critical benchmarking in the determination of bias is a conservative approach.

*Intercomparison between analytical methods is a technique endorsed by Reg. Guide 5.14, "Validation of Calculational Methods for Nuclear Criticality Safety".

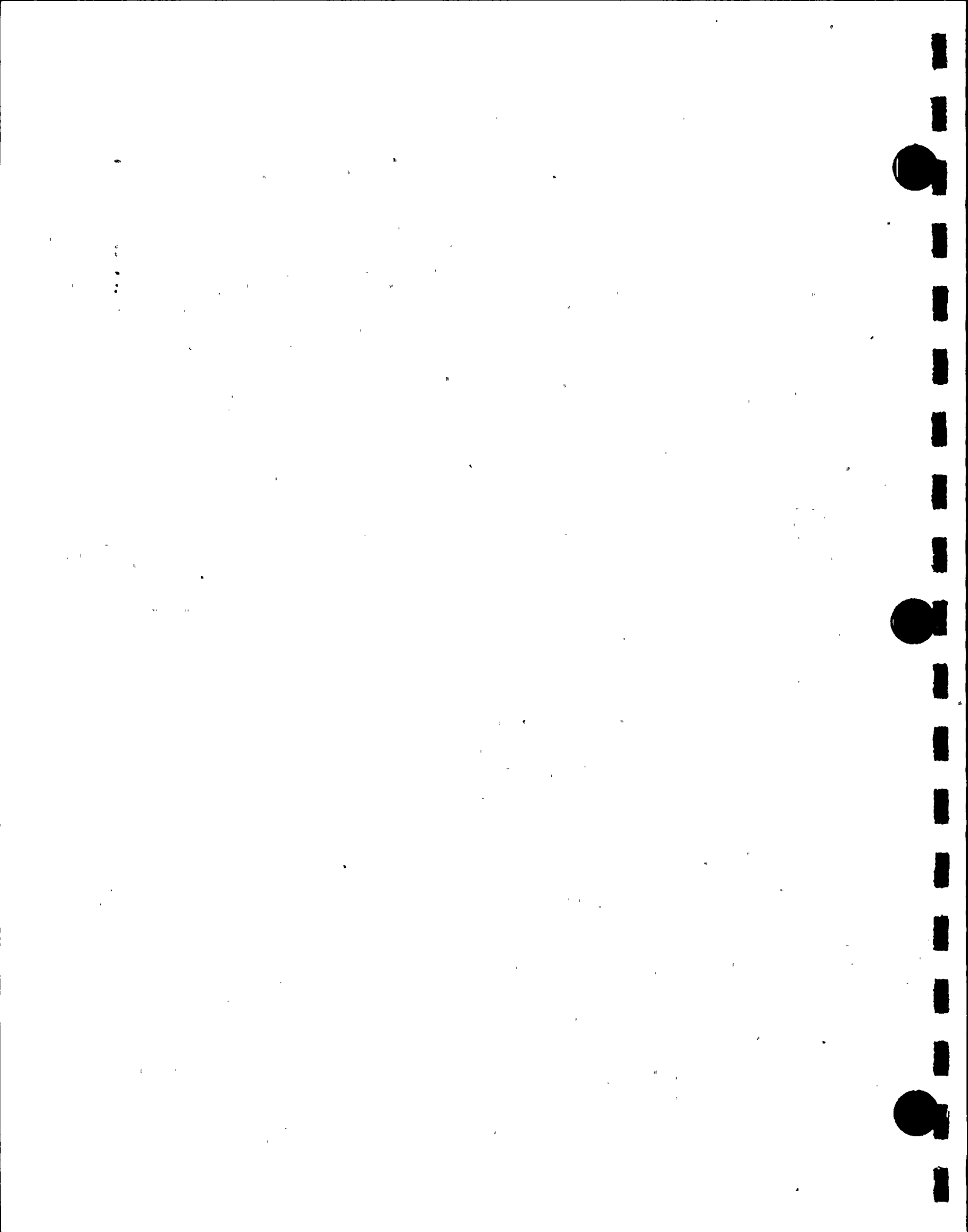


REFERENCES TO APPENDIX A

1. Green, Lucious, Petrie, Ford, White, and Wright, "PSR-63-/NITAWL-1 (code package) NITAWL Modular Code System For Generating Coupled Multigroup Neutron-Gamma Libraries from ENDF/B", ORNL-TM-3706, Oak Ridge National Laboratory, November 1975.
2. R.M. Westfall et. al., "SCALE: A Modular System for Performing Standardized Computer Analysis for Licensing Evaluation", NUREG/CR-0200, 1979.
3. A. Ahlin, M. Edenius, and H. Haggblom, "CASMO - A Fuel Assembly Burnup Program", AE-RF-76-4158, Studsvik report.

A. Ahlin and M. Edenius, "CASMO - A Fast Transport Theory Depletion Code for LWR Analysis", ANS Transactions, Vol. 26, p. 604, 1977.

"CASMO-3 A Fuel Assembly Burnup Program, Users Manual", Studsvik/NFA-87/7, Studsvik Energitechnik AB, November 1986
4. M.N. Baldwin et al., "Critical Experiments Supporting Close Proximity Water Storage of Power Reactor Fuel", BAW-1484-7, The Babcock & Wilcox Co., July 1979.
5. M. Edenius and A. Ahlin, "CASMO-3: New Features, Benchmarking, and Advanced Applications", Nuclear Science and Engineering, 100, 342-351, (1988)
6. M.G. Natrella, Experimental Statistics, National Bureau of Standards, Handbook 91, August 1963.
7. R.W. Westfall and J. H. Knight, "SCALE System Cross-section Validation with Shipping-cask Critical Experiments", ANS Transactions, Vol. 33, p. 368, November 1979.
8. S.E. Turner and M.K. Gurley, "Evaluation of NITAWL-KENO Benchmark Calculations for High Density Spent Fuel Storage Racks", Nuclear Science and Engineering, 80(2):230-237, February 1982.



9. J.C. Manaranche, et. al., "Dissolution and Storage Experiment with 4.75% U-235 Enriched UO_2 Rods", Nuclear Technology, Vol. 50, pp 148, September 1980
10. S.R. Bierman, et. al., "Critical Separation between Subcritical Clusters of 4.29 Wt. % ^{235}U Enriched UO_2 Rods in Water with Fixed Neutron Poisons", Batelle Pacific Northwest Laboratories, NUREG/CR/0073, May 1978 (with August 1979 errata).
11. A.M. Hathout, et. al., "Validation of Three Cross-section Libraries Used with the SCALE System for Criticality Analysis", Oak Ridge National Laboratory, NUREG/CR-1917, 1981.



Table 1

RESULTS OF 27-GROUP (SCALE) NITAWL-KENO-5a CALCULATIONS
OF B&W CRITICAL EXPERIMENTS

| Experiment
Number | Calculated
k_{eff} | σ |
|----------------------|-------------------------|--------------------|
| I | 0.9932 | ± 0.0016 |
| II | 0.9915 | ± 0.0015 |
| III | 0.9916 | ± 0.0013 |
| IX | 0.9918 | ± 0.0014 |
| X | 0.9923 | ± 0.0015 |
| XI | 0.9919 | ± 0.0014 |
| XII | 0.9961 | ± 0.0015 |
| XIII | 0.9960 | ± 0.0015 |
| XIV | 0.9817 | ± 0.0015 |
| XV | 0.9843 | ± 0.0014 |
| XVI | 0.9912 | ± 0.0015 |
| XVII | 0.9866 | ± 0.0013 |
| XVIII | 0.9904 | ± 0.0014 |
| XIX | 0.9861 | ± 0.0013 |
| XX | 0.9934 | ± 0.0013 |
| XXI | 0.9874 | ± 0.0014 |
| Mean | 0.9910 | $\pm 0.0014^{(1)}$ |
| Bias | 0.0090 | $\pm 0.0033^{(2)}$ |
| Bias (95%/95%) | 0.0090 | ± 0.0021 |

(1) Calculated from individual standard deviations.

(2) Calculated from k_{eff} values and used as reference.

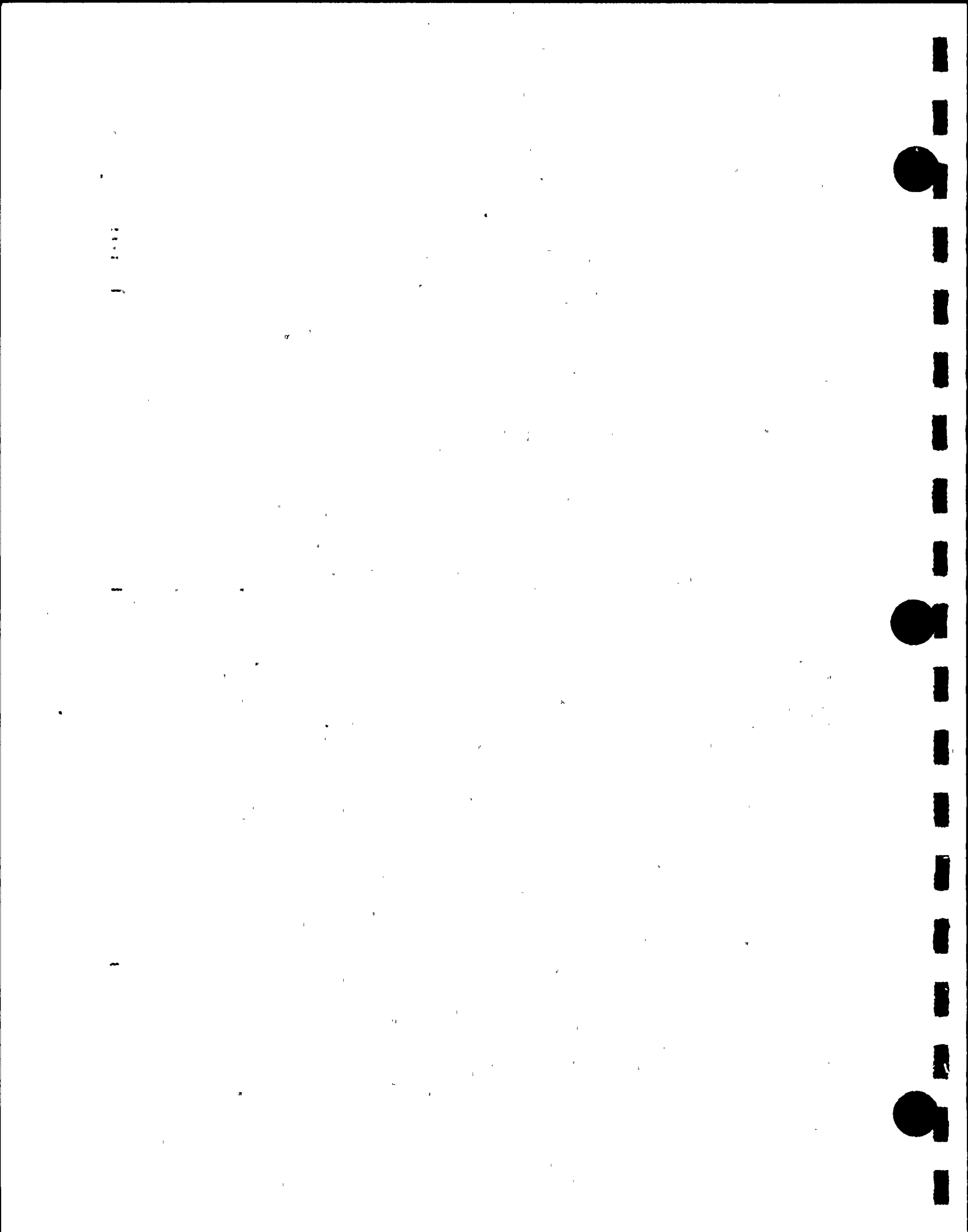


Table 2

RESULTS OF 27-GROUP (SCALE) NITAWL-KENO-5a CALCULATIONS
OF FRENCH and BNWL CRITICAL EXPERIMENTS

| French Experiments | | |
|----------------------------|------------------------|-------------------------|
| Separation
Distance, cm | Critical
Height, cm | Calculated
k_{eff} |
| 0 | 23.8 | 1.0231 ± 0.0036 |
| 2.5 | 24.48 | 1.0252 ± 0.0043 |
| 5.0 | 31.47 | 1.0073 ± 0.0013 |
| 10.0 | 64.34 | 0.9944 ± 0.0014 |
| BNWL Experiments | | |
| Case | Expt. No. | Calculated
k_{eff} |
| No Absorber | 004/032 | 0.9964 ± 0.0034 |
| SS Plates (1.05 B) | 009 | 0.9988 ± 0.0038 |
| SS Plates (1.62 B) | 011 | 1.0032 ± 0.0033 |
| SS Plates (1.62 B) | 012 | 0.9986 ± 0.0036 |
| SS Plates | 013 | 0.9980 ± 0.0038 |
| SS Plates | 014 | 0.9936 ± 0.0036 |
| Zr Plates | 030 | 1.0044 ± 0.0035 |
| Mean | | 0.9990 ± 0.0037 |

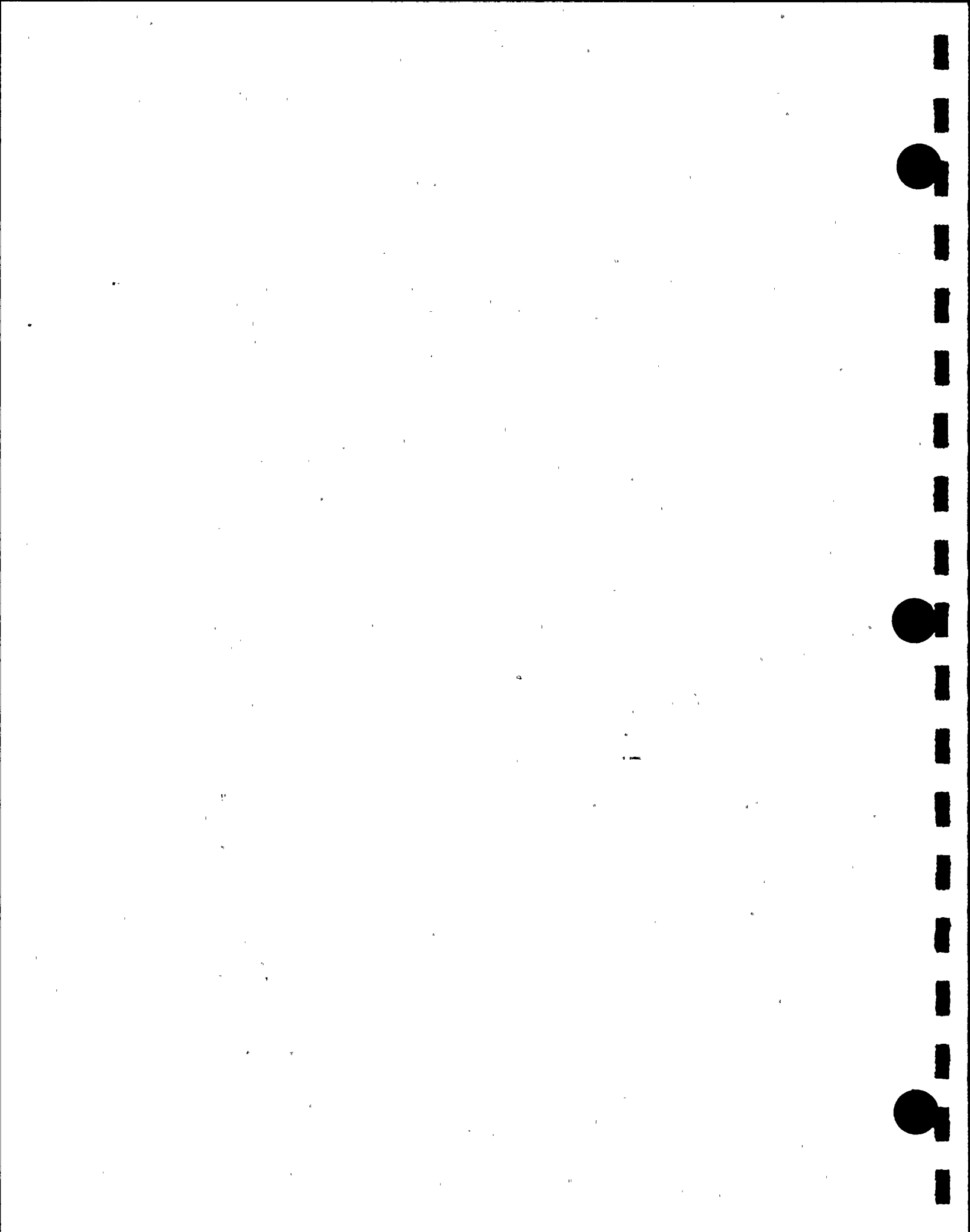


Table 3

RESULTS OF CASMO-3 AND NITAWL-KENO-5a
BENCHMARK (INTERCOMPARISON) CALCULATIONS

| Enrichment ⁽¹⁾
Wt. % U-235 | NITAWL-KENO-5a ⁽²⁾ $k_{\infty}^{(1)}$ | CASMO-3 | $ \delta k $ |
|--|--|---------|--------------|
| 2.5 | 0.8385 \pm 0.0016 | 0.8379 | 0.0006 |
| 3.0 | 0.8808 \pm 0.0016 | 0.8776 | 0.0032 |
| 3.5 | 0.9074 \pm 0.0016 | 0.9090 | 0.0016 |
| 4.0 | 0.9311 \pm 0.0016 | 0.9346 | 0.0035 |
| 4.5 | 0.9546 \pm 0.0018 | 0.9559 | 0.0013 |
| 5.0 | 0.9743 \pm 0.0018 | 0.9741 | 0.0002 |
| | | Mean | 0.0017 |

(1) Infinite array of assemblies typical of high-density spent fuel storage racks.

(2) k_{∞} from NITAWL-KENO-5a corrected for bias of 0.0090 δk .



5.0 THERMAL-HYDRAULIC CONSIDERATIONS

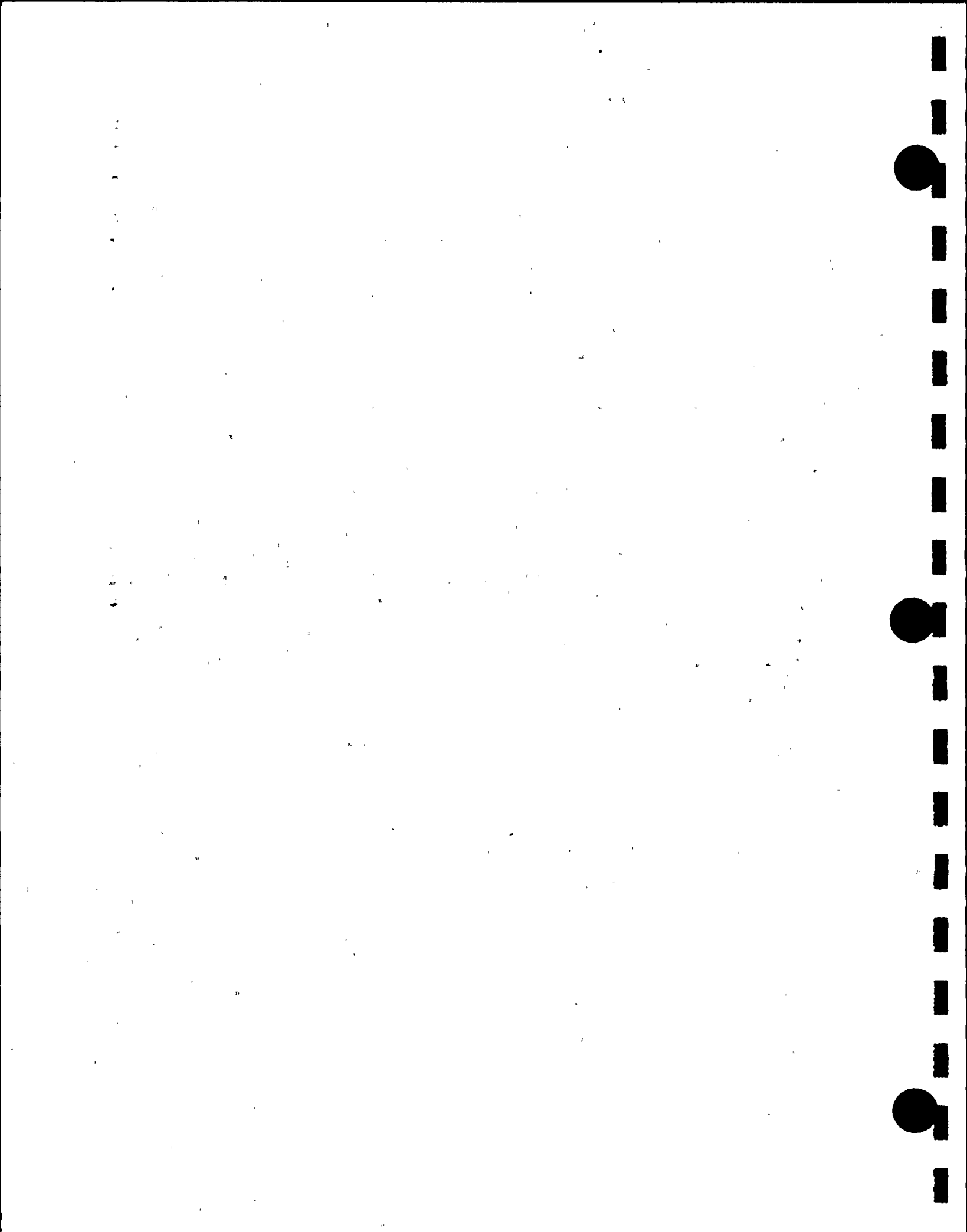
5.1 Introduction

A primary objective in the design of the high density spent fuel storage racks for the Donald C. Cook spent fuel pool is to ensure adequate cooling of the fuel assembly cladding. In the following section a brief synopsis of the design basis, the method of analysis, and the numerical results is provided.

Similar methods of thermal-hydraulic analysis have been used in previous licensing efforts on high density spent fuel racks for Fermi 2 (Docket 50-341), Quad Cities 1 and 2 (Dockets 50-254 and 50-265), Rancho Seco (Docket 50-312), Grand Gulf Unit 1 (Docket 50-416), Oyster Creek (Docket 50-219), Virgil C. Summer (Docket 50-395), Diablo Canyon 1 and 2 (Docket Nos. 50-275 and 50-323), Byron Units 1 and 2 (Docket 50-454, 455), St. Lucie Unit One (Docket 50-335), Millstone Point I (50-245), Vogtle Unit 2 (50-425), Kuosheng Units 1 & 2 (Taiwan Power Company), Ulchin Unit 2 (Korea Electric Power Company), J.A. FitzPatrick (New York Power Authority) and TMI Unit 1 (GPU Nuclear).

The analyses to be carried out for the thermal-hydraulic qualification of the rack array may be broken down into the following categories:

- (i) Pool decay heat evaluation and pool bulk temperature variation with time.
- (ii) Determination of the maximum pool local temperature at the instant when the bulk temperature reaches its maximum value.



- (iii) Evaluation of the maximum fuel cladding temperature to establish that bulk nucleate boiling at any location resulting in two phase conditions environment around the fuel does not occur.
- (iv) Evaluation of the time-to-boil if all heat rejection paths through the cooling and cleanup are lost.
- (v) Compute the effect of a blocked fuel cell opening on the local water and maximum cladding temperature.

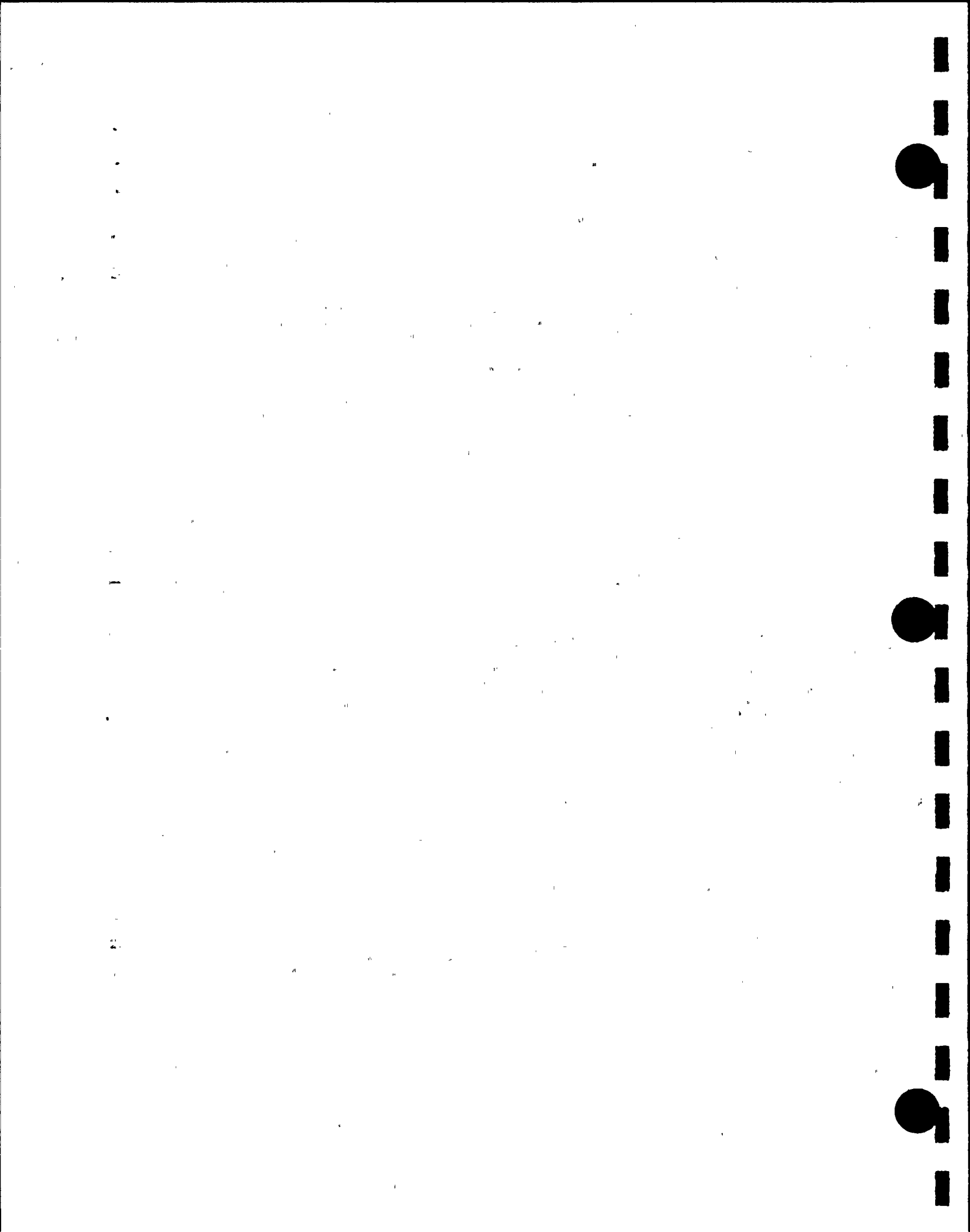
The following sections present a synopsis of the methods employed to perform such analyses and a final summary of the results.

5.2 Spent Fuel Cooling System Description

The principal functions of the Spent Fuel Cooling System are the removal of decay heat from the spent fuel stored in the pool it serves and maintaining the clarity of, and a low activity level in, the water of the pool. Cleanup of pool water is accomplished by diverting part of the flow, maintained for removal of decay heat, through filters and/or demineralizers as described in Section 9.4 of UFSAR.

5.2.1 System Functions

The Spent Fuel Pool Cooling System is designed to remove from the spent fuel pool the heat generated by stored spent fuel elements. The system serves the spent fuel pool which is shared between the two units.



The system design incorporates two separate cooling trains. System piping is arranged so that failure of any pipeline does not drain the spent fuel pool below the top of the stored fuel elements.

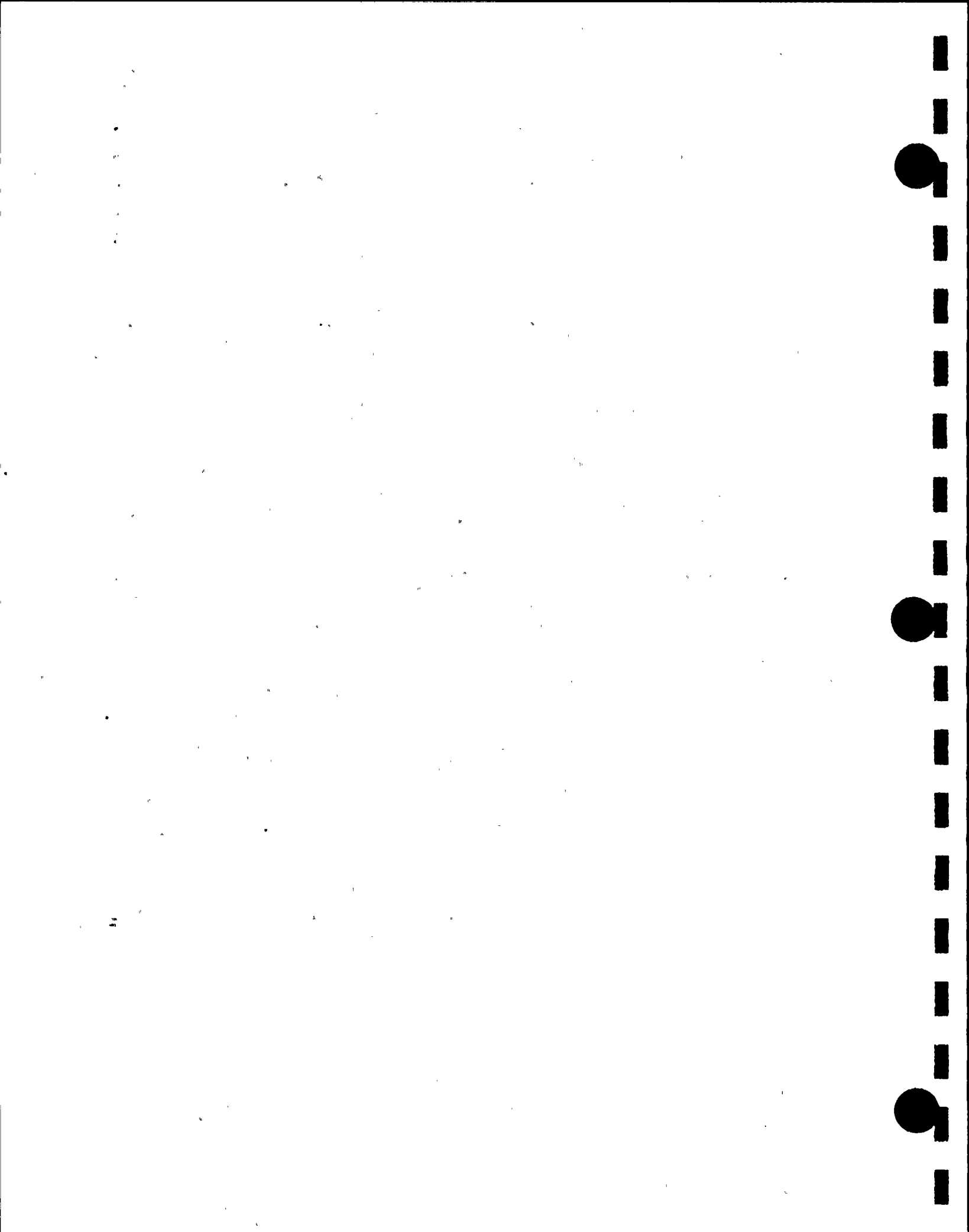
5.2.2 System Description

Each of the two cooling loops in the Spent Fuel Pool Cooling System consists of a pump, heat exchanger, strainer, piping, associated valves and instrumentation. The pump draws water from the pool, circulates it through the heat exchanger and returns it to the pool. Component cooling water cools the heat exchanger.

The clarity and purity of the spent fuel pool water is maintained by passing approximately 100 gpm of the cooling flow through a filter and demineralizer. Skimmers are provided to prevent dust and debris from accumulating on the surface of the water.

The refueling water purification pump and filter can be used separately or in conjunction with the spent fuel pool demineralizer to regain refueling water clarity after a crud burst in either unit. This can prevent loss of time during refueling due to poor visibility. The system is also used to maintain water quality in the Refueling Water Storage Tanks of both units.

The spent fuel pool filter/demineralizer is downstream of the spent fuel pool cooler. As a result, the pool purification components are subjected to water temperatures which correspond to the cooler outlets (less than 140°F). All elements of the purification system, including the resins, are qualified for 200°F design temperature.



The spent fuel pool pump suction lines penetrate the spent fuel pool wall above the fuel assemblies stored in the pool to prevent loss of water as a result of a suction line rupture. The pool is initially filled with water at the same boron concentration (2400 ppm) as in the refueling water storage tank.

The spent fuel pool is located outside the reactor containment. During refueling the water in the pool can be isolated from that in the re-fueling canal by a weir gate so that there is only a very small amount of interchange of water as fuel assemblies are transferred.

5.2.3 Performance Requirements

The first design basis of the system is based on the normal refueling operation with a normal batch of 80 assemblies being removed from the unit each time.

The second design basis for the system considers that it is possible to unload the reactor vessel (193 fuel assemblies) for maintenance or inspection at a time when a maximum of 3518 spent fuel assemblies are assumed already stored in the spent fuel pool.

5.3 Decay Heat Load Calculations

The decay heat load calculation is performed in accordance with the provisions of USNRC Branch Technical Position ASB9-2, "Residual Decay Energy for Light Water Reactors for Long Term Cooling", Rev. 2, July, 1981. For purposes of this licensing



11 11 11 11 11

11

11

application, it is assumed that the pool contains an inventory accumulated through scheduled discharges from 1975 to 2009 (Table 1.1.1). Further, since the decay heat load increases monotonically with reactor exposure time, an upper bound of 1260 full power operation days (approximately 3.5 years) is assumed for all stored fuel. The cumulative decay heat load is computed for the instance of hypothetical normal discharge (21B in Table 1.1.1) in the year 2009. As shown in Table 5.4.1, the ratio of this decay heat load due to the inventory of previously stored fuel to the average assembly operating power β is 0.3303.

This decay heat load is assumed to remain invariant for the duration of the pool temperature evaluations performed in the wake of normal and full core offloads discussed below.

5.4 Discharge Scenarios

The following discharge scenarios are examined:

Case 1: Normal discharge

A normal batch of 80 assemblies with 1260 days of reactor exposure time at full power is discharged in the pool at the end of a normal 18 month operating cycle. There are 43 previously discharged batches in the pool. As described later, the normal discharge is assumed to occur at the rate of approximately 4 assemblies per hour after 168 hours of decay in the reactor. One fuel pool cooling train is active and running. One cooling train contains one heat exchanger and one fuel pool pump.

This case is run with the design fuel pool water flow rate (2300 gpm) and actual available flow rate (2800 gpm). These two cases are labelled as Case 1a and Case 1b, respectively.

Case 2: Normal discharge

Same as Case 1 except two fuel pool cooling trains are operating.



0 1 2 3 4 5 6 7 8 9

10

Case 3: Back-to-Back Full core offload

The full core offload condition corresponds to the emergency reactor offload condition wherein the shutdown of a reactor occurs 30 days after the other reactor shutdown for a normal refueling. Two cooling trains are assumed to be operating in parallel after the shutdown. The decay time of the core in the reactor and the rate of discharge to the pool are the same as in Case 1.

Case 4:

Same as Case 3 except only one cooling train is in operation. This case is listed for reference only; it is not a design basis case by the Donald C. Cook Technical Specification or the USNRC guidelines (NUREG-0800).

Detailed data on the three cases are given in Table 5.4.1 to 5.4.3.

5.5 Bulk Pool Temperature

In order to perform the analysis conservatively, the heat exchangers are assumed to be fouled to their design maximum. Thus, the temperature effectiveness, p , for the heat exchanger utilized in the analysis is the lowest postulated value calculated from heat exchanger thermal hydraulic codes. p is assumed constant in the calculation.

The mathematical formulation can be explained with reference to the simplified heat exchanger alignment of Figure 5.5.1.

Referring to the spent fuel pool/cooler system, the governing differential equation can be written by utilizing conservation of energy:

$$C \frac{dT}{dt} = Q_L - Q_{HX} \quad (5-1)$$

$$Q_L = P_{\text{cons}} + Q(\tau) - Q_{EV}(T, t_a)$$



where:

- C: Thermal capacitance of the pool (net water volume times water density and times heat capacity), Btu/°F.
- Q_L : Heat load to the heat exchanger, Btu/hr.
- $Q(\tau)$: Heat generation rate from recently discharged fuel, which is a specified function of time, τ , Btu/hr.
- $P_{cons} = \beta P_o$: Heat generation rate from "old" fuel, Btu/hr. (P_o = average assembly operating power, Btu/hr.)
- Q_{HX} : Heat removal rate by the heat exchanger, Btu/hr.
- $Q_{EV}(T, t_a)$: Heat loss to the surroundings, which is a function of pool temperature T and ambient temperature t_a , Btu/hr.

Q_{HX} is a non-linear function of time if we assume the temperature effectiveness p is constant during the calculation. Q_{HX} can, however, be written in terms of effectiveness p as follows:

$$Q_{HX} = W_t C_t p (T - t_i) \quad (5-2)$$

$$p = \frac{t_o - t_i}{T - t_i}$$

where:

- W_t : Coolant flow rate, lb./hr.
- C_t : Coolant specific heat, Btu/lb.°F.
- p : Temperature effectiveness of heat exchanger.



T: Pool water temperature, °F

t_i: Coolant inlet temperature, °F

t_o: Coolant outlet temperature, °F

p is obtained by rating the heat exchanger on a Holtec proprietary thermal/hydraulic computer code. Q(τ) is specified according to the provisions of "USNRC Branch Technical Position ASB9-2, "Residual Decay Energy for Light Water Reactors for Long Term Cooling", Rev. 2, July, 1981. Q(τ) is a function of decay time, number of assemblies, and in-core exposure time. During the fuel transfer, the heat load in the pool will increase with respect to the rate of fuel transfer and equals to Q(τ) after the fuel transfer.

Q_{EV} is a non-linear function of pool temperature and ambient temperature. Q_{EV} contains the heat evaporation loss through the pool surface, natural convection from the pool surface and heat conduction through the pool walls and slab. Experiments show that the heat conduction takes only about 4% of the total heat loss [5.5.1], therefore, can be neglected. The evaporation heat and nature convection heat loss can be expressed as:

$$Q_{EV} = m \Gamma A_s + h_c A_s \theta \quad (5-3)$$

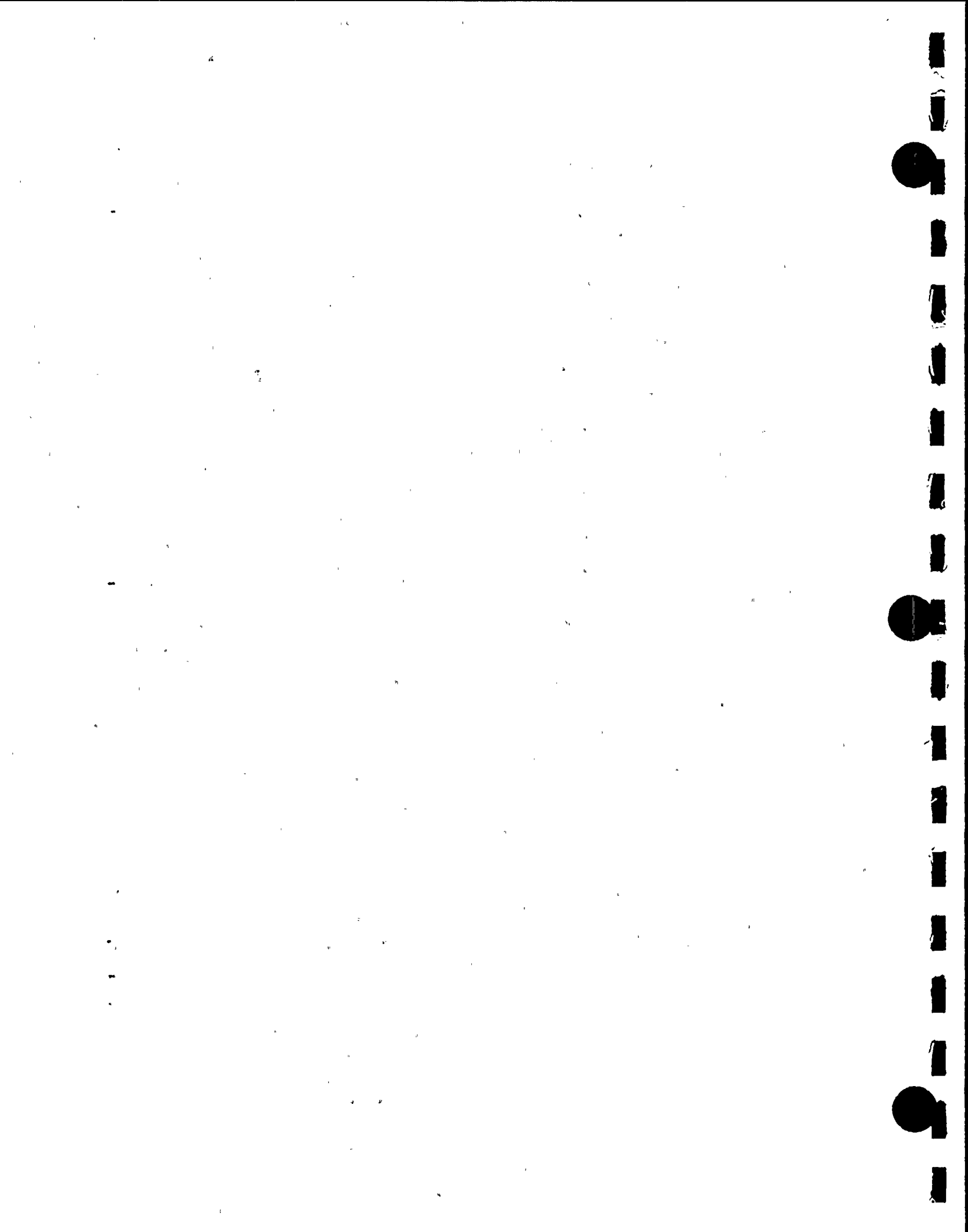
where:

m: Mass evaporation rate, lb./hr. ft.²

Γ: Latent heat of pool water, Btu/lb.

A_s: Pool surface area, ft.²

h_c: Convection heat transfer coefficient at pool surface, Btu/ft.² hr. °F



$\theta = T - t_a$: The temperature difference between pool water and ambient air, °F

The mass evaporation rate m can be obtained as a non-linear function of θ . We, therefore, have

$$m = h_D(\theta) (W_{ps} - W_{as}) \quad (5-4)$$

where:

W_{ps} : Humidity ratio of saturated moist air at pool water surface temperature T .

W_{as} : Humidity ratio of saturated moist air at ambient temperature t_a

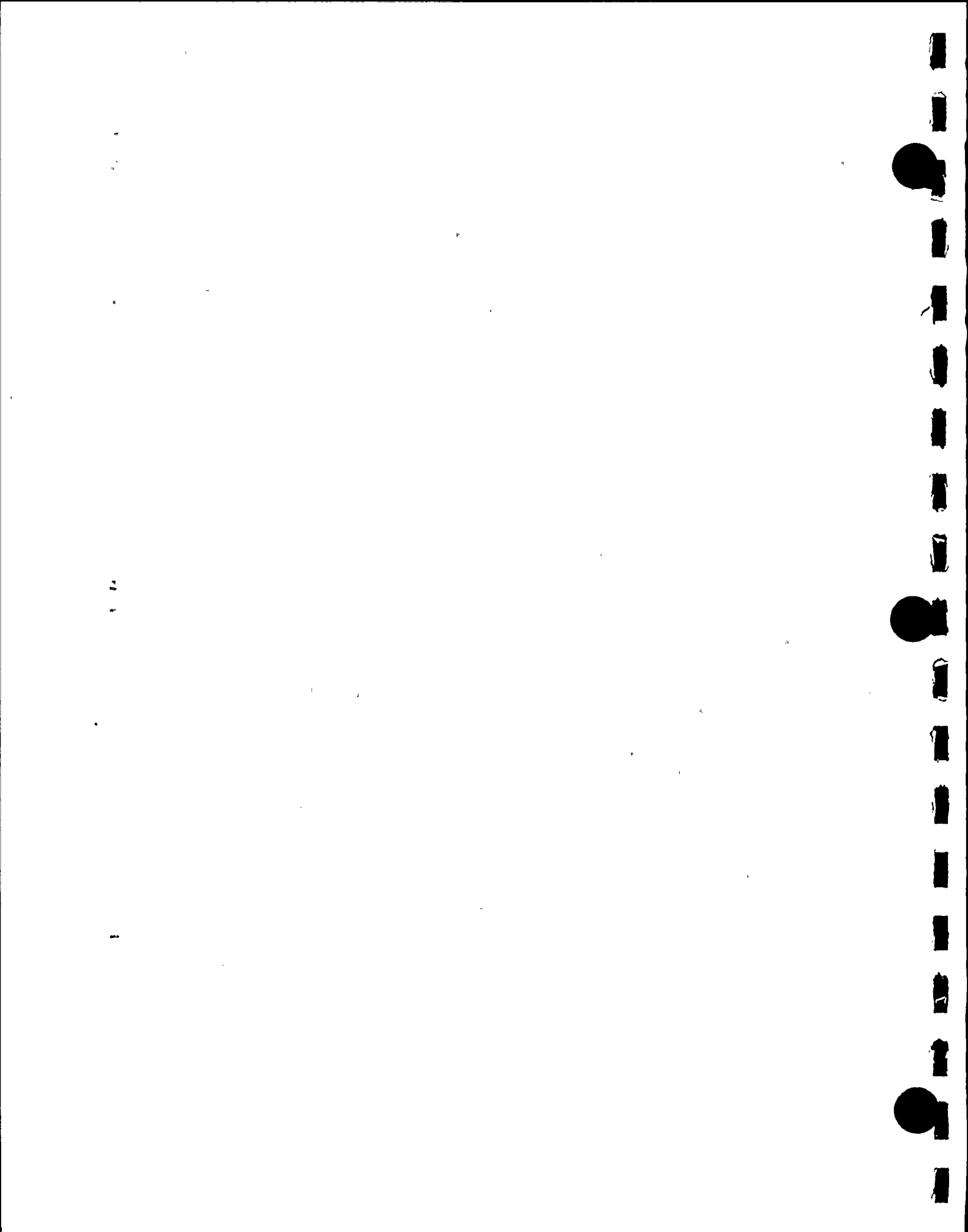
$h_D(\theta)$: Diffusion coefficient at pool water surface. h_D is a non-linear function of θ , lb./hr. ft.² °F

The non-linear single order differential equation (5-1) is solved using Holtec's Q.A. validated numerical integration code "ONEPOOL".

Figures 5.5.2 through 5.5.6 provide the bulk pool temperature profiles for the normal discharge, and full core offload scenarios respectively. Table 5.5.1 gives the peak water temperature, coincident time, and coincident heat load to the cooler and coincident heat loss to the ambient for three cases.

The next step in the analysis is to determine the temperature rise profile of the pool water if all forced indirect cooling modes are suddenly lost. Make-up water is provided with a fire hose.

Clearly, the most critical instant of loss-of-cooling is when pool water has reached its maximum value. It is assumed that cooling water is added through a fire hose at the rate of G lb./hr. The



cooling water is at temperature, t_{cool} . The governing enthalpy balance equation for this condition can be written as

$$[C + G(C_t)(\tau - \tau_0)] \frac{dT}{d\tau} = P_{cons} + Q(\tau + \tau_{ins}) + G(C_t)(t_{cool} - T) - Q_{EV}$$

where water is assumed to have specific heat of unity, and the time coordinate τ is measured from the instant maximum pool water temperature is reached. τ_0 is the time coordinate when the direct addition (fire hose) cooling water application is begun. τ_{ins} is the time coordinate measured from the instant of reactor shutdown to when maximum pool water temperature is reached. T is the dependent variable (pool water temperature). For conservatism, Q_{EV} is assumed to remain constant after pool water temperature reaches and rises above 170°F.

A Q.A. validated numerical quadrature code is used to integrate the foregoing equation. The pool water heat up rate, time-to-boil, and subsequent water evaporation-time profile are generated and compiled for safety evaluation.

Assuming no make-up water ($G = 0$), the time-to-boil output results are presented in Table 5.5.2. Figures 5.5.6 through 5.5.10 show the plot of the inventory of water in the pool after loss-of-coolant-to-the-pool condition begins.

It is seen from Table 5.5.2 that sufficient time to introduce manual cooling measures exists and the available time is consistent with other PWR reactor installations.



5.6 Local Pool Water Temperature

In this section, a summary of the methodology, calculations and results for local pool water temperature is presented.

5.6.1 Basis

In order to determine an upper bound on the maximum fuel cladding temperature, a series of conservative assumptions are made. The most important assumptions are listed below:

- O The fuel pool will contain spent fuel with varying time-after-shutdown (τ_s). Since the heat emission falls off rapidly with increasing τ_s , it is conservative to assume that all fuel assemblies are from the latest batch discharged simultaneously in the shortest possible time and they all have had the maximum postulated years of operating time in the reactor. The heat emission rate of each fuel assembly is assumed to be equal and maximum.
- O As shown in the pool layout drawings, the modules occupy an irregular floor space in the pool. For the hydrothermal analysis, a circle circumscribing the actual rack floor space is drawn (Fig. 5.6.1). It is further assumed that the cylinder with this circle as its base is packed with fuel assemblies at the nominal layout pitch.
- O The actual downcomer space around the rack module group varies. The nominal downcomer gap available in the pool is assumed to be the total gap available around the idealized cylindrical rack; thus, the maximum resistance to downward flow is incorporated into the analysis (Figs. 5.6.2 and 5.6.3) (i.e. minimum gap between the pool wall and rack module, including seismic kinematic effect).
- O No downcomer flow is assumed to exist between the rack modules.

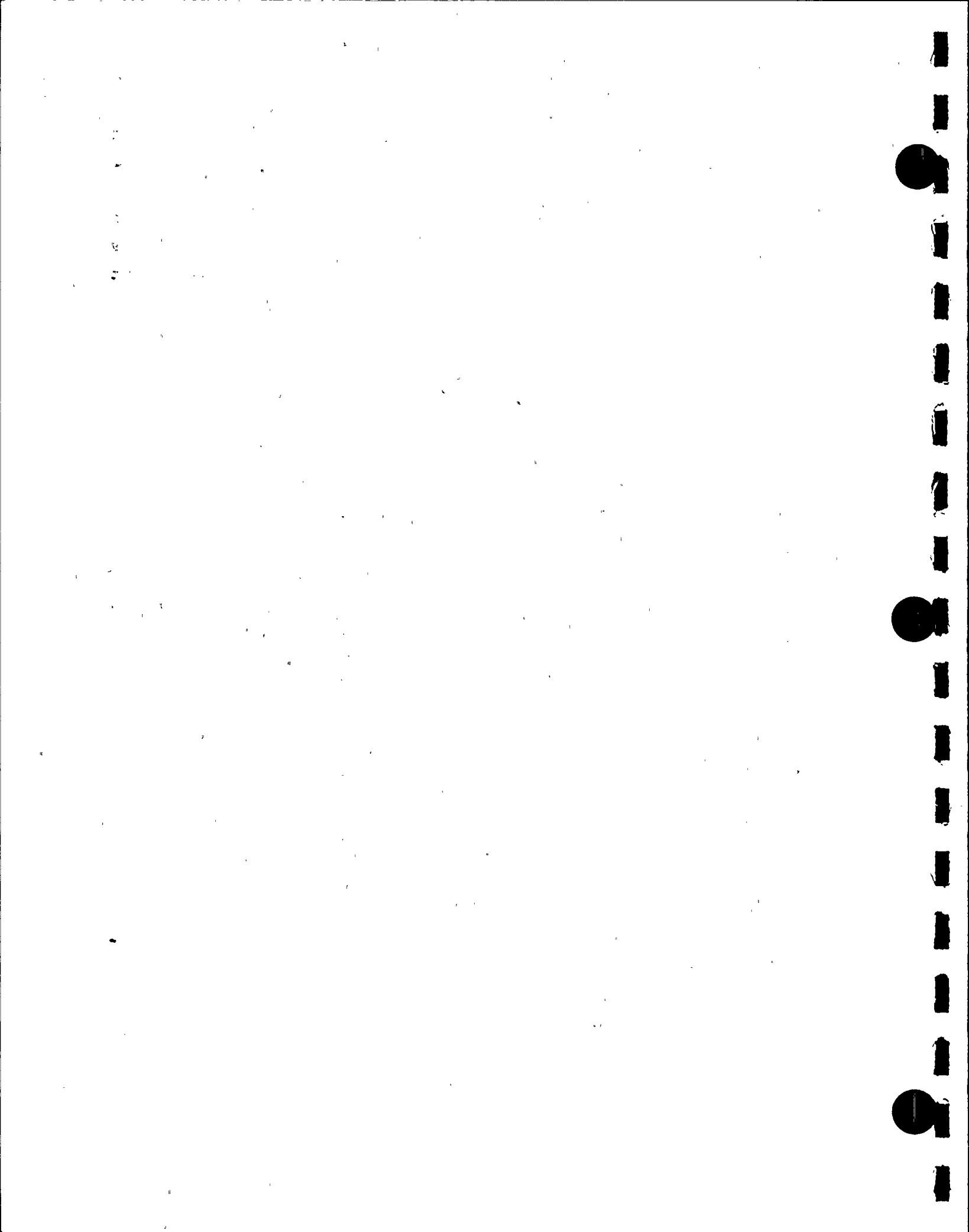


- O The ANF 17x17 fuel assembly has been used in the analysis which, from the thermal-hydraulic standpoint, bounds all types of fuel bundles utilized in the Donald C. Cook reactor.
- O No heat transfer is assumed to occur between pool water and the surroundings (wall, etc.)

5.6.2 Model Description

In this manner, a conservative idealized model for the rack assemblage is obtained. The water flow is axisymmetric about the vertical axis of the circular rack assemblage, and thus, the flow is two-dimensional (axisymmetric three-dimensional). Fig. 5.6.2 shows a typical "flow chimney" rendering of the thermal hydraulics model. The governing equation to characterize the flow field in the pool can now be written. The resulting integral equation can be solved for the lower plenum velocity field (in the radial direction) and axial velocity (in-cell velocity field), by using the method of collocation. The hydrodynamic loss coefficients which enter into the formulation of the integral equation are also taken from well-recognized sources (Ref. 5.6.1) and wherever discrepancies in reported values exist, the conservative values are consistently used. Reference 5.6.2 gives the details of mathematical analysis used in this solution process.

After the axial velocity field is evaluated, it is a straightforward matter to compute the fuel assembly cladding temperature. The knowledge of the overall flow field enables pinpointing of the storage location with the minimum axial flow (i.e, maximum water outlet temperatures). This is called the most "choked" location. In order to find an upper bound on the temperature in a typical cell, it is assumed that it is located at the most choked location. Knowing the global plenum velocity field, the revised



axial flow through this choked cell can be calculated by solving the Bernoulli's equation for the flow circuit through this cell. Thus, an absolute upper bound on the water exit temperature and maximum fuel cladding temperature is obtained. In view of these aforementioned assumptions, the temperatures calculated in this manner overestimate the temperature rise that will actually occur in the pool. Holtec's computer code THERPOOL*, based on the theory of Ref. 5.6.2, automates this calculation. The analysis procedure embodied in THERPOOL has been accepted by the Nuclear Regulatory Commission on several dockets. The Code THERPOOL for local temperature analyses includes the calculation of void generations. The effect of void on the conservation equation, crud layer in the clad, flux trap temperature due to gamma heating, and the clad stress calculation when a void exists, are all incorporated in THERPOOL. The peaking factors are given in Table 5.6.1.

5.7 Cladding Temperature

The maximum specific power of a fuel array q_A can be given by:

$$q_A = q F_{xy} \quad (1)$$

where:

F_{xy} = radial peaking factor

q = average fuel assembly specific power

* THERPOOL has been used in qualifying the spent fuel pools for Enrico Fermi Unit 2 (1980), Quad Cities I and II (1981), Oyster Creek (1984), V.C. Summer (1984), Rancho Seco (1983), Grand Gulf I (1985), Diablo Canyon I and II (1986), among others.



The maximum temperature rise of pool water in the most disadvantageously placed fuel assembly is computed for all loading cases. Having determined the maximum local water temperature in the pool, it is now possible to determine the maximum fuel cladding temperature. A fuel rod can produce F_z times the average heat emission rate over a small length, where F_z is the axial rod peaking factor. The axial heat distribution in a rod is generally a maximum in the central region, and tapers off at its two extremities.

It can be shown that the power distribution corresponding to the chopped cosine power emission rate is given by

$$q(x) = q_A \sin \frac{\pi (a + x)}{h + 2a}$$

where:

h : active fuel length

a : chopped length at both extremities in the power curve

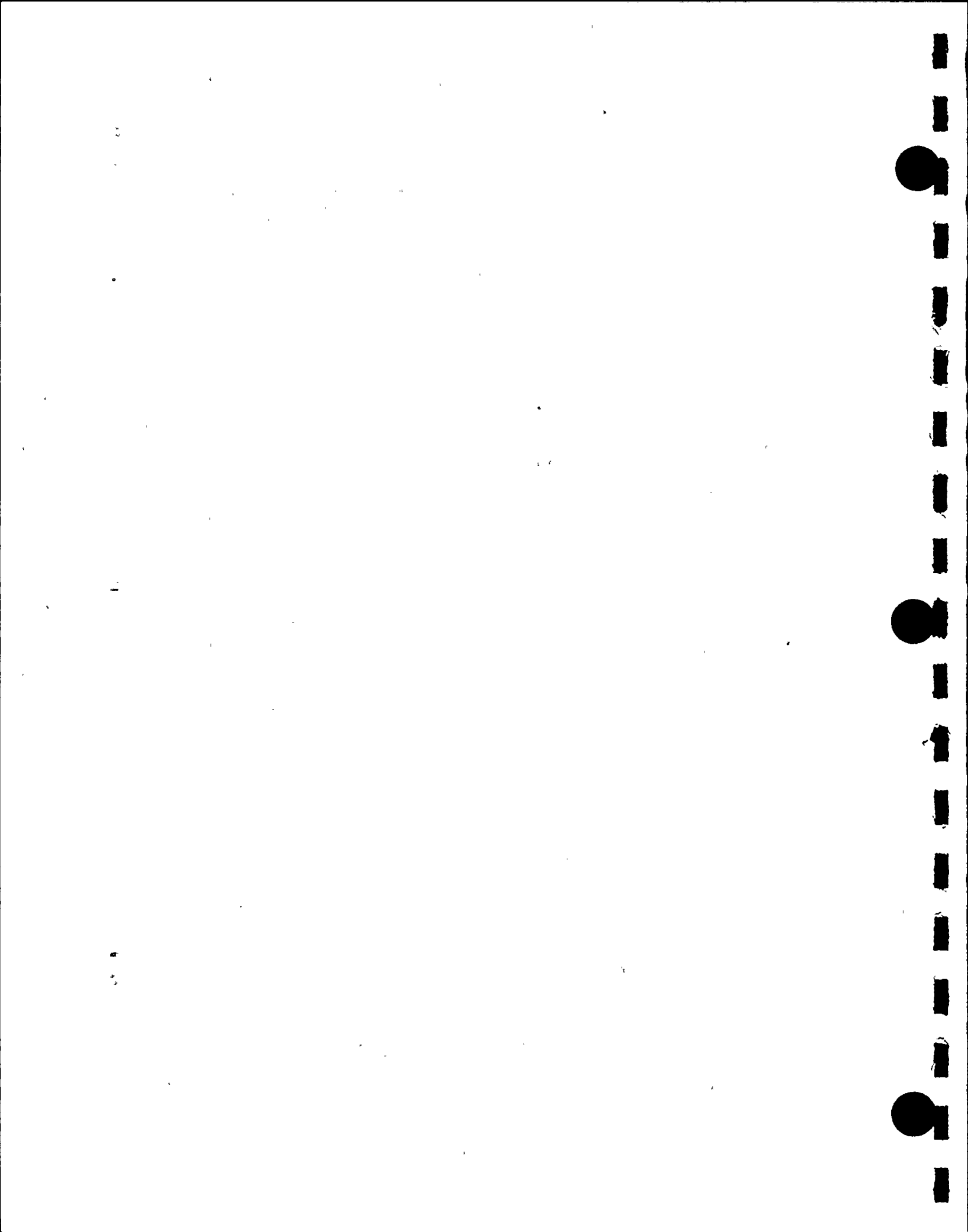
x : axial coordinate with origin at the bottom of the active fuel region

The value of a is given by

$$a = \frac{h z}{1 - 2z}$$

where:

$$z = \frac{1}{\pi F_z} - \left[\frac{1}{\pi^2 F_z^2} - \frac{1}{\pi F_z} + \frac{2}{\pi^2} \right]^{1/2}$$



where F_z is the axial peaking factor.

The cladding temperature T_c is governed by a third order differential equation which has the form of

$$\frac{d^3 T}{dx^3} + \alpha_1 \frac{d^2 T}{dx^2} - \alpha_2 \frac{dT}{dx} = f(x)$$

where α_1 , α_2 and $f(x)$ are functions of x , and fuel assembly geometric properties. The solution of this differential equation with appropriate boundary conditions provides the fuel cladding temperature and local water temperature profile.

In order to introduce some additional conservatism in the analysis, we assume that the fuel cladding has a crud deposit which results in .005 $^{\circ}\text{F}\cdot\text{sq.ft.}\cdot\text{hr/Btu}$ of crud resistance, which covers the entire surface.

Table 5.6.2 provides the key input data for local temperature analysis. The results of maximum local pool water temperature and minimum local fuel cladding temperature are presented in Table 5.7.1.

The local boiling temperature of water is approximately 242°F at 26' below the free water surface and higher at lower elevations.

The location where the local water temperature reaches its maximum value is deeper than 26' below the free water surface, where the coincident boiling temperature of water is greater than 242°F . It is shown that the local pool water temperature is lower than the local boiling point and therefore, nucleate boiling will not occur.



Finally, it is noted that the fuel cladding temperature is considerably lower than the temperatures to which the cladding is subjected inside the reactor. Therefore, it is concluded that there is sufficient margin against fuel cladding failure in the spent fuel pool.

5.8 Blocked Cell Analysis

Calculations are also performed assuming that 50% of the top opening in the thermally limiting storage cell is blocked due to a horizontally placed (misplaced) fuel assembly. The corresponding maximum local pool water temperature and local fuel cladding temperature data are also presented in Table 5.7.1.

There is also no incidence of localized nucleate boiling of the pool water or potential for fuel cladding damage.

5.9 References for Section 5

- 5.6.1 General Electric Corporation, R&D Data Books, "Heat Transfer and Fluid Flow", 1974 and updates.
- 5.6.2 Singh, K.P. et al., "Method for Computing the Maximum Water Temperature in a Fuel Pool Containing Spent Nuclear Fuel", Heat Transfer Engineering, Vol. 7, No. 1-2, pp. 72-82 (1986).

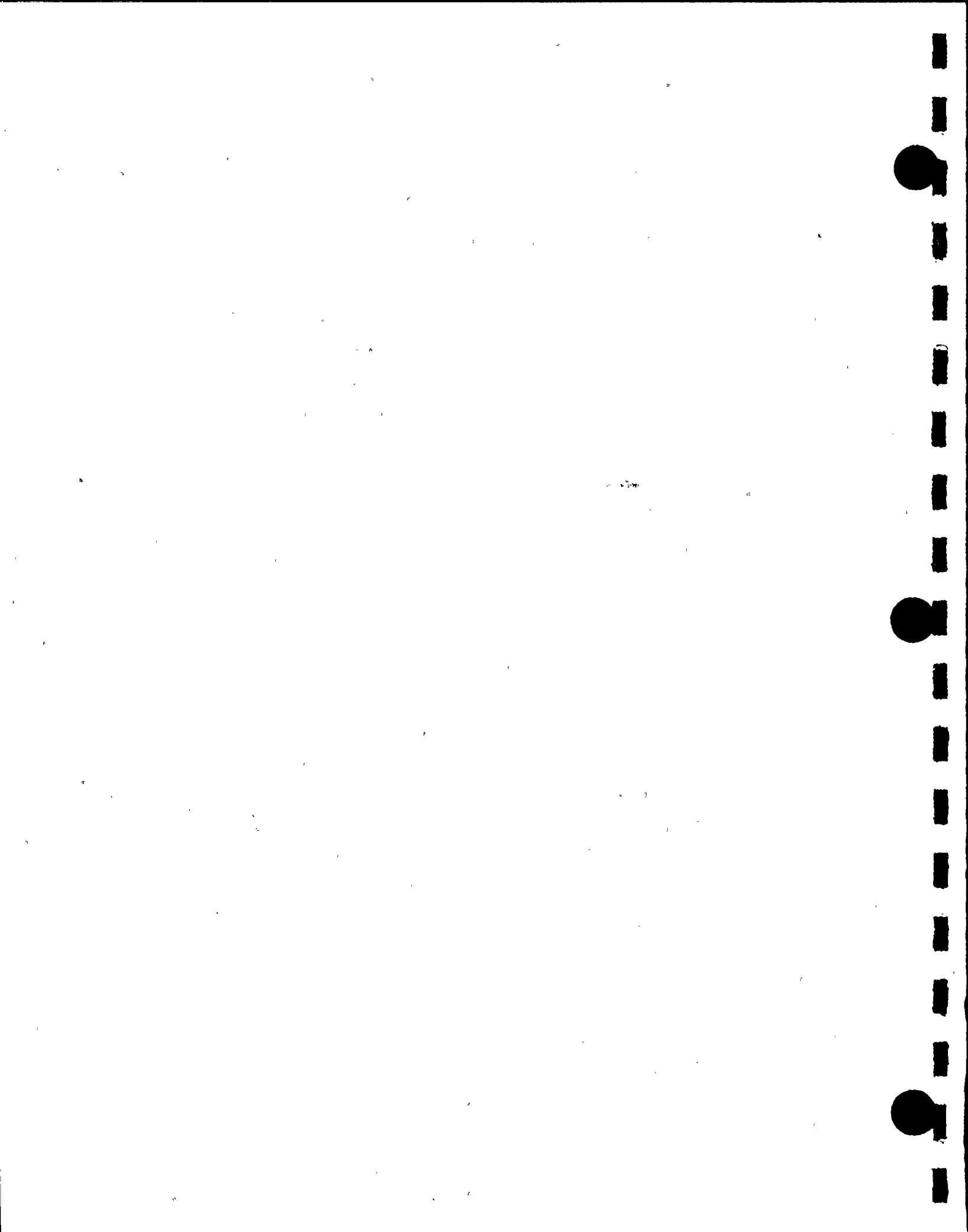


Table 5.4.1

FUEL SPECIFIC POWER AND POOL CAPACITY DATA

| | |
|---|------------------|
| Total water volume of Pool: | 635645 gallons |
| Specific Operating Power of
a Fuel Assembly: | 60.3E+06 Btu/hr. |
| Dimensionless decay power of
"old" discharges: | 0.3303 |



Table 5.4.2
DATA FOR SCENARIOS 1 through 4

| <u>CASE NO.</u> | <u>1a</u> | <u>1b</u> | <u>2</u> | <u>3</u> | <u>4</u> |
|---|-----------|-----------|----------|----------|----------|
| Pool thermal capacity
$C \times 10^{-6}$, Btu/ $^{\circ}$ F | 4.241 | 4.241 | 4.241 | 4.241 | 4.241 |
| No. of Cooling Trains | 1 | 1 | 2 | 2 | 1 |
| No. of Discharges
Considered for the
Analysis | 1 | 1 | 1 | 2 | 2 |
| Time between
Shutdowns, hr. | --- | --- | --- | 720 | 720 |
| Cooler Inlet Temp.,
$^{\circ}$ F | 108.4 | 108.4 | 103.9 | 101.4 | 104.7 |
| Coolant Flow Rate/
cooler, 10^6 lb./hr. | 1.49 | 1.49 | 1.49 | 1.49 | 1.49 |
| Fuel Pool Water
Flow Rate, 10^6
lb./hr. | 1.14 | 1.40 | 1.14 | 1.14 | 1.14 |
| Temperature
Effectiveness/
cooler, p | 0.3970 | 0.43 | 0.3975 | 0.3979 | 0.3987 |

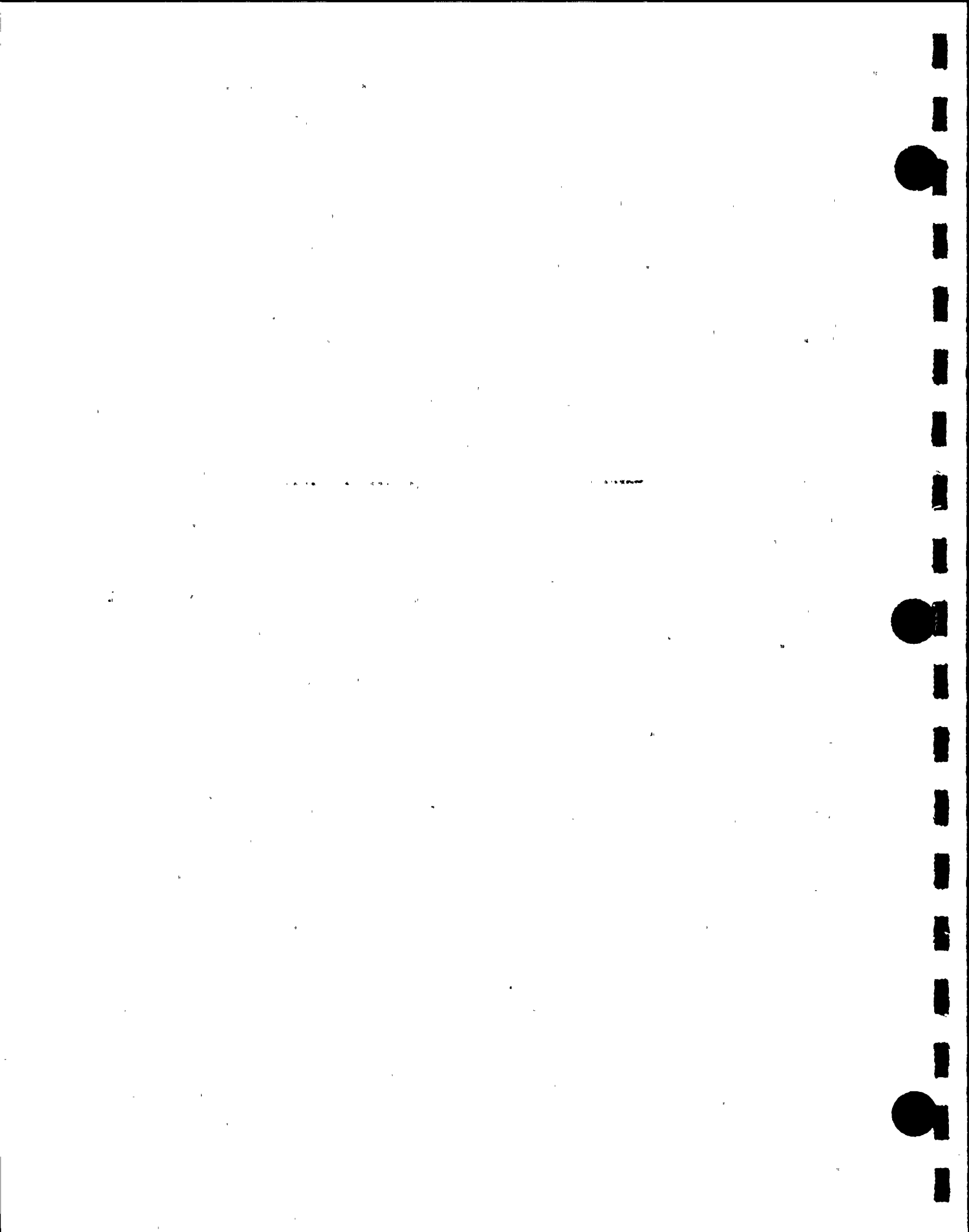


Table 5.4.3
DATA FOR SCENARIOS 1 THROUGH 4

| Case
No. | Discharge
ID | No. of
Assemblies | Time After
Shutdown when
Transfer Begins
(hrs) | Offload
Time
(hrs) | Expo.
Time
(hrs) |
|----------------|----------------------------|----------------------|---|--------------------------|------------------------|
| 1a
or
1b | Discharge 1 | 80 | 168 | 19.07 | 30240 |
| 2 | Discharge 1 | 80 | 168 | 19.07 | 30240 |
| 3 | Discharge 1 | 80 | 168 | 19.07 | 30240 |
| 3
or
4 | Discharge 2
(Full Core) | 80
113 | 168 | 46.00 | 10080
30240 |



Table 5.5.1

POOL BULK TEMPERATURE AND HEAT LOAD DATA

| Case
No. | Coincident
Cooler Duty
10^6 Btu/hr. | T_{max}
Max. Pool
Bulk Temp.,
$^{\circ}\text{F}$ | Time
Coincident
to T_{max}
(after
reactor
shutdown) | Coincident
Evaporation
Heat Loss,
10^6 Btu/hr. |
|-------------|---|--|---|---|
| 1a | 30.241 | 159.54 | 207 | 3.00 |
| 1b | 30.69 | 156.31 | 206 | 2.578 |
| 2 | 32.787 | 131.57 | 198 | 0.689 |
| 3 | 50.690 | 143.84 | 222 | 1.395 |
| 4 | 45.04 | 176.91 | 225 | 6.887 |

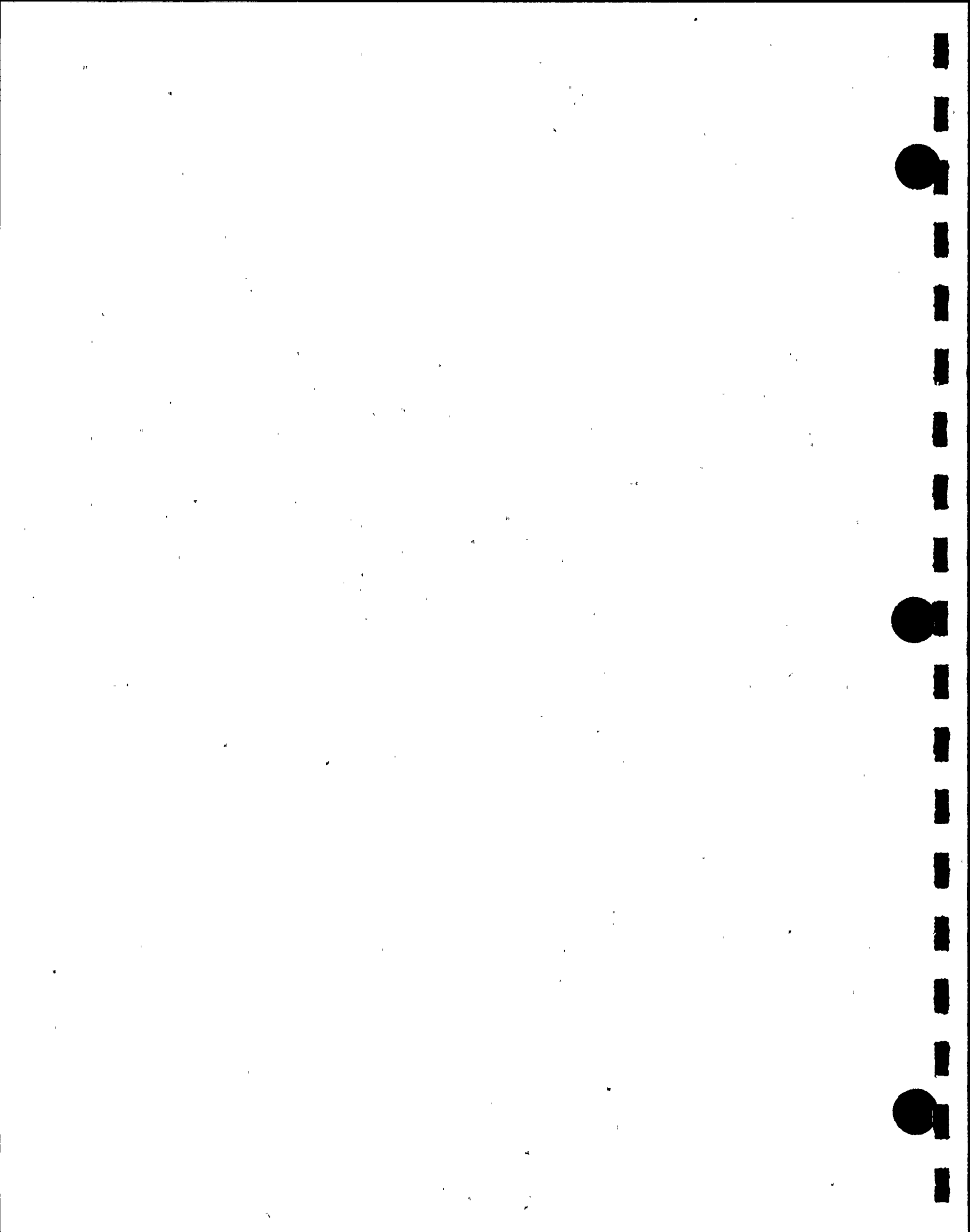


Table 5.5.2

TIME-TO-BOIL FOR VARIOUS DISCHARGE SCENARIOS

| <u>Case Number</u> | Time-to-Boil (hours)
<u>G = 0 GPM</u> |
|--------------------|--|
| 1a | 7.82 |
| 1b | 8.27 |
| 2 | 11.52 |
| 3 | 5.74 |
| 4 | 3.02 |



Table 5.6.1

PEAKING FACTOR DATA

| | |
|------------------------------|------|
| Radial Bundle Peaking Factor | 1.65 |
| Total peaking factor | 2.40 |



Table 5.6.2

DATA FOR LOCAL TEMPERATURE

| | |
|--|------|
| Type of Fuel Assembly | PWR |
| Fuel Cladding Outer Diameter, inches | 0.36 |
| Fuel Cladding Inside Diameter, inches | 0.31 |
| Storage Cell inside Dimension, inches | 8.75 |
| Active fuel length, inches | 144 |
| No. of Fuel Rods/Assembly | 264 |
| Operating Power per Fuel Assembly
$P_0 \times 10^{-6}$, Btu/hr | 60.3 |
| Cell pitch, inches | 8.97 |
| Cell height, inches | 168 |
| Plenum radius, feet | 29.3 |
| Min. Bottom height, inches | 4.75 |
| Min. gap between pool wall
and outer rack periphery, inches | 1.5 |

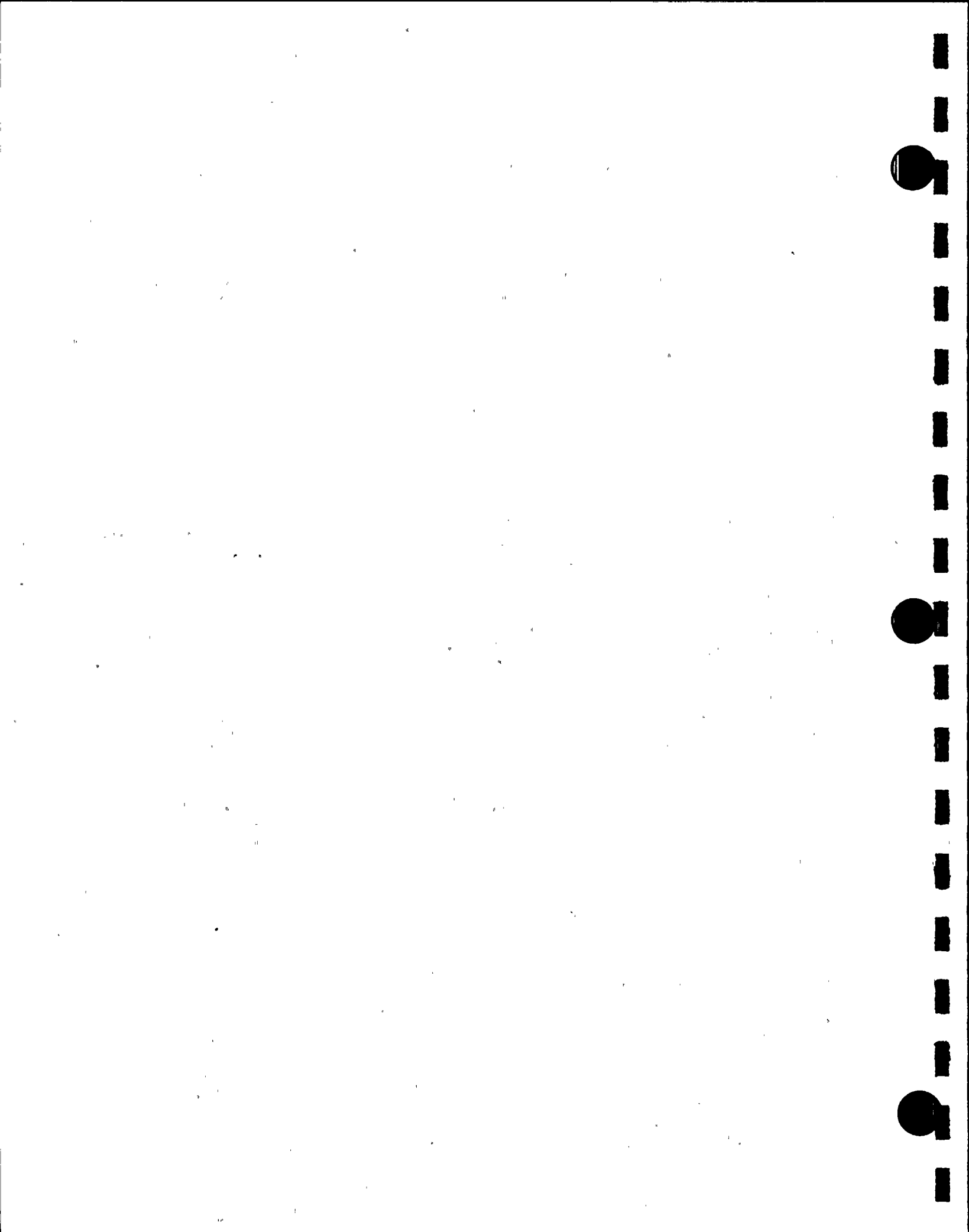


Table 5.7.1

LOCAL AND CLADDING TEMPERATURE OUTPUT DATA FOR
THE MAXIMUM POOL WATER CONDITION (Case a)

| <u>Condition</u> | <u>Water Temp., °F</u> | <u>Temp., °F</u> |
|------------------|------------------------|------------------|
| No blockage | 168.0 | 212.9 |
| 50% blockage | 219.2 | 246.9 |



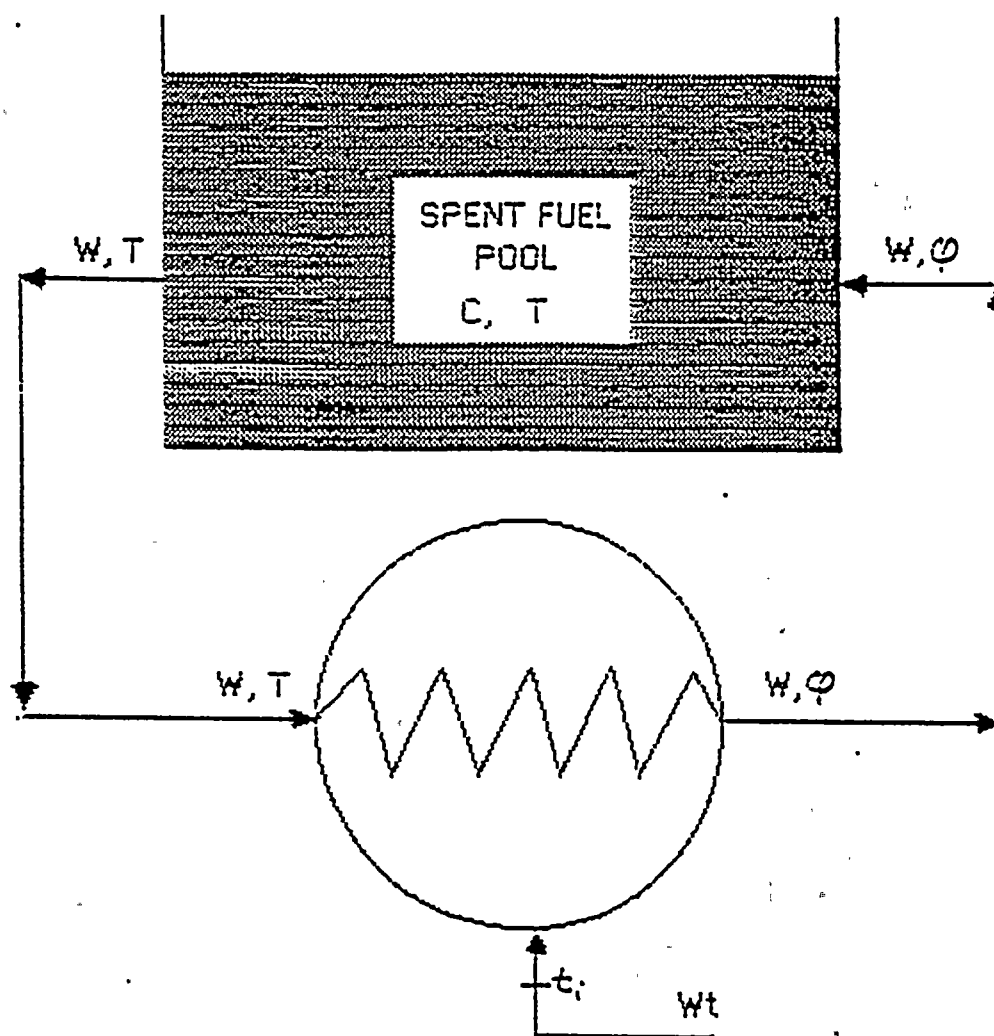


FIGURE 5.5.1

Pool Bulk Temperature Model



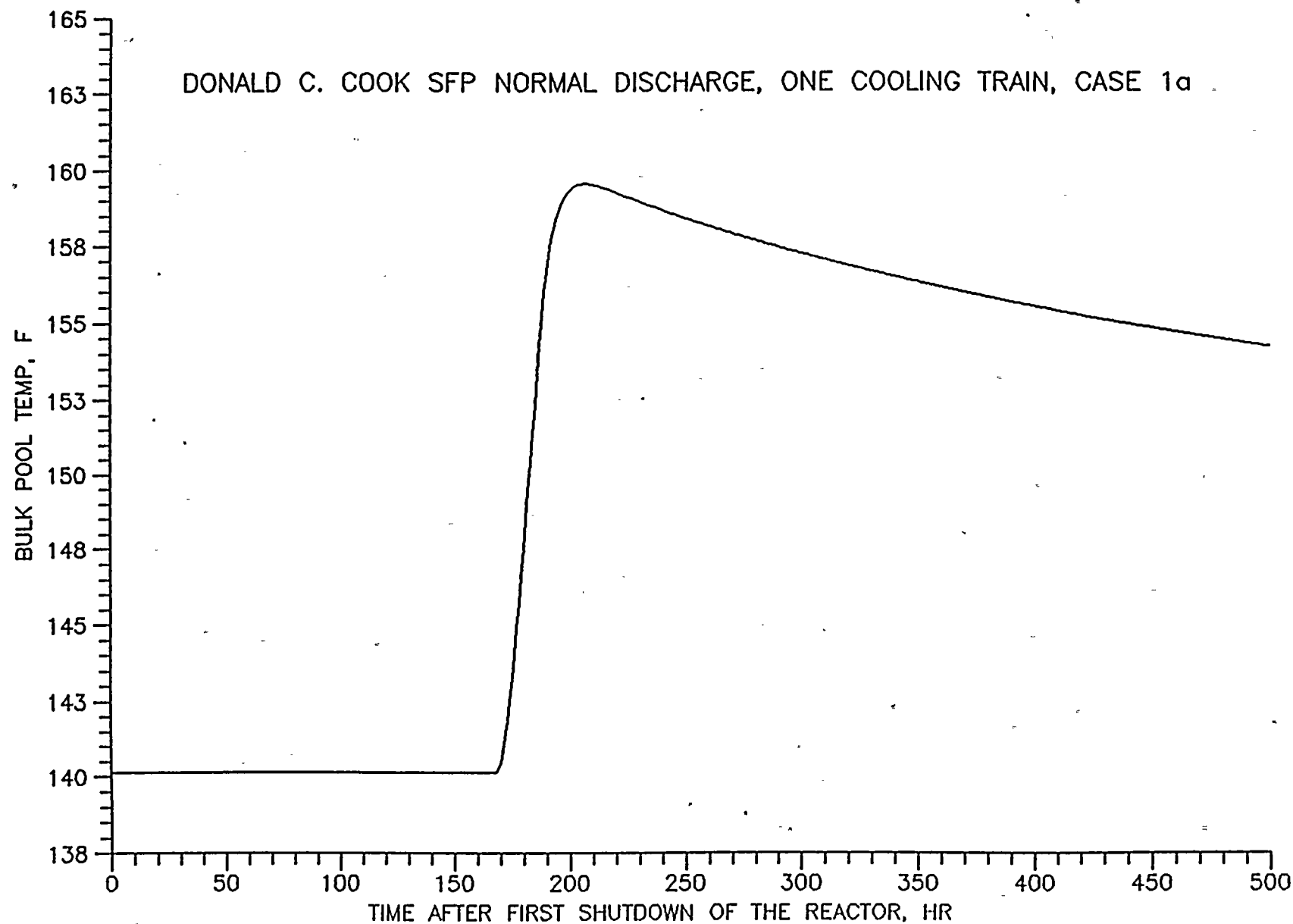


FIGURE 5.5.2



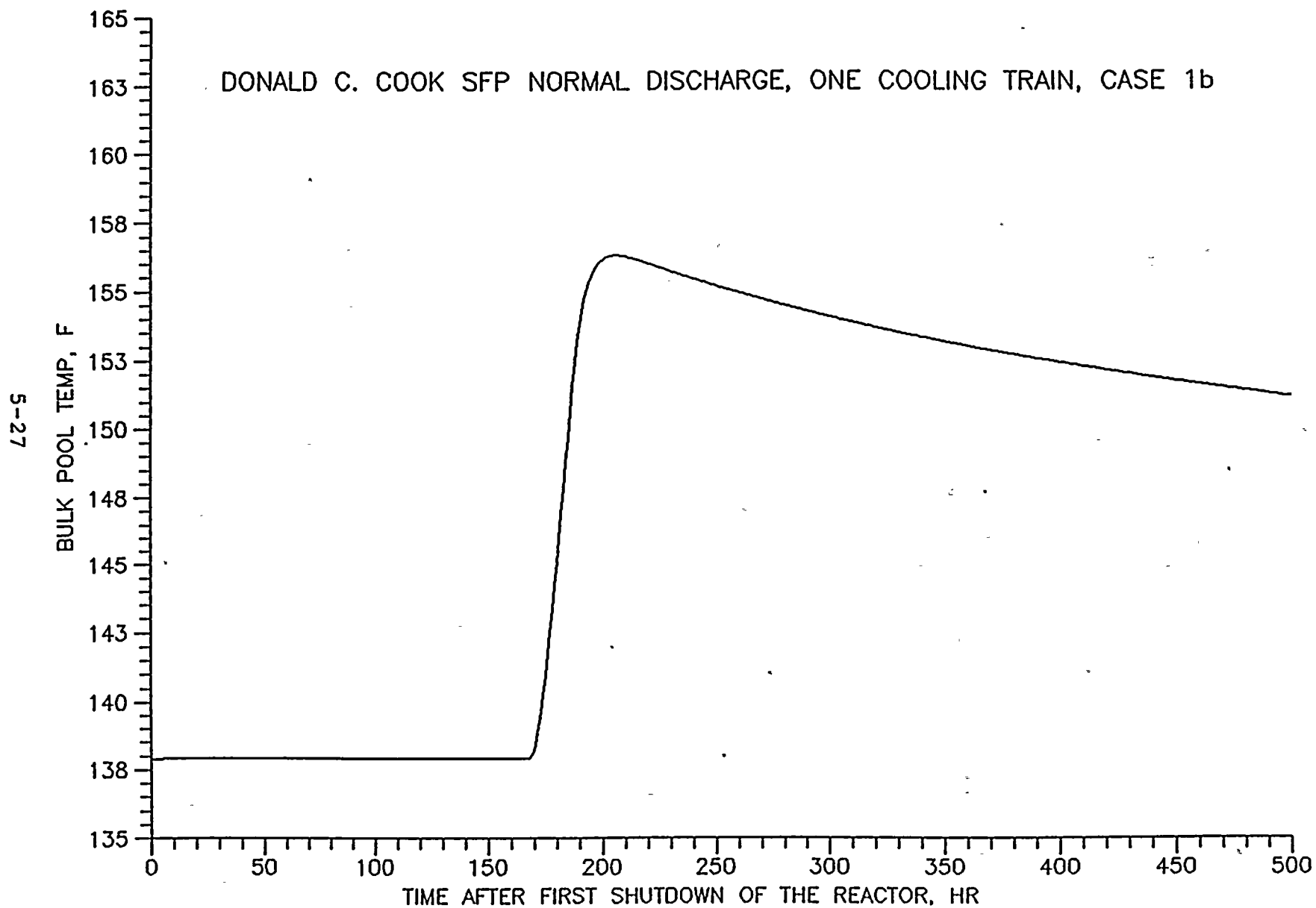


FIGURE 5.5.3



5-28

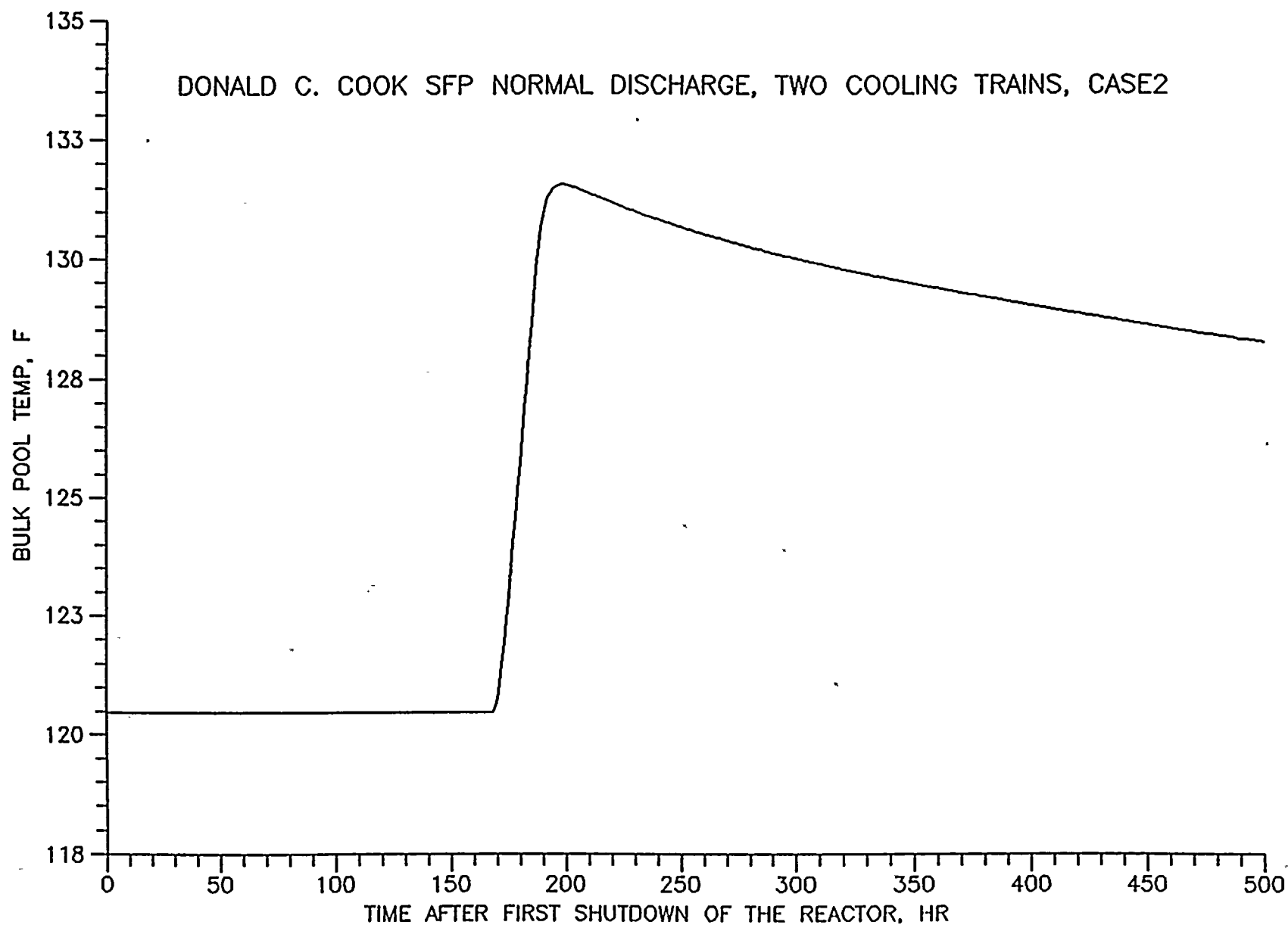


FIGURE 5.5.4

5-29

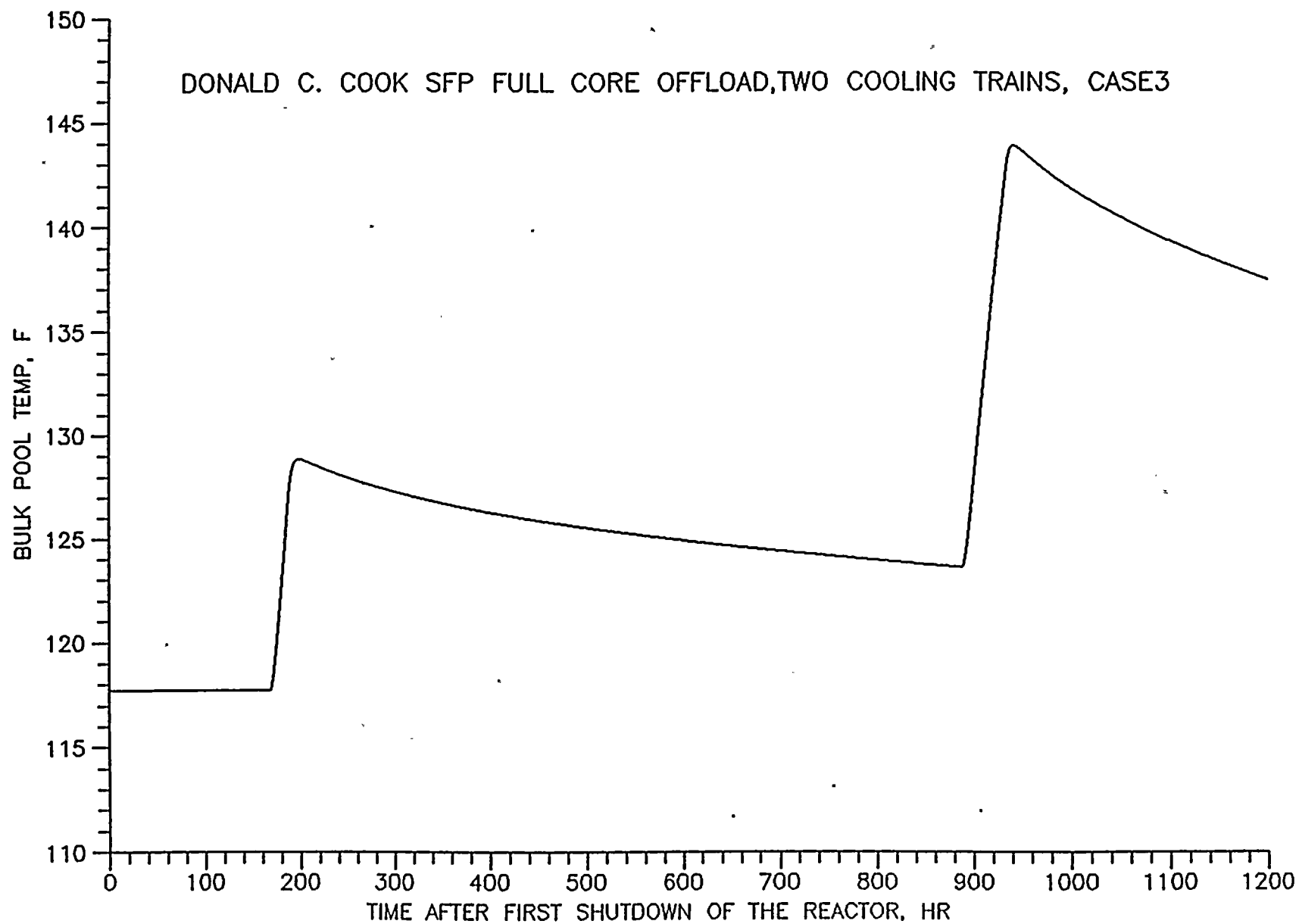


FIGURE 5.5.5



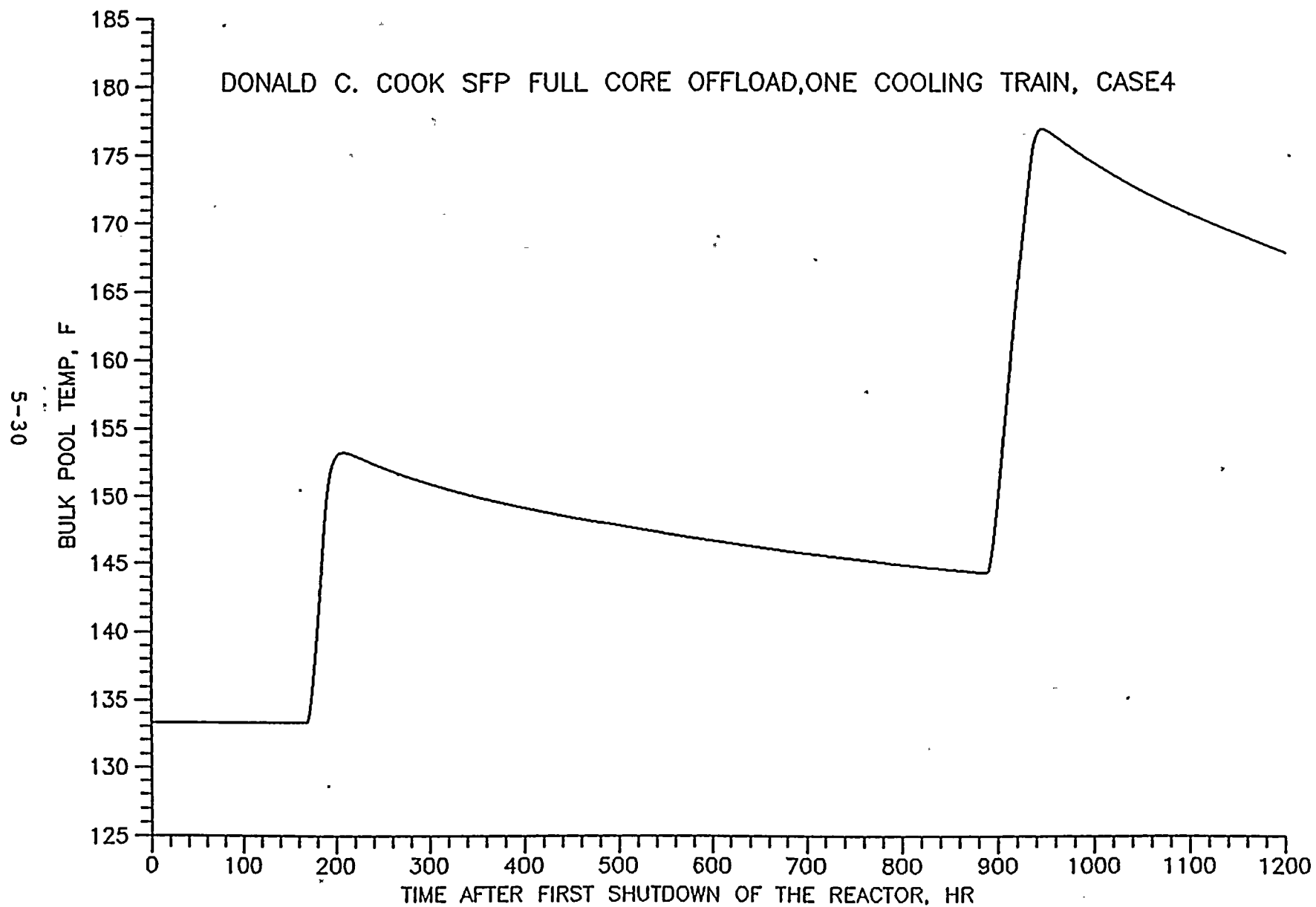


FIGURE 5.5.6



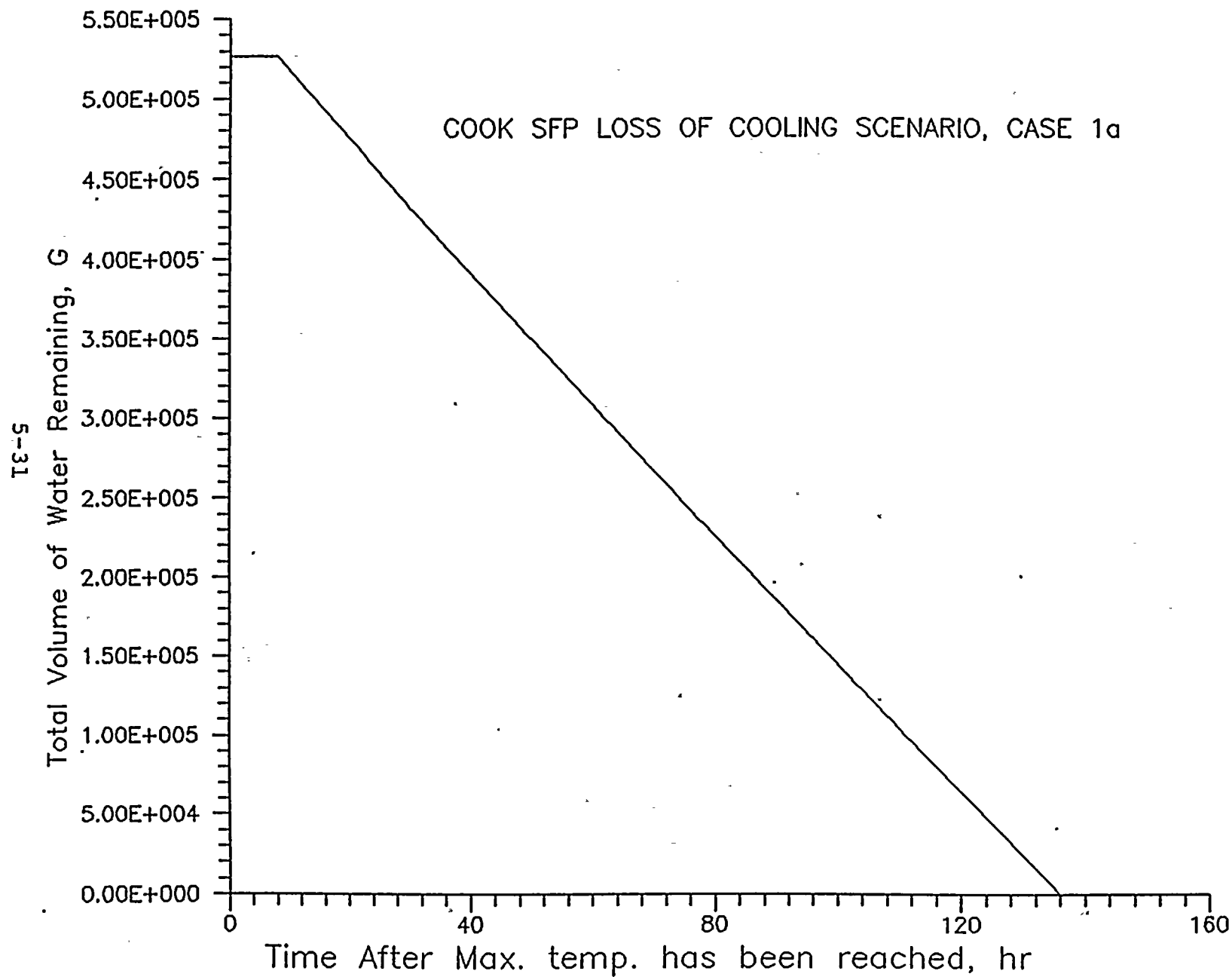
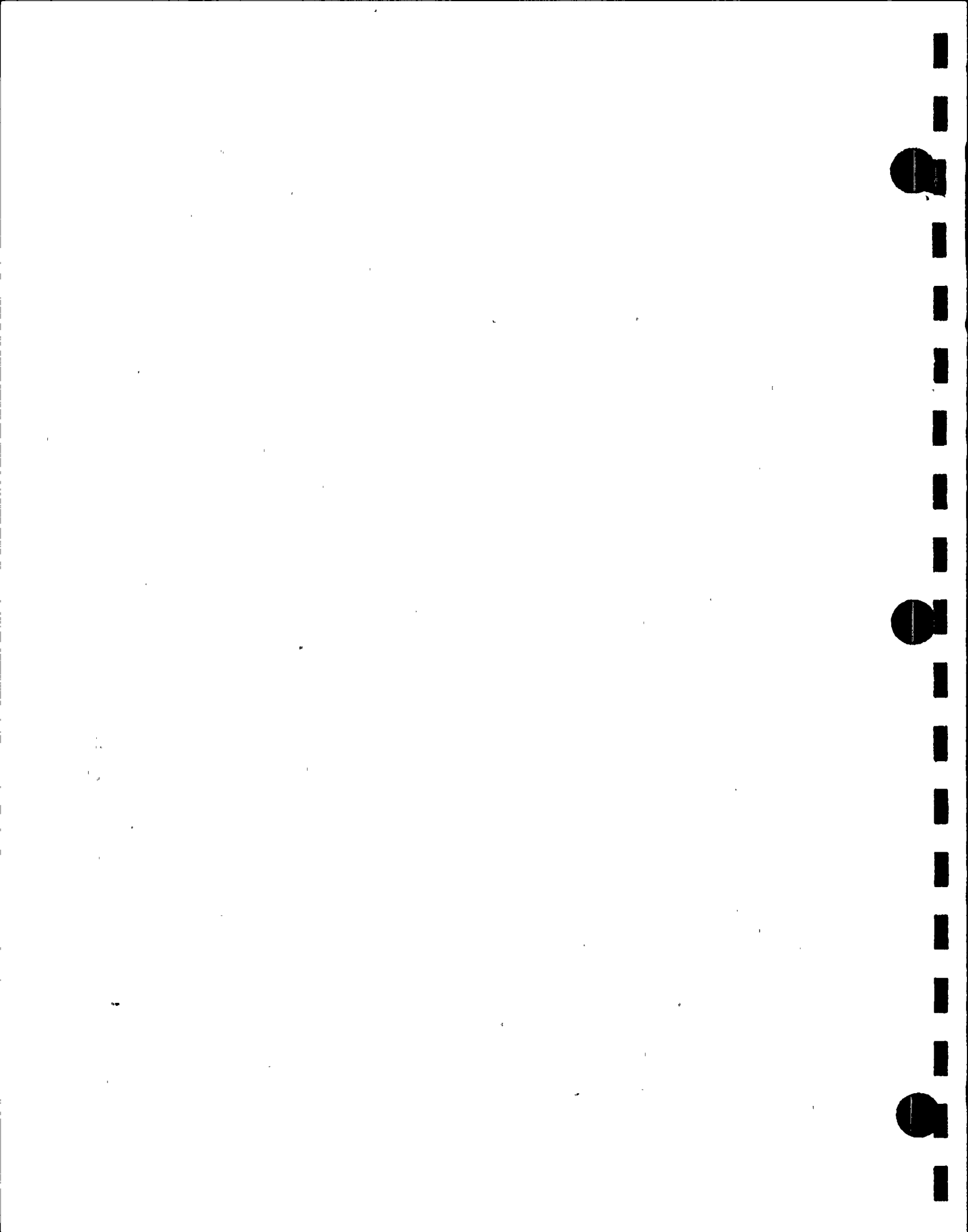


FIGURE 5.5.7



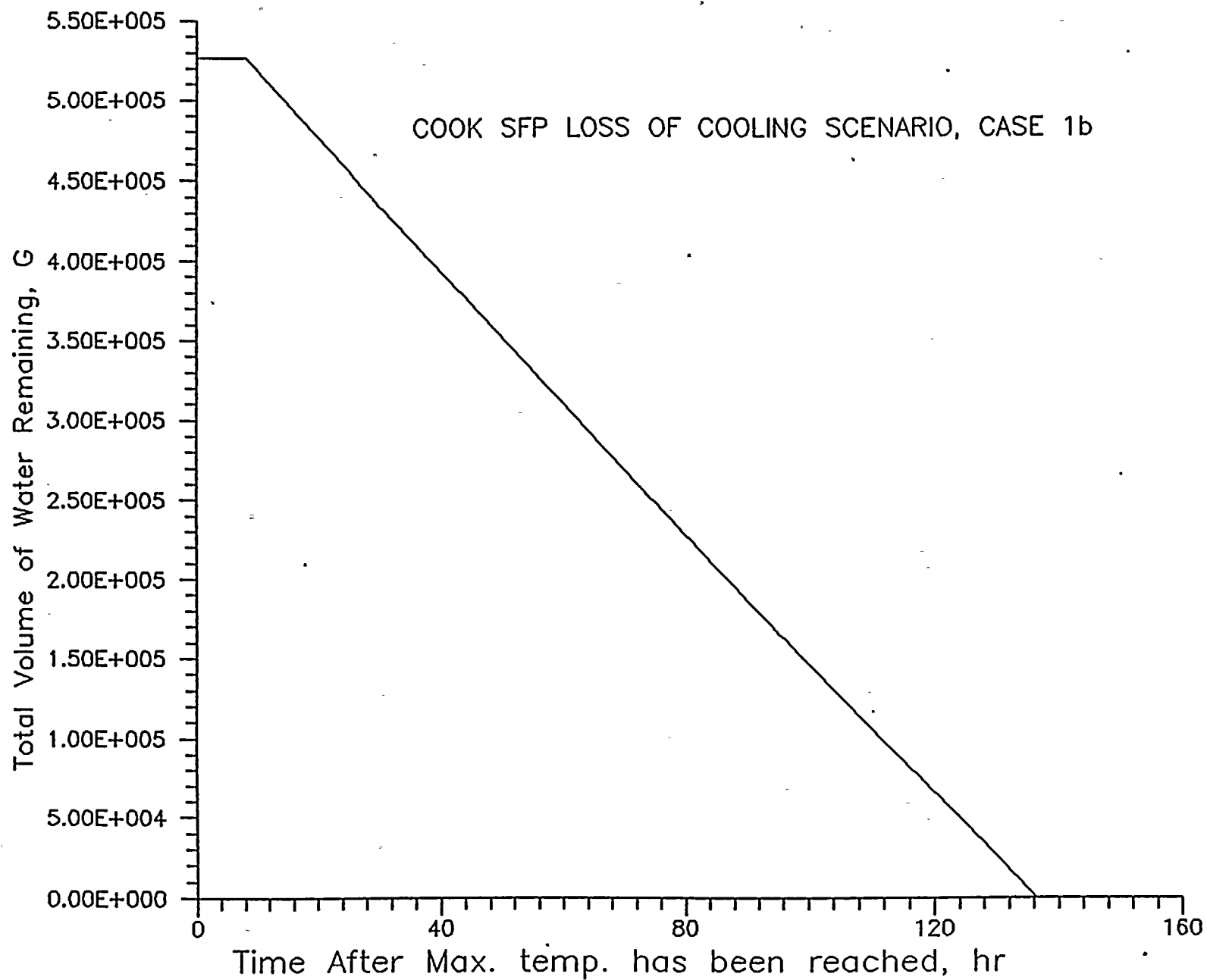


FIGURE 5.5.8



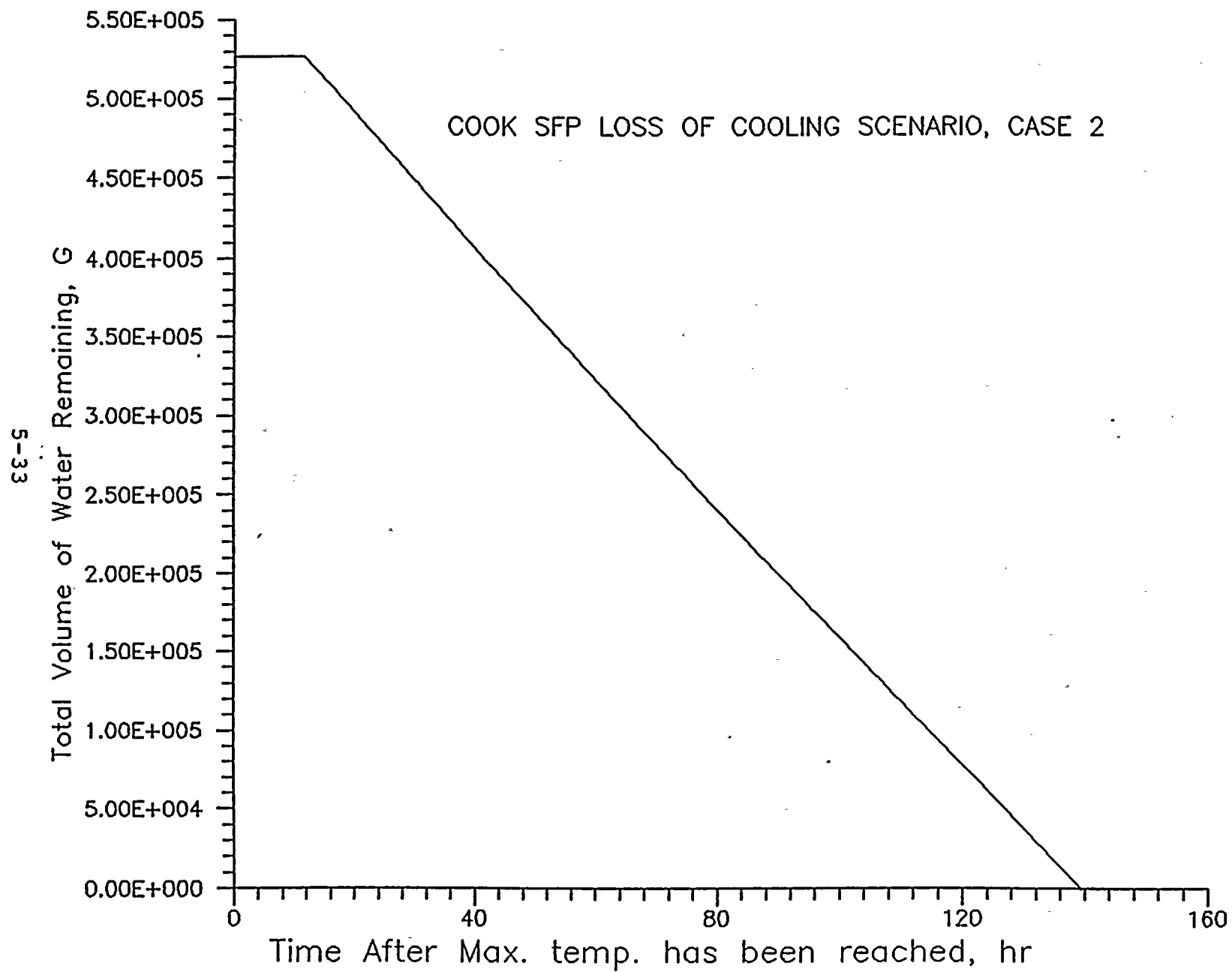


FIGURE 5.5.9



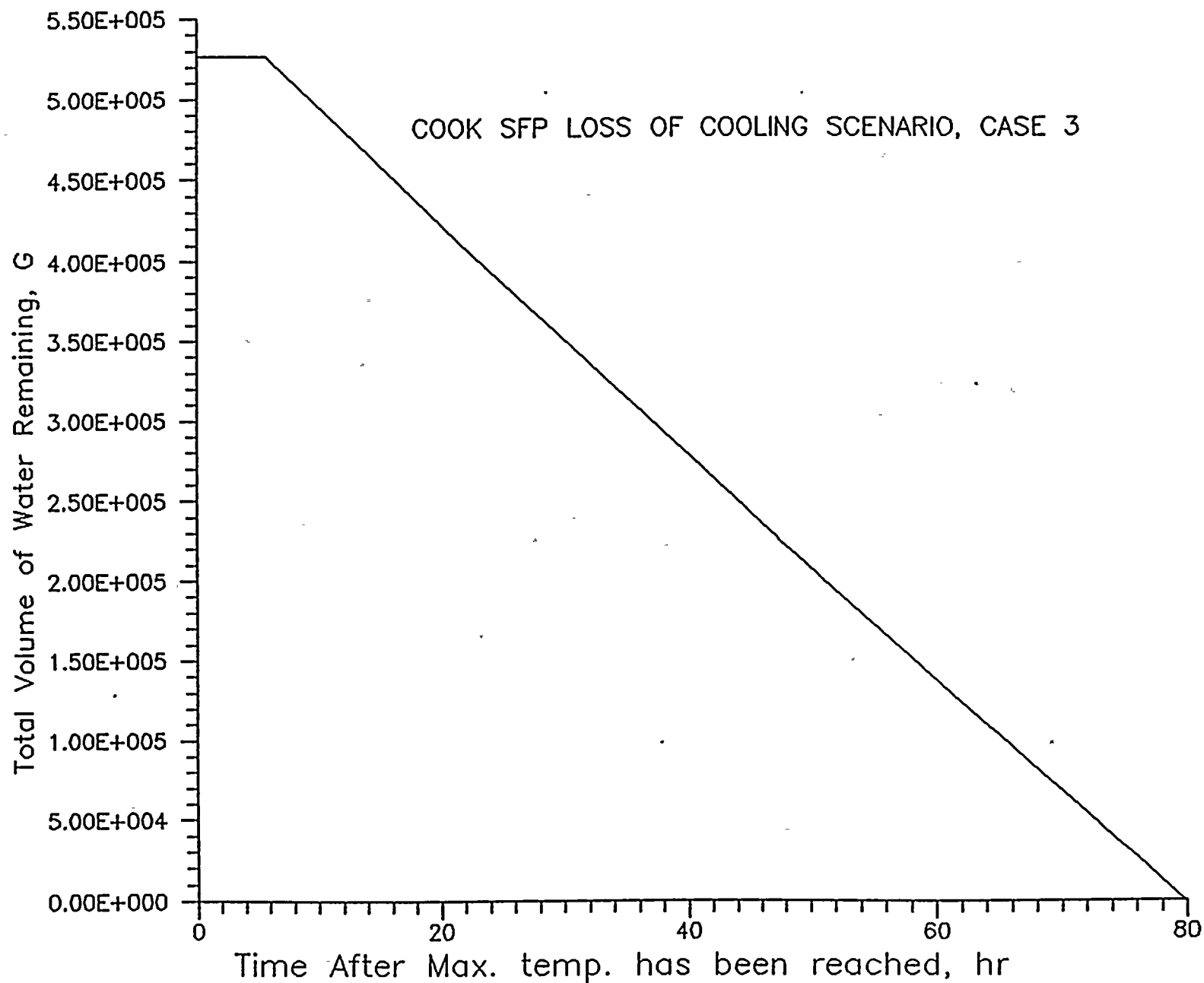


FIGURE 5.5.10



58-5

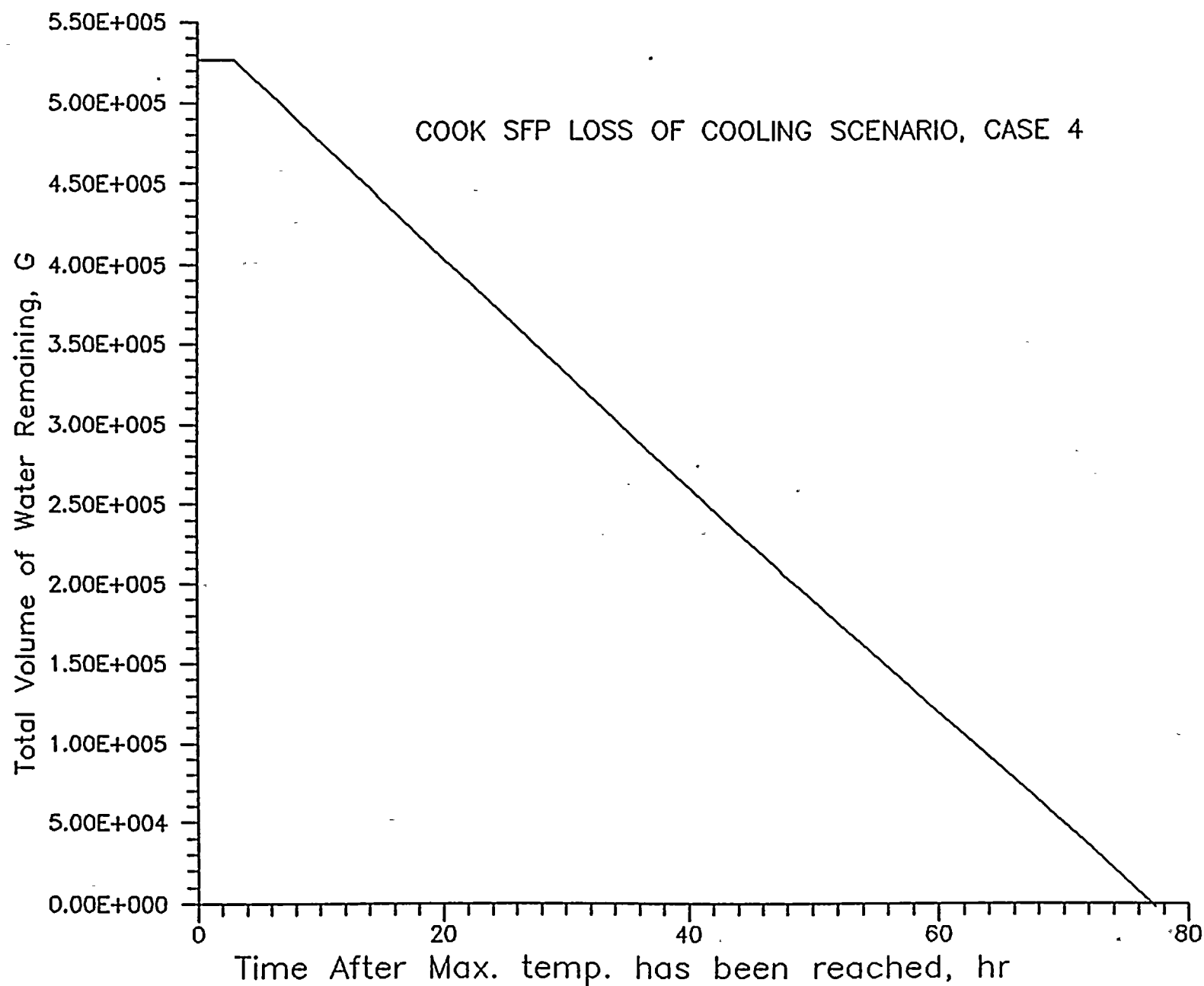


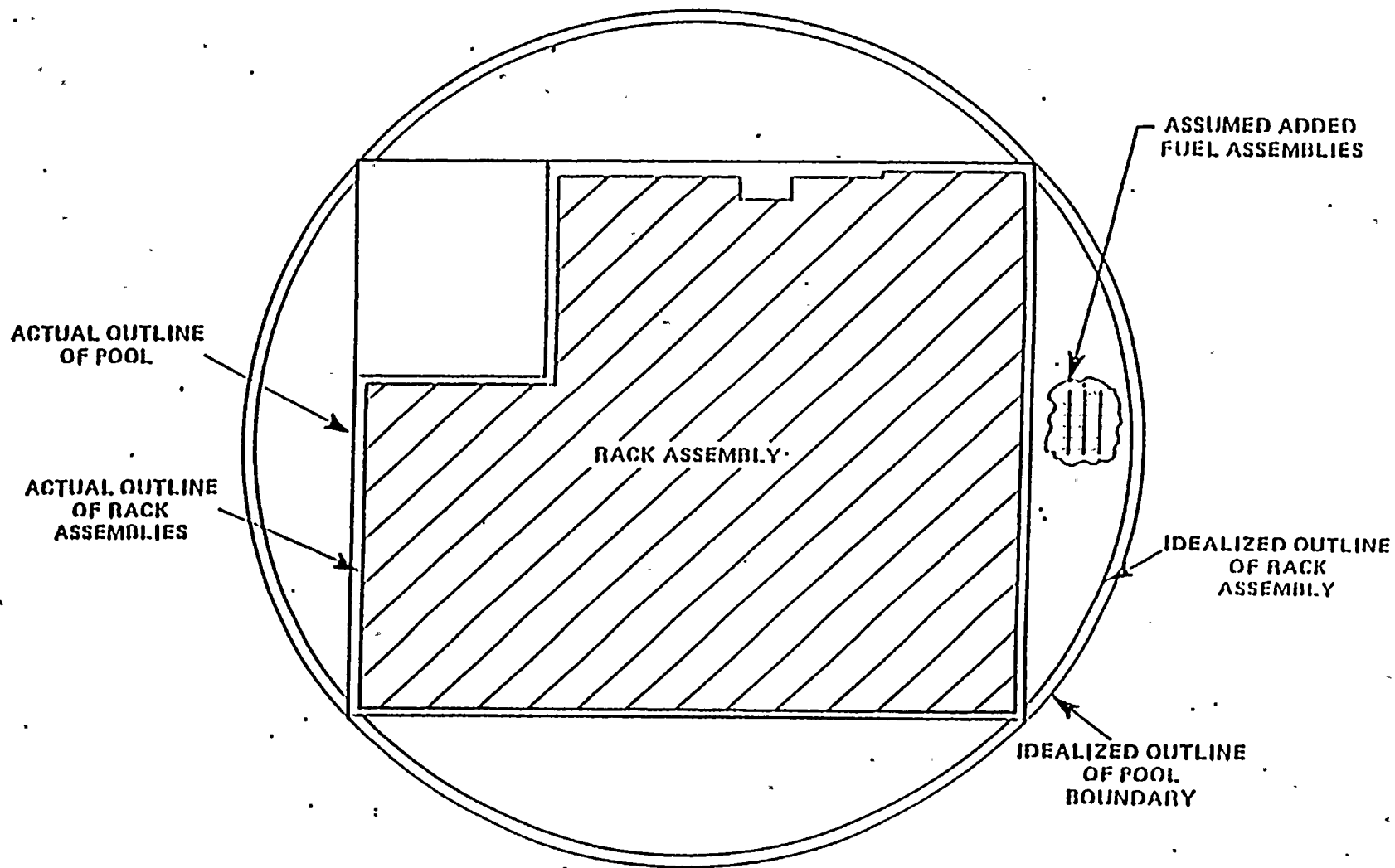
FIGURE 5.5.11



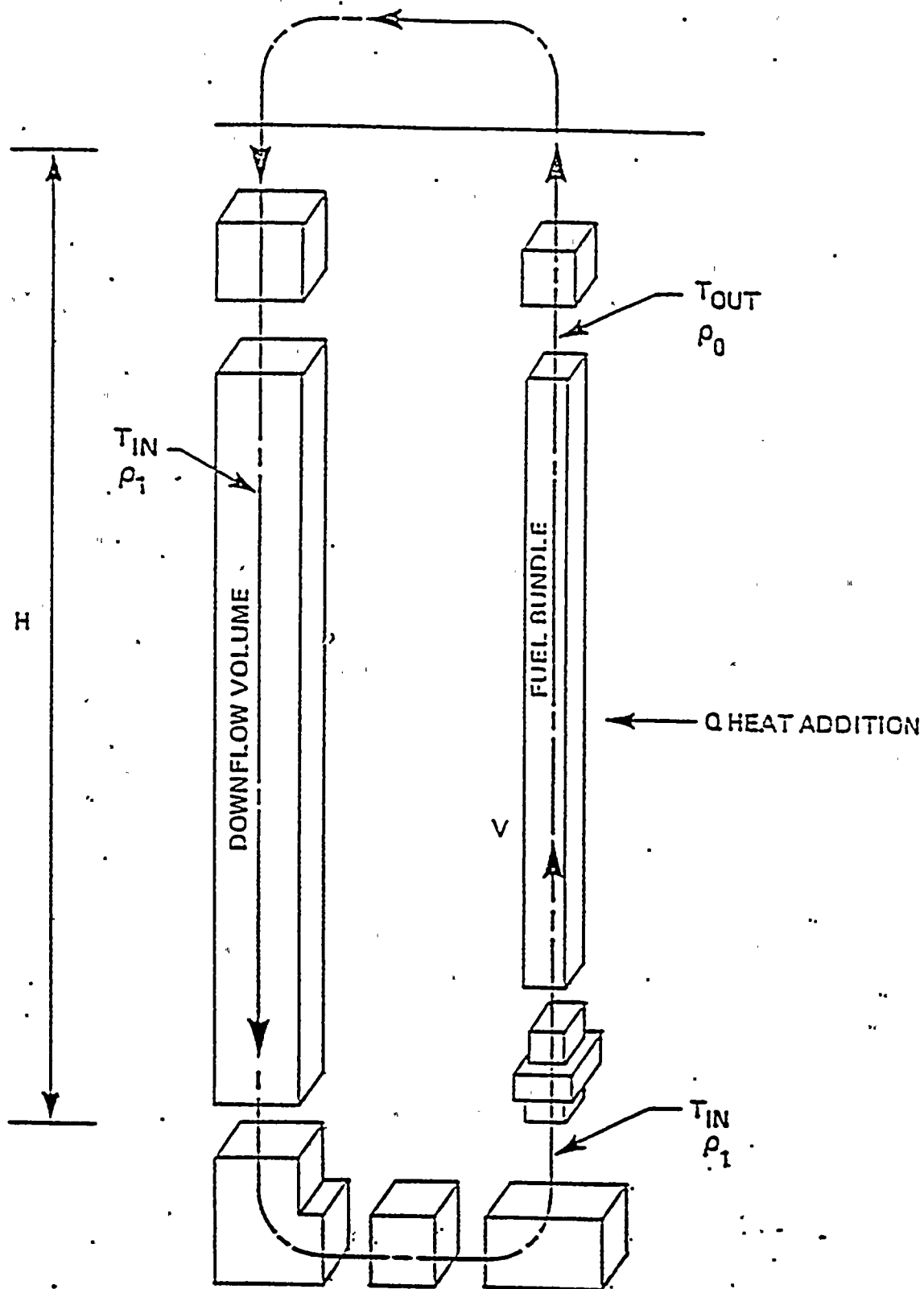
5-36

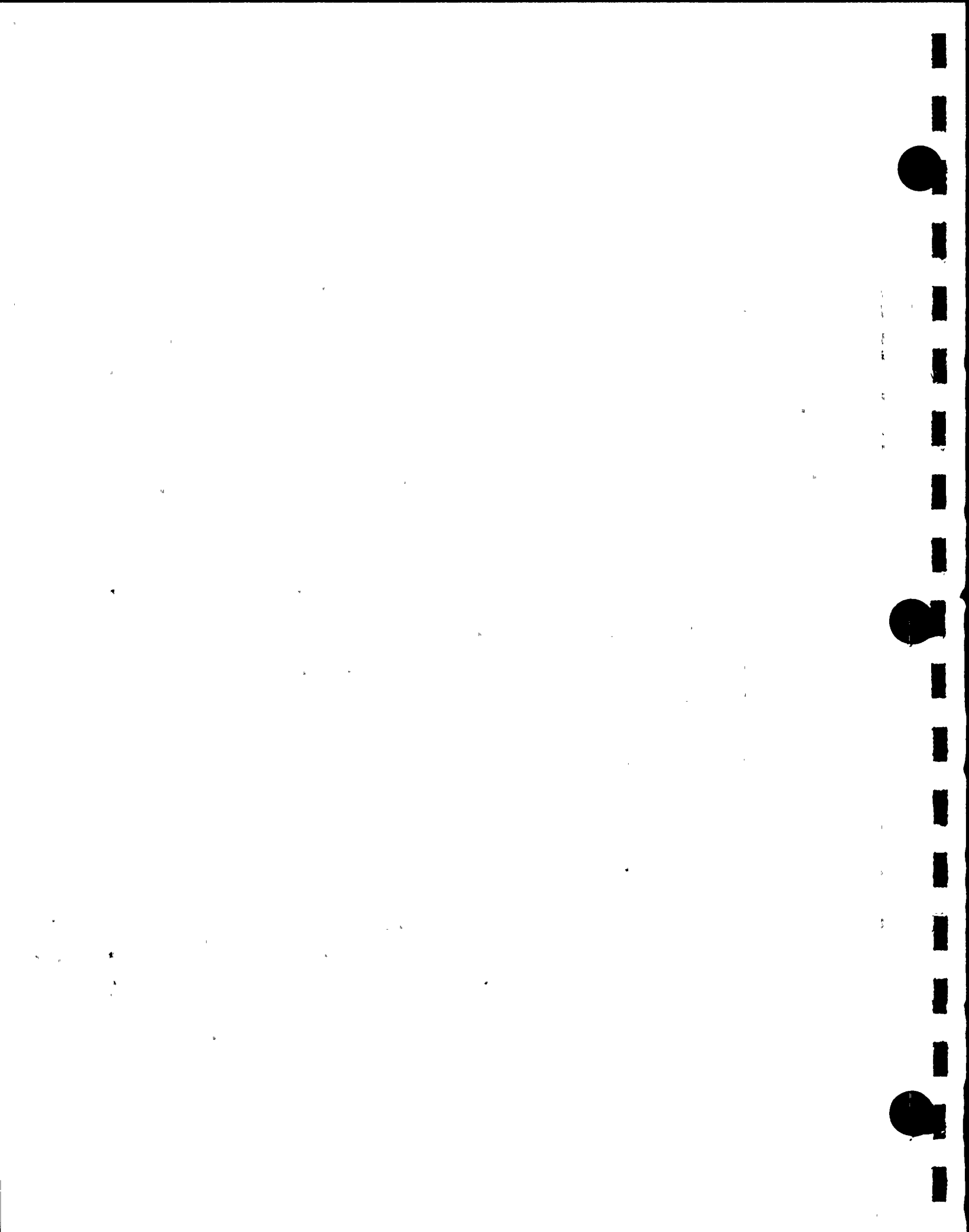
IDEALIZATION OF RACK ASSEMBLY

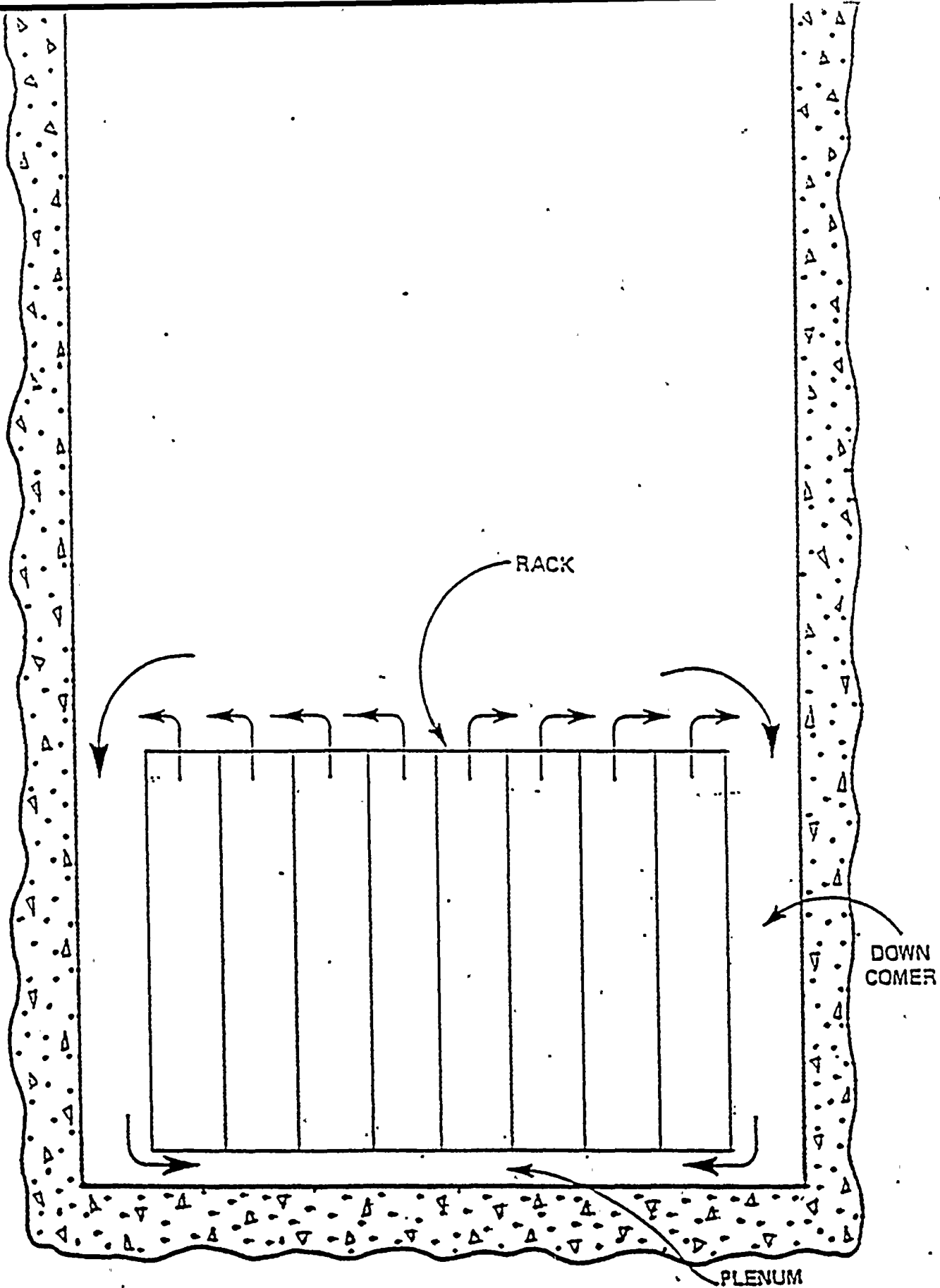
FIGURE 5.6.1

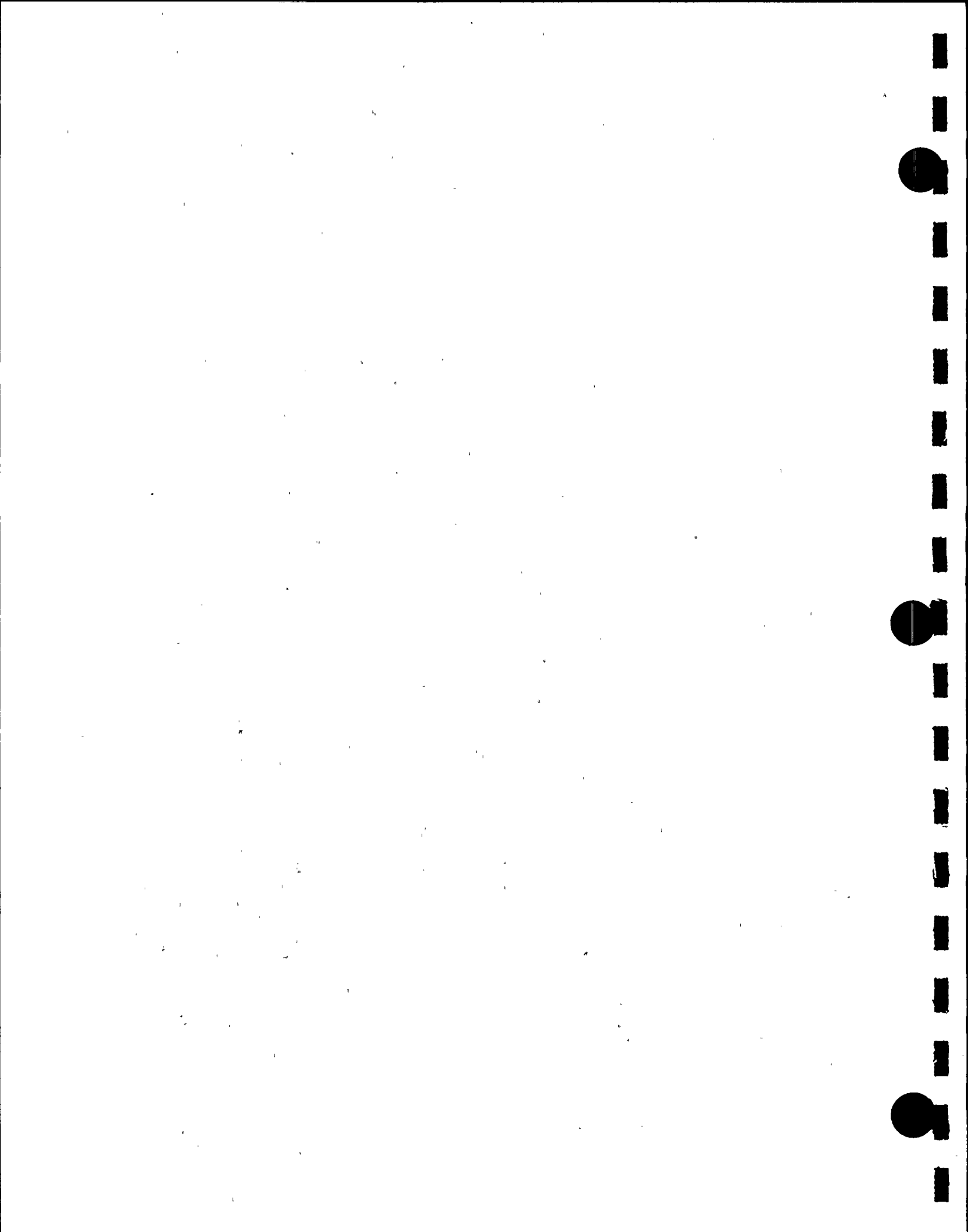












6.0 STATIC AND DYNAMIC ANALYSIS OF RACK STRUCTURE

6.1 Introduction

The purpose of this section is to present analyses which demonstrate the structural adequacy of the Donald C. Cook spent fuel high density rack design under normal storage and the postulated accident loading conditions as defined by and following the guidelines of the USNRC Standard Review Plan (Ref. 6.1.1). The method of analysis presented uses a time-history integration method similar to that previously used in the licensing reports on high density spent fuel racks for Enrico Fermi Unit 2 (USNRC Docket No. 50-341), Quad Cities 1 and 2 (USNRC Docket Nos. 50-254 and 50-265), Rancho Seco (USNRC Docket No. 50-312), Grand Gulf Unit 1 (USNRC Docket No. 50-416), Oyster Creek (USNRC Docket No. 50-219), V.C. Summer (USNRC Docket No. 50-395), Diablo Canyon Units 1 and 2 (USNRC Docket Nos. 50-275 and 50-323), Vogtle Unit 2 (USNRC Docket No. 50-425) and Millstone Point Unit 1 (USNRC Docket No. 50-245). The analyses carried out for the Donald C. Cook racks are considerably more elaborate and exhaustive in scope and substance than those performed in the aforementioned dockets, and reflect advances in 3-D fuel rack simulation technology in the past two years. The details are presented later in this section, after the essential elements of the dynamic model are fully explained.

The results show that the high density spent fuel racks are structurally adequate to resist the postulated stress combinations associated with level A, B, C, and D conditions as defined in Refs. 6.1.1, 6.1.2, and 6.1.3.



6.2 Analysis Outline

The principal steps in performing the seismic analysis of Donald C. Cook racks are summarized below:

- a. Develop statistically independent synthetic time histories for three orthogonal directions which satisfy USNRC SRP3.8.4. Two time histories are considered to be statistically independent if their normalized correlation coefficient is less than 0.15.
- b. Prepare a three-dimensional dynamic model of the fuel rack which embodies all elastostatic characteristics and structural nonlinearities of the Donald C. Cook rack modules.
- c. Perform a series of 3-D dynamic analyses on a limiting module geometry type from those listed in Tables 2.1.1 and 2.1.3 and for varying physical conditions (such as coefficient of friction, extent of cells containing fuel assemblies, and proximity of other racks).
- d. Perform stress analysis for the critical case from the dynamic analysis runs made in the foregoing steps. Demonstrate compliance with ASME Code Section III, subsection NF (Ref. 6.1.2) limits.
- e. Carry out a degree-of-freedom (DOF) reduction procedure on the single rack 3-D model such that the kinematic responses calculated by the reduced DOF (model RDOFM) are in agreement with the baseline model of step (b) above. This reduced DOF model is also truly three-dimensional.
- f. Prepare a whole pool multi-rack dynamic model by compiling the RDOFM's of all rack modules in the pool, and by including all fluid coupling interactions among them, as well as those between the racks and pool walls. This 3-D multi-module simulation is referred to as a Whole Pool Multi-Rack (WPMR) model.



- g. Perform a 3-D Whole Pool Multi-Rack (WPMR) analysis to demonstrate that all kinematic criteria for Donald C. Cook rack modules are satisfied (see Section 6.8), and that pedestal compressive loads are comparable to the loads used for structural qualification per item d above. Section 6.8 gives the criteria which need to be checked.

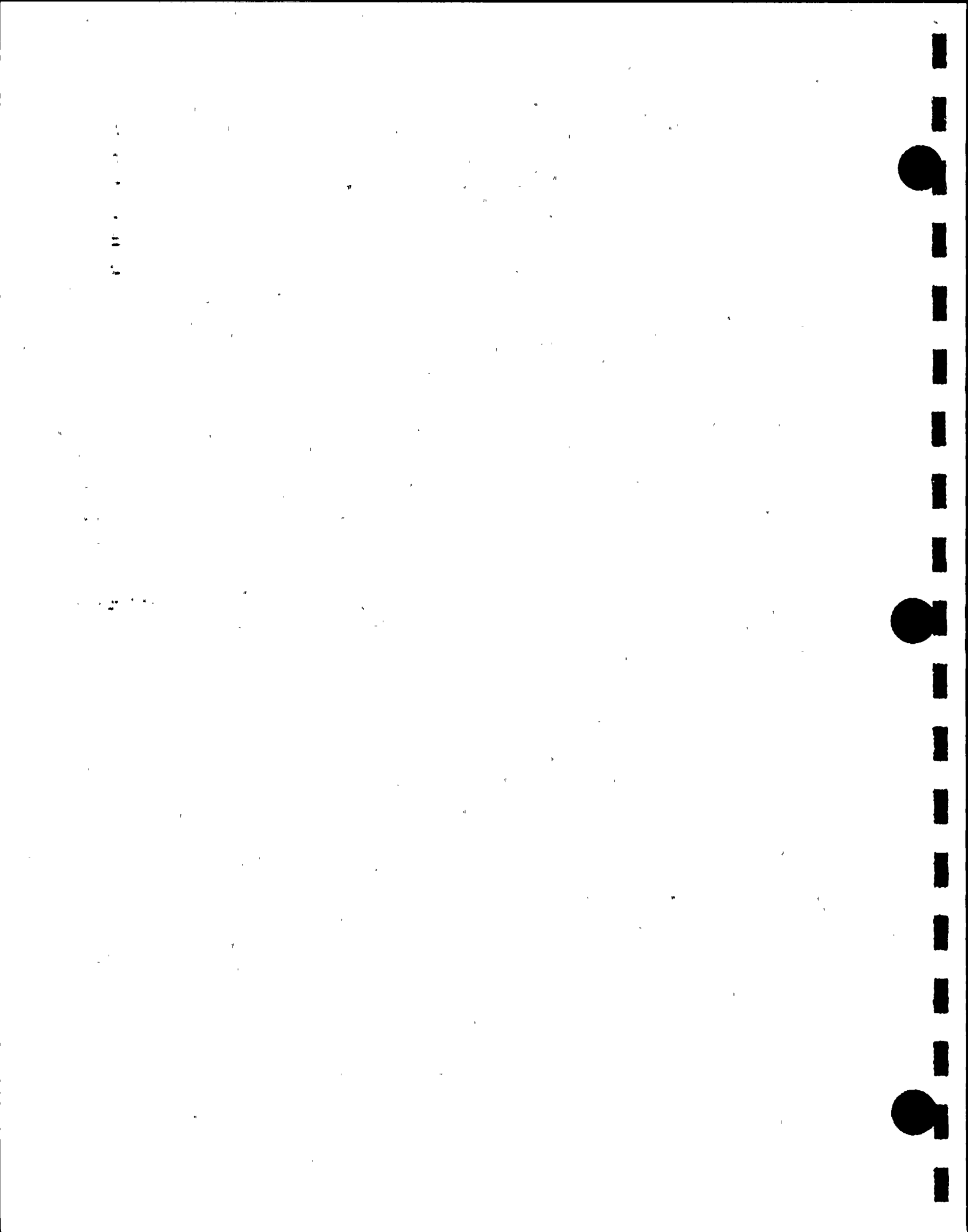
For the Donald C. Cook racks, the principal kinematic criteria are (i) no rack to pool wall impact, and (ii) no rack-to-rack impact in the cellular region of the racks.

Figure 6.2.1 shows a pictorial view of the rack module. It is noted that the baseplate extends beyond the cellular region envelope, thus ensuring that the inter-rack impact, if any, would first occur at the baseplate elevation. The baseplate of the rack modules is structurally qualifiable to withstand large in-plane impact loads.

We describe each of the above analysis steps in some detail in the following sub-sections with special emphasis on the baseline 3-D dynamic model which is the building block for all subsequent analyses. We also present the results of the analysis in the concluding sub-section.

6.3 Artificial Slab Motions

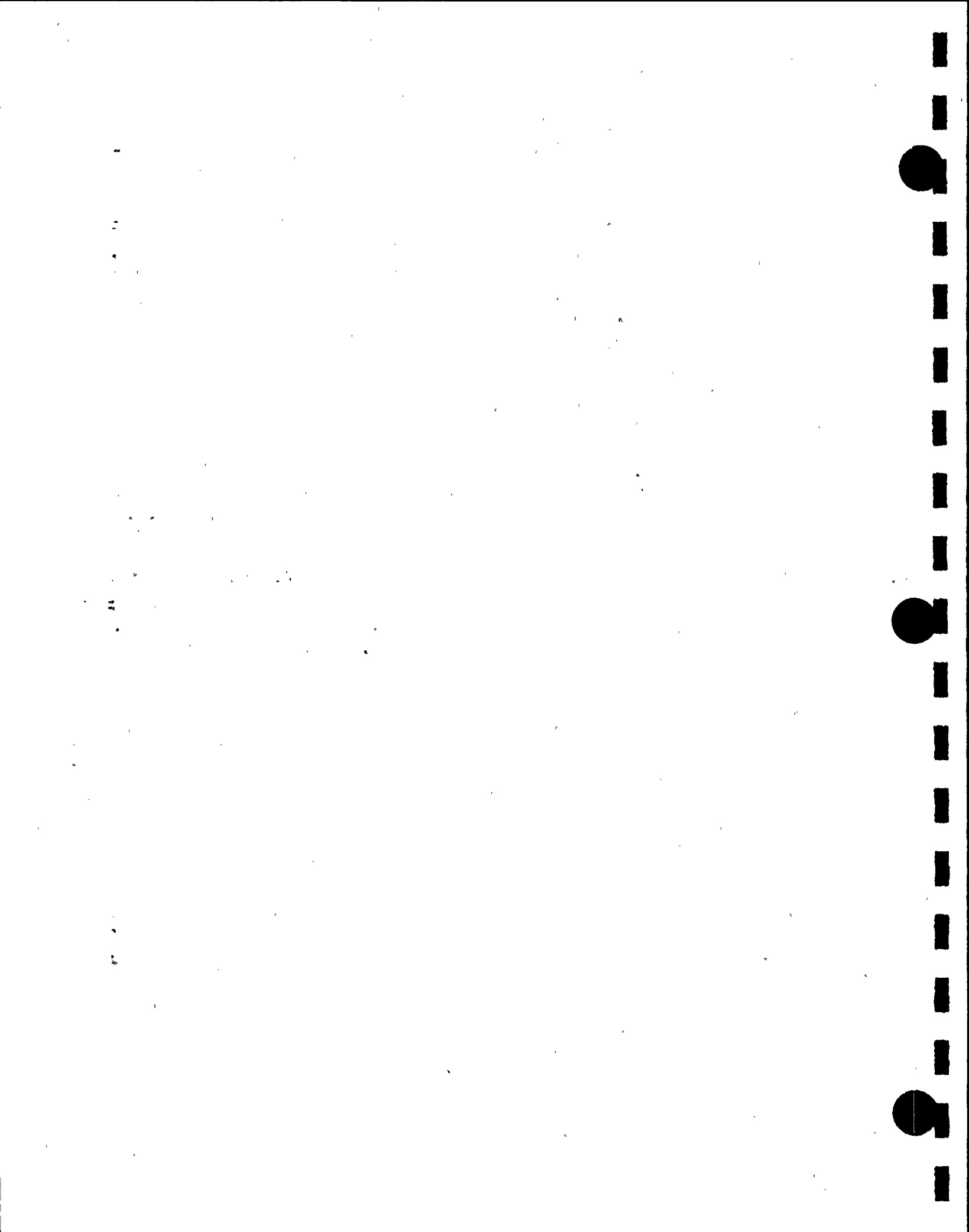
The UFSAR provides a single response spectrum in the horizontal direction and a single response spectrum in the vertical direction (2/3 of the horizontal) for the Design Basis Earthquake (DBE). A corresponding pair of spectra are provided for the Operating Basis Earthquake (OBE).



Holtec's Q.A. validated time history generation code GENEQ [6.3.1] was used to generate three synthetic statistically independent time histories for the North-South, East-West and vertical directions, respectively, from the two response spectra. 5% damping is used for the DBE condition. Figures 6.3.1 - 6.3.3 show the DBE time history plots. Response spectra corresponding to these time histories were also generated and are shown overlaid on the design spectra in Figures 6.3.4 - 6.3.6.

The normalized correlation coefficients p_{ij} between time histories i and j ($1 \equiv \text{N-S}$, $2 \equiv \text{E-W}$, $3 \equiv \text{vertical}$) are provided in Table 6.3.1.

The above analyses were repeated for the OBE spectra using 2% damping. Figures 6.3.7 - 6.3.9 present the time history plots, and Figures 6.3.10 - 6.3.12 show the comparison between the design spectra and the derived spectra. Table 6.3.1 also provides p_{ij} for the OBE time histories. It is noted that the enveloping requirement on the derived spectra and statistical non-coherence of artificial motions are unconditionally satisfied.



6.4 Outline of Single Rack 3-D Analysis

The spent fuel storage racks are Seismic Class I equipment. They are required to remain functional during and after a Design Basis Earthquake (Ref. 6.1.3). These racks are neither anchored to the pool floor nor attached to the sidewalls. The individual rack modules are not interconnected. Furthermore, a particular rack may be completely loaded with fuel assemblies (which corresponds to greatest rack inertia), or it may be completely empty. The coefficient of friction, μ , between the supports and pool floor is another indeterminate factor. According to Rabinowicz (Ref. 6.4.1), the results of 199 tests performed on austenitic stainless steel plates submerged in water show a mean value of μ to be 0.503 with a standard deviation of 0.125. The upper and lower bounds (based on twice the standard deviation) are thus 0.753 and 0.253, respectively. Analyses are therefore performed for single rack simulations using values of the coefficient of friction equal to 0.2 (lower limit) and 0.8 (upper limit), respectively. The bounding values of $\mu = 0.2$ and 0.8 have been found to bracket the upper limit of the module response in previous rerack projects.

A single rack 3-D analysis requires another key modelling assumption. This relates to the location and relative motion of neighboring racks. The gap between a peripheral rack and an adjacent pool wall is known, and the motion of the pool wall is prescribed without any ambiguity. However, another rack adjacent to the rack being analyzed is also free-standing and subject to motion during a seismic event. To conduct the seismic analysis of a given rack its physical interface with neighboring modules must be specified. The standard procedure in the single rack analysis is to specify that the neighboring racks move 180° out-of-phase in



1
2
3
4
5

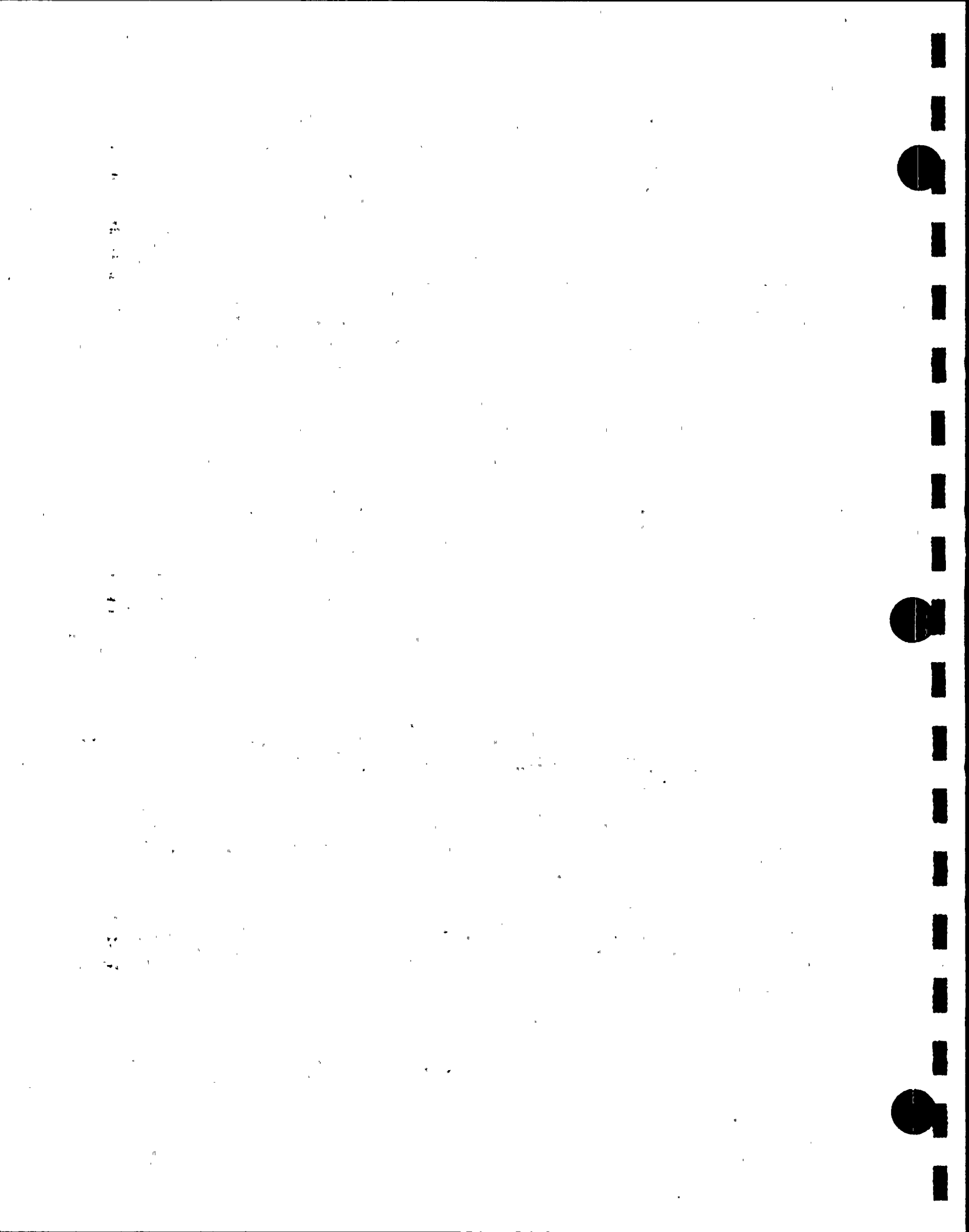
6

7
8
9

relation to the subject rack. Thus, the available gap before inter-rack impact occurs is one half of the physical gap. This "opposed phase motion" assumption increases the likelihood of predicting intra-rack impacts and is thus a conservative assumption. However, it also increases the relative contribution of fluid coupling terms, which depend on fluid gaps and relative movements of bodies, making the outright conservatism a less certain assertion. In fact, 3-D Whole Pool Multi-rack analyses carried out for Taiwan Power Company's Chin Shan Station, and for GPU Nuclear's Oyster Creek Nuclear Station show that the single rack simulations predict smaller rack displacement during seismic responses. Nevertheless, single rack analyses permit detailed evaluation of stress fields, and serve as a benchmark check for the much more involved, WPMR analysis results. In order to predict the limiting conditions of rack module seismic response within the framework of single rack analysis, module A4 (13x14) is analyzed. This is typical of the largest module, and is also a corner module. The corner module has larger rack-to-wall gaps which will minimize the fluid coupling.

The rack is considered fully loaded or half loaded, with limiting coefficients of friction; these simulations identify the worst case response for rack movement and for rack structural integrity. After completion of reracking, the gaps between the rack modules and those between the racks and walls will be in the manner of Figure 2.1.1. We show in this report that all single rack 3-D simulations predict that no rack-to-rack or rack-to-wall impacts will occur in the cellular region of the racks.

The seismic analyses were performed utilizing the time-history method. Pool slab acceleration data presented in the preceding sub-section was used.



The objective of the seismic analysis of single racks is to determine the structural response (stresses, deformation, rigid body motion, etc.) due to simultaneous application of the three statistically independent, orthogonal seismic excitations. Thus, recourse to approximate statistical summation techniques such as the "Square-Root-of-the-Sum-of-the-Squares" method (Ref. 6.4.2) is avoided. For nonlinear analysis, the only practical method is simultaneous application of the seismic loading to a nonlinear model of the structure.

The seismic analysis of a single rack is performed in three steps, namely:

1. Development of a nonlinear dynamic model consisting of inertial mass elements, spring, gap, and friction elements.
2. Generation of the equations of motion and inertial coupling and solution of the equations using the "component element method" (Refs. 6.4.3 and 6.4.4) to determine nodal forces and displacements. The Holtec computer code DYNARACK is used to solve the system of equations [6.4.5].
3. Computation of the detailed stress field in the rack just above the baseplate and in the support legs is made using the nodal forces calculated in the previous step. These stresses are checked against the design limits given in a later sub-section.

A brief description of the dynamic model follows.

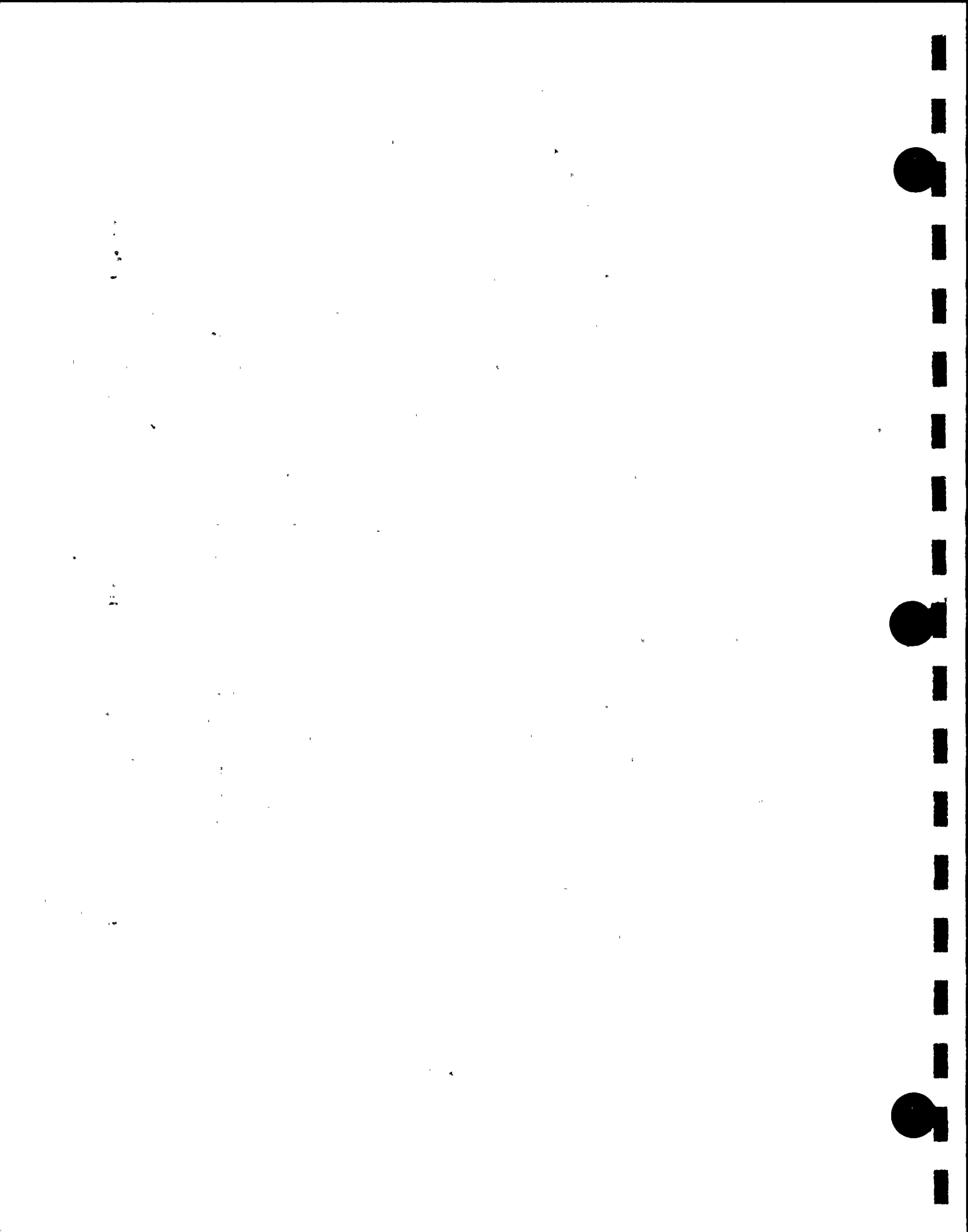
6.5 Dynamic Model for The Single Rack Analysis

Since the racks are not anchored to the pool slab or attached to the pool walls or to each other, they can execute a wide variety of motions. For example, the rack may slide on the pool floor

1 2 3 4 5 6 7 8 9 10 11 12 13 14 15 16 17 18 19 20 21 22 23 24 25 26 27 28 29 30 31 32 33 34 35 36 37 38 39 40 41 42 43 44 45 46 47 48 49 50 51 52 53 54 55 56 57 58 59 60 61 62 63 64 65 66 67 68 69 70 71 72 73 74 75 76 77 78 79 80 81 82 83 84 85 86 87 88 89 90 91 92 93 94 95 96 97 98 99 100



(so-called "sliding condition"); one or more legs may momentarily lose contact with the liner ("tipping condition"); or the rack may experience a combination of sliding and tipping conditions. The structural model should permit simulation of these kinematic events with inherent built-in conservatisms. Since the modules are designed to preclude the incidence of inter-rack impact in the cellular region, it is also necessary to include the potential for inter-rack impact phenomena in the analysis to demonstrate that such impacts do not occur. Lift-off of the support legs and subsequent liner impacts must be modelled using appropriate impact (gap) elements, and Coulomb friction between the rack and the pool liner must be simulated by appropriate piecewise linear springs. The elasticity of the rack structure, relative to the base, must also be included in the model even though the rack may be nearly rigid. These special attributes of rack dynamics require a strong emphasis on the modeling of the linear and nonlinear springs, dampers, and compression only stop elements. The term non-linear spring is the generic term to denote the mathematical element representing the situation where the restoring force exerted by the element is not linearly proportional to the displacement. In the fuel rack simulation the Coulomb friction interface between the rack support leg and the liner is a typical example of a non-linear spring. The model outline in the remainder of this subsection, and the model description in the following sub-section, describe the detailed modeling technique to simulate these effects, with considerable emphasis placed on the nonlinearity of the rack seismic response.



6.5.1 Assumptions

- a. The fuel rack structure is a folded metal plate assemblage welded to a baseplate and supported on four legs. An odd-shaped module may have more than four legs. The rack structure itself is a very rigid structure. Dynamic analysis of typical multi-cell racks has shown that the motion of the structure is captured almost completely by modelling the rack as a twelve degree-of-freedom structure, where the movement of the rack cross-section at any height is described in terms of six degrees-of-freedom of the rack base and six degrees of freedom defined at the rack top. The rattling fuel is modelled by five lumped masses located at H , $.75H$, $.5H$, $.25H$, and at the rack base, where H is the rack height as measured from the base.
- b. The seismic motion of a fuel rack is characterized by random rattling of fuel assemblies in their individual storage locations. Assuming a certain statistical coherence (i.e. assuming that all fuel elements move in-phase within a rack) in the vibration of the fuel assemblies exaggerates the computed dynamic loading on the rack structure. This assumption, however, greatly reduces the required degrees-of-freedom needed to model the fuel assemblies which are represented by five lumped masses located at different levels of the rack. The centroid of each fuel assembly mass can be located, relative to the rack structure centroid at that level, so as to simulate a partially loaded rack.
- c. The local flexibility of the pedestal is modelled so as to account for floor elasticity, and local rack elasticity just above the pedestal.
- d. The rack base support may slide or lift-off the pool floor.
- e. The pool floor has a specified time-history of seismic accelerations along the three orthogonal directions.
- f. Fluid coupling between rack and fuel assemblies, and between rack and wall, is simulated by introducing appropriate inertial coupling into the system kinetic energy. Inclusion of these effects uses the methods of Refs. 6.5.1 and 6.5.2 for rack/assembly coupling and for rack/rack coupling.

- g. Potential impacts between rack and fuel assemblies are accounted for by appropriate "compression only" gap elements between masses involved.
- h. Fluid damping due to viscous effects between rack and assemblies, and between rack and adjacent rack, is conservatively neglected.
- i. The supports are modeled as "compression only" elements for the vertical direction and as "rigid links" for transferring horizontal stress. The bottom of a support leg is attached to a frictional spring as described in sub-section 6.6. The cross-section inertial properties of the support legs are computed and used in the final computations to determine support leg stresses.
- j. The effect of sloshing is negligible at the level of the top of the rack and is hence neglected.
- k. The possible incidence of rack-to-wall or rack-to-rack impact is simulated by gap elements at the top and bottom of the rack in the two horizontal directions. The bottom elements are located at the baseplate elevation.
- l. Rattling of fuel assemblies inside the storage locations causes the "gap" between the fuel assemblies and the cell wall to change from a maximum of twice the nominal gap to a theoretical zero gap. Fluid coupling coefficients are based on the nominal gap.
- m. The form drag due to motion of the fuel assembly in the storage cell, or that due to movement of a rack in the pool, has been neglected in this analysis for added conservatism.
- n. The fluid coupling terms are based on opposed phase motion of adjacent modules.

Figure 6.5.1 shows a schematic of the model. Twelve degrees of freedom are used to track the motion of the rack structure. Figures 6.5.2 and 6.5.3, respectively, show the inter-rack impact springs (to track the potential for impact between racks or between rack and wall) and fuel assembly/storage cell impact



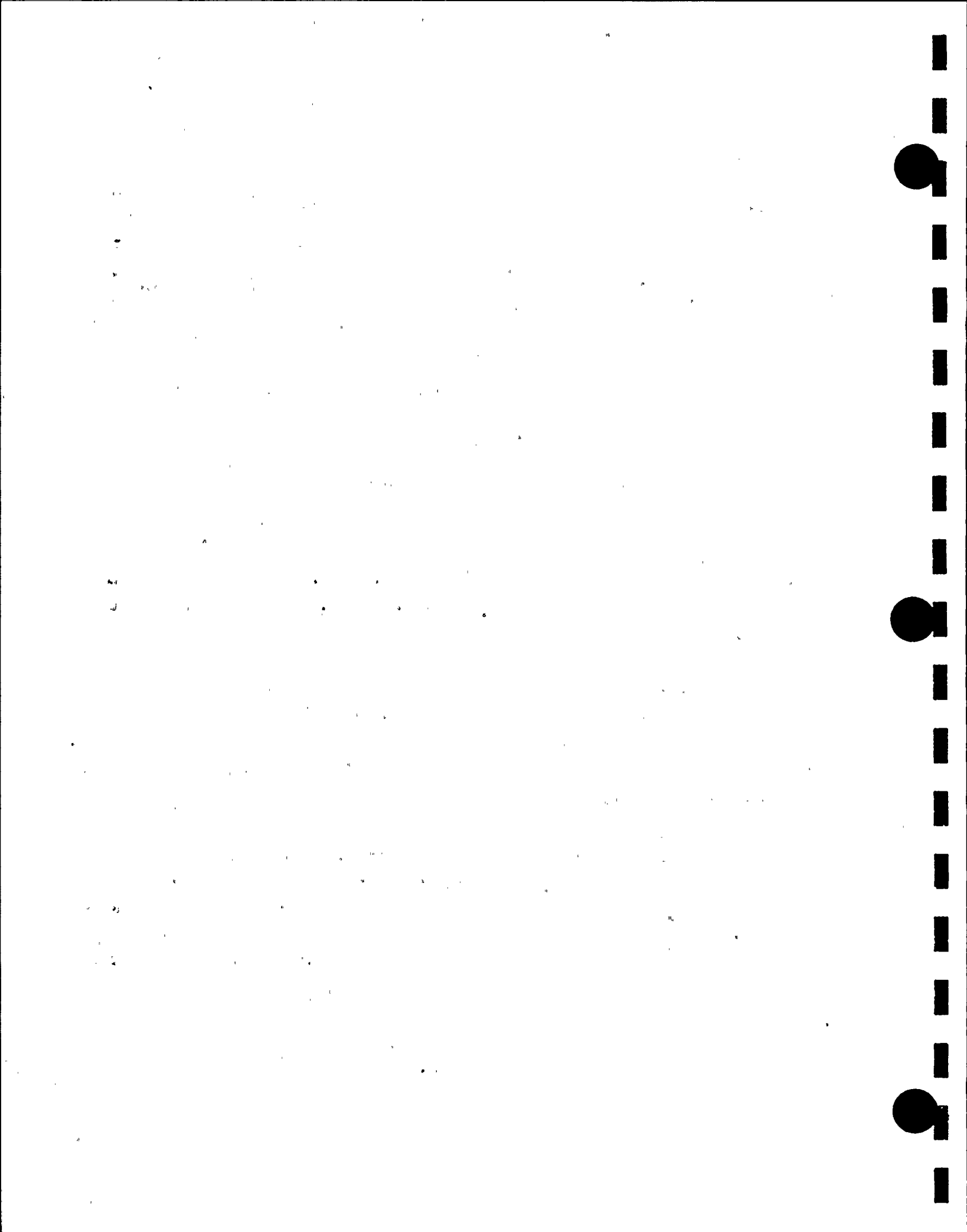
springs at a particular level. S_i ($i = 1, \dots, 4$) represent support locations, p_i represent absolute degrees-of-freedom, and q_i represent degrees-of-freedom relative to the slab. H is the height of the rack above the baseplate.

As shown in Figure 6.5.1, the model for simulating fuel assembly motion incorporates five rattling lumped masses. The five rattling masses are located at the baseplate, at quarter height, at half height, at three quarter height, and at the top of the rack. Two degrees-of-freedom are used to track the motion of each rattling mass in the horizontal plane. The vertical motion of each rattling mass is assumed to be the same as the rack base. Figures 6.5.4, 6.5.5, and 6.5.6 show the modelling scheme for including rack elasticity and the degrees of freedom associated with rack elasticity. In each plane of bending a shear and a bending spring are used to simulate elastic effects in accordance with Ref. 6.5.1. Table 6.6.2 gives spring constants for these bending springs as well as corresponding constants for extensional and torsional rack elasticity.

6.5.2 Model Description

The absolute degrees-of-freedom associated with each of the mass locations are identified in Figure 6.5.1 and in Table 6.5.1. The rattling masses (nodes 1*, 2*, 3*, 4*, 5*) are described by translational degrees-of-freedom q_7 - q_{16} .

$U_i(t)$ is the pool floor slab displacement seismic time-history. Thus, there are twenty-two degrees of freedom in the system. Not shown in Fig. 6.5.1 are the gap elements used to model the support legs and the impacts with adjacent racks.



6.5.3 Fluid Coupling

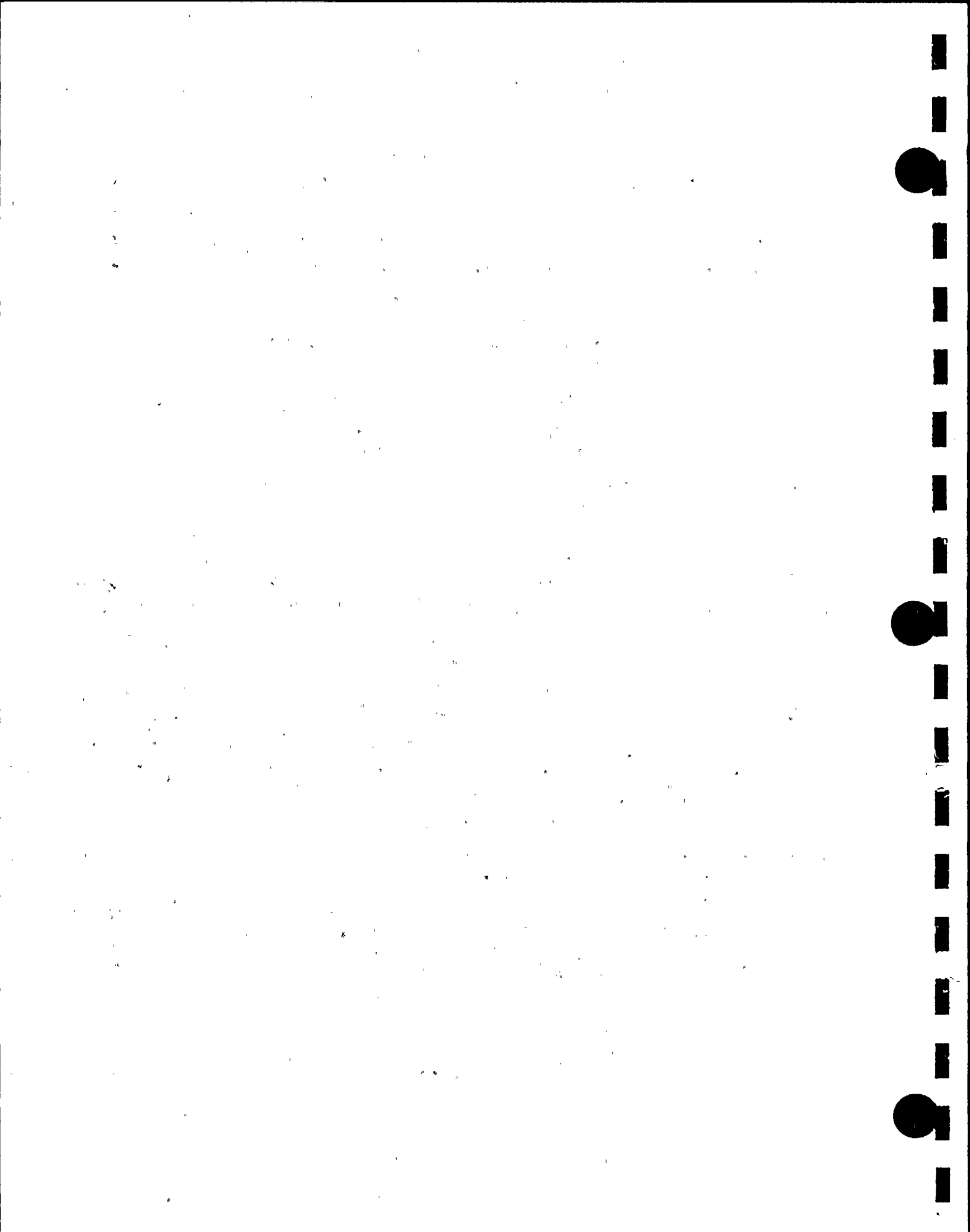
An effect of some significance requiring careful modeling is the "fluid coupling effect" (Refs. 6.5.1 and 6.5.2). If one body of mass (m_1) vibrates adjacent to another body (mass m_2), and both bodies are submerged in a frictionless fluid medium, then Newton's equations of motion for the two bodies have the form:

$$(m_1 + M_{11}) \ddot{X}_1 + M_{12} \ddot{X}_2 = \text{applied forces on mass } m_1 + O(\dot{x}_1^2)$$

$$M_{21} \ddot{X}_1 + (m_2 + M_{22}) \ddot{X}_2 = \text{applied forces on mass } m_2 + O(\dot{x}_2^2)$$

\ddot{X}_1 , \ddot{X}_2 denote absolute accelerations of masses m_1 and m_2 , respectively and the notation $O(\dot{x}^2)$ denotes non-linear terms which arise in the derivation.

M_{11} , M_{12} , M_{21} , and M_{22} are fluid coupling coefficients which depend on the shape of the two bodies, their relative disposition, etc. Fritz (Ref. 6.5.2) gives data for M_{ij} for various body shapes and arrangements. The above equations indicate that the effect of the fluid is to add a certain amount of mass to the body (M_{11} to body 1), and an external force which is proportional to the acceleration of the adjacent body (mass m_2). Thus, the acceleration of one body affects the force field on another. This force is a strong function of the interbody gap, reaching large values for very small gaps. This inertial coupling is called fluid coupling. It has an important effect in rack dynamics. The lateral motion of a fuel assembly inside the storage location will encounter this effect. So will the motion of a rack adjacent to another rack if the racks are closely spaced. These effects are included in the equations of motion. For example, the fluid



coupling is between nodes 2 and 2* in Figure 6.5.1. Furthermore, the rack equations contain coupling terms which model the effect of fluid in the gaps between adjacent racks. The coupling terms modeling the effects of fluid flowing between adjacent racks are computed assuming that all adjacent racks are vibrating 180° out of phase from the rack being analyzed. Therefore, only one rack is considered surrounded by a hydrodynamic mass computed as if there were a plane of symmetry located in the middle of the gap region.

Finally, fluid virtual mass is included in the vertical direction vibration equations of the rack; virtual inertia is also added to the governing equation corresponding to the rotational degree of freedom, $q_6(t)$ and $q_{22}(t)$.

6.5.4 Damping

In reality, damping (Ref. 6.5.3) of the rack motion arises from material hysteresis (material damping), relative intercomponent motion in structures (structural damping), and fluid viscous effects (fluid damping). In the analysis, a maximum of 1% structural damping is imposed on elements of the rack structure during OBE and DBE simulations. Material and fluid damping due to fluid viscosity are conservatively neglected. The dynamic model has the provision to incorporate form drag effects; however, no form drag has been used for this analysis.

6.5.5 Impact

Any fuel assembly node (e.g., 2*) may impact the corresponding structural mass node 2. To simulate this impact, four compression-only gap elements around each rattling fuel assembly



node are provided (see Figure 6.5.3). The compressive loads developed in these springs provide the necessary data to evaluate the integrity of the cell wall structure and stored array during the seismic event. Figure 6.5.2 shows the location of the impact springs used to simulate any potential for inter-rack or rack-to-wall impacts. Sub-section 6.6 gives more details on these additional impact springs. Since there are five rattling masses, a total of 20 impact springs are used to model fuel assembly-cell wall impact.

6.6 Assembly of the Dynamic Model

The cartesian coordinate system associated with the rack has the following nomenclature:

- x = Horizontal coordinate along the short direction of rack rectangular planform
- y = Horizontal coordinate along the long direction of the rack rectangular planform
- z = Vertical coordinate upward from the rack base

Table 6.6.1 lists all spring elements used in the 3-D single rack analysis.

If the simulation model is restricted to two dimensions (one horizontal motion plus vertical motion, for example) for the purposes of model clarification only, then a descriptive model of the simulated structure which includes gap and friction elements is shown in Figure 6.6.1.

The impacts between fuel assemblies and rack show up in the gap elements, having local stiffness K_I , in Figure 6.6.1. In Table 6.6.1, gap elements 5 through 8 are for the vibrating mass at the



top of the rack. The support leg spring rates K_S are modeled by elements 1 through 4 in Table 6.6.1. Note that the local compliance of the concrete floor is included in K_S . To simulate sliding potential, friction elements 2 plus 8 and 4 plus 6 (Table 6.6.1) are shown in Figure 6.6.1. The friction of the support/liner interface is modeled by a piecewise linear spring with a suitably large stiffness K_f up to the limiting lateral load, μN , where N is the current compression load at the interface between support and liner. At every time step during the transient analysis, the current value of N (either zero for lift-off condition, or a compressive finite value) is computed. Finally, the support rotational friction springs K_R reflect any rotational restraint that may be offered by the foundation. This spring rate is calculated using a modified Bousinesq equation and is included to simulate the resistive moment of the support to counteract rotation of the rack leg in a vertical plane. This rotation spring is also nonlinear, with a zero spring constant value assigned after a certain limiting condition of slab moment loading is reached.

The nonlinearity of these springs (friction elements 9, 11, 13, and 15 in Table 6.6.1) reflects the edging limitation imposed on the base of the rack support legs and the shifts in the centroid of load application as the rack rotates. If this effect is neglected, any support leg bending, induced by liner/baseplate friction forces, is resisted by the leg acting as a beam cantilevered from the rack baseplate. This leads to higher predicted loads at the support leg - baseplate junction than if the moment resisting capacity due to floor elasticity at the floor is included in the model.

The spring rate K_S , modeling the effective compression stiffness of the structure in the vicinity of the support, is computed from the equation:



The spring rate K_S , modeling the effective compression stiffness of the structure in the vicinity of the support, is computed from the equation:

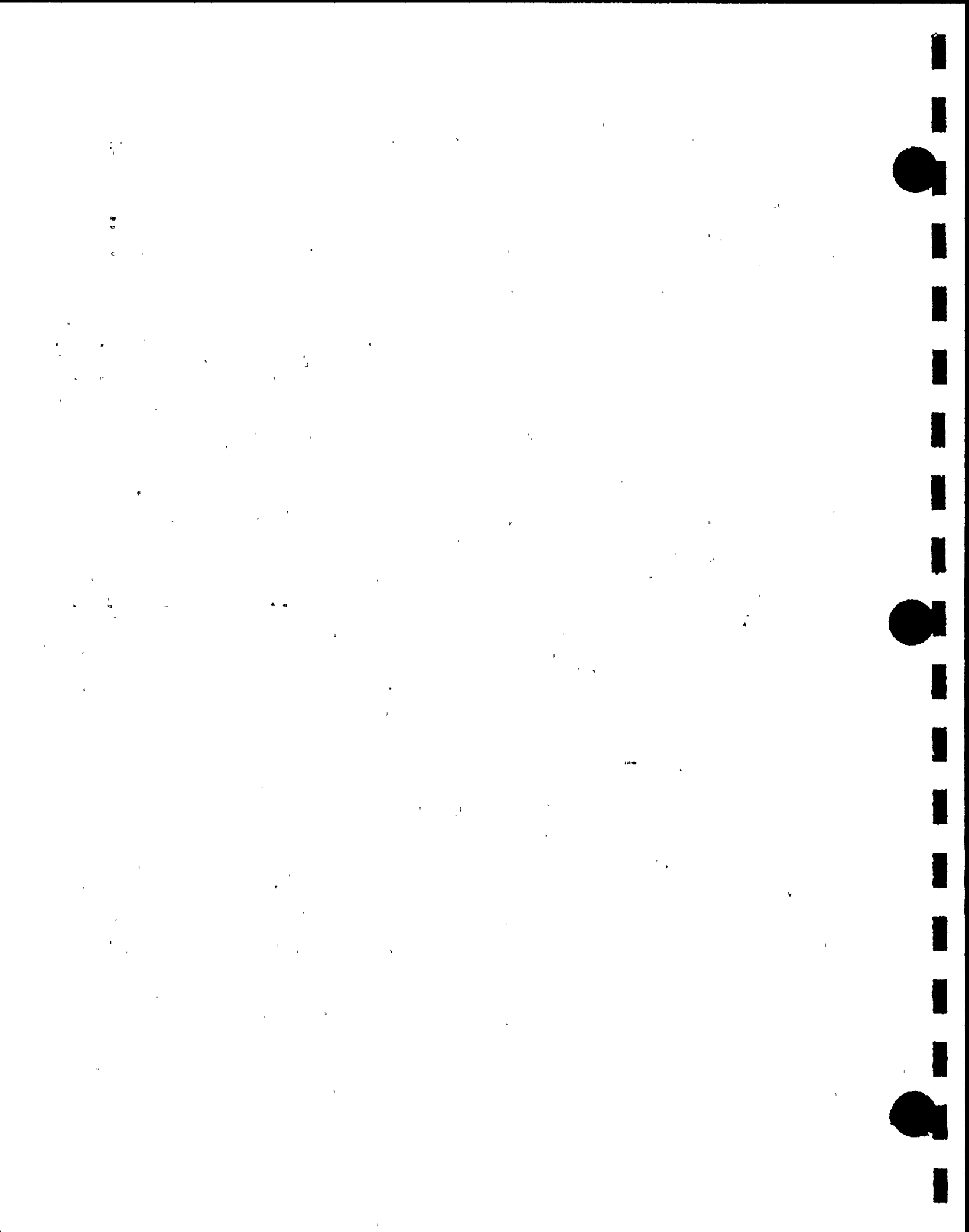
$$\frac{1}{K_S} = \frac{1}{K_1} + \frac{1}{K_2} + \frac{1}{K_3}$$

where:

- K_1 = spring rate of the support leg treated as a tension-compression member
- K_2 = local spring rate of pool slab
- K_3 = spring rate of folded plate cell structure above support leg

As described in the preceding section, the rack, along with the base, supports, and stored fuel assemblies, is modeled for the general three-dimensional (3-D) motion simulation by a twenty-two degree of freedom model. To simulate the impact and sliding phenomena expected, up to 64 nonlinear gap elements and 16 nonlinear friction elements are used. Gap and friction elements, with their connectivity and purpose, are also presented in Table 6.6.1. Table 6.6.2 lists representative values for a module used in the single rack dynamic simulations.

For the 3-D simulation of a single rack, all support elements (described in Table 6.6.1) are included in the model. Coupling between the two horizontal seismic motions is provided both by any offset of the fuel assembly group centroid which causes the rotation of the entire rack and/or by the possibility of lift-off of one or more support legs. The potential exists for the rack to be supported on one or more support legs during any instant of a complex 3-D seismic event. All of these potential events may be



simulated during a 3-D motion so that a mechanism exists in the model to simulate the real behavior.

6.7 Time Integration of the Equations of Motion

6.7.1 Time-History Analysis Using Multi-Degree of Freedom Rack Model

Having assembled the structural model, the dynamic equations of motion corresponding to each degree of freedom are written by using Lagrange's Formulation. The system kinetic energy can be constructed including contributions from the solid structures and from the trapped and surrounding fluid. A single rack is modelled in detail. The system of equations can be represented in matrix notation as:

$$[M] \{q''\} = \{Q\} + \{G\}$$

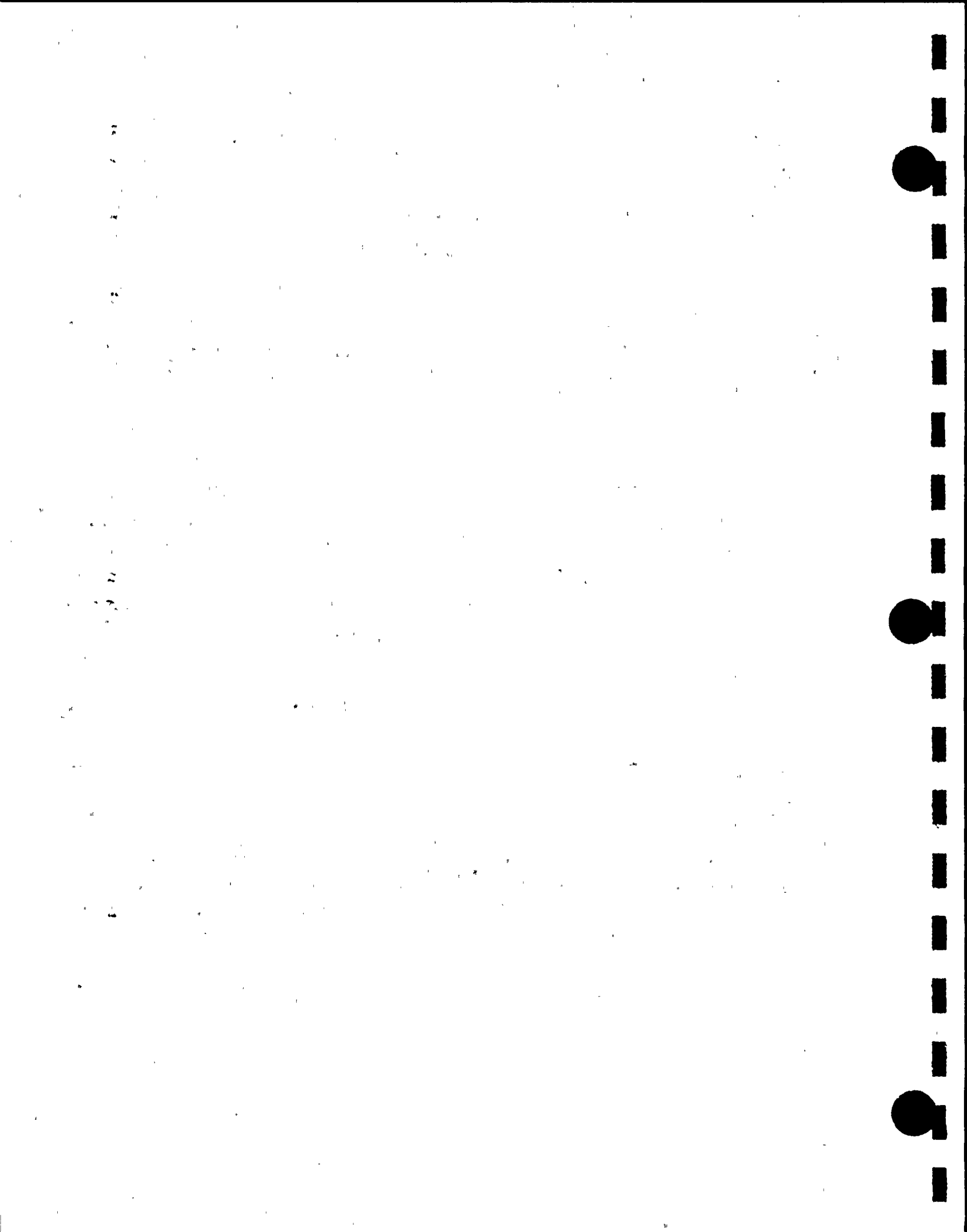
where:

- $[M]$ - total mass matrix;
- $\{q\}$ - the nodal displacement vector relative to the pool slab displacement; double prime stands for secondary derivations;
- $\{G\}$ - a vector dependent on the given ground acceleration;
- $\{Q\}$ - a vector dependent on the spring forces (linear and non-linear) and the coupling between masses.

The equation can be rewritten as

$$\{q''\} = [M]^{-1} \{Q\} + [M]^{-1} \{G\}$$

As noted earlier, in the numerical simulations run to verify structural integrity during a seismic event, the rattling fuel assemblies are assumed to move in phase. This will provide maximum impact force level, and induce additional conservatism in the time-history analysis.



This equation set is mass uncoupled, displacement coupled at each instant in time, and is ideally suited for numerical solution using a central difference scheme. The proprietary, USNRC accepted, computer program "DYNARACK"* is utilized for this purpose.

Stresses in various portions of the structure are computed from known element forces at each instant of time and the maximum value of critical stresses over the entire simulation is reported in summary form at the end of each run.

In summary, dynamic analysis of typical multi-cell racks has shown that the motion of the structure is captured almost completely by the behavior of a twenty-two degree of freedom structure; therefore, in this analysis model, the movement of the rack cross-section at any height is described in terms of the rack degrees of freedom ($q_1(t)$, ..., $q_6(t)$ and q_{17} - $q_{22}(t)$). The remaining degrees of freedom are associated with horizontal movements of the fuel assembly masses. In this dynamic model, five rattling masses are used to represent fuel assembly movement in the horizontal

* This code has been previously utilized in licensing of similar racks for Enrico Fermi Unit 2 (USNRC Docket No. 50-341), Quad Cities 1 and 2 (USNRC Docket Nos. 50-254 and 265), Rancho Seco (USNRC Docket No. 50-312), Oyster Creek (USNRC Docket No. 50-219), V.C. Summer (USNRC Docket No. 50-395), and Diablo Canyon 1 and 2 (USNRC Docket Nos. 50-275 and 50-323), St. Lucie Unit I (USNRC Docket No. 50-335), Byron Units I and II (USNRC Docket Nos. 50-454, 50-455), Vogtle 2 (USNRC Docket 50-425), and Millstone Unit 1 (USNRC Docket 50-245), Indian Point Unit 2 (USNRC Docket No. 50-247), among others.



plane. Therefore, the final dynamic model consists of twelve degrees of freedom for the rack plus ten additional mass degrees of freedom for the five rattling masses. The totality of fuel mass is included in the simulation and is distributed among the five rattling masses.

6.7.2 Evaluation of Potential for Inter-Rack Impact

Since racks are usually closely spaced, the simulation includes impact springs to model the potential for inter-rack impact. To account for this potential, yet still retain the simplicity of simulating only a single rack, gap elements are located on the rack at the top and at the baseplate level. Fig. 6.5.2 shows the location of these gap elements. The baseplate location is a designated potential impact region, and the impact springs located in this region are expected to register impact loads. However, the impact is disallowed in the cellular region of the racks. Therefore, the impact springs located at the top must not indicate any loads at any time during the seismic event.

6.8 Structural Acceptance Criteria

There are two sets of criteria to be satisfied by the rack modules:

a. Kinematic Criterion

This criterion seeks to ensure that the rack is a physically stable structure. The racks are designed to preclude inter-rack impacts in the cellular region. Therefore, physical stability of the rack is considered along with the criterion that inter-rack impact or rack-to-wall impacts in the cellular region do not occur.



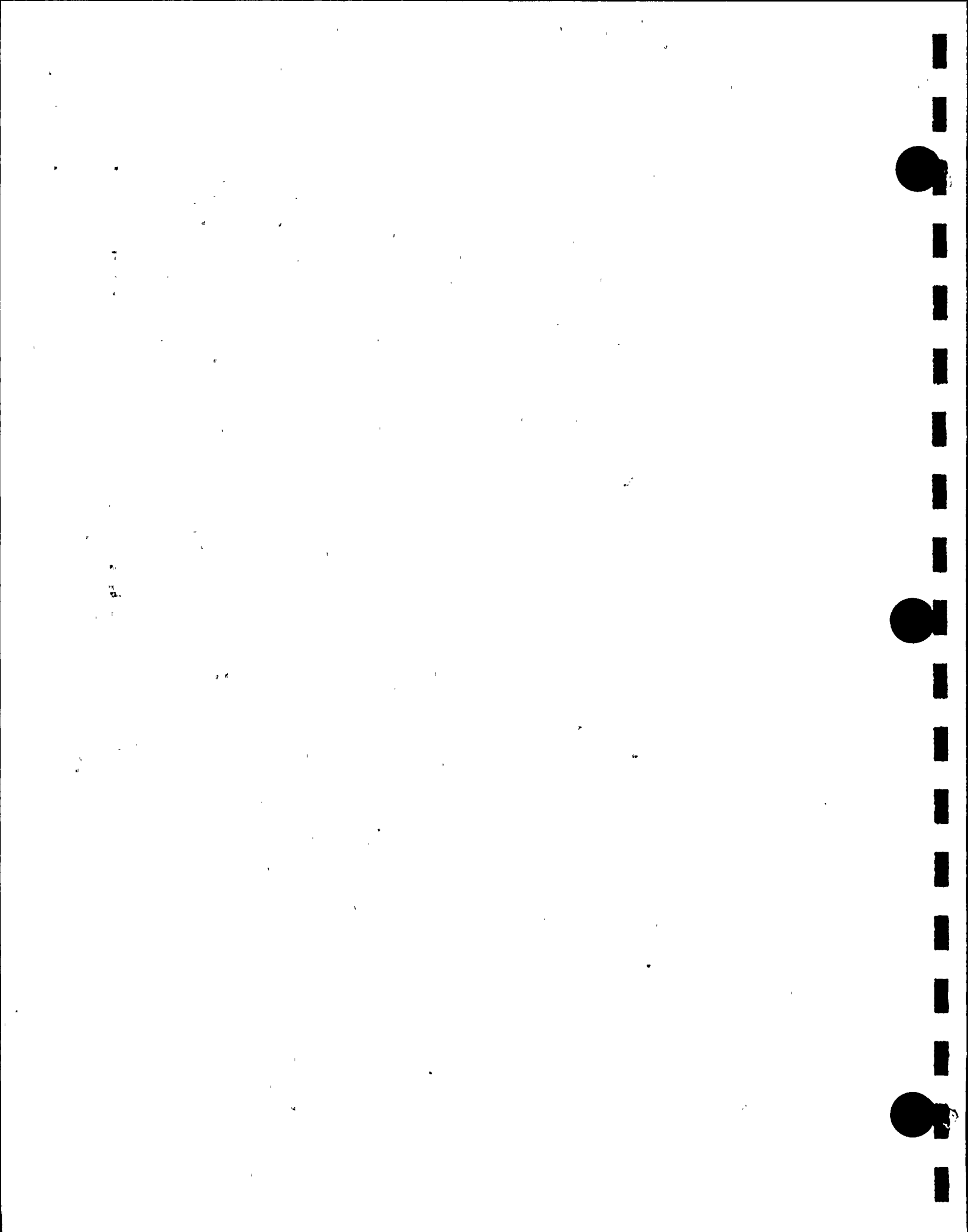
b. Stress Limits

The stress limits of the ASME Code, Section III, Subsection NF, 1989 Edition are used. The following loading combinations are applicable (Ref. 6.1.2) and are consistent with the plant UFSAR commitments.

| <u>Loading Combination</u> | <u>Stress Limit</u> |
|---|---|
| D + L | Level A service limits |
| D + L + T _O | |
| D + L + T _O + E | |
| D + L + T _a + E | Level B service limits |
| D + L + T _O + P _f | |
| D + L + T _a + E' | Level D service limits |
| D + L + F _d | The functional capability of the fuel racks should be demonstrated. |

The abbreviations in the table are those used in Section 3.8.4 of the Standard Review Plan and the "Review and Acceptance of Spent Fuel Storage and Handling Applications":

| | | |
|----------------|---|--|
| D | = | Dead weight-induced internal moments (including fuel assembly weight) |
| L | = | Live Load (not applicable for the fuel rack, since there are no moving objects in the rack load path). |
| F _d | = | Force caused by the accidental drop of the heaviest load from the maximum possible height. |
| P _f | = | Upward force on the racks caused by postulated stuck fuel assembly |
| E | = | Operating Basis Earthquake (OBE) |
| E' | = | Design Basis Earthquake (DBE) |



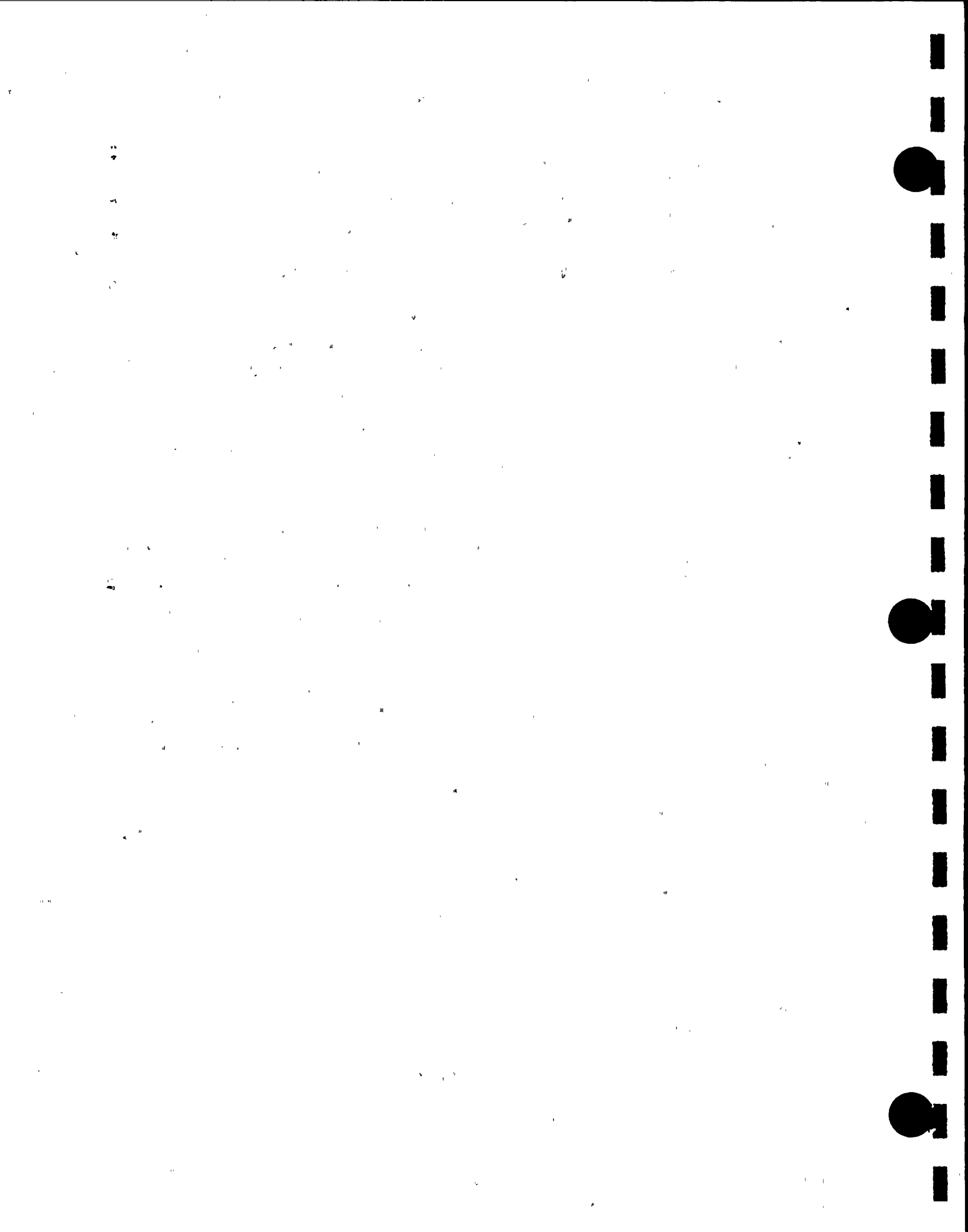
T_o = Differential temperature induced loads (normal operating or shutdown condition based on the most critical transient or steady state condition).

T_a = Differential temperature induced loads (the highest temperature associated with the postulated abnormal design conditions).

The conditions T_a and T_o cause local thermal stresses to be produced. For fuel rack analysis, only one scenario need be examined. The worst situation will be obtained when an isolated storage location has a fuel assembly which is generating heat at the maximum postulated rate. The surrounding storage locations are assumed to contain no fuel. The heated water makes unobstructed contact with the inside of the storage walls, thereby producing the maximum possible temperature difference between the adjacent cells. The secondary stresses thus produced are limited to the body of the rack; that is, the support legs do not experience the secondary (thermal) stresses. For rack qualification, T_o , T_a are the same.

6.9 Material Properties

The data on the physical properties of the rack and support materials, obtained from the ASME Boiler & Pressure Vessel Code, Section III, appendices, are listed in Table 6.9.1. Since the maximum pool bulk temperature is less than 200°F, this is used as the reference design temperature for evaluation of material properties.

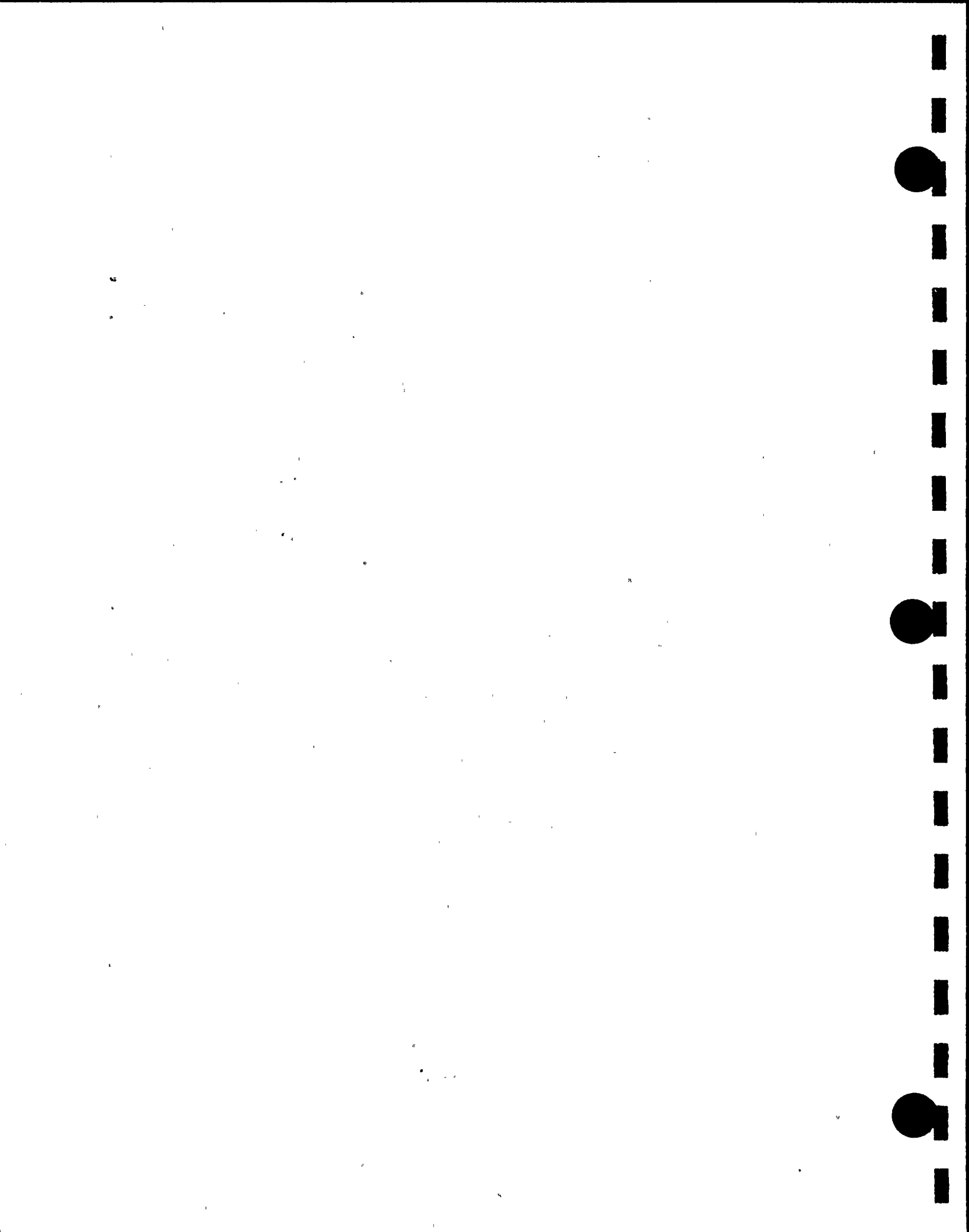


6.10 Stress Limits for Various Conditions

The following stress limits are derived from the guidelines of the ASME Code, Section III, Subsection NF [6.1.2], in conjunction with the material properties data of the preceding section. All parameters and terminology are in accordance with the Code.

6.10.1 Normal and Upset Conditions (Level A or Level B)

- a. Allowable stress in tension on a net section
 $= F_t = 0.6 S_y$ (S_y = yield stress at temperature)
 $F_t = (0.6) (25,000) = 15,000$ psi (rack material)
 F_t = is equivalent to primary membrane stresses
 $F_t = (.6) (25,000) = 15,000$ psi (upper part of support feet)
 $= (.6) (106,300) = 63,780$ psi (lower part of support feet)
- b. On the gross section, allowable stress in shear is:
 $F_v = .4 S_y$
 $(.4) (25,000) = 10,000$ psi (main rack body)
 $F_t = (.4) (25,000) = 10,000$ psi (upper part of support feet)
 $= (.4) (106,300) = 42,520$ psi (lower part of support feet)



c. Allowable stress in compression, F_a :

$$F_a = \frac{\left[1 - \frac{(kl)^2}{r^2} / 2C_c \right] S_y}{\left\{ \left(\frac{5}{3} \right) + \left[3 \left(\frac{kl}{r} \right) / 8C_c \right] - \left[\left(\frac{kl}{r} \right)^3 / 8C_c \right] \right\}}$$

where:

$$C_c = \left[\frac{(2\pi^2 E)^{1/2}}{S_y} \right]$$

l = unsupported length of component

k = length coefficient which gives influence of boundary conditions; e.g.

k = 1 (simple support both ends)
 = 1/2 (cantilever beam)
 = 2 (clamped at both ends)

E = Young's Modulus

r = radius of gyration of component

kl/r for the main rack body is based on the full height and cross section of the honeycomb region. Substituting numbers, we obtain, for both support leg and honeycomb region:

$F_a = 15,000$ psi (main rack body)
 $F_a = 15,000$ psi (upper part of support feet)
 $= 63,780$ psi (lower part of support feet)

d. Maximum allowable bending stress at the outermost fiber due to flexure about one plane of symmetry:

$F_b = 0.60 S_y = 15,000$ psi (rack body)
 $F_b = 15,000$ psi (upper part of support feet)
 $= 63,780$ psi (lower part of support feet)



e. Combined flexure and compression:

$$\frac{f_a}{F_a} + \frac{C_{mx} f_{bx}}{D_x F_{bx}} + \frac{C_{my} f_{by}}{D_y F_{by}} < 1$$

where:

f_a = Direct compressive stress in the section

f_{bx} = Maximum flexural stress along x-axis

f_{by} = Maximum flexural stress along y-axis

$C_{mx} = C_{my} = 0.85$

$$D_x = 1 - \frac{f_a}{F'_{ex}}$$

$$D_y = 1 - \frac{f_a}{F'_{ey}}$$

$$F'_{ex,ey} = \frac{12 \pi^2 E}{23 \left(\frac{kl}{r} \right)_{x,y}}$$

and the subscripts x,y reflect the particular bending plane of interest.

f. Combined flexure and compression (or tension):

$$\frac{f_a}{0.6S_y} + \frac{f_{bx}}{F_{bx}} + \frac{f_{by}}{F_{by}} < 1.0$$



The above requirement should be met for both the direct tension or compression case.

6.10.2 Level D Service Limits

Section F-1370 (ASME Section III, Appendix F), states that the limits for the Level D condition are the minimum of $1.2 (S_y/F_t)$ or $(0.7S_u/F_t)$ times the corresponding limits for Level A condition. S_u is the ultimate tensile stress at 200°F per Table 6.9.1. Since $1.2 S_y$ is greater than $0.7 S_u$ for the lower part of the support feet, the limit is 1.54 for the lower section under DBE conditions. The limit for the upper portion of the support foot is 2.0 under DBE conditions.

Instead of tabulating the results of the different stresses as dimensioned values, they are presented in a dimensionless form. These dimensionless stress factors are defined as the ratio of the actual developed stress to its specified limiting value. With this definition, the limiting value of each stress factor is 1.0 for the OBE and 2.0 (or 1.54) for the DBE condition.

6.11 Results for the Analysis of Spent Fuel Racks Using a Single Rack Model and 3-D Seismic Motion

A complete synopsis of the analysis of the single rack, subject to the postulated earthquake motions, is presented in a summary Table 6.11.1 which gives the bounding values of stress factors R_i ($i = 1 \dots 7$). The stress factors are defined as:

- | | | |
|-------|---|--|
| R_1 | = | Ratio of direct tensile or compressive stress on a net section to its allowable value (note support feet only support compression) |
| R_2 | = | Ratio of gross shear on a net section in the x-direction to its allowable value |



- R₃ = Ratio of maximum bending stress due to bending about the x-axis to its allowable value for the section
- R₄ = Ratio of maximum bending stress due to bending about the y-axis to its allowable value
- R₅ = Combined flexure and compressive factor (as defined in 6.10.1e above)
- R₆ = Combined flexure and tension (or compression) factor (as defined in 6.10.1f)
- R₇ = Ratio of gross shear on a net section in the y-direction to its allowable value.

As stated before, the allowable value of R_i (i = 1, 2, 3, 4, 5, 6, 7) is 1 for the OBE condition and 2 for the DBE (except for the lower section of the support where the factor is 1.54)

The dynamic analysis gives the maximax (maximum in time and in space) values of the stress factors at critical locations in the rack module. Values are also obtained for maximum rack displacements and for critical impact loads. Table 6.11.1 presents critical results for the stress factors, and for rack-to-fuel impact load. Table 6.11.2 presents maximum results for horizontal displacements at the top and bottom of the rack in the x and y direction. For single rack simulations "x" is always the short direction of the rack. In Table 6.11.2, for each run, both the maximum value of the sum of all support foot loadings (4 supports) as well as the maximum value on any single foot is reported. The table also gives values for the maximum vertical load and the corresponding net shear force at the liner at essentially the same time instant, and for the maximum net shear load and the corresponding vertical force at a support foot at essentially the same time instant.

The results presented in Tables 6.11.1 and 6.11.2 represent the totality of single rack runs carried out. The critical case for structural integrity calculations is included. Displacements at the baseplate level are minimal.

The single rack analysis for run A04 gave the highest stress factors for subsequent structural integrity calculations. Subsequent to the detailed analysis, pedestals adjacent to the pool walls were relocated from the corner cell to new locations 2 cells inboard from the edge. Since this relocation could affect the conclusions concerning rack structural integrity, the critical case of run A04 was re-considered using the new pedestal locations. The results of that re-analysis are presented in the tables as run A94. The detailed structural integrity computations reported herein are based on the critical case for the loading scenario investigated. Subsequent Whole Pool Multi-Rack analyses are also based on the final pedestal locations.

The results corresponding to DBE give the highest load factors. The critical load factors reported for the support feet are all for the upper segment of the foot for DBE simulations and are to be compared with the limiting value of 2.0. Results for the lower portion of the support foot are not critical and are not reported in the tables.

Analyses show that significant margins of safety exist against local deformation of the fuel storage cell due to rattling impact of fuel assemblies.



Overturning has also been considered. This has been done by assuming a multiplier of 1.5 on the DBE horizontal earthquakes (more conservative than required by the USNRC Standard Review Plan) and checking predicted displacements. The horizontal displacements do not grow to such an extent as to imply any possibility for overturning.

It is noted that the analyses of the Donald C. Cook plant fuel racks have included some asymmetrically loaded racks. The results of these studies can be used as bounding analyses for the case when a rack module is picked up and relocated when loaded asymmetrically with fuel assemblies. The results presented herein indicate that twisting or deformation that would cause loss of function or violation of safety margins will not occur during a planned rack relocation.

6.12 Impact Analyses

6.12.1 Impact Loading Between Fuel Assembly and Cell Wall

The local stress in a cell wall is conservatively estimated from the peak impact loads obtained from the dynamic simulations. Plastic analysis is used to obtain the limiting impact load. The limit load is calculated as 3125 lbs. per cell which is much greater than the loads obtained from any of the simulations.

6.12.2 Impacts Between Adjacent Racks

All of the dynamic analyses assume, conservatively, that the racks are isolated. However, the displacements obtained from the dynamic analyses are less than 50% of the rack-to-rack spacing or rack-to-wall spacing if the pool is assumed fully populated.



Therefore, we conclude that no impacts between racks or between racks and walls occur during the DBE event. This has been further proven by the Whole Pool Multi-Rack Analysis discussed in Section 6.14.

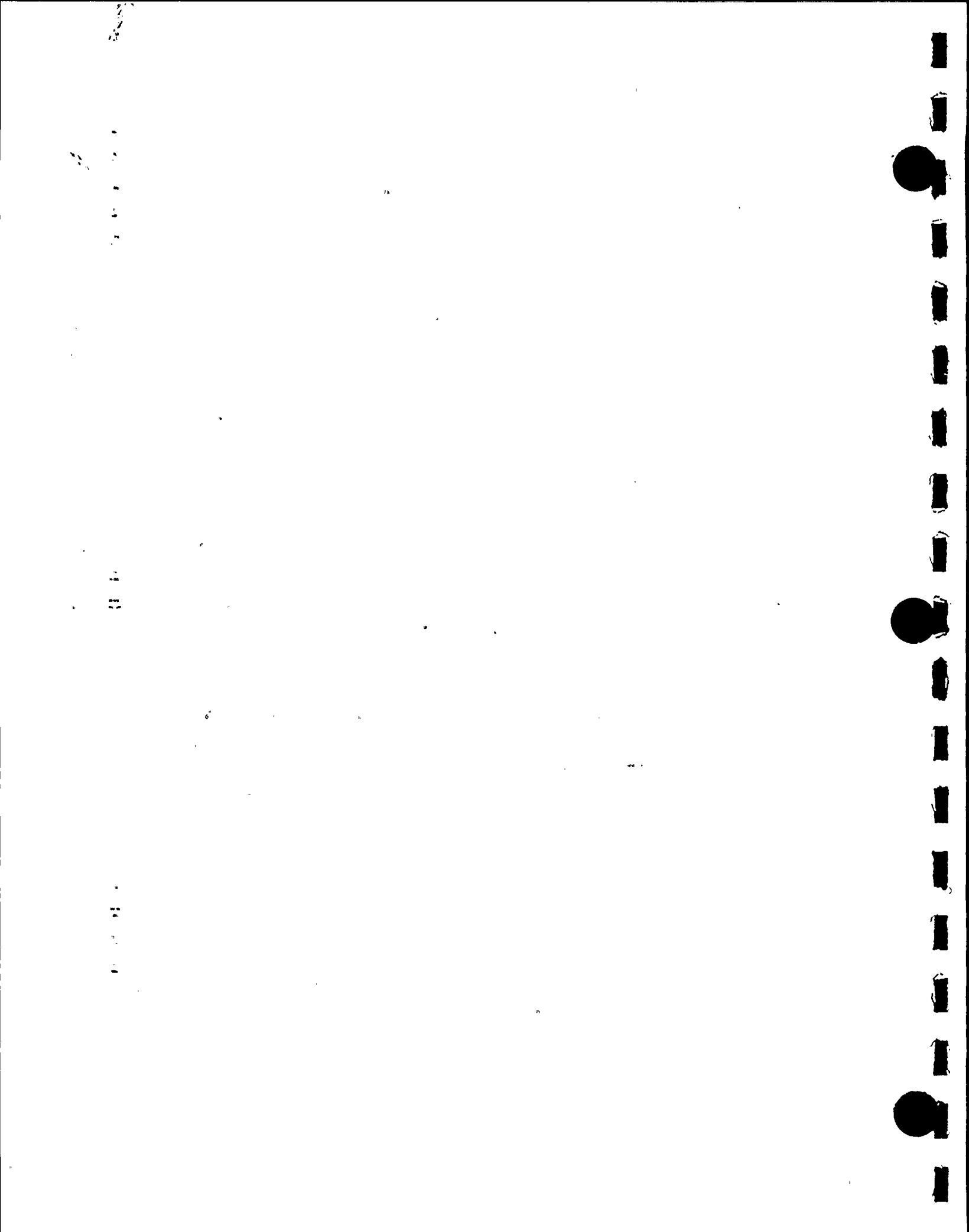
6.13 Weld Stresses

Critical weld locations under seismic loading are at the bottom of the rack at the baseplate connection and at the welds on the support legs. Results from the dynamic analysis using the simulation codes are surveyed and the maximum loading is used to qualify the welds on these locations.

6.13.1 Baseplate to Rack Welds and Cell-to-Cell Welds

Ref. [6.1.2] (ASME Code Section III, Subsection NF) permits, for the DBE condition, an allowable weld stress $\tau = .42 S_u = 29,820$ psi. Based on the worst case of all runs reported, the maximum weld stress for the baseplate to rack welds is 7605 psi for DBE conditions.

The weld between baseplate and support leg is checked using limit analysis techniques. The structural weld at that location is considered safe if the interaction curve between net force and moment is such that a derived function of F/F_y and M/M_y is below a limiting value of 1.0.



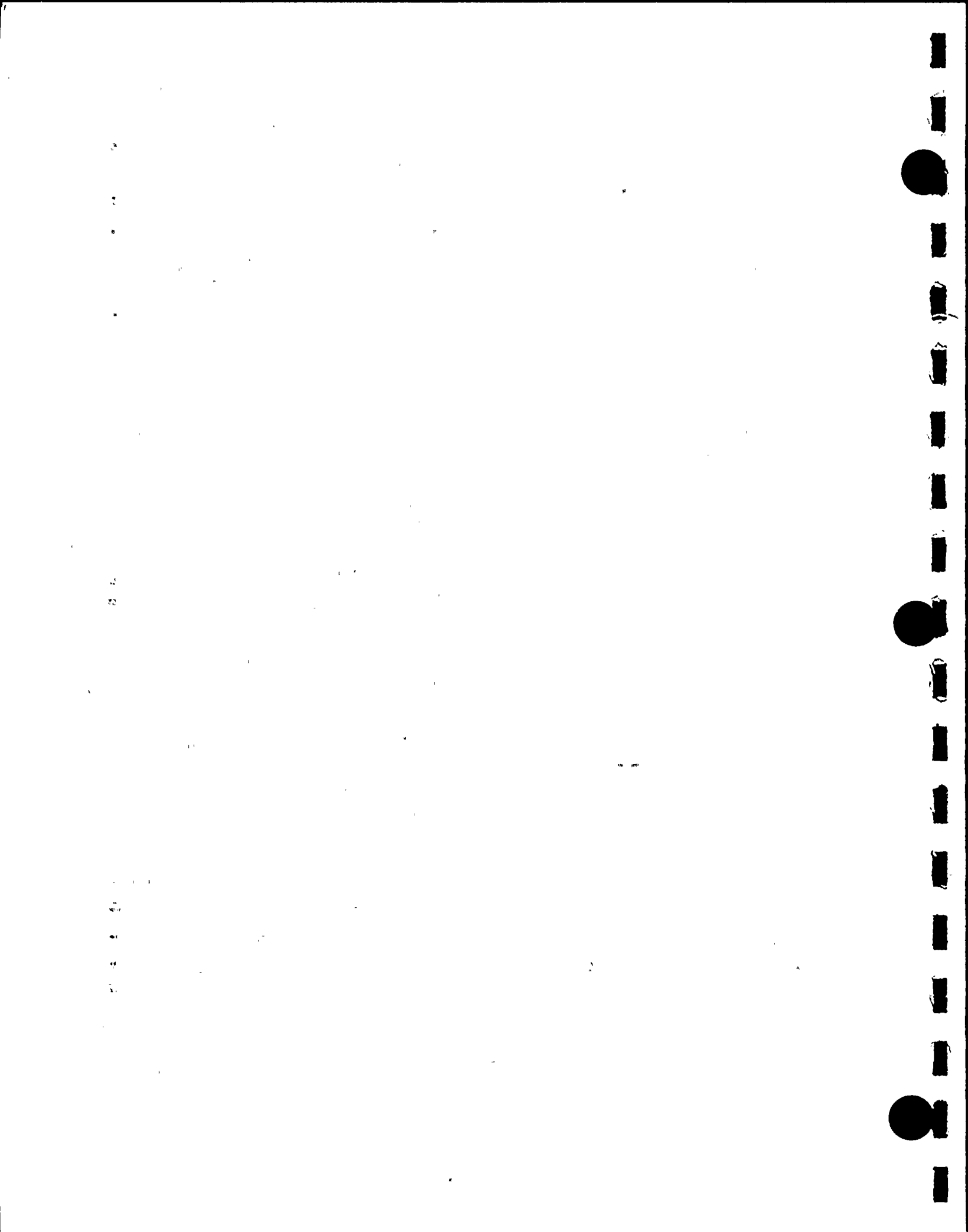
F_y , M_y are the limit load and moment under direct load only and direct moment only. F , M are the absolute values of the actual force and moments applied to the weld section. The calculated value is $.637 < 1.0$ based on the instantaneous peak loading. This value conservatively neglects any gussets in place to increase pedestal area and inertia.

The critical area that must be considered for cell-to-cell welds is the weld between the cells. This weld is discontinuous as we proceed along the cell length.

Stresses in the storage cell to storage cell welds develop along the length of each storage cell due to fuel assembly impact with the cell wall. This occurs if fuel assemblies in adjacent cells are moving out of phase with one another so that impact loads in two adjacent cells are in opposite directions which would tend to separate the channel from the cell at the weld. The critical load that can be transferred in this weld region for the DBE condition is calculated as 5273 lbs. at every fuel cell connection to adjacent cells. An upper bound to the load required to be transferred is 593 lbs. Where we have used a maximum impact load of 210 lbs. (obtained from Table 6.11.1), we have assumed two impact locations are supported by each weld region, and we have increased the load by $\sqrt{2}$ to account for 3-D effects.

6.13.2 Heating of an Isolated Cell

Weld stresses due to heating of an isolated hot cell are also computed. The assumption used is that a single cell is heated, over its entire length, to a temperature above the value associated with all surrounding cells. No thermal gradient in the



vertical direction is assumed, so that the results are conservative. Using the temperatures associated with this unit, analysis shows that the weld stresses along the entire cell length do not exceed the allowable value for a thermal loading condition. Section 7 reports the value for this thermal stress.

6.14 Whole Pool Multi-Rack (WPMR) Analysis

The single rack 3-D simulations presented in the preceding sections demonstrate the structural integrity, physical stability, and kinematic compliance (no rack-to-rack impact in the cellular region) of the rack modules. However, as noted before, prescribing the motion of the racks adjacent to the module being analyzed introduces an assumption of unpredictable import in the single rack modules. For closely spaced racks, it is possible to demonstrate kinematic compliance only by modelling all rack modules in one comprehensive simulation which is referred to as Whole Pool Multi-Rack (WPMR) model. In the WPMR analysis, DBE seismic load is applied (Ref. 6.1.3) and all racks are assumed fully loaded with fuel assemblies. The primary intent of the analysis is to confirm structural integrity conclusions from 3-D single rack analysis and to ensure that hydrodynamic effects not able to be modelled in a single rack analysis do not cause unanticipated structural impacts.

The cross coupling effects due to the movement of fluid from one interstitial (inter-rack) space to the adjacent one is modelled using classical potential flow theory and Kelvin's circulation theorem. This formulation has been reviewed and approved by the Nuclear Regulatory Commission, during the post-licensing multi-rack analysis for Diablo Canyon Unit I and II reracking project. The coupling coefficients are based on a consistent modelling of

1

2

3

4

5

6

7

8

9

10

11

12

13

14

15

16

17

18

19

20

21

22

23

24

25

26

27

28

29

30

31

32

33

34

35

36

37

38

39

40

41

42

43

44

45

46

47

48

49

50

51

52

53

54

55

56

57

58

59

60

61

62

63

64

65

66

67

68

69

70

71

72

73

74

75

76

77

78

79

80

81

82

83

84

85

86

87

88

89

90

91

92

93

94

95

96

97

98

99

100

101

102

103

104

105

106

107

108

109

110

111

112

113

114

115

116

117

118

119

120

121

122

123

124

125

126

127

128

129

130

131

132

133

134

135

136

137

138

139

140

141

142

143

144

145

146

147

148

149

150

151

152

153

154

155

156

157

158

159

160

161

162

163

164

165

166

167

168

169

170

171

172

173

174

175

176

177

178

179

180

181

182

183

184

185

186

187

188

189

190

191

192

193

194

195

196

197

198

199

200

201

202

203

204

205

206

207

208

209

210

211

212

213

214

215

216

217

218

219

220

221

222

223

224

225

226

227

228

229

230

231

232

233

234

235

236

237

238

239

240

241

242

243

244

245

246

247

248

249

250

251

252

253

254

255

256

257

258

259

260

261

262

263

264

265

266

267

268

269

270

271

272

273

274

275

276

277

278

279

280

281

282

283

284

285

286

287

288

289

290

291

292

293

294

295

296

297

298

299

300

301

302

303

304

305

306

307

308

309

310

311

312

313

314

315

316

317

318

319

320

321

322

323

324

325

326

327

328

329

330

331

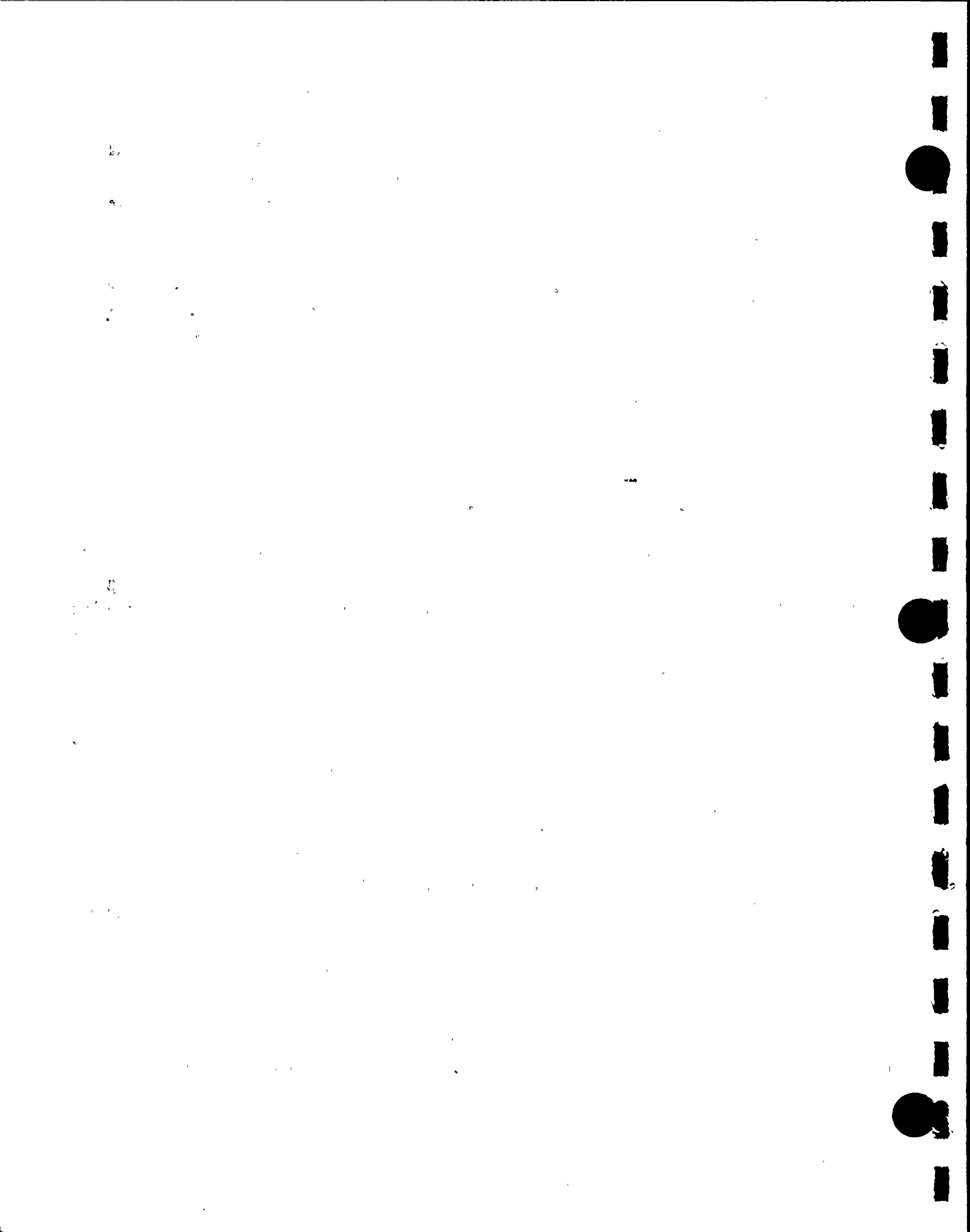
the fluid flow. While updating of the fluid flow coefficients, based on the current gap, is permitted in the algorithm, the analyses here are conservatively carried out using the constant nominal gaps that exist at the start of the seismic event.

Such a comprehensive WPMR model was prepared for the racks shown in the module layout drawing (Fig. 6.4.1). Computer code DYNARACK was used to perform the simulations.

In order to eliminate the last significant element of uncertainty in rack dynamic analyses, the friction coefficient was also ascribed to the support leg/pool bearing pad interface in a manner consistent with Rabinowicz's experimental data [6.4.1]. A set of friction coefficients were developed by a random number generator with Gaussian normal distribution characteristics. These random derived coefficients are imposed on each pedestal of each rack in the pool. The assigned values are then held constant during the entire simulation in order that the results are reproducible.

6.14.1 Multi-Rack Model

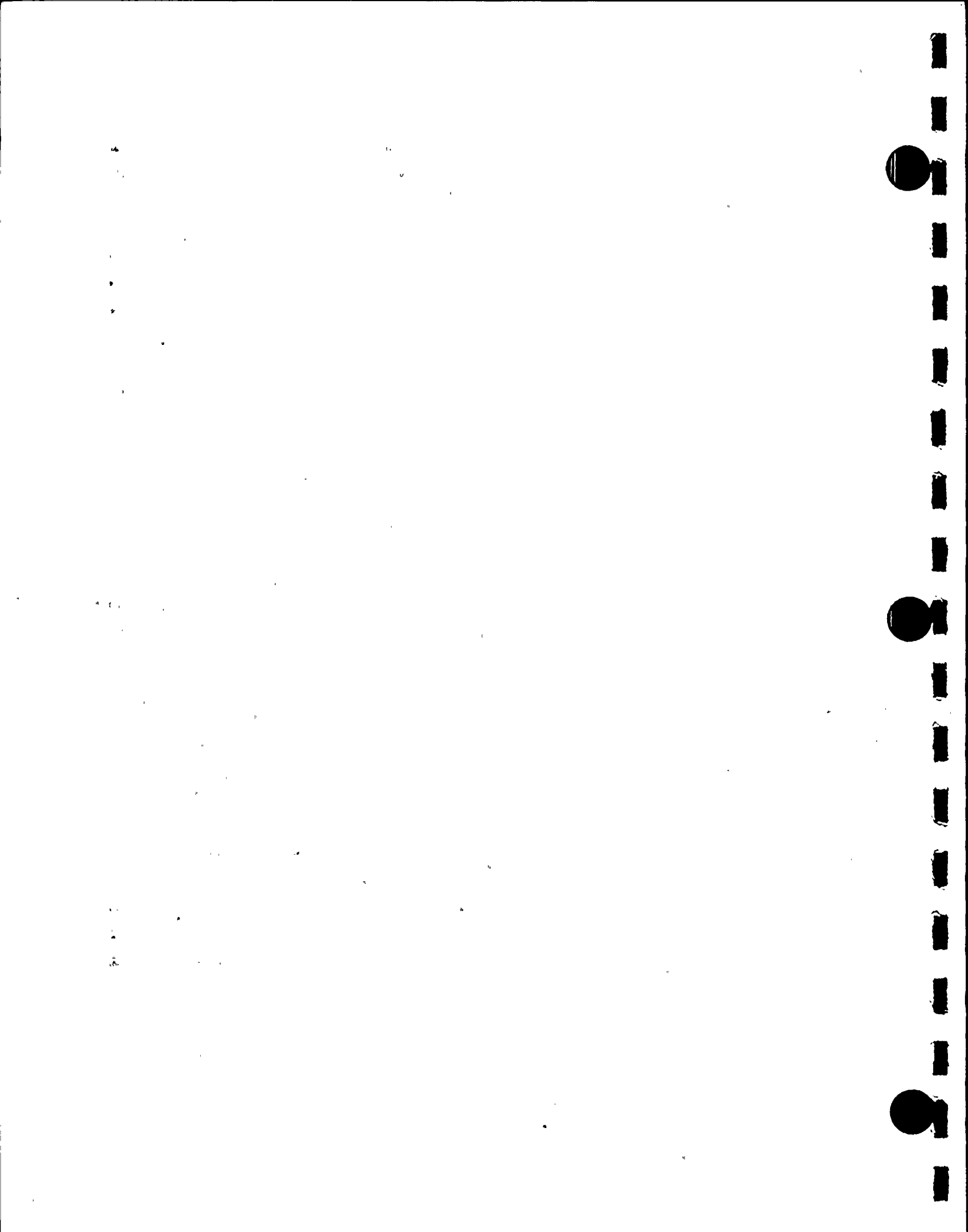
Figure 6.14.1 shows a planform view of the Donald C. Cook spent fuel pool. A rack and pedestal numbering scheme is set up in the figure. We set up a global x axis towards the East. Table 6.14.1 gives information on the number of cells per rack, and on the rack and fuel weights. All racks are assumed loaded with regular fuel. There are twenty-three racks in the pool. The cask area in the pool is modelled as a fictitious rack (Rack #24 in Figure 6.14.1). As noted previously, the presence of a fluid moving in the narrow gaps between racks and between racks and pool walls causes fluid coupling effects which cannot be modelled with a simulation using



only a single rack. Very simply, a single rack simulation can effectively include only the hydrodynamic effects due to contiguous racks when a certain set of assumptions is used for the motion of contiguous racks. In a multi-rack analysis the far field fluid coupling effects of all racks is accounted for using an appropriate model of the pool-rack fluid mechanics. For Donald C. Cook, the cask area was modelled assuming very large fluid gaps between racks 18 and 24 and between racks 23 and 24.

In the Whole Pool Multi-Rack analysis, used to investigate the interaction effects of all racks, we employ a reduced degree-of-freedom (RDOF) set for each rack plus its contained fuel. The purpose of the whole pool dynamic analysis, including the complete set of racks in the pool, is to determine whether effects, not able to be considered in a single rack analysis, alter any of the conclusions that are based on the results of the 22 DOF single rack analysis. In particular, the multi-rack analysis focusses on displacement excursions of each rack and on pedestal compressive loads. The Whole Pool Multi-Rack analysis is also utilized to investigate the possibility of impacts between racks or between racks and pool walls.

The reduced degree-of-freedom structural model for each rack is developed in a systematic way so that the important kinematic results from a dynamic analysis are in agreement with similar results from a solution obtained using the 22 DOF single rack model. The external hydrodynamic mass due to the presence of walls or adjacent racks is computed in a manner consistent with fundamental fluid mechanics principles and the use of a reduced



DOF fuel rack model [6.14.1]. The fluid flow model, used to obtain the whole pool hydrodynamic effect is site specific and reflects actual gaps and rack locations.

The whole pool multi-rack model includes many non-linear compression only gap elements. There are gap elements representing compression only pedestals (normally four pedestals are assumed for each rack), gap elements describing the impact potential of the fuel assembly-fuel rack interface, and gap elements tracking rack-to-rack or rack-to-wall impact potential at the top and bottom corners of the rack cell structure. In addition to the compression only gap elements, each pedestal has two friction springs associated with the compression spring. As noted previously, a random number generator is used to establish a friction coefficient for each pedestal at each instant when the pedestal is in contact with the liner.

The seismic excitation directions X and Y are shown in Figure 6.14.1. The critical DBE event that governs the behavior of the single rack analysis is applied to the 3-D multi-rack model in the appropriate directions. Three simulations have been carried out using coefficients of friction assumed to be 0.2, to be random with a mean of 0.5 at all pedestals, and to be 0.8, respectively.

6.14.2 Results of Multi-Rack Analysis

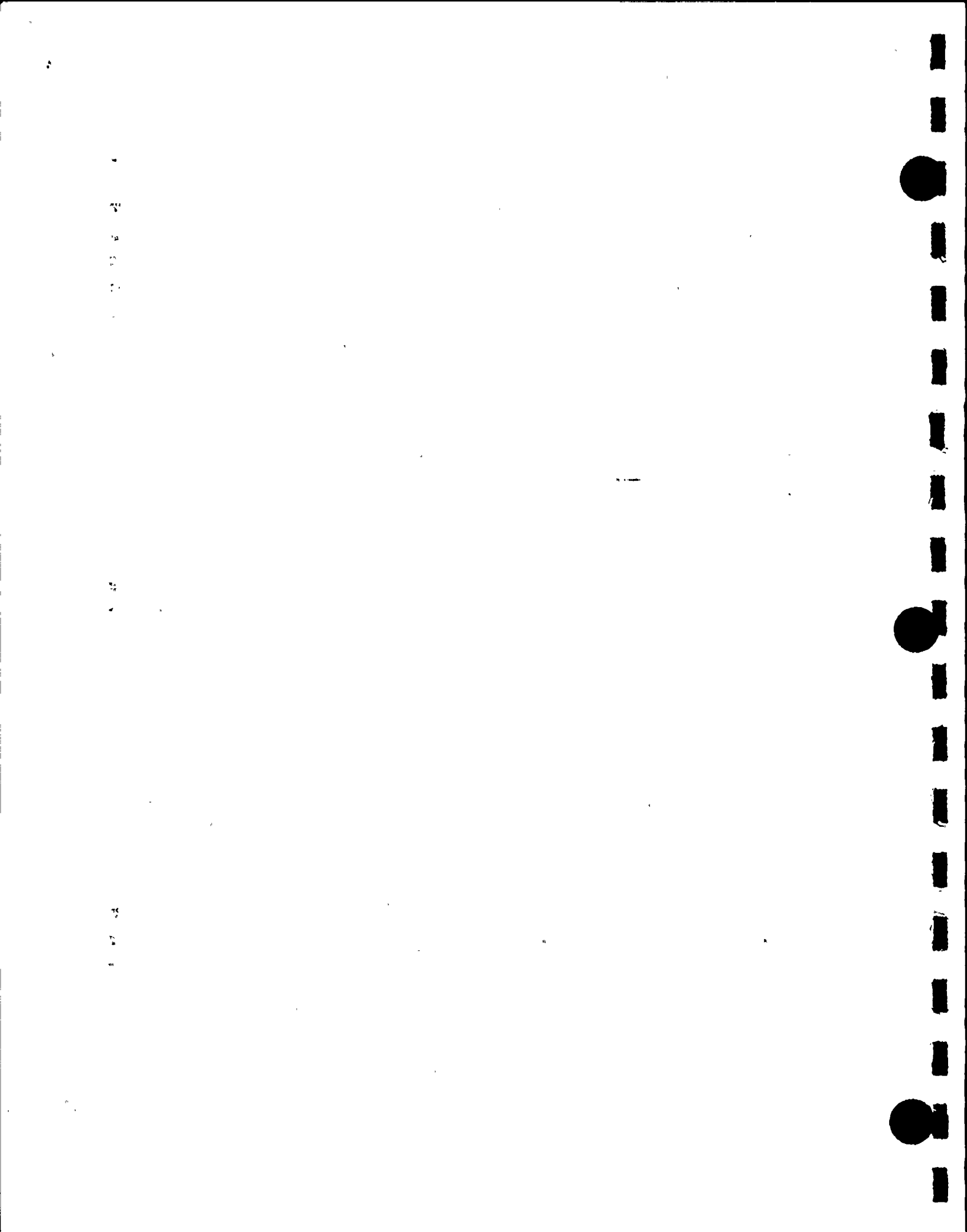
Tables 6.14.2 - 6.14.4 show the maximum corner absolute displacements at both the top and bottom of each rack in x and y directions from three multi-rack runs. In Table 6.14.5, the maximum displacements obtained from the three multi-rack simulations are compared with a single rack analysis. In all of

these tables, the results for fuel rack 24 can be ignored since there is no real rack at that location.

The absolute displacement values are higher than those obtained from single rack analysis. Thus, it appears essential to perform Whole Pool Multi-Rack analyses to verify that racks do not impact or hit the wall. Figures 6.14.2 - 6.14.5 show the time history of rack-to-rack gaps for the critical racks. It is shown that the rack-to-rack dynamic gaps are greater than 1.65" during a 15 second earthquake. Detailed examination of the rack-to-rack dynamic gaps show that the racks primarily move in-phase in all three simulations. That is, the entire assemblage of racks tends to move and minimize changes in rack-to-rack gaps.

Table 6.14.5 also presents peak pedestal compressive loads of all pedestals on the twenty-three real racks. In addition to a report of maximum pedestal loads, the time history of each pedestal load for each rack is archived for use in the structural evaluation of the fuel pool slab and the enveloping walls of the fuel pool.

It is noted that predicted maximum pedestal force from the multi-rack simulation giving the largest pedestal load (Run MP3 in Table 6.14.5) is lower than the result obtained from single rack analysis. The maximum instantaneous vertical foot load obtained from single rack analysis is 183300 lbs. From the Whole Pool Multi-Rack Run MP3, we find a peak single pedestal load of 180900 lbs. Because, detailed rack stress calculations are based on the single rack analysis results, no new structure concerns are identified by the scoping Whole Pool analysis and the overall structural integrity conclusions are confirmed.



6.15 Bearing Pad Analysis

To protect the slab from high localized dynamic loadings, bearing pads are placed between the pedestal base and the slab. Fuel rack pedestals impact on these bearing pads during a seismic event and the vertical pedestal loading is transferred to the liner. The bearing pad dimensions are set to ensure that the average pressure impacted to the slab surface due to a static load plus a dynamic impact load does not exceed the American Concrete Institute [6.15.1] limit on bearing pressures.

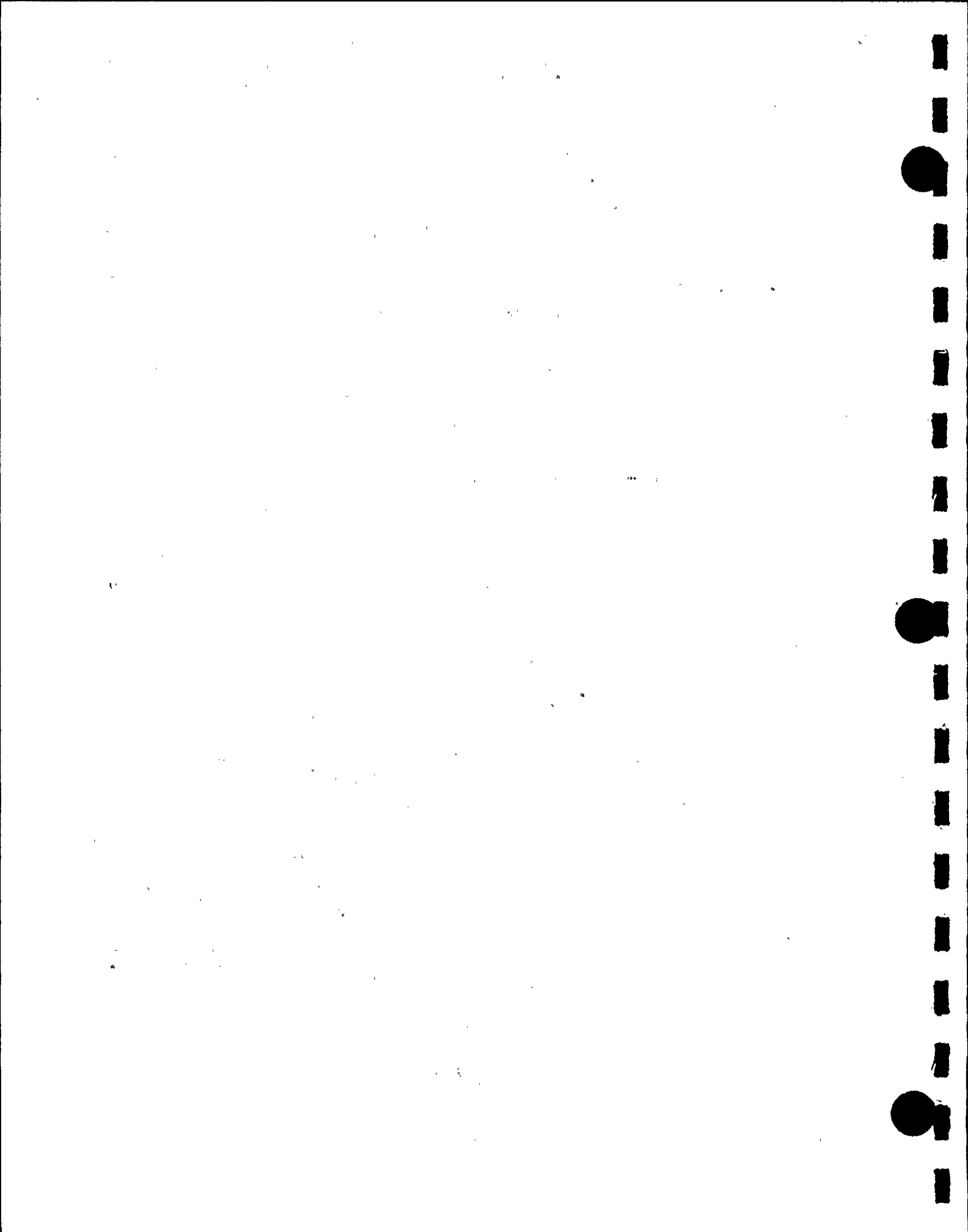
The time history results from the dynamic simulations for each pedestal are used to generate appropriate static and dynamic pedestal loads which are used to develop the bearing pad size.

From the whole pool multi-rack analysis, the worst case loading on a pedestal (instantaneous peak load) is 183,300 lbs. (see Table 6.14.5). For a 12" x 12" pad, this gives an average instantaneous pressure $p_a = 1273$ psi.

Section 10.15 of [6.15.1] gives the design bearing strength as

$$f_b = \phi (.85 f_c') \epsilon$$

where $\phi = .7$ and $f_c' = 3500$ psi for Donald C. Cook. $\epsilon = 1$ except when the supporting surface is wider on all sides than the loaded area. In that case, $\epsilon = (A_2/A_1)^{.5}$, but not more than 2. A_1 is the actual loaded area, and A_2 is an area greater than A_1 which is defined pictorially in the ACI commentary on Section 10.15. For Donald C. Cook, $1 \leq \epsilon \leq 2$; if we conservatively use $\epsilon = 1$, then $f_b = 2083$ psi which is in excess of the calculated pressure p_a . Thus, significant margin is provided by the bearing pads.



- 6.16 References for Section 6
- 6.1.1 USNRC Standard Review Plan, NUREG-0800 (1981).
- 6.1.2 ASME Boiler & Pressure Vessel Code, Section III, Subsection NF, appendices (1989).
- 6.1.3 USNRC Regulatory Guide 1.29, "Seismic Design Classification," Rev. 3, 1978.
- 6.3.1 Holtec Proprietary Report - Verification and User's Manual, Report HI-89364, January, 1990.
- 6.4.1 "Friction Coefficients of Water Lubricated Stainless Steels for a Spent Fuel Rack Facility," Prof. Ernest Rabinowicz, MIT, a report for Boston Edison Company, 1976.
- 6.4.2 USNRC Regulatory Guide 1.92, "Combining Modal Responses and Spatial Components in Seismic Response Analysis," Rev. 1, February, 1976.
- 6.4.3 "The Component Element Method in Dynamics with Application to Earthquake and Vehicle Engineering," S. Levy and J.P.D. Wilkinson, McGraw Hill, 1976.
- 6.4.4 "Dynamics of Structures," R.W. Clough and J. Penzien, McGraw Hill (1975).
- 6.4.5 Holtec Proprietary Reports: User's Manual, Report HI-89343, Revision 0; Theory, Reports HI-87162, Revision 1, and HI-90439, Revision 0; Verification, Report HI-87161, Revision 2.
- 6.5.1 "Dynamic Coupling in a Closely Spaced Two-Body System Vibrating in Liquid Medium: The Case of Fuel Racks," K.P. Singh and A.I. Soler, 3rd International Conference on Nuclear Power Safety, Keswick, England, May 1982.
- 6.5.2 R.J. Fritz, "The Effects of Liquids on the Dynamic Motions of Immersed Solids," Journal of Engineering for Industry, Trans. of the ASME, February 1972, pp 167-172.
- 6.5.3 USNRC Regulatory Guide 1.61, "Damping Values for Seismic Design of Nuclear Power Plants," 1973.



- 6.14.1 "Fluid Coupling in Fuel Racks: Correlation of Theory and Experiment", by B. Paul, Holtec Report HI-88243.
- 6.15.1 ACI 318-89, ACI 318R-89, Building Code Requirements for Reinforced Concrete, American Concrete Institute, Detroit, Michigan, 1989.

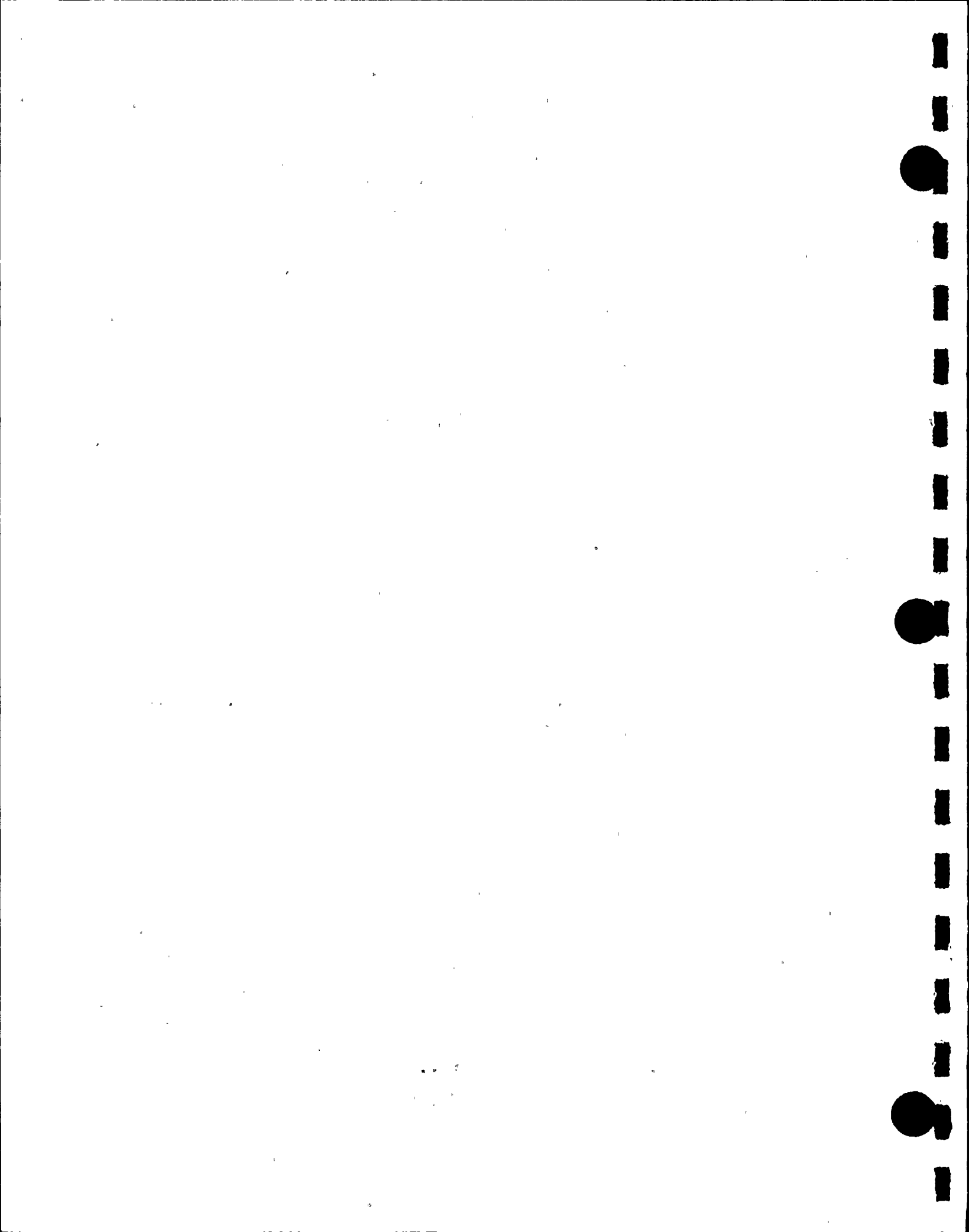


Table 6.3.1

CORRELATION COEFFICIENT

| <u>Time History Group</u> | <u>Value of ρ_{ij}</u> | |
|---------------------------|--|------------|
| | <u>DBE</u> | <u>OBE</u> |
| N-S and E-W (1,2) | 0.0146 | 0.1056 |
| N-S to Vertical (1,3) | 0.1269 | 0.0956 |
| E-W to Vertical (2,3) | 0.01016 | 0.1060 |



Table 6.5.1
DEGREES OF FREEDOM

| Location
(Node) | Displacement | | | Rotation | | |
|--------------------|--|-------|-------|------------|------------|------------|
| | U_x | U_y | U_z | θ_x | θ_y | θ_z |
| 1 | P1 | P2 | P3 | q4 | q5 | q6 |
| 2 | P17 | P18 | P19 | q20 | q21 | q22 |
| | Point 2 is assumed attached to rigid rack at the top most point. | | | | | |
| 2* | P7 | P8 | | | | |
| 3* | P9 | P10 | | | | |
| 4* | P11 | P12 | | | | |
| 5* | P13 | P14 | | | | |
| 1* | P15 | P16 | | | | |

where:

$$\begin{aligned}
 p_i &= q_i(t) + U_1(t) & i &= 1, 7, 9, 11, 13, 15, 17 \\
 &= q_i(t) + U_2(t) & i &= 2, 8, 10, 12, 14, 16, 18 \\
 &= q_i(t) + U_3(t) & i &= 3, 19
 \end{aligned}$$

$U_i(t)$ are the 3 known earthquake displacements.



Table 6.6.1
NUMBERING SYSTEM FOR GAP ELEMENTS AND FRICTION ELEMENTS

I. Nonlinear Springs (Gap Elements) (64 Total)

| <u>Number</u> | <u>Node Location</u> | <u>Description</u> |
|---------------|---|-------------------------------------|
| 1 | Support S1 | Z compression only element |
| 2 | Support S2 | Z compression only element |
| 3 | Support S3 | Z compression only element |
| 4 | Support S4 | Z compression only element |
| 5 | 2,2* | X rack/fuel assembly impact element |
| 6 | 2,2* | X rack/fuel assembly impact element |
| 7 | 2,2* | Y rack/fuel assembly impact element |
| 8 | 2,2* | Y rack/fuel assembly impact element |
| 9-24 | Other rattling masses for nodes 1*, 3*, 4* and 5* | |
| 25 | Bottom cross-section of rack (around edge) | Inter-rack impact elements |
| . | | Inter-rack impact elements |
| . | | Inter-rack impact elements |
| . | | Inter-rack impact elements |
| . | | Inter-rack impact elements |
| . | | Inter-rack impact elements |
| 44 | | Inter-rack impact elements |
| 45 | Top cross-section of rack (around edge) | Inter-rack impact elements |
| . | | Inter-rack impact elements |
| . | | Inter-rack impact elements |
| . | | Inter-rack impact elements |
| . | | Inter-rack impact elements |
| . | | Inter-rack impact elements |
| . | | Inter-rack impact elements |
| 64 | | Inter-rack impact elements |



Table 6.6.1 (continued)

NUMBERING SYSTEM FOR GAP ELEMENTS AND FRICTION ELEMENTS

II. Friction Elements (16 total)

| <u>Number</u> | <u>Node Location</u> | <u>Description</u> |
|---------------|----------------------|----------------------|
| 1 | Support S1 | X direction friction |
| 2 | Support S1 | Y direction friction |
| 3 | Support S2 | X direction friction |
| 4 | Support S2 | Y direction friction |
| 5 | Support S3 | X direction friction |
| 6 | Support S3 | Y direction friction |
| 7 | Support S4 | X direction friction |
| 8 | Support S4 | Y direction friction |
| 9 | S1 | X Slab moment |
| 10 | S1 | Y Slab moment |
| 11 | S2 | X Slab moment |
| 12 | S2 | Y Slab moment |
| 13 | S3 | X Slab moment |
| 14 | S3 | Y Slab moment |
| 15 | S4 | X Slab moment |
| 16 | S4 | Y Slab moment |



Table 6.6.2

TYPICAL INPUT DATA FOR RACK ANALYSES (lb-inch units)

| | |
|---|---|
| Support Foot Spring
Constant K_s (#/in.) | 4.91×10^6 |
| Frictional Spring
Constant K_f (#/in.) | 1.837×10^9 |
| Rack to Fuel Assembly
Impact Spring Constant (#/in.) | 1.38×10^5 (x-direction)
1.61×10^5 (y-direction) |
| Elastic Shear Spring for
Rack (#/in.) | 5.986×10^6 (x-direction)
4.866×10^6 (y-direction) |
| Elastic Bending Spring
for Rack (#-in./in.) | 5.458×10^{10} (x-z plane)
4.71×10^{10} (y-z plane) |
| Elastic Extensional Spring
(#/in.) | 4.074×10^7 |
| Elastic Torsional Spring
(#-in./in.) | 1.322×10^9 |
| Gaps (in.) (for hydrodynamic
calculations) | |

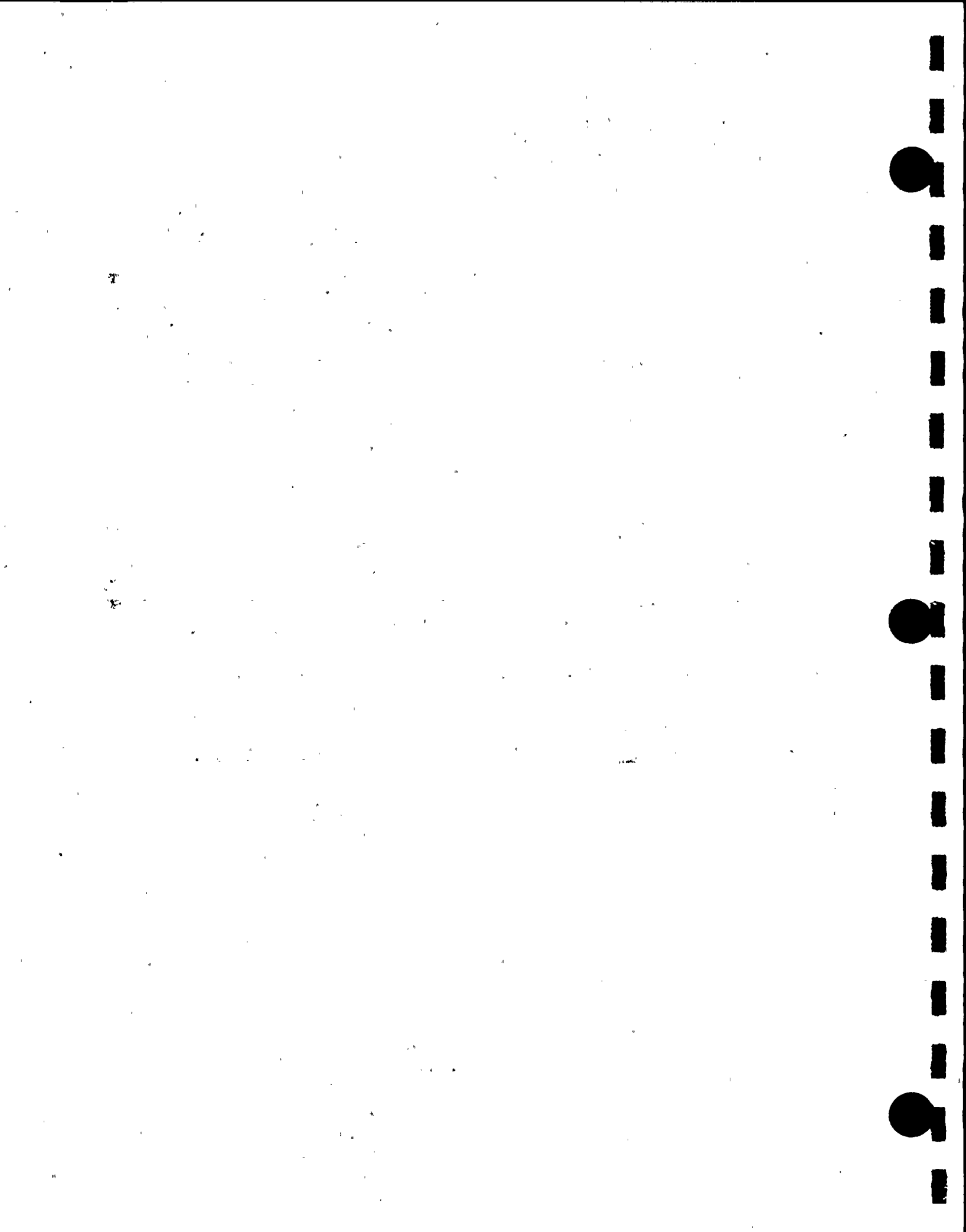


Table 6.9.1

RACK MATERIAL DATA (200°F)

| Material | Young's
Modulus
E (psi) | Yield
Strength
S _y (psi) | Ultimate
Strength
S _u (psi) |
|--------------------------|-------------------------------|---|--|
| 304 S.S. | 27.9 x 10 ⁶ | 25000 | 71000 |
| Section III
Reference | Table
I-6.0 | Table
I-2.2 | Table
I-3.2 |

SUPPORT MATERIAL DATA (200°F)

| Material | | | |
|---|-------------------------------|----------------|----------------|
| 1 SA-240, Type 304
(upper part of support
feet) | 27.9 x 10 ⁶
psi | 25,000
psi | 71000
psi |
| 2 SA-564-630
(age hardened at
1100°F) | 27.9 x 10 ⁶
psi | 106,300
psi | 140,000
psi |



Table 6.11.1
STRESS FACTORS AND RACK-TO-FUEL IMPACT LOAD

| Run | Remarks | Rack/Fuel
Impact Load
Per Cell at
Worst Location
Along Height
Critical
Location
(lbs) | | | | | | | |
|-----|--|--|---------------------------------|---------------------------------|---------------------------------|---------------------------------|---------------------------------|------------------------------------|--|
| | | R_1 | R_2 | R_3 | R_4 | R_5 | R_6 | R_7 | |
| a03 | DBE
$\mu = .2$
182 cells
loaded with
reg. fuel | 180.2
<u>.018</u>
.
<u>.274</u> | <u>.023</u>
.
<u>.074</u> | <u>.159</u>
.
<u>.167</u> | <u>.166</u>
.
<u>.161</u> | <u>.198</u>
.
<u>.417</u> | <u>.231</u>
.
<u>.442</u> | <u>.027*</u>
.
<u>.078**</u> | |
| a04 | DBE
$\mu = .8$
182 cells
loaded with
reg. fuel | 179.6
<u>.018</u>
.
<u>.284</u> | <u>.025</u>
.
<u>.079</u> | <u>.172</u>
.
<u>.214</u> | <u>.178</u>
.
<u>.172</u> | <u>.204</u>
.
<u>.431</u> | <u>.239</u>
.
<u>.460</u> | <u>.033</u>
.
<u>.095</u> | |
| a30 | $\mu = 0.2$
91 cells
loaded with
reg. fuel | 190
<u>.012</u>
.
<u>.181</u> | <u>.012</u>
.
<u>.046</u> | <u>.090</u>
.
<u>.118</u> | <u>.073</u>
.
<u>.106</u> | <u>.109</u>
.
<u>.281</u> | <u>.127</u>
.
<u>.299</u> | <u>.013</u>
.
<u>.052</u> | |
| a32 | $\mu = 0.2$
91 cells
loaded with
reg. fuel | 209.8
<u>.012</u>
.
<u>.176</u> | <u>.011</u>
.
<u>.049</u> | <u>.094</u>
.
<u>.112</u> | <u>.090</u>
.
<u>.110</u> | <u>.109</u>
.
<u>.271</u> | <u>.127</u>
.
<u>.289</u> | <u>.015</u>
.
<u>.049</u> | |
| a94 | Same as a04
with reloca-
ted pedestals | 174.8
<u>.018</u>
.
<u>.325</u> | <u>.018</u>
.
<u>.056</u> | <u>.168</u>
.
<u>.250</u> | <u>.121</u>
.
<u>.118</u> | <u>.187</u>
.
<u>.483</u> | <u>.219</u>
.
<u>.522</u> | <u>.032</u>
.
<u>.113</u> | |

* Upper values are for rack cell cross-section just above baseplate.

** Lower values are for support foot female cross-section just below attachment to baseplate.

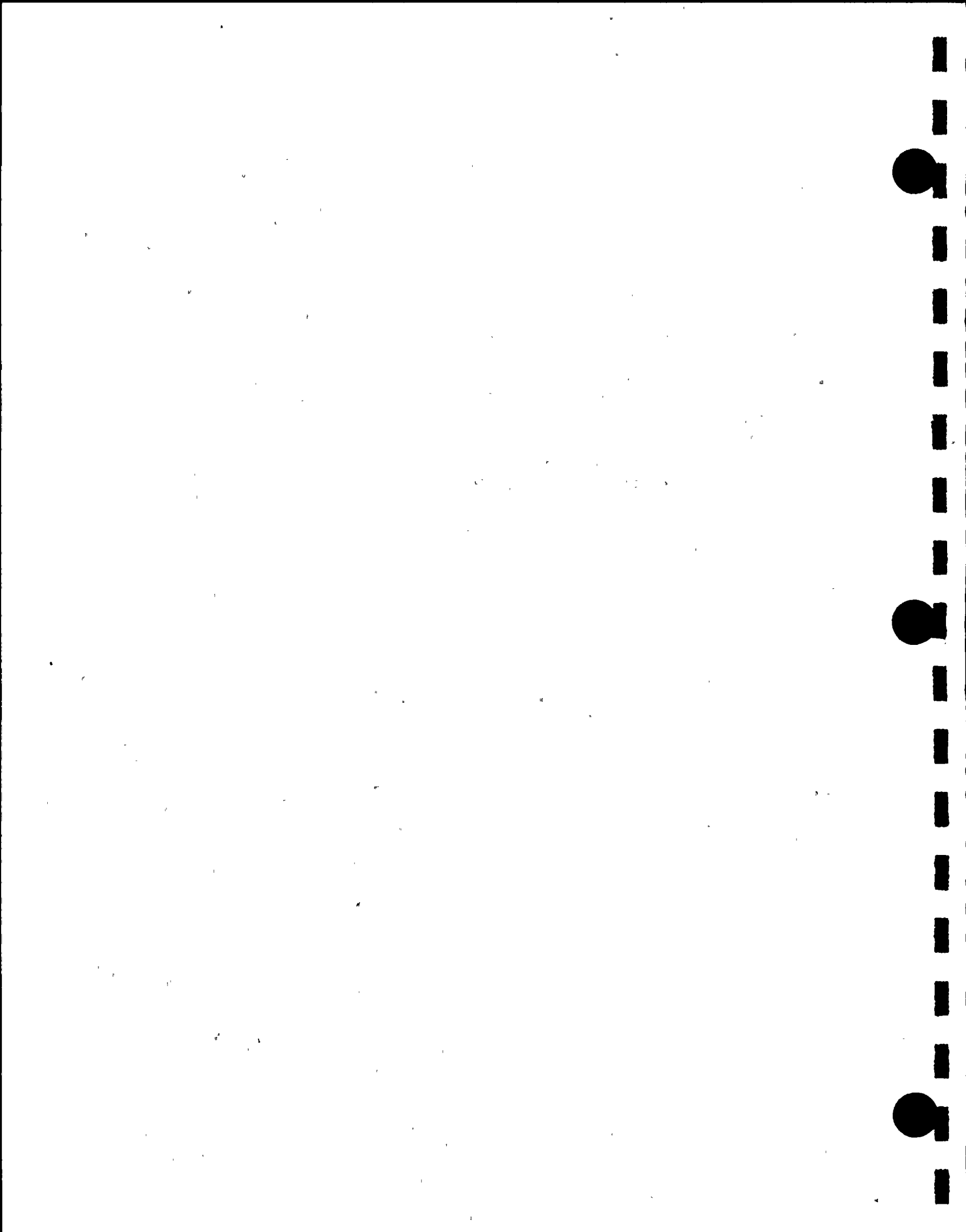


Table 6.11.2
Rack Displacements and Support Loads
(all loads are in lbs.)

| <u>RUN</u> | | <u>FLOOR LOAD</u>
(sum of all
support feet)
in a rack
(lbs.) | <u>MAXIMUM</u>
<u>VERTICAL</u>
<u>LOAD</u>
(1. foot)
(lbs.) | <u>MAXIMUM SHEAR*</u>
<u>LOAD AND</u>
<u>COINCIDENT</u>
<u>VERTICAL</u>
<u>LOAD</u> | <u>DX</u>
(in.) | <u>DY**</u>
(in.) |
|------------|---|--|---|---|--------------------|----------------------|
| a03 | Full load
$\mu = 0.2$
DBE, Reg. Fuel | 3.510×10^5 | 1.549×10^5 | 30212 (1.511×10^5) | .0609
.0084 | .0562
.0105 |
| a04 | Full load
$\mu = 0.8$
DBE, Reg. Fuel | 3.510×10^5 | 1.605×10^5 | 35832 (9.791×10^4) | .0679
.0015 | .0583
.0012 |
| a30 | Half load in
Pos. x
$\mu = 0.2$
DBE, Reg. Fuel | 1.883×10^5 | 1.021×10^5 | 20108 (1.005×10^5) | .0520
.0010 | .0450
.0008 |
| a32 | Half load in
Pos. y
$\mu = 0.2$
DBE, Reg. Fuel | 1.883×10^5 | 9.973×10^4 | 19389 (9.71×10^4) | .0482
.0055 | .0515
.0080 |
| a94 | Same as a04
with reloca-
pedestals | 3.508×10^5 | 1.833×10^5 | 44406 (1.4829×10^5) | .0678
.0014 | .0778
.0018 |

* The value in parenthesis is the vertical load at the instant when the shear load is maximum. The maximum vertical and shear loads generally do not occur at the same instant.

** Upper values are top movements; lower values are baseplate movements (not necessarily at the same time).

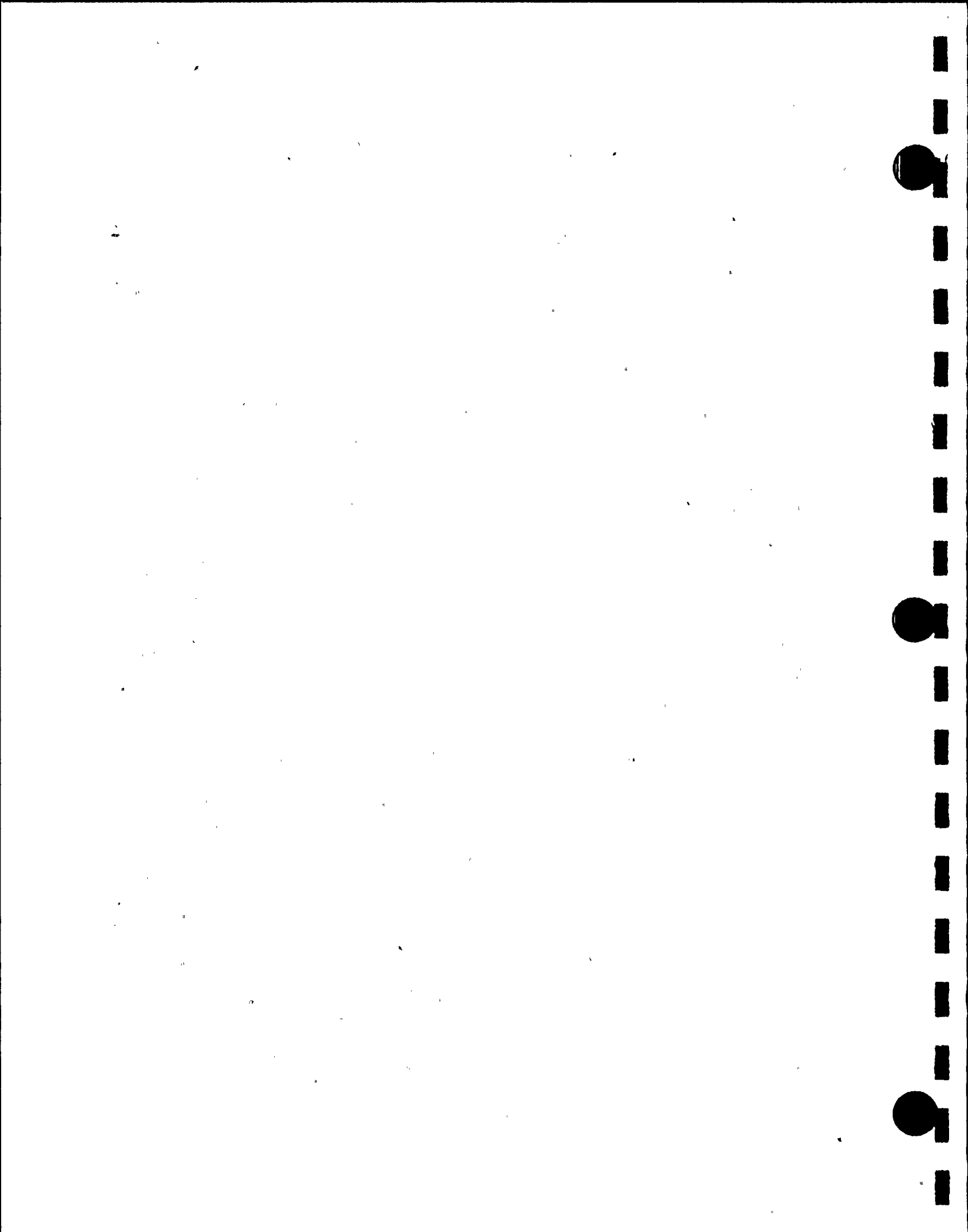


Table 6.14.1

RACK NUMBERING AND WEIGHT INFORMATION

| <u>Rack No.</u> | <u>No. of Cells</u> | <u>Weight of Rack, lb.</u> | <u>Weight of Fuel Assembly, lb.</u> |
|-----------------|---------------------|----------------------------|-------------------------------------|
| 1 | 182 | 25700 | 1550 |
| 2 | 168 | 23700 | 1550 |
| 3 | 168 | 23700 | 1550 |
| 4 | 182 | 25700 | 1550 |
| 5 | 182 | 25700 | 1550 |
| 6 | 182 | 25700 | 1550 |
| 7 | 156 | 22500 | 1550 |
| 8 | 144 | 20900 | 1550 |
| 9 | 144 | 20900 | 1550 |
| 10 | 156 | 22500 | 1550 |
| 11 | 156 | 22500 | 1550 |
| 12 | 156 | 22500 | 1550 |
| 13 | 143 | 20800 | 1550 |
| 14 | 132 | 19300 | 1550 |
| 15 | 132 | 19300 | 1550 |
| 16 | 143 | 20800 | 1550 |
| 17 | 143 | 20800 | 1550 |
| 18 | 143 | 20800 | 1550 |
| 19 | 182 | 25700 | 1550 |
| 20 | 168 | 23700 | 1550 |
| 21 | 168 | 23700 | 1550 |
| 22 | 166 | 23900 | 1550 |
| 23 | 120 | 17700 | 1550 |
| 24* | 0 | 0 | 0 |

* fictitious

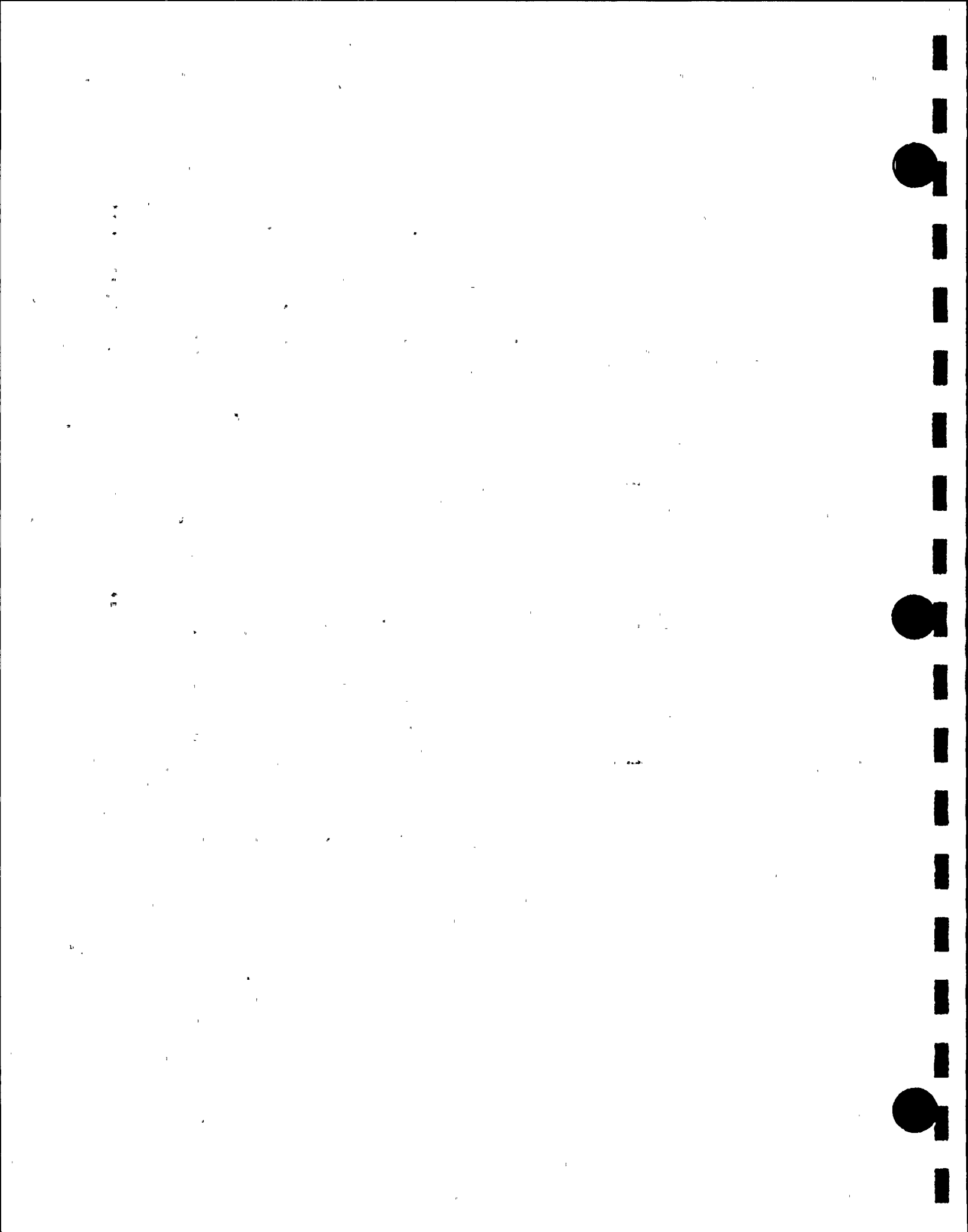


Table 6.14.2

MAXIMUM DISPLACEMENTS FROM WPMR RUN MP1
(Friction Coefficient = 0.2)

| rack | uxt | uyt | uxb | uyb |
|------|-----------|-----------|-----------|-----------|
| 1 | .7004E-01 | .7756E-01 | .6235E-01 | .7303E-01 |
| 2 | .7506E-01 | .5227E-01 | .6494E-01 | .3936E-01 |
| 3 | .8464E-01 | .7521E-01 | .6897E-01 | .6619E-01 |
| 4 | .5943E-01 | .5218E-01 | .4960E-01 | .3597E-01 |
| 5 | .5131E-01 | .5306E-01 | .4290E-01 | .4496E-01 |
| 6 | .6793E-01 | .9512E-01 | .5135E-01 | .9095E-01 |
| 7 | .4783E-01 | .8928E-01 | .3978E-01 | .7830E-01 |
| 8 | .4856E-01 | .7065E-01 | .3607E-01 | .5917E-01 |
| 9 | .4533E-01 | .6377E-01 | .3196E-01 | .5192E-01 |
| 10 | .3830E-01 | .5754E-01 | .2848E-01 | .4354E-01 |
| 11 | .4224E-01 | .5336E-01 | .3659E-01 | .4329E-01 |
| 12 | .6411E-01 | .9620E-01 | .4885E-01 | .8429E-01 |
| 13 | .7253E-01 | .1079E+00 | .6568E-01 | .9505E-01 |
| 14 | .4602E-01 | .1114E+00 | .3650E-01 | .9847E-01 |
| 15 | .3557E-01 | .1079E+00 | .2634E-01 | .9325E-01 |
| 16 | .3467E-01 | .9211E-01 | .2817E-01 | .8608E-01 |
| 17 | .5755E-01 | .4429E-01 | .5326E-01 | .3140E-01 |
| 18 | .1011E+00 | .1301E+00 | .8596E-01 | .9693E-01 |
| 19 | .6980E-01 | .1125E+00 | .6341E-01 | .8575E-01 |
| 20 | .8202E-01 | .8680E-01 | .6878E-01 | .6048E-01 |
| 21 | .8404E-01 | .1455E+00 | .6800E-01 | .1229E+00 |
| 22 | .8173E-01 | .1057E+00 | .7111E-01 | .9050E-01 |
| 23 | .5647E-01 | .6598E-01 | .4812E-01 | .6156E-01 |

uxt=absolute value of maximum rack corner displacement in
x-direction at rack top;
uyt=absolute value of maximum rack corner displacement in
y-direction at rack top;
uxb=absolute value of maximum rack corner displacement in
x-direction at rack baseplate;
uyb=absolute value of maximum rack corner displacement in
y-direction at rack baseplate.

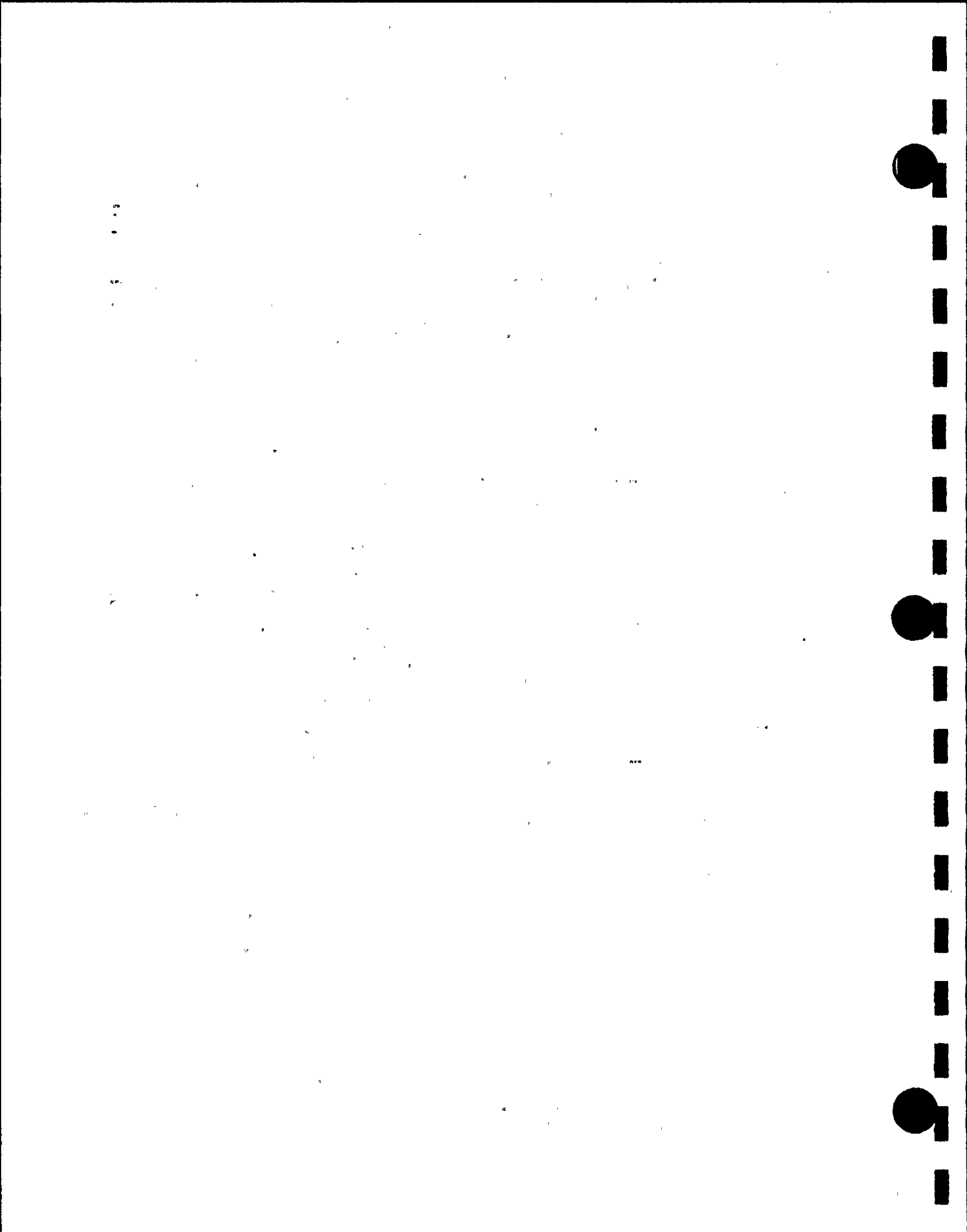


Table 6.14.3

MAXIMUM DISPLACEMENTS FROM WPMR RUN MP2
(Random Friction Coefficient)

| rack | uxt | uyt | uxb | uyb |
|------|-----------|-----------|-----------|-----------|
| 1 | .6524E-01 | .4772E-01 | .3373E-01 | .2303E-01 |
| 2 | .1423E+00 | .5829E-01 | .1442E+00 | .4598E-01 |
| 3 | .1247E+00 | .4122E-01 | .1161E+00 | .2566E-01 |
| 4 | .1860E+00 | .6628E-01 | .1859E+00 | .3161E-01 |
| 5 | .1106E+00 | .6379E-01 | .1091E+00 | .2673E-01 |
| 6 | .9642E-01 | .7250E-01 | .8330E-01 | .6348E-01 |
| 7 | .4742E-01 | .6267E-01 | .3334E-01 | .5443E-01 |
| 8 | .1801E+00 | .5755E-01 | .1819E+00 | .4534E-01 |
| 9 | .1275E+00 | .3974E-01 | .1207E+00 | .2115E-01 |
| 10 | .2336E+00 | .7640E-01 | .2336E+00 | .5527E-01 |
| 11 | .1710E+00 | .8644E-01 | .1712E+00 | .6245E-01 |
| 12 | .4015E-01 | .4740E-01 | .2869E-01 | .2678E-01 |
| 13 | .1088E+00 | .1034E+00 | .1030E+00 | .1040E+00 |
| 14 | .1439E+00 | .4029E-01 | .1282E+00 | .1865E-01 |
| 15 | .6218E-01 | .5620E-01 | .6029E-01 | .3386E-01 |
| 16 | .3322E+00 | .5413E-01 | .3374E+00 | .3677E-01 |
| 17 | .1727E+00 | .5385E-01 | .1727E+00 | .4896E-01 |
| 18 | .1269E+00 | .1958E+00 | .1223E+00 | .1913E+00 |
| 19 | .8411E-01 | .8106E-01 | .6365E-01 | .7508E-01 |
| 20 | .8402E-01 | .6480E-01 | .5976E-01 | .4419E-01 |
| 21 | .1280E+00 | .4742E-01 | .1281E+00 | .3530E-01 |
| 22 | .8427E-01 | .4951E-01 | .7430E-01 | .2335E-01 |
| 23 | .2389E+00 | .6471E-01 | .2388E+00 | .5758E-01 |

uxt=absolute value of maximum rack corner displacement in
x-direction at rack top;

uyt=absolute value of maximum rack corner displacement in
y-direction at rack top;

uxb=absolute value of maximum rack corner displacement in
x-direction at rack baseplate;

uyb=absolute value of maximum rack corner displacement in
y-direction at rack baseplate.

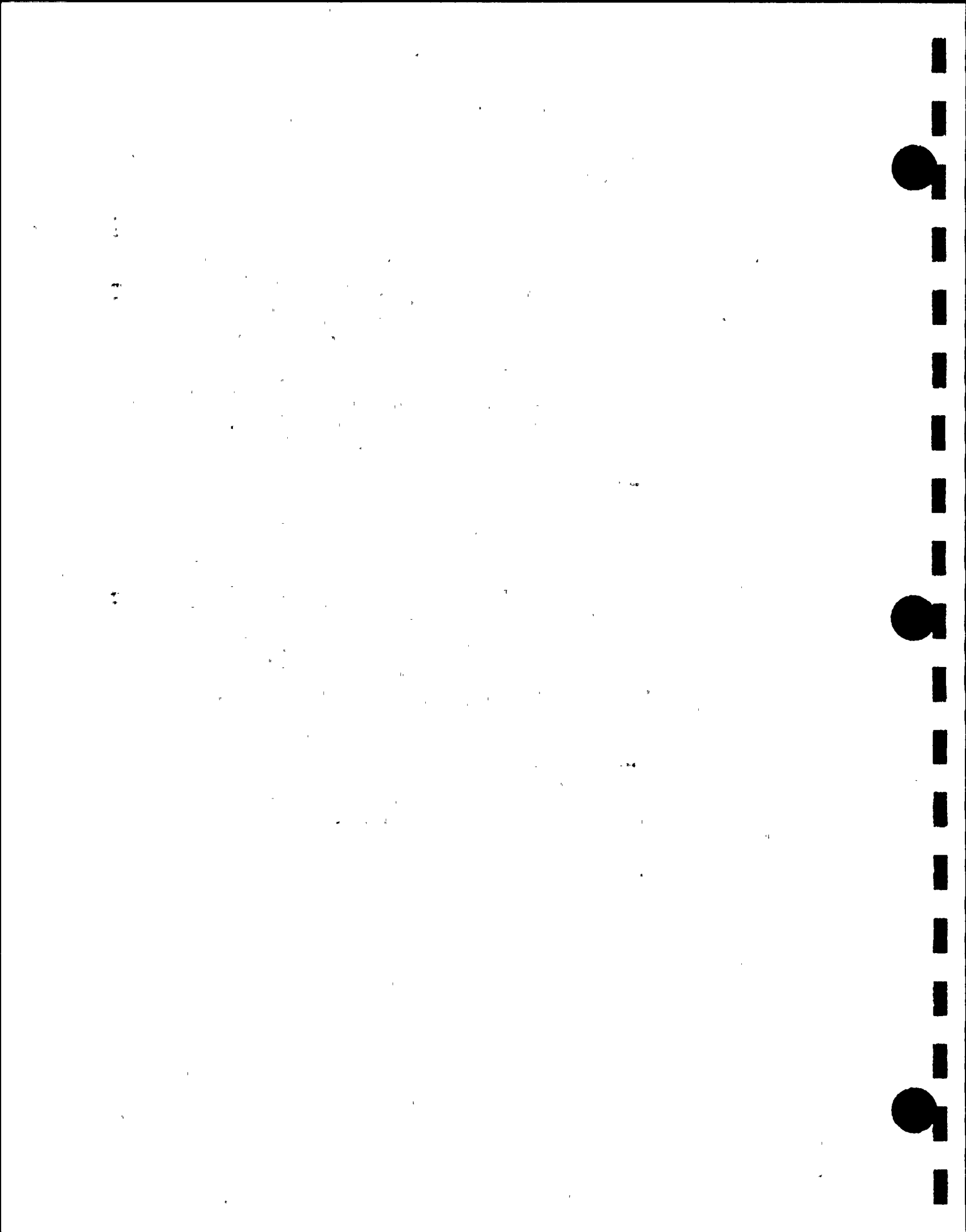


Table 6.14.4

MAXIMUM DISPLACEMENTS FROM WPMR RUN MP3
(Friction Coefficient=0.8)

| rack | uxt | uyt | uxb | uyb |
|------|-----------|-----------|-----------|-----------|
| 1 | .2035E+00 | .1702E+00 | .1987E+00 | .1774E+00 |
| 2 | .2751E+00 | .5173E-01 | .2732E+00 | .1658E-01 |
| 3 | .2637E+00 | .5740E-01 | .2638E+00 | .4010E-01 |
| 4 | .1363E+00 | .5449E-01 | .1321E+00 | .2788E-01 |
| 5 | .1333E+00 | .8237E-01 | .1273E+00 | .6876E-01 |
| 6 | .1720E+00 | .1514E+00 | .1609E+00 | .1617E+00 |
| 7 | .2425E+00 | .8747E-01 | .2461E+00 | .8782E-01 |
| 8 | .1785E+00 | .6039E-01 | .1784E+00 | .4260E-01 |
| 9 | .1519E+00 | .4434E-01 | .1506E+00 | .3129E-01 |
| 10 | .8112E-01 | .5007E-01 | .7887E-01 | .2883E-01 |
| 11 | .1146E+00 | .7975E-01 | .1117E+00 | .5071E-01 |
| 12 | .1005E+00 | .1602E+00 | .9143E-01 | .1601E+00 |
| 13 | .1604E+00 | .1310E+00 | .1633E+00 | .1073E+00 |
| 14 | .7786E-01 | .7618E-01 | .7823E-01 | .5953E-01 |
| 15 | .8616E-01 | .5521E-01 | .8214E-01 | .3148E-01 |
| 16 | .9843E-01 | .4780E-01 | .1024E+00 | .2903E-01 |
| 17 | .8975E-01 | .7115E-01 | .9063E-01 | .7056E-01 |
| 18 | .1418E+00 | .4416E+00 | .1089E+00 | .4526E+00 |
| 19 | .1959E+00 | .1720E+00 | .1922E+00 | .1806E+00 |
| 20 | .2741E+00 | .5563E-01 | .2727E+00 | .3118E-01 |
| 21 | .2117E+00 | .5159E-01 | .2120E+00 | .2287E-01 |
| 22 | .2361E+00 | .6081E-01 | .2242E+00 | .3986E-01 |
| 23 | .1016E+00 | .7703E-01 | .1033E+00 | .7364E-01 |

uxt=absolute value of maximum rack corner displacement in
x-direction at rack top;

uyt=absolute value of maximum rack corner displacement in
y-direction at rack top;

uxb=absolute value of maximum rack corner displacement in
x-direction at rack baseplate;

uyb=absolute value of maximum rack corner displacement in
y-direction at rack baseplate.

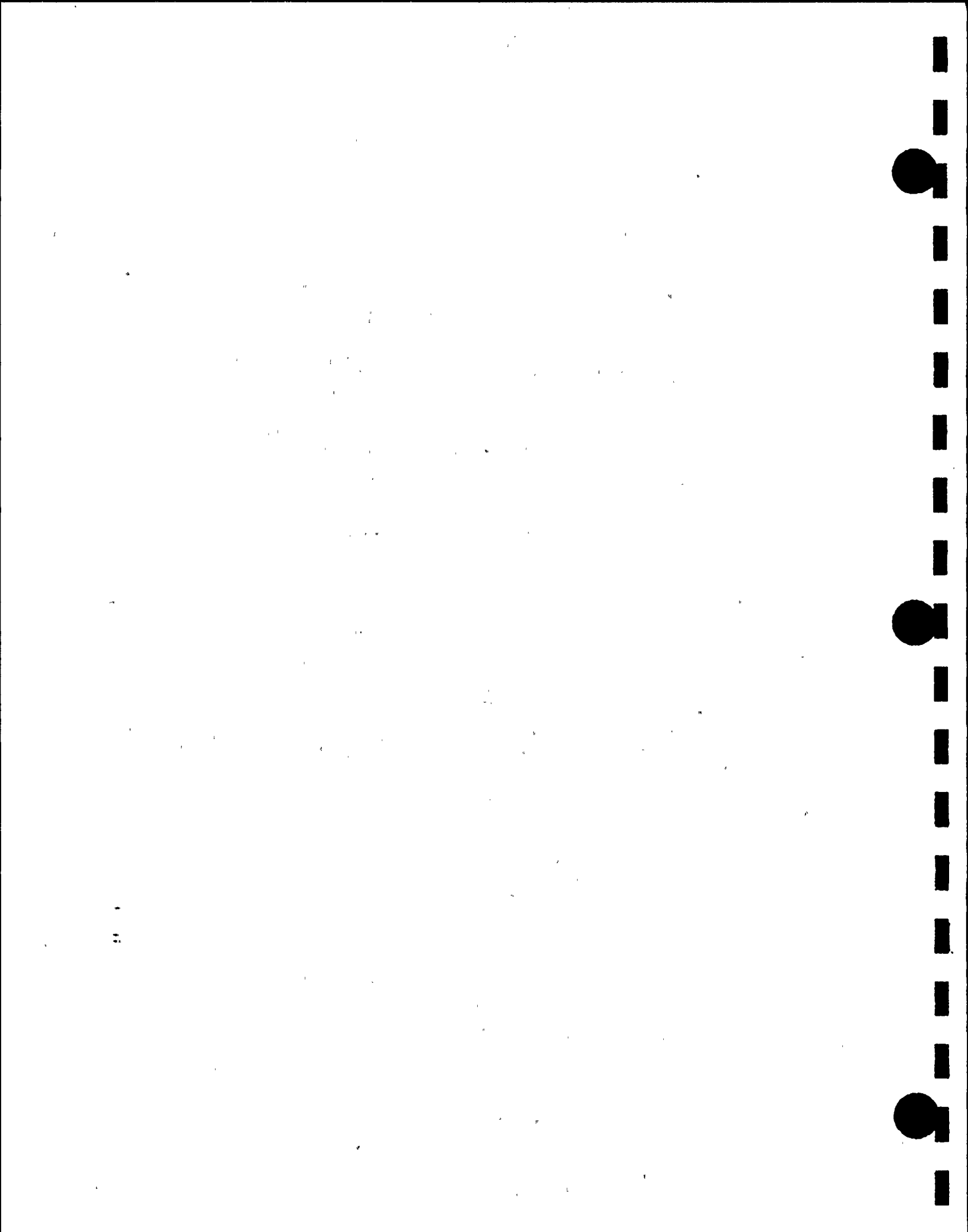
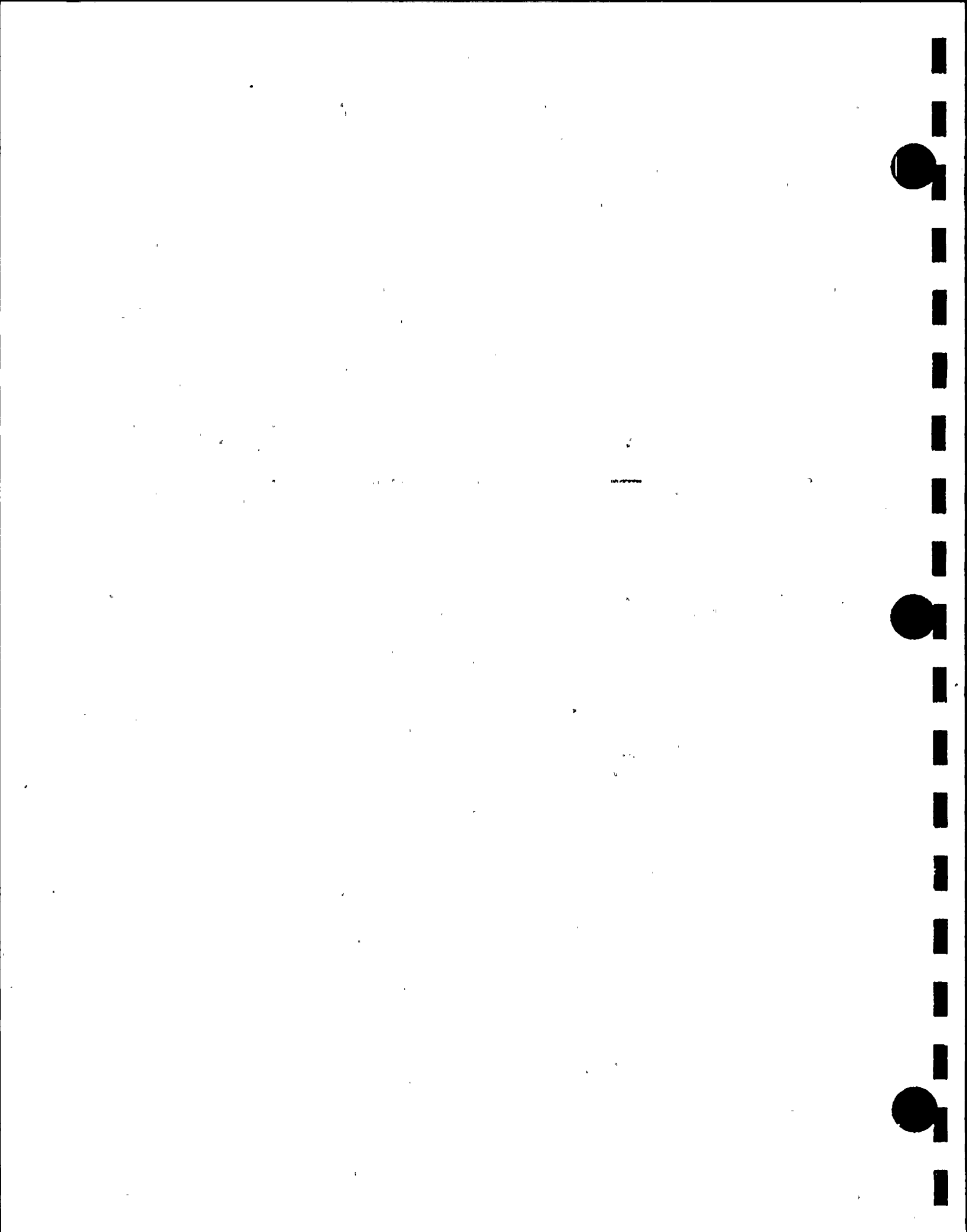


Table 6.14.5

MAXIMUM RACK DISPLACEMENT AND FOOT LOAD

| <u>Run</u> | <u>Remarks</u> | <u>Maximum
Rack Corner
Displacement
inch</u> | <u>Maximum
Foot
Pedestal
Force, lbs.</u> |
|------------|-------------------------|--|--|
| a94 | Single Rack
Analysis | 0.0778 | 183,300 |
| MP1 | WPMR, $\mu = 0.2$ | 0.1455 (Rack #21 in y) | 157,400
(Rack #19, Foot 4) |
| MP2 | WPMR, Random μ | 0.3322 (Rack #16 in x) | 170,900
(Rack #19, Foot 4) |
| MP3 | WPMR, $\mu = 0.8$ | 0.4416 (Rack #18 in y) | 180,900
(Rack #5, Foot 2) |

μ = friction coefficient



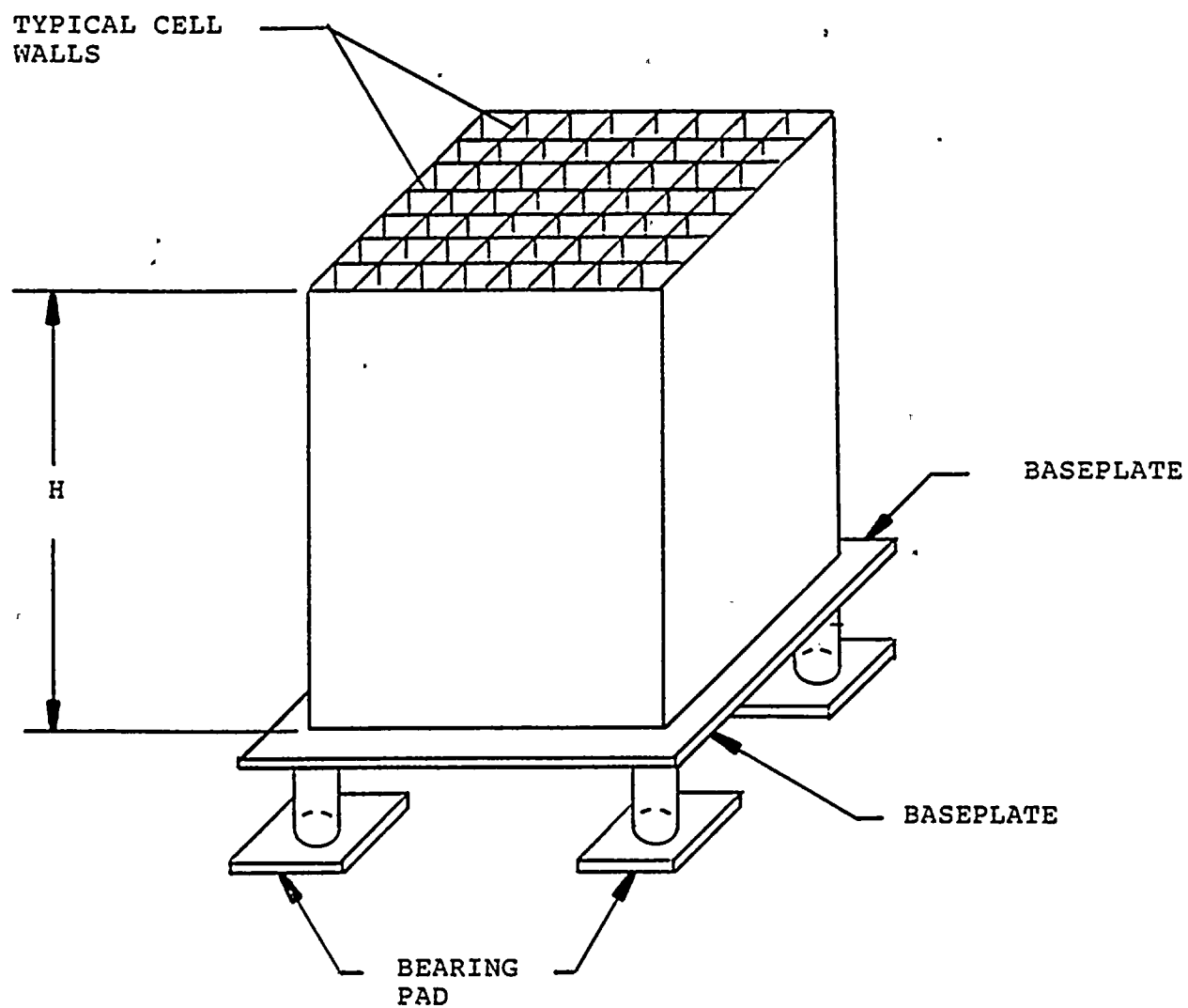
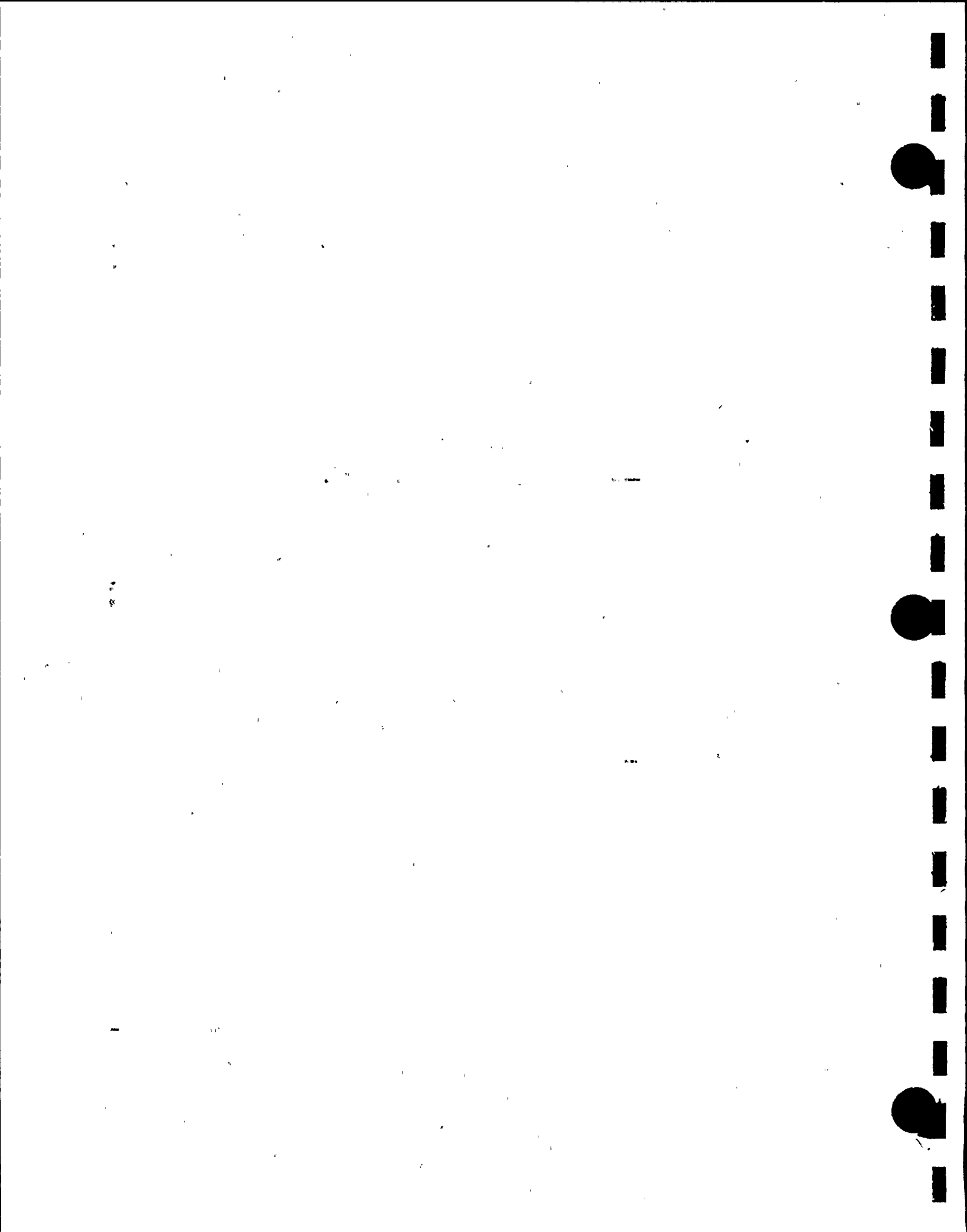


Figure 6.2.1 Pictorial View of Rack Structure



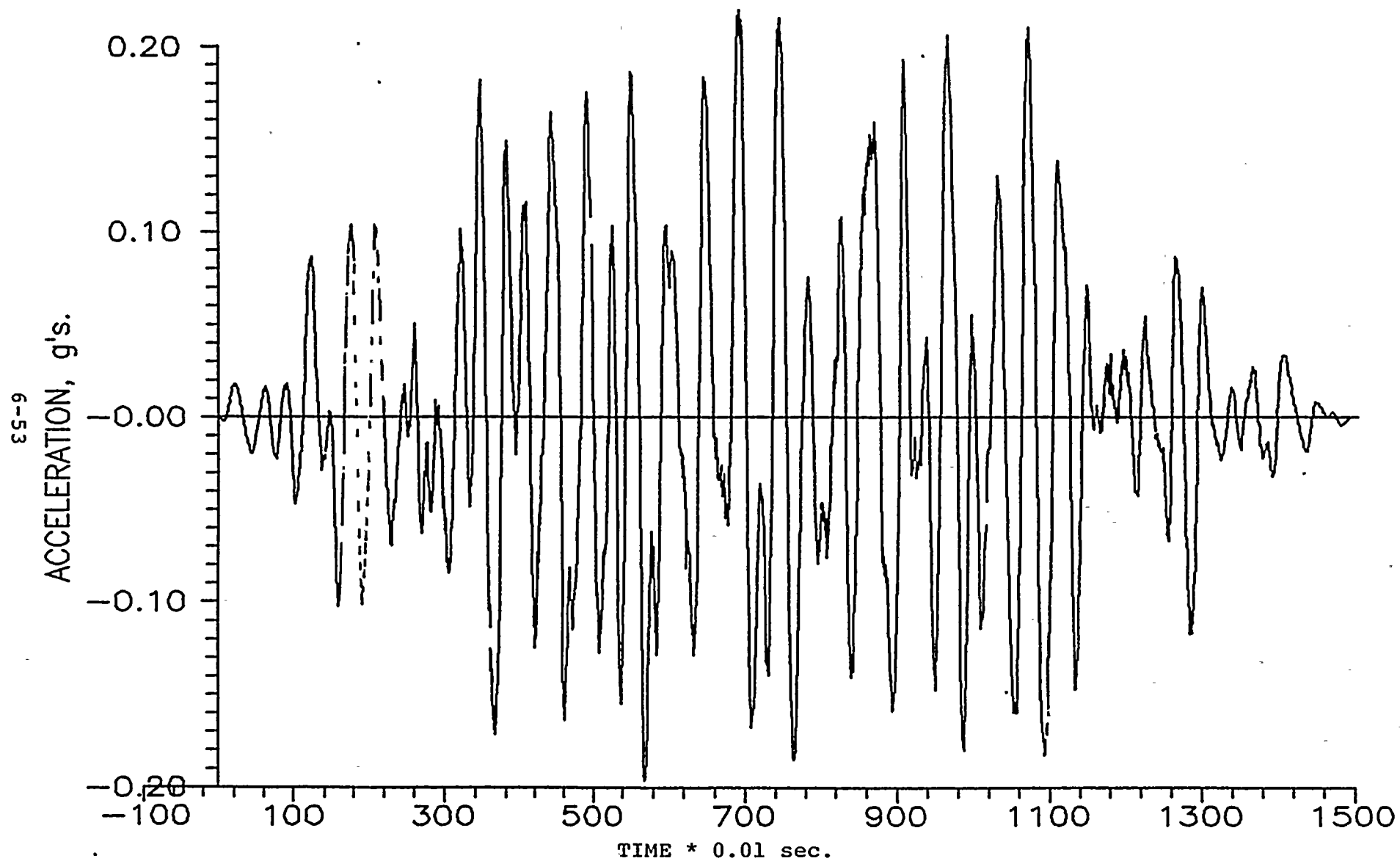
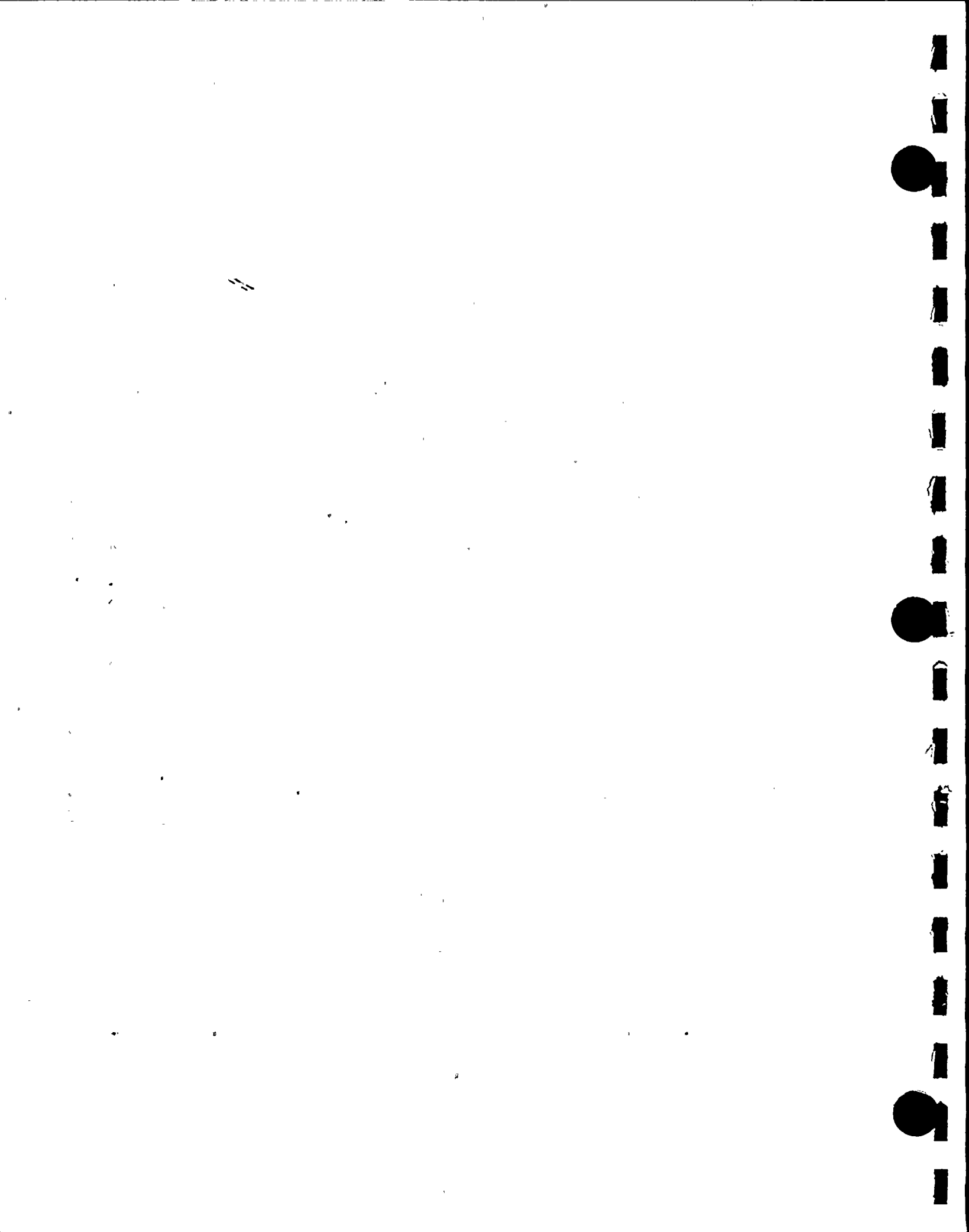


FIGURE 6.3.1 DBE - N-S ACCELERATION TIME-HISTORY



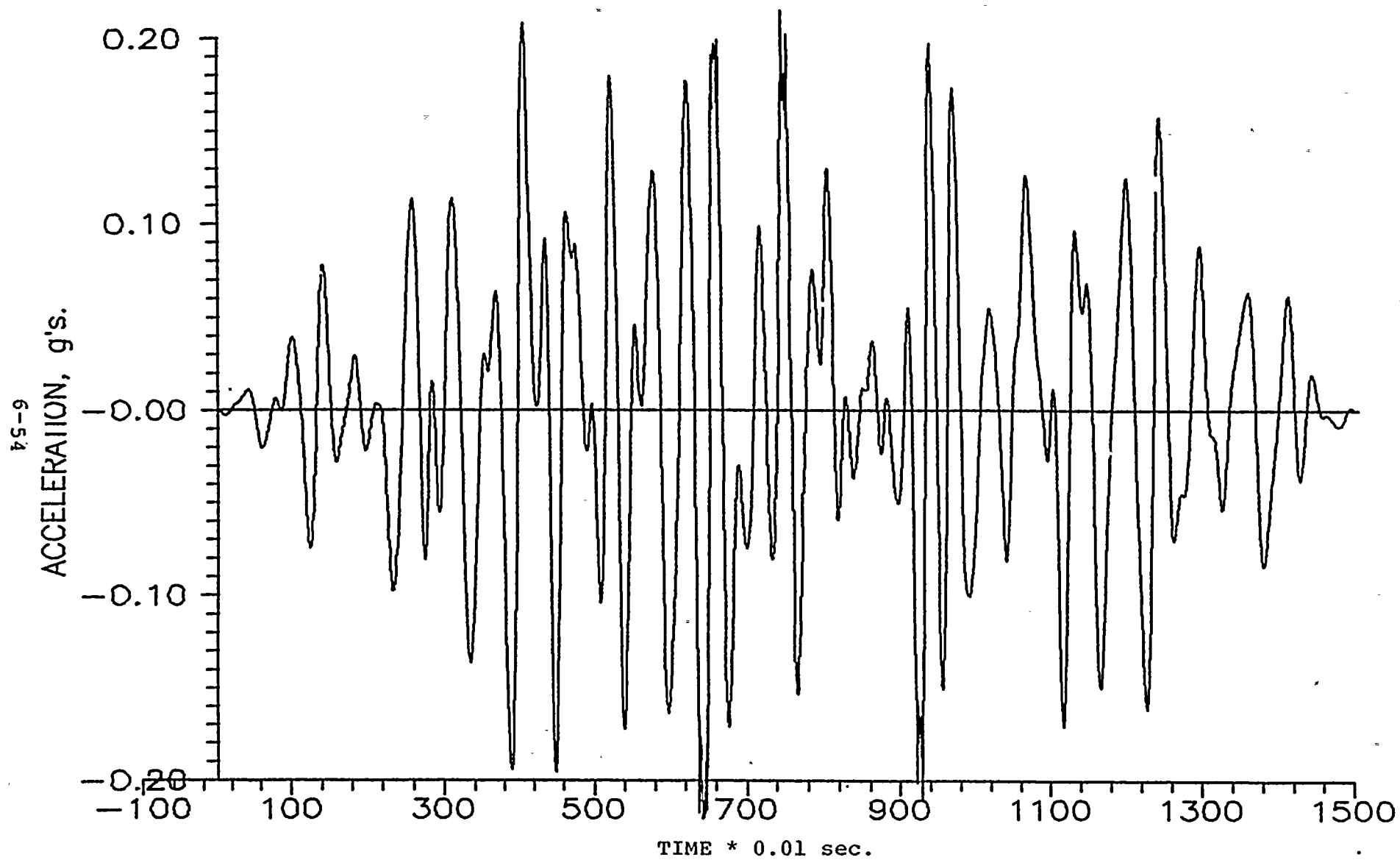
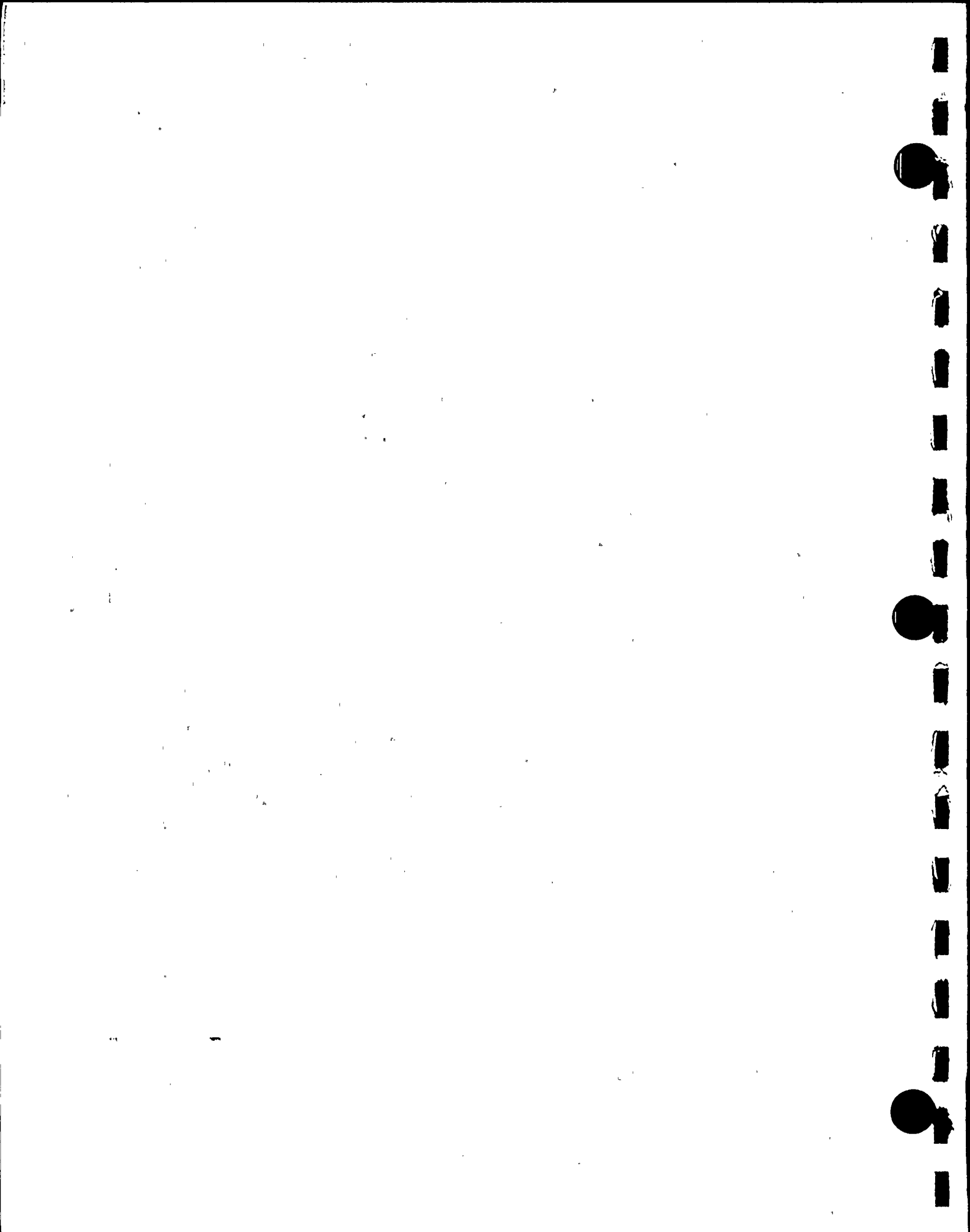


FIGURE 6.3.2 DBE E-W ACCELERATION TIME HISTORY



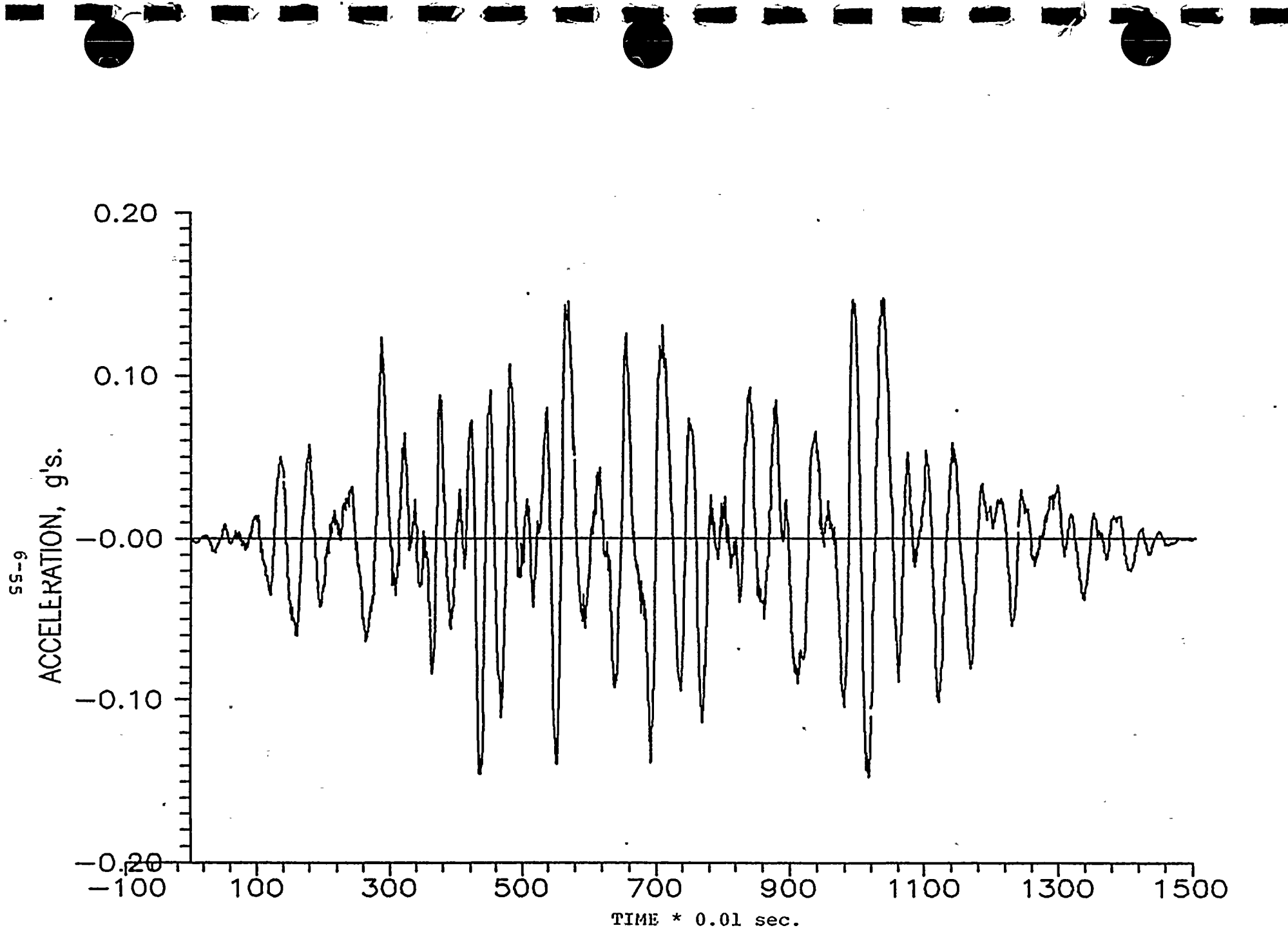
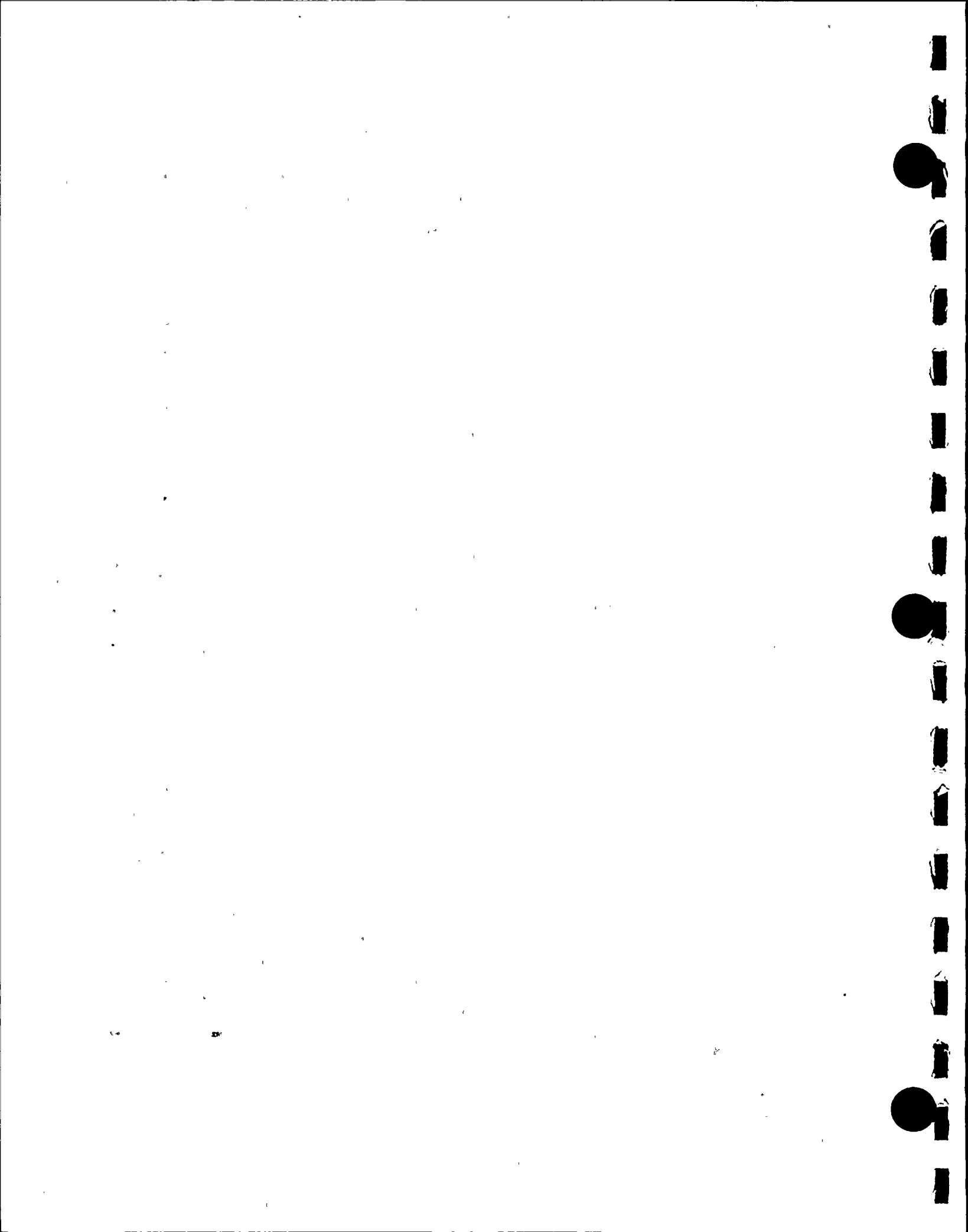


FIGURE 6.3.3 DBE - VERTICAL ACCELERATION TIME HISTORY



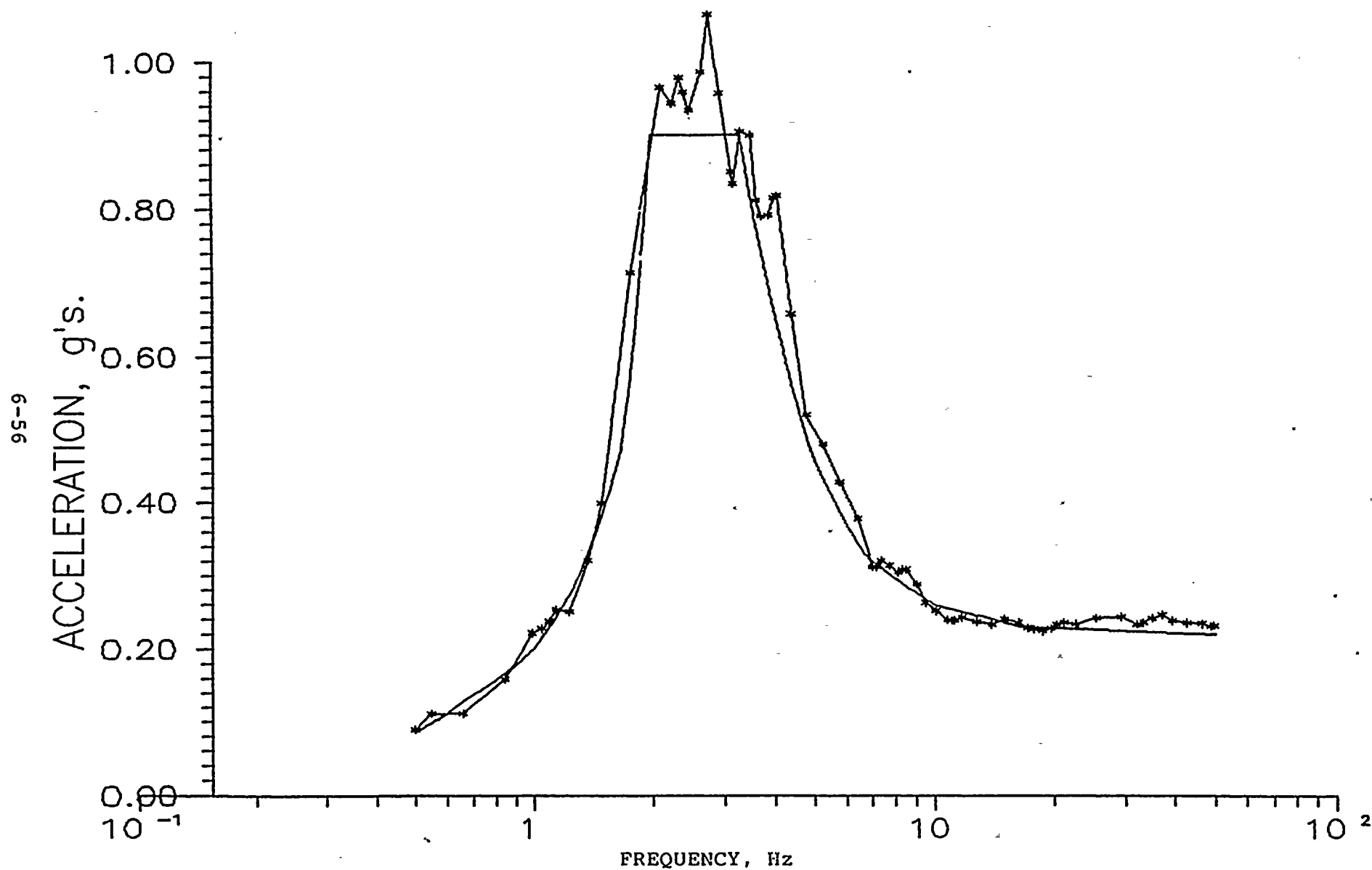


FIGURE 6.3.4 HORIZONTAL DESIGN SPECTRUM AND
N-S TIME HISTORY SPECTRUM (5% damping)



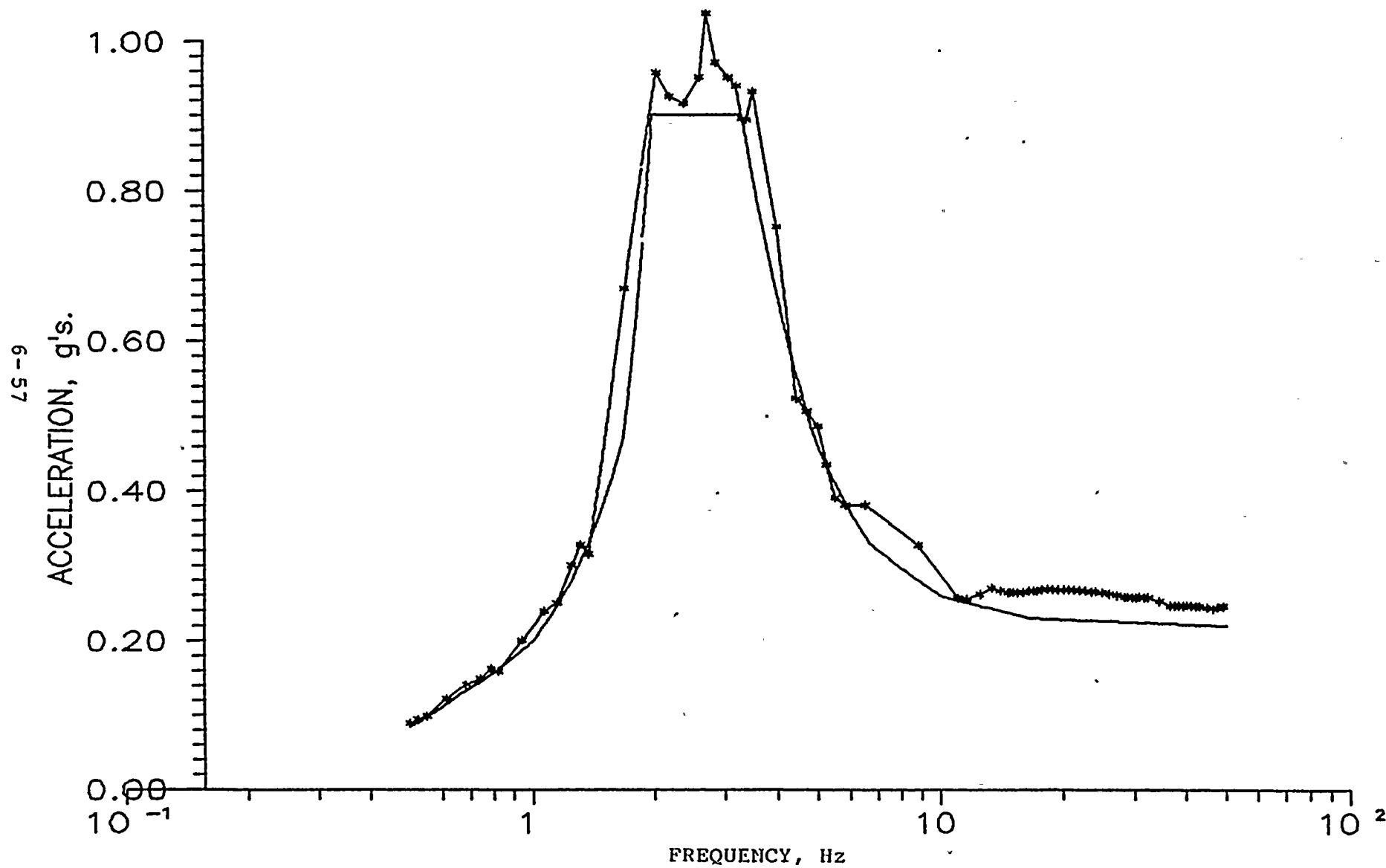
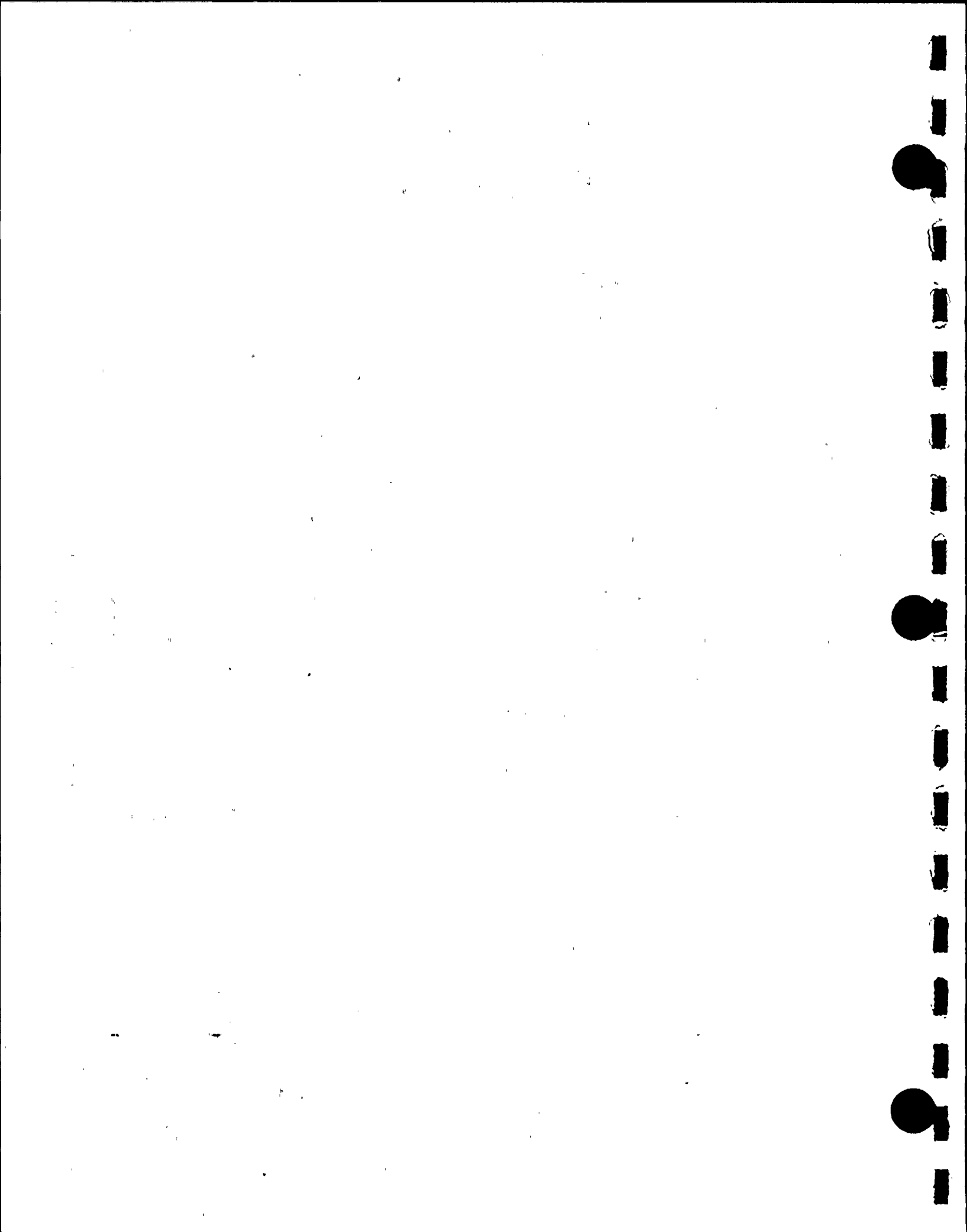


FIGURE 6.3.5 HORIZONTAL DESIGN SPECTRUM AND E-W
TIME HISTORY SPECTRUM (5% damping)



85-9

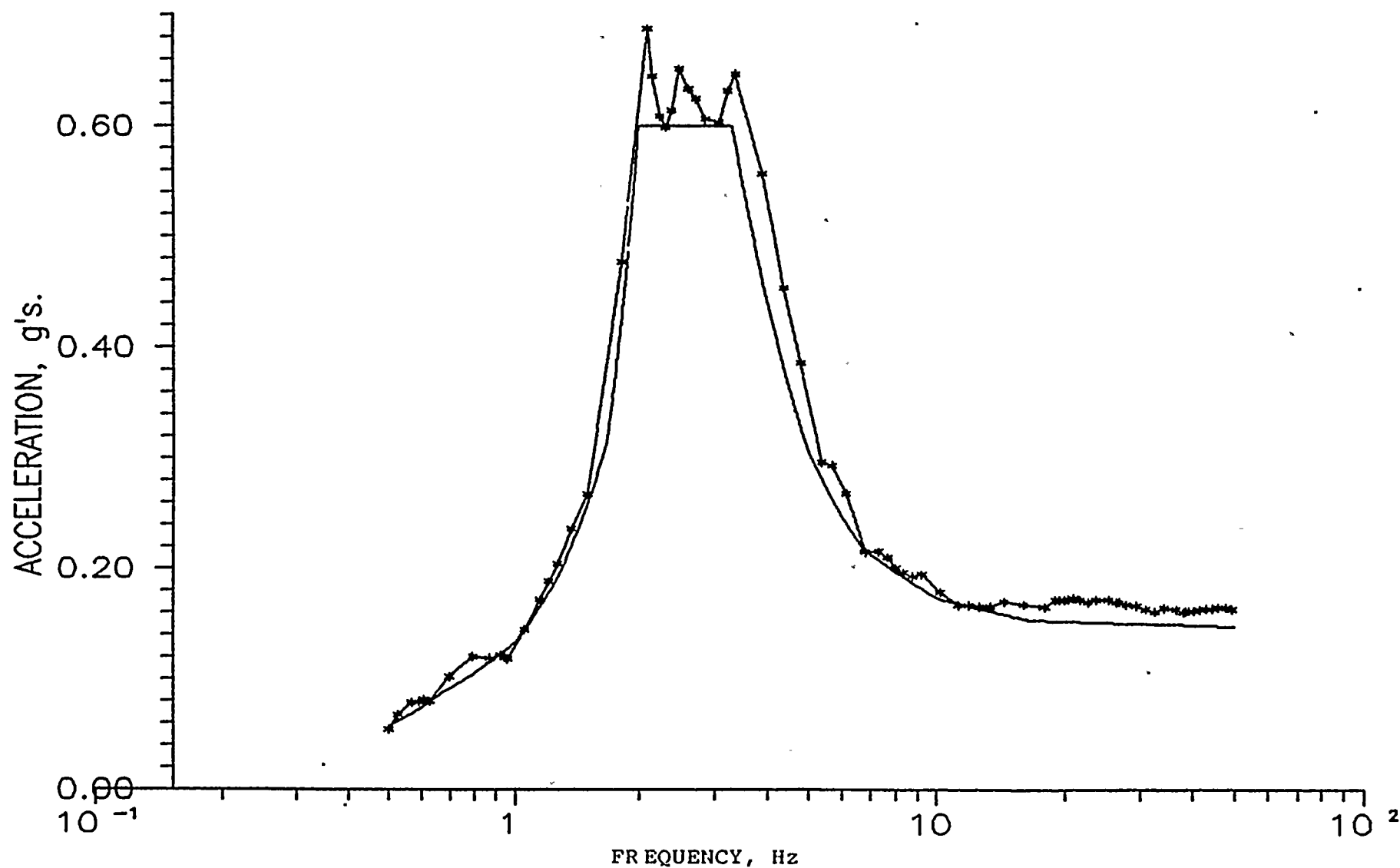
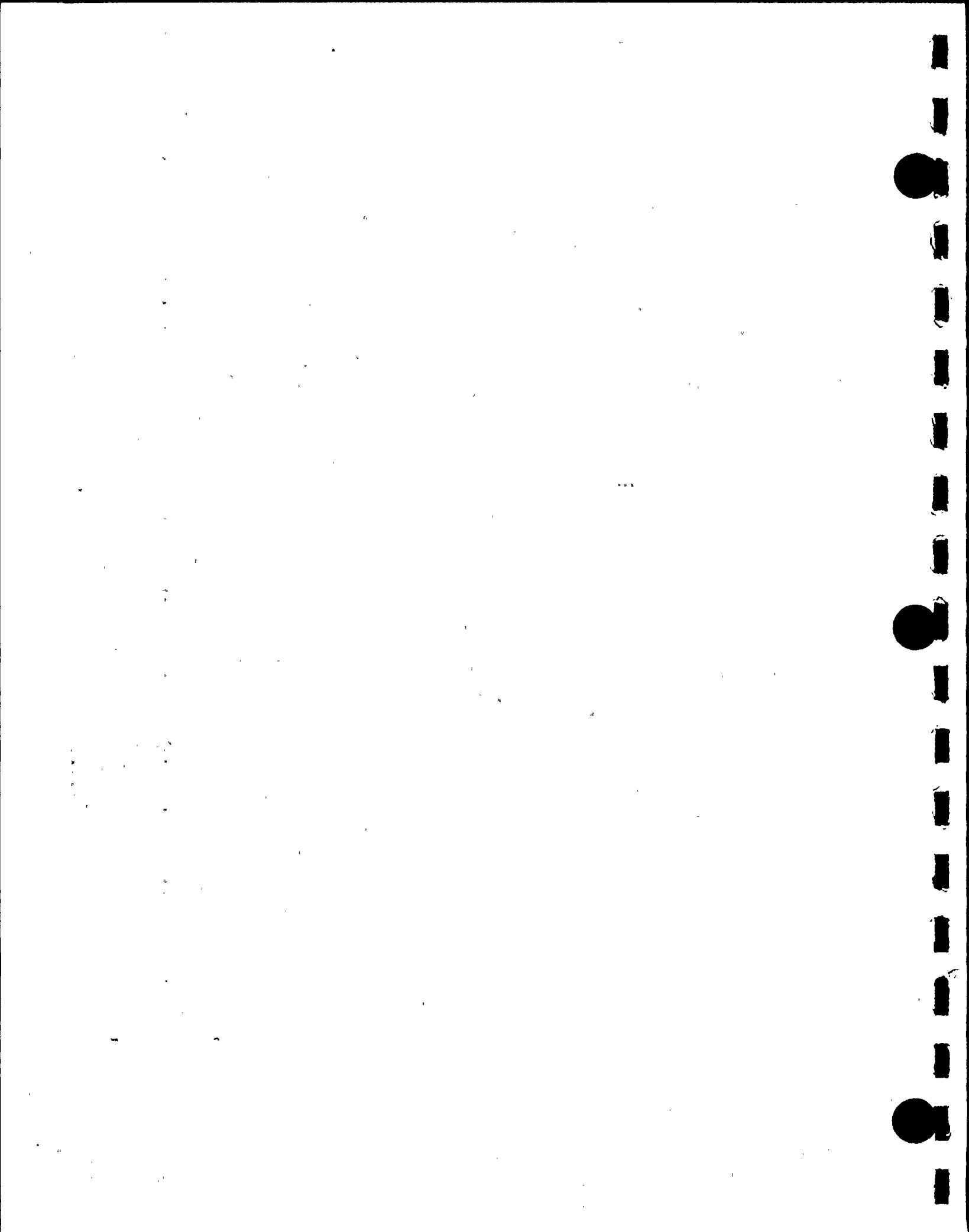


Figure 6.3.6 VERTICAL DESIGN AND TIME HISTORY DERIVED SPECTRA
(5% damping)



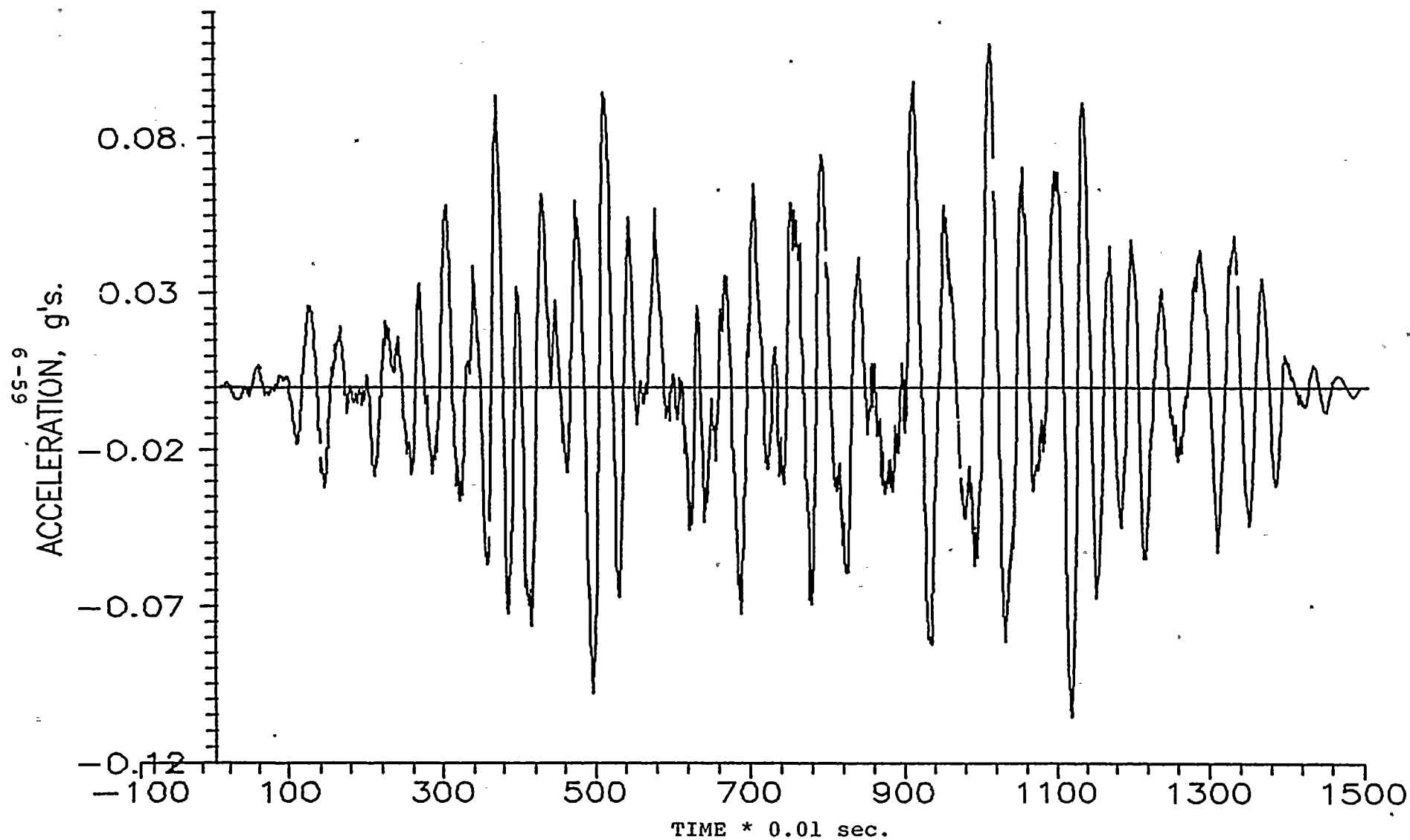
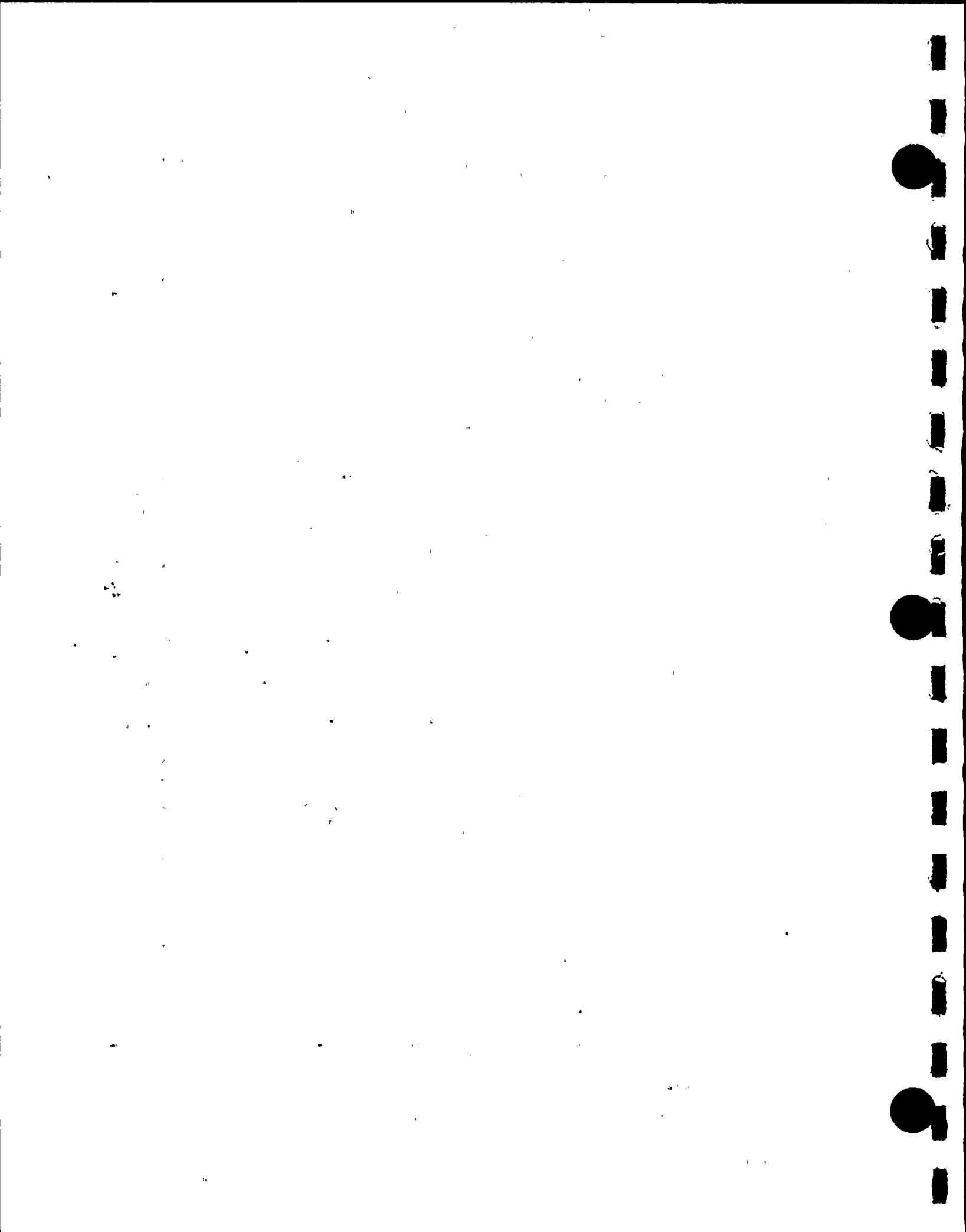


FIGURE 6.3.7 OBE - N-S ACCELERATION TIME HISTORY



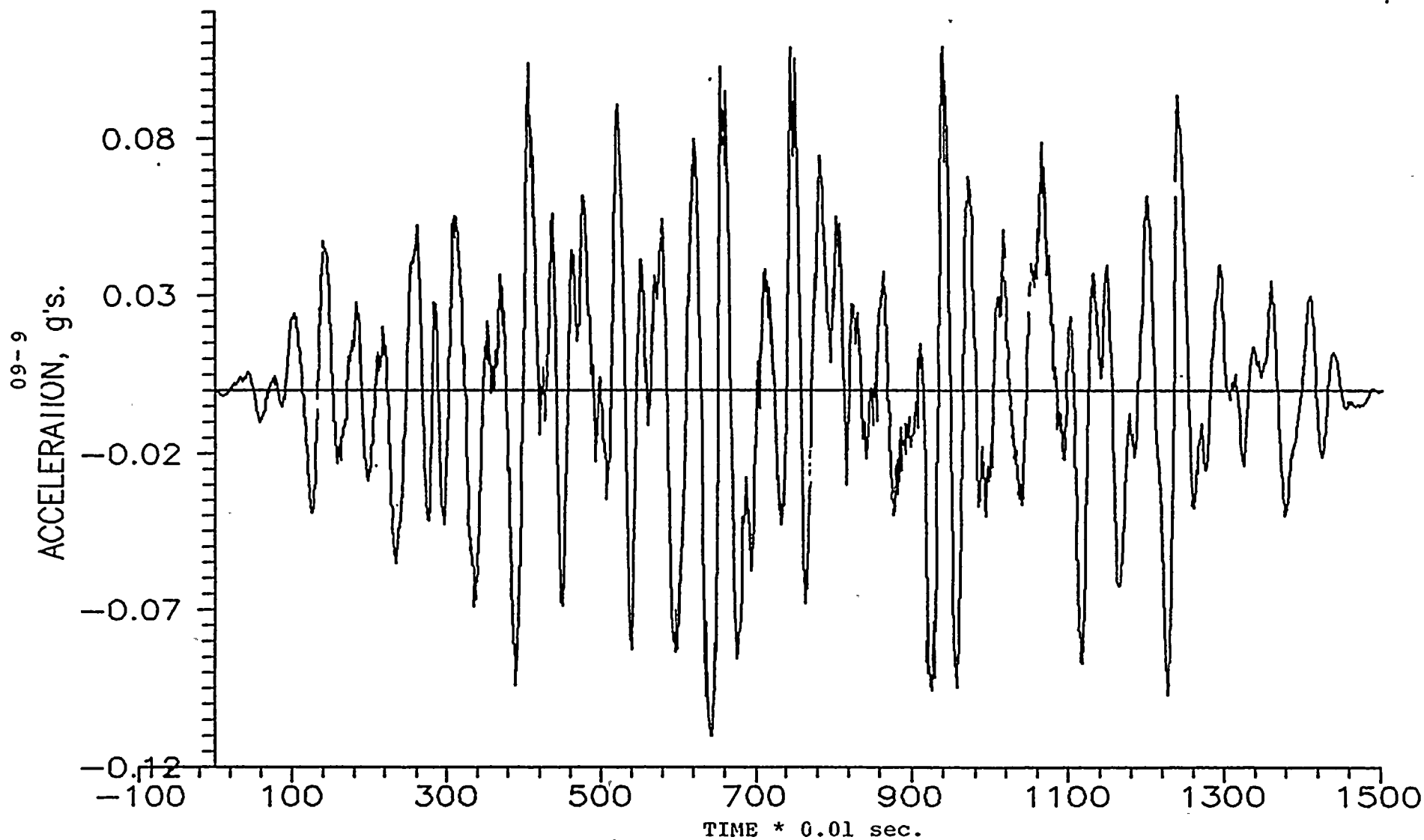
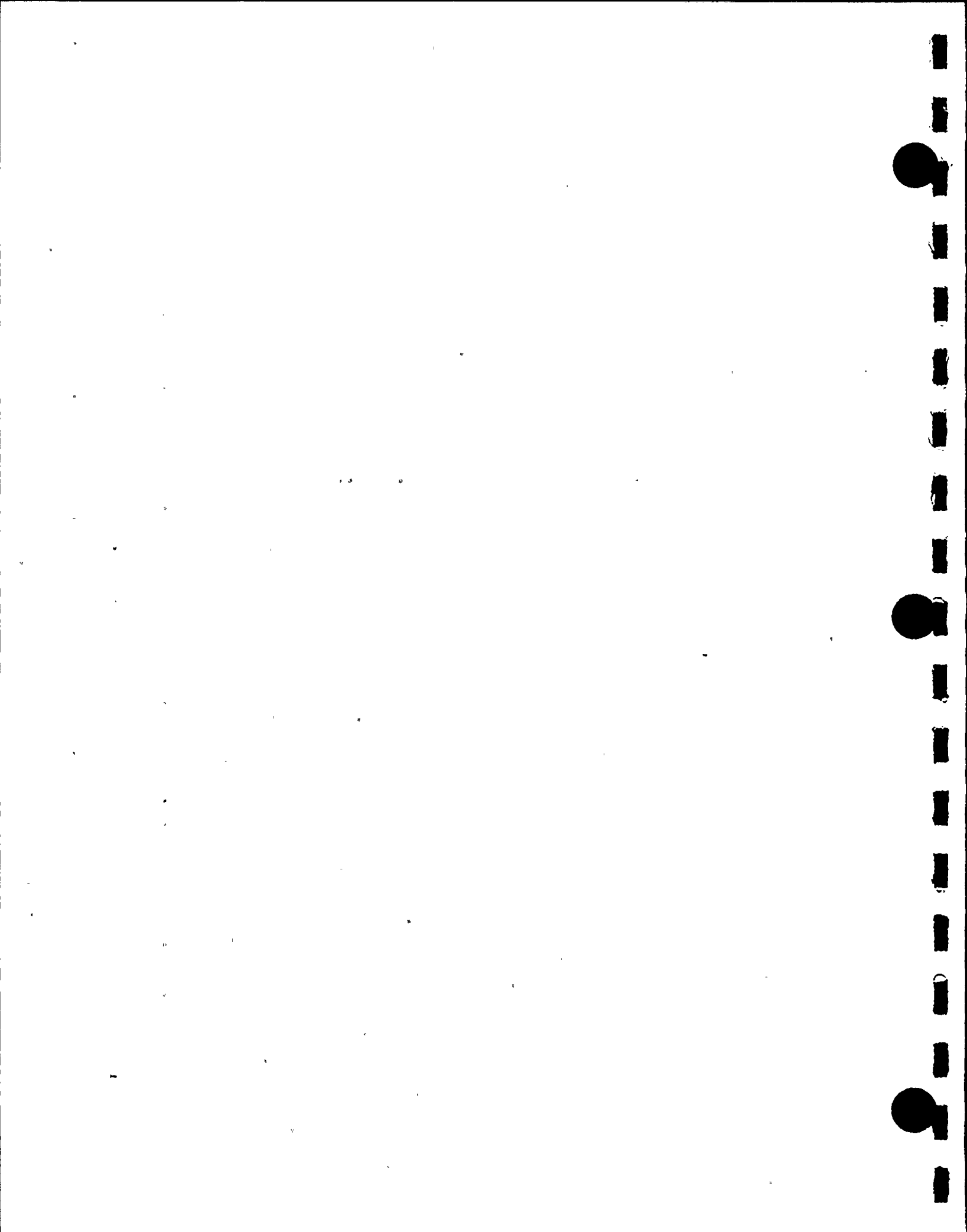


FIGURE 6.3.8 OBE - E-W ACCELERATION TIME HISTORY



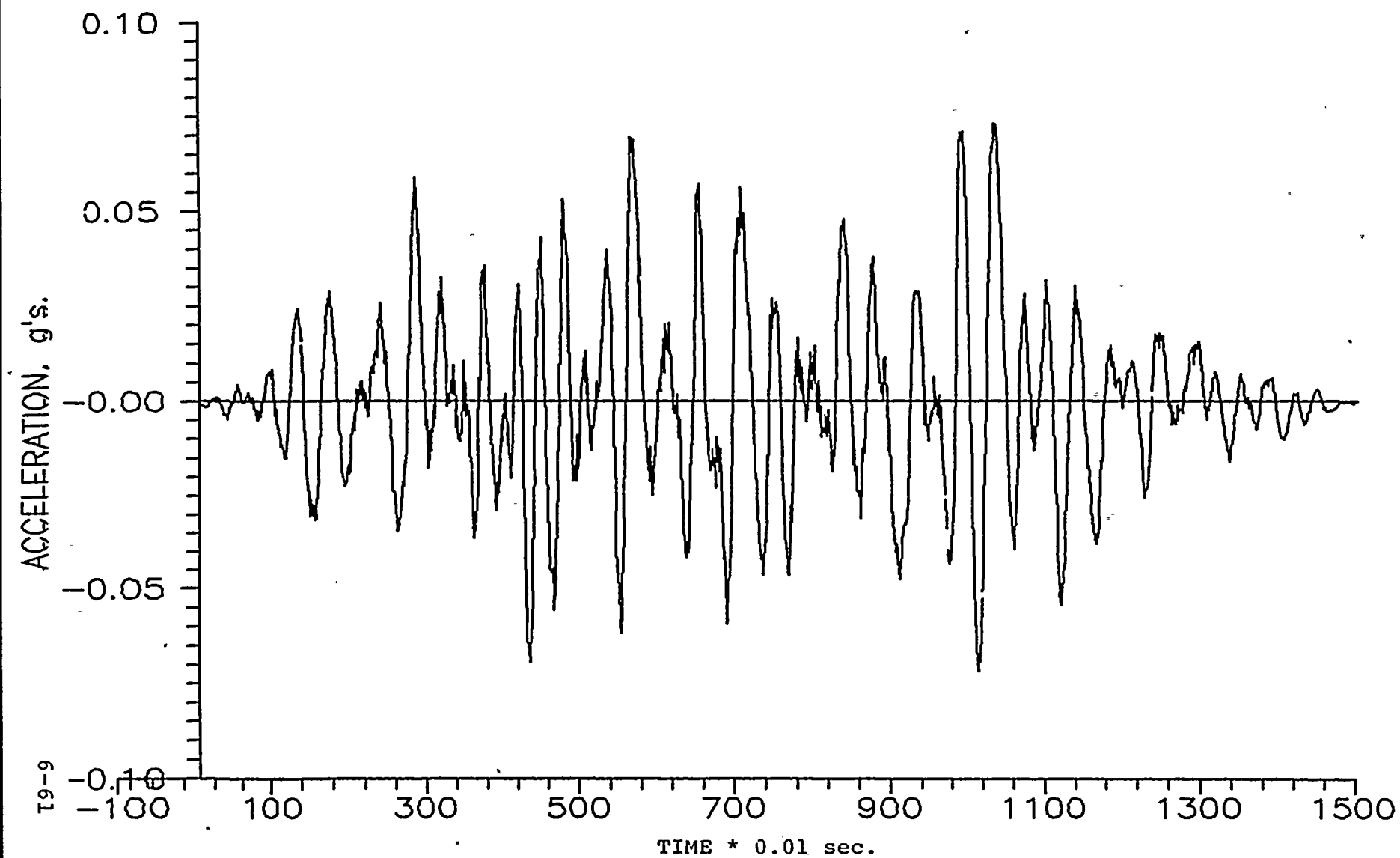
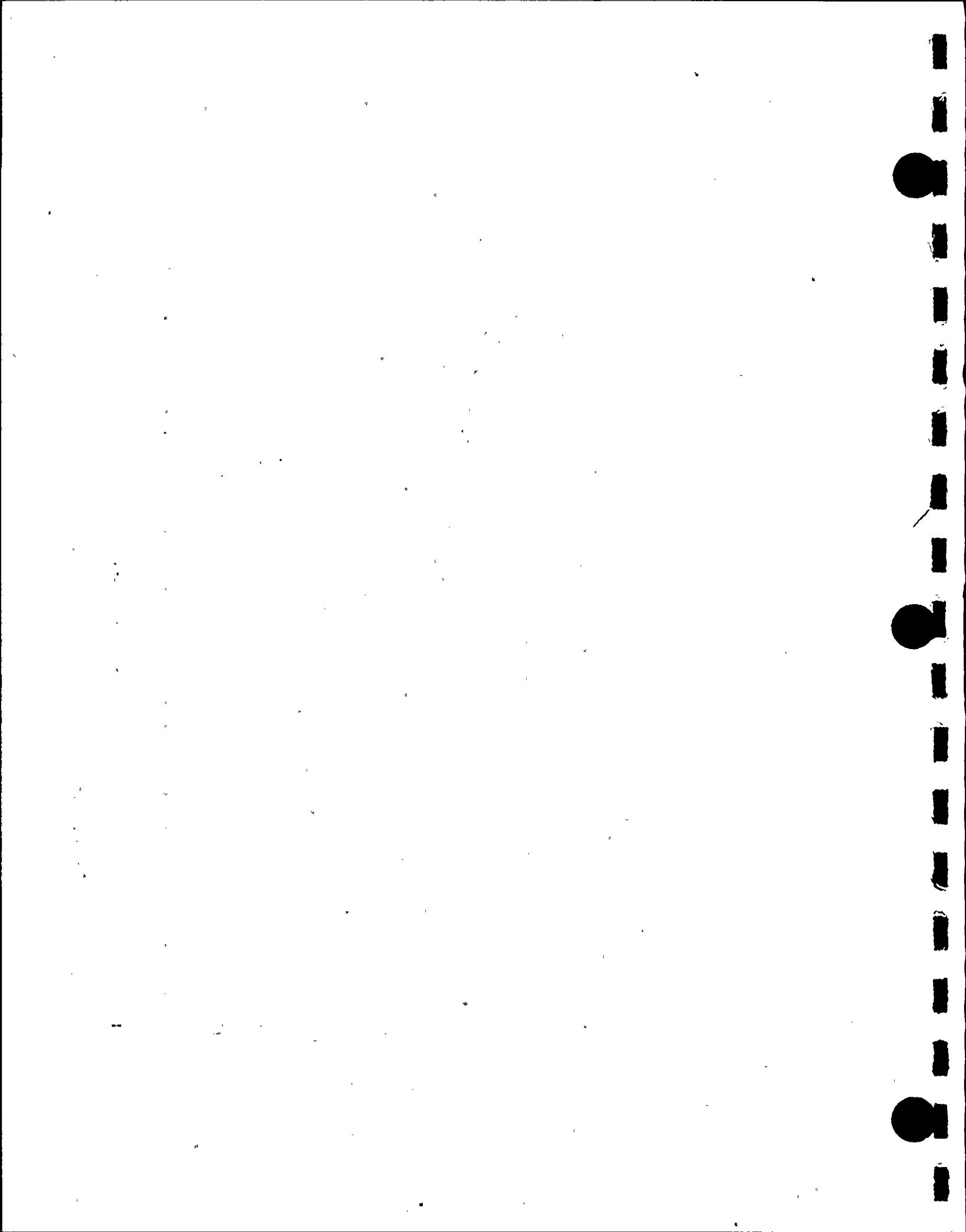


FIGURE 6.3.9 OBE - VERTICAL ACCELERATION TIME HISTORY



6-62

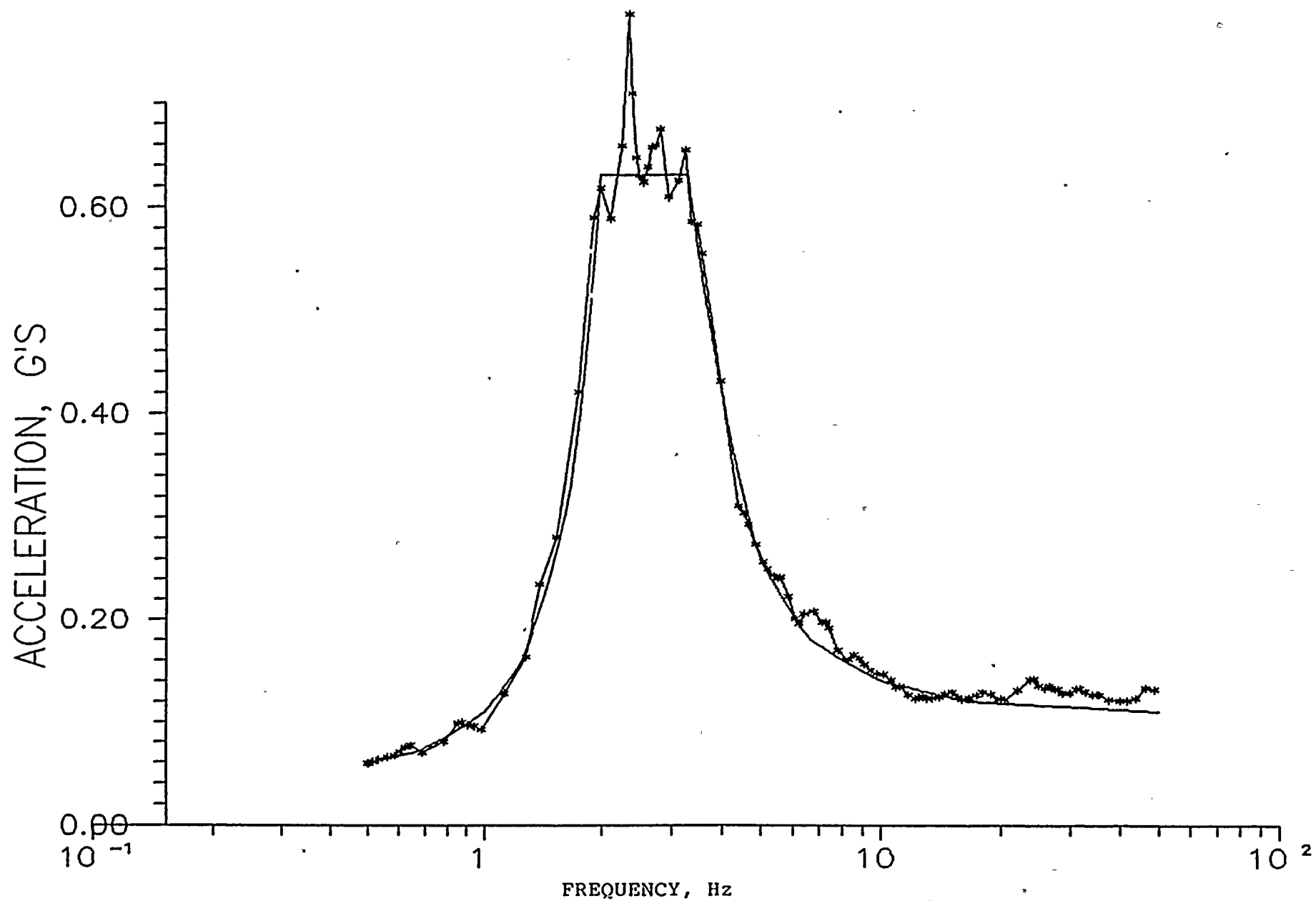
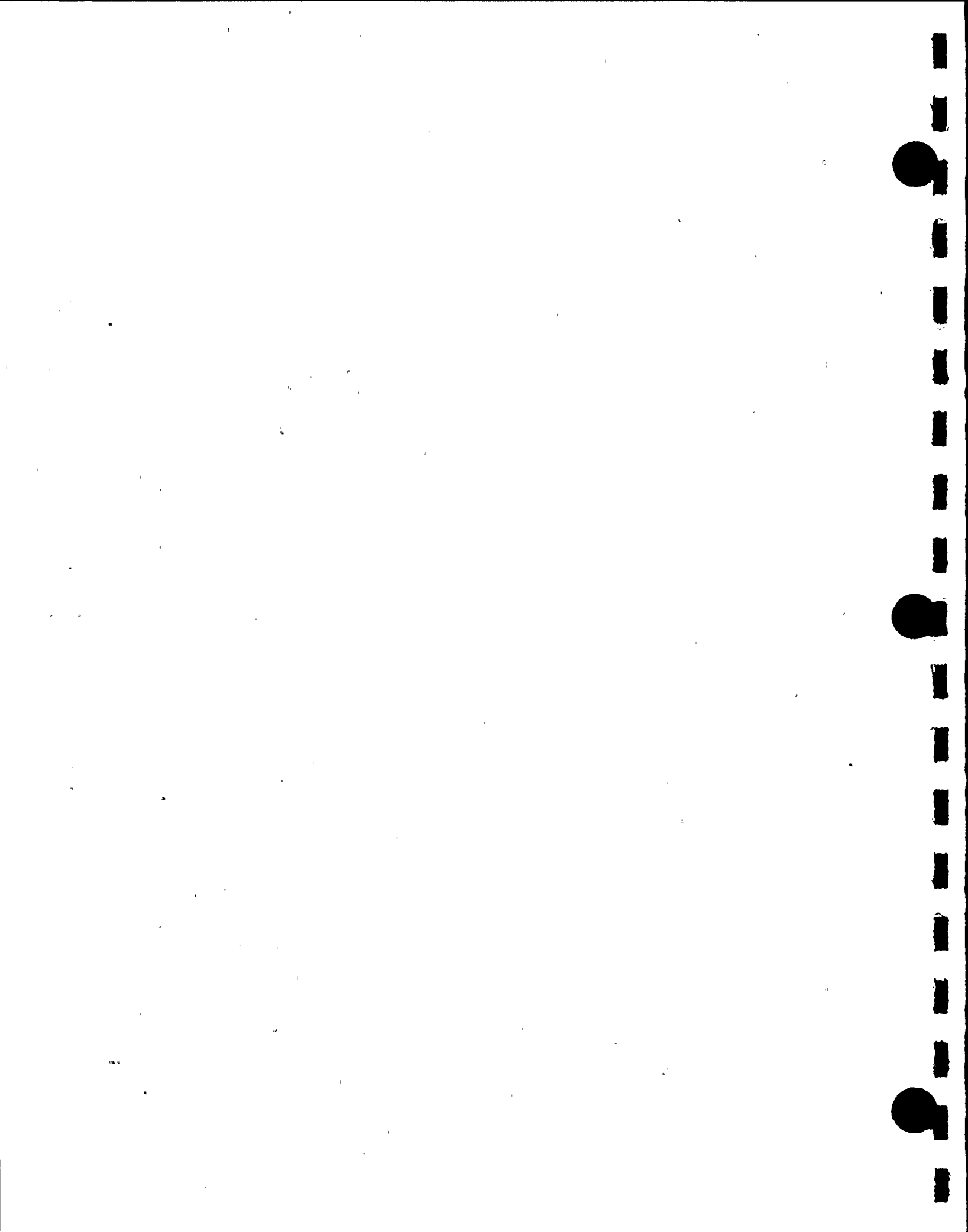


Figure 6.3.10 HORIZONTAL DESIGN SPECTRUM AND TIME HISTORY DERIVED N-S SPECTRUM (2% damping)



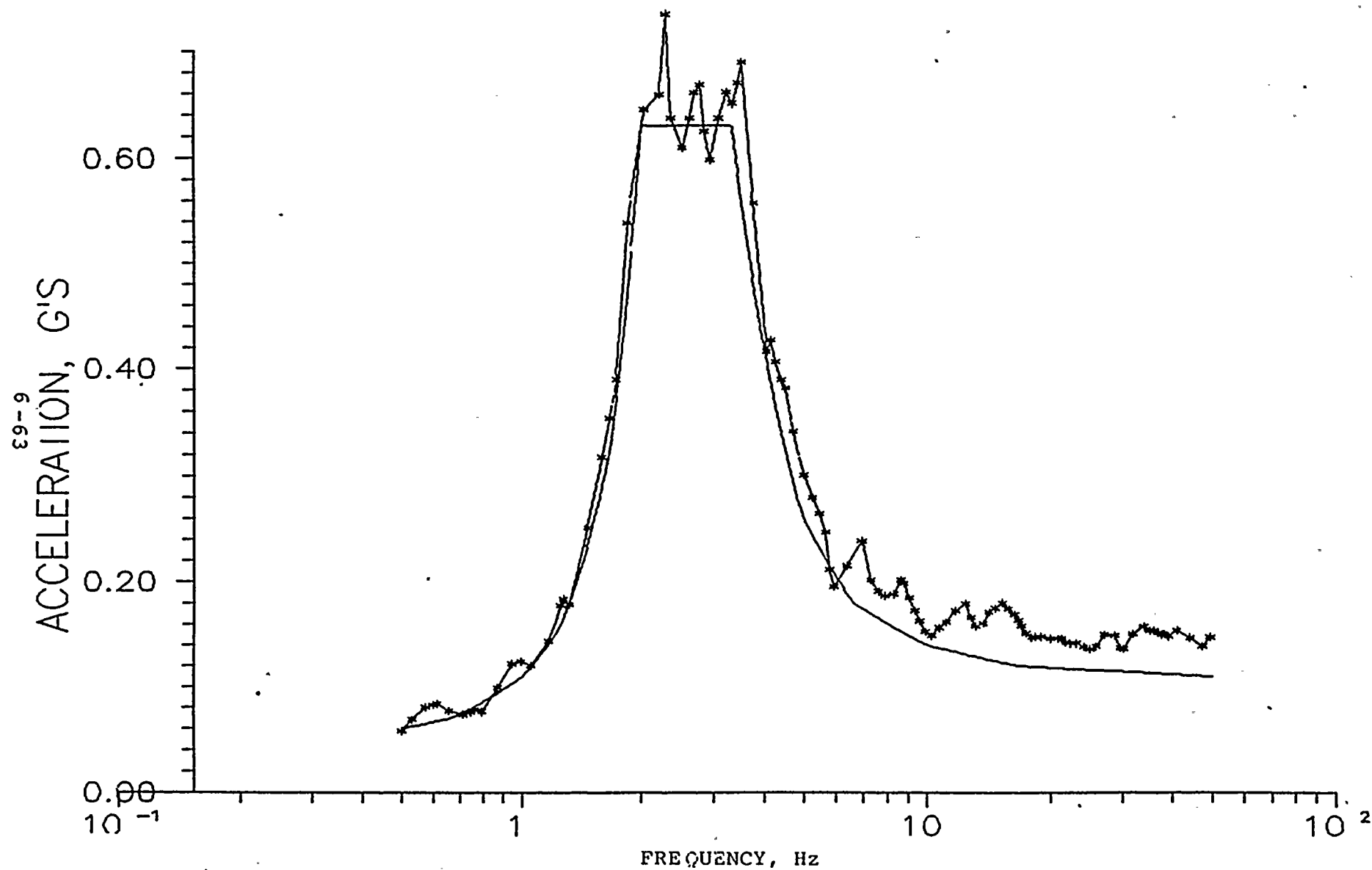
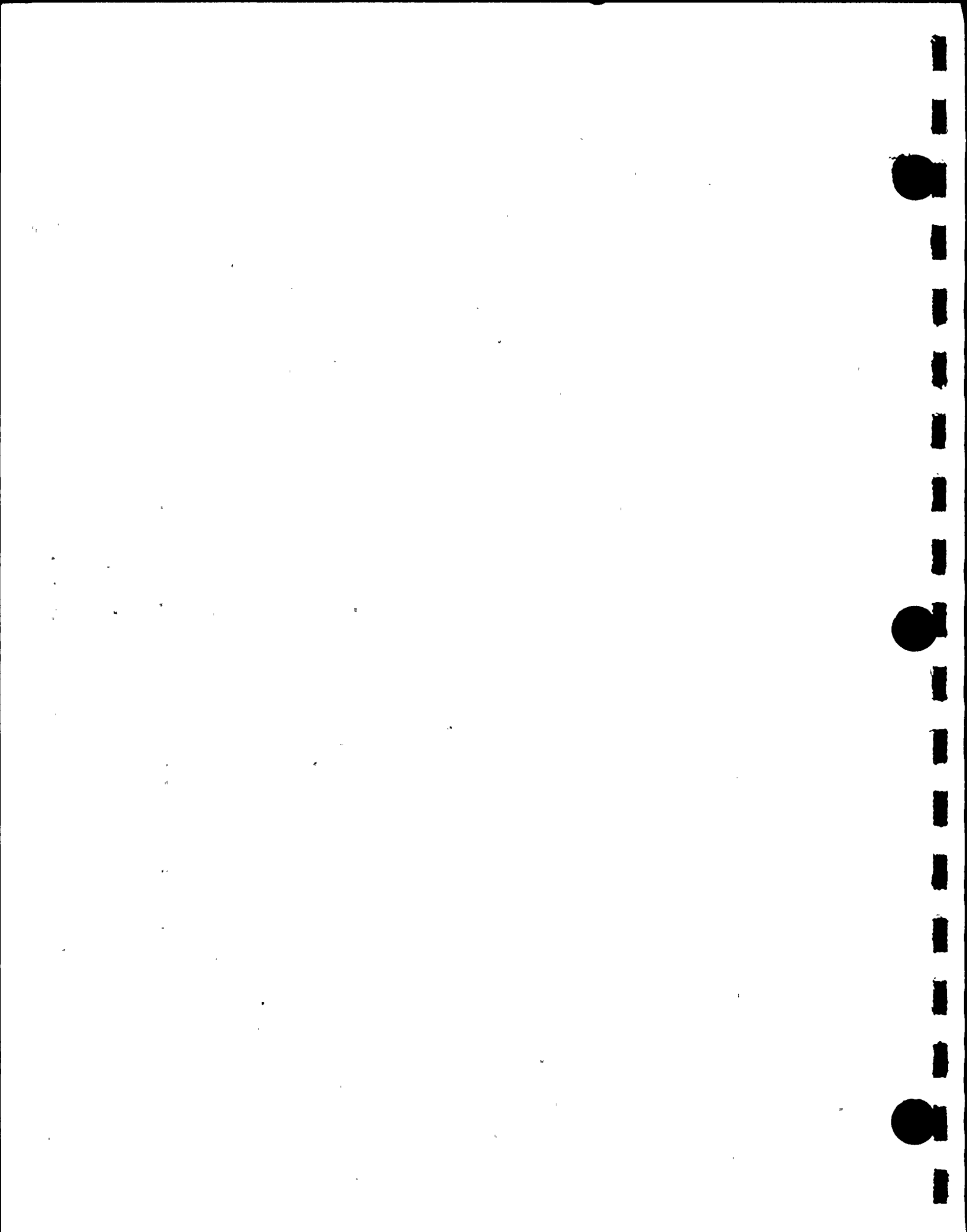


Figure 6.3.11 HORIZONTAL DESIGN SPECTRUM AND E-W
TIME HISTORY'S DERIVED SPECTRUM (2% damping)



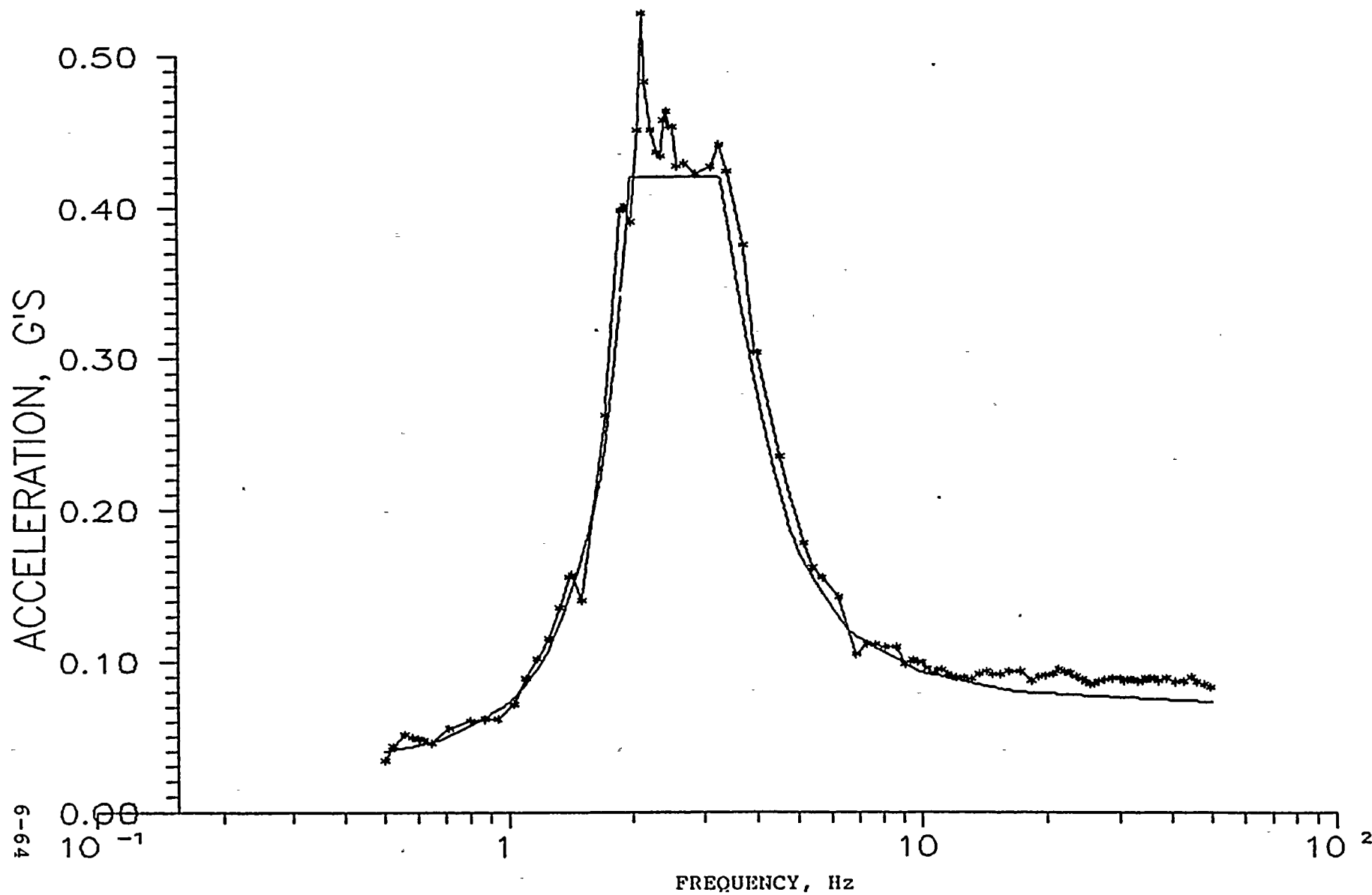


Figure 6.3.12 VERTICAL DESIGN AND TIME HISTORY
DERIVED SPECTRA (2% damping)



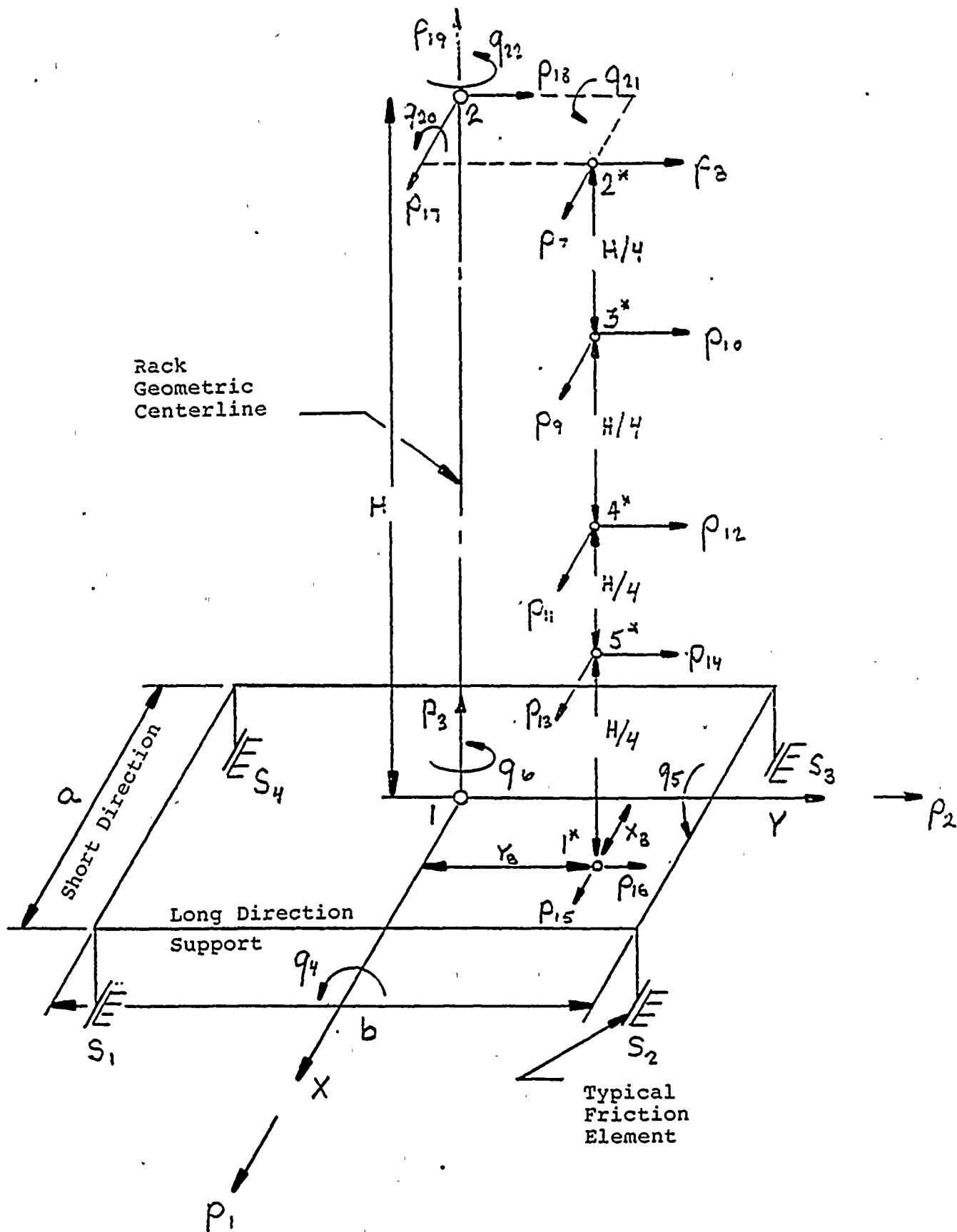
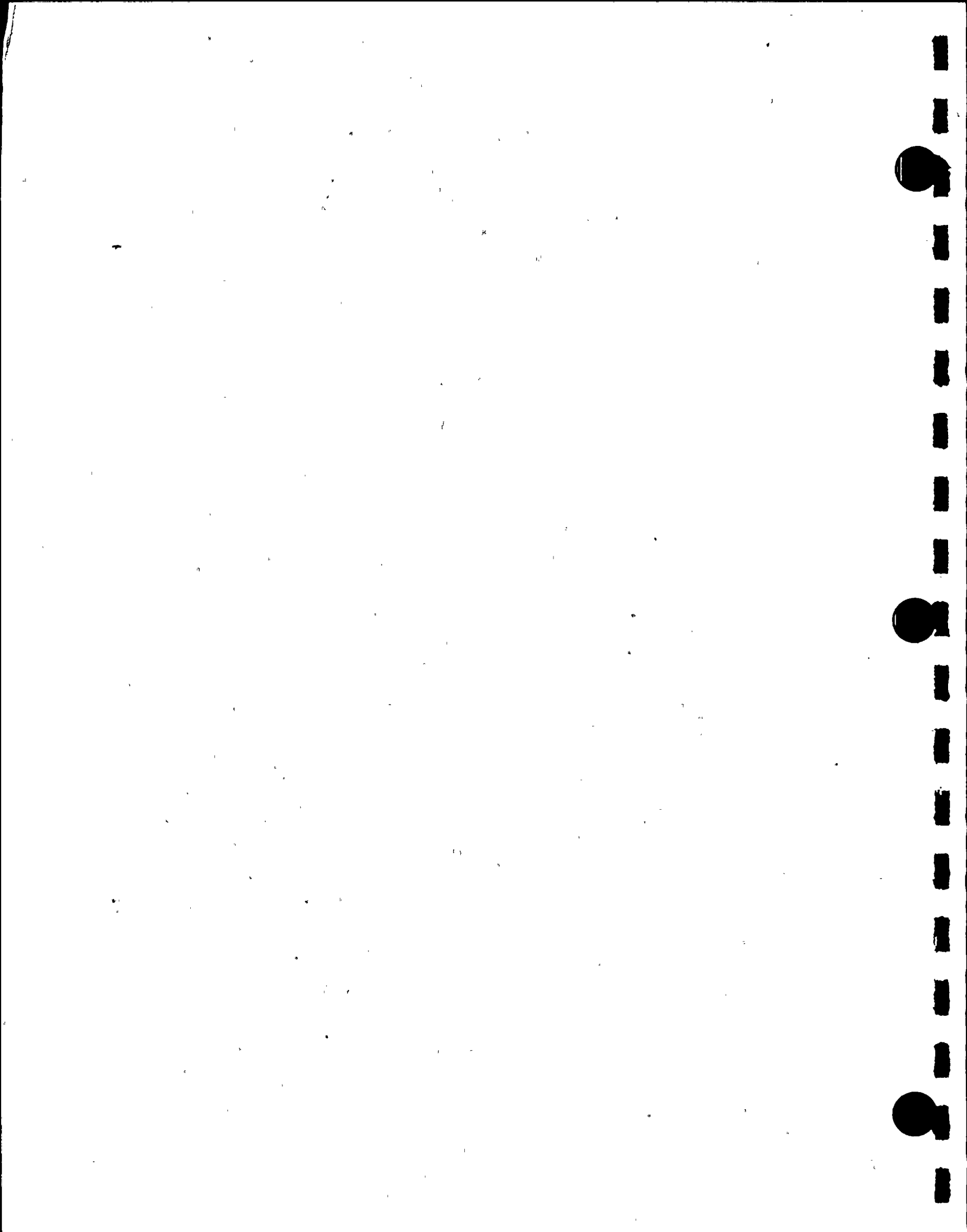


Figure 6.5.1 SCHEMATIC MODEL FOR DYNARACK



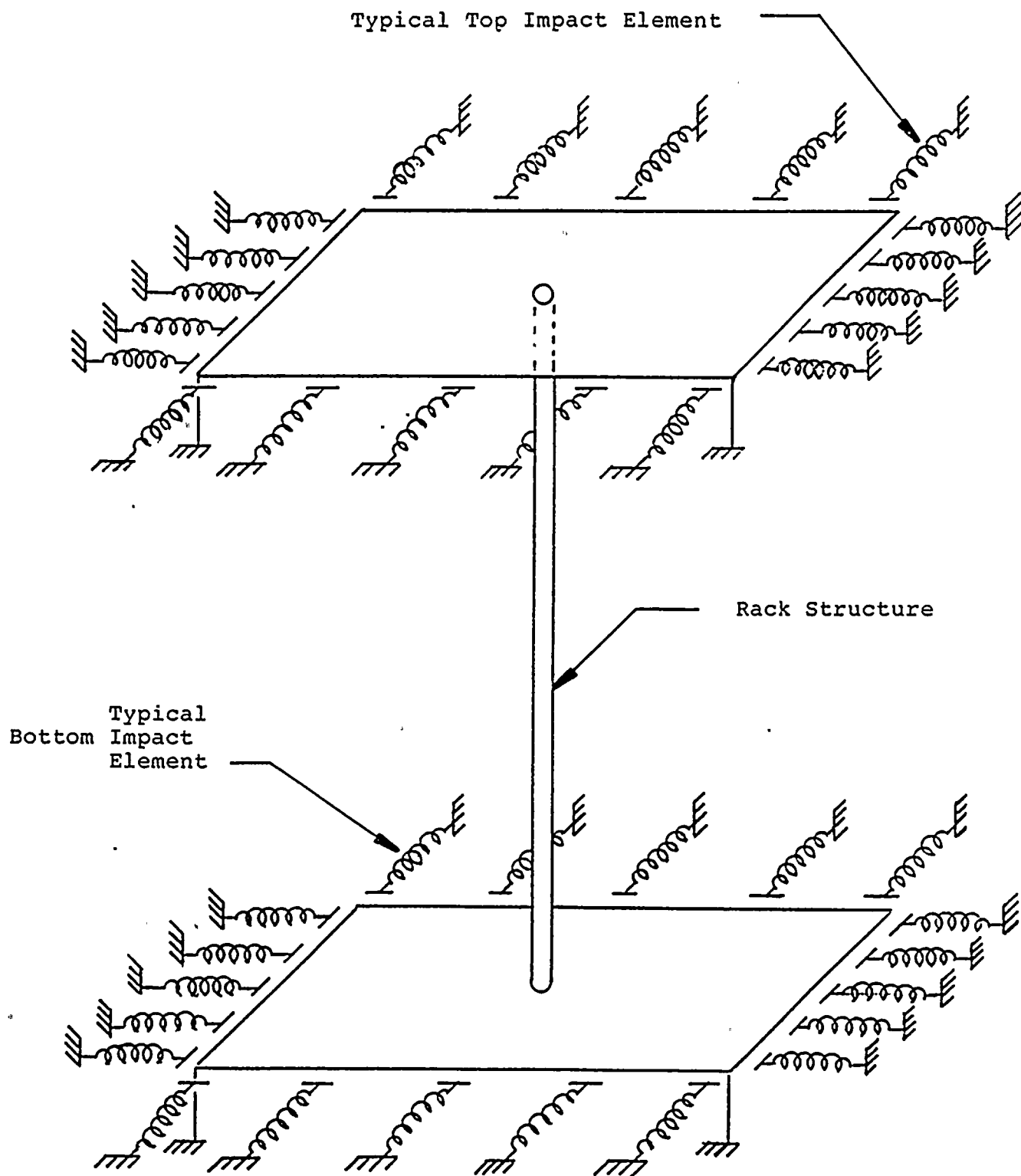
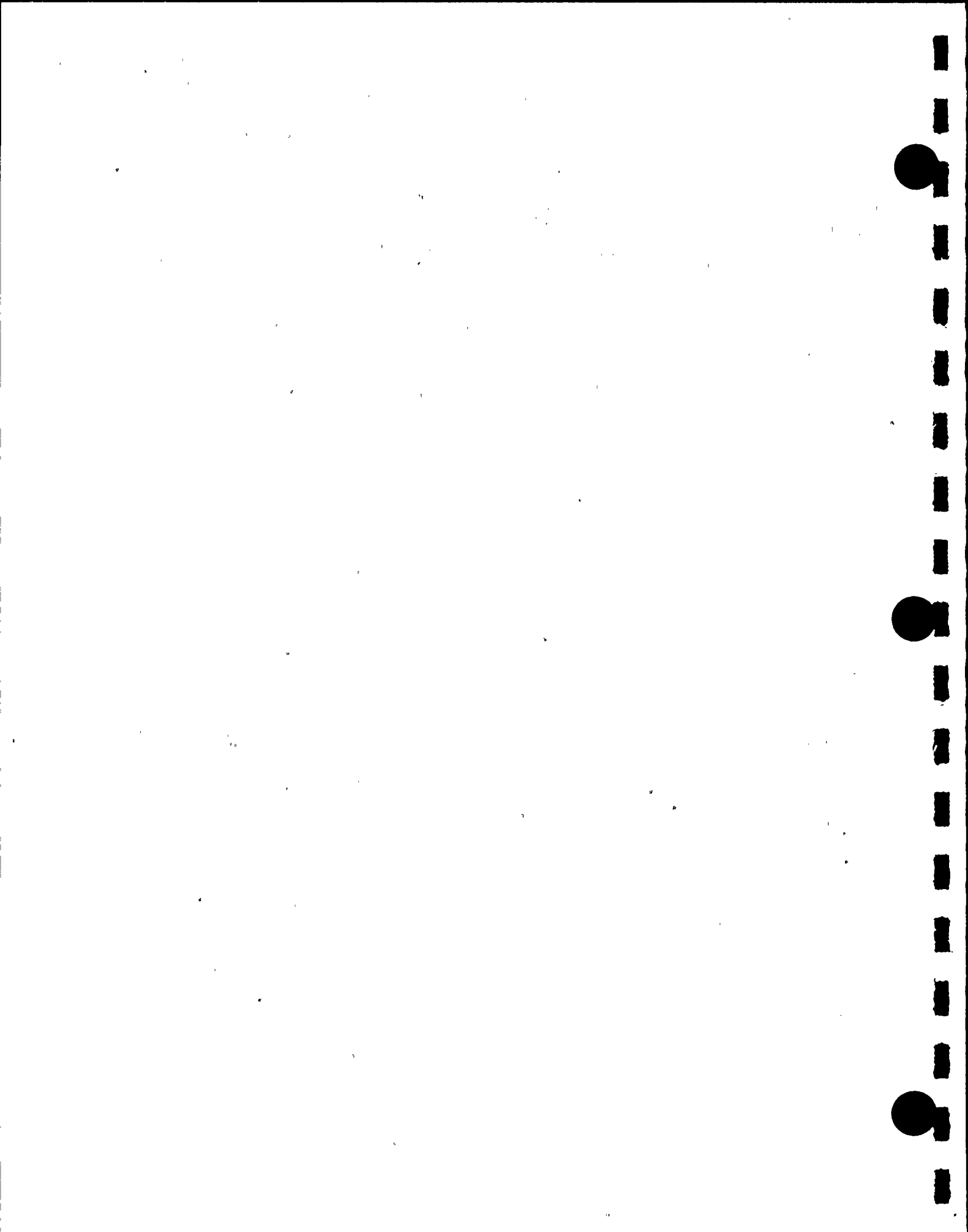


Figure 6.5.2 RACK-TO-RACK IMPACT SPRINGS



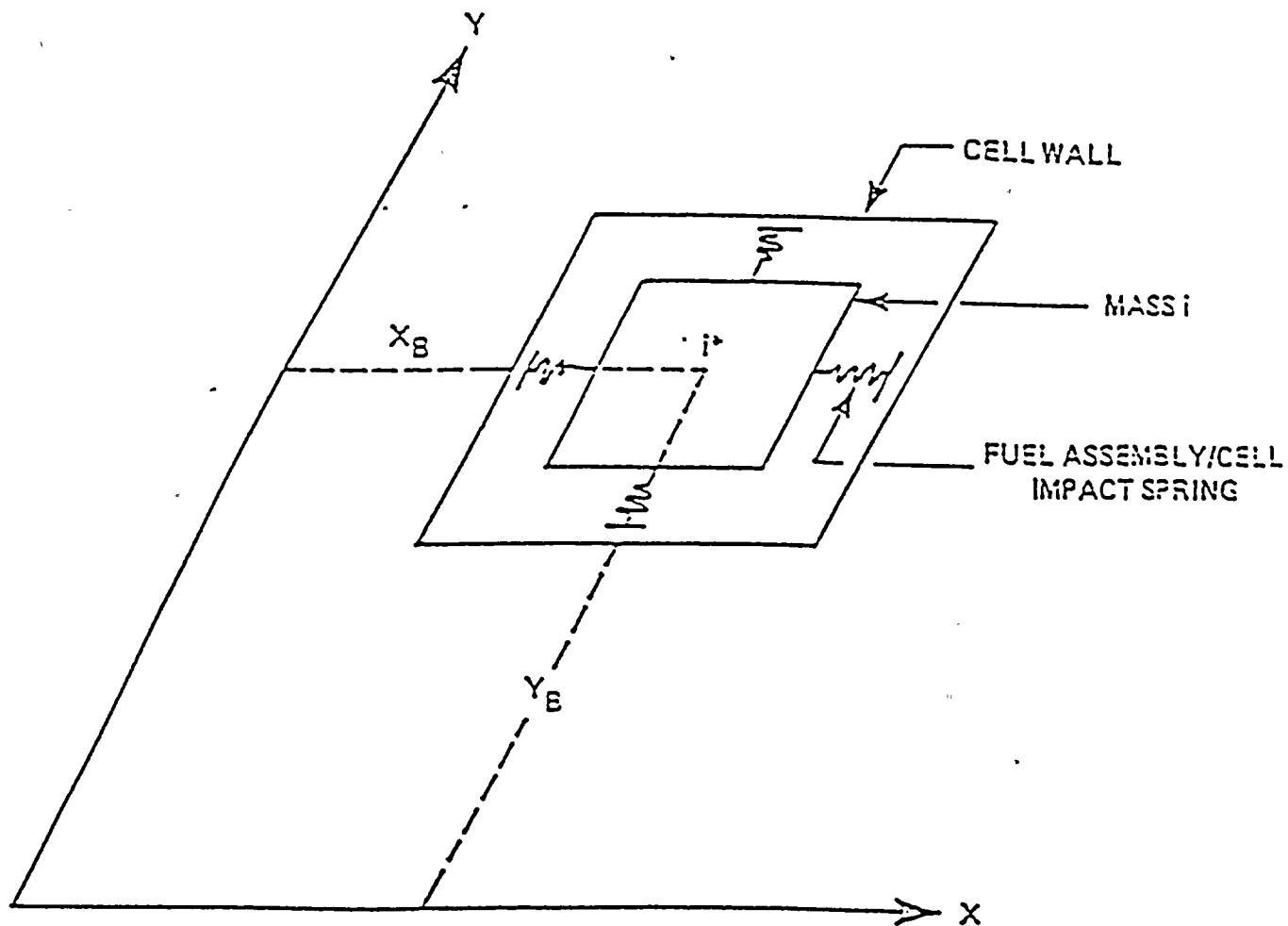
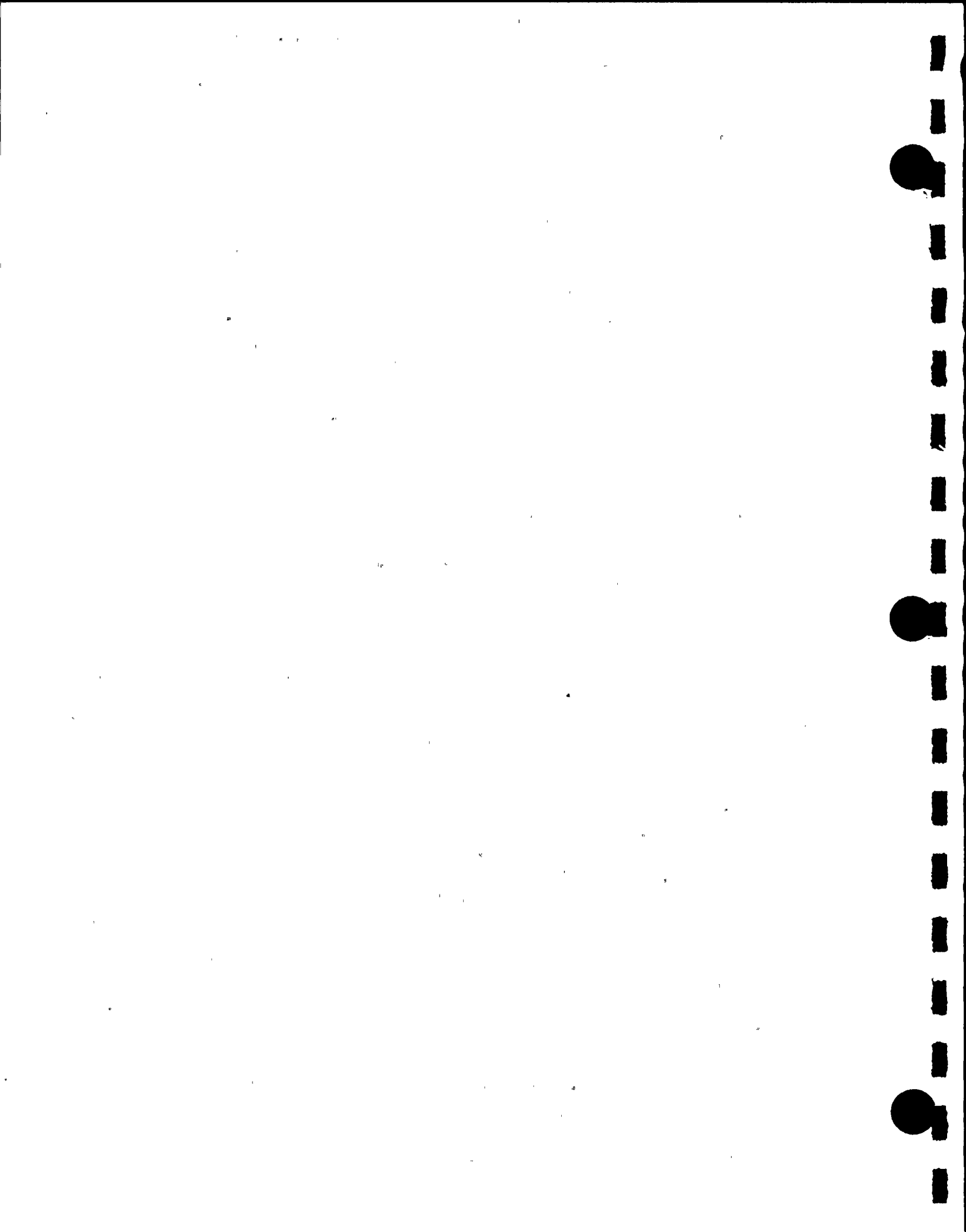


FIGURE 6.5.3 IMPACT SPRING ARRANGEMENT
AT NODE i



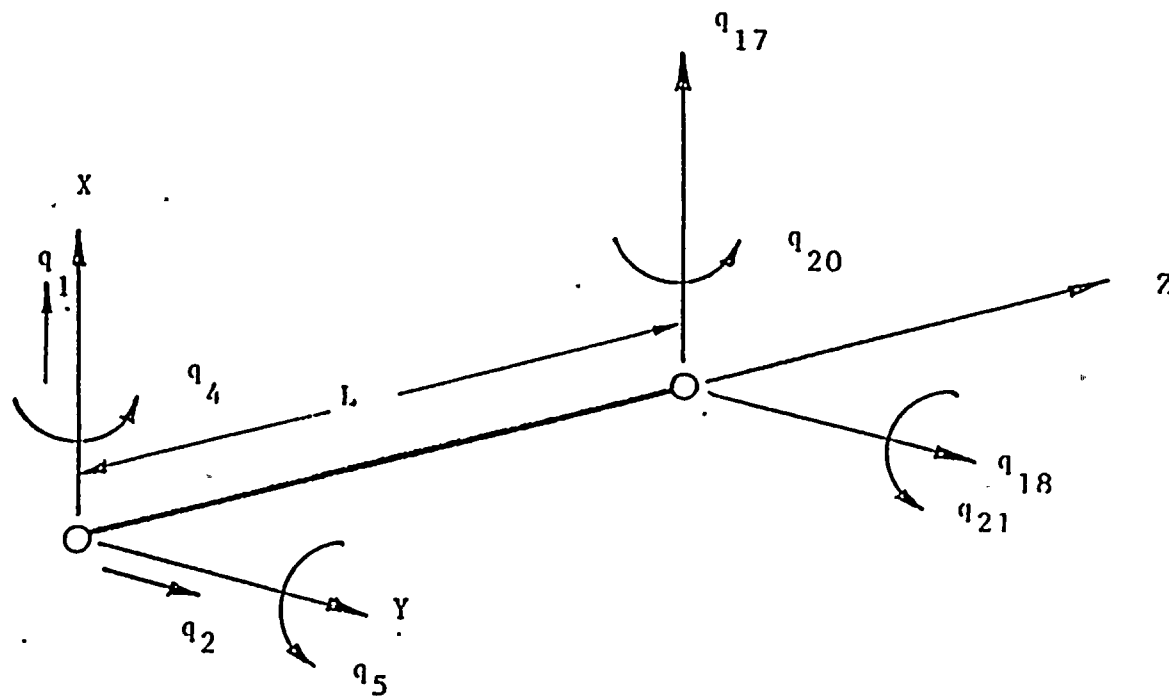


Figure 6.5.4

DEGREES OF FREEDOM MODELLING RACK MOTION



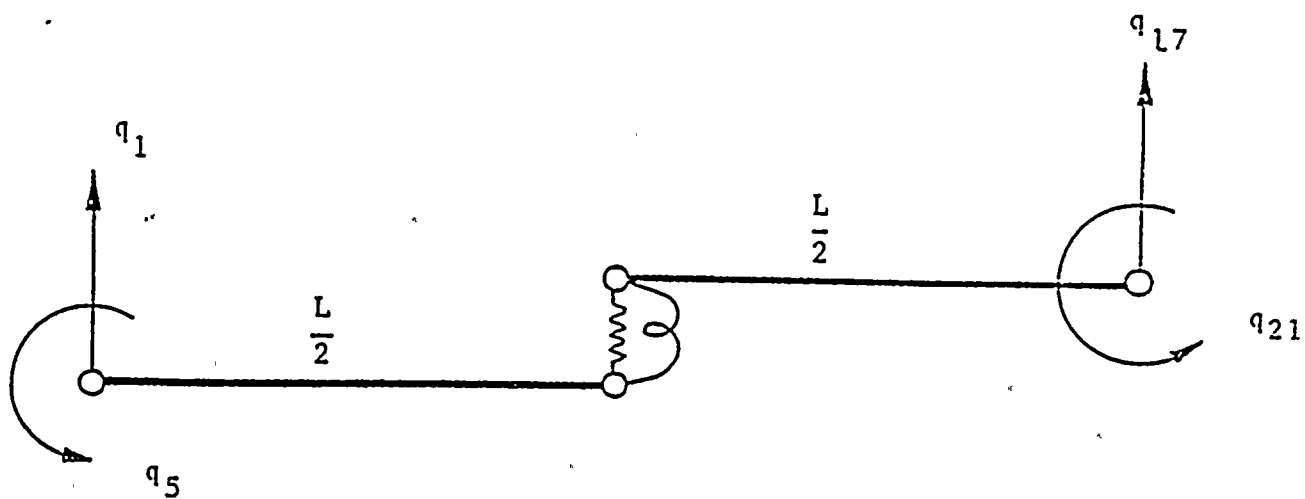


FIGURE 6.5.5 RACK DEGREES OF FREEDOM FOR X-Z PLANE BENDING



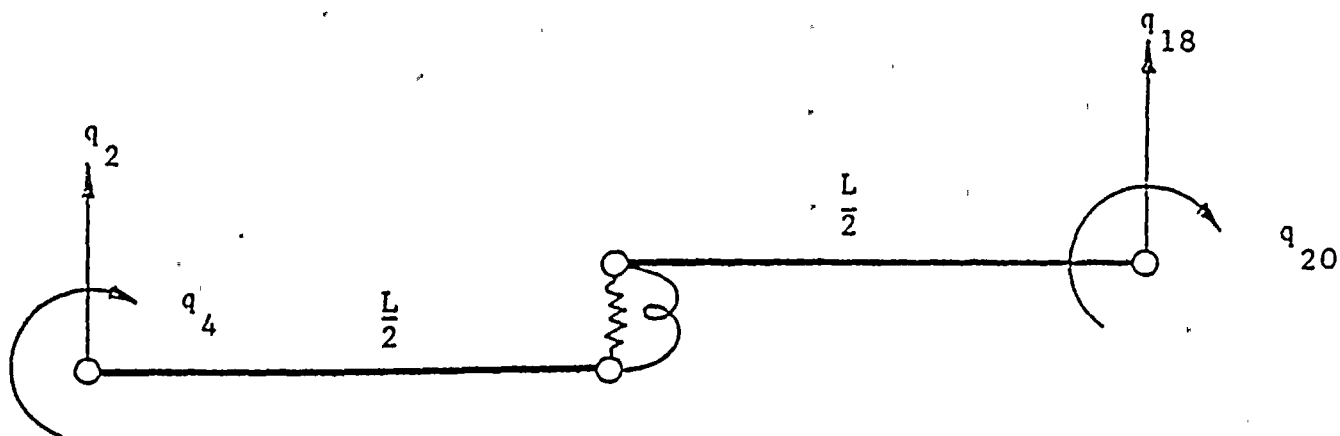
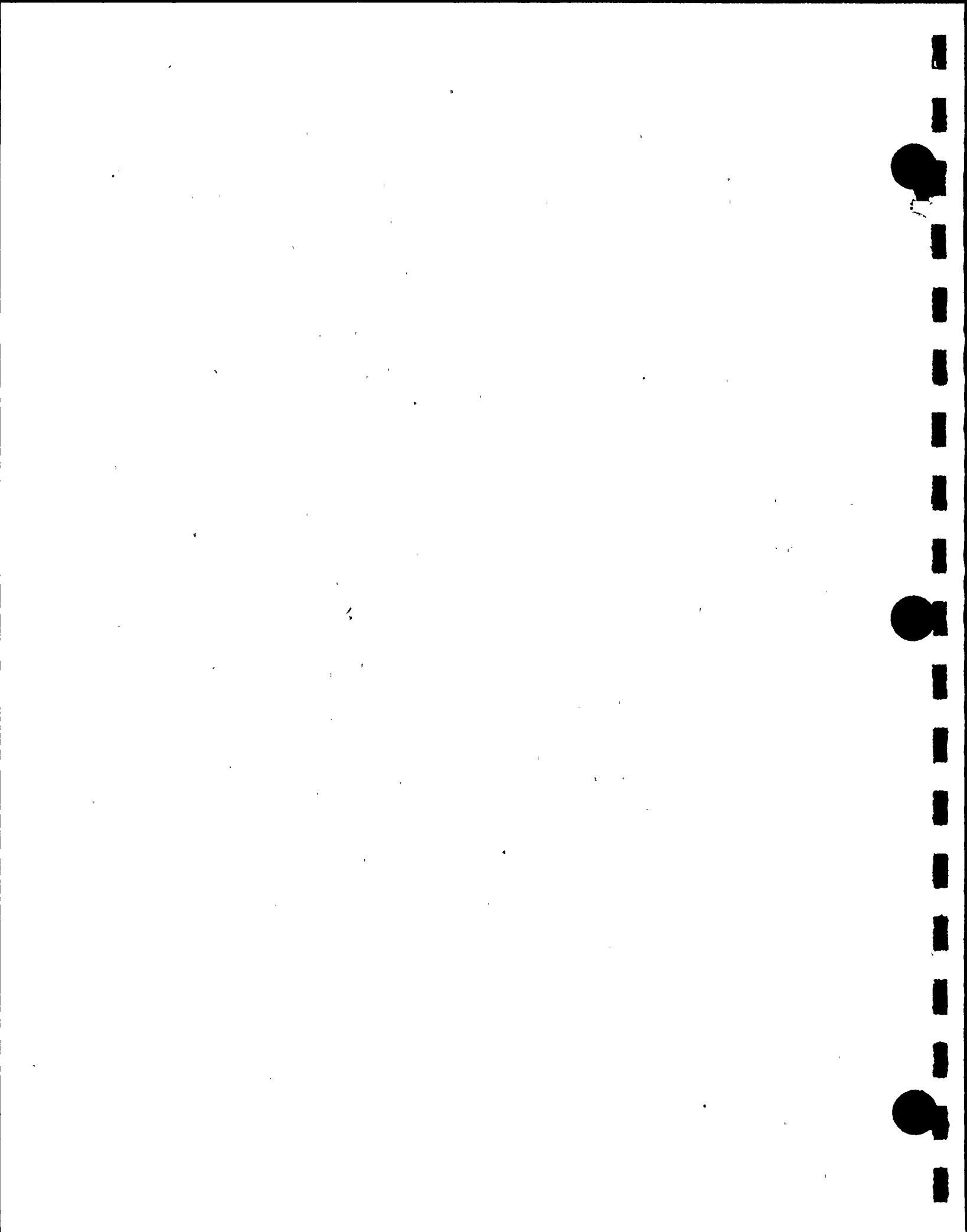


FIGURE 6.5.6 RACK DEGREES OF FREEDOM FOR Y-Z PLANE BENDING



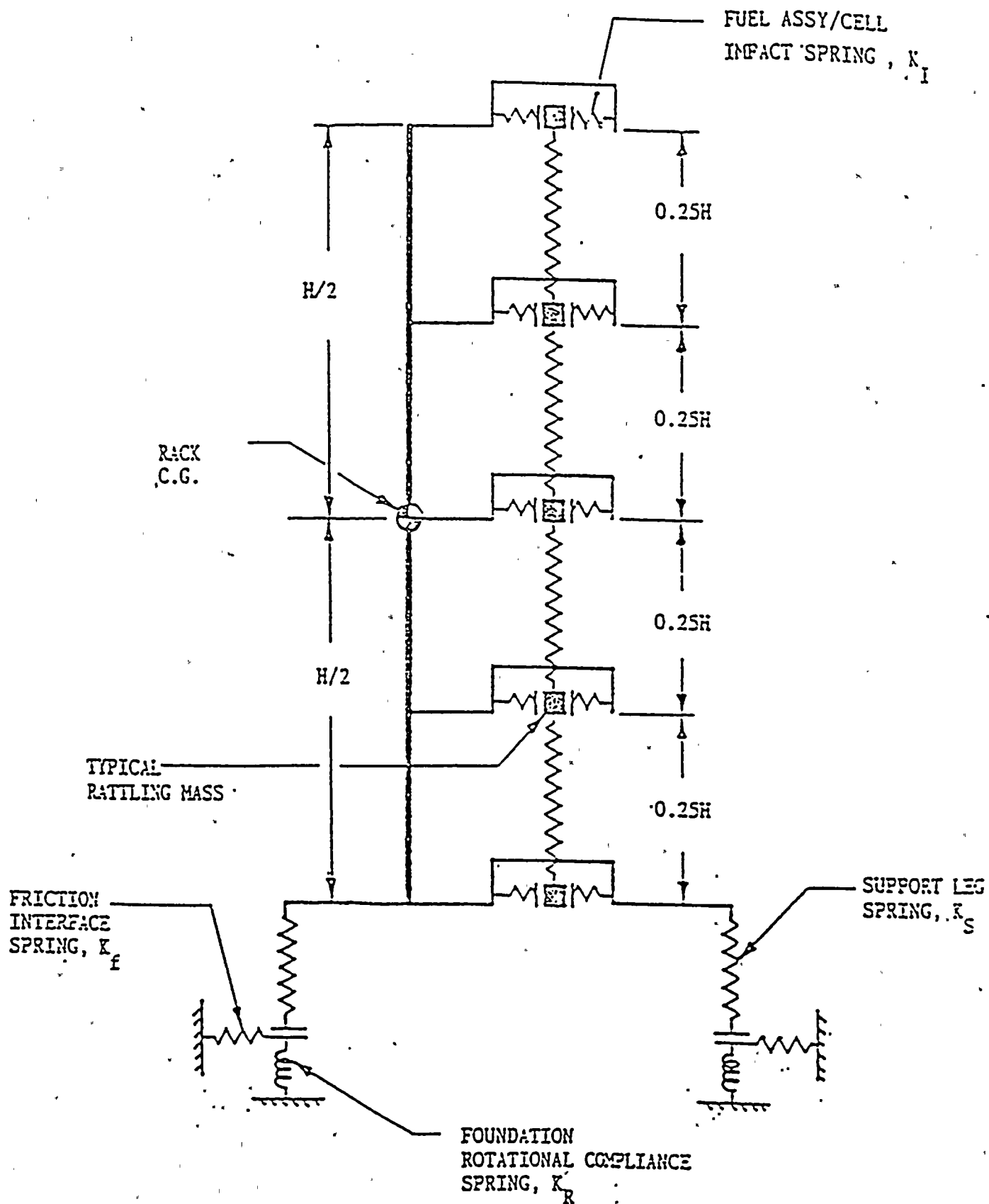
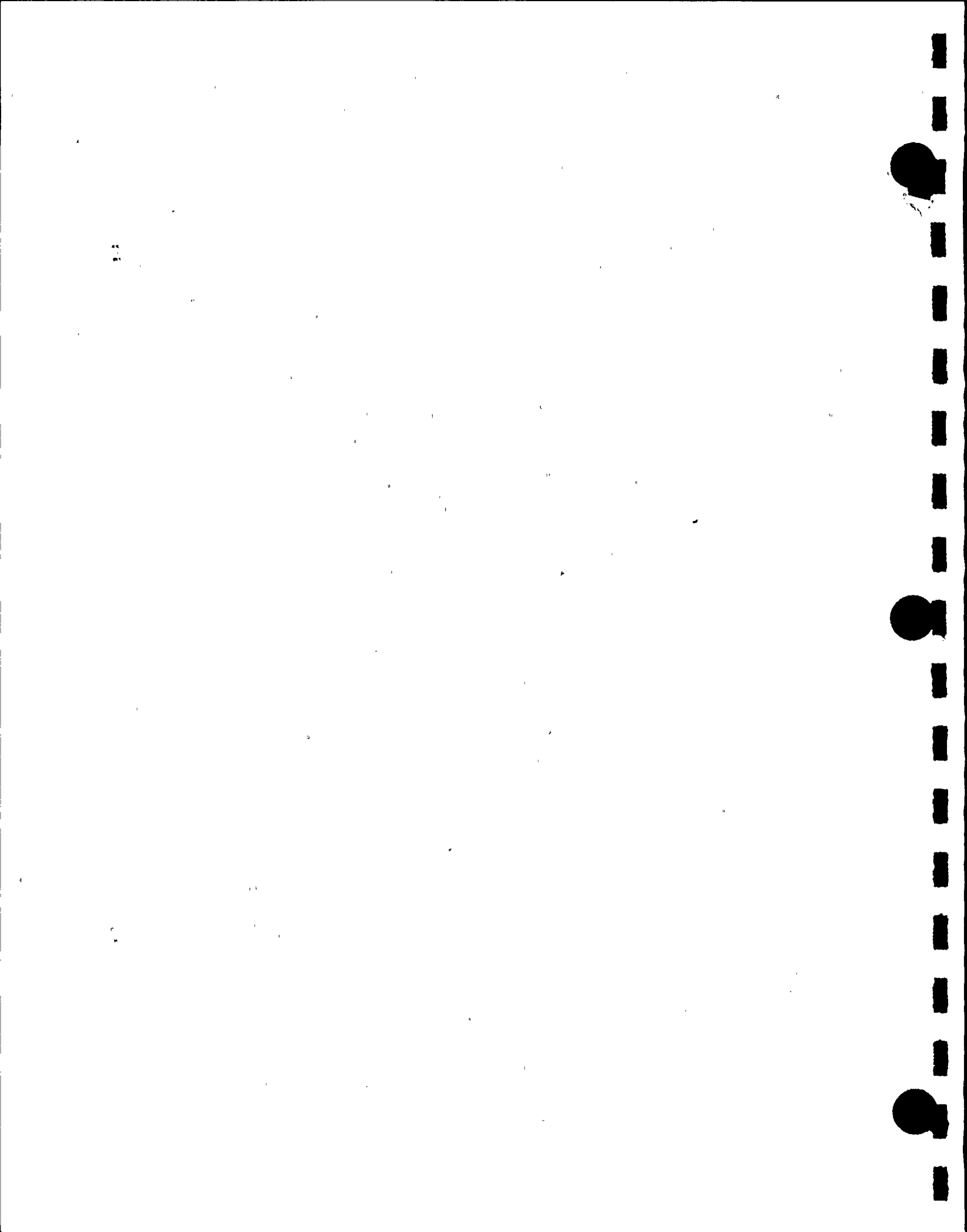


FIGURE 6.6.1 2-D VIEW OF RACK MODULE



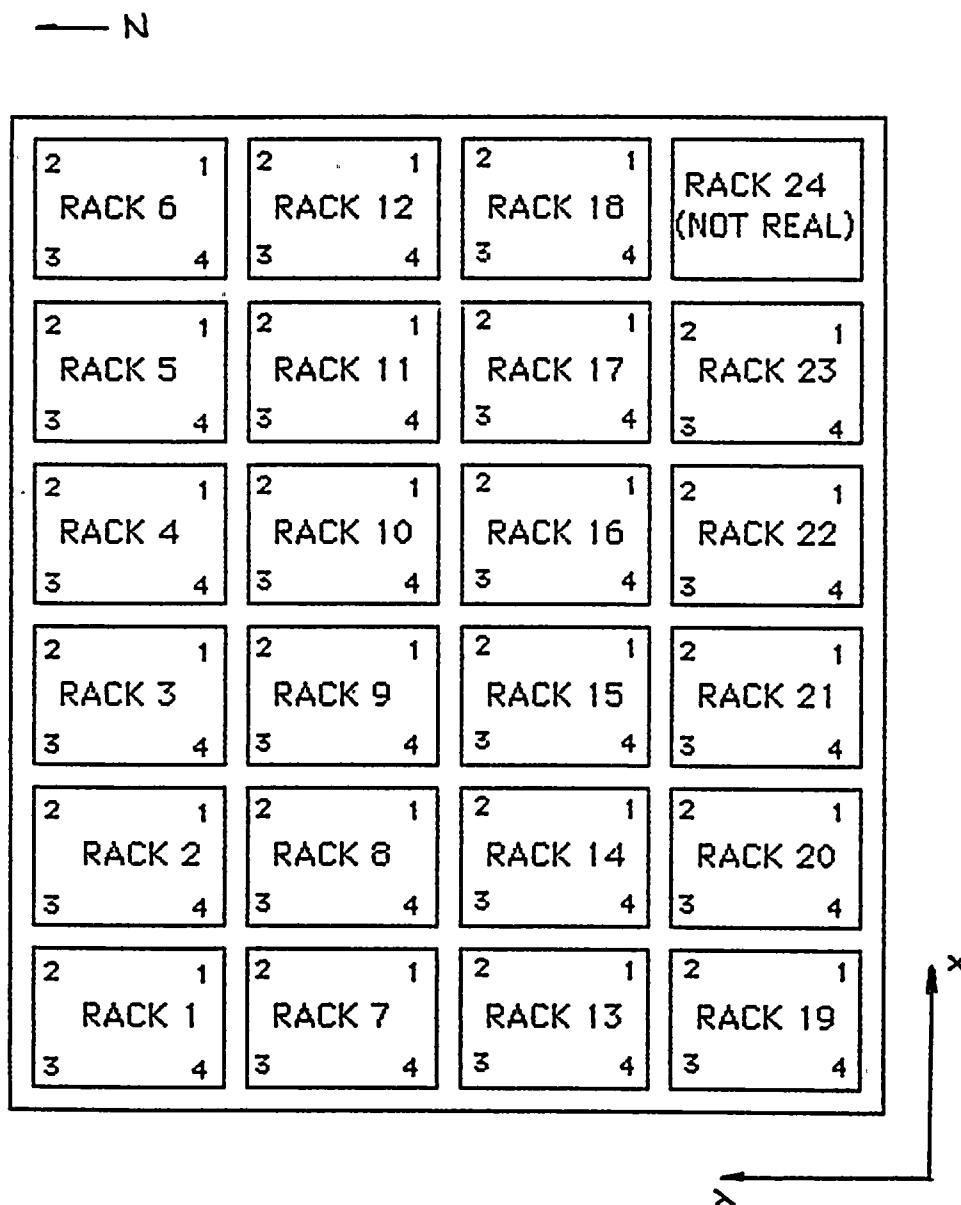
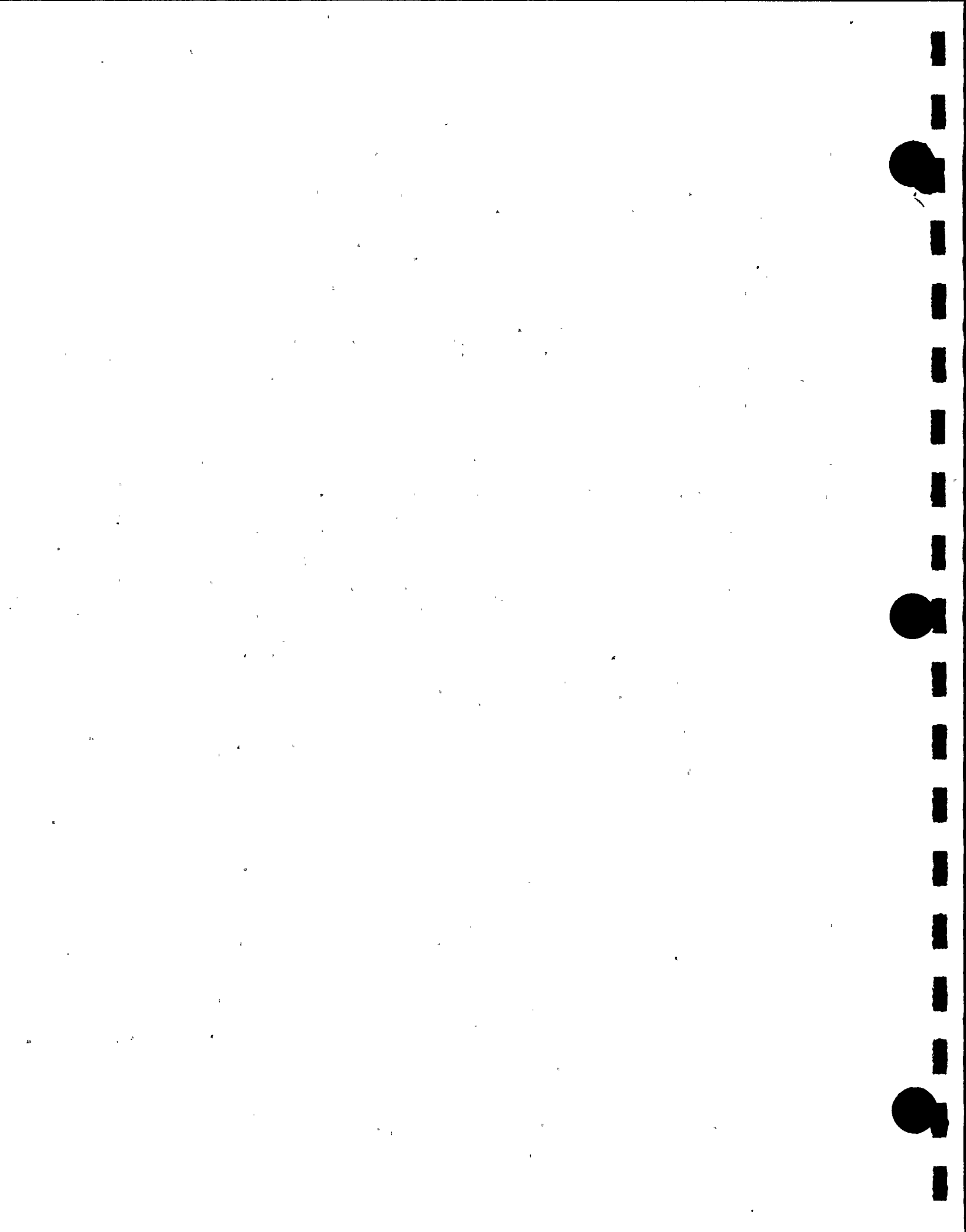


FIGURE 6.14.1 RACK AND FOOT PEDESAL NUMBERING FOR
D. C. COOK MULTI-RACK MODEL



6-73

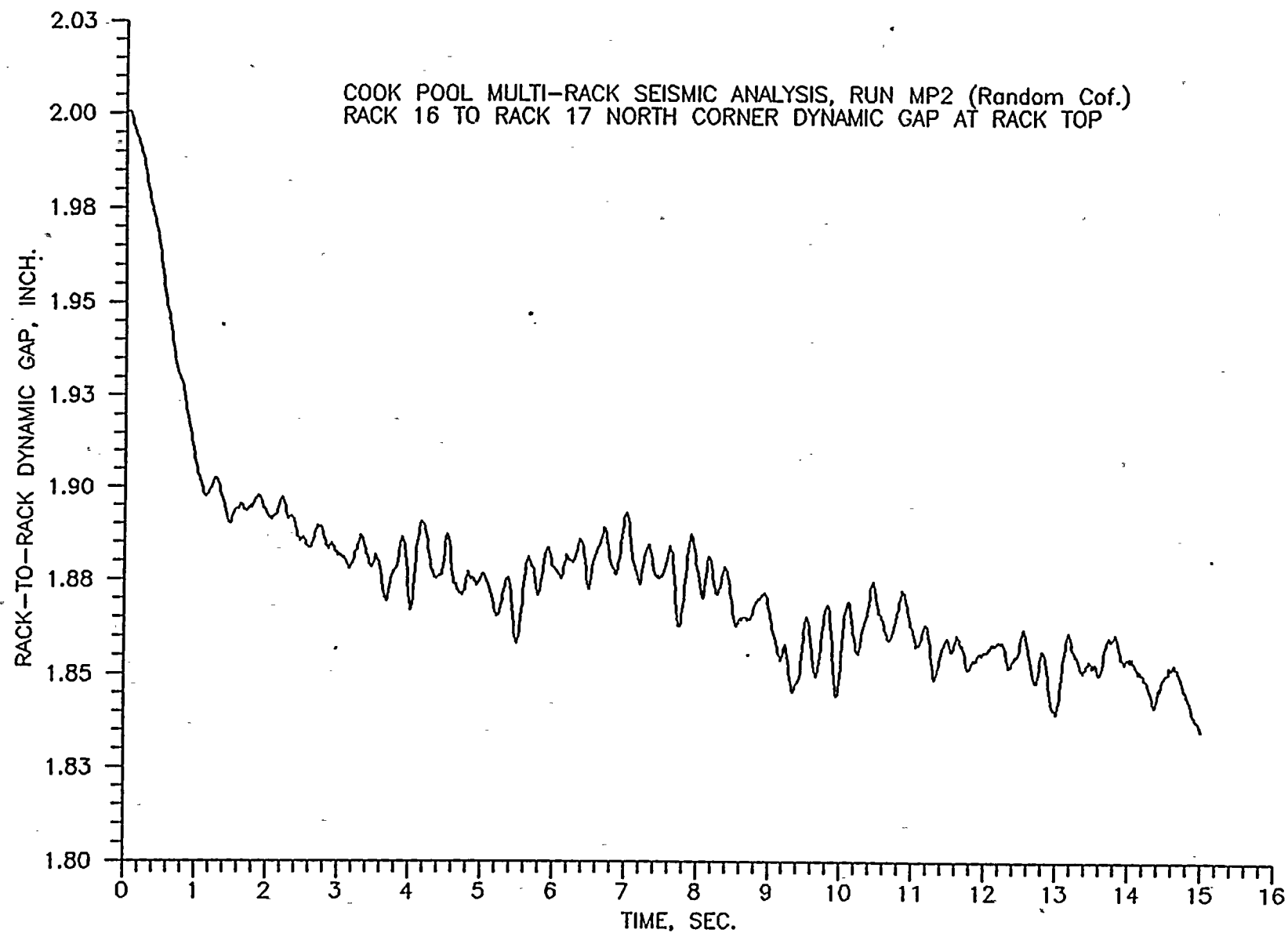
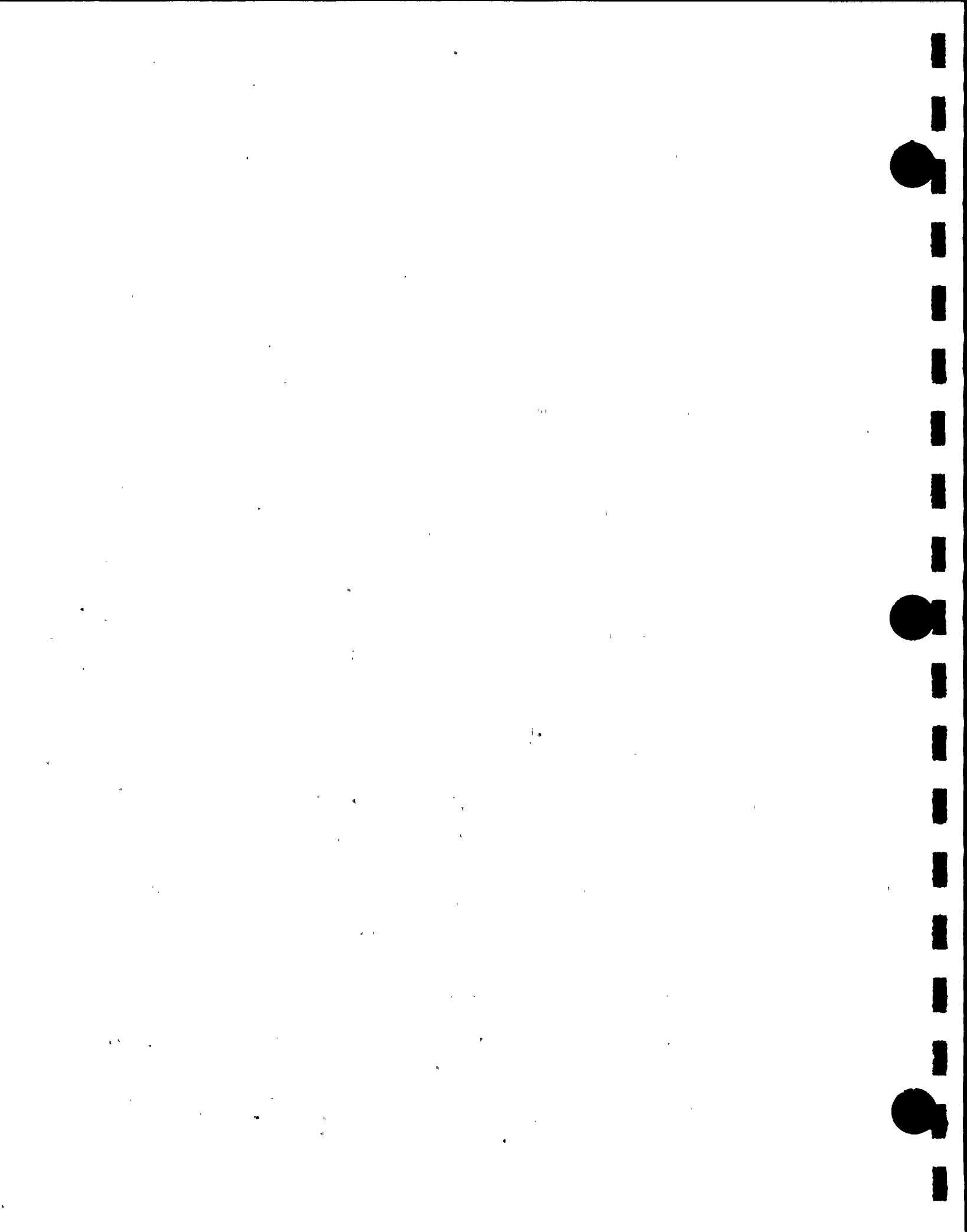


FIGURE 6.14.2



6-74

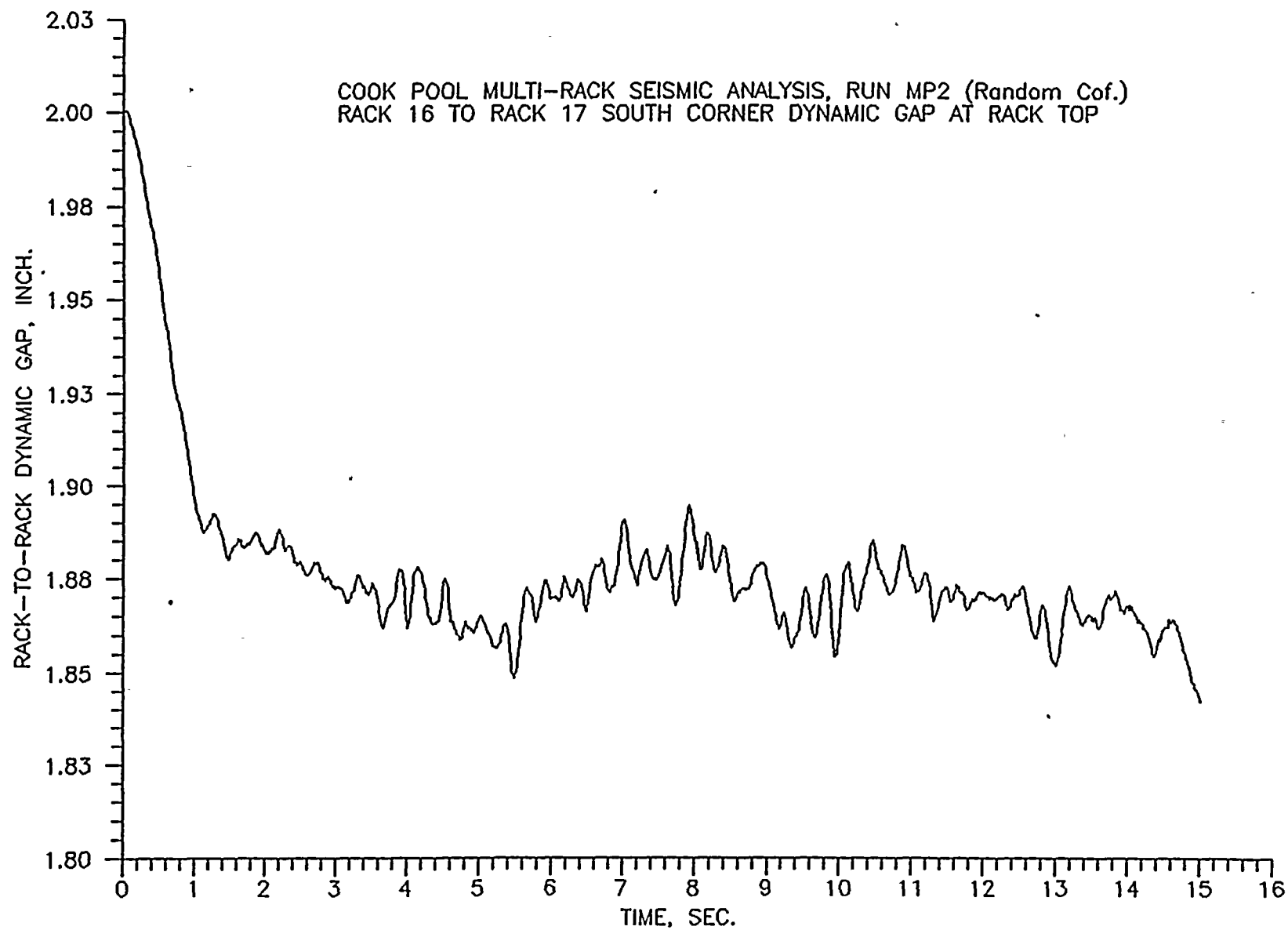
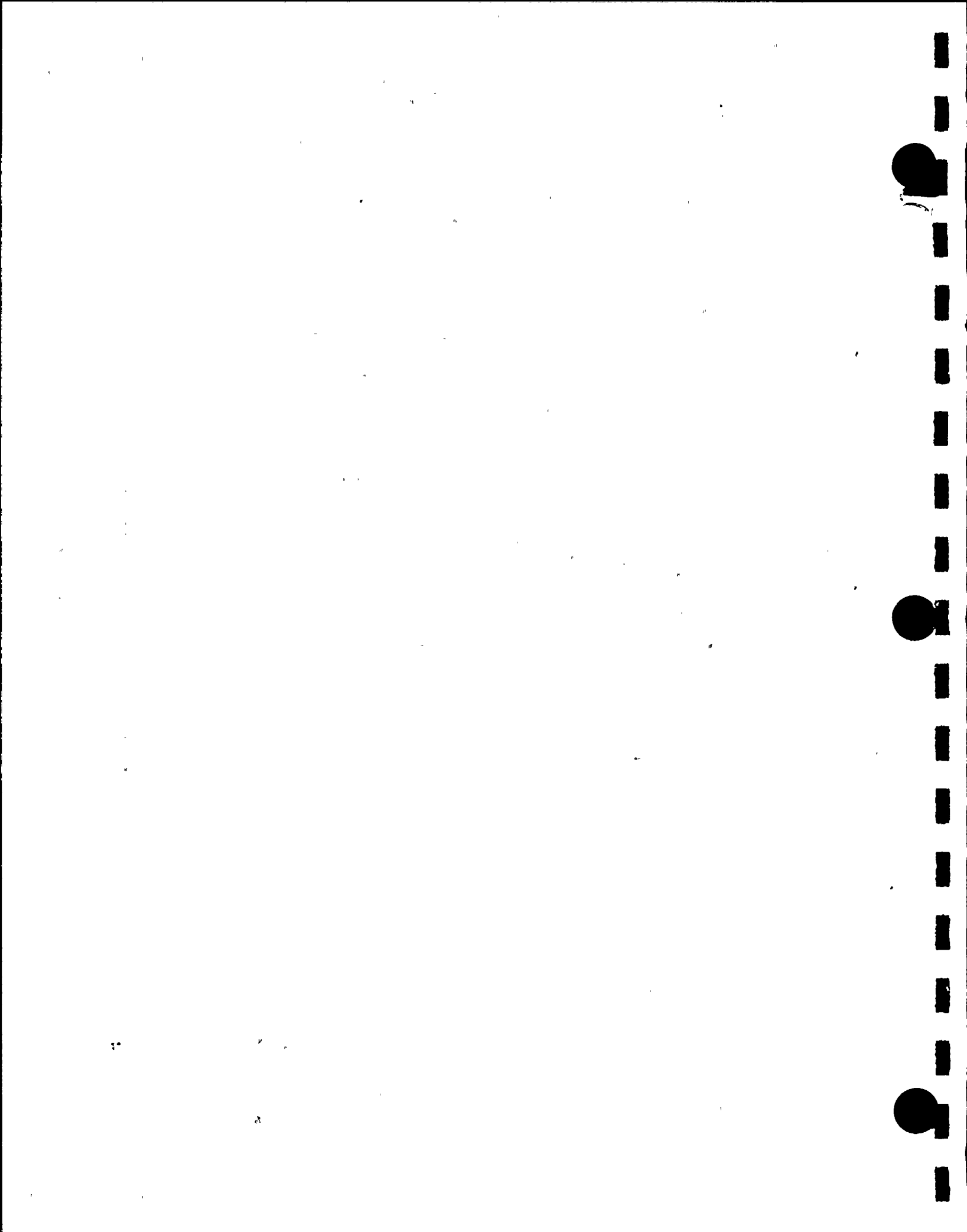


FIGURE 6.14.3



SL-9

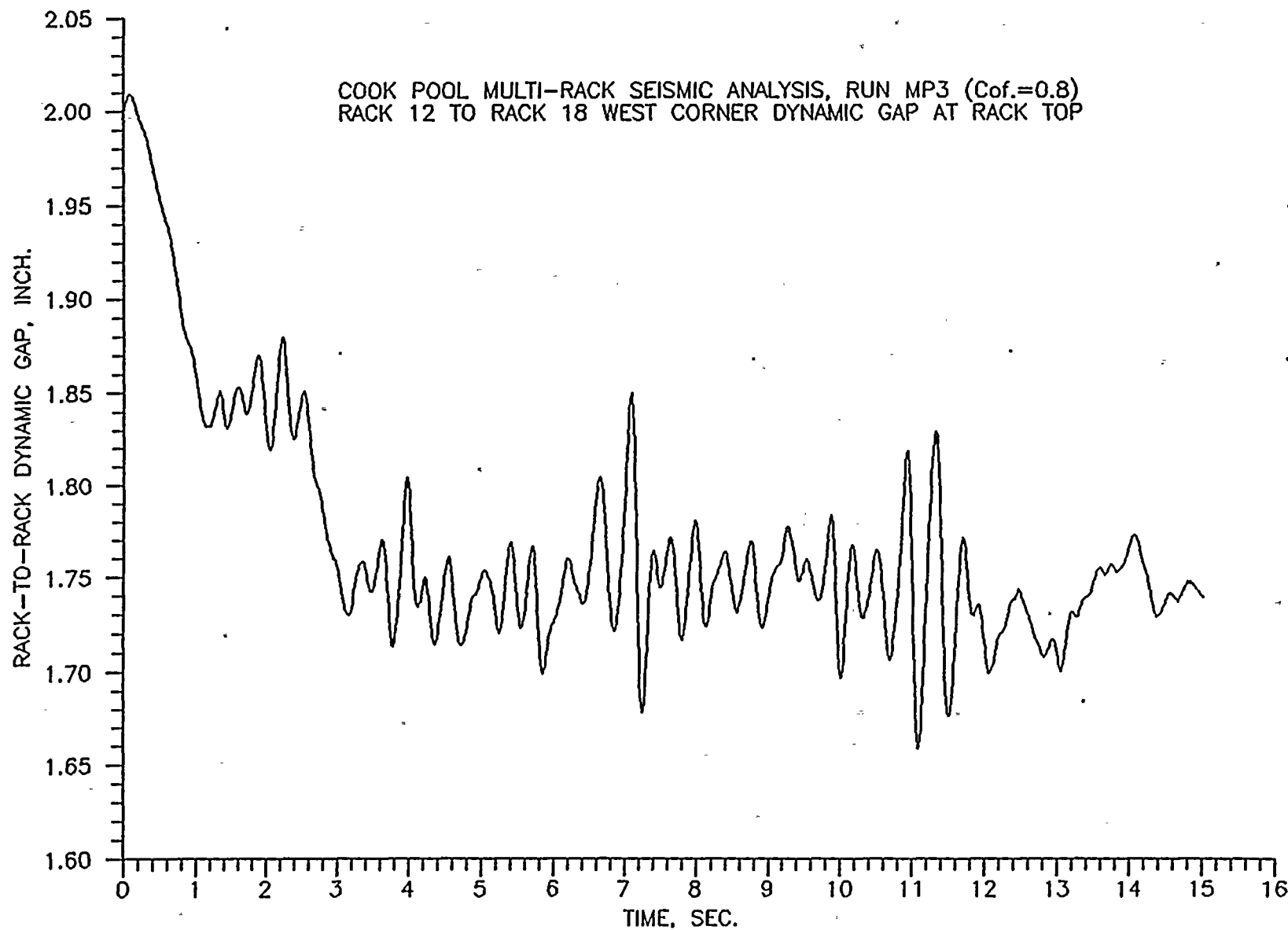


FIGURE 6.14.4



97-9

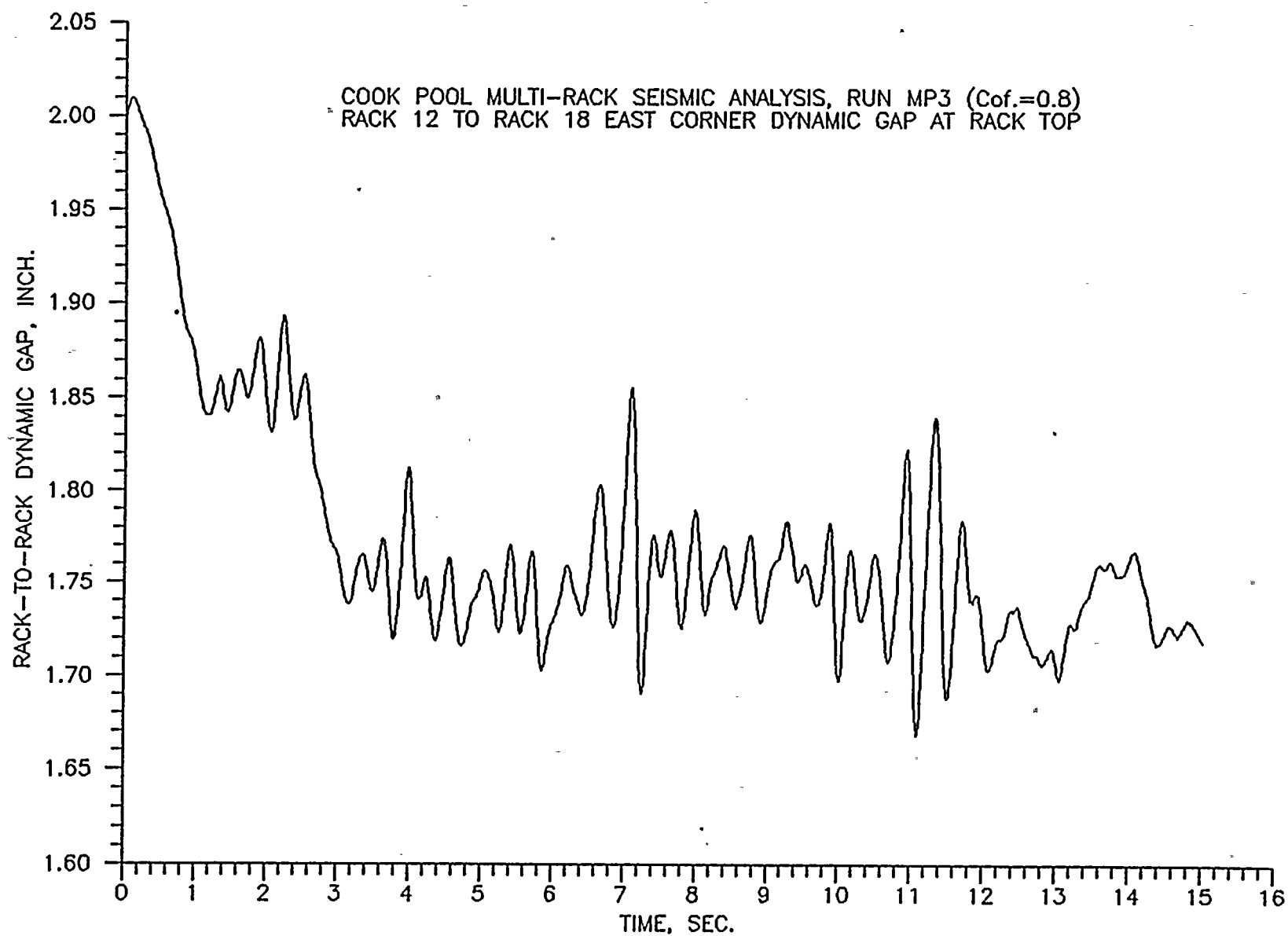


FIGURE 6.14.5



7.0 ACCIDENT ANALYSIS AND MISCELLANEOUS STRUCTURAL EVALUATIONS

7.1 Introduction

This section provides results of accident analyses performed to demonstrate regulatory compliance of the new fuel racks.

There are several types of accidents which could potentially affect the spent fuel storage pool. Installation of the proposed high density racks will enable the storage of increased amounts of spent fuel in the Donald C. Cook spent fuel pool. Accordingly, accidents involving the spent fuel pool have been evaluated to ensure that the proposed spent fuel pool modification does not change the present degree of assurance to public health and safety. The following accidents and miscellaneous structural evaluations have been considered:

- Refueling accident - Dropped Fuel
- Local Cell Wall Buckling
- Analysis of Welded Joints due to Isolated Hot Cell
- Crane Uplift Load

7.2 Refueling Accidents

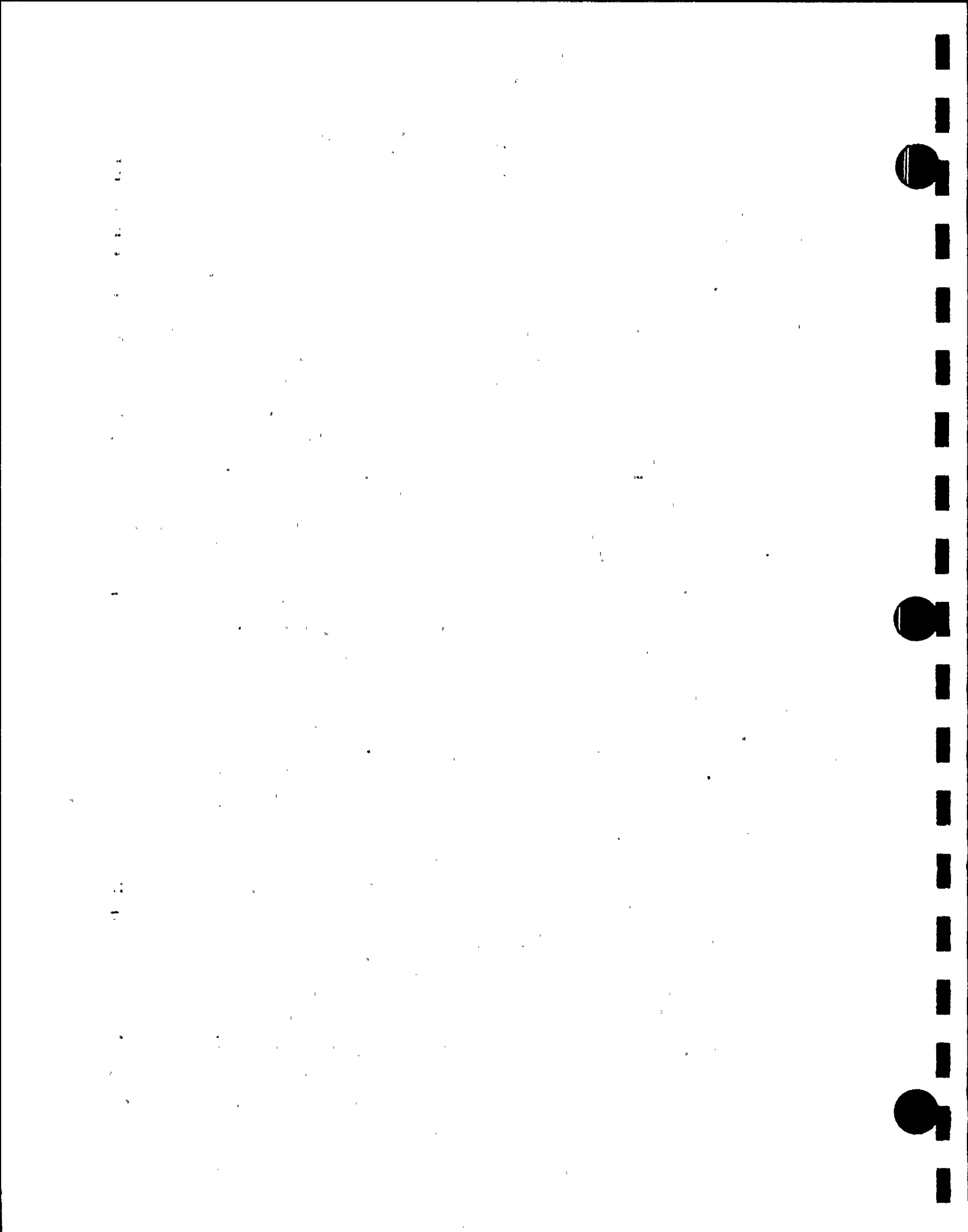
This section considers three (3) accidents associated with the handling of fuel assemblies.

7.2.1 Dropped Fuel Assembly

The consequences of dropping a new or spent fuel assembly as it is being moved over stored fuel is discussed below.

a. Dropped Fuel Assembly Accident I

A fuel assembly is dropped from 36" above the top of a storage location and impacts the base of the module. Local failure of the baseplate is acceptable; however, the rack design should ensure that gross structural failure does not occur and the subcriticality of the adjacent fuel assemblies is not violated. Calculated



results show that there will be no change in the spacing between cells. Local deformation of the baseplate in the neighborhood of the impact will occur, but the dropped assembly will be contained and not impact the liner. We show that the maximum movement of the baseplate toward the liner after the impact is less than 1.52". The load transmitted to the liner through the support by such an accident is well below that caused by seismic loads.

b. Dropped Fuel Assembly Accident II

One fuel assembly is (assumed dry weight. = 1550 lbs.) dropped from 36" above the top of the rack and impacts the top of the rack. This is a more severe condition than the currently postulated drop of 1616 lbs. from a height of 15" above the top of the rack. Permanent deformation of the rack is acceptable, but is required to be limited to the top region such that the rack cross-sectional geometry at the level of the top of the active fuel (and below) is not altered. Analysis shows that although local deformation occurs, it is confined to a region above the active fuel area. The region of permanent deformation is to a depth 5.34" below the top of the rack.

c. Dropped Fuel Assembly Accident III.

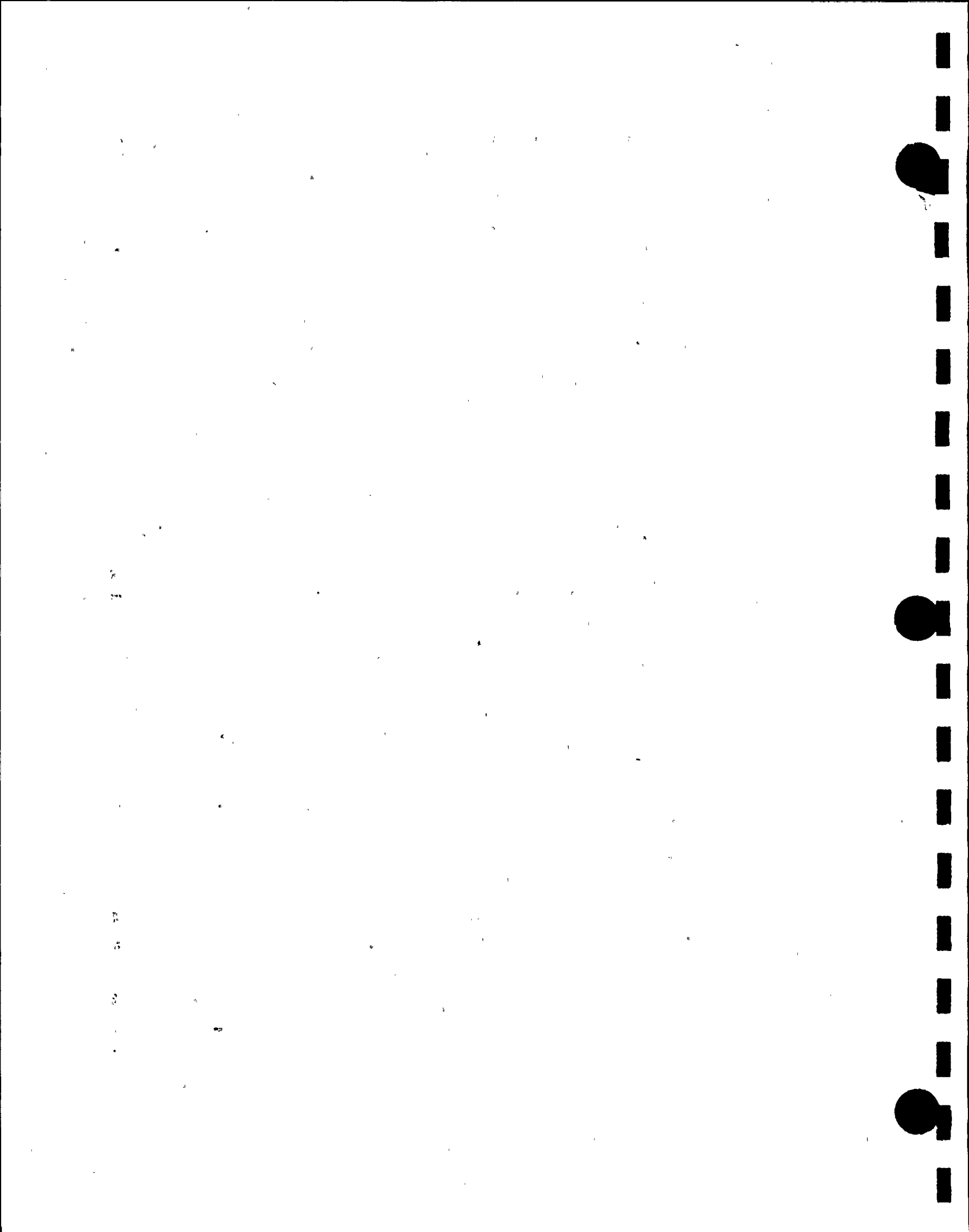
This postulated accident is identical to (b) above except that the fuel assembly is assumed to drop in an inclined manner on top of the rack. Analyses show that the straight drop case (case b above) bounds the results.

7.3 Local Buckling of Fuel Cell Walls

This subsection and the next one presents details on the secondary stresses produced by buckling and by temperature effects.

The allowable local buckling stresses in the fuel cell walls are obtained by using classical plate buckling analysis. The following formula for the critical stress has been used based on a width of cell "b": (See Figure 7.3.1.)

$$\sigma_{cr} = \frac{\beta \pi^2 E t^2}{12 b^2 (1 - \mu^2)}$$



where $E = 27.9 \times 10^6$ psi, $\mu = 0.3$, (Poisson's ratio), $t = .075$ ", $b = 8.75$ ". The factor β is suggested in (Ref. 7.3.1) to be 4.0 for a long panel.

For the given data

$$\sigma_{cr} = 7411 \text{ psi}$$

It should be noted that this stability calculation is based on the applied stress being uniform along the entire length of the cell wall. In the actual fuel rack, the compressive stress comes from consideration of overall bending of the rack structures during a seismic event and as such is negligible at the rack top and maximum at the rack bottom. It is conservative to apply the above equation to the rack cell wall if we compare σ_{cr} with the maximum compressive stress anywhere in the cell wall. As shown in Section 6, the local buckling stress limit of 7411 psi is not violated anywhere in the body of the rack modules, since the maximum compressive stress in the outermost cell is $\sigma = 3585$ psi. (From Table 6.11.1 for $R6 = .239$, the stress at the base of the rack under combined direct plus bending loads is $\sigma = R6 \times$ allowable stress).

7.4 Analysis of Welded Joints in Rack due to Isolated Hot Cell

In this subsection, in-rack welded joints are examined under the loading conditions arising from thermal effects due to an isolated hot cell.

A thermal gradient between cells will develop when an isolated storage location contains a fuel assembly emitting maximum postulated heat, while the surrounding locations are empty. We can obtain a conservative estimate of weld stresses along the length of an isolated hot cell by considering a beam strip (a cell wall) uniformly heated and restrained from growth along one long



edge. The strip is subject to a uniform temperature rise $\Delta T = 59.66^\circ\text{F}$. The temperature rise has been calculated from the difference of the maximum local water temperature and bulk water temperature in the spent fuel pool. (see Tables 5.5.1 and 5.7.1). Then, using a shear beam theory, we can calculate an estimate of the maximum value of the average shear stress in the strip (see Figure 7.4.1).

The final result for wall maximum shear stress, under conservative restraint assumptions, is given as

$$\tau_{\max} = \frac{E \alpha T}{.931}$$

where $\alpha = 9.5 \times 10^{-6} \text{ in/in } ^\circ\text{F}$

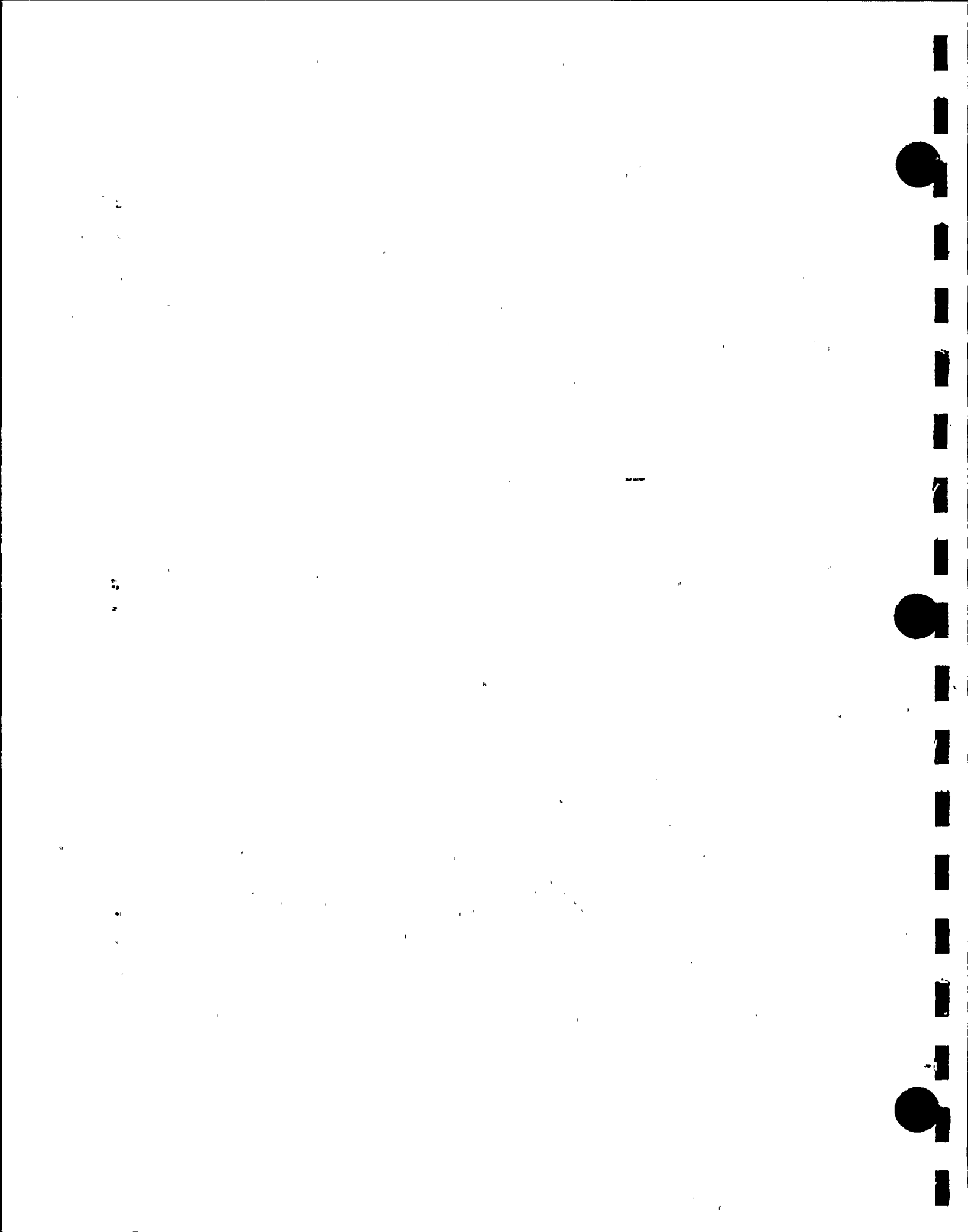
Therefore, we obtain an estimate of maximum weld shear stress in an isolated hot cell as

$$\tau_{\max} = 16984.8$$

Since this is a secondary thermal stress, it is appropriate to compare this to the allowable weld shear stress for a faulted event $\tau < .42S_u = 29820 \text{ psi}$. In the fuel rack, this maximum stress occurs near the top of the rack and does not interact with any other critical stress.

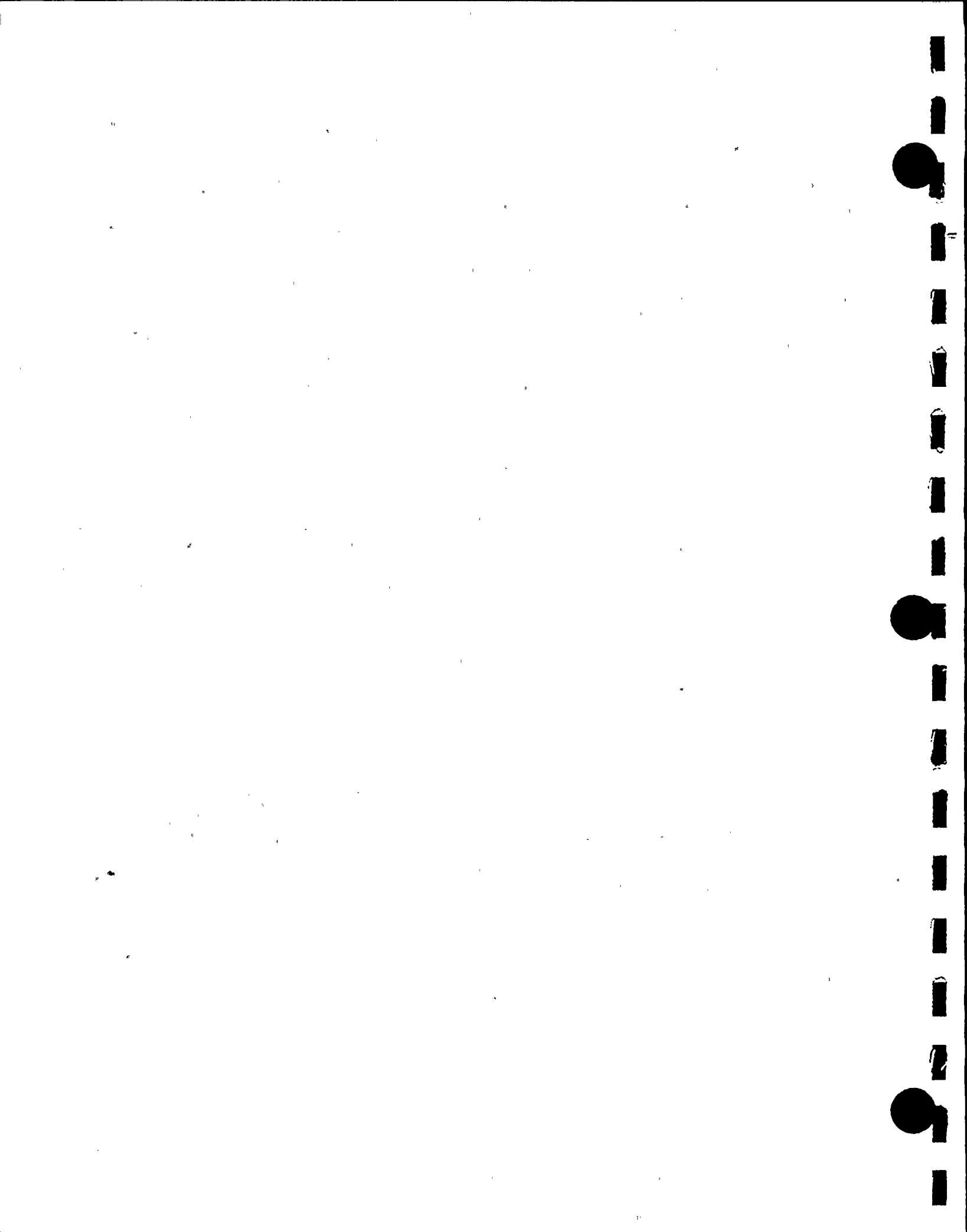
7.5 Crane Uplift Load of 3000 lb.

A local uplift load of 3000 lb. (UFSAR limit is 2950 lb.) will not induce any uplift stresses in the rack which are more severe than the limiting conditions discussed in the foregoing. This choice of load should be an upper bound load on the maximum load that can be applied to a struck fuel assembly during removal.



7.6 References for Section 7

- 7.3.1 "Strength of Materials", S.P. Timoshenko, 3rd Edition, Part II, pp 194-197 (1956).



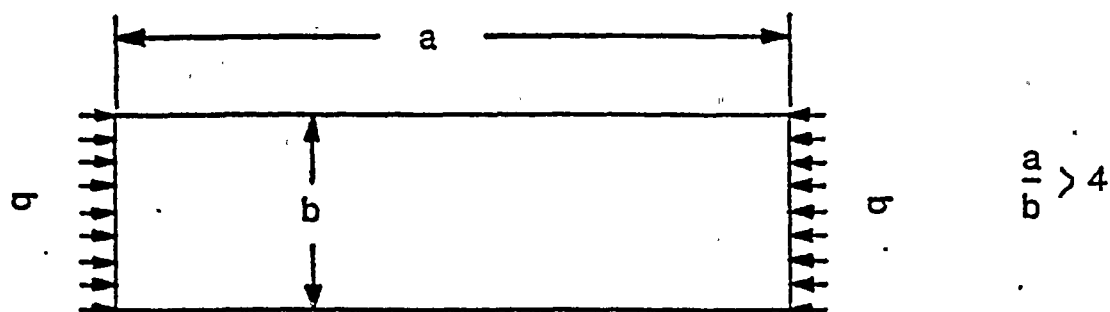


FIGURE 7.3.1

LOADING ON RACK WALL

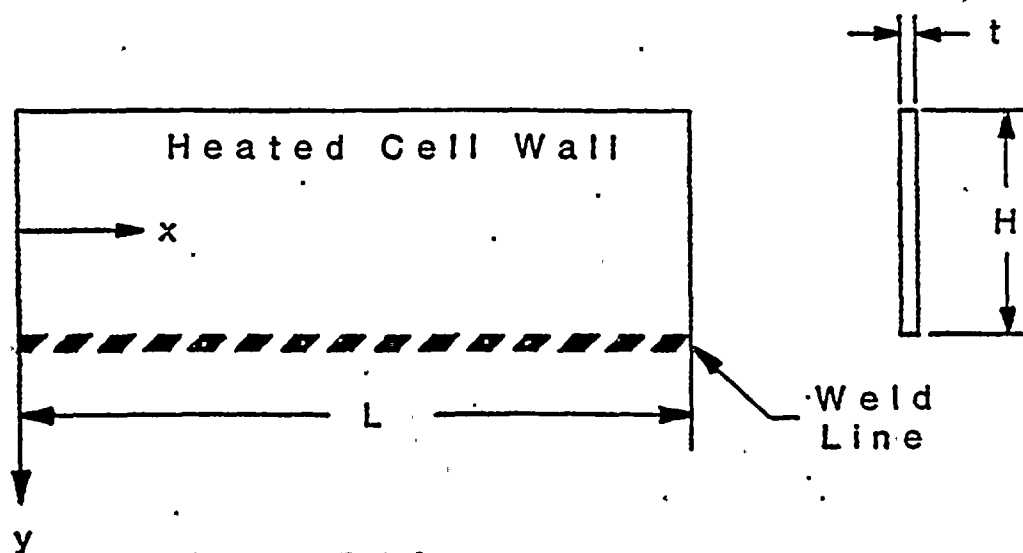
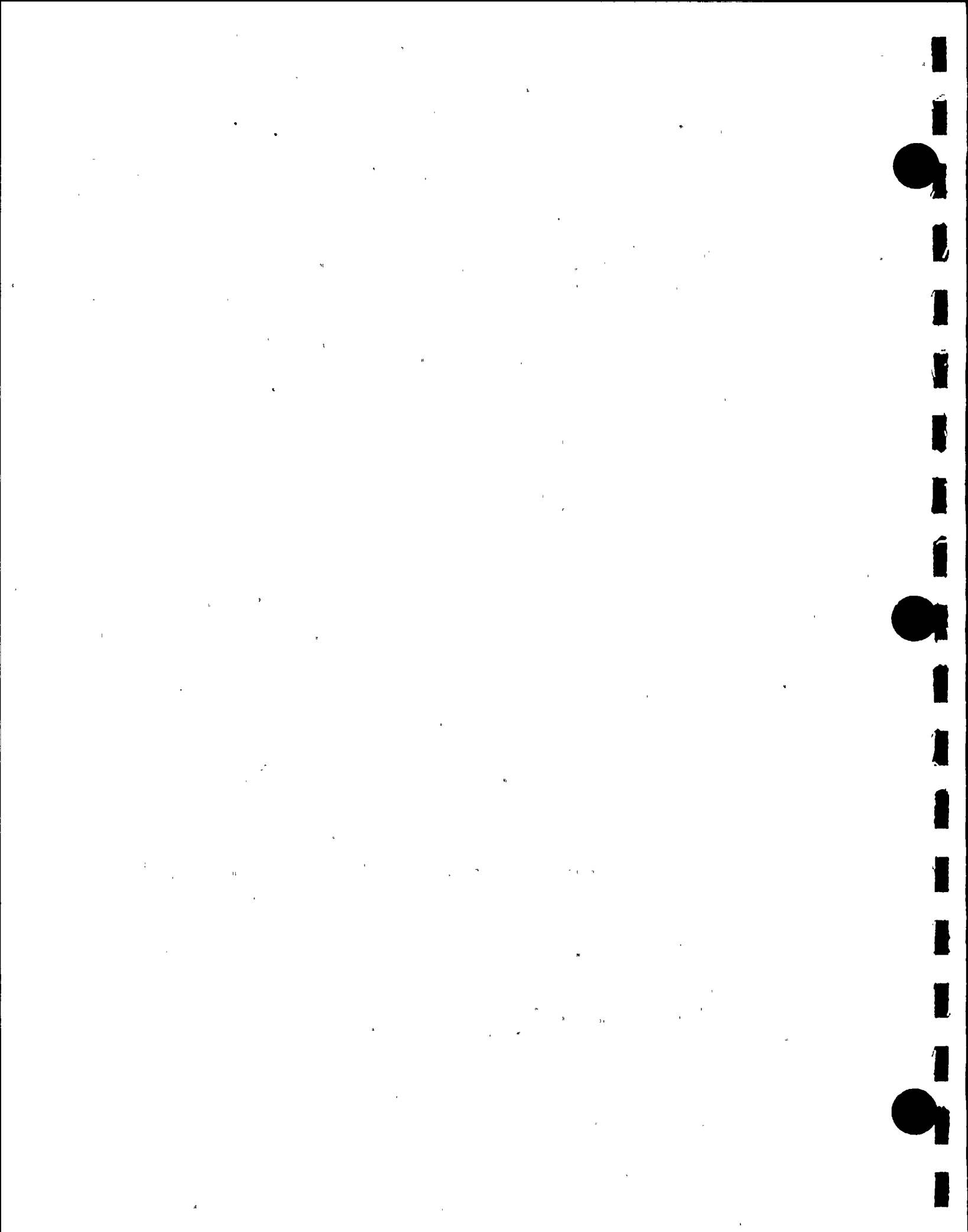


FIGURE 7.4.1

WELDED JOINT IN RACK



8.0 STATIC AND DYNAMIC ANALYSIS OF FUEL POOL STRUCTURE

8.1 Introduction

The Donald C. Cook spent fuel pool is a safety related, seismic category I, reinforced concrete structure. In this section an abstract of the analysis to demonstrate the structural adequacy of the pool structure is presented. The object of the analysis is to demonstrate the compliance of the pool slab and confining walls to the applicable design codes and to NRC regulations for the condition of increased loadings due to high density fuel storage. The loading on the pool structure is produced by the following discrete components:

a) Static Loading

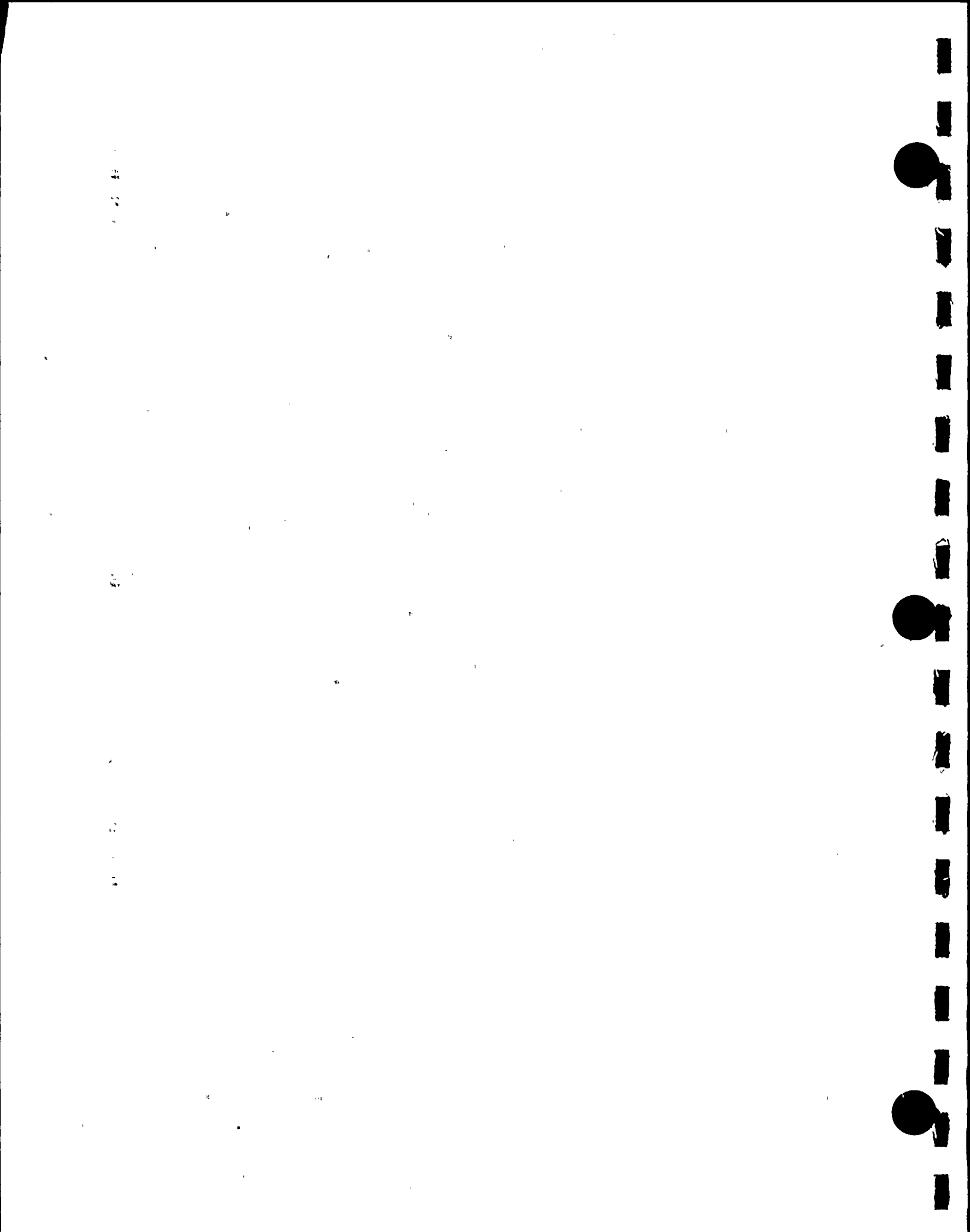
- 1) Dead weight of pool structure plus pool water (including hydraulic pressure on the pool walls).
- 2) Dead weight of the rack modules and fuel assemblies stored therein.

b) Dynamic Loading

- 1) Vertical loads transmitted by the rack support pedestals to the slab during a DBE or OBE event.
- 2) Inertia loads due to the slab, pool walls and contained water mass which arise during a DBE or OBE event.

c) Thermal Loading

- 1) Mean temperature rise and temperature gradient across the pool slab and the pool walls due to temperature differential between the pool water and the atmosphere external to the slab and walls.

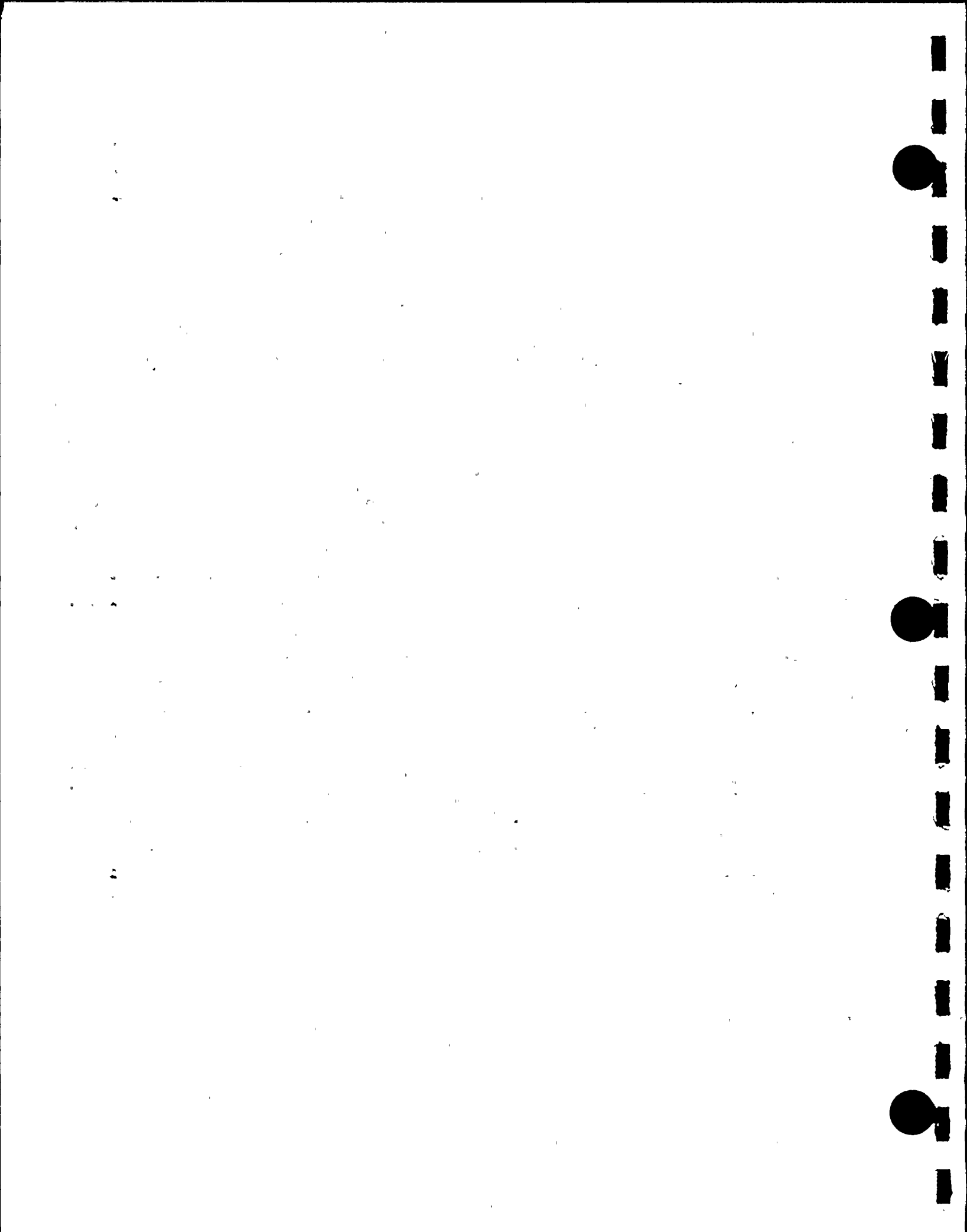


The spent fuel pool is analyzed using the finite element method. The results for the above load components are combined using factored load combinations mandated by NUREG-0800, the Standard Review Plan (SRP), Section 3.8.4 (Ref. 8.1.1). It is demonstrated that for the critical factored load combinations, structural integrity is maintained when the fuel pool is assumed to be fully loaded with high density fuel racks with all storage locations occupied by fuel assemblies. The general purpose finite element code ANSYS (Ref. 8.1.2) is utilized to perform the analysis.

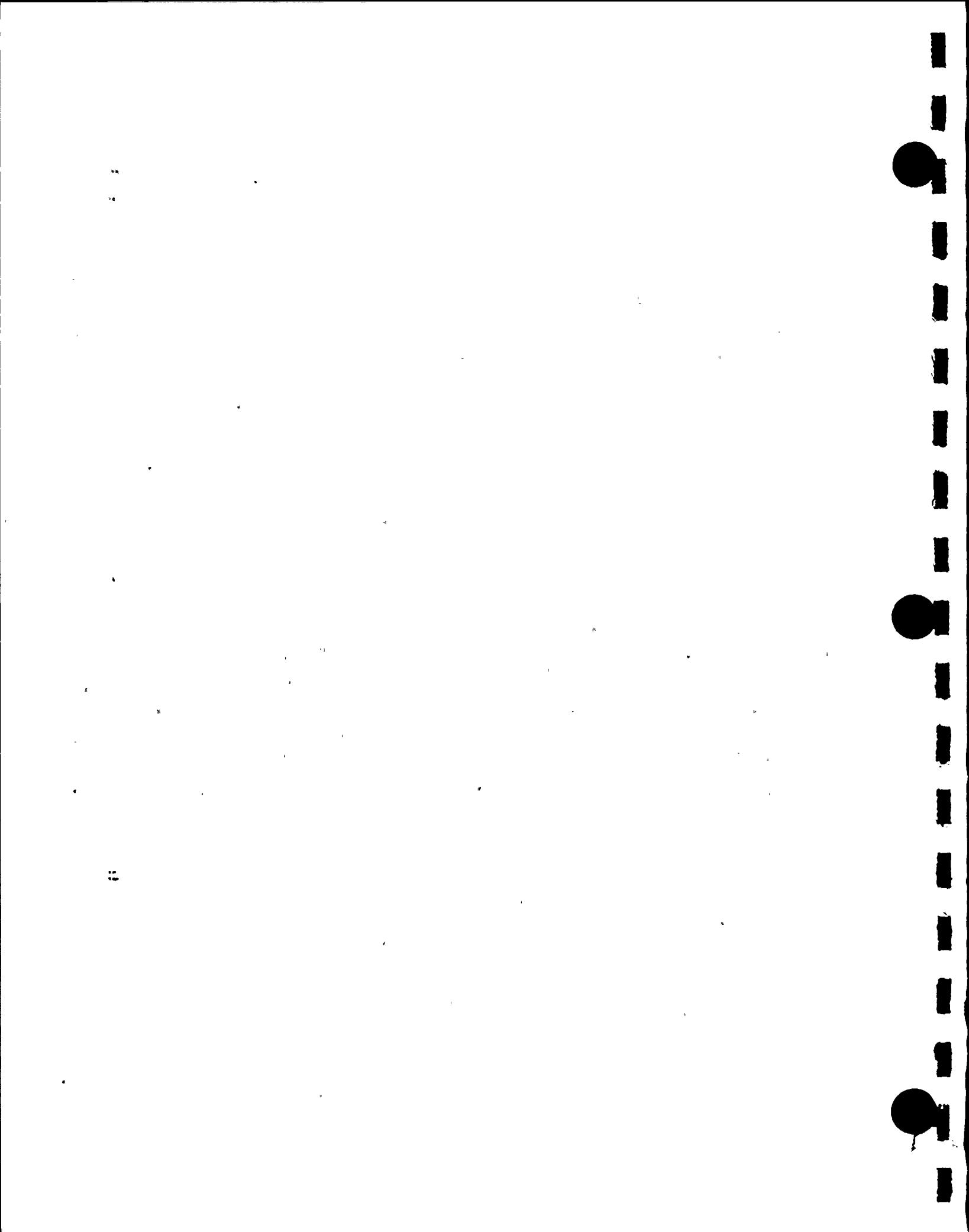
The critical regions examined are the fuel pool slab and the most critical wall sections adjoining the pool slab. Both moment and shear capacities of the critical regions are checked for structural integrity. Also evaluated is local punching integrity in the vicinity of a fuel rack bearing pad. Structural capacity evaluations are carried out in accordance with the requirements of the American Concrete Institute (ACI) (Refs. 8.1.3 and 8.1.4). In this analysis, the load factors of SRP Section 3.8.4 have been used together with the allowable concrete and reinforcement loads as called for by the American Concrete Institute. This constitutes the most conservative approach to the structural qualification of the pool structure based on a static load qualification method.

8.2 General Features of the Model

The fuel pool model is constructed using information from design basis Donald C. Cook auxiliary building structural drawings. A description of the portion of the pool modelled for analysis is given in the following.



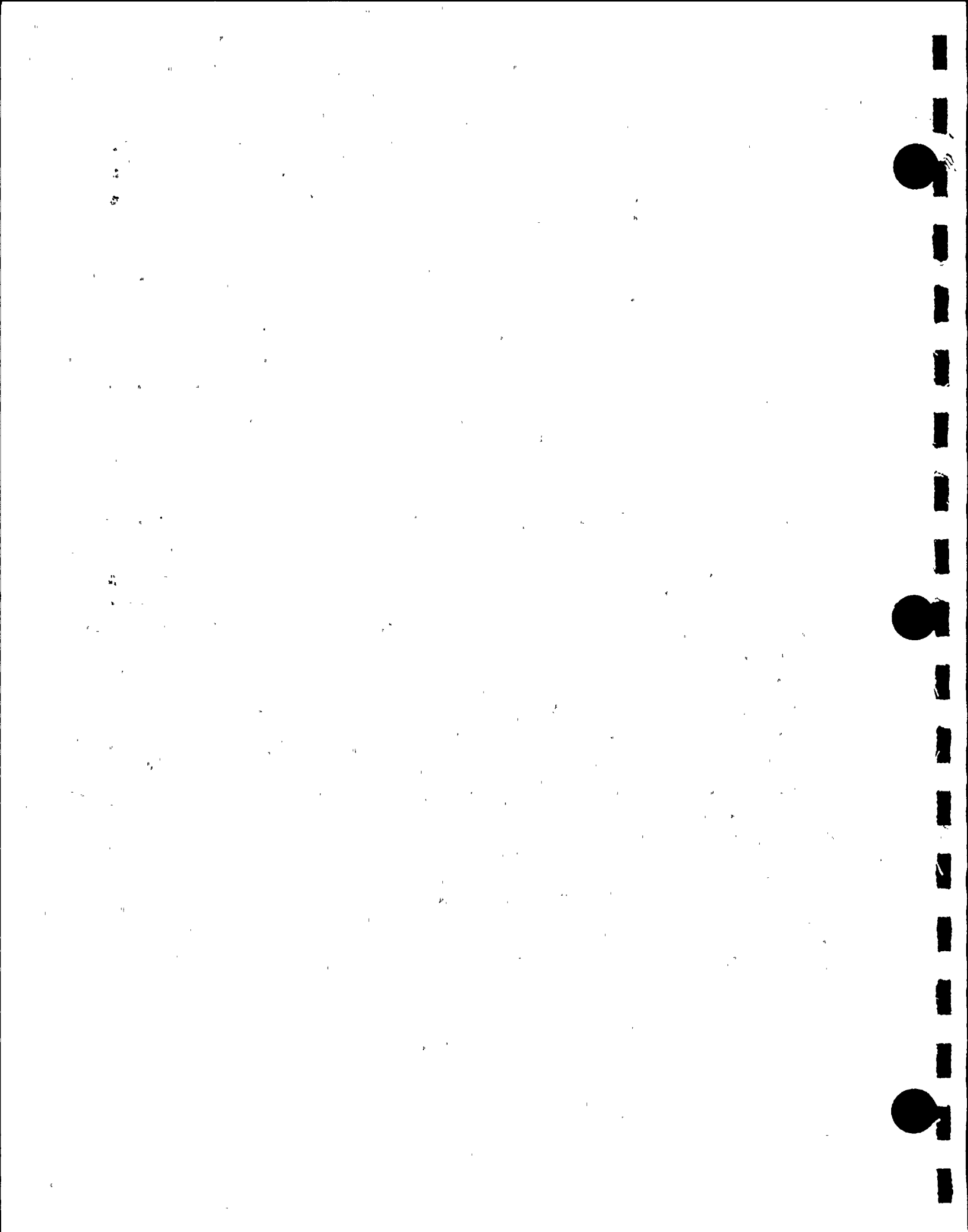
The fuel pool slab is a 5'-2 1/2" thick reinforced concrete slab with inside dimensions 39'-1 9/16" wide and 58'-3 1/8" long. The slab is located at elevation 600'-605'-2 1/2" and its long direction is aligned along the plant East-West direction. The East edge of the slab has a 5'-2" thick vertical reinforced wall which extends above the slab and is modeled to level 650'. The West edge of the slab has a 6' thick wall from level 605'-2 1/2" to level 650'. The West wall separates the fuel pool from the fuel transfer canal which is not modelled; however, the discontinuity in the wall structure in the center of the West wall is included. All wall modeling is done to level 650', and we assume free edges at this level. The North wall is a 6' thick wall extending from the slab to level 650'. The South edge of the slab has a 5' thick wall extending up to level 650'. It is clear from the above description that the South wall has the largest length to thickness ratio, and therefore, may represent a limiting condition of structural strength. The foundation mat is at elevation 584' and the pool slab and upper walls are supported on the foundation mat by walls and columns around the periphery. The North edge of the slab is supported by a continuous 3'-0" thick wall, while the East edge is partially supported along its length by a 2'-6" thick wall. There are three vertical columns located at the Southeast and Southwest corner of the slab, and intermediate along the South edge. There is also a portion of a wall below the South edge at one location. The floor slab has interior vertical support provided by a 2'-0" thick vertical wall providing vertical restraint in both the North-South and East-West direction over a substantial length of slab. In addition, there is a 25' span standard W14 x 158 wide flange beam from the slab North edge supporting wall to give additional pool slab support. This propped beam is skewed toward the East 16' from the North edge.



The entire beam (the straight part plus the skewed part) is supported vertically by four TS10" x 10" square tubes. Each tubular column has also been stiffened by four 8" x 3/8" plates. Figure 8.2.1 shows a schematic of the above geometry.

The pool slab is assumed to be loaded with 23 high density fuel racks having a total of 3616 cells. For analysis purposes, each cell is assumed to contain a 1550 lb. weight fuel assembly. As noted previously, all fuel pool walls above the pool slab are assumed to have a free edge at level 650'. Lateral restraint is provided to the vertical walls at certain locations above the 605' level. This restraint simulates the effect of adjacent structure which is not included in the modelled envelope. Figures 8.2.2 and 8.2.3 show layouts of the entire 3-D finite element model. The gridwork in different regions shows the totality of elements used. Shell elements are used to model the slab and walls, while beam elements are used to model the columns.

The finite element model is constructed using the ANSYS classical shell element STIF63 and the beam element STIF44 of the ANSYS finite element code. The shell element thickness in the various regions of the structure is the actual thickness of the structure at the location. The finite element model is prepared for the analysis of both mechanical load and thermal load. The effects of the reinforced concrete (cracked or uncracked) are accounted for in the finite element model by establishing an appropriate effective modulus for each shell element and effective inertias for the column elements. Effective moduli are defined for each local in-plane axis for the shell elements. The different moduli reflect the fact that different reinforcement geometries may be used in perpendicular directions of the plate-like sections when



the different concrete section assumptions (cracked or uncracked) are applied to the slab and walls. Only major reinforcement which affects the plate and shell-like behavior of the structure is incorporated into the definition of the effective moduli; additional local reinforcement in various areas of the pool structure are neglected in the defining of the effective moduli. However, such local reinforcement is accounted for in the strength evaluation after results are obtained. The non-homogeneous nature of the reinforcement is taken into account by defining different material types as necessary to reflect the varying values of effective moduli in different regions. The concrete section assumptions (cracked or uncracked) are fully in accordance with the requirements of American Concrete Institute (Refs. 8.1.3 and 8.1.4). In accordance with Ref. 8.1.4, we assume uncracked section properties for the mechanical load analyses (including load factors). For the thermal analyses, it is shown that the thermal gradients will always yield a cracked section if the uncracked stiffness is used; therefore, an iterative solution is used to show that cracked section properties should be used for the thermal analyses.

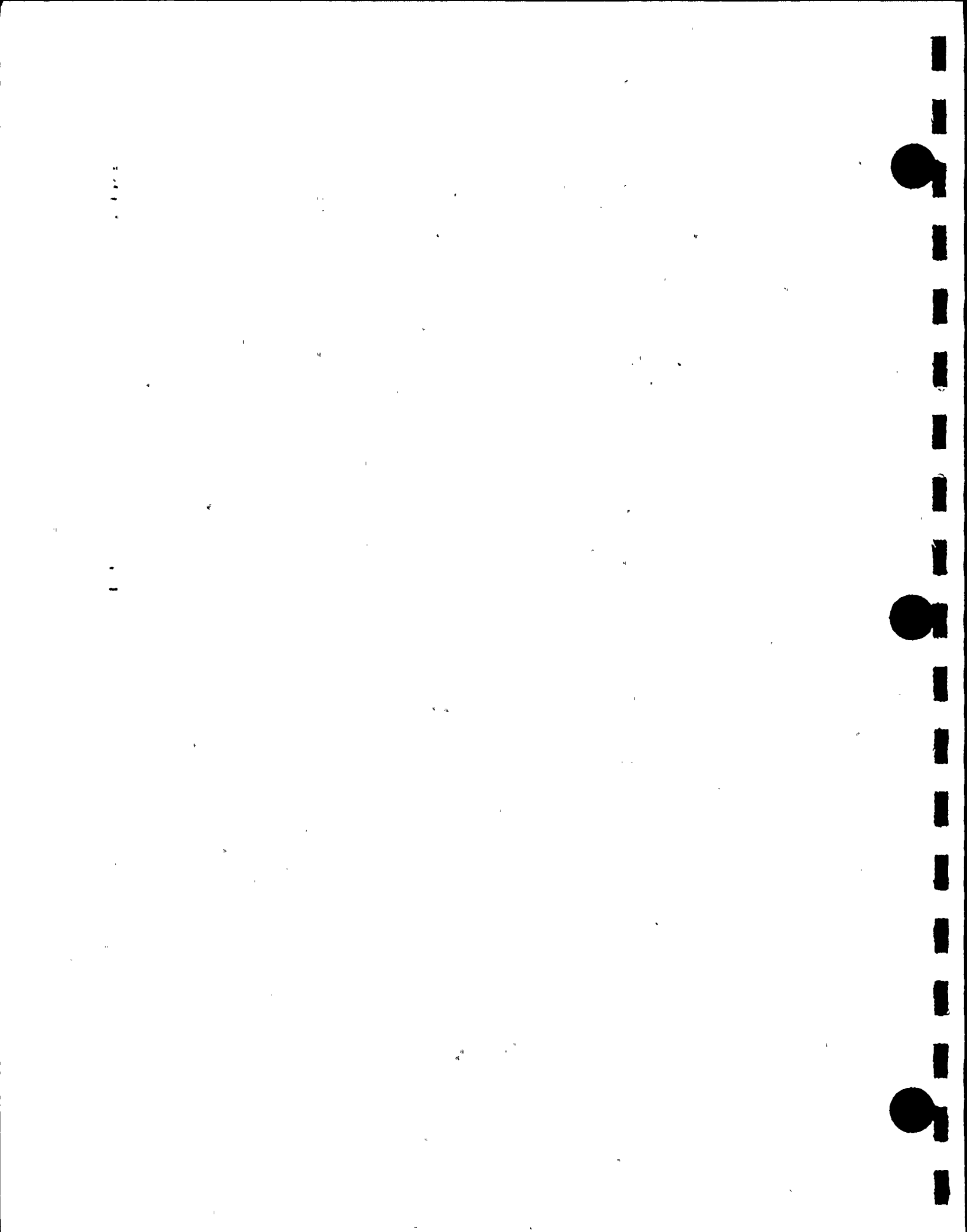
The effective properties for the elements used in the finite element model are calculated using standard procedures for reinforced concrete sections to define equivalent effective homogeneous materials having the appropriate stiffness and strength.



8.3 Loading Conditions

In order to evaluate the response due to the different load mechanisms outlined in Section 8.1, the following finite element analyses are carried out. Six loading cases are defined below which enable us to obtain the moments and shears for factored loadings by linear combination.

1. Dead loading from concrete, reinforcement and 40' of hydrostatic head. The loading is applied as a 1.0g vertical gravitational load for the structure and a surface pressure on the slab and walls for the hydrostatic head.
2. Dead loading due to weights of rack plus full fuel load. These loads are applied as a uniform static pressure applied to the slab.
3. Seismic vertical loading due to racks plus fuel load applied as an effective sustained pressure on the floor slab pedestals. The loading applied is obtained from the 3-D whole pool multi-rack analysis described in Section 6 of this report. From the results of that analysis, we take the stored time history of each pedestal load and define an effective sustained pool pressure load which yields the same total impulse over the time duration of the seismic event. The details of developing this effective sustained pressure load are presented later. We develop effective sustained vertical pressure loads for both OBE and DBE events and then perform appropriate finite element analyses.
4. Seismic horizontal loading due to structure weight (including reinforcement). The loading is applied as a 1g horizontal and vertical acceleration applied to the structure plus a hydrodynamic pressure equivalent to an acceleration of all of the water mass against the weakest wall. The acceleration level is obtained from the applicable response spectra and is taken as the peak g level on the spectra at frequencies above the lowest natural frequency for the structure. A separate ANSYS frequency analysis simulation is carried out to establish the dynamic characteristics of the structure.



5. Seismic horizontal load due to shear loads from each of the pedestals. This loading is obtained by using the static + effective dynamic loads developed for case 3 above and assuming a coefficient of friction = .8. The direction of these loads is set so as to develop stresses that maximize the load combinations necessary to satisfy structural integrity requirements discussed below. In this load case we also impose a lateral pressure on the weakest pool wall to simulate hydrodynamic effects from fluid coupling due to rack motion relative to the wall.
6. A mean temperature rise plus a thermal gradient is applied across the walls and floor slab to simulate the heating effect of the water in the pool. This gradient is calculated based on the maximum wall temperature deduced from the pool bulk temperature calculations for the licensing basis scenarios presented in Section 5 of this report.

For subsequent discussion of structural integrity checks using various mandated load combinations, we refer to the above individual finite element load cases as "case 1-6", respectively. As noted above, in addition to the static analyses using the developed finite element model, we also perform a frequency analysis of the pool structure assuming that all contained fluid is attached to the pool slab. Uncracked section properties are used here. This frequency analysis is used to determine the lowest pool structural frequencies so as to establish appropriate seismic amplifiers to apply to load cases 1 and 4. These seismic



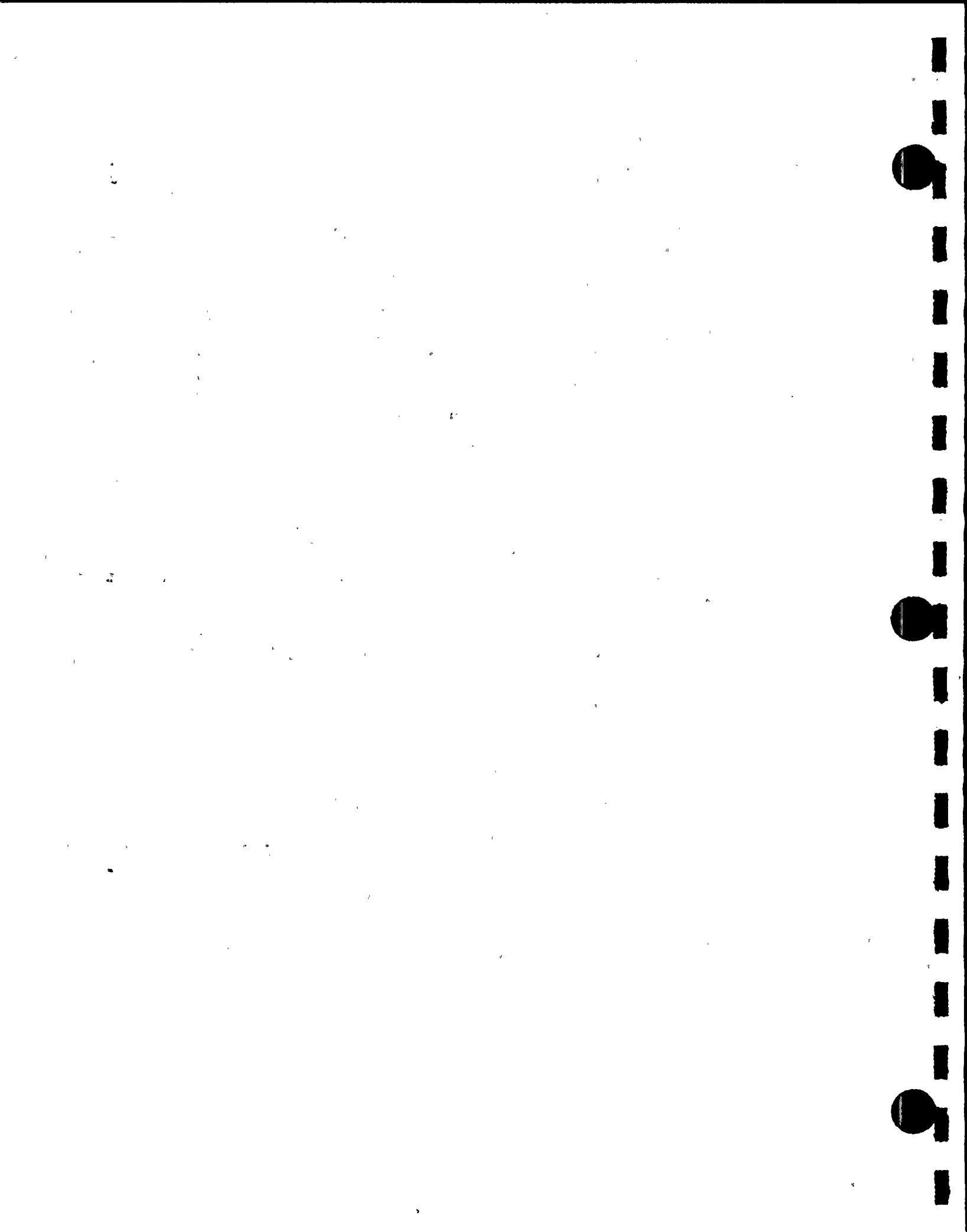
amplifiers are obtained from the response spectra of the seismic event and multiply the results of load cases 1 and 4 when forming the mandated load combinations.

As noted above, the case 3 loading involves the determination of an effective pressure load to represent the seismic load on the slab due to the racks plus fuel. The method of determination of this effective pressure is described below.

As noted previously, the Holtec 3-D dynamic simulation code DYNARACK is used to simulate the seismic response of the entire fuel pool containing multiple racks. The vertical load time history from each pedestal on each rack is saved in an archival file. For the pool slab structural analysis, which is based on static analyses, we compute an effective static load increment based on averaging of the time history. Figure 8.3.1 is used to illustrate the concept where the total pedestal load is considered as the static load (F_S in Figure 8.3.1 plus a time varying component). Note that in Figure 8.3.1 a zero load during a portion of the time means that the pedestal has lifted off. We define an effective static load for the purposes of pool static analysis and structural qualification as follows:

- a. From the archival pedestal load time history we may, at each point in time, determine the total pool load F_T by summing the total loads for each pedestal.
- b. At each point in time i , we can define the dynamic load increment for the pool as $F_T - F_S = DF_i$ where F_S now represents the total static load on the slab. We keep track of the number of time points i where $DF_i > 0$.
- c. An equivalent static pool load (seismic adder to the static pool load) is defined as

$$\text{SEISMIC ADDER} = \text{SUM}DF_i / \text{SUM}NI_i$$



where $SUMDF_I$ is the sum of all of the non zero DF_I and $SUMN_i$ is the total number of points in the time history where the dynamic pool load increment is greater than zero.

- d: In forming the appropriate load combinations mandated for structural integrity checks, the calculated "seismic adder" divided by the pool area, is used as the effective seismic pressure on the slab.

Of all loading conditions mandated in Ref. 8.1.1, the factored loads which apply to this structure and are deemed critical are:

- A. $1.4D + 1.9E$
- B. $.75 (1.4D + 1.9E + 1.7T_o)$
- C. $D + E' + T_o$

where:

D = Dead load
E' = Design Basis Earthquake (DBE)
E = Operating Basis Earthquake (OBE)
T_o = Steady State Thermal Load

The appropriate load cases are formed from the individual finite element analyses as follows:

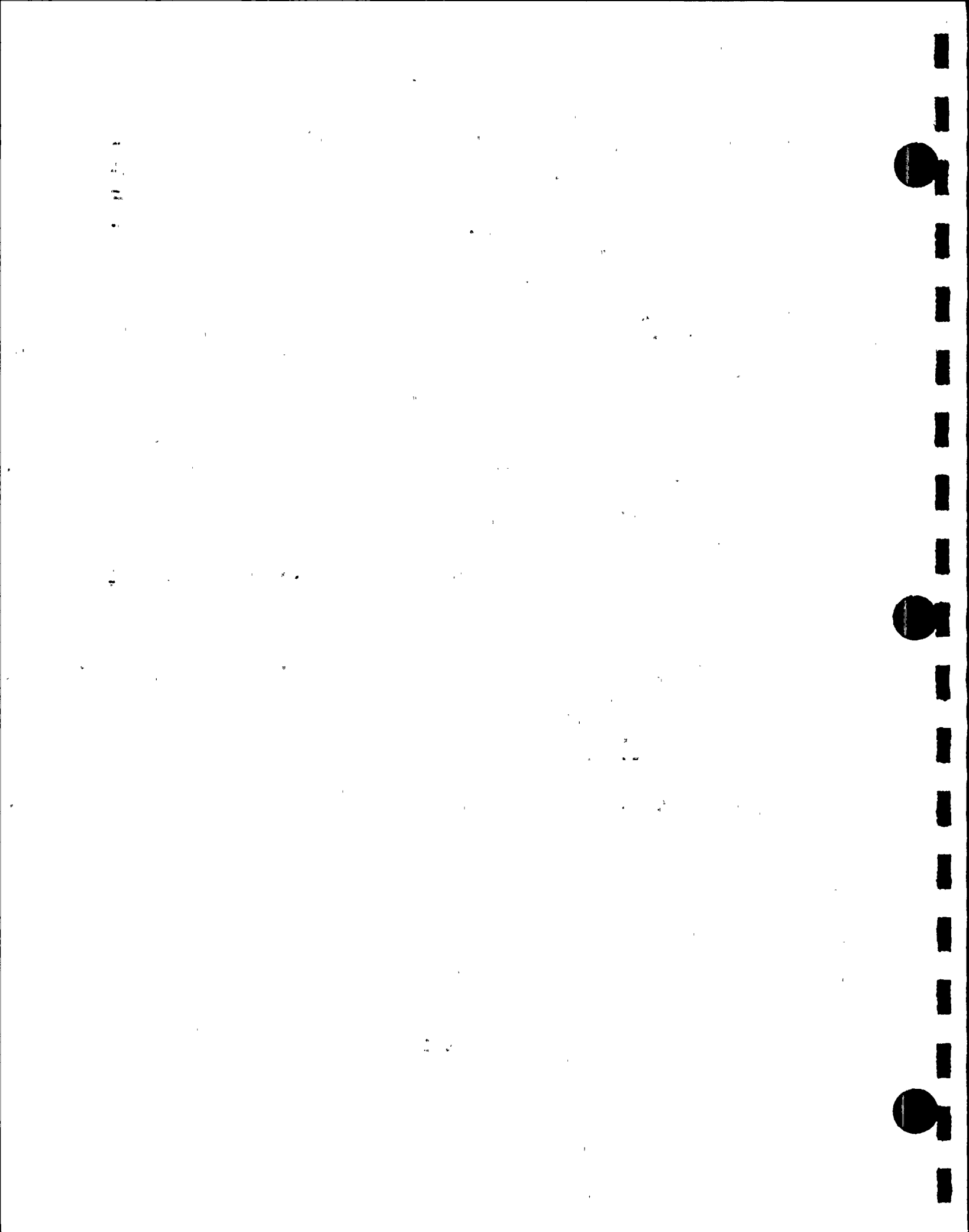
D = case 1 + case 2

E' = DBE amplifier x case 1 + DBE amplifier x case 4 + case 3
(for DBE) + case 5 (for DBE)

E = OBE amplifier x case 1 + OBE amplifier + case 4 + case 3
(for OBE) + case 5 (for OBE)

T_o = case 6

Load combinations are formed using absolute values where necessary so as to maximize critical stress resultants.



As noted above, for analysis of fuel pool structural integrity, the seismic amplifiers are based on the peak g level responses at the lowest resonant frequency that are obtained from the plant acceleration response spectrum. We show that this is conservative.

8.4 Results of Analyses

The ANSYS postprocessing capability is used to form the appropriate load combinations identified above and to establish the critical bending moments in various sections of the pool structure. The ultimate moments for each section are computed using allowable limit strength levels as described in Ref. 8.1.3. For Donald C. Cook, the following limit strengths for concrete and for reinforcement are used in the computation of limit (ultimate) moments.

concrete $\sigma_c = 3500$ psi (compression)
reinforcement = $\sigma_y = 40000$ psi (tension/compression)

In each section, we define the safety margin for bending as the ultimate bending moment divided by the calculated bending moment (from the ANSYS postprocessing of the required load cases). Table 8.4.1 summarizes the results obtained from the finite element analyses and shows minimum safety margins on each section of the structure. Note that these are safety margins based on the factored load conditions as mandated in Ref. 8.1.1 and need only satisfy a limit ≥ 1.0 .

12

11



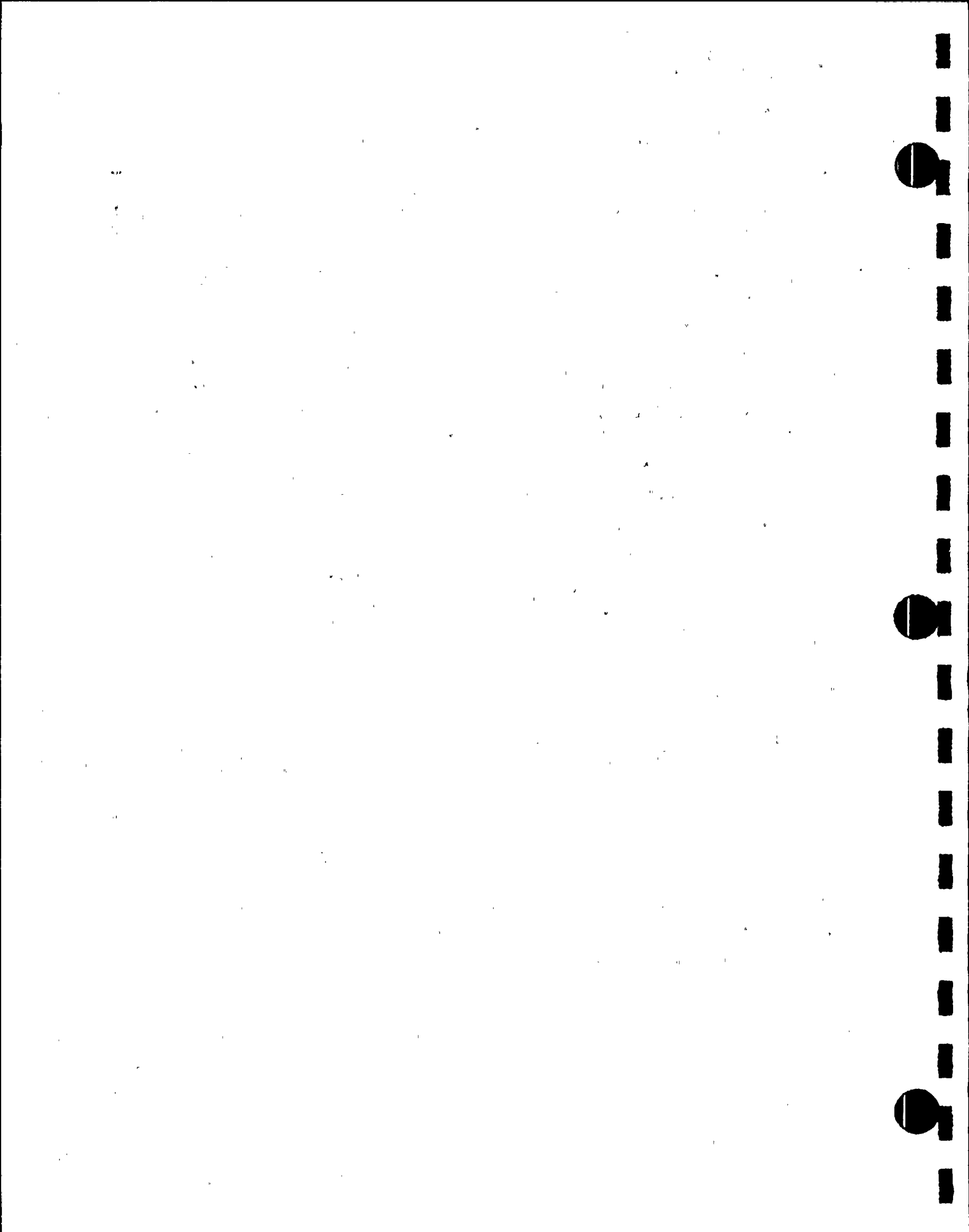
The floor slab perimeter is also checked against gross shear failure under factored load conditions. Local bearing strength and punching shear calculations are performed in accordance with (Ref. 8.1.3).

8.5 Pool Liner

The pool liner is subject to in-plane strains due to movement of the rack support feet during the seismic event. Calculations are made to establish that the liner will not fail due to cyclic straining caused by the rack foot loading. An ANSYS analysis of a liner plate section subjected to vertical and horizontal static pedestal loading is carried out. The time history result for the pedestal loading is then used to evaluate the number of stress cycles to be expected in the liner for each event. The cumulative damage factor (CDF) is computed and shown to be less than 1.0 in critical regions of the liner and attachment locations. The number of stress cycles used in the CDF evaluation is based on 1 DBE and 20 OBE events.

8.6 Conclusions

Critical regions affected by loading the fuel pool completely with high density racks are examined for structural integrity under bending and shearing action. It is determined that adequate safety factors exist assuming that all racks are fully loaded with normal (unconsolidated) fuel and that the factored load combinations are checked against the appropriate structural design strengths. It is also shown that local frictional loading on the liner results in in-plane stresses that are low enough so that liner fatigue is not a concern.



8.7 References for Section 8

- 8.1.1 NUREG-0800, SRP for Review of Safety Analysis Reports for Nuclear Power Plants, Section 3.8.4, July 1981.
- 8.1.2 ANSYS User's Manual, Swanson Analysis Rev. 4.3, 1987.
- 8.1.3 ACI 318-89, ACI 318R-89, Building Code Requirements for Reinforced Concrete, American Concrete Institute, Detroit, Michigan.
- 8.1.4 ACI349.1R-80, Reinforced Concrete Design for Thermal Effects on Nuclear Power Plant Structures, 1981.



Table 8.4.1

SAFETY FACTORS FOR BENDING OF POOL STRUCTURE REGIONS

| <u>REGION</u> | <u>FACTOR OF SAFETY*</u> |
|---------------|--------------------------|
| Slab | 1.23 |
| North Wall | 1.00 |
| East Wall | 1.08 |
| South Wall | 1.26 |
| West Wall | 1.05 |

* The factors of safety have been obtained using conservative assumptions on mechanical and thermal load distribution. They represent factors of safety over the values required by NUREG-0800.



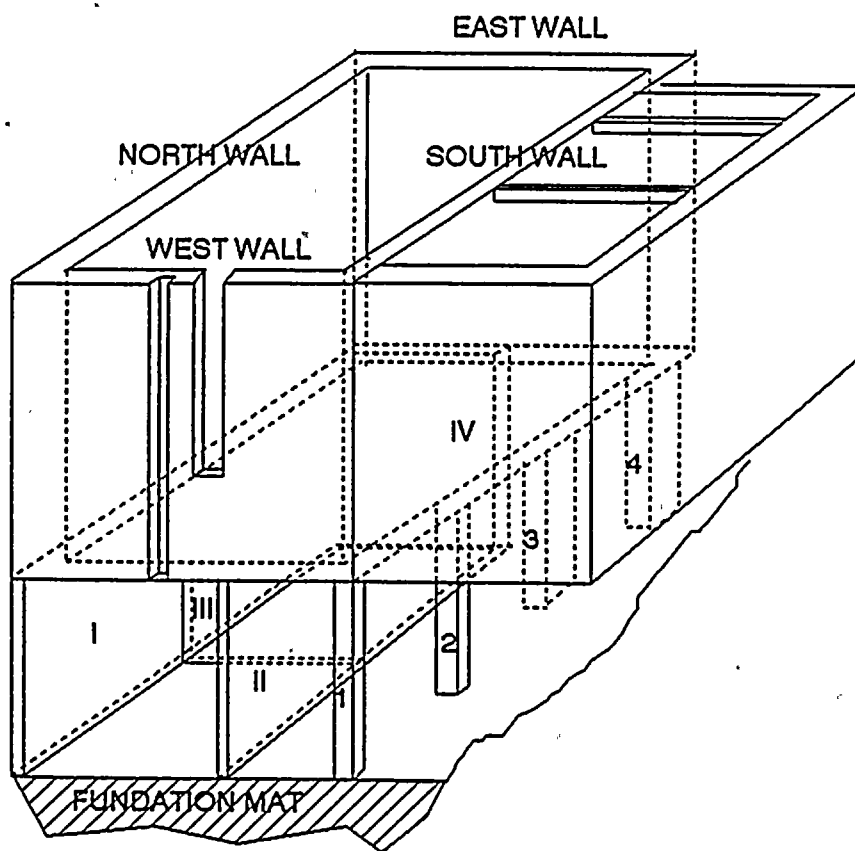
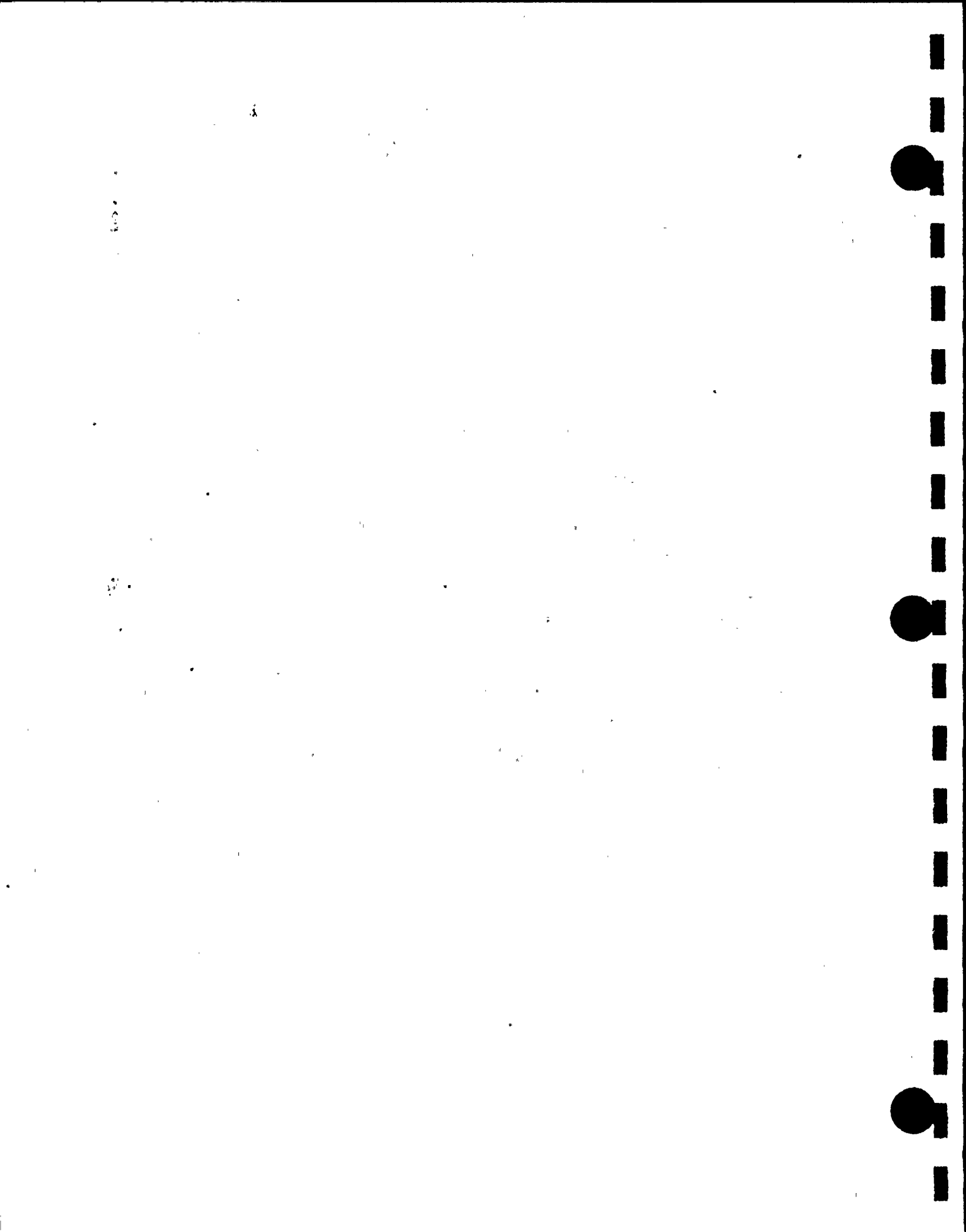


FIGURE 8.2.1 ISOMETRIC VIEW OF COOK SPENT FUEL POOL



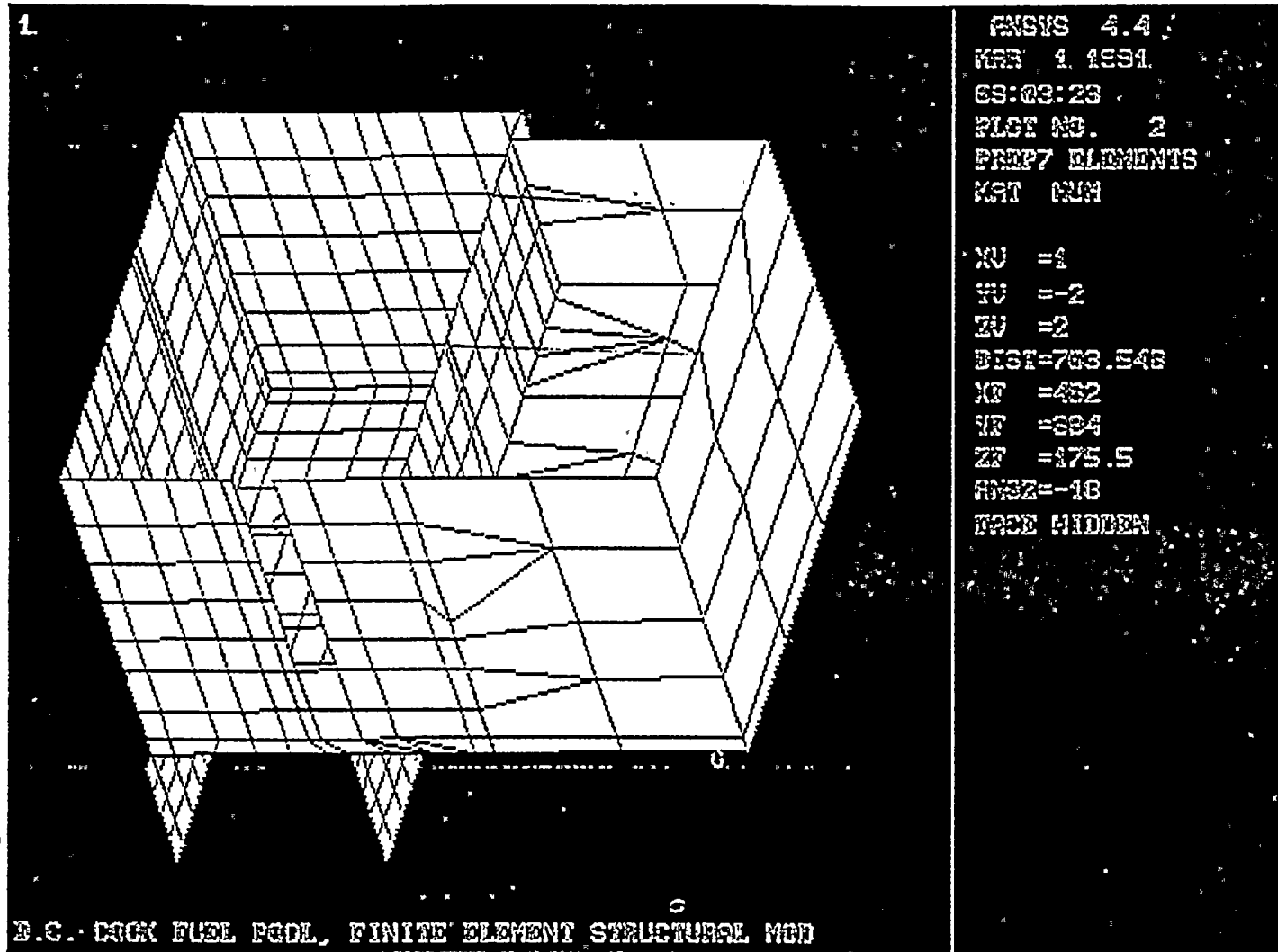


FIGURE 8.2.2

OVERALL FINITE MODEL OF COOK POOL
TOP VIEW



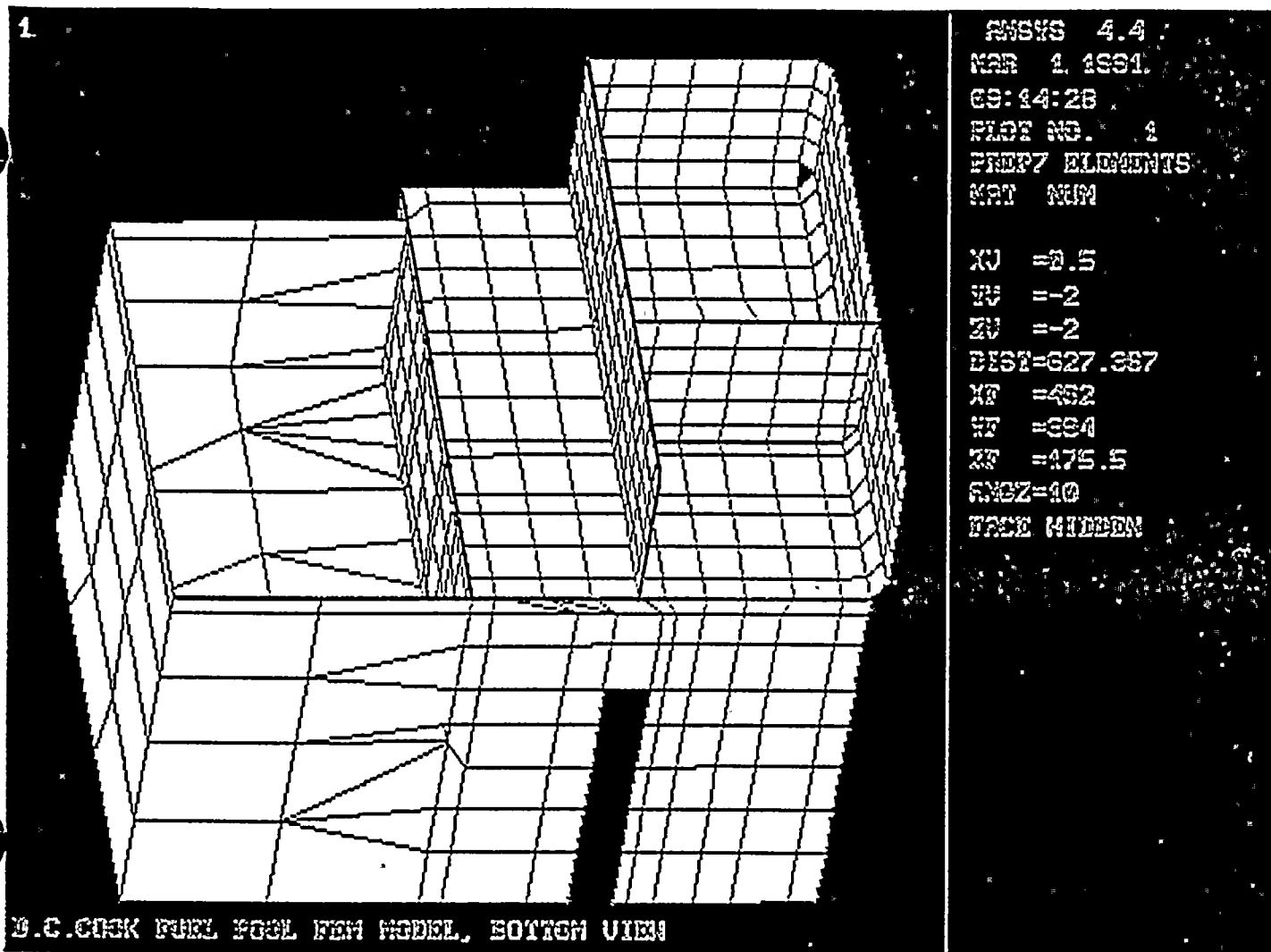
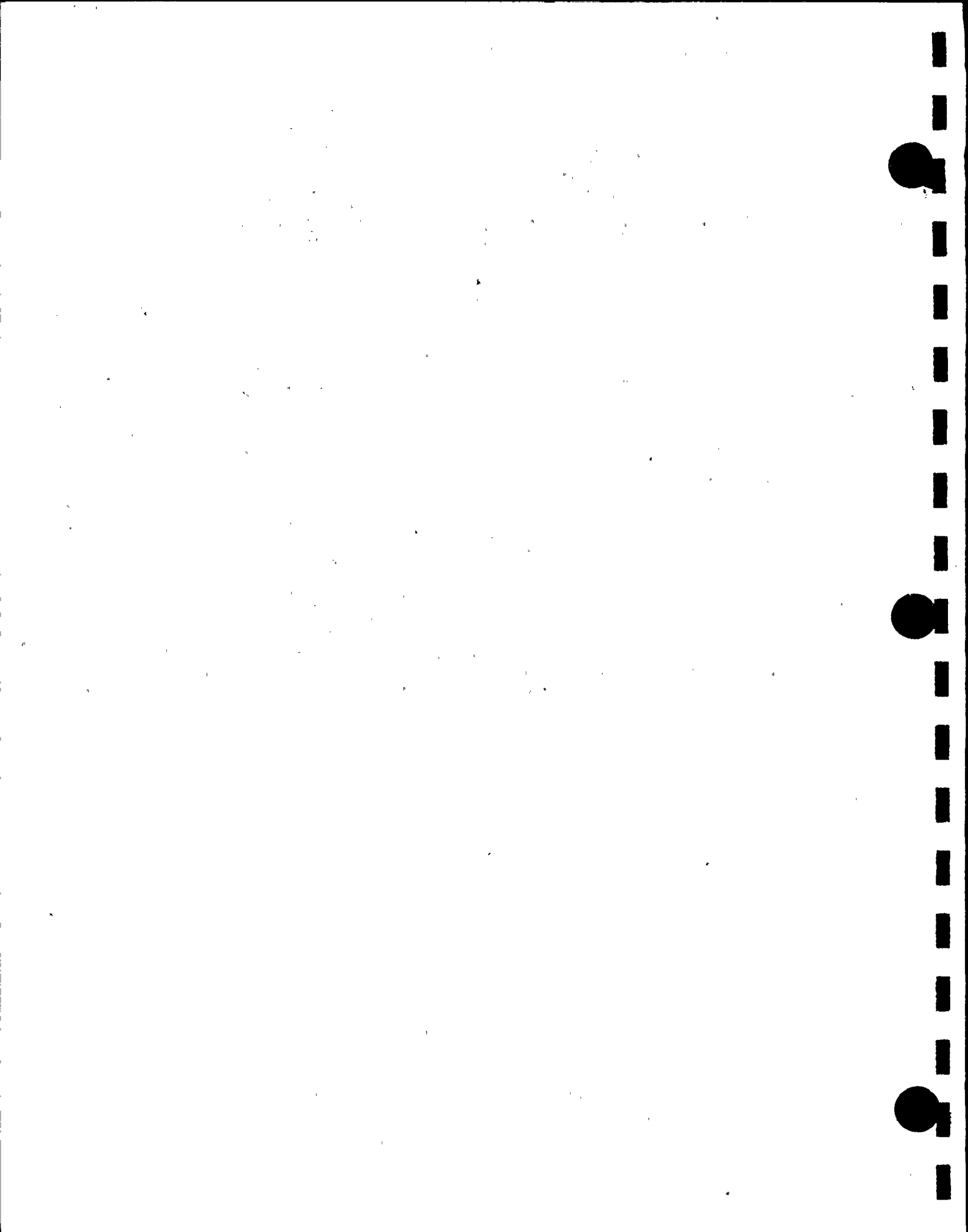


FIGURE 8.2.3

OVERALL FINITE MODEL OF COOK POOL
 BOTTOM VIEW



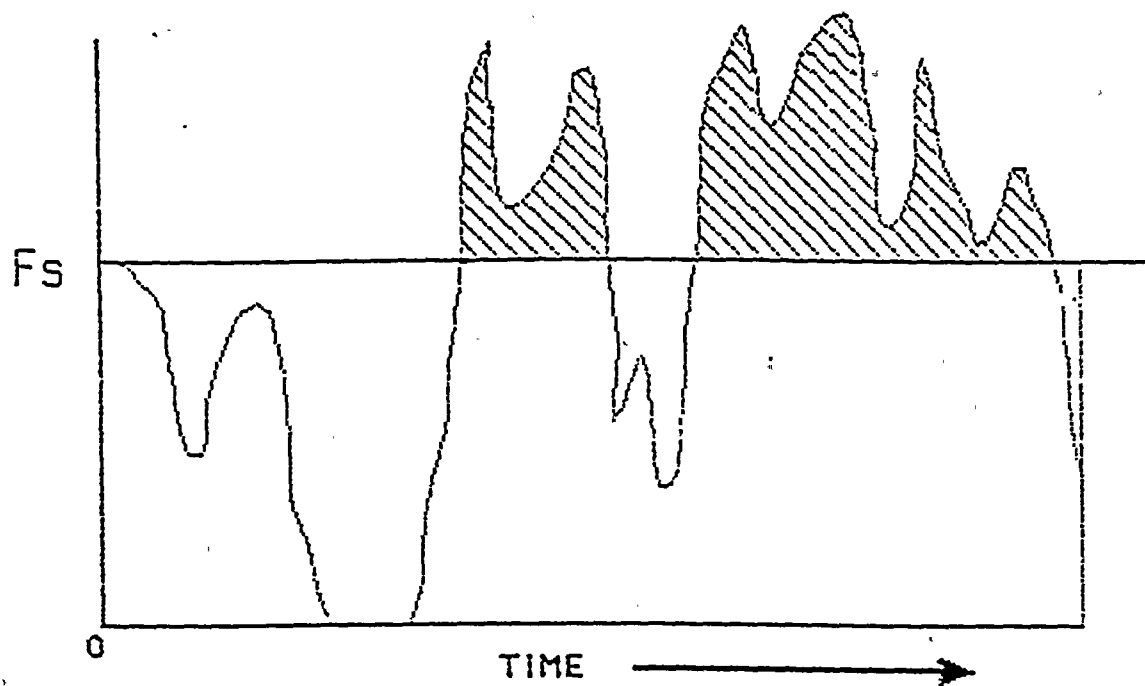
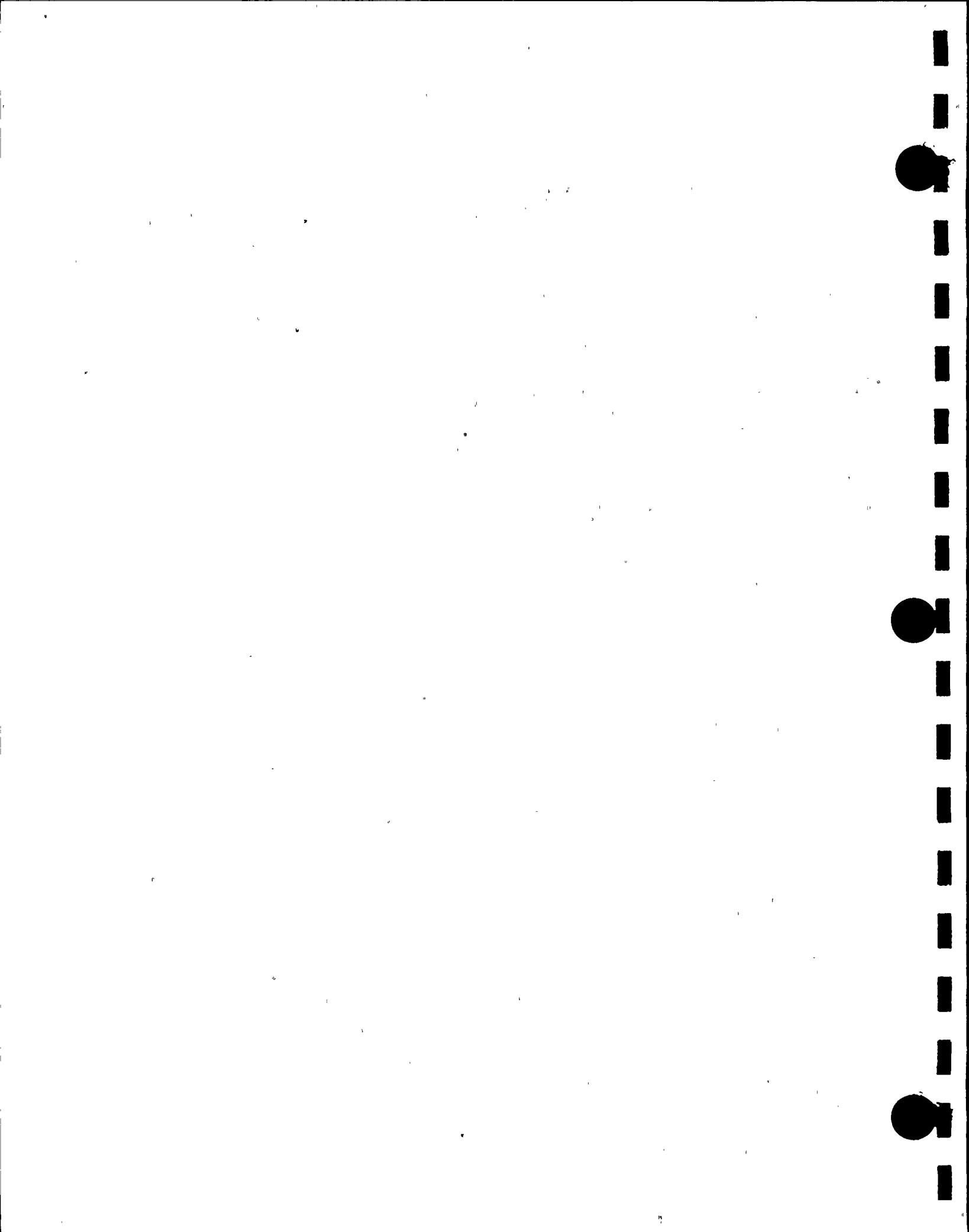


FIGURE 8.3.1 PEDESTAL LOAD VS. TIME
(Positive Load Means Pedestal in
Contact with Liner)



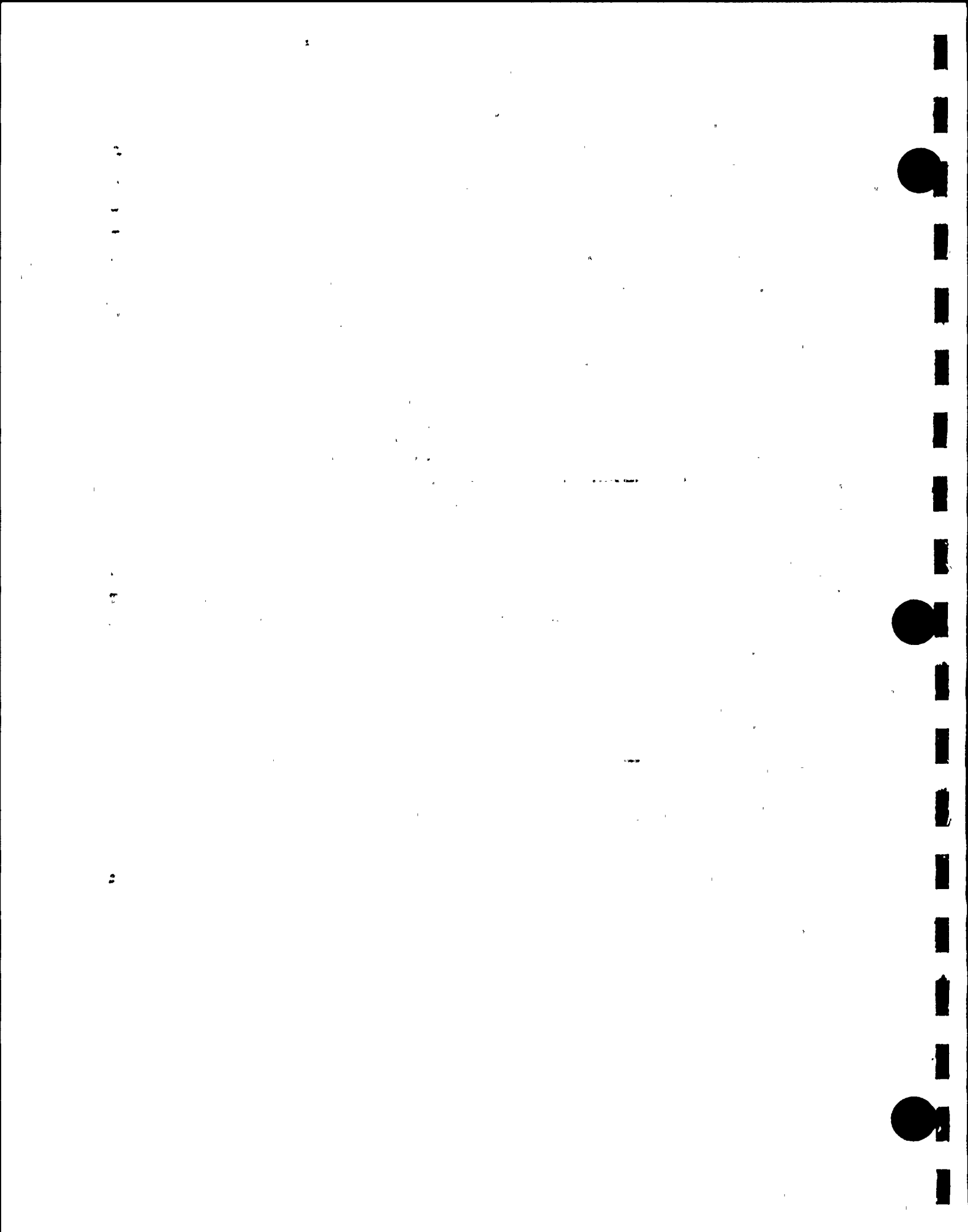
9.0 RADIOLOGICAL EVALUATION

9.1 Fuel Handling Accident

9.1.1 Assumptions and Source Term Calculations

An evaluation of the consequences of a fuel handling accident has been made for fuel of 5.0 wt% initial enrichment burned to 60,000 MWD/MTU, with the reactor conservatively assumed to have been operating at 3411 MW thermal power (38.8 MWD/KgU specific power) prior to reactor shutdown. Except for the fuel enrichment and discharge burnup, the assumptions used in the evaluation are the same as those previously reviewed and accepted by the USNRC. As in the previous evaluation, the fuel handling accident was conservatively assumed to result in the release of the gaseous fission products contained in the fuel-rod gaps of all the rods in the peak-power fuel assembly at the time of the accident. Gap inventories of fission products available for release were estimated using both the assumptions identified in Regulatory Guide 1.25⁽¹⁾ and those in NUREG/CR-5009⁽²⁾. NUREG/CR-5009 has confirmed that the Reg Guide 1.25 assumptions remain conservative for extended burnup except for I-131, for which the release fraction was reported to be 20% higher.

Most of the gaseous fission products having a significant impact on the off-site doses are the short-lived nuclides of Iodine and Xenon which reach saturation inventories during in-core operation. These inventories depend primarily on the fuel specific power over the few months immediately preceding reactor shutdown. In the highest power assembly, the specific power and hence the inventory of Iodine and Xenon will be directly related to the peaking factor (assumed to be 1.65 per Reg. Guide 1.25).



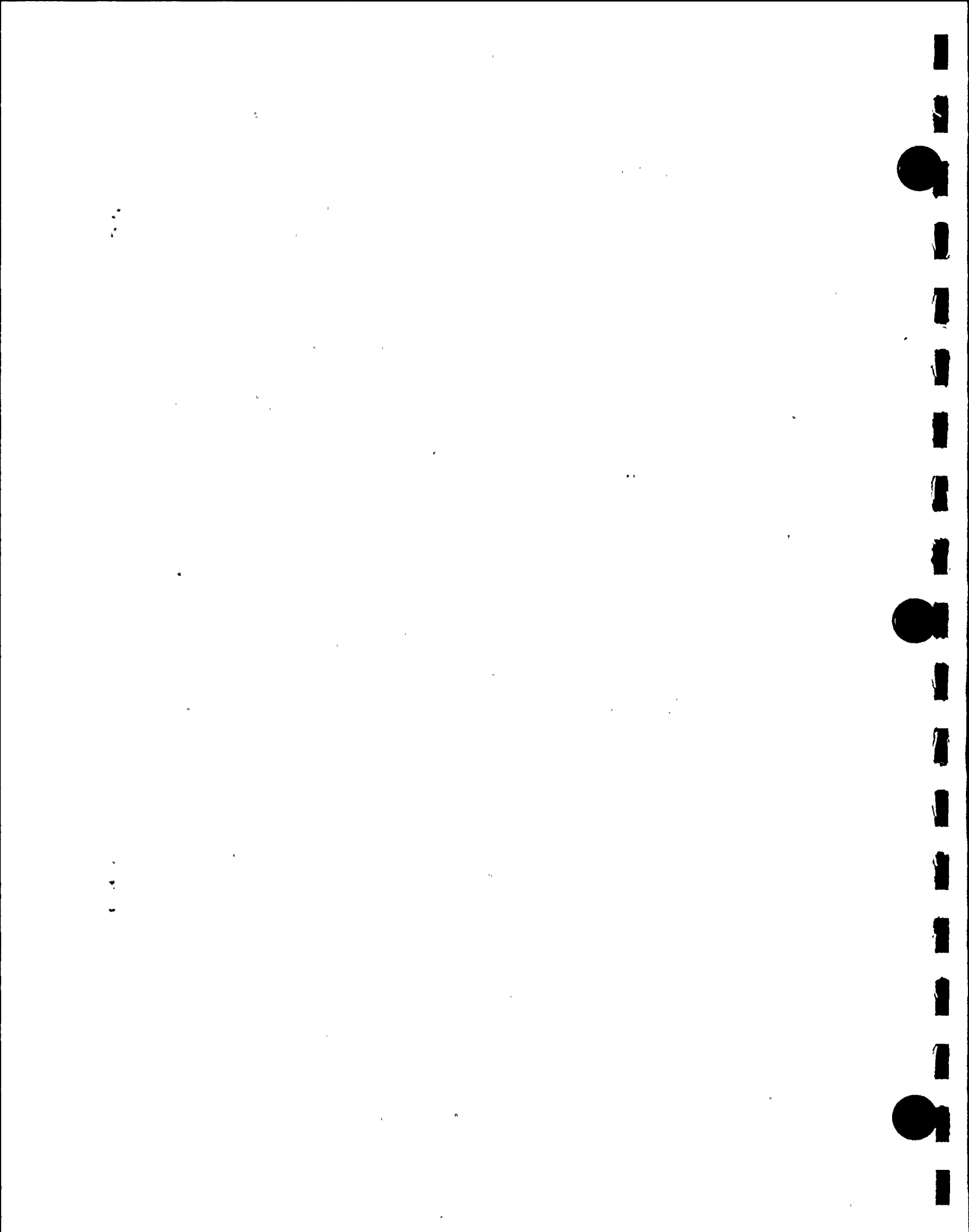
The inventory of long-lived Kr-85 (10.73 year half-life), however, is nearly proportional to the accumulated fuel discharge burnup and hence is independent of the peaking factor. Because Kr-85 is a weak beta emitter, it has only a minor impact on off-site doses, primarily affecting the whole-body beta dose. The off-site radiological consequences are dominated by the short-lived radionuclides (which are at saturation concentration independent of fuel burnup). In the present analysis, the calculated doses are higher and more conservative than those of the previous evaluation because (1) the analyses reported here use higher gap inventories based on Reg Guide 1.25 assumptions and (2) the use of the up-dated ORIGEN-2 code⁽³⁾ for calculating the fission product inventories. Results of the evaluation confirm that the off-site doses remain within the regulatory limits.

The present evaluation uses values for the 2-hour atmospheric dispersion factor (X/Q) and filter efficiencies that have previously been reviewed and accepted. Core inventories of fission products were estimated with the ORIGEN-2 code based upon a reactor power of 3411 MWt and fuel with an initial enrichment of 5.0% U-235 burned to 60,000 MWD/MTU. Calculations were made for 100 hours cooling time as the source term for the fuel handling accident. The release fraction of the core inventories assumed to be in the gap by both the Reg Guide 1.25 and NUREG/CR5009 assumptions are listed in Table 9.1.

The following equation, from Reg Guide 1.25, was used to calculate the thyroid dose (D) from the inhalation of radioiodine,

$$D = \sum_i \frac{F_g I_i F P B R_i (x/Q)}{DF_p DF_f} \quad \text{Rads}$$

summed over all Iodine radionuclides.



F_g = fraction of fuel rod
Iodine inventory in gap
space

B = Breathing rate =
 3.47×10^{-4} cubic
meters per second

I_i = core Iodine radio-nu-
clide inventory at time
of the accident (cu-
ries)

R_i = Dose conversion
factor (rads/curie)
from Reg. Guide 1.25

F = fraction of core dam-
aged so as to release
Iodine in the rod gap
(1/193)

(X/Q) = atmospheric
diffusion factor
(3.15×10^{-4} sec/m³)

P = Core peaking factor
(1.65)

DF_p = effective Iodine
decontamination
factor for pool
water (= 150)

DF_f = effective Iodine
decontamination factor
for filters (= 10)

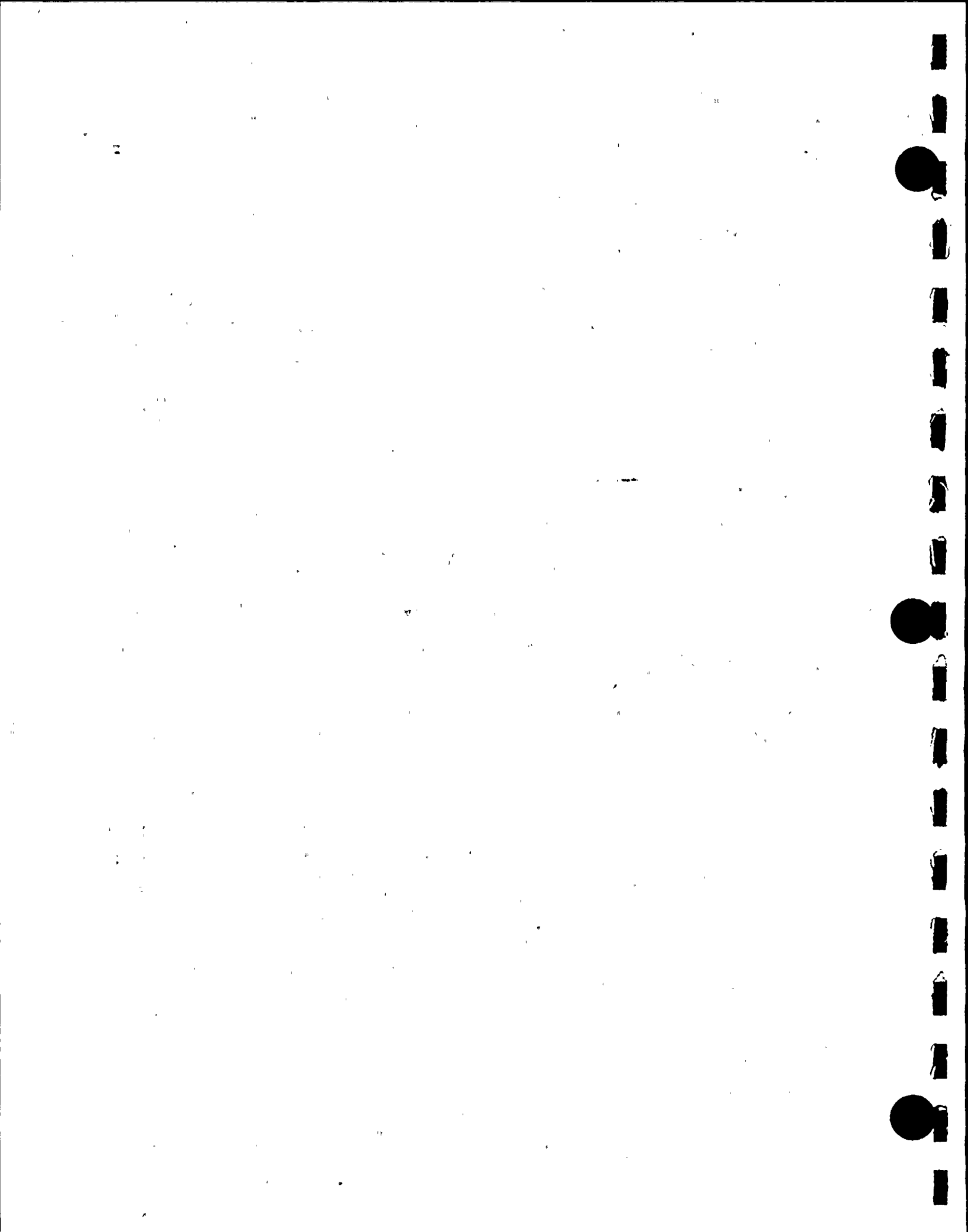
The gap inventories listed in Table 9-1 are the product of I_i
(core inventory) and F_g (the fraction existing in the gap).

The function used to calculate the external whole body dose from
beta (D_β) or gamma (D_γ) radiation in the cloud uses many of the
terms defined above and is given by:

$$D_\beta = \sum_i 0.23 (x/Q) F P G_i E_{\beta_i} \quad \text{and}$$

$$D_\gamma = \sum_i 0.25 (x/Q) F P G_i E_{\gamma_i}$$

where G_i is the gap inventory of the gaseous radionuclides of Xe
and Kr and the functions above are summed over all the noble gases.
 E_β and E_γ are the average energies of decay (beta and gamma
radiation respectively) for the various radionuclides. These
functions assume the noble gas decontamination factors in water and
the charcoal filters are 1.0. The gap inventories of radioiodine



make a negligible contribution to the whole body doses, D_β or D_γ , because of the large decontamination factors appropriate to the iodines.

9.1.2 Results

A summary of the assumptions used to evaluate the fuel handling accident is given in Table 9-2. The minimum time after shutdown when fuel assemblies would be moved was conservatively assumed to be 100 hours as identified in the Technical Specifications. At 100 hours after shutdown, the two-hour dose at the site boundary, for a fuel handling accident releasing all of the gaseous fission product radioactivity in the gaps of all rods in the highest power assembly, are as follows:

Two-Hour Site Boundary Dose

| | <u>NUREG/CR-5009
Method</u> | <u>Reg. Guide
1.25</u> | <u>Previous
Analysis</u> |
|-------------------------------------|---------------------------------|----------------------------|------------------------------|
| Inhalation thyroid dose = | 7.07 Rads | 5.97 Rads | 2.15 |
| Whole body beta dose, D_β = | 0.36 Rads | 0.70 Rads | - |
| Whole body gamma dose, D_γ = | 0.31 Rads | 0.58 Rads | 0.51 |

These doses are well within the limits of 10 CFR Part 100 in conformance with the acceptance criteria of SRP 15.7.4. (Rev.1, July 1981)⁽⁴⁾.

100-100000

100-100000

100-100000



9.2 Solid Radwaste

The necessity for resin replacement is determined primarily by the requirement for water clarity and the resin is normally changed about once a year. No significant increase in the volume of solid radioactive wastes is expected with the expanded storage capacity. During reracking operations, a certain amount of additional resins may be generated by the pool cleanup system on a one-time basis (perhaps 10 to 30 cubic feet).

9.3 Gaseous Releases

Gaseous releases from the fuel storage area of the auxiliary building are combined with other plant exhausts. Normally, the contribution from the fuel storage area of the auxiliary building is negligible compared to the other releases and no significant increases are expected as a result of the expanded storage capacity.

9.4 Personnel Exposures

During normal operations, personnel working in the fuel storage area may be exposed to radiation from the spent fuel pool. Operating experience has shown that the area radiation dose rates, which originate primarily from radionuclides in the pool water, are generally less than 1 mrem/hr but may temporarily increase to 2.5 - 3 mrem/hr during refueling operations. No evidence has been observed of any crud deposition around the edges of the pool that might cause local areas of high radiation.



Radiation levels in zones surrounding the pool are not expected to be significantly affected. Existing shielding around the pool (water depth and concrete walls) provide more than adequate protection, despite the slightly closer approach to the walls of the pool.

Typical concentrations of radionuclides in the pool water are shown in Table 9.3. During fuel reload operations, the concentrations will increase due to crud deposits spalling from spent fuel assemblies and to activities carried into the pool from the primary system. While these effects may increase the concentrations (as much as a factor of 10), the pool cleanup system soon reduces the concentrations to the normal operating range. No evidence has been seen of any significantly higher radiation doses near the edge of the pool that might suggest the accumulation of crud deposits.

Operating experience has shown that there have been negligible concentrations of airborne radioactivity and no increases are expected as a result of the expanded storage capacity. Area monitors for airborne activities are available in the immediate vicinity of the spent fuel pool.

No increase in radiation exposure to operating personnel is expected and therefore neither the current health physics program nor the area monitoring systems need to be modified.

9.5 Anticipated Exposure During Reracking

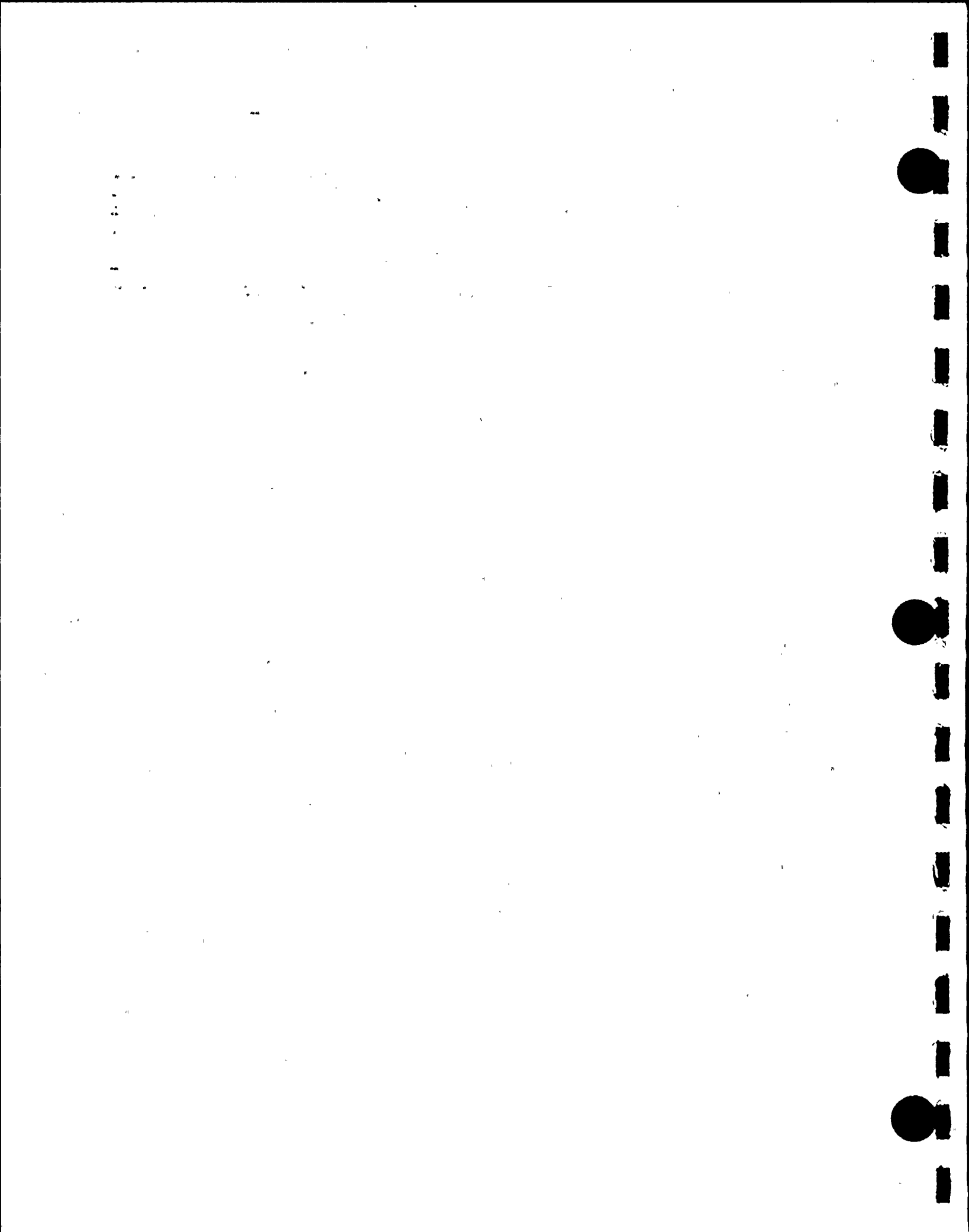
Total occupational exposure for the reracking operation is estimated to be between 6 and 11 person-rem, as indicated in Table 9.4. While individual task efforts and exposures may differ from those in Table 9.4, the total is believed to be a reasonable estimate for planning purposes. Divers will be necessary to remove



certain underwater appurtenances. These appurtenances are well removed for the stored fuel which minimizes the radiation dose rate to the divers. Careful monitoring and adherence to pre-prepared procedures will assure that the radiation dose to the divers will be maintained ALARA. All of the reracking operation will utilize detailed procedures prepared with full consideration of ALARA principles. Similar operations have been performed in a number of facilities in the past and there is every reason to believe that reracking can be safely and efficiently accomplished at the Donald C. Cook Nuclear Plant, with minimum radiation exposure to personnel.

The existing radiation protection program at the Cook Nuclear Plant is adequate for the reracking operations. Where there is a potential for significant airborne activity, continuous air samplers will be in operation. Personnel wear protective clothing and, if necessary, respiratory protective equipment. Activities are governed by a Radiation Work Permit and personnel monitoring equipment will be assigned to each individual. As a minimum, this includes thermoluminescent dosimeters and pocket dosimeters. Additional personnel monitoring equipment (i.e., extremity badges or alarming dosimeters) may be utilized as required. Work, personnel traffic, and the movement of equipment will be monitored and controlled to minimize contamination and to assure that exposures are maintained ALARA.

In reracking, the existing storage racks will be removed, decontaminated as much as possible by washing and wipe-downs, packaged and shipped to a licensed processing/disposal facility. Shipping containers and procedures will conform to Federal DOT regulations and the requirements of any State DOT office through which the shipment may pass.



9.6 References for Section 9

1. Reg. Guide 1.25 (AEC Safety Guide 25), "Assumptions used for evaluating the potential radiological consequences of a fuel handling accident in the fuel handling and storage facility for boiling and pressurized water reactors".
2. C.E. Beyer, et al., "Assessment of the Use of Extended Burnup Fuel in Light Water Power Reactors", NUREG/CR-5009, Pacific Northwest Laboratory (PNL-6258).
3. A.G. Croff, "A User's Manual for the ORIGEN2 Computer Code", ORNL/TM-7175, July 1980 (ORIGEN = ORNL Isotope Generation and Depletion)
4. Section 15.7.4, "Radiological Consequences of Fuel Handling Accidents" NUREG-0800, Section 15.7.4, Rev. 1 July 1981

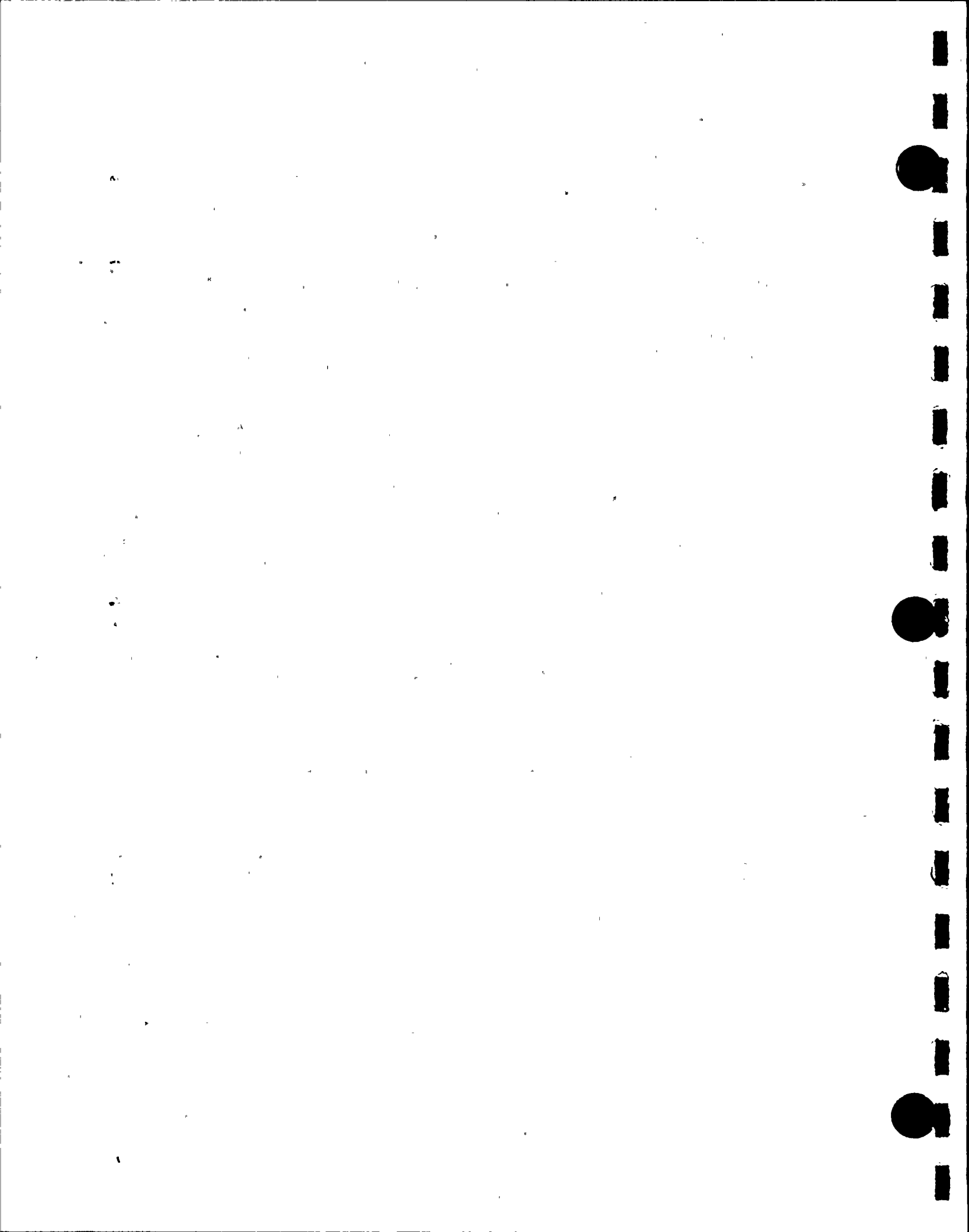


Table 9-1 INVENTORIES AND CONSTANTS OF SIGNIFICANT
FISSION PRODUCT RADIONUCLIDES

| NUCLIDE | SHUTDOWN
CORE
INVENTORY
CURIES | DECAY
CONST.
λ , 1/HR | TOTAL GAP INVENTORY, CURIES | | DOSE
CONVERSION
RI | E_{β} (MEV) | E_{γ} (MEV) |
|---------|---|-------------------------------------|-----------------------------|-----------------|--------------------------|-------------------|--------------------|
| | | | NUREG/CR-5009 | Reg. Guide 1.25 | | | |
| | | | 100 hrs | 100 hrs | | | |
| I-131 | 9.0 E+7 | 3.591E-3 | 7.5 E+6 | 6.3 E+6 | 1.48E+6 | 0.186 | 0.389 |
| I-132 | 1.3 E+8 | 3.013E-1 | Negligible* | Negligible | 5.35E+4 | - | - |
| I-133 | 1.8 E+8 | 3.332E-2 | 6.3 E+5* | 6.3 E+5 | 4.0 E+5 | 0.419 | 0.597 |
| I-134 | 1.9 E+8 | 7.905E-1 | Negligible* | Negligible | 2.5 E+4 | - | - |
| I-135 | 1.7 E+8 | 1.048E-1 | Negligible* | Negligible | 1.24E+5 | 0.394 | 1.456 |
| | | | | | | | |
| Kr-85M | 1.9 E+7 | 1.547E-1 | Negligible* | Negligible | | - | - |
| Kr-85 | 1.4 E+6 | 7.376E-6 | 2.0 E+5 | 4.2 E+5 | | 0.251 | 0.002 |
| Kr-87 | 3.6 E+7 | 5.451E-1 | Negligible | Negligible | | - | - |
| Kr-88 | 5.0 E+7 | 2.442E-1 | Negligible | Negligible | | - | - |
| | | | | | | | |
| Xe-131M | 1.0 E+6 | 2.427E-3 | 7.9 E+4* | 7.9 E+4 | | - | 0.163 |
| Xe-133M | 5.6 E+6 | 1.319E-2 | 1.5 E+5* | 1.5 E+5 | | - | 0.233 |
| Xe-133 | 1.8 E+8 | 5.506E-3 | 5.1 E+6 | 1.0 E+7 | | 0.102 | 0.081 |
| Xe-135 | 3.9 E+7 | 7.626E-2 | Negligible | Negligible | | 0.309 | 0.262 |

* NO RELEASE FRACTION GIVEN - ASSUMED SAME AS REG. GUIDE 1.25

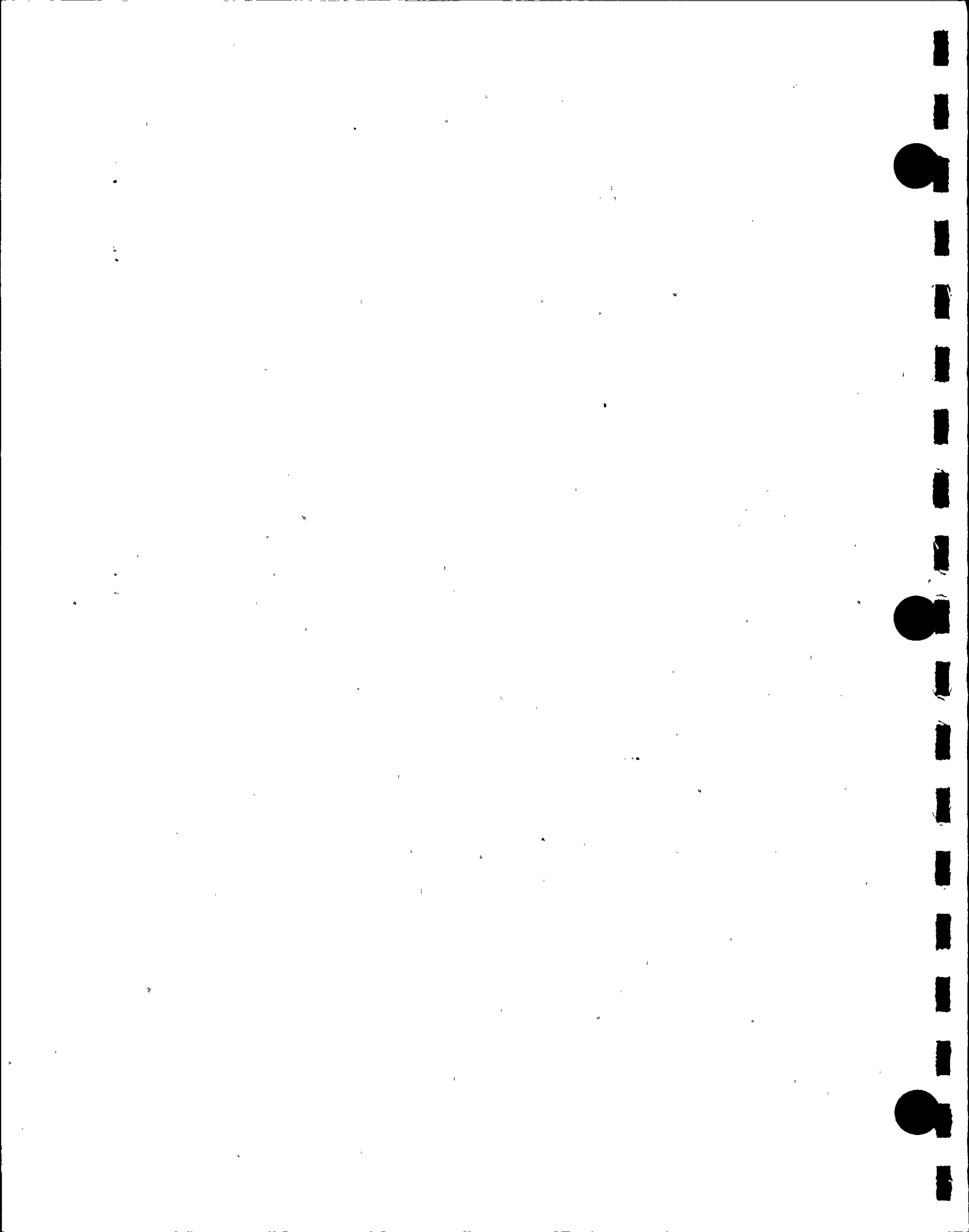


Table 9.2

DATA AND ASSUMPTIONS FOR THE EVALUATION
OF THE FUEL HANDLING ACCIDENT

| 1. <u>Source Term Assumptions</u> | <u>VALUES</u> |
|---|--|
| Core power level, MWT | 3411 |
| Fuel burnup, MWD/MTU | 60,000 |
| Analytical method | ORIGEN |
| 2. <u>Release Assumptions</u> | |
| Number of failed fuel rods | all rods in 1
of 193 assemblies |
| Fraction of core inventory released to gap (NUREG/CR-5009 % release of Iodine-131 is reported to be 20% higher) | <u>Reg. Guide 1.25</u>
% of the Iodine - 10
% of the Xenon - 10
% of Kr-85 - 30 |
| Assumed power peaking factor | 1.65 |
| Inventory in gap available for release | Table 9.1 |
| Pool decontamination factors | |
| For Iodines | 150 |
| For noble gases | 1 |
| Filter decontamination factors | |
| For Iodines | 10 |
| For noble gases | 1 |
| Atmospheric Dispersion, (x/Q) | $3.15 \times 10^{-4} \text{ sec/m}^3$ |
| Breathing rate | $3.47 \times 10^{-4} \text{ m}^3/\text{sec}$ |

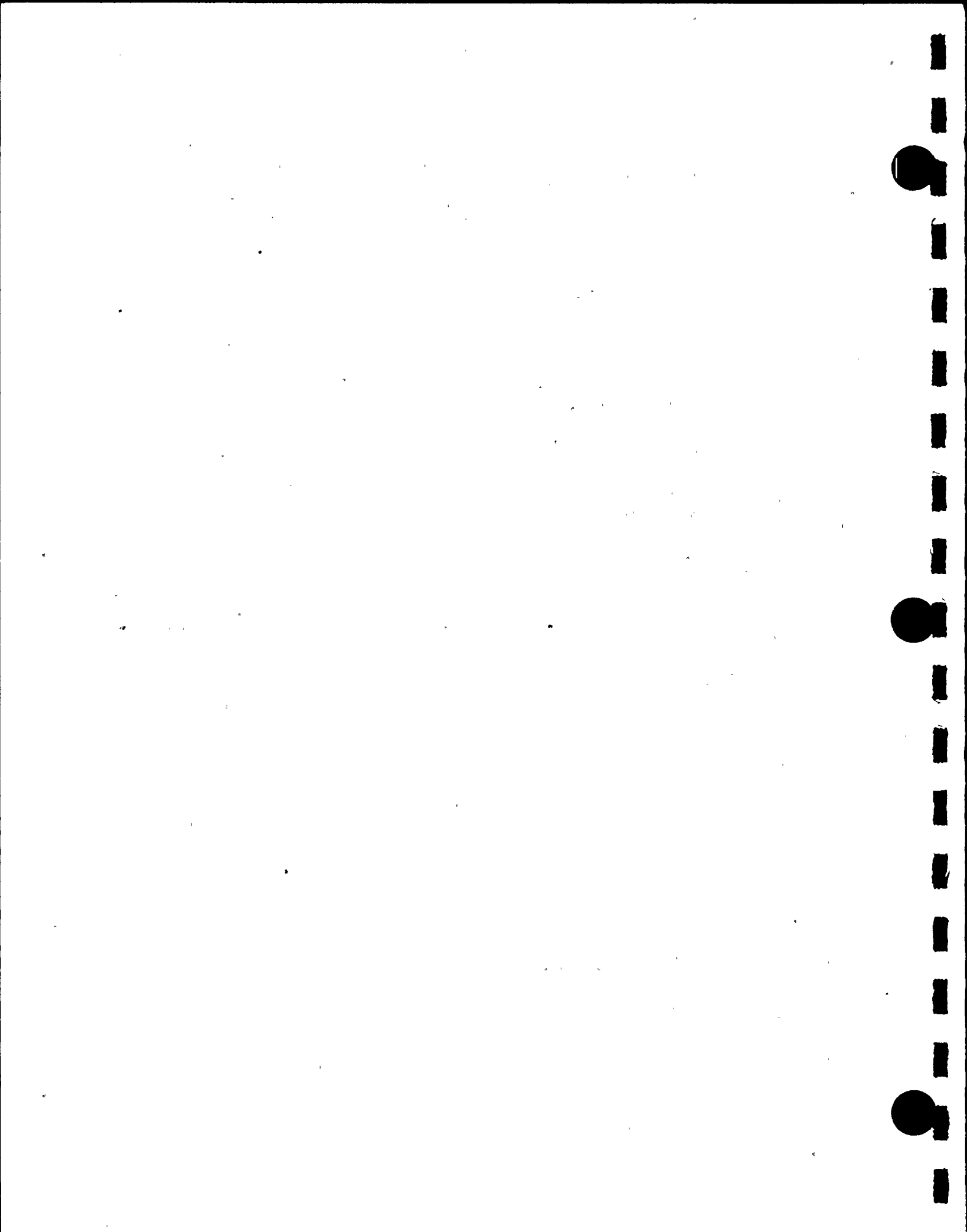


Table 9.3 Typical Concentrations of Radionuclides
in the Spent Fuel Pool Water

| <u>Nuclide</u> | Concentration |
|----------------|-------------------------------------|
| | <u>$\mu\text{Ci/ml}$</u> |
| Ag-110M | 4.6×10^{-5} |
| Co-58 | 1.5×10^{-5} |
| Co-60 | 4.4×10^{-5} |
| Cs-134 | 3.2×10^{-4} |
| Cs-137 | 6.4×10^{-4} |

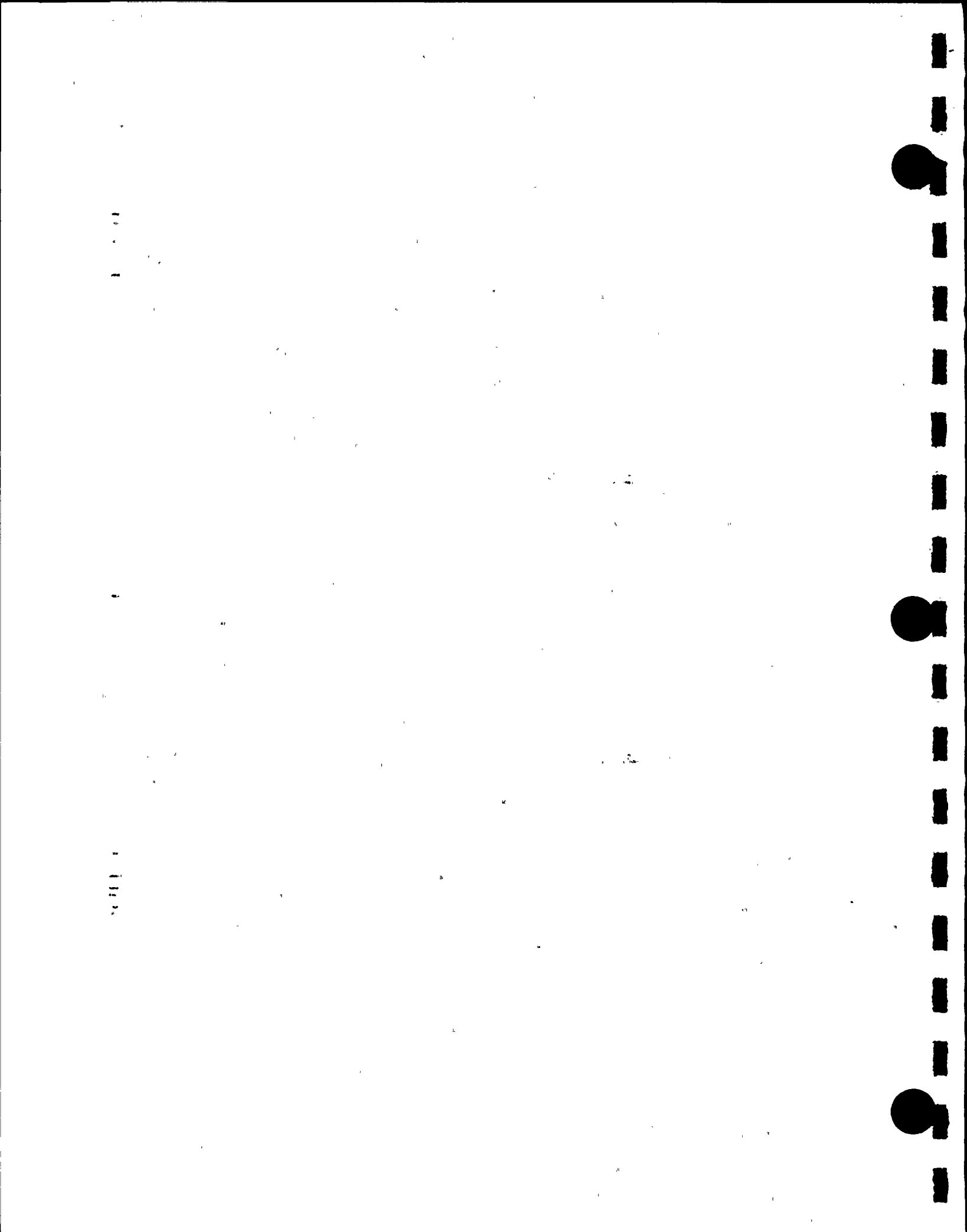


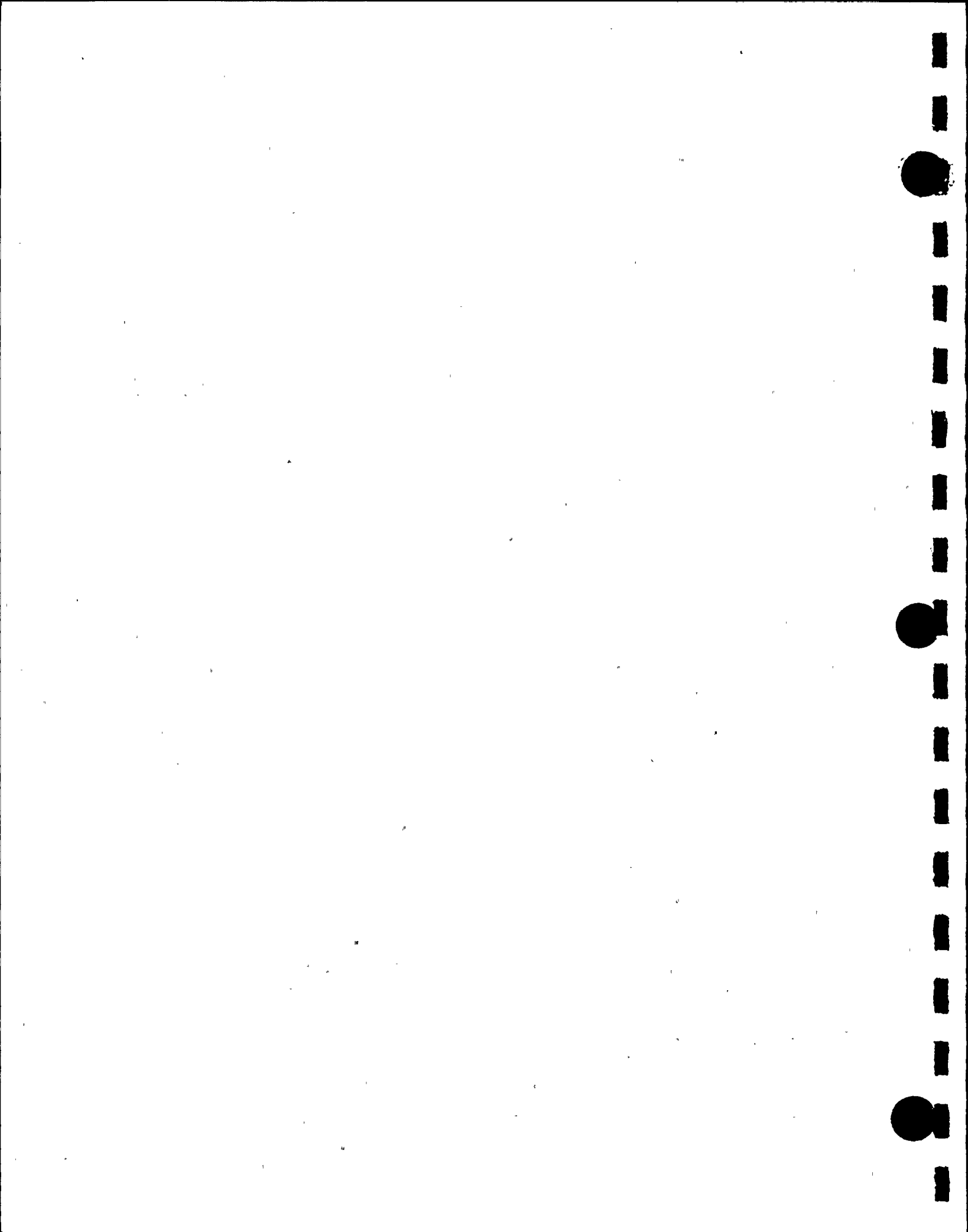
Table 9.4

PRELIMINARY ESTIMATE OF PERSON-REM EXPOSURES
DURING RERACKING

| <u>Step</u> | <u>Number of
Personnel</u> | <u>Hours</u> | <u>Estimated
Exposure⁽¹⁾</u> |
|---|--------------------------------|--------------|---|
| Remove empty racks | 5 | 40 | 0.5 to 1.0 |
| Wash and Decon racks | 3 | 10 | 0.08 to 0.2 |
| Clean and Vacuum Pool | 3 | 25 | 0.3 to 0.6 |
| Remove underwater
appurtences | 4 | 5 | 0.4 to 0.8 |
| Partial installation
of new rack modules | 5 | 20 | 0.25 to 0.5 |
| Move fuel to new racks | 2 | 150 | 0.8 to 1.5 |
| Remove remaining racks | 5 | 120 | 1.5 to 3.0 |
| Wash and Decon racks | 3 | 30 | 0.2 to 0.4 |
| Install remaining new
rack modules | 5 | 35 | 0.4 to 0.8 |
| Prepare old racks for
shipment | 4 | 80 | 1.0 to 2.0 ⁽²⁾ |
| Total Exposure, person-rem | | | 6 to 12 |

(1) Assumes minimum dose rate of 2 1/2 mR/hr (expected) to a maximum of 5 mR/hr, except for pool vacuuming operations which assumes 4 to 8 mR/hr and diving operations which assume 20 to 40 mR/hr.

(2) Maximum expected exposure, although details of preparation and packaging of old racks for shipment have not yet been determined.



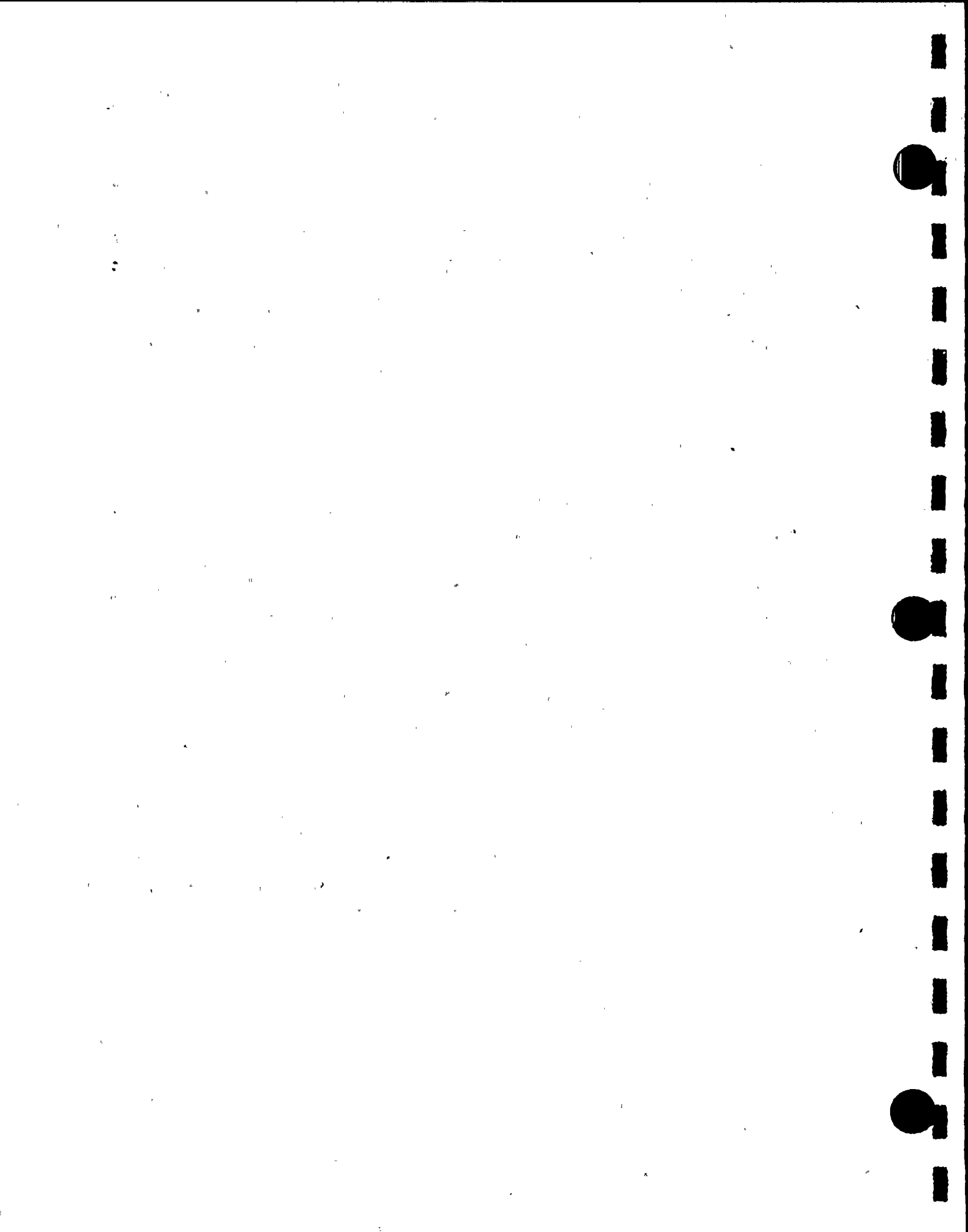
10.0 IN-SERVICE SURVEILLANCE PROGRAM

10.1 Purpose

This section describes the programmatic commitments made by Indiana Michigan Power Company (I&M) for in-service surveillance of the Boral neutron absorption material to comply with the provisions of Section IV (8) of the OT Position Paper (Ref. 10.1.1).

All material used within a storage system for spent nuclear fuel are qualified to a level of performance predicated upon calculated worst case environmental conditions and are based on accelerated testing of the materials to levels of service life corresponding to that environment. Because such environmental compatibility testing in the laboratory conditions is accelerated, it is prudent that each of the system components be monitored to some extent throughout the service life to assure that the actual in-service performance remains within acceptable parameters as defined by the accelerated testing. For many of the materials, monitoring throughout the service life is relatively easy, however, the neutron absorbing material is encased in a stainless steel jacket precluding a direct visual or physical examination during the in-service condition.

The coupon surveillance program presented herein is intended to provide a definitive assessment of the present physical integrity of the neutron absorber, as well as inferential information to detect future degradation.



The coupon surveillance procedure consists of preparing twelve neutron absorber coupons carefully encased in a stainless steel metal jacket, and suspending them from a "coupon tree".

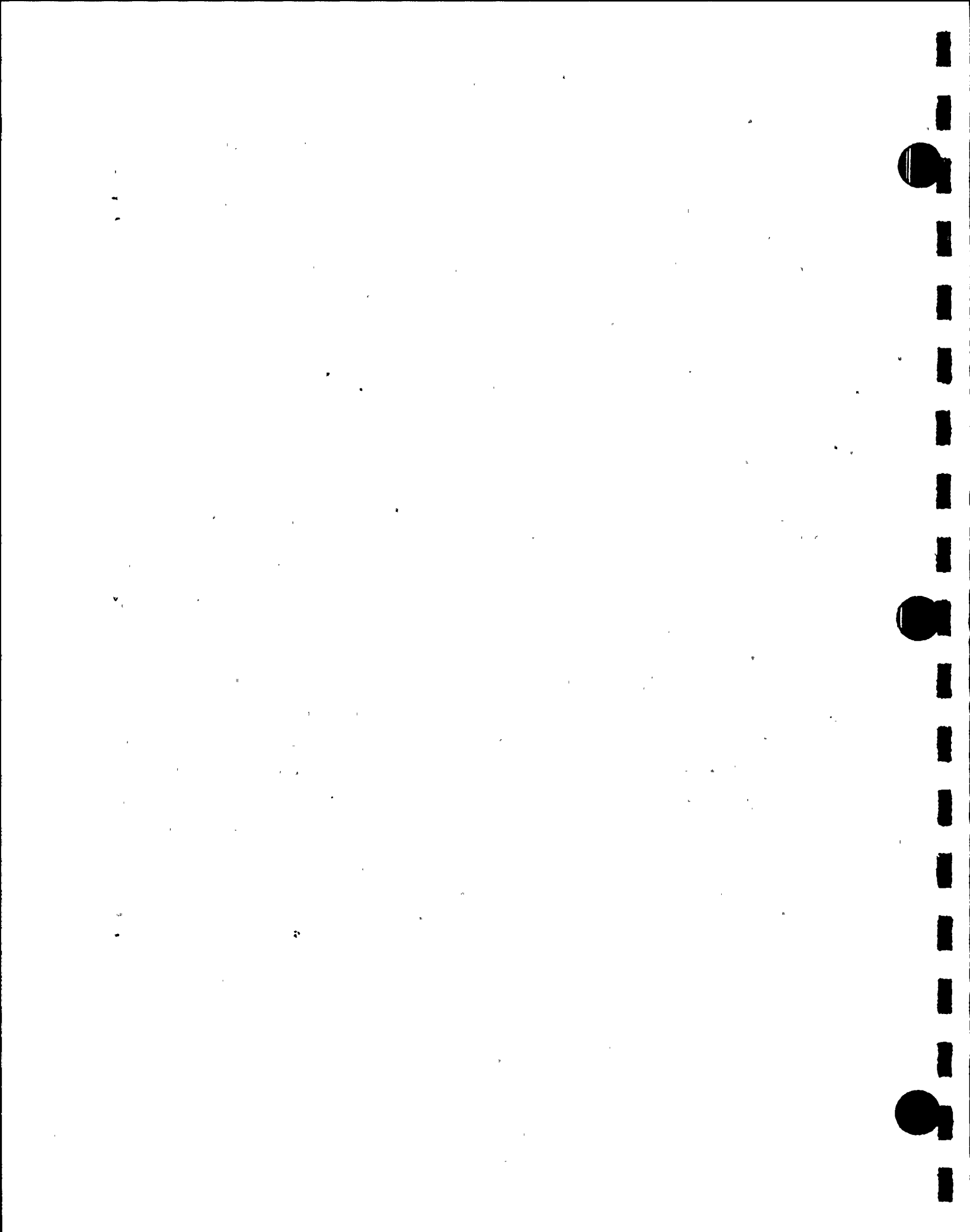
The coupon tree is placed in the center of a group of freshly discharged fuel assemblies each time a new batch is discharged to the pool. The group of assemblies surrounding the coupon tree shall be those which have the above-average values of radial peaking factor. The object, of course, is to subject this "tree" to the maximum radiation exposure in the fuel pool in the minimum amount of time.

Further details are provided in the following.

10.2 Coupon Surveillance

10.2.1 Description of Test Coupons

The neutron absorber used in the surveillance program shall be representative of the material used within the storage system. It shall be of the same composition, produced by the same method, and certified to the same criteria as the production lot neutron absorber. The sample coupon shall be the same thickness as the neutron absorber used within the storage system and shall meet the referenced Holtec drawing dimensional requirements. Each neutron absorber specimen shall be encased in a stainless steel jacket of an alloy identical to that used in the storage system, formed so as to encase the neutron absorbing material and fix it in a position and with tolerances similar to that for the storage racks. The jacket would be similar to that for the storage racks.



The jacket would be closed by quick disconnect clamps or screws with lock nuts in such a manner as to retain its form throughout the use period and also allow rapid and easy opening without contributing mechanical damage to the neutron absorber specimen contained therein.

Consistent with the USNRC OT Position Paper [reference 10.1.1], requirements of a statistically acceptable sample size, a total of twelve jacketed neutron absorber specimens, shall be used.

10.2.2 Benchmark Data

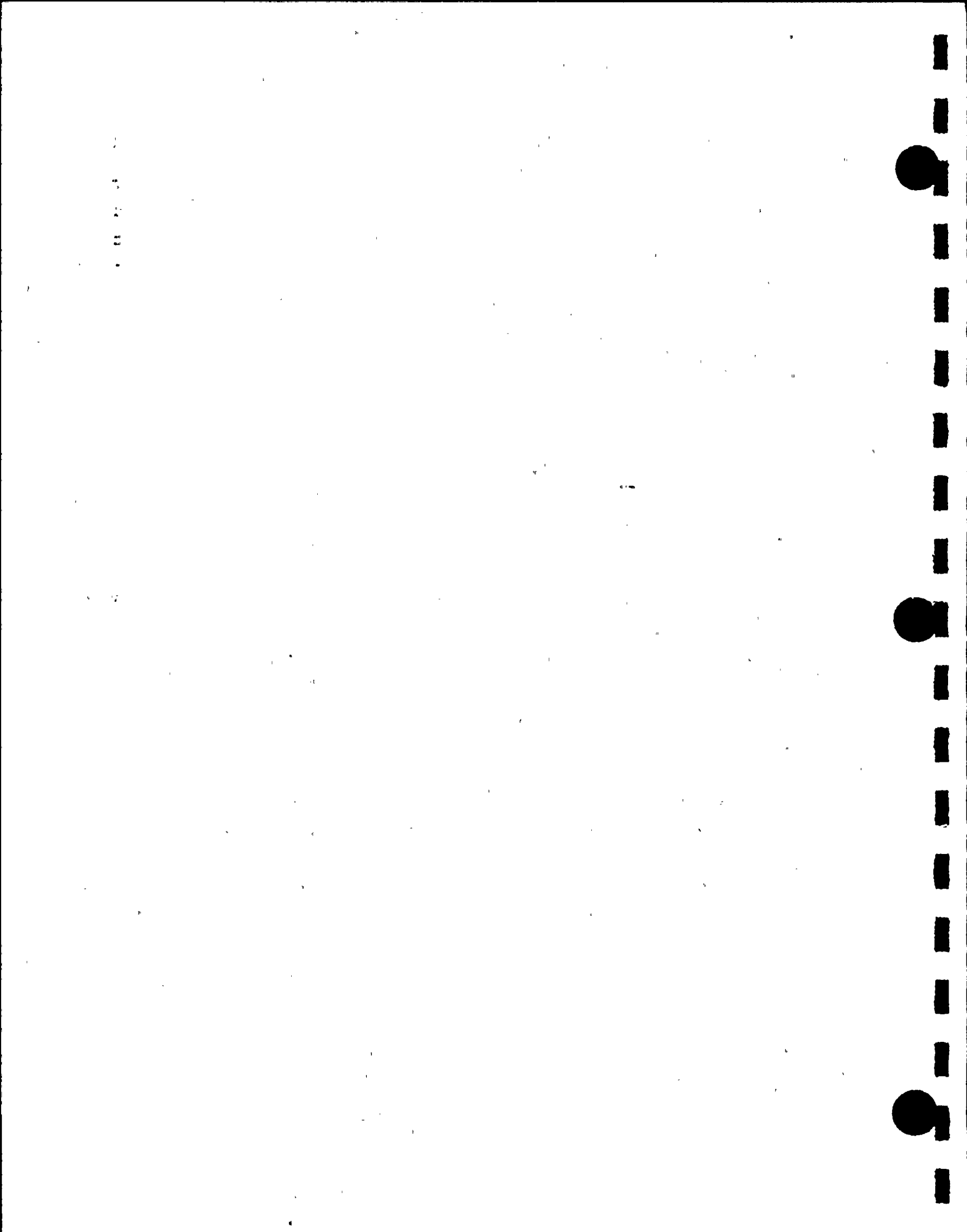
The following benchmark tests shall be performed on test coupons derived from the same production run as the actual neutron absorber panels.

- (i) Length, width, thickness and weight measurements
- (ii) Wet chemistry
- (iii) Neutron attenuation measurement (optional)

10.2.3 Coupon Reference Data

Prior to encasing the coupons, each coupon shall be carefully calibrated. Their width, thickness, length and weight shall be carefully measured and recorded. The wet chemistry will be performed on a strip taken from the same Boral plates from which the coupons are made to provide a benchmark B-10 loading data.

Three points on each coupon will be designated for neutron attenuation measurement. Neutron attenuation measurements at those three points will be made and recorded.



10.2.4 Accelerated Surveillance

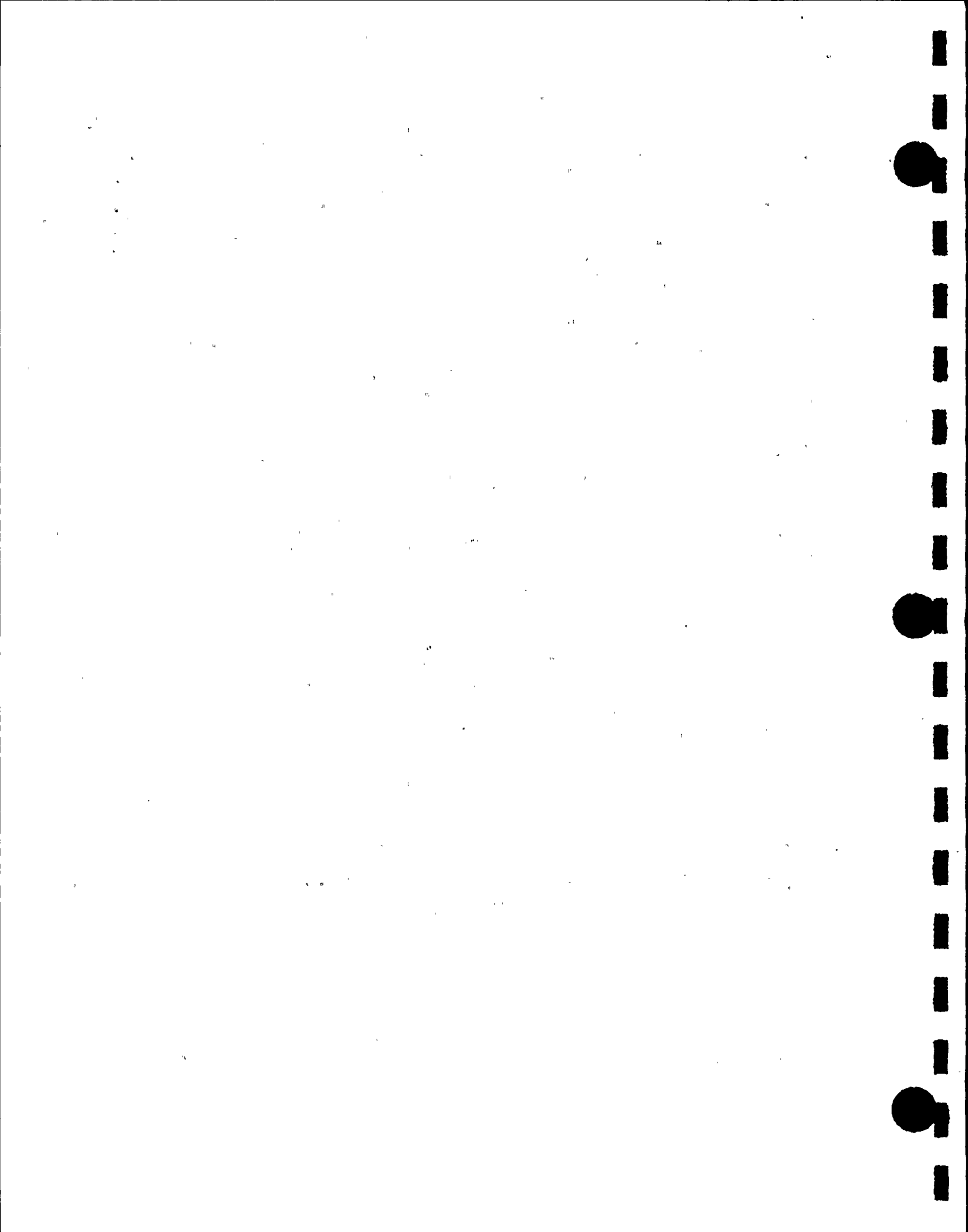
At the time of the first off-load of spent fuel, the coupon tree is surrounded by storage cells containing fuel assemblies from the peak power region of the reactor core. At the time of the second off-load of the fuel assemblies, the tree is withdrawn from the fuel pool and one coupon is taken for evaluation. The specimen strip is replaced in the fuel pool in a new location, where it is again surrounded by peak power region fuel assemblies. The storage cell that was vacated may now be used to store a fuel assembly. This arrangement is repeated at the first two off-loads of fuel and after that, every third outage. By evaluation of the specimens, an accelerated monitor of environmental effects on the neutron absorber will be obtained.

10.2.5 Post-Irradiation Tests

Coupons removed from the pool will be tested for dimensional, neutron attenuation, and wet chemistry changes using the same procedures which were used in initial benchmarking to minimize the potential for instrument errors.

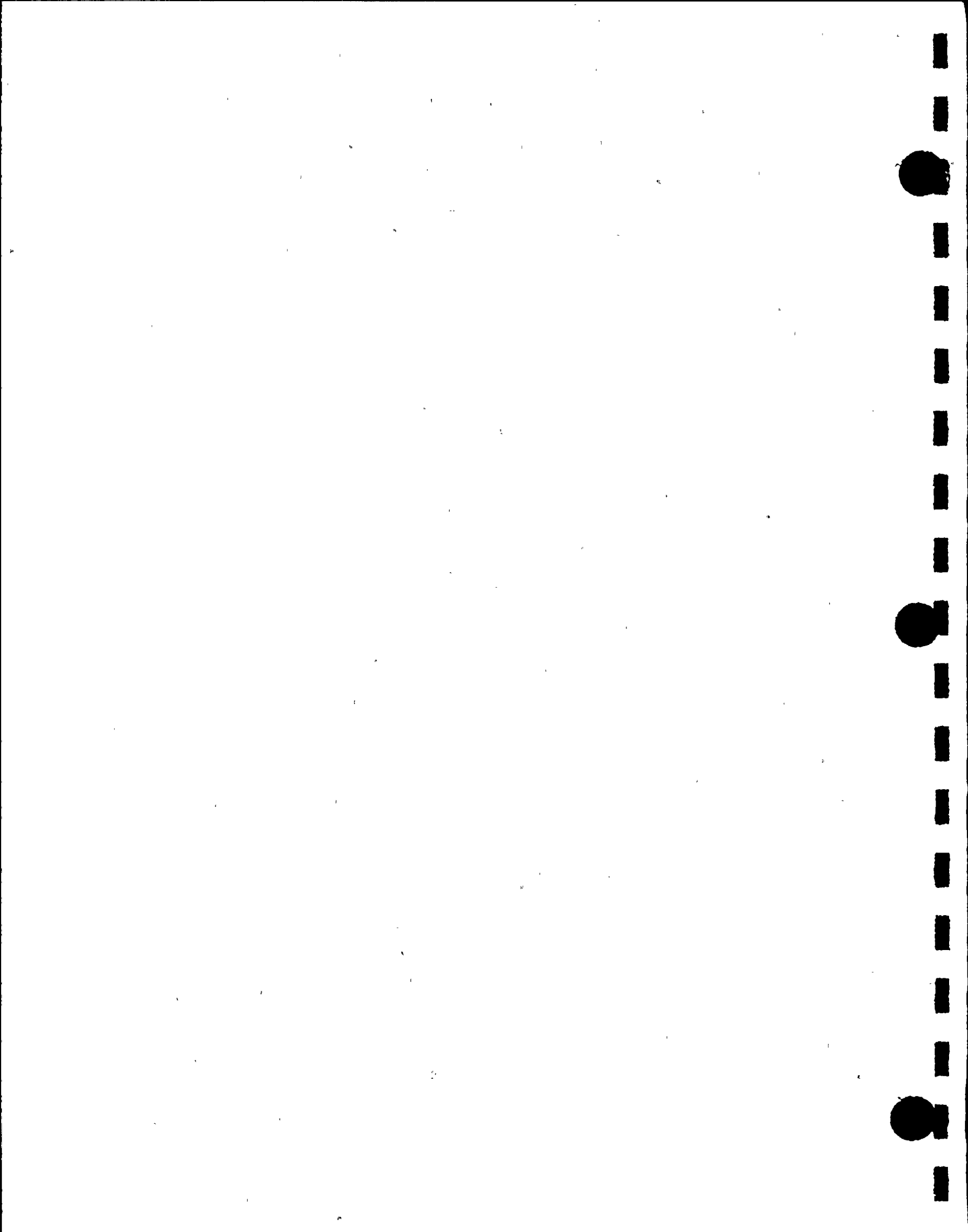
10.2.6 Acceptance Criteria

A plant procedure will be developed to execute the commitments made in this licensing submittal. Equipment requirements, step-by-step instructions for executing inspections and acceptance criteria will be described in that procedure for use by plant personnel.



10.3 References for Section 10

- 10.1.1 OT Position for Review and Acceptance of Spent Fuel Storage and Handling Applications", by Brian K. Grimes, USNRC, April 14, 1978, and Revision dated January 18, 1979.



11.0 ENVIRONMENTAL COST/BENEFIT ASSESSMENT

11.1 Introduction

The specific need to increase the existing storage capacity of the spent fuel pool at the Donald C. Cook Nuclear Plant is based on the continually-increasing inventory in the pool, the prudent requirement to maintain full-core offload capability, and a lack of viable economic alternatives.

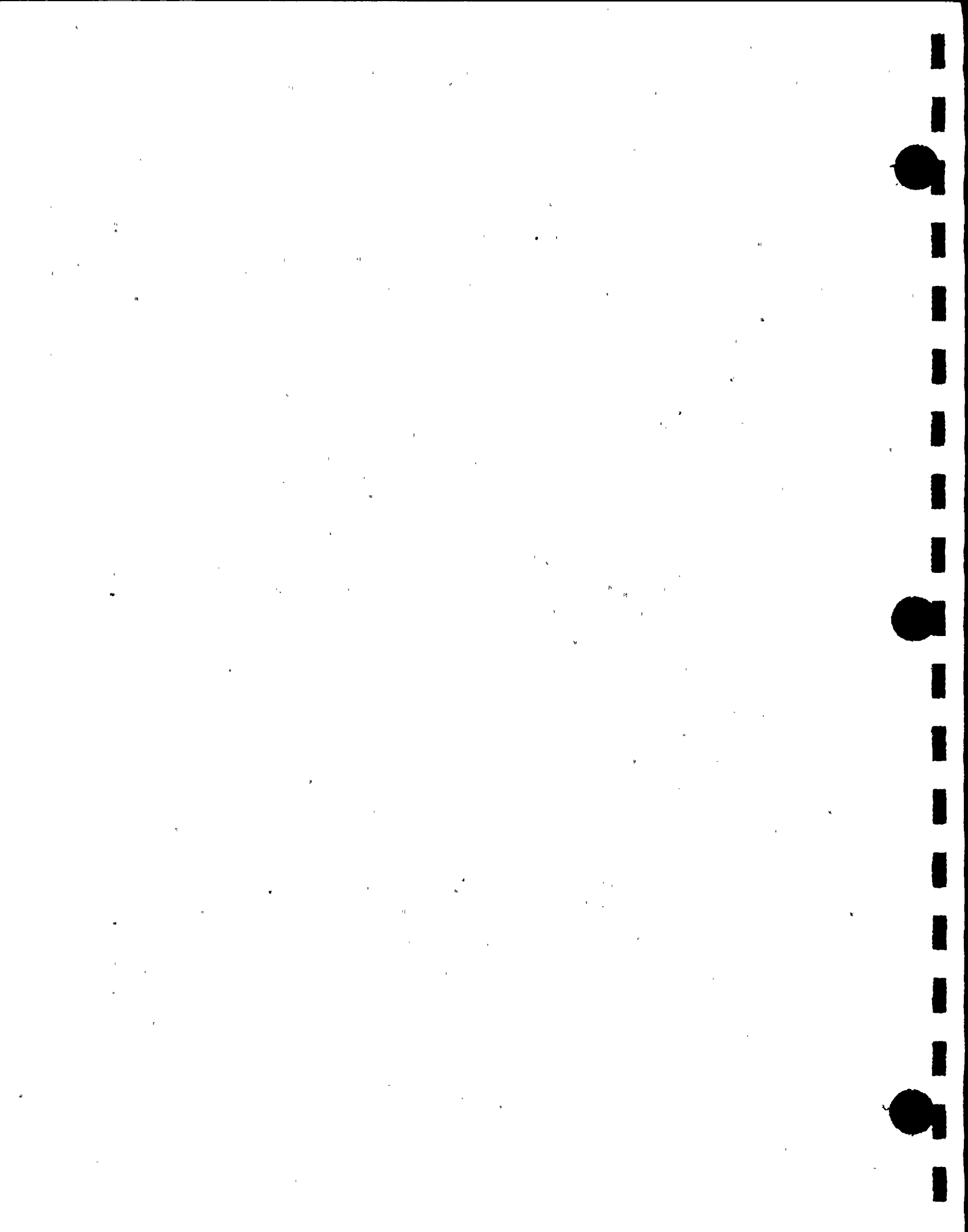
The inventory increase can be inferred from the fuel assembly discharge schedule contained in Table 11.1.

The proposed project contemplates the reracking of spent fuel pool with free-standing, high density, poisoned spent fuel racks. The engineering design and licensing will be completed for a full reracking of the pool, which is currently only partially racked. Engineering and design will also be completed to accommodate consolidated fuel. The licensing effort for consolidated fuel will, however, be pursued at a later date if consolidation is chosen to accommodate future storage needs.

11.2 Project Cost Assessment

The total capital cost for the rerack project is estimated to be approximately \$14.1 million.

Many alternatives were considered prior to proceeding with reracking, which is not the only technical option available to increase on-site storage capacity. Reracking does, however, enjoy a cost advantage over other technologies, as shown:



| <u>Type of Storage</u> | <u>Capital Costs</u>
<u>\$/KgU</u> |
|------------------------|---------------------------------------|
| Rerack | \$20 ⁽¹⁾ |
| Fuel consolidation | \$20 - 34 ⁽²⁾ |
| Dry cask storage | \$45 - 110 ⁽²⁾ |
| Storage vault | \$40 - 90 ⁽²⁾ |
| New pool | \$115 ⁽³⁾ |

There are no acceptable alternatives to develop off-site spent fuel storage capacity for the Cook Nuclear Plant. First, there are no commercial independent spent fuel storage facilities operating in the U.S. Second, the adoption of the Nuclear Waste Policy Act (NWPAct) created a de facto throw-away nuclear fuel cycle. Since the cost of spent fuel reprocessing is not offset by the salvage value of the residual uranium, reprocessing represents an added cost for the nuclear fuel cycle which already includes the NWPAct Nuclear Waste Fund fees. In any event, there are no domestic reprocessing facilities. Third, I&M has no other operating power plant; therefore, shipment of spent fuel from the Cook Nuclear Plant to other system nuclear power plants is not possible. Fourth, at \$600,000 per day replacement power cost, shutting down the Cook Nuclear Plant is many times more expensive than simply reracking the existing spent fuel pools.

(1) From EPRI NF-3580, May 1984

(2) From DOE RW-0220, "Final Version Dry Cask Storage Study," February 1989

(3) Actual estimated cost per KgU of storage space gained for this project

42.1

11.3 Resource Commitment

The expansion of the spent fuel pool capacity is expected to require the following primary resources:

Stainless steel 360 tons.

Boral Neutron Absorber 30 tons, of which 30 tons are Boron Carbide Powder and 20 tons are aluminum.

The requirements for stainless steel and aluminum represent a small fraction of total world output of these metals (less than .0001%). Although the fraction of world production of Boron Carbide required for the fabrication is somewhat higher than that of stainless steel or aluminum, it is unlikely that the commitment of Boron Carbide to this project will affect other alternatives. Experience has shown that the production of Boron Carbide is highly variable and depends upon need, and can easily be expanded to accommodate worldwide needs.

11.4 Environment Assessment

Due to the additional heat-load arising from increased spent fuel pool inventory, the anticipated maximum bulk pool temperature increases from a previously-licensed 140°F to approximately 160°F, as detailed in the calculations described in Section 5.0 of this report. The resultant total heat-load (worst case) is 35.5 million BTU/HR, which is less than 0.5% of the total plant heat loss to the environment.

The net result of the increased heat loss and water vapor emission (due to increased evaporation) to the environment is negligible.

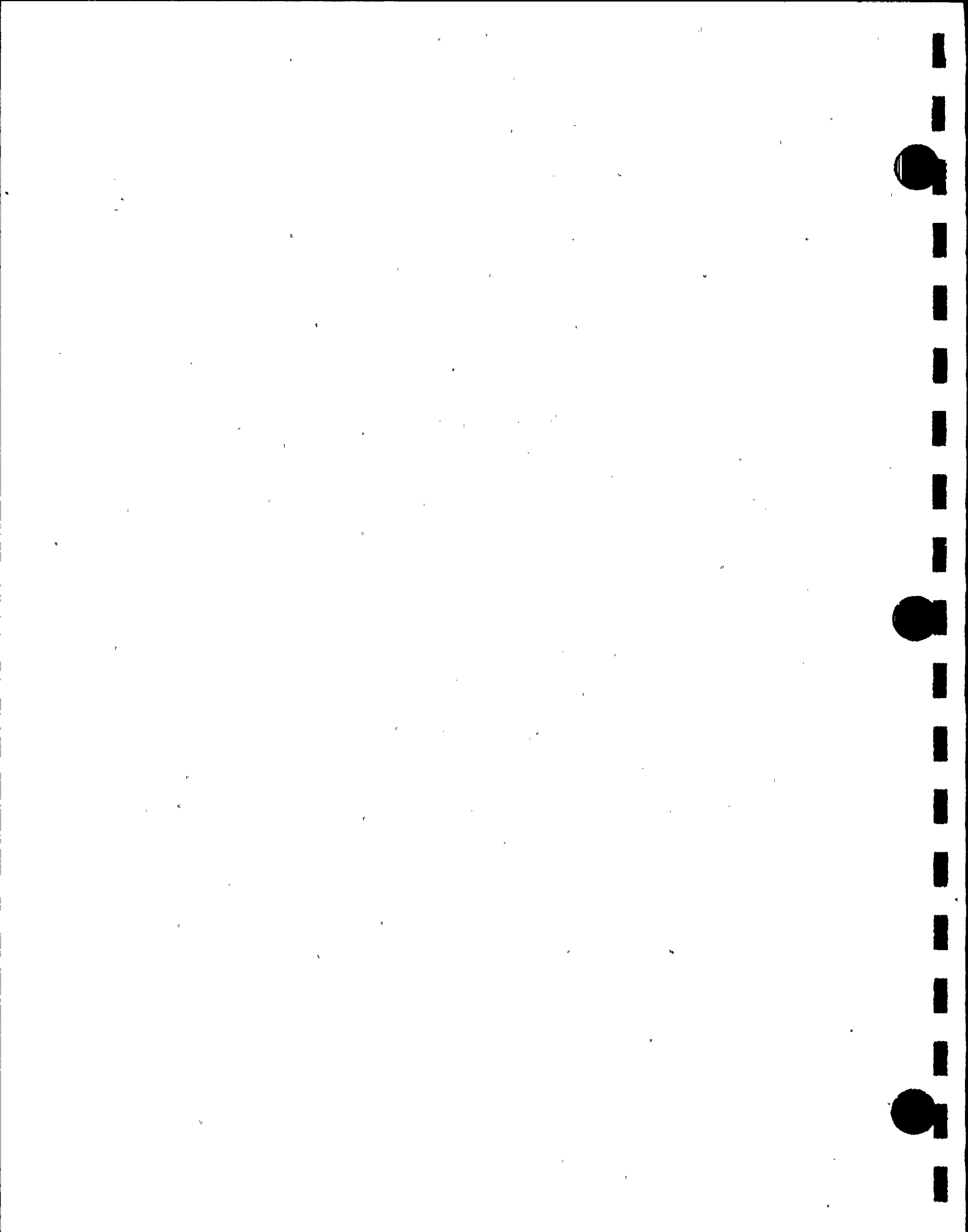


Table 11.1

DONALD C. COOK NUCLEAR PLANT
WORST CASE SPENT FUEL INVENTORY

| <u>YEAR</u> | <u>ASSEMBLIES
IN STORAGE</u> | |
|-------------|----------------------------------|---|
| 1991 | 1362 | |
| 1992 | 1518 | |
| 1993 | 1678 | |
| 1994 | 1838 | |
| 1995 | 1918 | Lose full core discharge capability with current capacity |
| 1996 | 1998 | |
| 1997 | 2158 | Lose normal discharge capability with current capacity |
| 1998 | 2318 | |
| 1999 | 2318 | |
| 2000 | 2478 | |
| 2001 | 2638 | |
| 2002 | 2798 | |
| 2003 | 2798 | |
| 2004 | 2958 | |
| 2005 | 3118 | |
| 2006 | 3198 | |
| 2007 | 3278 | |
| 2008 | 3438 | Lose full core discharge capability with proposed rerack |
| 2009 | 3598 | |
| 2010 | 3678 | Lose normal discharge capability with proposed rerack |
| 2011 | 3758 | |
| 2012 | 3918 | |
| 2013 | 4078 | |
| 2014 | 4158 | |
| 2015 | 4351 | |
| 2016 | 4431 | |
| 2017 | 4624 | |

